

The Study of Rhodium and Ruthenium Complexes for the Activation and  
Functionalization of Non-Polar Bonds

Samantha Anne Burgess  
Southborough, MA

Bachelors of Science Chemistry, Muhlenberg College, 2009

A Dissertation presented to the Graduate Faculty  
of the University of Virginia in Candidacy for the Degree of  
Doctor of Philosophy

Department of Chemistry

University of Virginia  
June, 2014

**ABSTRACT**

BURGESS, SAMANTHA A. The Study of Rhodium and Ruthenium Complexes for the Activation and Functionalization of Non-Polar Bonds. (Under the direction of Professor T. Brent Gunnoe).

The increasing global demand for fossil resources has amplified the importance of more efficient catalytic processes to convert hydrocarbons into higher value chemicals. Thus, the activation and subsequent functionalization of covalent bonds (*e.g.*, C–H, H–H, and Si–H) is a primary focus of the catalysis community. The activation of H–H, Si–H and C–H bonds by 1,2-addition across M–X (X = OR, NR<sub>2</sub>) bonds of d<sup>6</sup> and d<sup>8</sup> complexes has been reported, and these stoichiometric reactions are of interest for incorporation into catalytic cycles for hydrogenation, hydrosilylation or C–H functionalization. In this thesis, studies of 1,2-addition of Y–H bonds (Y = C, H, or Si) across a metal–alkoxide and amido bonds are reported.

The Rh(III) complexes [(<sup>t</sup>bpy)<sub>2</sub>Rh(OMe)(L)][X]<sub>n</sub> (<sup>t</sup>bpy = 4,4'-di-*tert*-butyl-2,2'-bipyridyl; L = MeOH, n = 2, X = OTf (OTf = trifluoromethanesulfonate) and TFA (TFA = trifluoroacetate); L = TFA, n = 1, X = OTf) have been shown to activate dihydrogen. Kinetic studies of this reaction reveal a first-order dependence on the Rh(III) methoxide complex and a dependence on dihydrogen that is between zero- and first-order. Combined experimental and computational studies have led to a proposed mechanism for hydrogen activation by [(<sup>t</sup>bpy)<sub>2</sub>Rh(OMe)(MeOH)][OTf][TFA] that involves MeOH dissociation, H<sub>2</sub> coordination, and 1,2-addition of dihydrogen across a Rh methoxide bond. The analogous complexes bearing TFA counterions, [(<sup>t</sup>bpy)<sub>2</sub>Rh(OMe)(L)][TFA]<sub>n</sub>

(L = MeOH, n = 2; L = TFA, n = 1), activate Si–H bonds of Et<sub>3</sub>SiH presumably by the 1,2-addition of a Si–H bond across a Rh methoxide bond.

The Rh(III) aniline complex [(<sup>Mes</sup>NNN)Rh(Me)(NH<sub>2</sub>Ph)(OTf)][OTf] (<sup>Mes</sup>NNN = 2,6-diacetylpyridinebis(2,4,6-trimethylaniline)) was synthesized. Deprotonation of coordinated aniline to give the corresponding anilido complex was not successful. For example, treatment of [(<sup>Mes</sup>NNN)Rh(Me)(NH<sub>2</sub>Ph)(OTf)][OTf] with NHEt<sub>2</sub> results in formation of the Rh(I) amido complex (<sup>Mes</sup>NNN)Rh(NEt<sub>2</sub>).

The C–H activation of benzene and catalytic ethylene hydrophenylation using a cationic Ru(II) metal complex, [(HC(pz<sup>5</sup>)<sub>3</sub>)Ru(P(OCH<sub>2</sub>)<sub>3</sub>CEt)(NCMe)Ph][BAR'<sub>4</sub>] (HC(pz<sup>5</sup>)<sub>3</sub> = tris(5-methyl-pyrazolyl)methane; BAR'<sub>4</sub> = tetrakis[3,5-bis(trifluoromethyl)phenyl]borate), has been pursued. Studies of our previously reported charge neutral Ru(II) ethylene hydrophenylation catalysts, TpRu(L)(NCMe)Ph [Tp = hydridotris(pyrazolyl)borate; L = CO, PMe<sub>3</sub>, P(OCH<sub>2</sub>)<sub>3</sub>CEt or P(OCH<sub>2</sub>)<sub>2</sub>(OCCH<sub>3</sub>)], suggest that accessing a less electron-rich cationic version of TpRu(P(OCH<sub>2</sub>)<sub>3</sub>CEt)(NCMe)Ph would give higher turnover numbers of ethylbenzene. Studies of catalytic ethylene hydrophenylation using the cationic Ru(II) complex [(HC(pz<sup>5</sup>)<sub>3</sub>)Ru(P(OCH<sub>2</sub>)<sub>3</sub>CEt)(NCMe)Ph][BAR'<sub>4</sub>] supports this hypothesis. The reaction of [(HC(pz<sup>5</sup>)<sub>3</sub>)Ru(P(OCH<sub>2</sub>)<sub>3</sub>CEt)(NCMe)Ph][BAR'<sub>4</sub>] (0.025 mol% relative to benzene) in benzene with C<sub>2</sub>H<sub>4</sub> (15 psi) at 90 °C gives 565 turnovers of ethylbenzene after 131 hours. This corresponds to an approximate one-pass 95% yield based on ethylene, and is a 28-fold improvement compared to the charge neutral catalyst TpRu(P(OCH<sub>2</sub>)<sub>3</sub>CEt)(NCMe)Ph. Under identical conditions, [(HC(pz<sup>5</sup>)<sub>3</sub>)Ru(P(OCH<sub>2</sub>)<sub>3</sub>CEt)(NCMe)Ph][BAR'<sub>4</sub>] is only 1.3 times less active than

TpRu(P(OCH<sub>2</sub>)<sub>3</sub>CEt)(NCMe)Ph, but the increased stability of the cationic Ru(II) catalyst allows higher temperatures (up to 175 °C) to be employed, which significantly enhance the rate by ~42-fold.

## ACKNOWLEDGEMENTS

First and foremost, I would like to thank my advisor Dr. T. Brent Gunnoe. Without your guidance, endless ideas and enthusiasm, my PhD research would not have been successful. I appreciate all that you have taught me over the course of the last five years. I am grateful for the secure funding that you have provided me throughout my graduate career. I would also like to thank my committee, Dr. Harman, Dr. Fraser, Dr. Demas and Dr. Davis for taking time out of their busy schedules to read my thesis and be a part of my defense.

I would like to thank all the Gunnoe Group members past and present. You are the only people who truly understand what this experience has entailed. I greatly appreciate your willingness to read countless drafts of my thesis chapters and papers and provide feedback on my presentations. To those Gunnoe lab students who have yet to graduate, I know you can do it! Steve, I have enjoyed working with you not only in the Keane lab at Muhlenberg but also as a member of the Gunnoe Group. I could not have asked for a better person to work alongside in our Vigor glovebox. Thank you for your endless help, encouragement, and for all the laughs we have shared over the years. It is going to be very strange not to work with you next year. Kathleen, I will miss your company and our conversations. We have an extremely tough project and I know that you will be successful.

There are a number of past members of the Gunnoe lab who I would especially like to thank. First, I would like to thank Dr. Evan Joslin for being a good friend throughout graduate school. Thank you for pulling me out of the lab to attend football games, girl's nights, GSASC events, and recruiting me to be a member of the Huskey

Committee. I would also like to thank Evan for always providing me with a positive insight and encouragement. My last year has been extremely lonely without having Evan as my orthogonal desk buddy. Also, thank you so much Evan for letting me run catalysis with your complex  $[(HC(pz^5)_3)Ru(P(OCH_2)_3OCEt)(NCMe)Ph][BAR'_4]$ . It was a joy to have a project that actually worked!

I would also like to thank Dr. Mark Pouy for everything he has taught me whether it was related to kinetic studies, organic reactions, Kaleidagraph, MestReNova, or ChemDraw shortcuts. Also thank you for all the Gunnoe lab social events that you organized during your time as a postdoc. I would also like to thank “my Hercules” Dr. Jeremy Andreatta. I appreciate your continual willingness to stop what you were doing to help me lift or open something that I was not strong enough to do on my own. To Dr. Laurel Goj Habgood, thank you so much for all the advice and encouragement you have provided. I greatly enjoyed the time that I was able to spend with you during your research sabbaticals at UVA. Dr. Joanna Webb, I am still in shock that our Dalton review has actually been published. Thank you so much for enduring this with me. Dr. Tamara Bolaño, I am glad that I was finally able to get your bismethoxide complex to display interesting reactivity.

I would like to thank Dr. Jeff Ellena for the enormous amount of help he has provided. I appreciate his willingness to help me set up obscure NMR experiments and observe nuclei such as  $^{15}N$  and  $^{29}Si$  that are not routinely observed in our department. I am especially grateful to Jeff for allowing me to monopolize the Burger during my fourth and fifth years of graduate school so that I could run all my  $H_2$  activation arrays. I am

thankful for your patience especially when I made mistakes, which made your job more difficult.

I would like to thank Dr. Michal Sabat for always taking a look at my tiny Rh crystals and managing to give me publishable X-ray crystal structures. Also, thank you to Dr. Bill Myers at the University of Richmond for running HRMS analysis of my complexes.

I would also like to thank other students outside of the Gunnoe lab who have helped make the last five years more enjoyable. Anusa Thapa, thank you for being the best roommate I could ask for. Thank you for enduring my neat-freak tendencies and for teaching me about your Nepalese culture. Thank you for your willingness to go for hikes, play in the snow, or celebrate a birthday with me. Thank you to Jared Pienkos and Mike Ferracane for being my study buddies during our first year. Thank you for spending long hours in our “club house” room in the chemistry library explaining stereochemistry and organic transition states to me. Thank you to Morgan Bolden and Joe Houck for hosting all the football tailgates. Thank you to all the Harman lab members, especially Jared Pienkos, Ben Liebov, and Vic Zottig, for always letting me use your equipment or borrow a chemical. I would also like to thank Ben for being another past Dr. Keane group member to reminisce with.

Thank you to all the departmental administrative staff (Susie, Cindy, Eddie, Debbie, Victoria, Valerie, and Joe) for making the lives of chemistry graduate students a lot easier. Also thank you to Danny Via for being the best stockroom manager we could ask for. A special thank you to Jerry and Larry for promptly fixing everything that broke in lab. I also really appreciate the custodial staff for keeping our labs clean.

I would like to thank my undergraduate research advisor Dr. Joseph Keane for opening my eyes to synthetic chemistry and inspiring me to pursue research. I am also very thankful for all the experiences that I was provided while studying chemistry at Muhlenberg College.

Most importantly, I would like to thank my family for all their love and support. I appreciate all the opportunities that my parents have provided me with during my lifetime. Thank you Mom, Dad, Stephen, and David for withstanding me and being the best parents and brothers that I could ever ask for. Thank you to my Aunt Donna and Uncle Wayne. I have greatly enjoyed spending Thanksgiving and other holidays at your house during my graduate school career. Aunt Donna thank you for being my shopping buddy and Uncle Wayne I really appreciate all the delicious homemade meals you have prepared for me. I would like to thank my Grandma and Grannie for always thinking of me. I would like to thank my Nanny who passed away in December of 2010 for inspiring me to be a strong woman and to always pursue my dreams.

## TABLE OF CONTENTS

<b>LIST OF SCHEMES .....</b>	<b>XI</b>
<b>LIST OF FIGURES .....</b>	<b>XVII</b>
<b>LIST OF TABLES .....</b>	<b>XXI</b>
<b>1 Introduction.....</b>	<b>1</b>
<b>1.1 Brief Introduction.....</b>	<b>1</b>
<b>1.2 Hydrocarbon Functionalization .....</b>	<b>2</b>
1.2.1 Hydrocarbon Functionalization by Hydrogen Atom Abstraction .....	6
1.2.2 Hydrocarbon Functionalization by C–H Activation .....	7
1.2.3 Homogeneous Catalysis for RH Functionalization .....	9
1.2.4 Proposed Catalytic Cycle for Hydrocarbon Functionalization .....	13
<b>1.3 1,2-CH-Addition by Early Metal Imido Complexes.....</b>	<b>16</b>
1.3.1 Zr Imido Complexes.....	16
1.3.2 Tantalum, Vanadium, and Tungsten Imido Complexes.....	21
1.3.3 (PNP)Scandium imido complex.....	24
<b>1.4 Activation of H–H and C–H Bonds by Late Transition Metal Heteroatom   Complexes .....</b>	<b>25</b>
1.4.1 H <sub>2</sub> Activation by Late Transition Metal Complexes.....	25
1.4.2 Intramolecular C–H Activation by Late Transition Metal Complexes .....	28
1.4.3 1,2-CH-Addition by d <sup>6</sup> Metal Amido and Anilido Complexes.....	31
1.4.4 Arene C–H Activation by d <sup>8</sup> M–Heteroatom Complexes.....	38
<b>1.5 M–R Functionalization.....</b>	<b>42</b>
<b>1.6 Summary and Thesis Outline .....</b>	<b>44</b>
<b>1.7 References.....</b>	<b>48</b>
<b>2 Synthesis and Characterization of Rh(III) Anilido, Hydroxide and Methoxide Complexes.....</b>	<b>58</b>
<b>2.1 Introduction .....</b>	<b>58</b>
<b>2.2 Results and Discussion .....</b>	<b>63</b>
2.2.1 Synthesis of Rh(III) Aniline and Anilido Compounds .....	63
2.2.2 Synthesis of Rh(III)–OH, H <sub>2</sub> O, OMe and MeOH Compounds.....	73
2.2.3 Reactivity of [( <sup>t</sup> bpy) <sub>2</sub> Rh(X) <sub>2</sub> ] <sup>+</sup> (X = NHPH, OH, OMe) with MOTf (M = Ag, Tl, Na) Salts.....	84
2.2.4 Discussion of X-ray Crystal Data for Aniline and Anilido Complexes .....	91
<b>2.3 Attempted Arene H/D Exchange using (<sup>t</sup>bpy)<sub>2</sub>Rh(OH)<sub>2</sub>][OTf] (7).....</b>	<b>93</b>

	IX
2.4	Conclusions ..... 96
2.5	Experimental Section ..... 96
2.6	References ..... 112
<b>3</b>	<b>1,2-Addition of Dihydrogen Across Rh(III)–OMe Bonds .....117</b>
3.1	Introduction .....117
3.2	Results and Discussion .....121
3.3	Conclusions .....157
3.4	Experimental Section .....158
3.5	References .....173
<b>4</b>	<b>Work in Progress: Si–H Activation Across Rh(III)–OMe Bonds .....177</b>
4.1	Introduction ..... 177
4.2	Results and Discussion ..... 180
4.2.1	Characterization of the Organic Reaction Products ..... 184
4.2.2	Identity of the Rh–H Complexes ..... 187
4.2.3	Control Reactions ..... 192
4.3	Summary and Future Work..... 193
4.4	Experimental Section ..... 194
4.5	References ..... 196
<b>5</b>	<b>Synthesis of Rh–Heteroatom Complexes with Pyridine-Diimine Ligand.....199</b>
5.1	Introduction .....199
5.2	Results and Discussion .....202
5.2.1	Synthesis of 2,6-diacetylpyridinebis(2,4,6-trimethylaniline) .....202
5.2.2	Synthesis of ( <sup>Mes</sup> NNN)Rh(Cl) and Oxidation to ( <sup>Mes</sup> NNN)Rh(Me)(OTf) <sub>2</sub> ..203
5.2.3	Synthesis of [( <sup>Mes</sup> NNN)Rh(Me)(OTf)(NH <sub>2</sub> Ph)][OTf] ( <b>4</b> ) .....207
5.2.4	Synthesis of ( <sup>Mes</sup> NNN)Rh(NEt <sub>2</sub> ) ( <b>5</b> ).....209
5.3	Treatment of [( <sup>Mes</sup> NNN)Rh(Me)(OTf)(NH <sub>2</sub> Ph)][OTf] ( <b>4</b> ) with Base.....217
5.3.1	Reactivity of (MesNNN)Rh(NEt <sub>2</sub> ) ( <b>5</b> ) .....220
5.4	Initial Exploration of Other NNN Complexes .....221
5.5	Conclusions .....221
5.6	Possible Future Work .....222
5.7	Experimental.....224
5.8	References..... 228

<b>6 Hydrophenylation of Ethylene using a Cationic Ru(II) Catalyst: Comparison to a Neutral Ru(II) Catalyst</b> .....	<b>230</b>
<b>6.1 Introduction</b> .....	<b>230</b>
<b>6.2 Results and Discussion</b> .....	<b>234</b>
6.2.1 Synthesis of Ru(II) Poly(pyrazolyl) Alkane Complexes .....	234
6.2.2 Catalytic Ethylene Hydrophenylation.....	238
6.2.3 Degenerate NCMe/NCCD <sub>3</sub> Exchange .....	251
6.2.4 Stoichiometric C–D Activation of C <sub>6</sub> D <sub>6</sub> .....	254
6.2.5 Other Olefin Hydroarylation Reactions .....	257
<b>6.3 Conclusion</b> .....	<b>259</b>
<b>6.4 Future Work</b> .....	<b>260</b>
<b>6.5 Experimental</b> .....	<b>265</b>
<b>6.6 References</b> .....	<b>276</b>
<b>7 Summary and Future Outlook</b> .....	<b>281</b>
<b>7.1 Activation of Nonpolar Bonds by 1,2-Addition across Rh–X (X = OR, NHR) Bonds</b> .....	<b>281</b>
7.1.1 Rh(III) Heteroatom Complexes Supported by Bipyridyl and Pyridine-Diimine Ligands for 1,2-Addition of C–H, H–H and Si–H Bonds .....	282
7.1.2 Future Synthetic Targets .....	283
<b>7.2 Ethylene Hydrophenylation Using a Ru(II) Complex Supported by a Charge Neutral Poly(pyrazolyl) Alkane Ligands</b> .....	<b>285</b>
7.2.1 Future Directions .....	287
<b>7.3 References</b> .....	<b>288</b>

## LIST OF SCHEMES

## CHAPTER 1

Scheme 1.1. Proposed cycle for catalytic hydrocarbon functionalization.....	2
Scheme 1.2. The current method for the synthesis of phenol.....	6
Scheme 1.3. C–H bond cleavage by hydrogen atom abstraction (X = O, OR, NR, etc.)..	7
Scheme 1.4. Mechanism for metal mediated C–H activation.....	9
Scheme 1.5. Differences in the transition states for 1,2-CH-addition versus $\sigma$ -bond metathesis.....	9
Scheme 1.6. Proposed catalytic cycle for the conversion of alkanes to alcohols or alkyl chlorides using the Pt(II) Shilov catalyst.....	10
Scheme 1.7. Conversion of methane to methyl trifluoroacetate (MeTFA) using KX (X = F, Cl, Br or I) and NH <sub>4</sub> IO <sub>3</sub> .....	11
Scheme 1.8. Proposed catalytic cycle for hydrocarbon functionalization incorporating 1,2-CH-addition across M=O or M–OR bonds.....	15
Scheme 1.9. The functionalization step for the catalytic cycle shown in Scheme 1.8. ....	15
Scheme 1.10. Overall reaction of Cp <sub>2</sub> Zr(CH <sub>3</sub> )(NHR) [R = 4- <i>tert</i> -butylphenyl (Ar <sup>t</sup> Bu) or <i>tert</i> -butyl ( <sup>t</sup> Bu)] with benzene.....	16
Scheme 1.11. Benzene C–H activation by reaction intermediate, Cp <sub>2</sub> Zr(NR)( $\eta^2$ -C,H-benzene) showing the involvement of the lone pair in C–H activation.....	17
Scheme 1.12. Rotation about the Zr–N bond enables proper orientation of the NH for H atom transfer to the methyl ligand.....	18
Scheme 1.13. Proposed mechanism for the reaction of ( <sup>t</sup> Bu <sub>3</sub> SiNH) <sub>3</sub> Zr(CH <sub>3</sub> ) and C <sub>6</sub> D <sub>6</sub> ..	18
Scheme 1.14. Calculated activation barriers for the addition of H <sub>2</sub> across a Zr=NH versus Zr–NH <sub>2</sub> bonds of (NH <sub>2</sub> ) <sub>2</sub> Zr=NH. <sup>88</sup> .....	20
Scheme 1.15. 1,2-CH-addition of RH across Zr=NR bonds of (RNH) <sub>2</sub> Zr=NR showing the four-centered transition state.....	20
Scheme 1.16. Two-step reductive elimination of methane from ( <sup>t</sup> Bu <sub>3</sub> SiNH) <sub>3</sub> ZrCH <sub>3</sub> .....	21
Scheme 1.17. Proposed mechanism for R'H elimination from ( <sup>t</sup> Bu <sub>3</sub> SiNH) <sub>3</sub> TaR' and subsequent H/D exchange (RDS = rate determining step). Rates of R'H elimination at 183 °C are shown.....	23
Scheme 1.18. Calculated reaction pathway for the activation of alkanes (RH) by (R'O) <sub>2</sub> Ti=NR' and calculated $\Delta G$ for methane adduct formation.....	23
Scheme 1.19. Reaction of [( <sup>t</sup> Bu <sub>3</sub> SiN=) <sub>3</sub> WH]K with CH <sub>3</sub> I and CD <sub>3</sub> I to produce tungsten methyl amido complexes via the formation of an intermediate methane adduct.....	24
Scheme 1.20. Plausible mechanism for the activation of dihydrogen by (PCP)Ru(CO)(NH <sub>2</sub> ).....	26
Scheme 1.21. Activation of dihydrogen by (PCP)Pd(OR) (R = H or CH <sub>3</sub> ).....	27
Scheme 1.22. Pt(s) catalyzes the addition of H <sub>2</sub> to the Pt–NHPh bond of ( <sup>t</sup> bpy)Pt(Me)(NHP).....	28
Scheme 1.23. Intramolecular C–H activation by (PCP)Ru(CO)(NH <sub>2</sub> ) and (PCP)Ru(CO)(Me) to produce methane and cyclometalated complex.....	30
Scheme 1.24. Calculated energetics (DFT) for H <sub>2</sub> and CH <sub>4</sub> activation by (PCP')Ru(CO)(NH <sub>2</sub> ).....	31

Scheme 1.25. Proposed mechanism for benzene H/D exchange encompassing the 1,2-addition of benzene C–D bonds across Ru–X bond of TpRu(PMe <sub>3</sub> ) <sub>2</sub> XH (X = O or NPh).....	32
Scheme 1.26. DFT [B3LYP/ CEP-31G(d)] calculated free energies of activation for C <sub>6</sub> H <sub>6</sub> C–H activation across the Ru–OH bond of (Tab)Ru(PH <sub>3</sub> )(OH)(η <sup>2</sup> -C <sub>6</sub> H <sub>6</sub> ) and the Ru–Me bond of (Tab)Ru(PH <sub>3</sub> )(Me)(η <sup>2</sup> -C <sub>6</sub> H <sub>6</sub> ) [Tab = tris(azo)borate].....	33
Scheme 1.27. Calculated free energies for C <sub>6</sub> H <sub>6</sub> C–H activation using the model complex (Tab)Ru(PH <sub>3</sub> ) <sub>2</sub> (OH) (Tab = tris(azo)borate). .....	33
Scheme 1.28. Proposed mechanism for benzene C–H activation by (acac) <sub>2</sub> Ir(OMe)(L) (L = py or CH <sub>3</sub> OH). .....	34
Scheme 1.29. Isophthalic acid H/D exchange in the presence and absence (value in parentheses) of 1 mol% catalyst. ....	36
Scheme 1.30. Proposed mechanism for nucleophilic C–H activation of water-soluble arenes using (IPI)Ru(OH) <sub>n</sub> (H <sub>2</sub> O) <sub>m</sub> (R = CO <sub>2</sub> H or OH). ....	36
Scheme 1.31. Reaction profile for C–H activation by 18-electron octahedral complexes showing that $\Delta E^\ddagger_{\text{tot}} = \Delta E_{\text{lig}} + \Delta E_{\text{coord}} + \Delta E^\ddagger_{\text{clv}}$ . ....	37
Scheme 1.32. Proposed mechanism for arene C–H bond activation with (PNP)Rh(OR) (R = H or CH <sub>2</sub> CF <sub>3</sub> ; R'H = arene). .....	39
Scheme 1.33. Proposed mechanism for indene C–H activation by [(COD)Rh(μ-OH)] <sub>2</sub> (TFE = 2,2,2-trifluoroethanol, Solv = H <sub>2</sub> O or TFE). .....	41
Scheme 1.34. Benzene C–H activation by (BIAN)Pt(OH) <sub>2</sub> catalyzed by <i>in situ</i> generated Pt(0) particles.....	41
Scheme 1.35. Baeyer–Villiger oxy-insertion pathway for methanol formation from MTO and IO <sub>4</sub> <sup>−</sup> . .....	43
Scheme 1.36. Lumiflavin derivative has been shown to catalyze the reaction of MTO with H <sub>2</sub> O <sub>2</sub> .....	43
Scheme 1.37. Generic illustration of the Rh and Ru complexes described in Chapters 2, 3, 4, 5 and 6. ....	47

## CHAPTER 2

Scheme 2.1. Transition metal heteroatom complexes exhibit bifunctional character. ....	63
Scheme 2.2. Synthesis of [( <sup>t</sup> bpy) <sub>2</sub> Rh(Me)(NH <sub>2</sub> Ph)][BAR' <sub>4</sub> ][OTf] ( <b>1</b> ). .....	64
Scheme 2.3. Synthesis of [( <sup>t</sup> bpy) <sub>2</sub> Rh(Me)(NHPh)][BAR' <sub>4</sub> ] ( <b>2</b> ). .....	67
Scheme 2.4. Synthesis of [( <sup>t</sup> bpy) <sub>2</sub> Rh(NH <sub>2</sub> Ph) <sub>2</sub> ][OTf] <sub>3</sub> ( <b>3</b> ). .....	68
Scheme 2.5. Deprotonation of [( <sup>t</sup> bpy) <sub>2</sub> Rh(NH <sub>2</sub> Ph) <sub>2</sub> ][OTf] <sub>3</sub> ( <b>3</b> ) to give [( <sup>t</sup> bpy) <sub>2</sub> Rh(NHPh) <sub>2</sub> ][OTf] ( <b>5</b> ). .....	71
Scheme 2.6. Synthesis of [( <sup>t</sup> bpy) <sub>2</sub> Rh(OH) <sub>2</sub> ][OTf] ( <b>7</b> ). .....	74
Scheme 2.7. Synthesis of [( <sup>t</sup> bpy) <sub>2</sub> Rh(H <sub>2</sub> O) <sub>2</sub> ][OTf] <sub>3</sub> ( <b>8</b> ). .....	77
Scheme 2.8. Synthesis of [( <sup>t</sup> bpy) <sub>2</sub> Rh(OMe)(Cl)]Cl ( <b>9</b> ). .....	78
Scheme 2.9. Synthesis of [(bpy) <sub>2</sub> Rh(OR) <sub>2</sub> ][PF <sub>6</sub> ] (R = H, Me) by addition of excess CsOH·H <sub>2</sub> O to [(bpy) <sub>2</sub> Rh(py)(Cl)][PF <sub>6</sub> ]. .....	82
Scheme 2.10. The synthesis of [( <sup>t</sup> bpy) <sub>2</sub> Rh(OH)(H <sub>2</sub> O)][OTf] <sub>2</sub> ( <b>12</b> ). .....	85
Scheme 2.11. Addition of MOTf (M = Tl or Ag) to a CH <sub>3</sub> CN solution of [( <sup>t</sup> bpy) <sub>2</sub> Rh(NHPh) <sub>2</sub> ][OTf] ( <b>5</b> ) leads to formation of [( <sup>t</sup> bpy) <sub>2</sub> Rh(NHPh)(NH <sub>2</sub> Ph)][OTf] <sub>2</sub> ( <b>14</b> ) via <i>in situ</i> generated HOTf.....	89

Scheme 2.12. Proposed benzene H/D exchange using $[(^1\text{bpy})_2\text{Rh}(\text{OH})_2]\text{OTf}$ ( <b>7</b> ) and a Lewis acid (LA).....	94
Scheme 2.13. General depiction of reaction conditions for H/D exchange reactions between benzene and deuterated solvents in the presence of 10 mol% $[(^1\text{bpy})_2\text{Rh}(\text{OH})_2]\text{OTf}$ .....	95

### CHAPTER 3

Scheme 3.1. The oxidative addition of dihydrogen across M–X (X = OR, NR <sub>2</sub> or SR) bonds. ....	117
Scheme 3.2. The 1,2-addition of dihydrogen across M–X (X = OR, NR <sub>2</sub> or SR) bonds. ....	118
Scheme 3.3. Mechanism for metal mediated heterolytic cleavage of H <sub>2</sub> in the hydrogenation of aldehydes, ketone and imines. (X = O, N). ....	118
Scheme 3.4. A reported example of hydrogenolysis of diaryl ethers. <sup>7</sup> .....	118
Scheme 3.5. Synthesis of $[(^1\text{bpy})_2\text{Rh}(\text{OMe})_2]\text{OTf}$ ( <b>1</b> ).....	122
Scheme 3.6. The reaction of $[(^1\text{bpy})_2\text{Rh}(\text{OMe})_2][\text{OTf}]$ ( <b>1</b> ) with HTFA (1 equivalent) leads to the formation of three products.....	124
Scheme 3.7. Intramolecular proton transfer between the methoxide and methanol ligands of $[(^1\text{bpy})_2\text{Rh}(\text{OMe})(\text{MeOH})][\text{OTf}][\text{TFA}]$ ( <b>4</b> ). ....	128
Scheme 3.8. The reaction of complexes <b>4</b> and <b>5</b> ultimately leads to the formation of $[(^1\text{bpy})_2\text{Rh}(\text{H})(\text{TFA})][\text{OTf}]$ ( <b>6</b> ).....	131
Scheme 3.9. The oxidative addition of HTFA or HCl to the Rh(I) complexes $[(^1\text{bpy})_2\text{Rh}]^+$ gives the hydride complexes $[(^1\text{bpy})_2\text{Rh}(\text{H})(\text{TFA})]^+$ and $[(^1\text{bpy})_2\text{Rh}(\text{H})(\text{Cl})]^+$ respectively. ....	132
Scheme 3.10. The reaction of $[(^1\text{bpy})_2\text{Rh}(\text{H})(\text{TFA})][\text{OTf}]$ ( <b>6</b> ) with CH <sub>2</sub> Cl <sub>2</sub> leads to the formation of a second hydride species, $[(^1\text{bpy})_2\text{Rh}(\text{H})(\text{Cl})][\text{TFA}]$ ( <b>7</b> ), and excess CH <sub>2</sub> Cl <sub>2</sub> leads to the formation of $[(^1\text{bpy})_2\text{Rh}(\text{Cl})_2][\text{TFA}]$ ( <b>8</b> ).....	133
Scheme 3.11. The reaction of $[(^1\text{bpy})_2\text{Rh}(\text{H})(\text{TFA})][\text{OTf}]$ ( <b>6</b> ) with excess CH <sub>2</sub> Br <sub>2</sub> leads to the formation of $[(^1\text{bpy})_2\text{Rh}(\text{Br})_2][\text{TFA}]$ ( <b>9</b> ) without observation of an intermediate hydride species.....	136
Scheme 3.12. Monitoring the rate of coordinated MeOH exchange with free CD <sub>3</sub> OD gives rate of MeOH dissociation (see Table 3.3).....	142
Scheme 3.13. Monitoring the rate of MeOH exchange with coordinated CD <sub>3</sub> OD of $[(^1\text{bpy})_2\text{Rh}(\text{OCD}_3)(\text{CD}_3\text{OD})][\text{OTf}][\text{TFA}]$ gives the rate of CD <sub>3</sub> OD dissociation....	143
Scheme 3.14. Proposed pathway for the formation of HD, H <sub>2</sub> and Rh–H during the reaction of $[(^1\text{bpy})_2\text{Rh}(\text{OMe})(\text{MeOH})][\text{OTf}][\text{TFA}]$ ( <b>4</b> ) with D <sub>2</sub> after the initial formation of $[(^1\text{bpy})_2\text{Rh}(\text{D})(\text{TFA})]^+$ . ....	145
Scheme 3.15. Proposed mechanism for H <sub>2</sub> activation by $[(^1\text{bpy})_2\text{Rh}(\text{OMe})(\text{MeOH})][\text{TFA}][\text{OTf}]$ ( <b>4</b> ).....	147

Scheme 3.16. Alternative mechanism for dihydrogen activation involving the oxidative addition of dihydrogen. ....	148
Scheme 3.17. Alternative mechanism for dihydrogen activation involving deprotonation of $\eta^2$ -H <sub>2</sub> by free MeOH. ....	148
Scheme 3.18. Calculated reaction pathway for H <sub>2</sub> activation by the model [(bpy) <sub>2</sub> Rh(OMe)(MeOH)] <sup>2+</sup> complex (kcal/mol). ....	150
Scheme 3.19. Methanol assisted H <sub>2</sub> activation and M06/6-311++G(2d,2p)[LANL2TZ(f)] energies in THF solvent (kcal/mol). ....	154
Scheme 3.20. Rate laws based on proposed mechanisms. ....	155

## CHAPTER 4

Scheme 4.1. Hydrosilylation of olefins is used to synthesize alkylsilanes. ....	177
Scheme 4.2. Chalk-Harrod mechanism for transition metal catalyzed hydrosilylation. ....	178
Scheme 4.3. Mechanism for d <sup>0</sup> transition metal catalyzed hydrosilylation involving $\sigma$ -bond metathesis. ....	178
Scheme 4.4. Toste and co-workers proposed mechanism for hydrosilylation using (PPh) <sub>3</sub> Re(O) <sub>2</sub> I. ....	179
Scheme 4.5. Si-H bond activation using ( <sup>i</sup> Pr <sub>3</sub> NNN)Ir $\equiv$ N. ....	179
Scheme 4.6. Synthesis of [(tbpy) <sub>2</sub> Rh(OMe) <sub>2</sub> ][TFA] ( <b>1</b> ). ....	181
Scheme 4.7. The addition of HTFA (1 equiv.) to [( <sup>t</sup> bpy) <sub>2</sub> Rh(OMe) <sub>2</sub> ][TFA] ( <b>1</b> ) leads to the formation of four products. ....	181
Scheme 4.8. The final products from the reaction of [( <sup>t</sup> bpy) <sub>2</sub> Rh(OMe)(L)] <sup>n+</sup> (L = MeOH, n = 2 TFA, ( <b>3</b> ); L = TFA, n = TFA, ( <b>4</b> )) with Et <sub>3</sub> SiH are [( <sup>t</sup> bpy) <sub>2</sub> Rh(H)(TFA)][TFA], Et <sub>3</sub> SiOMe and Et <sub>3</sub> SiOH. ....	183
Scheme 4.9. Et <sub>3</sub> SiOMe and Et <sub>3</sub> SiOH are observed as the organic products from the activation of Et <sub>3</sub> SiH using [( <sup>t</sup> bpy) <sub>2</sub> Rh(OMe)(L)] <sup>n+</sup> [L = MeOH, n = 2 TFA, ( <b>3</b> ); L = TFA, n = TFA, ( <b>4</b> )]. ....	185
Scheme 4.10. Proposed mechanism for the reaction of Et <sub>3</sub> SiH with [( <sup>t</sup> bpy) <sub>2</sub> Rh(OMe)(MeOH)][TFA] <sub>2</sub> ( <b>3</b> ), and [( <sup>t</sup> bpy) <sub>2</sub> Rh(OMe)(TFA)][TFA] ( <b>4</b> ). ....	191
Scheme 4.11. [( <sup>t</sup> bpy) <sub>2</sub> Rh(H)(TFA)][TFA] ( <b>6</b> ) and [( <sup>t</sup> bpy) <sub>2</sub> Rh(H)(Et <sub>3</sub> SiOH)][TFA] ( <b>8</b> ) are not in equilibrium. ....	192
Scheme 4.12. Control reaction between Et <sub>3</sub> SiH and MeOH. ....	193
Scheme 4.13. Control reaction between Et <sub>3</sub> SiH and MeOH in the presence of HTFA. ....	193

## CHAPTER 5

Scheme 5.1. Benzene C-H activation by ( <sup>i</sup> Pr <sub>3</sub> NNN)IrMe. ....	200
Scheme 5.2. Si-H and H <sub>2</sub> activation by ( <sup>i</sup> Pr <sub>3</sub> NNN)Ir $\equiv$ N. ....	201
Scheme 5.3. Oxidative addition of C-Cl bonds to ( <sup>p-anisyl</sup> NNN)Rh(Cl). ....	201
Scheme 5.4 Synthesis of 2,6-diacetylpyridinebis(2,4,6-trimethylaniline) ( <sup>Mes</sup> NNN) ( <b>1</b> ). ....	202
Scheme 5.5. Synthesis of ( <sup>Mes</sup> NNN)Rh(Cl) ( <b>2</b> ). ....	204
Scheme 5.6. Synthesis of ( <sup>Mes</sup> NNN)Rh(Me)(OTf) <sub>2</sub> ( <b>3</b> ). ....	206
Scheme 5.7. Synthesis of [( <sup>Mes</sup> NNN)Rh(Me)(NH <sub>2</sub> Ph)(OTf)][OTf] ( <b>4</b> ). ....	207

Scheme 5.8. The addition of Et <sub>2</sub> NH to [( <sup>Mes</sup> NNN)Rh(Me)(NH <sub>2</sub> Ph)(OTf)][OTf] ( <b>4</b> ) leads to the formation of the Rh(I)-amido complex ( <sup>Mes</sup> NNN)Rh(NEt <sub>2</sub> ) ( <b>5</b> ).....	210
Scheme 5.9. Proposed mechanism for the formation of ( <sup>Mes</sup> NNN)Rh(NEt <sub>2</sub> ) ( <b>5</b> ). .....	211
Scheme 5.10. Free Et <sub>2</sub> NH is in rapid chemical exchange with the coordinated amido ligand of ( <sup>Mes</sup> NNN)Rh(NEt <sub>2</sub> ) ( <b>5</b> ). .....	214
Scheme 5.11. The planar geometry of amido ligand is a result of the orthogonal orientation of the nitrogen p-orbital for the amido. The orthogonal orientation leads to a two-center interaction giving not net bond. ....	216
Scheme 5.12. A three-center interaction would be observed if the p-orbital of the pyridyl nitrogen, Rh dπ and p-orbital of the amido nitrogen are coplanar. ....	216
Scheme 5.13. Attempted synthesis of ( <sup>Mes</sup> NNN)Rh(Me)(NHPh)(OTf). .....	218
Scheme 5.14. Oxidation of ( <sup>Mes</sup> NNN)Rh(NEt <sub>2</sub> ) ( <b>5</b> ) by HOTf to form the Rh(III) complex ( <sup>Mes</sup> NNN)Rh(H)(OTf) <sub>2</sub> . .....	220
Scheme 5.15. 1,2-CH-addition of benzene by a proposed [3,3'-diaryl-1,1'-pyridine-2,6-diylbis(imidazole-2-ylidene)]Rh(NHPh)Cl <sub>2</sub> complex. ....	223
Scheme 5.16. Comparison of ( <sup>Mes</sup> NNN)Rh(Me)(NHPh)(OTf) to proposed [3,3'-diaryl-1,1'-pyridine-2,6-diylbis(imidazole-2-ylidene)]Rh complex. ....	223
Scheme 5.17. Proposed Rh(I) heteroatom complex for 1,2-CH-addition.....	224

## CHAPTER 6

Scheme 6.1. Catalytic cycle for transition metal catalyzed olefin hydroarylation that incorporates olefin insertion and aromatic C–H activation. ....	231
Scheme 6.2. Formation of the complexes TpRu(L)(η <sup>3</sup> -C <sub>3</sub> H <sub>4</sub> Me) [L = CO, PMe <sub>3</sub> , P(OCH <sub>2</sub> ) <sub>3</sub> CEt, and P(OCH <sub>2</sub> ) <sub>2</sub> (OCCH <sub>3</sub> )]. ....	232
Scheme 6.3. Previously reported TpRu(P(OCH <sub>2</sub> ) <sub>3</sub> CEt)(NCMe)Ph gives 20 TONs of ethylbenzene at 90 °C whereas [(HC(pz <sup>5</sup> ) <sub>3</sub> )Ru(P(OCH <sub>2</sub> ) <sub>3</sub> CEt)(NCMe)Ph][BAR' <sub>4</sub> ], gives 565 TONs of ethylbenzene.....	233
Scheme 6.4. Synthesis of [(HC(pz' <sub>3</sub> )Ru(P(OCH <sub>2</sub> ) <sub>3</sub> CEt)(NCMe)Ph]Br ( <b>1</b> ).....	235
Scheme 6.5. Synthesis of [(HC(pz <sup>5</sup> ) <sub>3</sub> )Ru(P(OCH <sub>2</sub> ) <sub>3</sub> CEt)(NCMe)Ph][BAR' <sub>4</sub> ] ( <b>6</b> ).....	237
Scheme 6.6. Ethylene hydrophenylation using [(HC(pz <sup>5</sup> ) <sub>3</sub> )Ru(P(OCH <sub>2</sub> ) <sub>3</sub> CEt)(NCMe)Ph][BAR' <sub>4</sub> ] ( <b>6</b> ) (0.025 mol%) gives ethylbenzene in 95% yield based on ethylene as a limiting reagent .....	239
Scheme 6.7. Independent synthesis of [(HC(pz <sup>5</sup> ) <sub>3</sub> )Ru(P(OCH <sub>2</sub> ) <sub>3</sub> CEt)(η <sup>3</sup> -C <sub>3</sub> H <sub>4</sub> Me)][BAR' <sub>4</sub> ] ( <b>7</b> ).....	242
Scheme 6.8. The proposed deactivation pathway for [(HC(pz <sup>5</sup> ) <sub>3</sub> )Ru(P(OCH <sub>2</sub> ) <sub>3</sub> CEt)(NCMe)Ph][BAR' <sub>4</sub> ] ( <b>6</b> ) involves ethylene C–H activation. ....	243
Scheme 6.9. Proposed catalytic cycle for ethylene hydrophenylation using [(HC(pz <sup>5</sup> ) <sub>3</sub> )Ru(P(OCH <sub>2</sub> ) <sub>3</sub> CEt)(NCMe)Ph][BAR' <sub>4</sub> ] ( <b>6</b> ).....	248
Scheme 6.10. C <sub>6</sub> D <sub>5</sub> CH <sub>2</sub> CH <sub>2</sub> D is the major product from the catalytic reaction of [(HC(pz <sup>5</sup> ) <sub>3</sub> )Ru(P(OCH <sub>2</sub> ) <sub>3</sub> CEt)(NCMe)Ph][BAR' <sub>4</sub> ] ( <b>6</b> ) with C <sub>6</sub> D <sub>6</sub> and 25 psig C <sub>2</sub> H <sub>4</sub> . .....	249

Scheme 6.11. A KIE ( $k_H/k_D$ ) of 1.8(3) was determined by comparing the TOF for ethylbenzene product for identical catalytic reactions one using $C_6H_6$ and the other using $C_6D_6$ .	250
Scheme 6.12. The reaction of $[(HC(pz^5)_3)Ru(P(OCH_2)_3CEt)(NCMe)Ph][BAR'_4]$ ( <b>6</b> ) with a 1:1 molar ratio $C_6H_6$ to $C_6D_6$ leads to the formation of four isotopologues of ethylbenzene.	251
Scheme 6.13. Proposed pathway for C–D activation of benzene by $TpRu(L)(NCMe)Ph$ [ $L = CO, P(OCH_2)_3CEt$ , and $P(OCH_2)_2(OCCH_3)$ ].	253
Scheme 6.14. Degenerate NCMe/NCCD <sub>3</sub> exchange using $[(HC(pz^5)_3)Ru(P(OCH_2)_3CEt)(NCMe)Ph][BAR'_4]$ ( <b>6</b> ).	254
Scheme 6.15. Stoichiometric C–D Activation of $C_6D_6$ using $[(HC(pz^5)_3)Ru(P(OCH_2)_3CEt)(NCMe)Ph][BAR'_4]$ ( <b>6</b> ).	256
Scheme 6.16. Catalysis with ethylbenzene gives 1,3 and 1,4-diethylbenzene in a 2 to 1 ratio.	258
Scheme 6.17. Catalytic reaction between ethylene and furan.	258
Scheme 6.18. Synthesis of $(\eta^6\text{-}p\text{-cymene})Ru(CO)Br_2$ ( <b>8</b> ).	261
Scheme 6.19. The reaction of $(\eta^6\text{-}p\text{-cymene})Ru(CO)Br_2$ ( <b>8</b> ) with $Ph_2Mg[THF]_2$ leads to the formation of an asymmetric Ru binuclear complex ( <b>9</b> ).	262
Scheme 6.20. Synthesis of $(HC(pz^5)_3)Ru(CO)Br_2$ ( <b>10</b> ).	264
Scheme 6.21. Possible synthesis of $[(HC(pz^5)_3)Ru(CO)Br_2][TiOTf]_2$ ( <b>11</b> ) and $[(HC(pz^5)_3)Ru(CO)(NCMe)(Ph)_2]Br$ ( <b>12</b> ).	265

## CHAPTER 7

Scheme 7.1. Proposed catalytic cycles for hydrocarbon functionalization incorporating 1,2-CH-addition across $M=O$ or $M-OR$ bonds.	281
Scheme 7.2. Energy level diagram to showing the predicted differences in $\Delta G_{coord}$ for C–H, Si–H and H–H bonds.	284
Scheme 7.3. Proposed catalyst recycling of MSN-supported $[(HC(pz^5)_3)Ru(P(OCH_2)_3CEt)(NCMe)Ph][BAR'_4]$ .	288

## LIST OF FIGURES

## CHAPTER 1

Figure 1.1. Depiction of  $Zr\equiv NR$  triple bond with positive charge on imido nitrogen and  $Zr=NR$  resonance structure with negative charge on the imido nitrogen..... 17

## CHAPTER 2

- Figure 2.1. Molecular orbital diagram showing that there is no net  $M-X$   $\pi$ -bond if d-orbitals are filled ( $M$  = transition metal,  $X$  = OR, NHR, SR, etc.)..... 58
- Figure 2.2.  $^1H$  NMR spectrum of  $[(^t\text{bpy})_2\text{Rh}(\text{Me})(\text{NH}_2\text{Ph})][\text{BAR}'_4][\text{OTf}]$  (**1**) in  $\text{CD}_3\text{NO}_2$ . ..... 65
- Figure 2.3. ORTEP diagram (50% probability) of  $[(^t\text{bpy})_2\text{Rh}(\text{Me})(\text{NH}_2\text{Ph})][\text{BAR}'_4][\text{OTf}]$  (**1**). ..... 66
- Figure 2.4.  $^1H$  NMR spectrum of  $[(^t\text{bpy})_2\text{Rh}(\text{Me})(\text{NHPh})][\text{BAR}'_4]$  (**2**) in  $\text{CD}_3\text{CN}$ . ..... 67
- Figure 2.5.  $^1H$  NMR spectrum of  $[(^t\text{bpy})_2\text{Rh}(\text{NH}_2\text{Ph})_2][\text{OTf}]_3$  (**3**) in  $\text{CD}_3\text{NO}_2$ .  $^{15}\text{NH}_2\text{Ph}$  resonance  $[(^t\text{bpy})_2\text{Rh}(^{15}\text{NH}_2\text{Ph})_2][\text{OTf}]_3$  (**3- $^{15}\text{N}$** ) is shown in the inset. .... 69
- Figure 2.6. ORTEP diagram (50% probability) of  $[(^t\text{bpy})_2\text{Rh}(\text{NH}_2\text{Ph})_2][\text{BAR}'_4]_3$  (**4**). ..... 70
- Figure 2.7.  $^1H$  NMR spectrum of  $[(^t\text{bpy})_2\text{Rh}(\text{NH}_2\text{Ph})_2][\text{OTf}]$  (**5**) in  $\text{CD}_3\text{CN}$ .  $^{15}\text{NHPh}$  resonance  $[(^t\text{bpy})_2\text{Rh}(^{15}\text{NHPh})_2][\text{OTf}]$  (**5- $^{15}\text{N}$** ) is shown in the inset. .... 72
- Figure 2.8. ORTEP diagram (30% probability) of  $[(^t\text{bpy})_2\text{Rh}(\text{NHPh})_2][\text{BAR}'_4]$  (**6**). ..... 73
- Figure 2.9.  $^1H$  NMR spectrum of  $[(^t\text{bpy})_2\text{Rh}(\text{OH})_2][\text{OTf}]$  (**7**) in  $\text{CD}_2\text{Cl}_2$ .  $\text{H}_2\text{O}$  is observed at 1.61 ppm. .... 75
- Figure 2.10. ORTEP diagram (50% probability) of  $[(^t\text{bpy})_2\text{Rh}(\text{OH})_2][\text{OTf}]$  (**7**). ..... 76
- Figure 2.11.  $^1H$  NMR spectrum of  $[(^t\text{bpy})_2\text{Rh}(\text{H}_2\text{O})_2][\text{OTf}]_3$  (**8**) in  $\text{CD}_2\text{Cl}_2$ . ..... 77
- Figure 2.12.  $^1H$  NMR spectrum of  $[(^t\text{bpy})_2\text{Rh}(\text{OMe})(\text{Cl})]\text{Cl}$  (**9**) in  $\text{CD}_3\text{CN}$ . ..... 79
- Figure 2.13. ORTEP diagram (50% probability) of  $[(\text{tbpy})_2\text{Rh}(\text{OMe})(\text{Cl})]\text{Cl}$  (**9**). ..... 80
- Figure 2.14.  $^1H$  NMR spectrum of  $[(\text{bpy})_2\text{Rh}(\text{OH})_2][\text{PF}_6]$  (**10**) in  $\text{CD}_3\text{CN}$ . ..... 82
- Figure 2.15.  $^1H$  NMR spectrum of  $[(\text{bpy})_2\text{Rh}(\text{OMe})_2][\text{PF}_6]$  (**11**) in  $\text{CD}_2\text{Cl}_2$ . ..... 83
- Figure 2.16. ORTEP diagram (30% probability) of  $[(\text{bpy})_2\text{Rh}(\text{OMe})_2][\text{PF}_6]$  (**11**). ..... 84
- Figure 2.17.  $^1H$  NMR spectrum of  $[(^t\text{bpy})_2\text{Rh}(\text{OH})(\text{H}_2\text{O})][\text{OTf}]_2$  (**12**) in  $\text{CD}_3\text{CN}$ . ..... 86
- Figure 2.18.  $^1H$  NMR spectra demonstrating the slight differences in the chemical shifts of the methoxide resonance of  $[(^t\text{bpy})_2\text{Rh}(\text{OMe})(\text{MeOH})][\text{OTf}]_2$  (**13**) for the reaction of  $[(^t\text{bpy})_2\text{Rh}(\text{OMe})_2]\text{Cl}$  with different MOTf salts ( $M$  = Tl, Ag or Na). ..... 87
- Figure 2.19.  $^1H$  NMR spectrum of  $[(^t\text{bpy})_2\text{Rh}(\text{NHPh})(\text{NH}_2\text{Ph})][\text{OTf}]_2$  (**14**) in  $\text{CD}_3\text{CN}$ . . 90
- Figure 2.20. ORTEP diagram (30% probability) of  $[(\text{bpy})_2\text{Rh}(\text{NHPh})(\text{NH}_2\text{Ph})][\text{OTf}]_2$  (**14**). ..... 91
- Figure 2.21. Comparison of bond angles and lengths data from X-ray crystal structures of the synthesized Rh(III) aniline and anilido complexes  $[(^t\text{bpy})_2\text{Rh}(\text{Me})(\text{NH}_2\text{Ph})_2][\text{OTf}][\text{BAR}'_4]$  (**1**)  $[(^t\text{bpy})_2\text{Rh}(\text{NH}_2\text{Ph})_2][\text{BAR}'_4]_3$  (**4**),  $[(^t\text{bpy})_2\text{Rh}(\text{NHPh})_2][\text{BAR}'_4]$  (**6**) and  $[(^t\text{bpy})_2\text{Rh}(\text{NHPh})(\text{NH}_2\text{Ph})][\text{OTf}]_2$  (**14**). ..... 93

## CHAPTER 3

Figure 3.1. Transition metal heteroatom complexes that have been reported to mediate dihydrogen activation.....	120
Figure 3.2. $^1\text{H}$ NMR spectrum of $[(^t\text{bpy})_2\text{Rh}(\text{OMe})_2]\text{OTf}$ ( <b>1</b> ) in $\text{CD}_3\text{CN}$ .....	122
Figure 3.3. ORTEP diagram (50% probability) of $[(^t\text{bpy})_2\text{Rh}(\text{OMe})_2]\text{BAR}'_4$ ( <b>2</b> ).....	123
Figure 3.4. $^1\text{H}$ NMR spectrum of $[(\text{tbpy})_2\text{Rh}(\text{MeOH})_2][\text{OTf}][\text{TFA}]_2$ ( <b>3</b> ) in $\text{CD}_2\text{Cl}_2$ .....	125
Figure 3.5. $^1\text{H}$ NMR spectrum of soluble protonation products $[(^t\text{bpy})_2\text{Rh}(\text{OMe})(\text{MeOH})][\text{OTf}][\text{TFA}]$ ( <b>4</b> ) and $[(^t\text{bpy})_2\text{Rh}(\text{OMe})(\text{TFA})][\text{OTf}]$ ( <b>5</b> ) in $\text{THF-}d_8$ . ....	126
Figure 3.6. ORTEP diagram (50% probability) of $[(^t\text{bpy})_2\text{Rh}(\text{OMe})(\text{MeOH})][\text{OTf}][\text{TFA}]$ ( <b>4</b> ).....	127
Figure 3.7. Stacked $^1\text{H}$ NMR spectra plot for the variable temperature $^1\text{H}$ NMR study of $[(^t\text{bpy})_2\text{Rh}(\text{OMe})(\text{MeOH})][\text{OTf}][\text{TFA}]$ ( <b>4</b> ).....	129
Figure 3.8 $^1\text{H}$ NMR spectrum of $[(\text{tbpy})_2\text{Rh}(\text{H})(\text{TFA})][\text{OTf}]$ ( <b>6</b> ) in $\text{THF-}d_8$ . ....	132
Figure 3.9. $^1\text{H}$ NMR spectrum of $[(^t\text{bpy})_2\text{Rh}(\text{H})(\text{Cl})][\text{TFA}]$ ( <b>7</b> ) in acetone- $d_6$ with the baseline cropped between -0.40 to -13.20 ppm. ....	134
Figure 3.10. $^1\text{H}$ NMR spectrum of $[(^t\text{bpy})_2\text{Rh}(\text{Cl})_2][\text{TFA}]$ ( <b>8</b> ) in $\text{CD}_3\text{CN}$ . ....	135
Figure 3.11. $^1\text{H}$ NMR spectrum of $[(^t\text{bpy})_2\text{Rh}(\text{Br})_2][\text{TFA}]$ ( <b>9</b> ) in $\text{CD}_3\text{CN}$ . ....	137
Figure 3.12. Disappearance of starting material (complexes <b>4</b> and <b>5</b> ) under variable pressure of dihydrogen.....	138
Figure 3.13. Representative plot of $\ln$ of total starting material (complexes <b>4</b> and <b>5</b> ) versus time under 30 psig dihydrogen. ....	139
Figure 3.14. A plot of $k_{\text{obs}}$ versus concentration of methanol for the activation of dihydrogen by complexes <b>4</b> and <b>5</b> . ....	140
Figure 3.15. Plot of $k_{\text{obs}}$ versus $[\text{CD}_3\text{OD}]$ for the exchange of coordinated MeOH of $[(^t\text{bpy})_2\text{Rh}(\text{OMe})(\text{MeOH})][\text{OTf}][\text{TFA}]$ ( <b>4</b> ) with free $\text{CD}_3\text{OD}$ .....	143
Figure 3.16. $^1\text{H}$ NMR stack plot showing the formation of HD, $\text{H}_2$ , and the hydride resonance of $[(^t\text{bpy})_2\text{Rh}(\text{H})(\text{TFA})]\text{OTf}$ ( <b>6</b> ) for the reaction of complexes <b>4</b> and <b>5</b> with $\text{D}_2$ . ....	146
Figure 3.17. Dihydrogen coordination and 1,2-addition transition-state structures (bond lengths are in Å).....	151

## CHAPTER 4

Figure 4.1. $^1\text{H}$ NMR spectrum of soluble protonation products $[(^t\text{bpy})_2\text{Rh}(\text{OMe})(\text{MeOH})][\text{TFA}]_2$ ( <b>3</b> ) and $[(^t\text{bpy})_2\text{Rh}(\text{OMe})(\text{TFA})][\text{TFA}]$ ( <b>4</b> ) in $\text{THF-}d_8$ . ....	182
Figure 4.2. $^1\text{H}$ NMR spectrum in $\text{THF-}d_8$ of the final product mixture from the reaction of $\text{Et}_3\text{SiH}$ with $[(^t\text{bpy})_2\text{Rh}(\text{OMe})(\text{L})]^{n+}$ ( $\text{L} = \text{MeOH}$ , $n = 2$ TFA, ( <b>3</b> ); $\text{L} = \text{TFA}$ , $n =$ TFA, ( <b>4</b> )).....	183

Figure 4.3. Partial $^1\text{H}$ NMR spectrum for the product mixture from the activation of Si–H of $\text{Et}_3\text{SiH}$ by $[(^t\text{bpy})_2\text{Rh}(\text{OMe})(\text{L})]^{n+}$ (L = MeOH, n = 2 TFA, <b>(3)</b> ; L = TFA, n = TFA, <b>(4)</b> ). .....	186
Figure 4.4. $^1\text{H}$ NMR spectrum of $\text{Et}_3\text{SiOH}$ in $\text{THF-}d_8$ . .....	187
Figure 4.5. Possible identities of the hydride complex with observed resonance at –14 ppm. ....	189
Figure 4.6. Stacked $^1\text{H}$ NMR spectra plot for the activation of Si–H bonds of $\text{Et}_3\text{SiH}$ by $[(^t\text{bpy})_2\text{Rh}(\text{OMe})(\text{MeOH})][\text{TFA}]_2$ ( <b>(3)</b> ) and $[(^t\text{bpy})_2\text{Rh}(\text{OMe})(\text{TFA})][\text{TFA}]$ ( <b>(4)</b> ) showing the changes in the ethyl resonances with time. ....	190

## CHAPTER 5

Figure 5.1 $^1\text{H}$ NMR spectrum of 2,6-diacetylpyridinebis(2,4,6-trimethylaniline) ( $^{\text{Mes}}\text{NNN}$ ) ( <b>(1)</b> ) in $\text{CDCl}_3$ . ....	203
Figure 5.2. $^1\text{H}$ NMR spectrum of $(^{\text{Mes}}\text{NNN})\text{Rh}(\text{Cl})$ ( <b>(2)</b> ) in $\text{THF-}d_8$ . ....	205
Figure 5.3. $^1\text{H}$ NMR spectrum of $(^{\text{Mes}}\text{NNN})\text{Rh}(\text{Me})(\text{OTf})_2$ ( <b>(3)</b> ) in $\text{CD}_2\text{Cl}_2$ . ....	206
Figure 5.4. $^1\text{H}$ NMR spectrum of $[(^{\text{Mes}}\text{NNN})\text{Rh}(\text{Me})(\text{NH}_2\text{Ph})(\text{OTf})][\text{OTf}]$ ( <b>(4)</b> ) in $\text{CD}_2\text{Cl}_2$ . ....	208
Figure 5.5. ORTEP diagram (30% probability) of $[(^{\text{Mes}}\text{NNN})\text{Rh}(\text{Me})(\text{NH}_2\text{Ph})(\text{OTf})][\text{OTf}]$ ( <b>(4)</b> ). ....	209
Figure 5.6. $^1\text{H}$ NMR spectrum of $(^{\text{Mes}}\text{NNN})\text{Rh}(\text{NEt}_2)$ ( <b>(5)</b> ) in $\text{THF-}d_8$ . ....	213
Figure 5.7. ORTEP diagram (50% probability) of $(^{\text{Mes}}\text{NNN})\text{Rh}(\text{NEt}_2)$ ( <b>(5)</b> ). ....	215

## CHAPTER 6

Figure 6.1. ORTEP diagram of $[(\text{HC}(\text{pz}^5)_3)\text{Ru}(\text{P}(\text{OCH}_2)_3\text{CEt})(\text{NCMe})\text{Ph}]\text{Cl}$ ( <b>(5-Cl)</b> ) (35% probability). ....	237
Figure 6.2. Catalytic hydrophenylation of ethylene (15 psi) using 0.01 mol% (relative to benzene) $[(\text{HC}(\text{pz}^5)_3)\text{Ru}(\text{P}(\text{OCH}_2)_3\text{CEt})(\text{NCMe})\text{Ph}][\text{BAR}'_4]$ ( <b>(6)</b> ) at 90, 105, 150 and 175 °C. ....	239
Figure 6.3. Allyl Coupling Diagram for $[(\text{HC}(\text{pz}^5)_3)\text{Ru}(\text{P}(\text{OCH}_2)_3\text{CEt})(\eta^3\text{-C}_3\text{H}_4\text{Me})][\text{BAR}'_4]$ ( <b>(7)</b> ). ....	242
Figure 6.4. Partial $^1\text{H}$ NMR spectrum of the non-volatiles from a catalytic ethylene hydrophenylation reaction using $[(\text{HC}(\text{pz}^5)_3)\text{Ru}(\text{P}(\text{OCH}_2)_3\text{CEt})(\text{NCMe})\text{Ph}][\text{BAR}'_4]$ ( <b>(6)</b> ). ....	244
Figure 6.5. $^1\text{H}$ NMR spectrum of $[(\text{HC}(\text{pz}^5)_3)\text{Ru}(\text{P}(\text{OCH}_2)_3\text{CEt})(\eta^3\text{-C}_3\text{H}_4\text{Me})][\text{BAR}'_4]$ ( <b>(7)</b> ) in $\text{CD}_2\text{Cl}_2$ . ....	245
Figure 6.6. Catalytic ethylene hydrophenylation by $[(\text{HC}(\text{pz}^5)_3)\text{Ru}(\text{P}(\text{OCH}_2)_3\text{CEt})(\text{NCMe})\text{Ph}][\text{BAR}'_4]$ ( <b>(6)</b> ) (0.01 mol%, 90 °C) at variable ethylene pressures. ....	246
Figure 6.7. TOF for ethylbenzene production for catalytic ethylene hydrophenylation using $[(\text{HC}(\text{pz}^5)_3)\text{Ru}(\text{P}(\text{OCH}_2)_3\text{CEt})(\text{NCMe})\text{Ph}][\text{BAR}'_4]$ ( <b>(6)</b> ) (0.01 mol%) versus psi $\text{C}_2\text{H}_4$ . ....	247
Figure 6.8. Representative plot of degenerate $\text{NCCH}_3/\text{NCCD}_3$ exchange for $[(\text{HC}(\text{pz}^5)_3)\text{Ru}(\text{P}(\text{OCH}_2)_3\text{CEt})(\text{NCMe})\text{Ph}][\text{BAR}'_4]$ ( <b>(6)</b> ) at 88 °C. ....	253
Figure 6.9. Eyring plot of degenerate $\text{NCMe} / \text{NCCD}_3$ exchange for $[(\text{HC}(\text{pz}^5)_3)\text{Ru}(\text{P}(\text{OCH}_2)_3\text{CEt})(\text{NCMe})\text{Ph}][\text{BAR}'_4]$ ( <b>(6)</b> ). ....	254

Figure 6.10. Representative plot of stoichiometric C–D activation of C <sub>6</sub> D <sub>6</sub> by [(HC(pz <sup>5</sup> ) <sub>3</sub> )Ru(P(OCH <sub>2</sub> ) <sub>3</sub> CEt)(NCMe)Ph][[BAr' <sub>4</sub> ]] ( <b>6</b> ) in THF- <i>d</i> <sub>8</sub> with 30 equivalents of C <sub>6</sub> D <sub>6</sub> at 90 °C.....	257
Figure 6.11. <sup>1</sup> H NMR spectrum of (η <sup>6</sup> - <i>p</i> -cymene)Ru(CO)Br <sub>2</sub> ( <b>8</b> ) in CDCl <sub>3</sub> .....	261
Figure 6.12. ORTEP diagram of (η <sup>6</sup> - <i>p</i> -cymene)Ru(μ-Br) <sub>3</sub> Ru(CO) <sub>2</sub> Ph ( <b>9</b> ).....	262
Figure 6.13. <sup>1</sup> H NMR spectrum of (η <sup>6</sup> - <i>p</i> -cymene)Ru(μ-Br) <sub>3</sub> Ru(CO) <sub>2</sub> (Ph) ( <b>9</b> ) in CDCl <sub>3</sub> .....	263
Figure 6.11. <sup>1</sup> H NMR spectrum of (η <sup>6</sup> - <i>p</i> -cymene)Ru(CO)Br <sub>2</sub> ( <b>8</b> ) in CDCl <sub>3</sub> .....	261
Figure 6.12. ORTEP diagram of (η <sup>6</sup> - <i>p</i> -cymene)Ru(μ-Br) <sub>3</sub> Ru(CO) <sub>2</sub> Ph ( <b>9</b> ).....	262
Figure 6.13. <sup>1</sup> H NMR spectrum of (η <sup>6</sup> - <i>p</i> -cymene)Ru(μ-Br) <sub>3</sub> Ru(CO) <sub>2</sub> (Ph) ( <b>9</b> ) in CDCl <sub>3</sub> .....	263
Figure 6.14. <sup>1</sup> H NMR spectrum of (HC(pz <sup>5</sup> ) <sub>3</sub> )Ru(CO)Br <sub>2</sub> ( <b>10</b> ) in CD <sub>3</sub> CN.....	264

## CHAPTER 7

Figure 7.1. Ligands for future Rh(III) synthetic targets.....	285
Figure 7.2. [(HC(pz <sup>5</sup> ) <sub>3</sub> )Ru(P(OCH <sub>2</sub> ) <sub>3</sub> CEt)(NCMe)Ph][[BAr' <sub>4</sub> ]] supported on a mesoporous silica nanoparticle (MSN).....	288

## LIST OF TABLES

## CHAPTER 2

Table 2.1. Conditions investigated for benzene H/D exchange using [( <sup>t</sup> bpy) <sub>2</sub> Rh(OH) <sub>2</sub> ][OTf] (7) in the presence of Lewis acid. ....	94
Table 2.2. Deuterium incorporation into C <sub>6</sub> D <sub>6</sub> using [( <sup>t</sup> bpy) <sub>2</sub> Rh(OH) <sub>2</sub> ][OTf] (7) (10 mol% relative to benzene) in acidic solvents at 180 °C. ....	95

## CHAPTER 3

Table 3.1. Average <i>k</i> <sub>obs</sub> from the first-order fits to kinetic plots for the reaction of 4 and 5 with H <sub>2</sub> at 68 °C (see Figure 3.12). ....	139
Table 3.2. Average <i>k</i> <sub>obs</sub> from the first-order decay plots of the reaction of protonation product with H <sub>2</sub> (45 psig) and added MeOH (0, 3, and 5 equiv.) at 68 °C. ....	140
Table 3.3. Average <i>k</i> <sub>obs</sub> from the first-order decay plots for the exchange of coordinated MeOH of [( <sup>t</sup> bpy) <sub>2</sub> Rh(OMe)(MeOH)][OTf][TFA] (4) with CD <sub>3</sub> OD at 68 °C. ....	142

## CHAPTER 5

Table 5.1. Investigated bases for the synthesis of [( <sup>Mes</sup> NNN)Rh(Me)(NHPH)(OTf)]. ....	219
---	-----

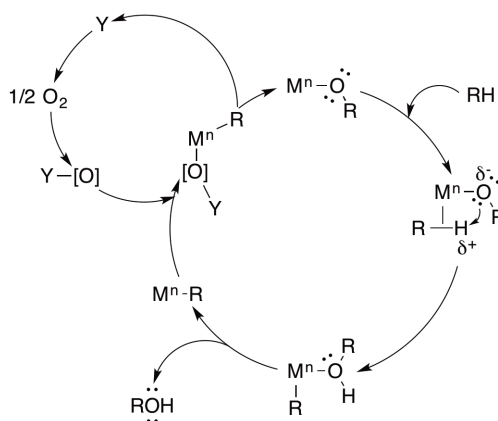
## CHAPTER 6

Table 6.1. Comparison of Ru(III/II) potentials and TONs for ethylene hydrophenylation using TpRu(L)(NCMe)(Ph) [L = CO, PMe <sub>3</sub> , P(OCH <sub>2</sub> ) <sub>3</sub> CEt or P(OCH <sub>2</sub> ) <sub>2</sub> (OCCH <sub>3</sub> )] complexes. <sup>17,39</sup> ....	232
Table 6.2. Comparison of TOF for ethylbenzene production for catalytic ethylene hydrophenylation using Ru(II) complexes. ....	241
Table 6.3. Comparison of TOF for ethylbenzene production for catalytic ethylene hydrophenylation using [(HC(pz <sup>5</sup> ) <sub>3</sub> )Ru(P(OCH <sub>2</sub> ) <sub>3</sub> CEt)(NCMe)Ph][BAR' <sub>4</sub> ] (6) (0.01 mol%) and varying pressures of C <sub>2</sub> H <sub>4</sub> . ....	247

## 1 Introduction

### 1.1 Brief Introduction

The activation and functionalization of covalent bonds (e.g., C–H, H–H, Si–H) is of prime interest to the catalysis community. For example, the functionalization of hydrocarbons is a cornerstone of the chemical industry,<sup>1-6</sup> and catalytic hydrogenation is important for the production of pharmaceutical, agricultural products and many other materials.<sup>7</sup> Despite the importance of catalytic hydrocarbon functionalization, many current processes operate at high temperature and pressure and often occur with low yields.<sup>2</sup> We have been working toward a new catalytic cycle for hydrocarbon functionalization (Scheme 1.1). The cycle consists of two steps; the 1,2-addition of a C–H bond across a M–alkoxide or amide bond followed by oxygen atom or nitrene insertion into a M–alkyl bond to regenerate the starting metal complex and release functionalized product. Examples of 1,2-CH-addition of hydrocarbons are rare and the reactions are not well understood.<sup>6</sup> This thesis is focused on the 1,2-addition of C–H, H–H, and Si–H bonds across Rh(I) and Rh(III) heteroatom bonds.



**Scheme 1.1.** Proposed cycle for catalytic hydrocarbon functionalization. A similar cycle for C–N bond formation could be drawn for a metal amide complex with insertion of a nitrene into the metal–alkyl bond.

## 1.2 Hydrocarbon Functionalization

The economy of the United States is heavily dependent on a reliable supply of oil. Every day the United States spends \$1 billion dollars on oil imports.<sup>8</sup> A ceiling of 75 million barrels of oil per day was reached in 2005; since then, oil production has idled and has failed to meet the rising demand despite an increase in price around 15% per year since 1998 (from \$15/barrel in 1998 to \$140/barrel in 2008).<sup>8,9</sup> The ever-increasing cost of crude oil and concerns over CO<sub>2</sub> emissions have led to a search for a more environmentally benign energy resource. Natural gas offers the potential for positive environmental benefits because it contains more energy per unit carbon than other fossil fuels.<sup>10</sup> Currently, 25% of the electricity in the United States comes from natural gas power plants.<sup>8</sup> This figure is on the rise as a result of the recent push for hydraulic fracking. New shale oil resources have enabled the United States to surpass Russia and Saudi Arabia for total petroleum and natural gas production.<sup>11</sup>

Methane, the major component of natural gas (~85% by volume), can be utilized as an alternative fuel source for transportation and as a feedstock for the production of chemicals. Unfortunately, transportation of this flammable, low boiling point ( $-161.6\text{ }^{\circ}\text{C}$  at 1 atm) gaseous resource is both difficult and expensive.<sup>10-14</sup>

After Russia, the United States is the second largest producer of natural gas.<sup>13</sup> Despite this, the United States is also the largest importer of natural gas.<sup>13</sup> In the United State natural gas is utilized in the residential and commercial sectors (35%), industrial sector (32%) and to produce electricity (30%). Natural gas is not heavily used in the transportation sector (0.15%) as a result of the high cost of compressed natural gas vehicles.<sup>10</sup> Building an infrastructure of pipelines could facilitate the use of natural gas as a transportation fuel, but the infrastructure is expensive, and there are environmental and health concerns. Methane (the major component of natural gas) is a known to be a greenhouse gas.<sup>13</sup> As a result, one concern with natural gas pipelines is loss during transport. In developing countries, natural gas pipelines lose  $\geq 5\%$  during transport whereas in developed nations far less ( $\leq 1\%$ ) is lost during transport.<sup>13</sup> In some locations, underwater pipelines are utilized to transport natural gas. Undersea pipelines are only viable for short distances and in shallow waters.<sup>13</sup> TransCanada and ExxonMobil had plans to build a pipeline on the north face of Alaska to transport natural gas; however, the costly project was canceled in 2010.<sup>15</sup>

Liquefied Natural Gas (LNG) is an expensive method to transport natural gas overseas or distances greater than 4,000 km.<sup>10,13</sup> This involves the port side liquefaction of natural gas at  $-162\text{ }^{\circ}\text{C}$ . This step alone accounts for 50% of the total cost of LNG.<sup>13</sup> The remaining 50% is divided equally between shipping and regasification.<sup>13</sup> LNG is

shipped on massive insulated tankers (size of three football fields) and reheated to convert to a gas upon arrival at the destination.<sup>13</sup> There are concerns with the safety of LNG transportation. In addition, LNG infrastructure is extremely expensive. For example, ExxonMobil and Qatar Petroleum each contributed \$12 billion towards the production of LNG infrastructure with a ~16,000 barrels of natural gas per day capacity.<sup>13</sup>

Gas to liquid (GTL) technology refers to the conversion of natural gas to liquid products.<sup>13</sup> The liquid product can be shipped less expensively than liquefied natural gas. Fischer–Tropsch technology is utilized for GTL. Fischer–Tropsch was developed in the 1920s in Germany using coal as a feedstock.<sup>13</sup> The process was also utilized in South Africa during Apartheid. The fuel produced by Fischer–Tropsch is however, clean burning and free of most pollutants (especially sulfur pollutants). Fischer–Tropsch synthesis is both energy and capital intensive. Mixtures of product are obtained along with large amount of CO<sub>2</sub> thus contributing to global warming. The major drawback to current GTL processes is the costly infrastructure. For example, Sasol and Qatar Petroleum constructed a \$18 billion GTL facility in Qatar capable of producing 140,000 barrels equivalents/day.<sup>13</sup> The production of the plant exceeded the estimated cost by three fold.<sup>13</sup> Recently, ExxonMobil abandoned the production of a 154,000 barrel equivalents/day capacity plant due to costs.<sup>13</sup>

As a result of the cost and difficulty associated with transporting methane, a substantial amount is lost each year to natural gas flares. In 2004, it was estimated that over 100 billion m<sup>3</sup> of natural gas were flared.<sup>16</sup> This amount of wasted natural gas could have met the energy needs of both Germany and France.<sup>16</sup> In addition to simply wasting

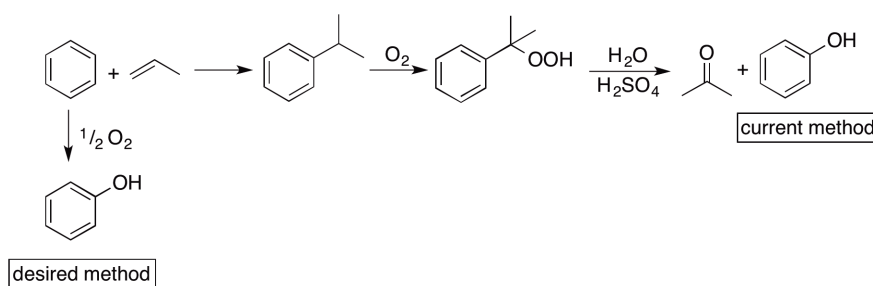
natural gas, flaring results in the release of approximately 400 million tons of CO<sub>2</sub> into the atmosphere each year.<sup>17</sup> A solution to avoid the wasting methane would be to convert methane to methanol (MTM). Methanol can be used as an easily transportable fuel, as a feedstock for the synthesis of commodity chemicals such as ethylene and propylene, or converted to gasoline or diesel fuel.<sup>13</sup>

Although the partial oxidation of methane with  $\frac{1}{2}$  O<sub>2</sub> to methanol is enthalpically favorable ( $\Delta H_{\text{rxn}} = -31$  kcal/mol), a large barrier must be overcome due to the inert nature of methane. Methane has strong C–H bonds (bond dissociation energy = 104 kcal/mol), and the C–H bonds are covalent.<sup>5</sup> Methane is a weak base, and coordination to a metal center is typically weak. The products from the oxidation of alkanes, such as methane, are typically more reactive than the starting alkane, and over oxidation is a common issue.<sup>18</sup>

As discussed above, current routes for the conversion of methane to methanol involve the formation of carbon monoxide and hydrogen (syn-gas, CO + H<sub>2</sub>), which are then converted to methanol.<sup>19</sup> Fischer–Tropsh synthesis involved in this indirect MTM process requires high temperatures (~800 °C) and pressures (~514 psi).<sup>19</sup> A MTM process that operates at moderate temperatures ( $\leq 250$  °C) and pressure ( $\leq 500$  psi) is desired. To be scalable, the overall yield and efficiency must out-perform the existing technology while reducing capital costs. To avoid an energy intensive process, the development of a transition metal catalyst that allows for the selective conversion of methane to methanol under mild conditions is required.<sup>6</sup>

Despite the emphasis placed on the conversion of MTM in this section, the functionalization of higher alkanes is also of interest. Cracking, the conversion of alkanes

such as ethane, propane and butane (other components of natural gas) to olefins, is accomplished by heating at high temperature ( $\sim 850$  °C).<sup>20,21</sup> It is desirable to develop more benign conditions for the direct partial oxidation of all alkanes to alcohols. In addition, it would be beneficial to develop conditions for the partial oxidation of benzene to phenol. The current method for the synthesis of phenol uses propene, an expensive hydrocarbon, and occurs via a radical reaction involving a peroxy species (Scheme 1.2).<sup>19</sup> With the current method, phenol and acetone are generated in a 1:1 mixture. Since the demand for acetone is less than the demand for phenol the generated acetone is often viewed as waste.



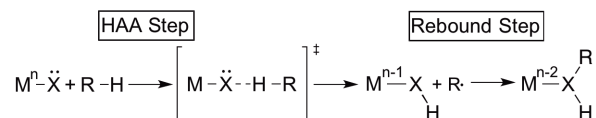
**Scheme 1.2.** The current method for the synthesis of phenol involving the formation of cumene from benzene and propene. Acidic oxidation of cumene yields phenol.

### 1.2.1 Hydrocarbon Functionalization by Hydrogen Atom Abstraction

Hydrogen atom abstraction (HAA) is a radical method for hydrocarbon functionalization. Organic radicals (*e.g.*,  $HO^\cdot$  or  $RO^\cdot$ ), metal-oxo( $O^{2-}$ )/oxyl( $O^-$ )/oxene( $O^0$ ), metal-imide ( $NR^{2-}$ )/imidyl( $NR^\cdot$ )/nitrene( $NR^0$ ) and metal alkoxide complexes have been reported to perform hydrocarbon functionalization by a process that involves HAA.<sup>5,4,22-34</sup> The transition metal mediated HAA reactions are proposed to occur by initial net hydrogen atom transfer to generate a new O–H or N–H bond and

carboradical with concomitant formal reduction of the metal center (Scheme 1.3). Further formal reduction of the metal center by one electron occurs in a “rebound step,” which allows for the formation of an O–C or N–C bond.<sup>35</sup>

The selectivity for these radical reactions is often governed by C–H bond strengths, with weaker bonds typically reacting more rapidly ( $3^\circ \text{CH} > 2^\circ \text{CH} > 1^\circ \text{CH}$ ). The bond dissociation energy (BDE) of the products are often weaker than those of the hydrocarbon starting material, and therefore preferential reactivity with the product is often observed. This is especially troublesome for the functionalization of  $\text{CH}_4$  to methanol because the BDE of  $\text{CH}_4$  (104 kcal/mol) is much greater than that of methanol (96 kcal/mol). Also, since the HAA step involves cleavage of a C–H bond, formation of an X–H bond, and generation of a transient carboradical, the rate of reaction is often governed by the relative C–H and X–H bond dissociation energies. As a result, most transition metal oxo, nitrene or alkoxide complexes that functionalize C–H bonds by this route are incapable of reaction with BDEs  $> 100$  kcal/mol.



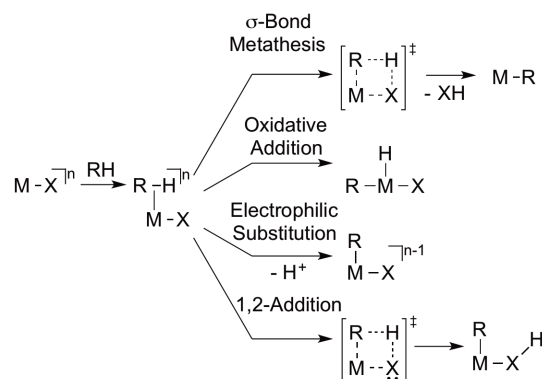
**Scheme 1.3.** C–H bond cleavage by hydrogen atom abstraction (X = O, OR, NR, etc.).

### 1.2.2 Hydrocarbon Functionalization by C–H Activation

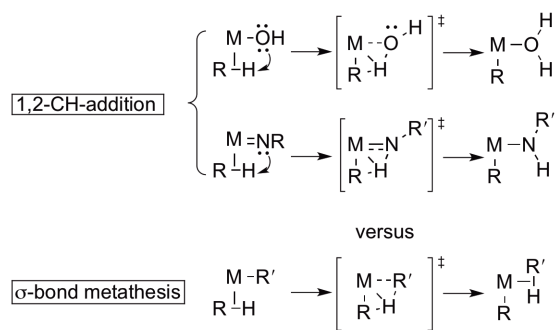
Hydrogen atom abstraction differs from C–H activation since the latter does not generate radicals or formally reduce the metal. Several mechanisms have been elucidated for non-radical, transition metal-mediated C–H bond activation, including oxidative addition, electrophilic substitution,  $\sigma$ -bond metathesis and 1,2-addition across metal–

heteroatom bonds (Scheme 1.4). The activation of C–H bonds by  $\sigma$ -bond metathesis proceeds by concerted M–C and C–H bond breaking and bond formation via a four-centered transition state. Oxidative addition occurs when a C–H bond adds to a metal to form new hydride and hydrocarbyl ligands with a formal increase in oxidation state of the metal by +2.<sup>36</sup> Electrophilic substitution involves coordination of a C–H bond with subsequent loss of a proton to a non-coordinated base. Variants of these mechanistic paradigms have been distinguished by the nature of the hydrogen transferred or activated (deprotonation or hydrogen atom abstraction), whether or not a *bona fide* hydrocarbon adduct is formed, whether the base is internal (*i.e.*, coordinated) or external.<sup>37-40</sup>

The 1,2-CH-addition across a M–X bond, where X is a formally anionic or dianionic ligand (*e.g.*, imido, hydroxide, amido) and possesses at least one lone pair, has features similar to the classic  $\sigma$ -bond metathesis and electrophilic substitution reactions; however, the ligand receiving the hydrogen (X in Scheme 1.4) possesses a lone pair or polarized  $\pi$ -bond electron pair (in the starting complex), making the four-centered transition state a six-electron core (*cf.* the four-centered/four-electron unit for  $\sigma$ -bond metathesis of C–H across a metal–alkyl moiety).<sup>39,41-44</sup> Similar to electrophilic substitution, the coordinated C–H bond is activated to transfer a proton, but in the 1,2-addition reaction the proton is transferred to an "internal" base (*i.e.*, a ligand). Given that the bonding interactions between the metal and X can impact the energetics of the 1,2-CH-addition and that the geometric constraints are different, we believe that 1,2-CH-addition across a M–X bond is best considered as mechanistically distinct from electrophilic substitution. Herein, 1,2-CH-addition refers to the 1,2-CH-addition across a M–X bond.



**Scheme 1.4.** Mechanism for metal mediated C–H activation.

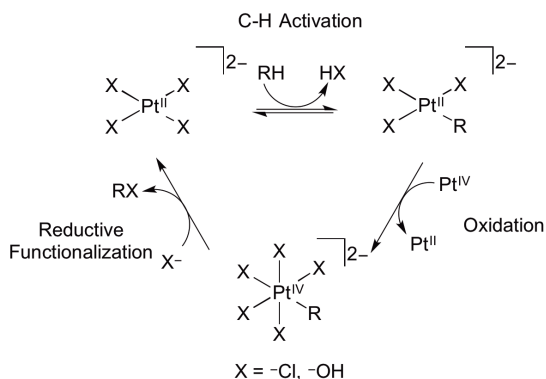


**Scheme 1.5.** Differences in the transition states for 1,2-CH-addition versus  $\sigma$ -bond metathesis.

### 1.2.3 Homogeneous Catalysis for RH Functionalization

Many examples of heterogeneous systems for the catalytic oxidation of alkanes have been reported.<sup>45-52</sup> These systems often suffer from low selectivity. Homogeneous catalysts offer the opportunity to fine tune selectivity and as a result, we believe they offer a more viable strategy to functionalize hydrocarbons. In 1970, Shilov reported the reaction of alkanes (including methane) with Pt(II) salts in aqueous solutions to generate alcohols and alkyl chlorides (Scheme 1.6).<sup>21,53</sup> The catalytic cycle requires two oxidation states of Pt: Pt(II) for the C–H activation step and Pt(IV) for the functionalization step. The major limitation of the Shilov system is that an expensive Pt(IV) salt is used as a

stoichiometric oxidant to perform the Pt(II/IV) oxidation. A commercially viable alternative oxidant has not yet been discovered.<sup>54,55</sup>



**Scheme 1.6.** Proposed catalytic cycle for the conversion of alkanes to alcohols or alkyl chlorides using the Pt(II) Shilov catalyst.

Periana and coworkers have reported the conversion of  $\text{CH}_4$  to methyl bisulfate using a  $(\text{bpym})\text{Pt}(\text{Cl}_2)$  ( $\text{bpym} = 2,2'$ -bipyrimidine) in concentrated  $\text{H}_2\text{SO}_4$ .<sup>18</sup> Greater than 70% yield of methyl bisulfate was obtained. The oxidant for the  $(\text{bpym})\text{Pt}(\text{Cl}_2)$  system is  $\text{S}^{+6}$  (from  $\text{SO}_4^{2-}$  or  $\text{SO}_3$ ), which is less expensive than the Pt(IV) oxidant used in the Shilov system. The bisulfate serves as a protecting group against over-oxidation since reactivity with methyl bisulfate is  $\geq 100$  times slower than  $\text{CH}_4$ .<sup>18</sup> Methyl bisulfate can be hydrolyzed to methanol. Unfortunately the  $(\text{bpym})\text{Pt}(\text{Cl}_2)$  catalyst is inhibited after the production of  $\sim 1$  M methyl bisulfate, and this concentration is too low for industrial scale up. Dilution of the sulfuric acid renders product removal more facile but the activity of electrophilic Pt catalysts is inhibited in non-superacidic acids. Variations of the  $(\text{bpym})\text{Pt}(\text{Cl}_2)$  system using catalysts based on electrophilic  $\{\text{Hg}(\text{II}), \text{Tl}(\text{III}), \text{Pd}(\text{II}), \text{Au}(\text{I})\}$  in  $\text{H}_2\text{SO}_4$  to generate methyl bisulfate have been reported but suffer the same drawback.<sup>12,56,57</sup>



electrophilic main group salts  $\text{Tl}(\text{TFA})_3$  and  $\text{Pb}(\text{TFA})_4$  in HTFA at 180 °C to generate the corresponding trifluoroacetate ester.<sup>59</sup> Experimental and computational studies support a mechanism involving slow irreversible electrophilic C–H activation.

The borylation of hydrocarbons using catalysts based on Fe, W, Re, Rh, Ir, has been reported.<sup>60</sup> Covalent metal boron bonds react with inert C–H bonds to form a functionalization product containing a coupled hydrocarbyl and boryl ligand.<sup>61</sup> Electronic factors favor the functionalization of methyl C–H bonds.<sup>61,62</sup> Hydrocarbon borylation reactions are favorable because B–C bonds are stronger than the B–B or B–H.<sup>61</sup> The reaction of an alkane with borane is thermodynamically favorable (exothermic by 3 to 4 kcal/mol).<sup>61,62</sup> The observed low barriers for C–H cleavage are attributed to the combination of the p orbital on the boryl ligand and  $\sigma$ -donation from the electropositive boron.<sup>61,62</sup>

Hartwig and coworkers have reported the formation of 1-alkylborane ester from alkanes with bis(pinacolato)diborane using the  $\text{Cp}^*\text{Rh}$  catalyst  $\text{Cp}^*\text{Rh}^*(\text{C}_6\text{Me}_6)$ .<sup>63</sup> After 80 h at 150 °C 144 turnovers (TO) of product are obtained.<sup>63</sup> Examples Ir catalysts for C–H borylation have also been reported.<sup>61</sup> For the Ir systems, bipyridine ligands led to more reactive catalysts than bisphosphine ligated Ir complexes.<sup>61</sup> For example, the combination of  $[\text{Ir}(\text{COD})(\text{OMe})]_2$  and 4,4'-di-*tert*-butylbipyridine catalyze regioselective borylation of aromatic C–H bonds using a 1:1 ratio of borane and arene at room temperature in high yields.<sup>64</sup>

The dehydrogenation of alkanes to form alkenes, serves as important hydrocarbon functionalization reaction. Industrially heterogeneous catalysts are used to dehydrogenate alkanes at high temperatures (500 °C to 900 °C).<sup>65</sup> These reaction are plagued by low

selectivity, olefin isomerization, and cracking (C–C bond cleavage).<sup>65</sup> Homogeneous catalysts for alkane dehydrogenation have afforded for increased product selectivity and operate under milder conditions.<sup>65</sup> The first homogeneous alkane dehydrogenation catalyst  $(\text{PAr}_3)\text{ReH}_7$  was independently reported by Crabtree and Felkin.<sup>66-70</sup>  $[\text{P}(p\text{-FC}_6\text{H}_4)_3]\text{ReH}_7$  showed the highest reactivity achieving 1.6 TO in 10 minutes at 30 °C.<sup>66</sup> The dehydrogenation of cyclooctane using Ir and Ru pentahydride complexes with *tert*-butylethylene (TBE) as the hydrogen acceptor were later reported.<sup>66</sup> These catalyst offered improved reactivity relative to  $[\text{P}(p\text{-FC}_6\text{H}_4)_3]\text{ReH}_7$ .<sup>67</sup> The development of Ir catalysts with pincer based ligands has led to increased TO and increased thermal stability of the catalysts.<sup>65</sup> At 200 °C, 12 TO/minute were obtained using  $(^{\text{tBu}}\text{PCP})\text{IrHCl}$  ( $^{\text{tBu}}\text{PCP} = 2,6\text{-(CH}_2\text{P}^{\text{tBu}}\text{Bu}_2)_2\text{C}_6\text{H}_3$ ) as a catalyst for the dehydrogenation of cyclooctane with TBE as a hydrogen acceptor.<sup>71-74</sup>  $(^{\text{tBu}}\text{PCP})\text{IrHCl}$  remained active for 1 week without decomposition.<sup>71-74</sup>  $(^{\text{tBu}}\text{PCP})\text{IrHCl}$  is also active in open system reactions where hydrogen is extruded; however, lower TO are observed.<sup>73,74</sup>

Replacement of the carbon of the methylene bridge of PCP with oxygen resulted in a catalyst with increased activity  $(^{\text{tBu}}\text{POCOP})\text{IrHCl}$  ( $^{\text{tBu}}\text{POCOP} = \eta^3\text{-(1,3-OP}^{\text{tBu}}\text{Bu}_2)_2\text{C}_6\text{H}_3$ ). Relative to the PCP analogue, the activity for the transfer dehydrogenation of cyclooctane has increased by nearly an order of magnitude using  $(^{\text{tBu}}\text{POCOP})\text{IrHCl}$ .<sup>75,65</sup>

#### 1.2.4 Proposed Catalytic Cycle for Hydrocarbon Functionalization

Two key steps are involved in hydrocarbon functionalization using a metal catalyst via C–H activation. The first step involves C–H bond breaking to generate a M–R complex; C–X (X = OR, NHR, halide, etc.) bond formation occurs in the second step.

Most reported catalysts for hydrocarbon functionalization are electrophilic and function by a Shilov type pathway consisting of C–H activation, oxidation and reductive functionalization by nucleophilic addition to an electrophilic hydrocarbyl ligand (Scheme 1.6). Lewis bases inhibit these electrophilic catalysts including coordinating solvents.<sup>18,57</sup> Even weak acids such as acetic acid can be problematic, and the electrophilic catalysts often require superacidic media. Less Lewis acidic metals are unable to do the reductive functionalization step because of prohibitively high activation barriers.

We have proposed a new strategy for hydrocarbon functionalization using middle transition metals. The proposed pathway for C–H functionalization involves an initial 1,2-CH-addition across metal–X (X = OH, OR, NHR) bonds (Scheme 1.8). In Pathway A of Scheme 1.8, 1,2-CH-addition occurs across a metal–oxo bond. This step is followed by C–O reductive elimination to produce a functionalized product. The starting metal–oxo is then regenerated by oxidation of the metal center. A similar cycle could be proposed for C–N bond formation when starting with a metal-imido complex. In this case, the oxidation step would employ a nitrene transfer reagent. Alternatively, as shown in Pathway B of Scheme 1.8, 1,2-CH-addition could occur across a metal–alkoxide or –amido (alkoxide is shown) bond to form a coordinated alcohol or amine, respectively. The starting metal–alkoxide or –amido is subsequently reformed via alcohol or amine dissociation and subsequent oxygen atom or nitrene insertion into the M–alkyl bond. The functionalization step can occur without change in formal oxidation state of the metal center, but also can proceed via a metal oxo or nitrene intermediate (Scheme 1.9).

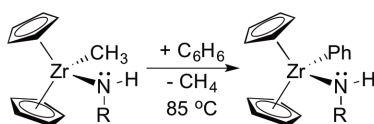


hydroxides? The remainder of the introduction provides an overview of 1,2-addition reactions using early metal imido complexes and late transition metal amido and alkoxo complexes. A discussion of the functionalization step is also included.

### 1.3 1,2-CH-Addition by Early Metal Imido Complexes

#### 1.3.1 Zr Imido Complexes

The 1,2-addition of C–H bonds was first reported with early transition metal  $d^0$  imido complexes that are generated *in situ*. For example, Bergman and co-workers reported that heating (85 °C) the zirconium methyl amide complexes  $\text{Cp}_2\text{Zr}(\text{CH}_3)(\text{NHR})$  [ $\text{R} = 4\text{-tert-butylphenyl}$  ( $\text{Ar}^t\text{Bu}$ ) or *tert*-butyl ( $^t\text{Bu}$ ),  $\text{Cp} = \text{cyclopentadienyl}$ ] in benzene results in the elimination of methane to form the transient species  $\text{Cp}_2\text{Zr}=\text{NR}$  (Scheme 1.10).<sup>76</sup> Subsequent benzene C–H activation leads to the formation of  $\text{Cp}_2\text{Zr}(\text{NH}^t\text{Bu})(\text{Ph})$ .<sup>76</sup> The two possible resonance structures for a  $d^0$  Zr(IV) imido complex are shown in Figure 1.1. The  $\text{Zr}=\text{N}-\text{R}$  resonance structure (right side of Figure 1.1) dominates as indicated by the Kohn-Sham HOMO-1 and HOMO of  $\text{Cp}_2\text{Zr}(\text{NR})(\eta^2\text{-C,H-benzene})$ , which suggests that substantial electron density is located on the imido nitrogen.<sup>76,77</sup> As shown in Scheme 1.11, the lone pair on the imido likely plays a key role in the benzene C–H activation step.



**Scheme 1.10.** Overall reaction of  $\text{Cp}_2\text{Zr}(\text{CH}_3)(\text{NHR})$  [ $\text{R} = 4\text{-tert-butylphenyl}$  ( $\text{Ar}^t\text{Bu}$ ) or *tert*-butyl ( $^t\text{Bu}$ )] with benzene.

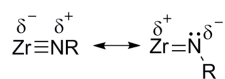
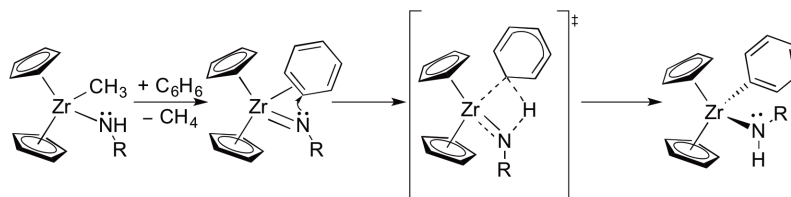


**Figure 1.1.** Depiction of  $\text{Zr} \equiv \text{NR}$  triple bond with positive charge on imido nitrogen and  $\text{Zr} = \text{NR}$  resonance structure with negative charge on the imido nitrogen.



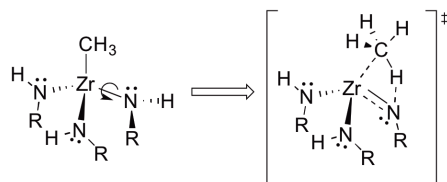
**Scheme 1.11.** Benzene C–H activation by reaction intermediate,  $\text{Cp}_2\text{Zr}(\text{NR})(\eta^2\text{-C}_6\text{H}_6)$  showing the involvement of the lone pair in C–H activation.

$\text{Cp}_2\text{Zr}(\text{CH}_3)(\text{NHR})$  is only reported to activate aromatic C–H bonds; however, Wolczanski and co-workers reported zirconium imido complexes generated from  $(^t\text{Bu}_3\text{SiNH})_3\text{ZrR}$  ( $\text{R} = \text{Me}, \text{Ph}, \text{C}_6\text{H}_{11}$ ) that are capable of activating alkanes.<sup>78,79</sup> For example, upon heating  $(^t\text{Bu}_3\text{SiNH})_3\text{Zr}(\text{CD}_3)$  and  $\text{CH}_4$  in cyclohexane,  $\text{CD}_3\text{H}$  and  $(^t\text{Bu}_3\text{SiNH})_3\text{Zr}(\text{CH}_3)$  are produced. In addition,  $(^t\text{Bu}_3\text{SiNH})_3\text{Zr}(\text{CH}_3)$  and free cyclohexane are observed when  $(^t\text{Bu}_3\text{SiNH})_3\text{Zr}(\text{Cy})$  ( $\text{Cy} = \text{cyclohexyl}$ ) is pressurized with methane in  $\text{C}_6\text{D}_{12}$ .

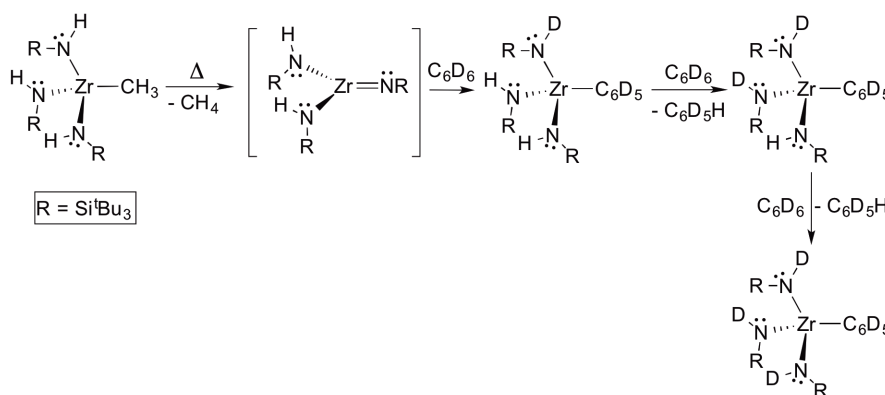
The reactivity of  $(^t\text{Bu}_3\text{SiNH})_3\text{ZrR}$  ( $\text{R} = \text{Me}, \text{Ph}, \text{C}_6\text{H}_{11}$ ) complexes with hydrocarbons was studied in detail. Thermolysis of  $(^t\text{Bu}_3\text{SiNH})_3\text{Zr}(\text{CH}_3)$  in benzene produces  $(^t\text{Bu}_3\text{SiNH})_3\text{Zr}(\text{Ph})$  and methane. Kinetic studies of this reaction indicate a first-order dependence on  $(^t\text{Bu}_3\text{SiNH})_3\text{ZrCH}_3$  and a zero-order dependence on benzene. A  $\Delta H^\ddagger = 25.9(4)$  kcal/mol and  $\Delta S^\ddagger = -7(1)$  eu were obtained from an Eyring plot (87 – 127 °C) of methane elimination from  $(^t\text{Bu}_3\text{SiNH})_3\text{Zr}(\text{CH}_3)$ . Rotation of the N–H bond of the amido ligand in the transition state is necessary to enable hydrogen transfer to the methyl ligand (Scheme 1.12). This constrained transition state is proposed to be responsible for

the negative entropy. Wolczanski and co-workers were able to provide evidence for the formation of the Zr-imido complex by trapping the imido as a THF adduct,  $(\text{THF})(^t\text{Bu}_3\text{SiNH})_2\text{Zr}=\text{NSi}^t\text{Bu}_3$ , when heating  $(^t\text{Bu}_3\text{SiNH})_3\text{Zr}(\text{Ph})$  in THF.<sup>80</sup>

Experimental results for the reaction of  $(^t\text{Bu}_3\text{SiNH})_3\text{Zr}(\text{CH}_3)$  with  $\text{C}_6\text{D}_6$  support the reaction mechanism shown in Scheme 1.13. Rate-determining hydrogen abstraction from an amido ligand of  $(^t\text{Bu}_3\text{SiNH})_3\text{Zr}(\text{CH}_3)$  by the methyl ligand leads to the formation of the transient imido complex,  $(^t\text{Bu}_3\text{SiNH})_2\text{Zr}=\text{NSi}^t\text{Bu}_3$ . Subsequent C–D activation of  $\text{C}_6\text{D}_6$  by  $(^t\text{Bu}_3\text{SiNH})_2\text{Zr}=\text{NSi}^t\text{Bu}_3$  yields  $(^t\text{Bu}_3\text{SiNH})_2(^t\text{Bu}_3\text{SiND})\text{Zr}(\text{C}_6\text{D}_5)$ . Deuteration of multiple amido ligands was observed suggesting that the reaction is reversible.



**Scheme 1.12.** Rotation about the Zr–N bond enables proper orientation of the NH for H atom transfer to the methyl ligand.

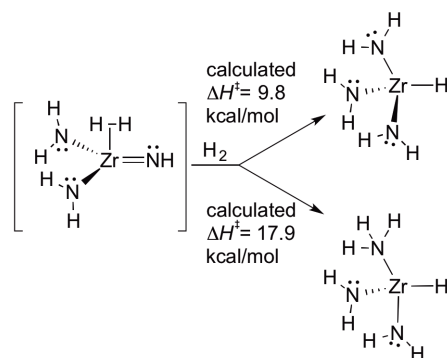


**Scheme 1.13.** Proposed mechanism for the reaction of  $(^t\text{Bu}_3\text{SiNH})_3\text{Zr}(\text{CH}_3)$  and  $\text{C}_6\text{D}_6$ .

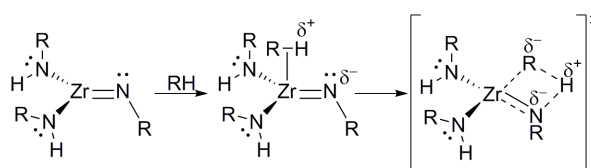
Both experimental computational evidence suggest that the ability of early metal imido complexes to activate C–H bonds is enhanced by having more than one imido

ligand coordinated to a central  $d^0$  transition metal ion.<sup>80-85</sup> This is referred to as " $\pi$ -loading."<sup>86</sup> The presence of multiple  $\pi$ -donor (imido or related) ligands on the early transition metal center leads to a competition for  $d\pi$ - $p\pi$  interactions resulting in an increase in negative charge localization on the  $\pi$ -donor ligand(s). For example, the presence of multiple  $\pi$ -donor ligands in  $(^t\text{Bu}_3\text{SiNH})_2\text{Zr}=\text{NSi}^t\text{Bu}_3$  results in a competition between the  $\pi$ -donor ligands for  $d\pi$ - $p\pi$  intermediates with Zr; this enhances the polarity of Zr=NR bonds and may enhance the rate of C–H activation by  $(^t\text{Bu}_3\text{SiNH})_2\text{Zr}=\text{NSi}^t\text{Bu}_3$  (and related complexes).<sup>87</sup>

An in-depth computational study of  $\text{H}_2$  activation using the model complex  $(\text{H}_2\text{N})_2\text{Zr}=\text{NH}$  has been reported.<sup>88</sup> As shown in Scheme 1.14, from the  $\text{H}_2$  adduct  $(\text{H}_2\text{N})_2(\text{H}_2)\text{Zr}=\text{NH}$  the calculated activation barrier for  $\text{H}_2$  addition across the Zr– $\text{NH}_2$  bond (17.9 kcal/mol) is more substantial than addition across the Zr=NH bond (9.8 kcal/mol). A Mulliken population analysis of methane activation by  $(\text{H})_2\text{M}=\text{NH}$  reveals that  $\sim 0.2 e^-$  are transferred from methane to the metal center upon coordination of methane. This results in the polarization of the coordinated C–H bond ( $\text{C}^{\delta-}\text{H}^{\delta+}$ ).<sup>89</sup> This polarization is induced by the imido basicity ( $\text{M}^{\delta+}=\text{N}^{\delta-}$ ) in the 4-centered transition state interaction (Scheme 1.15).



**Scheme 1.14.** Calculated activation barriers for the addition of  $\text{H}_2$  across a  $\text{Zr}=\text{NH}$  versus  $\text{Zr}-\text{NH}_2$  bonds of  $(\text{NH}_2)_2\text{Zr}=\text{NH}$ .<sup>88</sup>



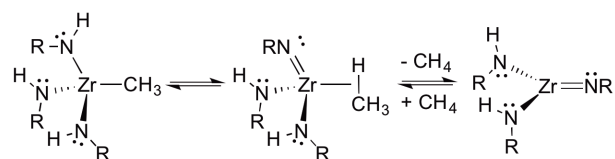
**Scheme 1.15.** 1,2-CH-addition of  $\text{RH}$  across  $\text{Zr}=\text{NR}$  bonds of  $(\text{RNH})_2\text{Zr}=\text{NR}$  showing the four-centered transition state.

An *ab initio* computational study focused on the comparative reactivity of the congeneric series of Group 4 imido complexes  $(\text{H})_2\text{M}=\text{NH}$  ( $\text{M} = \text{Ti}, \text{Zr}, \text{Hf}$ ) has been reported.<sup>89</sup> The calculated activation barriers for methane activation with  $(\text{H})_2\text{M}=\text{NH}$  follow the order  $\text{Hf} < \text{Zr} < \text{Ti}$ , while the exothermicity of methane activation was found to increase as the metal becomes heavier ( $\text{Ti} > \text{Zr} > \text{Hf}$ ). If it is assumed that the N–H bond energies are of similar magnitude for the  $(\text{H})_2\text{M}=\text{NH}$  complexes, the strength of the incipient metal–methyl bond must contribute to the observed differences in activation energy. Computational and experimental investigation of the microscopic reverse, methane elimination, support this assumption because the barriers for methane elimination is the highest for  $(\text{tBu}_3\text{SiNH})_3\text{Hf}(\text{CH}_3)$  ( $\Delta H_{\text{elim}}^\ddagger = 38.0 \text{ kcal/mol}$ ), intermediate for the zirconium complex ( $\Delta H_{\text{elim}}^\ddagger = 34.1 \text{ kcal/mol}$ ), and lowest for the titanium complex ( $\Delta H_{\text{elim}}^\ddagger = 23.4 \text{ kcal/mol}$ ).<sup>78,90</sup> In another computational (*ab initio*) study the C–H

activation barriers for methane activation by  $(X)_2Zr=NH$  ( $X = H > Cl > NH_2$ ) suggest that  $\pi$ -loading for the  $M=NR$  bond is responsible for the enhanced ability to cleave C–H bonds.<sup>89</sup>

Kinetic isotope effects (KIE) for the 1,2-elimination of  $CH_4$  and  $CH_3D$  from  $(^tBu_3SiNH)_3Zr(CH_3)$  and  $(^tBu_3SiND)_3Zr(CH_3)$  show a large primary  $k_H/k_D$  of 7.3(4) for N–H versus N–D abstraction consistent with a nearly linear transition state for H-atom transfer with similar amounts of C–H bond formation and N–H bond breaking.<sup>79</sup> The KIE for methane elimination suggests that a rotation about the Zr–N bond in the 4-centered transition state must occur to allow for H-atom transfer (Scheme 1.12).<sup>80</sup>

The rates of 1,2-RH-elimination from  $(^tBu_3SiNH)_3Zr(R)$  ( $R = CH_3, Ph, CH_2Ph, Cy$ ) complexes reveal an inverse dependence on the Zr–C bond strength suggesting a 2-step process for net R–H elimination (Scheme 1.16).<sup>80</sup> Faster 1,2-RH-elimination from  $(^tBu_3SiNH)_3Zr(R)$  was observed as the proton affinity of the hydrocarbon increased.



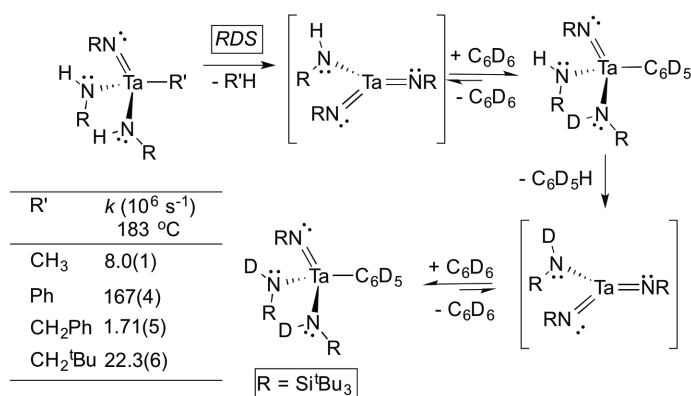
**Scheme 1.16.** Two-step reductive elimination of methane from  $(^tBu_3SiNH)_3ZrCH_3$ .

### 1.3.2 Tantalum, Vanadium, and Tungsten Imido Complexes

1,2-CH-addition by Ta, V and W imido complexes is known. For example, the activation of C–H bonds by  $(^tBu_3SiNH)_2(R)Ta=NSi^tBu_3$  ( $R = CH_3, Ph, CH_2Ph, CH_2^tBu$ ) complexes and  $(^tBu_3SiNH)_2(CH_3)V=NSi^tBu_3$  has been reported.<sup>85,91</sup>  $(^tBu_3SiNH)Ta(=NSi^tBu_3)_2$ , a reactive bis-imido intermediate generated by rate limiting

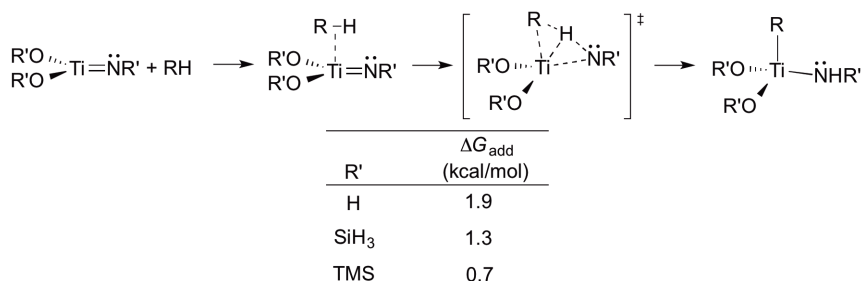
RH elimination, activates the C–D bond of C<sub>6</sub>D<sub>6</sub> to produce (<sup>t</sup>Bu<sub>3</sub>SiNH)(<sup>t</sup>Bu<sub>3</sub>SiND)(C<sub>6</sub>D<sub>5</sub>)Ta=NSi<sup>t</sup>Bu<sub>3</sub> (Scheme 1.17). CH<sub>4</sub> liberation from (<sup>t</sup>Bu<sub>3</sub>SiNH)(<sup>t</sup>Bu<sub>3</sub>SiND)(CH<sub>3</sub>)Ta=NSi<sup>t</sup>Bu<sub>3</sub> is observed at 180 °C and the addition of free <sup>t</sup>Bu<sub>3</sub>SiNH<sub>2</sub> does not impact the rate of methane release. A  $k_H/k_D$  of  $\geq 3.4(3)$  was determined for the loss of CH<sub>3</sub> from (<sup>t</sup>Bu<sub>3</sub>SiNH)<sub>2</sub>(CH<sub>3</sub>)Ta=NSi<sup>t</sup>Bu<sub>3</sub> versus CH<sub>3</sub>D loss from (<sup>t</sup>Bu<sub>3</sub>SiND)<sub>2</sub>(CH<sub>3</sub>)Ta=NSi<sup>t</sup>Bu<sub>3</sub>. For the V analogue, methane elimination from (<sup>t</sup>Bu<sub>3</sub>SiNH)<sub>2</sub>(CH<sub>3</sub>)V=NSi<sup>t</sup>Bu<sub>3</sub> at 80 °C was determined to proceed at a rate of  $11.4 \times 10^{-5} \text{ s}^{-1}$  and to exhibit a first-order dependence on V complex.

Substantial differences in  $\Delta G^\ddagger$ 's between Zr and Ta systems for the rate of 1,2-RH-elimination were observed. For example, methane elimination from (<sup>t</sup>Bu<sub>3</sub>SiNH)<sub>2</sub>(CH<sub>3</sub>)Ta=NSi<sup>t</sup>Bu<sub>3</sub> occurs with  $\Delta G^\ddagger = 37.7 \text{ kcal/mol}$  (183 °C) while methane elimination from the Zr complex (<sup>t</sup>Bu<sub>3</sub>SiNH)<sub>3</sub>ZrCH<sub>3</sub> has an activation energy of  $\Delta G^\ddagger = 28.5 \text{ kcal/mol}$  (97 °C). The tantalum complexes are more heavily  $\pi$ -loaded than zirconium due to six electron contribution from the two bonding imido ligands if pseudo-trigonal geometry is assumed following methane elimination. Moving from the Group 4 bis-amido/imido to the Group 5 amido/bis-imido involves the replacement of an amido with a more strongly  $\pi$ -donating imido. Possibly as a result of the increased  $\pi$ -loading, 1,2-addition to (RNH)Ta(NR)<sub>2</sub> is faster than to (RNH)<sub>2</sub>Zr(NR).



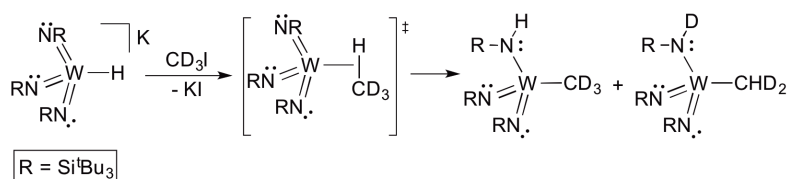
**Scheme 1.17.** Proposed mechanism for R'H elimination from (tBu<sub>3</sub>SiNH)<sub>3</sub>TaR' and subsequent H/D exchange (RDS = rate determining step). Rates of R'H elimination at 183 °C are shown.

Similar to the Zr–imido complexes, the metal electrophilicity and metal–imido bond polarity was determined to be vital for C–H activation. The calculated reaction coordinates for the C–H activation of a series of alkanes with (R'O)<sub>2</sub>Ti=NR' (R' = H, Si, TMS) reveal an increase in positive charge at Ti and a decrease of the Ti–imido bond order with larger R'.<sup>92</sup> A decrease in Ti–imido bond order coincides with an increase in Ti<sup>δ+</sup>N<sup>δ-</sup> bond polarization thus increasing the predilection for C–H activation. In addition, the ΔG for the formation of a methane adduct becomes more favorable with larger R' (Scheme 1.18).



**Scheme 1.18.** Calculated reaction pathway for the activation of alkanes (RH) by (R'O)<sub>2</sub>Ti=NR' and calculated ΔG for methane adduct formation.

Group VI  $d^0$  tris-imido complexes also activate C–H bonds. The reaction of  $[(^t\text{Bu}_3\text{SiN}=\text{)}_3\text{WH}]\text{K}$  with  $\text{CD}_3\text{I}$  produces  $\text{KI}$  and two tungsten isotopomers ( $60^\circ\text{C}$ ),  $(^t\text{Bu}_3\text{SiN}=\text{)}_2(^t\text{Bu}_3\text{SiNH})\text{WCD}_3$  and  $(^t\text{Bu}_3\text{SiN}=\text{)}_2(^t\text{Bu}_3\text{SiND})\text{WCDH}_2$  (Scheme 1.19).<sup>81</sup> However, the reaction of  $[(^t\text{Bu}_3\text{SiN}=\text{)}_3\text{WH}]\text{K}$  with  $\text{CH}_3\text{I}$  only produces  $(^t\text{Bu}_3\text{SiN}=\text{)}_2(^t\text{Bu}_3\text{SiNH})\text{WCH}_3$ . Using  $^2\text{H}$  NMR spectroscopy analysis of the  $\text{W}-\text{CD}_3$  and  $\text{W}-\text{CHD}_2$  isotopomer ratios, a  $k_{\text{H}}/k_{\text{D}}$  of 9.6(6) was determined. These results are consistent with the intermediacy of the coordinated alkane adduct  $(^t\text{Bu}_3\text{SiN}=\text{)}_3\text{W}(\text{CHD}_3)$ .



**Scheme 1.19.** Reaction of  $[(^t\text{Bu}_3\text{SiN}=\text{)}_3\text{WH}]\text{K}$  with  $\text{CH}_3\text{I}$  and  $\text{CD}_3\text{I}$  to produce tungsten methyl amido complexes via the formation of an intermediate methane adduct.

### 1.3.3 (PNP)Scandium Imido Complex

Pyridine C–H activation by a  $\text{Sc}(\text{III})$  imido complex has been reported.<sup>93</sup> Heating  $(\text{PNP})\text{Sc}(\text{NHAr})\text{Me}$  [ $\text{PNP} = (\text{bis}(2\text{-diisopropylphosphino-4-tolyl})\text{amide})$ ;  $\text{Ar} = 2,6\text{-diisopropylphenyl}$ ] at  $50^\circ\text{C}$  in the presence of pyridine results in the formation of methane and  $(\text{PNP})\text{Sc}(\text{NHAr})(\eta^2\text{-NC}_5\text{H}_4)$ . The calculated Mayer bond order of the imido intermediate  $(\text{PNP})(\text{pyridine})\text{Sc}=\text{NAr}$  that is responsible for C–H activation reveals that the  $\text{Sc}$ –imido linkage is intermediate between a double and triple bond. DFT orbital calculations suggest considerable charge polarization of the  $\text{Sc}$ –imido bond toward the nitrogen and, as a result, the C–H activation is similar to that of  $d^0$  imido complexes described above.

## 1.4 Activation of H–H and C–H Bonds by Late Transition Metal Heteroatom

### Complexes

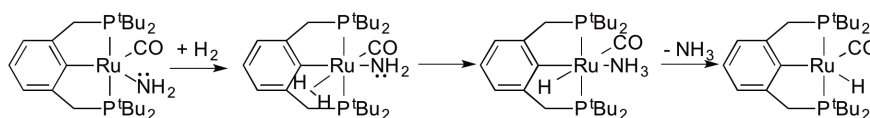
Despite the ability of early transition metal  $d^0$  imido complexes to facilitate 1,2-addition of arene and alkane C–H bonds, these systems failed to perform the necessary C–N reductive elimination to generate the desired functionalized product (Scheme 1.8). The large activation barrier for the reductive elimination step is attributed to the electropositive nature and lack of redox flexibility for these early transition metal complexes. The polarization of the M=NR was determined to be important in the 1,2-addition of C–H bonds involving the early metal  $d^0$  imido complexes. A number of late transition metal complexes with basic hydroxo and amido ligands have been reported,<sup>94,95</sup> suggesting that a late transition metal system for the 1,2-addition of C–H bonds across M–heteroatom bonds is potentially viable.<sup>41</sup>

#### 1.4.1 H<sub>2</sub> Activation by Late Transition Metal Complexes

The bond dissociation energies for C–H (104 kcal/mol for CH<sub>4</sub>) bonds and the H–H (104 kcal/mol) bond are of comparable magnitude; however, dihydrogen is a better ligand than methane. As a result, activation of H<sub>2</sub> is often more facile than methane activation. Several  $d^6$  Ru–X (X = OR, NHR) complexes have been reported to activate H<sub>2</sub>. Addition of dihydrogen across the Ru(II) amido bond of RuCl(PPh<sub>3</sub>)[ $\kappa^3$ -N(SiMe<sub>2</sub>CH<sub>2</sub>PPh<sub>2</sub>)<sub>2</sub>] results in the formation of the amine hydride complex RuCl(PPh<sub>3</sub>)H[ $\kappa^3$ -NH(SiMe<sub>2</sub>CH<sub>2</sub>PPh<sub>2</sub>)<sub>2</sub>].<sup>96</sup> Morris and co-workers have reported that the Ru(II) amido complex *trans*-RuH<sub>2</sub>(diphosphine)(tmen) (where diphosphine = *R*- or *S*-binap and tmen = NHCMe<sub>2</sub>CMe<sub>2</sub>NH<sub>2</sub>) activates dihydrogen to yield a complex in which the H–H bond distance is intermediate between protic-hydridic (*i.e.*, H <sup>$\delta^-$</sup> ···H <sup>$\delta^+$</sup> ) and

hydrogen bonding character.<sup>97</sup>

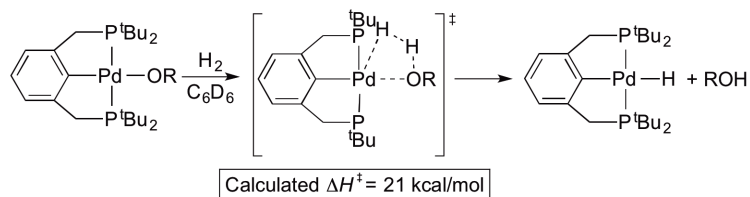
Our group reported the activation of dihydrogen using the Ru(II)–amido complex (PCP)Ru(CO)(NH<sub>2</sub>) [PCP = 2,6-(CH<sub>2</sub>P<sup>t</sup>Bu<sub>2</sub>)<sub>2</sub>C<sub>6</sub>H<sub>3</sub>] to generate (PCP)Ru(CO)(H) and free ammonia (Scheme 1.20).<sup>41</sup> The proposed reaction pathway involves the initial  $\eta^2$ -coordination of dihydrogen to Ru followed by intramolecular addition of H<sub>2</sub> across the Ru–NH<sub>2</sub> bond to form (PCP)Ru(CO)(H)(NH<sub>3</sub>). This intermediate species has been observed by NMR spectroscopy and independently prepared, but it has not been isolated. Dissociation of ammonia yields the final product (PCP)Ru(CO)(H).



**Scheme 1.20.** Plausible mechanism for the activation of dihydrogen by (PCP)Ru(CO)(NH<sub>2</sub>).

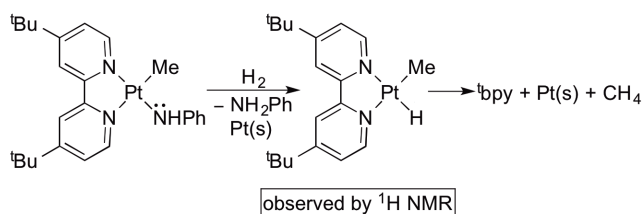
The 1,2-HH-addition of dihydrogen across d<sup>8</sup> M–X bonds has also been reported. Pd(II)–hydroxide and –methoxide complexes, (PCP)Pd(OR) [PCP = 2,6-(CH<sub>2</sub>P<sup>t</sup>Bu<sub>2</sub>)<sub>2</sub>C<sub>6</sub>H<sub>3</sub>, R = H, CH<sub>3</sub>], were reported by Goldberg and co-workers to activate dihydrogen to give (PCP)PdH and either water or methanol (Scheme 1.21).<sup>98,99</sup> Excess water (9 equivalents) is required to obtain reproducible kinetic data. The kinetic studies revealed a first order dependence on the concentration of H<sub>2</sub> and a half order dependence on the concentration of (PCP)Pd(OH). The initial formation of a dimer [(PCP)Pd(OH)]<sub>2</sub>·4H<sub>2</sub>O, that dissociates into the monomer (PCP)Pd(OH) and subsequently reacts with H<sub>2</sub> is consistent with these results.<sup>100</sup> DFT studies (BL3LYP) using <sup>Me</sup>PCP [<sup>Me</sup>PCP = 2,6-(CH<sub>2</sub>PCH<sub>3</sub>)<sub>2</sub>C<sub>6</sub>H<sub>3</sub>] as a model for PCP suggest that the

reaction involves the 1,2-addition of H<sub>2</sub> across the Pd–OR bond.



**Scheme 1.21.** Activation of dihydrogen by (PCP)Pd(OR) (R = H or CH<sub>3</sub>).

Studies of net H<sub>2</sub> addition across a Pt(II) anilido bond indicate that not all dihydrogen activation involving M–X bonds follow a concerted 1,2-addition mechanism. We have reported a Pt(II)–anilido complex (<sup>t</sup>bpy)Pt(Me)(NHPPh) (<sup>t</sup>bpy = 4,4-di-*tert*-butyl-2,2-dipyridyl) that reacts with H<sub>2</sub> to generate <sup>t</sup>bpy, NH<sub>2</sub>Ph and CH<sub>4</sub>.<sup>101,102</sup> Kinetic studies indicated that the reaction is zero-order in (<sup>t</sup>bpy)Pt(Me)(NHPPh), and an induction period was observed. The results of several tests suggest that Pt(s) likely formed *in situ* is a catalyst for the activation of H<sub>2</sub> (Scheme 1.22). For example, the addition of Hg suppressed the reaction, while the addition of Pt(s) accelerated the reaction rate. The results of a filtration test were also consistent with the formation of insoluble Pt(s). Dihydrogen activation across the Pt–NHPPh bond of (<sup>t</sup>bpy)Pt(Me)(NHPPh) and subsequent dissociation of aniline gives the intermediate (<sup>t</sup>bpy)Pt(Me)(H), which is observed directly by <sup>1</sup>H NMR spectroscopy. The net reductive elimination of methane from (<sup>t</sup>bpy)Pt(Me)(H) and dissociation of <sup>t</sup>bpy leads to the formation of Pt(s). Unfortunately, mechanistic details are unknown; it is possible that H<sub>2</sub> addition might occur across either the Pt–Me or Pt–NHPPh bond. However, the lone pair on the anilido provides a kinetic advantage for the addition of H<sub>2</sub> across the Pt–NHPPh bonds versus Pt–Me as suggested by the observation of (<sup>t</sup>bpy)Pt(Me)(H) and free aniline by NMR spectroscopy.



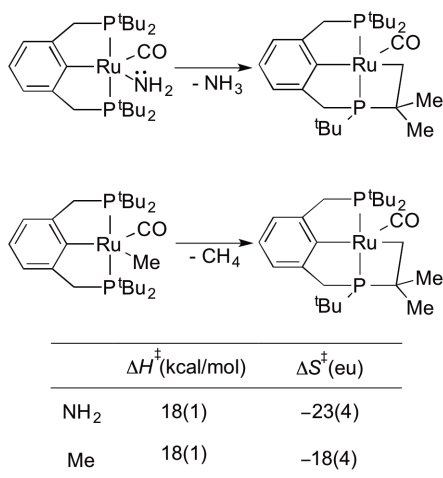
**Scheme 1.22.** Pt(s) catalyzes the addition of H<sub>2</sub> to the Pt–NHP bond of (t<sup>b</sup>py)Pt(Me)(NHP).

It is surprising that the H<sub>2</sub> activation across the Pd–OR bond of Goldberg and co-worker's (PCP)Pd(OR) is feasible whereas the reaction of dihydrogen with (t<sup>b</sup>py)Pt(Me)(NHP) does not occur by H<sub>2</sub> coordination and 1,2-addition across the Pt–NHP bond. A large  $\Delta H^\ddagger$  of 45 kcal/mol was calculated for the activation of dihydrogen by initial formation of (t<sup>b</sup>py)Pt(Me)(NHP)( $\eta^2$ -H<sub>2</sub>) and then subsequent addition of H<sub>2</sub> across the Pt–NHP bond to give (t<sup>b</sup>py)Pt(Me)(H) and aniline. The  $\Delta H^\ddagger$  for the analogous reaction using (PCP)Pd(OR) was approximately half the magnitude (21 kcal/mol). Changing the metal center, –NHP versus –OR, and the ancillary ligand likely result in the difference in activation barriers between (t<sup>b</sup>py)Pt(Me)(NHP) and (t<sup>Bu</sup>PCP)Pd(OR).<sup>5,101</sup> Calculations suggest that for this family of d<sup>8</sup> complexes, each parameter has similar impact on the H<sub>2</sub> addition barrier, which suggests substantial potential to tune such complexes for catalytic activity.

#### 1.4.2 Intramolecular C–H Activation by Late Transition Metal Complexes

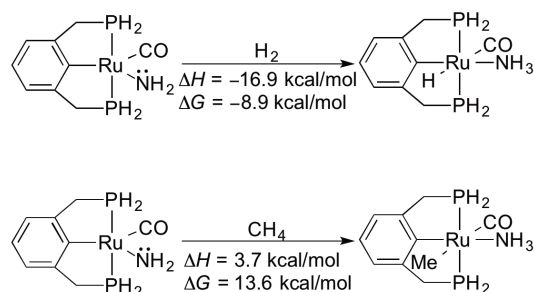
Dihydrogen may be easier to activate than many C–H bonds, but our group provided initial evidence that late transition metal amido or hydroxide (or related) complexes can perform C–H activation. The intramolecular C–H activation of a t<sup>Bu</sup> group on the PCP ligand of (PCP)Ru(CO)(NH<sub>2</sub>) served as the first example of C–H

activation by a  $d^6$  or  $d^8$  metal amido or hydroxide or alkoxide complex (Scheme 1.23).<sup>41</sup> The related complex (PCP)Ru(CO)(Me) also undergoes intramolecular C–H activation to produce methane and cyclometalated complex (Scheme 1.23). Kinetic studies of the two intramolecular C–H activation reactions were performed to obtain a direct comparison for C–H activation of a M–R versus M–X ( $X = \text{NR}_2$  or OR) bond. From these studies it was determined that the reaction is first order in (PCP)Ru(CO)(NH<sub>2</sub>). The C–H activation reaction using (PCP)Ru(CO)(Me) ( $k_{\text{obs}} = 3.2(1) \times 10^{-4} \text{ s}^{-1}$ ,  $\Delta G^\ddagger = 19 \text{ kcal/mol}$ ) was determined to be approximately five times faster at 50 °C than the activation with (PCP)Ru(CO)(NH<sub>2</sub>) ( $k_{\text{obs}} = 6.0(3) \times 10^{-5} \text{ s}^{-1}$ ,  $\Delta G^\ddagger = 20 \text{ kcal/mol}$ ). Identical  $\Delta H^\ddagger$  values [18(1) kcal/mol] were obtained from the Eyring plots of both complexes. However, the Eyring plots revealed different  $\Delta S^\ddagger$  values for the amido and methyl complexes [–23(4) eu and –18(4) eu, respectively] (Scheme 1.23). The identical  $\Delta H^\ddagger$  values indicate that the lone pair on the amido ligand offers no inherent kinetic advantage for the intramolecular C–H activation with (PCP)Ru(CO)X complexes. The entropic difference for the activation of H<sub>2</sub> by (PCP)Ru(CO)(Me) versus (PCP)Ru(CO)(NH<sub>2</sub>) is likely because alkanes are poor ligands; thus, CH<sub>4</sub> is more weakly bound to the (PCP)Ru(CO)(Me) versus ammonia for (PCP)Ru(CO)(NH<sub>2</sub>).



**Scheme 1.23.** Intramolecular C–H activation by (PCP)Ru(CO)(NH<sub>2</sub>) and (PCP)Ru(CO)(Me) to produce methane and cyclometalated complex.

DFT [B3LYP/SBK(d)] calculations using the model complex (PCP')Ru(CO)X (X = NH<sub>2</sub> or Me), which differs from PCP in the replacement of phosphine <sup>t</sup>Bu substituents with hydrogen, were performed in order to gain insight into why H<sub>2</sub> activation with (PCP)Ru(CO)NH<sub>2</sub> is observed experimentally but CH<sub>4</sub> C–H activation is not.<sup>41</sup> The activation of dihydrogen by (PCP)Ru(CO)NH<sub>2</sub> was calculated to be exothermic (–17 kcal/mol) and exergonic (–9 kcal/mol) whereas methane C–H activation is calculated to be endothermic (4 kcal/mol) and endergonic (14 kcal/mol) (Scheme 1.24). The large reduction in Ru–N bond strength upon conversion of the Ru–NH<sub>2</sub> bond to Ru–NH<sub>3</sub> ( $\Delta$ BDE = 40 kcal/mol), partially due to the loss of the amido–Ru  $\pi$ -bonding, essentially cancels out the 32 kcal/mol gain from breaking a methane C–H bond and forming Ru–CH<sub>3</sub> and Ru–NH<sub>2</sub> bonds. Net ligand-to-metal  $\pi$ -bond interaction is not viable for octahedral d<sup>6</sup> complexes; however, five-coordinate d<sup>6</sup> complexes in trigonal bipyramidal geometries possess an empty orbital which allows for efficient  $\pi$ -donation.<sup>103</sup>

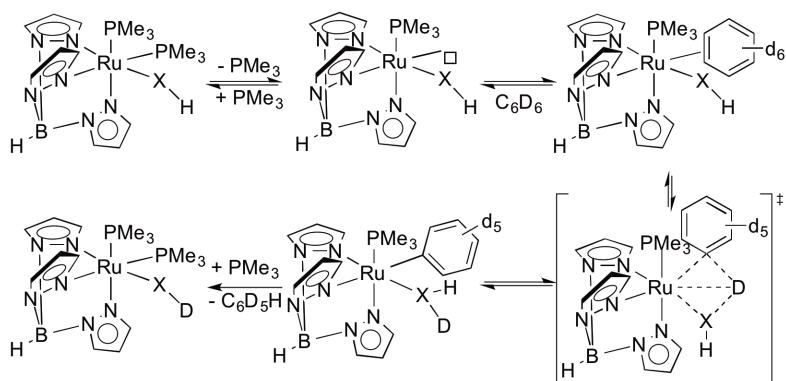


**Scheme 1.24.** Calculated energetics (DFT) for H<sub>2</sub> and CH<sub>4</sub> activation by (PCP')Ru(CO)(NH<sub>2</sub>).

### 1.4.3 1,2-CH-Addition by d<sup>6</sup> Metal Amido and Anilido Complexes

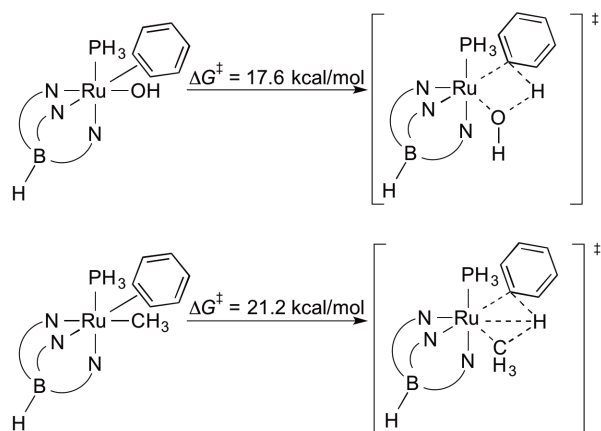
In the year following our report of intramolecular C–H activation by (PCP)Ru(CO)(NH<sub>2</sub>), our group and Periana, Goddard and co-workers independently reported the first examples of intermolecular C–H activation via 1,2-CH-addition of arenes across d<sup>6</sup> M–X (X = OR, NHR).

Our group has shown that heating (80 – 130 °C) TpRu(PMe<sub>3</sub>)<sub>2</sub>X (Tp = hydridotris(pyrazolyl)borate; X = OH or NH<sub>2</sub>) in C<sub>6</sub>D<sub>6</sub> leads to H/D exchange between the hydroxide or anilido ligands and C<sub>6</sub>D<sub>6</sub>.<sup>42-44</sup> The proposed mechanism (Scheme 1.25) is believed to involve dissociation of PMe<sub>3</sub> to provide a vacant coordination site for benzene, followed by 1,2-addition across the Ru–XH (X = O or NPh) to give TpRu(PMe<sub>3</sub>)(XHD)(C<sub>6</sub>D<sub>5</sub>). The addition of 1 equivalent of PMe<sub>3</sub> relative to TpRu(PMe<sub>3</sub>)<sub>2</sub>X (X = OH, NHPH) halts H/D exchange, presumably because PMe<sub>3</sub> competes with benzene for coordination to Ru. Kinetic studies indicate that the H/D exchange into the hydroxide ligand of TpRu(PMe<sub>3</sub>)<sub>2</sub>OH is first order with  $k_{\text{obs}} = 8.0(2) \times 10^{-5} \text{ s}^{-1}$  at 80 °C. The H/D exchange into the anilido ligand of TpRu(PMe<sub>3</sub>)<sub>2</sub>NHPH is much slower ( $k_{\text{obs}} = 1.4(2) \times 10^{-5} \text{ s}^{-1}$  at 130 °C).



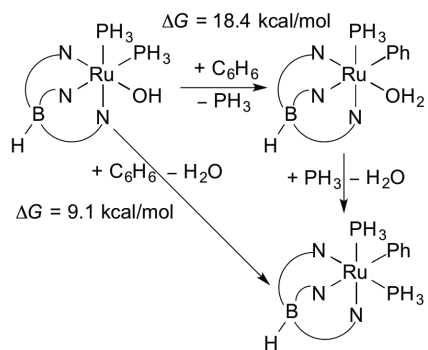
**Scheme 1.25.** Proposed mechanism for benzene H/D exchange encompassing the 1,2-addition of benzene C–D bonds across Ru–X bond of  $\text{TpRu}(\text{PMe}_3)_2\text{XH}$  ( $\text{X} = \text{O}$  or  $\text{NPh}$ ).

Density functional theory calculations [B3LYP/CEP-31G(d)] by Cundari and co-workers using  $(\text{Tab})\text{Ru}(\text{PH}_3)(\text{X})(\eta^2\text{-C}_6\text{H}_6)$  ( $\text{X} = \text{Me}$ ,  $\text{OH}$  or  $\text{NH}_2$ ;  $\text{Tab}$  = tris(azo)borate, a  $\text{Tp}$  model) indicate that the C–H activation occurs via a concerted process with no change in oxidation state involving a four-centered kite shaped transition state. A lower  $\Delta G^\ddagger$  was calculated when  $\text{X} = \text{OH}$  for benzene C–H activation from the benzene adduct  $(\text{Tab})\text{Ru}(\text{PH}_3)(\text{X})(\eta^2\text{-C}_6\text{H}_6)$  ( $\text{X} = \text{Me}$  or  $\text{OH}$ ) ( $\Delta\Delta G^\ddagger$  of 3.6 kcal/mol, Scheme 1.26). This calculation suggests that the lone pair on the hydroxide ligand offers a kinetic advantage for the hydrocarbon C–H activation.



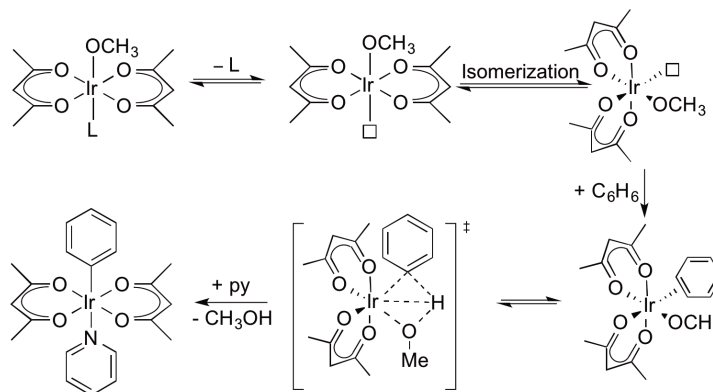
**Scheme 1.26.** DFT [B3LYP/ CEP-31G(d)] calculated free energies of activation for  $C_6H_6$  C–H activation across the Ru–OH bond of  $(\text{Tab})\text{Ru}(\text{PH}_3)(\text{OH})(\eta^2\text{-}C_6H_6)$  and the Ru–Me bond of  $(\text{Tab})\text{Ru}(\text{PH}_3)(\text{Me})(\eta^2\text{-}C_6H_6)$  [Tab = tris(azo)borate].

The 1,2-addition of benzene C–H bonds across Ru–OH or Ru–NHPh of  $\text{TpRu}(\text{PMe}_3)_2(\text{X})$  ( $\text{X} = \text{OH}, \text{NHPH}$ ) is thermodynamically disfavored as neither  $\text{TpRu}(\text{PMe}_3)(\text{Ph})(\text{XH})$  ( $\text{X} = \text{OH}$  or  $\text{NHPH}$ ) nor  $\text{TpRu}(\text{PMe}_3)_2\text{Ph}$  is observed. The calculations are in agreement with the formation of  $\text{TpRu}(\text{PMe}_3)_2(\text{NHPH})$  and  $C_6H_6$  when heating  $\text{TpRu}(\text{PMe}_3)_2\text{Ph}$  and aniline (130 °C) in  $C_6D_6$ . Additionally, DFT calculations [B3LYP/CEP-31G(d)] on  $(\text{Tab})\text{Ru}(\text{PH}_3)_2\text{OH}$  [Tab = tris(azo)borate] indicate that the reaction is endergonic (Scheme 1.27).<sup>43</sup>



**Scheme 1.27.** Calculated free energies for  $C_6H_6$  C–H activation using the model complex  $(\text{Tab})\text{Ru}(\text{PH}_3)_2(\text{OH})$  (Tab = tris(azo)borate).

Periana, Goddard and co-workers reported stoichiometric C–H activation of benzene with the iridium(III) methoxide complex  $(\text{acac})_2\text{Ir}(\text{OMe})(\text{L})$  ( $\text{acac} = \kappa^2\text{-O,O-acetylacetonate}$ ,  $\text{L} = \text{pyridine}$  or  $\text{CH}_3\text{OH}$ ) leading to the formation of  $(\text{acac})_2\text{Ir}(\text{Ph})(\text{py})$  and methanol in high yields (Scheme 1.28).<sup>104,105</sup> A 75% yield of  $(\text{acac})_2\text{Ir}(\text{Ph})(\text{py})$  and methanol is obtained after heating  $(\text{acac})_2\text{Ir}(\text{OMe})(\text{CH}_3\text{OH})$ , benzene, and pyridine at 160 °C for 10 minutes. The analogous reaction with  $(\text{acac})_2\text{Ir}(\text{OMe})(\text{py})$  results in increased yield of  $(\text{acac})_2\text{Ir}(\text{Ph})(\text{py})$  and methanol ( $\geq 95\%$ ); however, a higher temperature (180 °C) and a longer reaction time (4 h) is required.

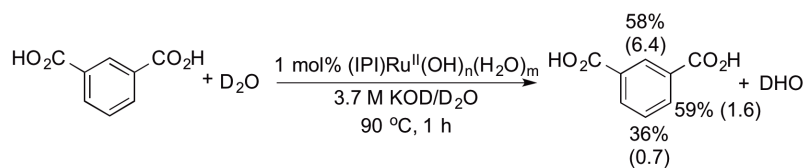


**Scheme 1.28.** Proposed mechanism for benzene C–H activation by  $(\text{acac})_2\text{Ir}(\text{OMe})(\text{L})$  ( $\text{L} = \text{py}$  or  $\text{CH}_3\text{OH}$ ).

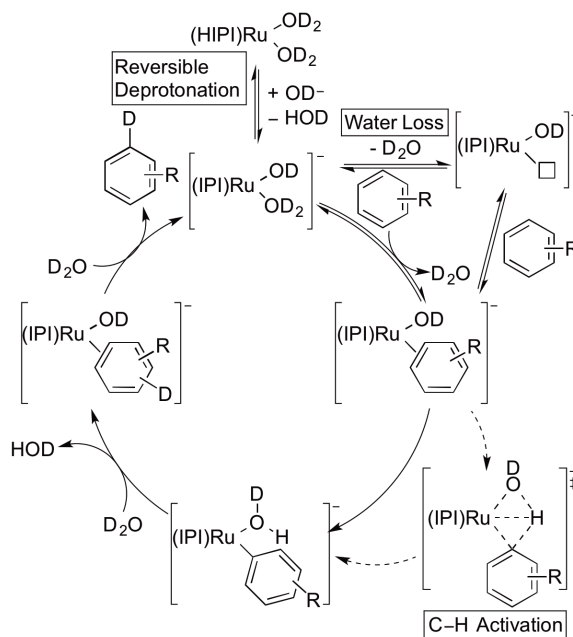
The proposed mechanism for benzene C–H activation by  $(\text{acac})_2\text{Ir}(\text{OMe})(\text{py})$  involves pyridine dissociation to give a five-coordinate intermediate, isomerization, benzene coordination, and benzene C–H bond cleavage via 1,2-addition across the Ir–OMe bond (Scheme 1.28). No kinetic isotope effect (KIE) is observed for the reaction of  $(\text{acac})_2\text{Ir}(\text{OH})(\text{py})$  with a mixture of  $\text{C}_6\text{H}_6$  and  $\text{C}_6\text{D}_6$  ( $k_{\text{H}}/k_{\text{D}} = 1.07 \pm 0.24$ ). A normal primary KIE is observed for the reaction of  $(\text{acac})_2\text{Ir}(\text{OH})(\text{py})$  with 1,3,5-trideuterobenzene ( $k_{\text{H}}/k_{\text{D}} = 2.65 \pm 0.56$ ). The observed KIE suggests the formation of the

arene complex is the rate-determining step. Computational data (DFT and Pipek-Mezey population analysis) for the reaction of  $(\text{acac})_2\text{Ir}(\text{OMe})(\text{py})$  and benzene indicate that the lone pair on the methoxide ligand participates in the C–H activation step providing support for a 1,2-CH-addition mechanism.<sup>39</sup> Unlike the reaction of  $\text{TpRu}(\text{PMe}_3)_2\text{X}$  ( $\text{X} = \text{OH}, \text{NHPH}$ ) with benzene, the benzene C–H activation by  $(\text{acac})_2\text{Ir}(\text{OMe})(\text{py})$  was calculated to be exergonic.

Periana, Goddard and co-workers have recently reported a Ru(II) hydroxide complex  $(\text{IPI})\text{Ru}^{\text{II}}(\text{OH})_n(\text{H}_2\text{O})_m$  ( $\text{IPI} = 2,6\text{-diimidizoylpyridine}$ ) for the H/D exchange reactions between C–H bonds of water-soluble aromatic substrates and KOD/D<sub>2</sub>O (Scheme 1.29).<sup>106</sup> The rate of H/D exchange reaction was determined to increase with increasing concentrations of KOD. This is quite surprising as one might anticipate that hydroxide might instead inhibit aromatic C–H coordination to Ru. The authors suggest that KOD increases the  $\pi$ -nucleophilicity of the Ru catalyst by deprotonating the protic sites of the IPI ligand. A first order dependence on both catalyst and substrate was determined from kinetic studies using isophthalic acid as a substrate. A  $\Delta H^\ddagger$  of 17.8(9) kcal/mol and a  $\Delta S^\ddagger$  of  $-19.6(3)$  eu were determined from the Eyring analysis of kinetic data collected between 60 °C and 80 °C. The H/D exchange reaction is proposed to occur by a mechanism involving the reversible deprotonation of  $(\text{IPI})\text{Ru}^{\text{II}}(\text{OH})_n(\text{H}_2\text{O})_m$  by KOD, followed by H<sub>2</sub>O dissociation, arene coordination, and C–H activation (Scheme 1.30).



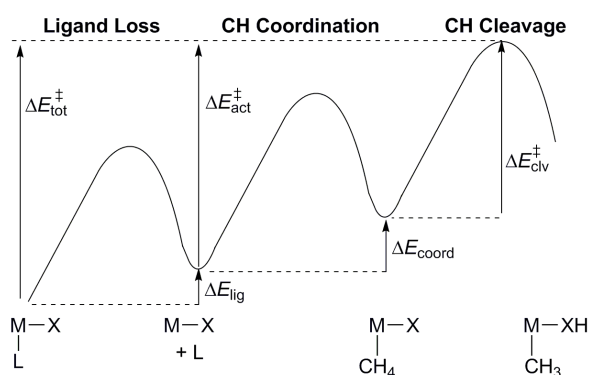
**Scheme 1.29.** Isophthalic acid H/D exchange in the presence and absence (value in parentheses) of 1 mol% catalyst.



**Scheme 1.30.** Proposed mechanism for nucleophilic C–H activation of water-soluble arenes using  $(\text{IPI})\text{Ru}(\text{OH})_n(\text{H}_2\text{O})_m$  ( $\text{R} = \text{CO}_2\text{H}$  or  $\text{OH}$ ).

DFT calculations (B3LYP, M06 and X3LYP) of the  $d^6$  complexes *cis*-(*acac*)<sub>2</sub>M(L)X and TpM(L)(CO)X ( $\text{M} = \text{Ir, Rh, Ru, Os}$ ;  $\text{X} = \text{CH}_3, \text{OH, OMe, NH}_2, \text{NMe}_2$ ;  $\text{L} = \text{pyridine}$ ) were performed to determine if the lone pair on X offers an intrinsic kinetic advantage for methane C–H activation.<sup>40</sup> The total activation energies ( $\Delta E_{\text{tot}}^\ddagger$ ) from the 18-electron precursors *cis*-(*acac*)<sub>2</sub>MX(py) and TpM(CO)(py)X (py = pyridine) to final C–H activation products *cis*-(*acac*)<sub>2</sub>M(HX)(CH<sub>3</sub>) and TpM(CO)(HX)(CH<sub>3</sub>) have

been calculated. These calculations are important because both *cis*-(*acac*)<sub>2</sub>Ir(L)X and TpRu(L)(CO)X have been demonstrated experimentally to mediate C–H activation.<sup>43,44,104,105,107-111</sup> As shown in Scheme 1.31,  $\Delta E_{\text{tot}}^{\ddagger}$  is the sum of  $\Delta E_{\text{lig}}$  (ligand loss) +  $\Delta E_{\text{coord}}$  (methane coordination) +  $\Delta E_{\text{clv}}^{\ddagger}$  (C–H cleavage). Ess et al. also calculated the activation energy for 1,2-CH-addition from the 5-coordinate intermediates following ligand dissociation ( $\Delta E_{\text{act}}^{\ddagger} = \Delta E_{\text{coord}} + \Delta E_{\text{clv}}^{\ddagger}$ ).



**Scheme 1.31.** Reaction profile for C–H activation by 18-electron octahedral complexes showing that  $\Delta E_{\text{tot}}^{\ddagger} = \Delta E_{\text{lig}} + \Delta E_{\text{coord}} + \Delta E_{\text{clv}}^{\ddagger}$ .

From the 5-coordinate (*acac*)<sub>2</sub>Ir–X species, the calculated  $\Delta E_{\text{act}}^{\ddagger}$  values increase in the following order X = CH<sub>3</sub> < OR < NR<sub>2</sub> (Table 1.1). The calculated  $\Delta E_{\text{act}}^{\ddagger}$  is negative when X = Me because the energy of (*acac*)<sub>2</sub>Ir–Me is greater than the energy for the CH<sub>4</sub> activation transition state. These calculations suggest that the lone pair on OR and NR<sub>2</sub> hinders C–H activation. This inhibition is likely because when X = OH, OMe, NH<sub>2</sub> or NMe<sub>2</sub>, (*acac*)<sub>2</sub>Ir–X adopts a trigonal-bipyramidal geometry that is a result of X-to-metal  $\pi$ -donation, the ground state energy is lowered by the ligand-to-metal  $\pi$ -donation and the  $\Delta G^{\ddagger}$  for methane activation relative to (*acac*)<sub>2</sub>Ir–Me is increased. From the 5-coordinate TpRu(CO)X the values for  $\Delta E_{\text{act}}^{\ddagger}$  from smallest to largest are X = OH < CH<sub>3</sub>  $\approx$  NR<sub>2</sub>  $\approx$

OMe. The trend differences for the  $\Delta E_{\text{act}}^{\ddagger}$  for the Ir(III) complexes versus the Ru(II) complexes suggests that there is no straightforward method to predict the relative influence of  $\pi$ -donor ligands on ground states and transition states.

The relative barrier heights for  $\Delta E_{\text{tot}}^{\ddagger}$  were calculated to be  $X = \text{NR}_2 \approx \text{CH}_3 \ll \text{OR}$  for  $(\text{acac})_2\text{IrX}$  and  $X = \text{NR}_2 \ll \text{CH}_3 \approx \text{OR}$  for  $\text{TpRu}(\text{CO})\text{X}$ . Similar to the calculated  $\Delta E_{\text{act}}^{\ddagger}$  values the trends differ from one metal to another. Unlike with the  $\Delta E_{\text{act}}^{\ddagger}$  values,  $\pi$ -donation is not a factor for  $\Delta E_{\text{tot}}^{\ddagger}$ , and as a result, the basic amido ligand appears to offer an advantage.

**Table 1.1.** DFT (MO6/B2) calculated  $\Delta E_{\text{act}}^{\ddagger}$  for  $(\text{acac})_2\text{IrX}$  ( $X = \text{Me}, \text{OH}$  or  $\text{NH}_2$ ) (See **Scheme 1.31** for  $\Delta E_{\text{act}}^{\ddagger}$  and  $\Delta E_{\text{clv}}^{\ddagger}$ ).

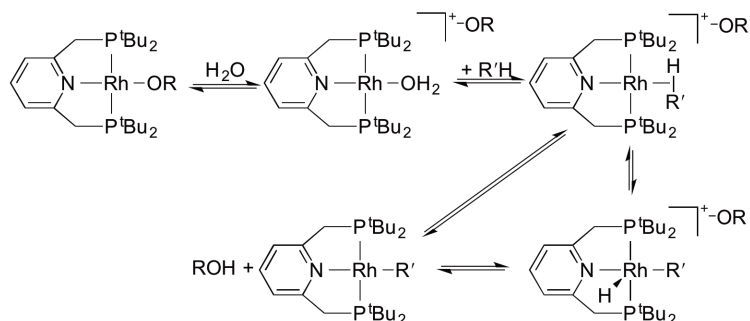
$\text{Ir}(\text{acac})_2\text{-X}$	$\longrightarrow$	$\text{Ir}(\text{acac})_2\text{X}$	$\longrightarrow$	$\text{Ir}(\text{acac})_2\text{XH}$
		$\begin{array}{c}   \\ \text{H}_3\text{C}-\text{H} \end{array}$		$\begin{array}{c}   \\ \text{CH}_3 \end{array}$
		$\Delta E_{\text{act}}^{\ddagger}$		$\Delta E_{\text{clv}}^{\ddagger}$
X	(kcal/mol)	(kcal/mol)		(kcal/mol)
CH <sub>3</sub>	-7.3	7.1		
OH	13.1	10.8		
NH <sub>2</sub>	19.9	NA <sup>a</sup>		

<sup>a</sup> No methane complex was observed with  $\text{NH}_2$ .

#### 1.4.4 Arene C–H Activation by $d^8$ M–Heteroatom Complexes

Several  $d^8$  M–X ( $X = \text{OR}, \text{NHR}$ ) systems for C–H activation have also been reported. Goldberg and co-workers have reported stoichiometric arene activation using the Rh(I) complexes  $(\text{PNP})\text{Rh}(\text{X})$  [ $\text{PNP} = 2,6\text{-}(\text{di-}i\text{-tert-butylphosphinomethyl})\text{pyridine}$ ;  $X = \text{OH}, \text{OCH}_2\text{CF}_3$ ] (Scheme 1.32).<sup>112,113</sup> Heating  $(\text{PNP})\text{Rh}(\text{OH})$  (60 °C) in benzene- $d_6$  for 95 h led to the formation of  $(\text{PNP})\text{Rh}(\text{C}_6\text{D}_5)$  in 60% yield. Similarly, heating  $(\text{PNP})\text{Rh}(\text{OCH}_2\text{CF}_3)$  in  $\text{C}_6\text{D}_6$  at a higher temperature for a longer period of time (100 °C, 158 h) led to the formation of  $(\text{PNP})\text{Rh}(\text{C}_6\text{D}_5)$  in 40% yield. The proposed mechanism for benzene C–H activation by  $(\text{PNP})\text{Rh}(\text{X})$  ( $R = \text{OH}, \text{OCH}_2\text{CF}_3$ ) does not involve 1,2-

CH-addition. Instead, the reaction is believed to proceed by initial heterolytic cleavage of the Rh–OR bond to generate uncoordinated hydroxide or alkoxide. Next, the arene coordinates to Rh to form (PNP)Rh( $\eta^2$ -CH-R'H), followed by C–H activation and proton transfer to the uncoordinated RO<sup>−</sup> group.



**Scheme 1.32.** Proposed mechanism for arene C–H bond activation with (PNP)Rh(OR) (R = H or CH<sub>2</sub>CF<sub>3</sub>; R'H = arene).

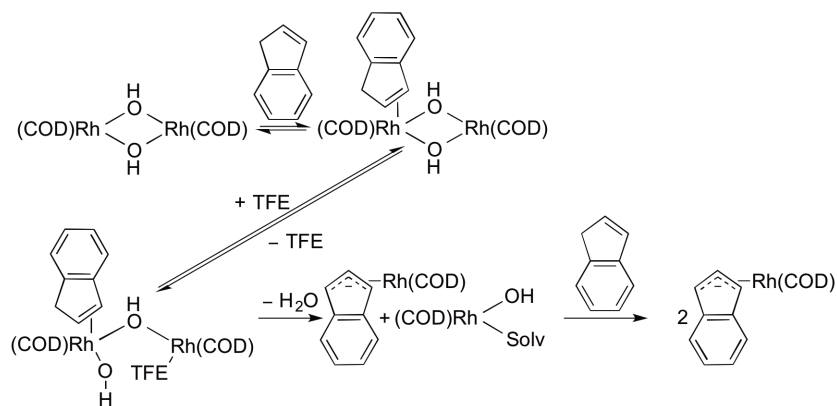
Another example of a d<sup>8</sup> Rh(I)–X complex performing arene C–H activation has been reported by Bercaw, Labinger and co-workers. The hydroxy-bridged rhodium dimer [( $\kappa^4$ -COD)Rh( $\mu$ -OH)]<sub>2</sub> (COD = 1,5-cyclooctadiene) has been shown to activate indene to form [(COD)Rh( $\eta^3$ -indenyl)] (Scheme 1.33).<sup>114</sup> Kinetic studies indicate that the reaction is first-order in Rh and indene. A two-term rate law is suggested because increasing the concentration of 2,2,2-trifluoroethanol (TFE) accelerates the formation of [(COD)Rh( $\eta^3$ -indenyl)] without effecting the first-order dependence on Rh or indene.

From KIE studies of the reaction of [(COD)Rh( $\mu$ -OH)]<sub>2</sub> with 1,1,3-trideuteroindene and perprotio-indene, C–H cleavage was determined to be the rate determining step because a primary KIE of  $k_H/k_D = 4.2(2)$  was obtained. A plausible reaction pathway for activation of indene by [( $\kappa^4$ -COD)Rh( $\mu$ -OH)]<sub>2</sub> that is consistent with

a first order dependence on the concentration of Rh and rate determining C–H activation would involve reversible indene coordination to the dimer, followed by C–H activation to yield water,  $[(\text{COD})\text{Rh}(\eta^3\text{-indenyl})]$ , and  $[(\text{COD})\text{Rh}(\text{OH})(\text{solv})]$  (solv =  $\text{H}_2\text{O}$  or TFE). A second equivalent of  $[(\text{COD})\text{Rh}(\eta^3\text{-indenyl})]$  could then be obtained by exchange with the solvent (Scheme 1.33). The specific mechanism for the C–H activation step has not been determined.

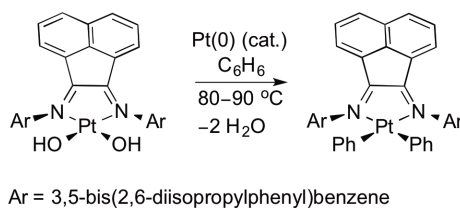
Labinger, Bercaw and co-workers have recently reported the C–H activation of indene and cyclopentadiene by the Ir analogue  $[(\text{COD})\text{Ir}(\mu\text{-OH})_2]$ .<sup>115</sup> Kinetic studies suggest that the C–H activation by both the Rh and Ir complexes proceed via similar pathways. The relative rates for indene C–H activation by  $[(\text{COD})\text{M}(\mu\text{-OH})_2]$  (M = Rh, Ir) at 50 °C are comparable, but differences in the activation parameters are observed.

The reaction with Ir has a larger  $\Delta H^\ddagger$  ( $\Delta\Delta H^\ddagger = 4.3(1)$  kcal/mol) and has a less favorable enthalpy than the reaction with the Rh analogue ( $\Delta\Delta S^\ddagger = 9.0$  eu). As a result, it has been suggested that the C–H activation occurs via a 1,2-addition across the M–OH (M = Rh, Ir) bonds. A 1,2-CH-addition mechanism offers support of larger  $\Delta H^\ddagger$  for Ir since the M–OH bond would be stronger than with Rh. The strong Ir–OH bond would be transformed to a weaker M–OH<sub>2</sub> bond.



**Scheme 1.33.** Proposed mechanism for indene C–H activation by  $[(\text{COD})\text{Rh}(\mu\text{-OH})]_2$  (TFE = 2,2,2-trifluoroethanol, Solv =  $\text{H}_2\text{O}$  or TFE).

Piers and co-workers have reported benzene C–H activation across the Pt(II)–OH bonds of the bulky diimine complex  $(\text{BIAN})\text{Pt}(\text{OH})_2$  (BIAN = bis(3,5-bis(2,6-diisopropylphenyl)benzene)-acenaphthenequinonediimine) at 80 – 90 °C to give a Pt(II) bisphenyl complex (Scheme 1.34). This reaction is related to the addition of dihydrogen to  $(^t\text{bpy})\text{Pt}(\text{Me})(\text{NHPh})$  in that it is accelerated by *in situ* generated Pt(s).<sup>101</sup> Mechanistic studies suggest that 1,2-CH(D)-addition across Pt–OH bonds occurs at low Pt concentrations, but at higher starting concentrations of Pt(II), *in situ* generated Pt(0) particles catalyze the net C–H(D) addition.



**Scheme 1.34.** Benzene C–H activation by  $(\text{BIAN})\text{Pt}(\text{OH})_2$  catalyzed by *in situ* generated Pt(0) particles.

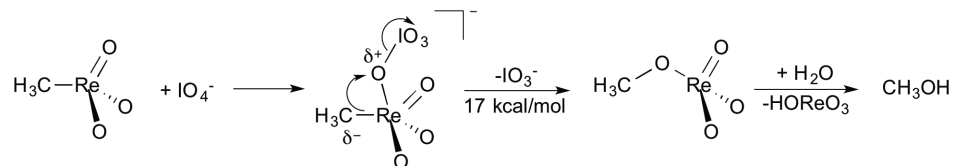
## 1.5 M–R Functionalization

Our proposed catalytic cycle for hydrocarbon functionalization, shown in Scheme 1.8, consists of the following two steps: C–H activation via a 1,2-addition across a M–X bond and hetero-functionalization of the M–alkyl group. The functionalization of M–R has not been observed for any of the systems described above that perform 1,2-addition.

In Pathway A of Scheme 1.8, C–O or C–N reductive elimination leads to formation of the functionalized product. Oxidation of the metal center by atom (O) or group (NR) transfer regenerates the starting M-oxo or M-nitrene complex. The activation barriers for the reductive elimination step are sufficiently large that functionalization via this type of mechanism is not likely viable for the early metal systems that perform 1,2-CH-addition. The reductive elimination step could be feasible for middle or late metal complexes; however, these transition metal oxo and nitrene complexes are typically in high oxidation states and are “electrophilic” making them prone to hydrogen atom abstraction. Also, nitrene and oxo ligands coordinated to high oxidation state metals are often not strongly basic. As shown in the alternative Pathway B of Scheme 1.8, functionalization could also occur via the oxygen atom or nitrene insertion into the M–alkyl bond. Oxy-functionalization of hydrocarbyl ligands of W(VI), Re(VII), Ni(II) and Pd(II) complexes have been reported.<sup>116-125</sup>

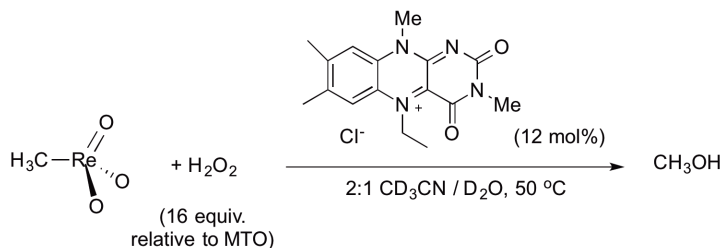
Oxy-insertion into the M–alkyl bond of methylrheniumtrioxo (MTO) to produce methanol is known.<sup>126</sup> Methanol is generated stoichiometrically when MTO is treated with an oxidant at room temperature.<sup>117</sup> Periana, Goddard and co-workers studied the mechanism of this transformation.<sup>117,127</sup> Computational studies suggest the rate determining step is a “Baeyer–Villiger” type oxygen insertion into the Re–Me bond of

MTO (Scheme 1.35). This pathway is calculated to have an activation barrier of 17 kcal/mol.<sup>127</sup>



**Scheme 1.35.** Baeyer–Villiger oxy-insertion pathway for methanol formation from MTO and  $\text{IO}_4^-$ .

An interesting extension to this work was recently reported. In nature, monooxygenases, with the assistance of flavin co-factors, catalyze Baeyer–Villiger type oxidations.<sup>128</sup> Flavins have been shown to serve as organocatalysts for the oxygen atom insertion into the  $\text{Re}-\text{CH}_3$  bond of MTO (Scheme 1.36)<sup>123</sup> The reaction of MTO with  $\text{H}_2\text{O}_2$  was determined to have a first order dependence on flavin catalyst. The O atom in the product was determined to originate from  $\text{H}_2\text{O}_2$  since performing both the uncatalyzed and catalyzed reactions with isotopically labeled  $\text{H}_2^{18}\text{O}_2$  gives  $^{18}\text{O}$  labeled methanol. Calculated energy barrier indicate an energetic advantage for the insertion of MTO into the flavin versus  $\text{H}_2\text{O}_2$ .



**Scheme 1.36.** Lumiflavin derivative has been shown to catalyze the reaction of MTO with  $\text{H}_2\text{O}_2$ .

We have recently reported that the  $W^{IV}$  complexes,  $Cp^*W(O)_2(CH_2SiMe_3)$  and  $Cp^*W(O)(\eta^2-O)_2(CH_2SiMe_3)$  ( $Cp^* = \eta^5$ -pentamethylcyclopentadienyl) carry out oxygen atom insertion.<sup>124</sup> The reaction of  $Cp^*W(O)_2(CH_2SiMe_3)$  with oxygen atom donors (e.g.,  $IO_4^-$ ,  $PhIO$ ,  $H_2O_2$ ) leads to the formation of  $TMSCH_2OH$  (TMS = trimethylsilyl). Oxygen insertion using  $Cp^*W(O)(\eta^2-O)_2(CH_2SiMe_3)$  is accelerated by NaOH or Brønsted acid; however, a greater acceleration is observed for addition of NaOH than acid. Several different pathways are believed to be operative for the oxygen insertion reaction using the  $Cp^*W^{IV}$  complexes, one of which is the organometallic Baeyer–Villiger (OMBV) pathway. The concerted insertion of an oxygen atom in the  $W-CH_2SiMe_3$  bond serves as the only other example of OMBV reaction besides that observed for MTO.

Recently, our lab has observed non-radical oxygen atom insertion into Fe(II) hydrocarbyl bonds.<sup>129</sup>  $Cp^*Fe[P(OCH_2)_3CET]_2Ph$  reacts with excess  $Me_3NO$  to form  $PhOH$  (after reaction with  $H_2O$  or  $HCl$ ) in an 85% yield.<sup>129</sup> Light is required, presumably to initiate the ligand exchange of phosphite with  $Me_3NO$ . During the reaction  $Cp^*$  is oxidized to 1,2,3,4-tetramethyl fulvene and the phosphite is oxidized to phosphate. The methyl analogue,  $Cp^*Fe[P(OCH_2)_3CET]_2Me$ , undergoes an analogous reaction with  $Me_3NO$  to generate  $MeOH$  in 25% yield. The oxygen atom insertion into Fe–R bonds of  $Cp^*Fe[P(OCH_2)_3CET]_2R$  ( $R = Ph, Me$ ) complexes is exciting because the related Fe complex  $Cp^*Fe(CO)(NCMe)Ph$  has been reported to activate C–H bonds.<sup>130</sup>

## 1.6 Summary and Thesis Outline

The 1,2-addition of C–H bonds has been reported with early metal  $d^0$  imido complexes that are generated *in situ*.<sup>76-79,81,85,92,131-135</sup> The polarization of the  $M=N$  bond in the early metal–imido systems is responsible for the observed reactivity with C–H

bonds. Low oxidation state late metal complexes with heteroatom ligands are able to disrupt the metal to ligand  $\pi$  bonding, thus enhancing the polar nature of the metal–heteroatom bonds. However, despite the ability of these complexes to activate inert C–H bonds, most notably methane, C–N reductive elimination to form a functionalized amine product has not been observed with early transition metal systems. This drawback led us to pursue late transition metal systems, and we and others have demonstrated 1,2-addition of C–H bonds across late transition metal–alkoxide and amido bonds.<sup>41,42,43,104,105,112,113,114,115</sup> Unfortunately, there are no reported examples of 1,2-CH-addition of alkane C–H bonds by late transition metal complexes.

The polarization of the M–heteroatom bond such that there is substantial negative charge on the heteroatom is important for 1,2-CH-addition by both the early and late metal systems. For late transition metals, the oxidation state is key because vacant  $d\pi$  orbitals likely result in –OR or –NR ligands that are insufficiently basic to activate C–H bonds. In addition, it might be necessary to avoid high oxidation state complexes that are active for undesirable HAA/ radical processes. Further research on 1,2-CH-addition to develop a better understanding of what promotes this reaction is necessary. For example, to what extent do the following factors influence the propensity toward C–H activation?

- 1) Metal oxidation state: Low oxidation states might enhance reactivity by providing more basic ligands “X,” but high oxidation states are likely to enhance the protic character of coordinated C–H bonds.
- 2) Identity of ligand X: More basic ligands are also likely better  $\pi$ -donors, which could stabilize coordinatively unsaturated intermediates. However, the

coordination of more basic ligands results in less electrophilic metal centers and might therefore increase the barrier for hydrocarbon coordination.

3) Identity of ancillary ligands: To what extent can reactivity be modulated by donor ability of ancillary ligands?

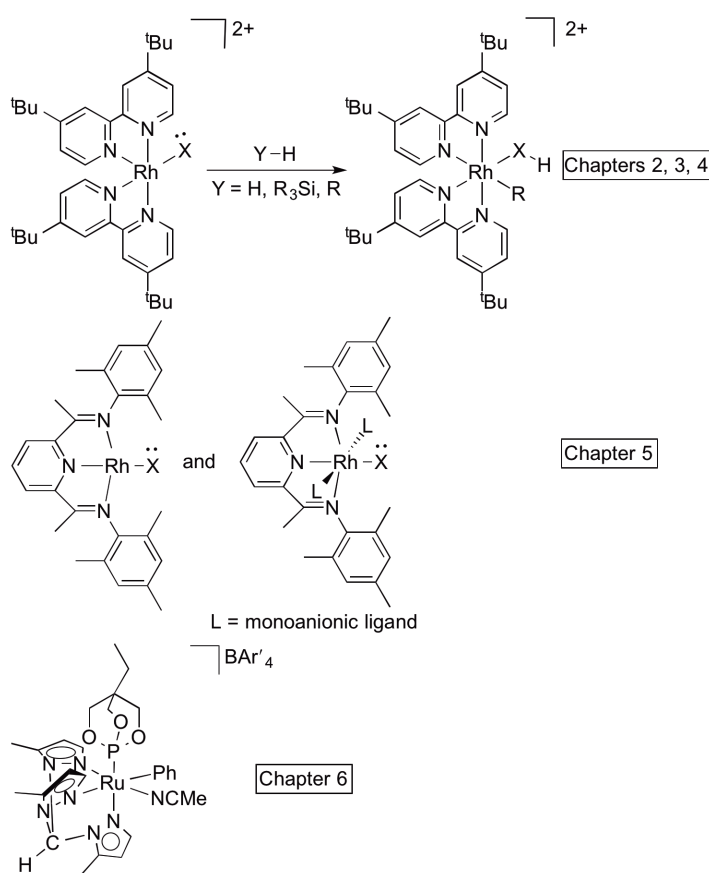
Also, many transition metal C–H activation reactions are selective for stronger C–H bonds (*e.g.*, terminal C–H bonds of alkanes). Whether this selectivity will be observed for Rh(III) metal complexes is unknown. These were motivating factors for the research in this thesis.

It was hypothesized that energetically favorable C–H activation of both arenes and alkanes would be possible using electrophilic Rh(III) heteroatom complexes. From the viewpoint of the oxy-functionalization step, there are no examples of isolable Rh(V) oxo so if a Rh(III) complexes that is active for 1,2-CH-addition can be developed perhaps Rh–O–R could be obtained. Presented herein is the synthesis of Rh(III) heteroatom complexes for the 1,2-addition of non-polar bonds.

Several design features were considered for the synthesized Rh(III) heteroatom complexes. First, octahedral Rh(III) complexes with well-defined coordination spheres and either one or two heteroatom ligands (OR, NHR) were targeted. Second, phosphine ligands were avoided due to their propensity to be oxidized. Lastly, N-based ligands were utilized to enhance the electrophilicity of the dicationic Rh(III) complexes.

An outline for the remainder of this thesis is as follows. Chapter 2 describes the synthesis and characterization of (<sup>R</sup>bpy)<sub>2</sub>Rh (R = <sup>t</sup>Bu, H) heteroatom complexes while Chapter 3 describes a detailed kinetic and mechanistic study of 1,2-addition of dihydrogen across (<sup>t</sup>bpy)<sub>2</sub>Rh(III)–OMe bonds (Scheme 1.37). Chapter 4 includes

preliminary results for Si–H activation by a  $(^t\text{bpy})_2\text{Rh(III)}\text{--OMe}$  complex (Scheme 1.37). Chapter 5 reports the synthesis of Rh(I) and Rh(III) heteroatom complexes bearing tetradentate aryl-substituted pyridine dimine ligands (Scheme 1.37). Lastly, Chapter 6 focuses on an extension of this work involving the C–H activation of benzene using a cationic Ru(II) metal complex. Chapter 6 will also present results from catalytic olefin hydroarylation.



**Scheme 1.37.** Generic illustration of the Rh and Ru complexes described in Chapters 2, 3, 4, 5 and 6.

## 1.7 References

1. Wittcoff, H. A.; Reuben, B. G.; Plotkin, J. S. *Industrial Organic Chemicals*. 2nd ed.; John Wiley and Sons: Hoboken, N.J. , 2004.
2. Conley, B. L.; Tenn, W. J.; Young, K. J. H.; Ganesh, S. K.; Meier, S. K.; Ziatdinov, V. R.; Mironov, O.; Oxgaard, J.; Gonzales, J.; Goddard, W. A.; Periana, R. A. *J. Mol. Cat. A: Chem.* **2006**, *251*, 8.
3. Goldberg, K. I.; Goldman, A. S., *Activation and Functionalization of C-H Bonds*. American Chemical Society: Washington, DC, 2004; Vol. 885.
4. Crabtree, R. H. *J. Chem. Soc. Dalton* **2001**, 2437.
5. Webb, J. R.; Bolaño, T. B.; Gunnoe, T. B. *ChemSusChem* **2011**, *4*, 37.
6. Webb, J. R.; Burgess, S. A.; Cundari, T. R.; Gunnoe, T. B. *Dalton Trans.* **2013**, *42*, 16646. Portions of this chapter were adapted from this manuscript.
7. *Handbook of Homogeneous Hydrogenation*. Wiley-VCH: Weinheim, Germany, 2007.
8. Murray, J.; King, D. *Nature* **2012**, *481*, 433.
9. Kerr, R. A. *Science* **2011**, *331*, 1510.
10. *The Future of Natural Gas: An Interdisciplinary MIT Study*; MIT: 2011.
11. Johnson, J. "The New King of Fossil Fuel." *Chem. Eng. News* **2013**, *42*, 27.
12. Periana, R. A.; Taube, D. J.; Evitt, E. R.; Loffler, D. G.; Wentreck, P. R.; Voss, G.; Masuda, T. *Science* **1993**, *259*, 340.
13. Olah, G. A.; Goeppert, A.; Surya Prakash, G. K. *Beyond Oil and Gas: the Methanol Economy*. Wiley-VCH: Weinheim, 2006.

14. *Annual Energy Review 2009*; U.S. Energy Information Administration: Washington, DC, 2010.
15. TransCanada, E. Alaska Pipeline Project.  
<http://www.thealaskapipelineproject.com/>.
16. Government Concentrates. *Chem. Eng. News* **2004**, *82*, 21.
17. Johnson, J. "Valuing Flared Natural Gas." *Chem. Eng. News* **2007**, *85*, 10.
18. Periana, R. A.; Taube, D. J.; Gamble, S.; Taube, H.; Satoh, T.; Fuji, H. *Science* **1998**, *280*, 560.
19. Olah, G. A.; Molnar, A. *Hydrocarbon Chemistry*. 2nd ed.; Wiley-Intersciences: New York, 2003.
20. Periana, R. A.; Bhalla, G.; Tenn, W. J.; Young, K. J. H.; Liu, X. Y.; Mironov, O.; Jones, C. J.; Ziatdinov, V. R. *J. Mol. Cat. A: Chem.* **2004**, *220*, 7.
21. Shilov, A. E.; Shul'pin, G. B. *Chem. Rev.* **1997**, *97*, 2879.
22. Sen, A., "Catalytic Activation of Methane and Ethane by Metal Compounds." In *Activation of Unreactive Bonds and Organic Synthesis*, Murai, S., Ed. Springer: Berlin, Germany, 1999; pp 47.
23. Jonas, R. T.; Stack, T. D. P. *J. Am. Chem. Soc.* **1997**, *119*, 8566.
24. Samuelsson, B.; Dahlen, S. E.; Lindgren, J. A.; Rouzer, C. A.; Serhan, C. N. *Science* **1987**, *237*, 1171.
25. Mayer, J. M. *Acc. Chem. Res.* **1998**, *31*, 441.
26. Goldsmith, C. R.; Jonas, R. T.; Stack, T. D. P. *J. Am. Chem. Soc.* **2001**, *124*, 83.
27. Au, S.-M.; Zhang, S.-B.; Fung, W.-H.; Yu, W.-Y.; Che, C.-M.; Cheung, K.-K. *Chem. Commun.* **1998**, 2677.

28. Che, C.-M. *Pure and Appl. Chem.* **1995**, *67*, 225.
29. Che, C.-M.; Yam, V. W.-W. *Adv. Inorg. Chem.* **1992**, *39*, 233.
30. Kogut, E.; Wiencko, H. L.; Zhang, L.; Cordeau, D. E.; Warren, T. H. *J. Am. Chem. Soc.* **2005**, *127*, 11248.
31. Wiese, S.; Badiei, Y. M.; Gephart, R. T.; Mossin, S.; Varonka, M. S.; Melzer, M. M.; Meyer, K.; Cundari, T. R.; Warren, T. H. *Angew. Chem. Int. Ed.* **2010**, *49*, 8850.
32. Badiei, Y. M.; Dinescu, A.; Dai, X.; Palomino, R. M.; Heinemann, F. W.; Cundari, T. R.; Warren, T. H. *Angew. Chem. Int. Ed.* **2008**, *47*, 9961.
33. Chen, M. S.; White, M. C. *Science* **2007**, *318*, 783.
34. Liu, W.; Huang, X. Y.; Cheng, M. J.; Nielsen, R. J.; Goddard, W. A.; Groves, J. T. *Science* **2012**, *337*, 1322.
35. Groves, J. T. *J. Chem. Educ.* **1985**, *62*, 928.
36. Sherry, A. E.; Wayland, B. B. *J. Am. Chem. Soc.* **1990**, *112*, 1259.
37. Vastine, B. A.; Hall, M. B. *J. Am. Chem. Soc.* **2007**, *129*, 12068.
38. Perutz, R. N.; Sabo-Etienne, S. *Angew. Chem. Int. Ed.* **2007**, *46*, 2578.
39. Oxgaard, J.; Tenn, I., W. J.; Nielson, R. J.; Periana, R. A.; Goddard III, W. A. *Organometallics* **2007**, *26*, 1565.
40. Ess, D. H.; Gunnoe, T. B.; Cundari, T. R.; Goddard III, W. A.; Periana, R. A. *Organometallics* **2010**, *29*, 6801.
41. Conner, D.; Jayaprakash, K. N.; Cundari, T. R.; Gunnoe, T. B. *Organometallics* **2004**, *23*, 2724.
42. Feng, Y.; Lail, M.; Barakat, K. A.; Cundari, T. R.; Gunnoe, T. B.; Petersen, J. L. *J. Am. Chem. Soc.* **2005**, *127*, 14174.

43. Feng, Y.; Lail, M.; Foley, N. A.; Gunnoe, T. B.; Barakat, K. A.; Cundari, T. R.; Petersen, J. L. *J. Am. Chem. Soc.* **2006**, *128*, 7982.
44. Cundari, T. R.; Grimes, T. V.; Gunnoe, T. B. *J. Am. Chem. Soc.* **2007**, *129*, 13172.
45. Raja, R.; Ratnasamy, P. *App. Catal. A.* **1997**, *158*, L7.
46. Forlani, O.; Rossini, S. *Mater. Chem. Phys.* **1992**, *31*, 155.
47. Maitra, A. M. *Appl. Catal. A.* **1993**, *104*, 11.
48. Bar-Nahum, I.; Khenkin, A. M.; Neumann, R. *J. Am. Chem. Soc.* **2004**, *126*, 10236.
49. Dinse, A.; Aigner, M.; Ulbrich, M.; Johnson, G. R.; Bell, A. T. *J. Catal.* **2012**, *288*, 104.
50. Arakawa, H.; Aresta, M.; Armor, J. N.; Barteau, M. A.; Beckman, E. J.; Bell, A. T.; Bercaw, J. E.; Creutz, C.; Dinjus, E.; Dixon, D. A.; Domen, K.; DuBois, D. L.; Eckert, J.; Fujita, E.; Gibson, D. H.; Goddard, W. A.; Goodman, D. W.; Keller, J.; Kubas, G. J.; Kung, H. H.; Lyons, J. E.; Manzer, L. E.; Marks, T. J.; Morokuma, K.; Nicholas, K. M.; Periana, R.; Que, L.; Rostrup-Nielson, J.; Sachtler, W. M. H.; Schmidt, L. D.; Sen, A.; Somorjai, G. A.; Stair, P. C.; Stults, B. R.; Tumas, W. *Chem. Rev.* **2001**, *101*, 953.
51. Blick, K.; Mitrelias, T. D.; Hargreaves, J. S. J.; Hutchings, G. J.; Joyner, R. W.; Kiely, C. J.; Wagner, F. E. *Catal. Lett.* **1998**, *50*, 211.
52. Dimitratos, N.; Lopez-Sanchez, J. A.; Hutchings, G. J. *Chem. Sci.* **2012**, *3*, 20.
53. Shilov, A. E.; Shulpin, G. B. *Russ. Chem. Rev.* **1987**, *56*, 442.
54. Stahl, S. S.; Labinger, J. A.; Bercaw, J. E. *Angew. Chem. Int. Ed.* **1998**, *37*, 2180.
55. Lersch, M.; Tilset, M. *Chem. Rev.* **2005**, *105*, 2471.

56. Jones, C. J.; Taube, D.; Ziatdinov, V. R.; Periana, R. A.; Nielson, R. J.; Oxgaard, J.; Goddard III, W. A. *Angew. Chem. Int. Ed.* **2004**, *43*, 4626.
57. Hashiguchi, B. G.; Bischof, S. M.; Konnick, M. M.; Periana, R. A. *Acc. Chem. Res.* **2012**, *45*, 885.
58. Fortman, G. C.; Boaz, N. C.; Munz, D.; Konnick, M. M.; Periana, R. A.; Groves, J. T.; Gunnoe, T. B. *J. Am. Chem. Soc.* **2014**, *136*, 8393.
59. Hashiguchi, B. G.; Konnick, M. M.; Bischof, S. M.; Gustafson, S. J.; Devarajan, D.; Gunsalus, N.; Ess, D. H.; Periana, R. A. *Science* **2014**, *343*, 1232.
60. Hartwig, J. F. "Catalytic, Thermal, Regioselective Functionalization of Alkanes and Arenes with Borane Reagents." In *Activation and Functionalization of C-H Bonds*, ACS: 2004; Vol. 885, pp 136.
61. Hartwig, J. F. *Acc. Chem. Res.* **2012**, *45*, 864.
62. Hartwig, J. F. *Chem. Soc. Rev.* **2011**, *40*, 1992.
63. Chen, H. Y.; Schlecht, S.; Semple, T. C.; Hartwig, J. F. *Science* **2000**, *287*, 1995.
64. Liskey, C. W.; Wei, C. S.; Pahls, D. R.; Hartwig, J. F. *Chem. Commun.* **2009**, 5603.
65. Findlater, M.; Choi, J.; Goldman, A. S.; Brookhart, M., Alkane Dehydrogenation. In *Alkane C-H Activation by Single-site Metal Catalysis*, Pérez, P. J., Ed. Springer: New York, 2012; pp 113.
66. Baudry, D.; Ephritikhine, M.; Felkin, H.; Holmessmith, R. *J. Chem. Soc., Chem. Comm.* **1983**, 788.
67. Felkin, H.; Fillebeenkhan, T.; Gault, Y.; Holmessmith, R.; Zakrzewski, J. *Tetrahedron Lett.* **1984**, *25*, 1279.

68. Felkin, H.; Fillebeenkhan, T.; Holmessmith, R.; Yingrui, L. *Tetrahedron Lett.* **1985**, *26*, 1999.
69. Burk, M. J.; Crabtree, R. H.; Parnell, C. P.; Uriarte, R. J. *Organometallics* **1984**, *3*, 816.
70. Burk, M. J.; Crabtree, R. H.; Mcgrath, D. V. *J. Chem. Soc., Chem. Comm.* **1985**, 1829.
71. Gupta, M.; Kaska, W. C.; Jensen, C. M. *Chem. Commun.* **1997**, 461.
72. Gupta, M.; Hagen, C.; Kaska, W. C.; Cramer, R. E.; Jensen, C. M. *J. Am. Chem. Soc.* **1997**, *119*, 840.
73. Lee, D. W.; Kaska, W. C.; Jensen, C. M. *Organometallics* **1998**, *17*, 1.
74. Ghosh, R.; Kanzelberger, M.; Emge, T. J.; Hall, G. S.; Goldman, A. S. *Organometallics* **2006**, *25*, 5668.
75. Gottker-Schnetmann, I.; White, P.; Brookhart, M. *J. Am. Chem. Soc.* **2004**, *126*, 1804.
76. Walsh, P. J.; Hollander, F. J.; Bergman, R. G. *J. Am. Chem. Soc.* **1988**, *110*, 8729.
77. Cundari, T. R. *J. Am. Chem. Soc.* **1992**, *114*, 7879.
78. Cummins, C. C.; Baxter, S. M.; Wolczanski, P. T. *J. Am. Chem. Soc.* **1988**, *110*, 8731.
79. Schaller, C. P.; Cummins, C. C.; Wolczanski, P. T. *J. Am. Chem. Soc.* **1996**, *118*, 591.
80. Cundari, T. R. *Organometallics* **1994**, *13*, 2987.
81. Schafer, D. F.; Wolczanski, P. T. *J. Am. Chem. Soc.* **1998**, *120*, 4881.

82. Schafer, D. F.; Wolczanski, P. T.; Lobkovsky, E. B. *Organometallics* **2011**, *30*, 6518.
83. Schafer, D. F.; Wolczanski, P. T.; Lobkovsky, E. B. *Organometallics* **2011**, *30*, 6539.
84. Benson, M. T.; Cundari, T. R.; Moody, E. W. *J. Organomet. Chem.* **1995**, *504*, 1.
85. Schaller, C. P.; Wolczanski, P. T. *Inorg. Chem.* **1993**, *32*, 131.
86. Chao, Y.-W.; Rodgers, P. M.; Wigley, D. E. *J. Am. Chem. Soc.* **1991**, *113*, 6326.
87. Lin, Z.; Hall, M. B. *Coord. Chem. Rev.* **1993**, *123*, 149.
88. Cundari, T. R. *Int. J. Quantum Chem* **1992**, 793.
89. Cundari, T. R. *J. Am. Chem. Soc.* **1992**, *114*, 10557.
90. Cundari, T. R.; Gordon, M. S. *J. Am. Chem. Soc.* **1993**, *115*, 4210.
91. With, J. D.; Horton, A. D. *Angew. Chem. Int. Ed.* **1993**, *32*, 903.
92. Cundari, T. R.; Klinckman, T. R.; Wolczanski, P. T. *J. Am. Chem. Soc.* **2002**, *124*, 1481.
93. Wicker, B. F.; Fan, H. J.; Hickey, A. K.; Crestani, M. G.; Scott, J.; Pink, M.; Mendiola, D. J. *J. Am. Chem. Soc.* **2012**, *134*, 20081.
94. Gunnoe, T. B. *Eur. J. Inorg. Chem.* **2007**, 1185.
95. Fox, D. J.; Bergman, R. G. *J. Am. Chem. Soc.* **2003**, *125*, 8984.
96. Fryzuk, M. D.; Montgomery, C. D.; Rettig, S. J. *Organometallics* **1991**, *10*, 467.
97. Abdur-Rashid, K.; Faatz, M.; Lough, A. J.; Morris, R. H. *J. Am. Chem. Soc.* **2001**, *123*, 7473.
98. Fulmer, G. R.; Muller, R. P.; Kemp, R. A.; Goldberg, K. I. *J. Am. Chem. Soc.* **2009**, *131*, 1346.

99. Fulmer, G. R.; Herndon, A. N.; Kaminsky, W.; Kemp, R. A.; Goldberg, K. I. *J. Am. Chem. Soc.* **2011**, *133*, 17713.
100. Johansson, R.; Ohrstrom, L.; Wendt, O. F. *Cryt. Growth Des.* **2007**, *7*, 1974.
101. Webb, J. R.; Pierpont, A. W.; Munro-Leighton, C.; Gunnoe, T. B.; Cundari, T. R.; Boyle, P. D. *J. Am. Chem. Soc.* **2010**, *132*, 4520.
102. Webb, J. R.; Figg, T. M.; Otten, B. M.; Cundari, T. R.; Gunnoe, T. B.; Sabat, M. *Eur. J. Inorg. Chem.* **2013**, *2013*, 4515.
103. Riehl, J. F.; Jean, Y.; Eisenstein, O.; Pelissier, M. *Organometallics* **1992**, *11*, 729.
104. Tenn, I., W. J.; Young, K. J. H.; Bhalla, G.; Oxgaard, J.; Goddard III, W. A.; Periana, R. A. *J. Am. Chem. Soc.* **2005**, *127*, 14172.
105. Tenn, I., W. J.; Young, K. J. H.; Oxgaard, J.; Nielson, R. J.; Goddard III, W. A.; Periana, R. A. *Organometallics* **2006**, *25*, 5173.
106. Hashiguchi, B. G.; Young, K. J. H.; Yousufuddin, M.; Goddard, W. A.; Periana, R. A. *J. Am. Chem. Soc.* **2010**, *132*, 12542.
107. Feng, Y.; Gunnoe, T. B.; Grimes, T. V.; Cundari, T. R. *Organometallics* **2006**, *25*, 5456.
108. Lail, M.; Bell, C. M.; Conner, D.; Cundari, T. R.; Gunnoe, T. B.; Petersen, J. L. *Organometallics* **2004**, *23*, 5007.
109. Lail, M.; Arrowood, B. N.; Gunnoe, T. B. *J. Am. Chem. Soc.* **2003**, *125*, 7506.
110. Oxgaard, J.; Muller, R. P.; Goddard III, W. A.; Periana, R. A. *J. Am. Chem. Soc.* **2004**, *126*, 352.
111. Oxgaard, J.; Periana, R. A.; Goddard, W. A. *J. Am. Chem. Soc.* **2004**, *126*, 11658.

112. Kloek, S. M.; Heinekey, D. M.; Goldberg, K. I. *Angew. Chem., Int. Ed.* **2007**, *46*, 4736.
113. Hanson, S. K.; Heinekey, D. M.; Goldberg, K. I. *Organometallics* **2008**, *27*, 1454.
114. Bercaw, J. E.; Hazari, N.; Labinger, J. A. *Organometallics* **2009**, *28*, 5489.
115. Ahmed, T. S.; Tonics, I. A.; Labinger, J. A.; Bercaw, J. E. *Organometallics* **2013**, *32*, 3322.
116. Brown, S. N.; Mayer, J. M. *J. Am. Chem. Soc.* **1996**, *118*, 12119.
117. Conley, B. L.; Ganesh, S. K.; Gonzales, J. M.; Tenn, W. J.; Young, K. J. H.; Oxgaard, J.; Goddard, W. A.; Periana, R. A. *J. Am. Chem. Soc.* **2006**, *128*, 9018.
118. Bischof, S. M.; Cheng, M. J.; Nielsen, R. J.; Gunnoe, T. B.; Goddard, W. A.; Periana, R. A. *Organometallics* **2011**, *30*, 2079.
119. Figg, T. M.; Cundari, T. R.; Gunnoe, T. B. *Organometallics* **2011**, *30*, 3779.
120. Koo, K. M.; Hillhouse, G. L.; Rheingold, A. L. *Organometallics* **1995**, *14*, 456.
121. Kamaraj, K.; Bandyopadhyay, D. *Organometallics* **1999**, *18*, 438.
122. Alsters, P. L.; Teunissen, H. T.; Boersma, J.; Spek, A. L.; Vankoten, G. *Organometallics* **1993**, *12*, 4691.
123. Pouy, M. J.; Milczek, E. M.; Figg, T. M.; Otten, B. M.; Prince, B. M.; Gunnoe, T. B.; Cundari, T. R.; Groves, J. T. *J. Am. Chem. Soc.* **2012**, *134*, 12920.
124. Mei, J. J.; Carsch, K. M.; Freitag, C. R.; Gunnoe, T. B.; Cundari, T. R. *J. Am. Chem. Soc.* **2013**, *135*, 424.
125. Cheng, M. J.; Bischof, S. M.; Nielsen, R. J.; Goddard, W. A.; Gunnoe, T. B.; Periana, R. A. *Dalton T* **2012**, *41*, 3758.

126. AbuOmar, M. M.; Hansen, P. J.; Espenson, J. H. *J. Am. Chem. Soc.* **1996**, *118*, 4966.
127. Gonzales, J. M.; Distasio, R.; Periana, R. A.; Goddard, W. A.; Oxgaard, J. *J. Am. Chem. Soc.* **2007**, *129*, 15794.
128. Mihovilovic, M. D. *Curr. Org. Chem.* **2006**, *10*, 1265.
129. Mei, J. *Unpublished Results* **2014**.
130. Kalman, S. E.; Petit, A.; Gunnoe, T. B.; Ess, D. H.; Cundari, T. R.; Sabat, M. *Organometallics* **2013**, *32*, 1797.
131. Hoyt, H. M.; Michael, F. E.; Bergman, R. G. *J. Am. Chem. Soc.* **2004**, *126*, 1018.
132. Cummins, C. C.; Schaller, C. P.; Duyne, G. D. V.; Wolczanski, P. T.; Chan, A. W. E.; Hoffman, R. *J. Am. Chem. Soc.* **1991**, *113*, 2985.
133. Schaller, C. P.; Bonanno, J. B.; Wolczanski, P. T. *J. Am. Chem. Soc.* **1994**, *116*, 4133.
134. Bennett, J. L.; Wolczanski, P. T. *J. Am. Chem. Soc.* **1997**, *119*, 10696.
135. Slaughter, L. M.; Wolczanski, P. T.; Klinckman, T. R.; Cundari, T. R. *J. Am. Chem. Soc.* **2000**, *122*, 7953.

## 2 Synthesis and Characterization of Rh(III) Anilido, Hydroxide and Methoxide Complexes

### 2.1 Introduction

When a  $\pi$ -donor heteroatom ligand is bound to a transition metal having a filled  $d\pi$  manifold, significant electron density is localized on a heteroatom.<sup>1,2,3</sup> This is because both M–X  $d\pi$  and M–X  $d\pi^*$  bonding orbitals are occupied, which results in a net single bond between the metal and ligand X (Figure 2.1).<sup>1-6</sup> Late transition metal alkoxide (OR), aryloxide (OAr) and amido (NHR) complexes in low oxidation states often exhibit nucleophilic and basic reactivity, and this feature has been utilized to facilitate diverse bond-breaking and bond-forming transformations.<sup>1-5,7</sup> This is similar to  $\pi$ -loading for high oxidation state early and middle transition metals with  $\pi$ -donor ligands. This occurs when a metal possesses more  $\pi$ -donor interactions than it has vacant  $d\pi$  orbitals.<sup>8,9</sup>

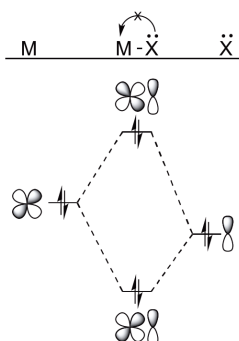


**Figure 2.1.** Molecular orbital diagram showing that there is no net M–X  $\pi$ -bond if d-orbitals are filled (M = transition metal, X = OR, NHR, SR, etc.).

An example of a reactive late transition metal–heteroatom complex (note: herein, a “heteroatom complex” will refer to a complex with a mono- or di-anionic  $\pi$ -donating

ligand such as alkoxide, amido, imido, oxo, etc.) was reported by Bergman and co-workers in their investigation of the Ru amido complex *trans*-(DMPE)<sub>2</sub>Ru(H)(NH<sub>2</sub>) [DMPE = 1,2-bis(dimethylphosphino)ethane].<sup>10</sup> The complex *trans*-(DMPE)<sub>2</sub>Ru(H)(NH<sub>2</sub>) was shown to deprotonate C–H bonds of cyclohexadiene and 9,10-dihydroanthracene, ultimately yielding benzene or anthracene, and after subsequent net hydride removal to produce (DMPE)<sub>2</sub>Ru(H)<sub>2</sub> and NH<sub>3</sub>. Other reactive d<sup>6</sup> Ru(II)–amido complexes have been reported. For example, we reported that the five coordinate Ru amido complex (PCP)Ru(CO)(NH<sub>2</sub>) [PCP = 2,6-(CH<sub>2</sub>P<sup>t</sup>Bu<sub>2</sub>)<sub>2</sub>C<sub>6</sub>H<sub>3</sub>] forms (PCP)Ru(CO)(C≡CPh) and ammonia when reacted with phenylacetylene.<sup>3</sup> The proposed reaction pathway involves initial deprotonation of phenylacetylene to yield the intermediate (PCP)Ru(CO)(NH<sub>3</sub>(C≡CPh), which then dissociates ammonia. Our group has investigated a series of TpRu(L)(L')(NHR) (L = L' = P(OMe)<sub>3</sub> or PMe<sub>3</sub>; L = CO, L' = PPh<sub>3</sub>; R = H, <sup>t</sup>Bu) complexes that contain basic amido ligands that facilitate intermolecular deprotonation of phenylacetylene resulting in the formation of Ru(II) phenylacetylene complexes.<sup>11</sup> In the case of R = H or <sup>t</sup>Bu, the ion pairs [TpRu(L)(L')(NH<sub>3</sub>)] [PhC<sub>2</sub>] can be observed.

Beyond the reactivity with phenylacetylene, TpRu(PMe<sub>3</sub>)<sub>2</sub>NHPh has been reported to undergo an S<sub>N</sub>2 reaction with ethyl bromide to form *N*-ethyl aniline and Ru–Br.<sup>11</sup> The Cu(I) anilido complexes (NHC)CuNHPh [NHC = *N*-heterocyclic carbene = 1,3-bis(2,6-diisopropylphenyl)imidazol-2-ylidene (IPr), 1,3-bis(2,6-diisopropylphenyl)imidazolin-2-ylidene (SIPr), 1,3-bis(2,4,6-trimethylphenyl)imidazol-2-ylidene (IMes)] and (dtbpe)CuNHPh [dtbpe = 1,2-bis(di-tertbutylphosphino)ethane] also

undergo  $S_N2$  reactions with ethyl bromide.<sup>12</sup> The  $S_N2$  reaction using the (NHC)CuNHPH complexes proceeded at room temperature whereas the reaction with TpRu(PMe<sub>3</sub>)<sub>2</sub>(NHPH) required heating at 80 °C. The reactivity of the (NHC)CuNHPH complexes was observed to decrease with increasing steric bulk of the NHC ligands (IMes > IPr > SIPr).

The electron rich amido ligand of the Ir(I) PNP amido complex Ir(PMe<sub>3</sub>)(PNP<sup>iPr</sup>) [PNP<sup>iPr</sup> = {N(CH<sub>2</sub>CH<sub>2</sub>P<sup>iPr</sup><sub>2</sub>)<sub>2</sub>}] undergoes *N*-alkylation when treated with MeOTf to give [(MePNP<sup>iPr</sup>)Ir(PMe<sub>3</sub>)]+[OTf].<sup>13</sup> The magnitude of the basicity of the amido ligand of (PNP<sup>iPr</sup>)Ir(L) (L = PMe<sub>3</sub>, CO or COE) is dependent on the identity of the ligand trans to the PNP nitrogen. Increasing  $\pi$ -acceptor ability of the trans ligand leads to lower pK<sub>a</sub> values.

Examples of reactive late transition metal hydroxide complexes have also been reported. For example, Milstein and co-workers reported the stoichiometric generation of H<sub>2</sub> and O<sub>2</sub> from H<sub>2</sub>O by successive thermal and photochemical steps using a bis-hydroxide Ru(II) pincer complex (PNN)Ru(CO)(OH)<sub>2</sub> [PNN = 2-(di-*tert*-butylphosphinomethyl)-6-diethylaminomethyl)pyridine].<sup>14</sup> Heating the Rh(III) porphyrin complex (tpp)RhCl (tpp = tetratolylporphyrinato dianion) in the presence of KOH leads to the formation of the reactive Rh hydroxide intermediate (tpp)Rh(OH).<sup>15</sup> The hydroxide ligand of (tpp)Rh(OH) acts as a reducing agent leading to the formation of (tpp)Rh(II) and H<sub>2</sub>O<sub>2</sub>.

Late transition metal heteroatom complexes have also been shown to activate dihydrogen and C–H bonds.<sup>7</sup> The Ru amido complex RuCl(PPh<sub>3</sub>)[ $\kappa^3$ -

N(SiMe<sub>2</sub>CH<sub>2</sub>PPh<sub>2</sub>)<sub>2</sub>] reported by Fryzuk and co-workers has been shown to activate dihydrogen.<sup>16</sup> Additionally, reversible intramolecular heterolytic splitting of dihydrogen has been shown using Ru(H)(NHCM<sub>2</sub>CMe<sub>2</sub>NH<sub>2</sub>)(R-binap) [binap = 1,1'-(binaphthalene-2,2'-diyl)bis(diphenylphosphine)].<sup>17</sup> The 1,2-addition of dihydrogen across the Rh–OMe bond of the Rh(III) complexes, [(<sup>t</sup>bpy)<sub>2</sub>Rh(OMe)(L)][X]<sub>n</sub> (<sup>t</sup>bpy = 4,4'-di-*tert*-butyl-2,2'-bipyridyl; L = MeOH, n = 2, X = OTf (OTf = trifluoromethanesulfonate) and TFA (TFA = trifluoroacetate); L = TFA, n = 1, X = OTf) will be discussed in Chapter 3. Goldberg and co-workers reported d<sup>8</sup> Pd(II)–hydroxide and methoxide complexes, (PCP)Pd(OR) (PCP = 2,6-(CH<sub>2</sub>P<sup>i</sup>Bu<sub>2</sub>)<sub>2</sub>C<sub>6</sub>H<sub>3</sub>, R = H, CH<sub>3</sub>), that activate H<sub>2</sub> to generate water or free methanol and (PCP)Pd(H).<sup>18,19</sup> Our group has demonstrated that *in situ* generated Pt(s) catalyzes the addition of dihydrogen across Pt–NHPPh bonds of (<sup>t</sup>bpy)Pt(Me)(NHPPh).<sup>20</sup> (PCP)Ru(CO)(NH<sub>2</sub>) performs both intramolecular addition of dihydrogen across the Ru–NH<sub>2</sub> bond and intramolecular C–H activation of a <sup>t</sup>Bu group on the PCP ligand leading to the formation of a cyclometalated complex and free ammonia.<sup>3</sup>

Examples of intermolecular arene C–H activation using d<sup>6</sup> metal–heteroatom complexes are known. H/D exchange between the hydroxide or anilido ligands of TpRu(PMe<sub>3</sub>)<sub>2</sub>X (X = OH or NHPPh) in C<sub>6</sub>D<sub>6</sub> at elevated temperatures (80 to 130 °C) has been reported by our group.<sup>21-23</sup> Periana, Goddard and co-workers reported an Ir(III) methoxide complex, (acac)<sub>2</sub>Ir(OMe)(L) (acac = κ<sup>2</sup>-O,O-acetylacetonate; L = pyridine or CH<sub>3</sub>OH), that performs stoichiometric C–H activation of benzene.<sup>24,25</sup> Examples of H/D exchange reactions between C–H bonds of water-soluble substrates (e.g., isophthalic acid) and KOD/D<sub>2</sub>O catalyzed by the Ru(II) hydroxide/aqua complex

(IPI)Ru<sup>II</sup>(OH)<sub>n</sub>(H<sub>2</sub>O)<sub>m</sub> (IPI is 2,6-diimidizoylpyridine) has been reported.<sup>26</sup> The reaction is accelerated by strongly basic solvent. The base is proposed to deprotonate protic ligands on (IPI)Ru(OH)<sub>n</sub>(H<sub>2</sub>O)<sub>m</sub> thereby increasing the  $\pi$ -nucleophilicity of the catalyst.

In addition to the d<sup>6</sup> M–heteroatom complexes described above, a few d<sup>8</sup> M–X (X = OR, NHR) complexes for the activation of arene C–H bonds have been reported. For example, Goldberg and co-workers have reported stoichiometric arene activation by the Rh(I) complex (PNP)Rh(X) [PNP = 2,6-(di-*tert*-butylphosphinomethyl)pyridine; X = OH, OCH<sub>2</sub>CF<sub>3</sub>].<sup>27,28</sup> The hydroxo-bridged Rh dimer [(COD)Rh( $\mu$ -OH)]<sub>2</sub> (COD = 1,5-cyclooctadiene) has been reported to activate indene to form [(COD)Rh( $\eta^3$ -indenyl)].<sup>29</sup> Furthermore, the Ir analogue [(COD)Ir( $\mu$ -OH)]<sub>2</sub> activates C–H bonds of indene and cyclopentadiene.<sup>30</sup> Additionally, 1,2-addition of benzene C–H bonds across the Pt(II)–OH bonds of (BIAN)Pt(OH)<sub>2</sub> (BIAN = bis(3,5-bis(2,6-diisopropylphenyl)benzene)-acenaphthenequinonediimine) to give water and (BIAN)Pt(Ph)<sub>2</sub> has been reported.<sup>31</sup> Similar to our report of H<sub>2</sub> activation by a Pt(II) anilido complex,<sup>20</sup> this reaction is accelerated by *in situ* generated Pt nanoparticles.

Transition metal heteroatom complexes with filled d $\pi$  orbitals have been reported to function as strongly basic moieties,<sup>3,10-13</sup> undergo S<sub>N</sub>2 reactions,<sup>11,12</sup> and mediate C–H and H–H bond activation.<sup>3,7,17,18-31</sup> A potential key for the reactivity of transition metal complexes is the bifunctional character, of an electrophilic metal and a basic/nucleophilic ligand (Scheme 2.1). We sought to synthesize electrophilic cationic or dicationic Rh(III) complexes with a general motif of bis-bipyridyl (bpy = 2,2'-bipyridyl) ligands and at

least one mono-anionic heteroatomic ligand such as –NHR or –OR. Such complexes should possess highly electrophilic metal centers yet retain basic/ nucleophilic ligands “Y.” It is our hypothesis that such complexes will engender reactivity with typically inert substrates such as hydrocarbons (C–H activation), dihydrogen and silanes (Si–H activation). Herein we report the synthesis, characterization and initial reactivity studies of (<sup>R</sup>bpy)<sub>2</sub>Rh(III) (R = <sup>t</sup>Bu, or H) aniline, anilido, hydroxide, aqua, methoxide and methanol complexes. The complexes [(<sup>t</sup>bpy)<sub>2</sub>Rh(OH)<sub>2</sub>][OTf], [(<sup>t</sup>bpy)<sub>2</sub>Rh(H<sub>2</sub>O)<sub>2</sub>][OTf]<sub>3</sub> and [(<sup>t</sup>bpy)<sub>2</sub>Rh(OH)(H<sub>2</sub>O)][OTf]<sub>2</sub> were initially synthesized by Dr. Tamara Bolaño.<sup>32</sup>



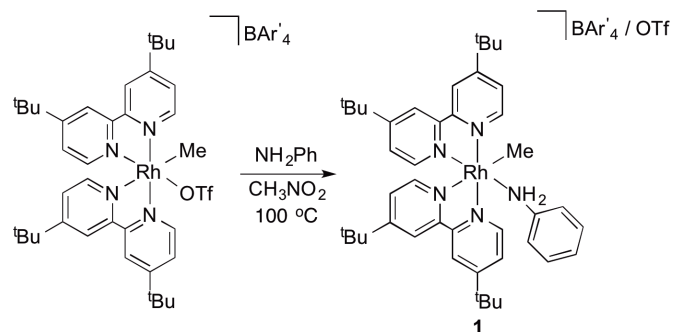
**Scheme 2.1.** Transition metal heteroatom complexes exhibit bifunctional character.

## 2.2 Results and Discussion

### 2.2.1 Synthesis of Rh(III) Aniline and Anilido Compounds

We have previously reported that the trifluoromethane sulfonate (OTf) ligand of [(<sup>t</sup>bpy)<sub>2</sub>Rh(Me)(OTf)][BAR'<sub>4</sub>] is labile and is substituted by H<sub>2</sub>O upon heating in THF to afford [(<sup>t</sup>bpy)<sub>2</sub>Rh(Me)(H<sub>2</sub>O)][BAR'<sub>4</sub>][OTf].<sup>33</sup> The OTf ligand of [(<sup>t</sup>bpy)<sub>2</sub>Rh(Me)(OTf)][BAR'<sub>4</sub>] can also be replaced by aniline to give [(<sup>t</sup>bpy)<sub>2</sub>Rh(Me)(NH<sub>2</sub>Ph)][BAR'<sub>4</sub>][OTf] (**1**) in 80% isolated yield (Scheme 2.2). Diastereotopic aniline NH doublets are observed at 6.19 and 5.85 ppm (<sup>2</sup>J<sub>H–H</sub> = 11 Hz) in the <sup>1</sup>H NMR spectrum of complex **1** (Figure 2.2). The methyl ligand of complex **1** is observed at 5.6 ppm (<sup>1</sup>J<sub>Rh–C</sub> = 22 Hz) in the <sup>13</sup>C NMR spectrum. The solid-state structure

of complex **1** was determined by single-crystal X-ray diffraction (Figure 2.3). The  $\text{CH}_3\text{-Rh-N}_{\text{aniline}}$  bond angle of complex **1** is  $88.0(1)^\circ$ . The  $\text{Rh-CH}_3$  bond length of complex **1** is  $2.063(3) \text{ \AA}$ , which is in close agreement with that of the previously reported structure  $[(^t\text{bpy})_2\text{Rh}(\text{Me})_2][\text{BAR}'_4][2.089(9) \text{ \AA}]$ .<sup>33</sup>



**Scheme 2.2.** Synthesis of  $[(^t\text{bpy})_2\text{Rh}(\text{Me})(\text{NH}_2\text{Ph})][\text{BAR}'_4][\text{OTf}]$  (**1**).

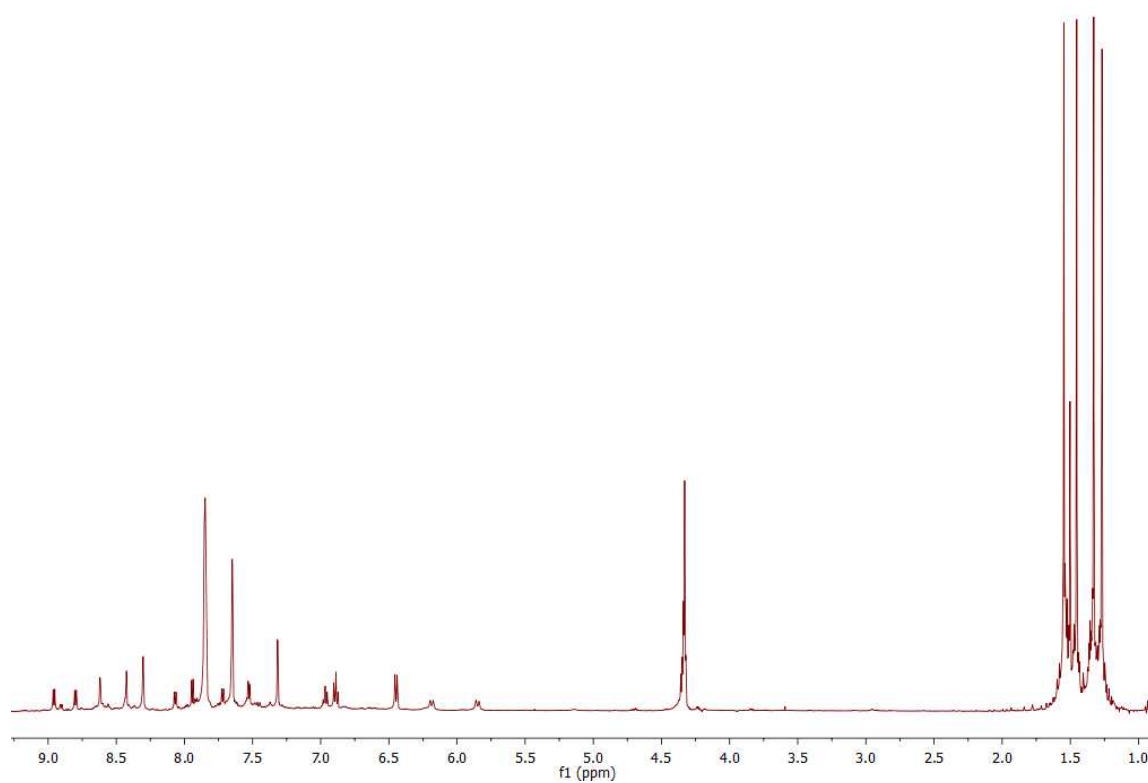


**Figure 2.2.**  $^1\text{H}$  NMR spectrum of  $[(\text{bpy})_2\text{Rh}(\text{Me})(\text{NH}_2\text{Ph})][\text{BAr}'_4][\text{OTf}]$  (**1**) in  $\text{CD}_3\text{NO}_2$ .

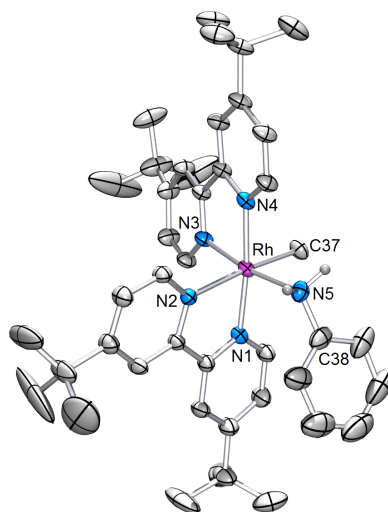
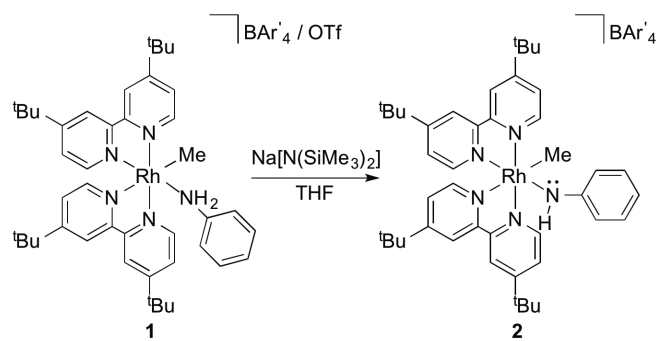


**Figure 2.3.** ORTEP diagram (50% probability) of  $[(^1\text{bpy})_2\text{Rh}(\text{Me})(\text{NH}_2\text{Ph})][\text{BAR}'_4][\text{OTf}]$  (**1**). Counterions and most hydrogen atoms are omitted for clarity. Selected bond lengths ( $\text{\AA}$ ): Rh–C37, 2.063(3); Rh–N1, 2.019(3); Rh–N2, 2.027(3); Rh–N3, 2.059(3); Rh–N4, 2.165(2); Rh–N5, 2.114(3); N5–C38, 1.429(5). Selected bond angles ( $^\circ$ ): C37–Rh–N5, 88.02(12); C38–N5–Rh, 119.4(2).

Deprotonation of the aniline ligand of  $[(^1\text{bpy})_2\text{Rh}(\text{Me})(\text{NH}_2\text{Ph})][\text{BAR}'_4][\text{OTf}]$  (**1**) with  $\text{Na}[\text{N}(\text{SiMe}_3)_2]$  (1 equiv.) gives  $[(^1\text{bpy})_2\text{Rh}(\text{Me})(\text{NHPh})][\text{BAR}'_4]$  (**2**) in 97% isolated yield (Scheme 2.3). The methyl resonance of complex **2** is observed at 1.38 ppm ( $^2J_{\text{Rh-H}} = 2$  Hz) in the  $^1\text{H}$  NMR spectrum (Figure 2.4). Depending on the exact conditions a broad *NH* resonance for complex **2** is sometimes observed at 5.88 ppm in the  $^1\text{H}$  NMR spectrum of **2** but other times it is not observed (Figure 2.4). The *NH* resonance has shifted upfield relative to complex **1** (6.19 and 5.85 ppm).



**Scheme 2.3.** Synthesis of  $[(t'bpv)_2Rh(Me)(NHPh)][BAR'_4]$  (**2**).

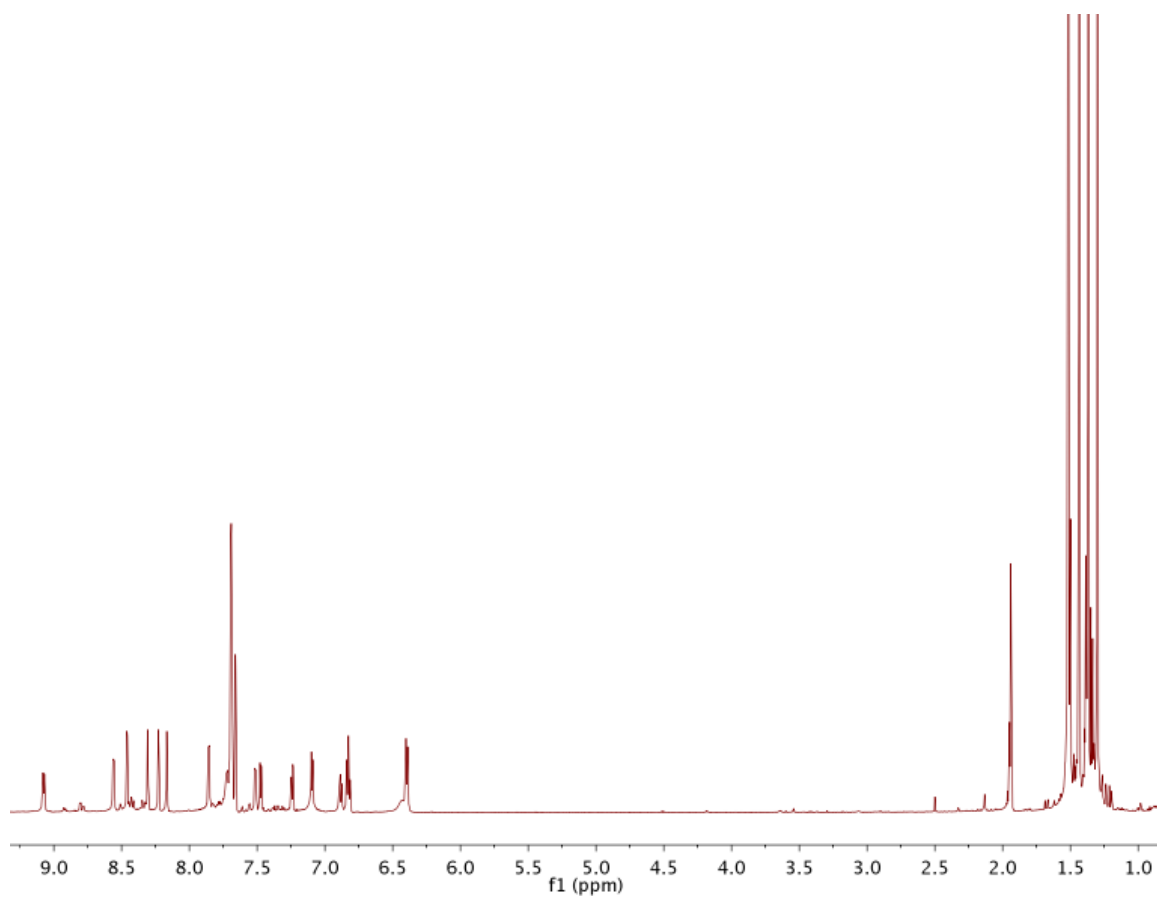
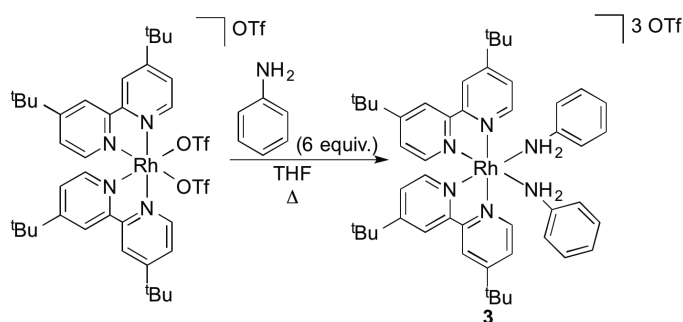


**Figure 2.4.**  $^1H$  NMR spectrum of  $[(t'bpv)_2Rh(Me)(NHPh)][BAR'_4]$  (**2**) in  $CD_3CN$ .

Analogues of complexes **1** and **2** bearing a second heteroatom ligand in place of the methyl ligand have also been prepared. Heating a THF solution of  $[(^t\text{bpy})_2\text{Rh}(\text{OTf})_2]\text{OTf}$  with an excess of aniline leads to the precipitation of  $[(^t\text{bpy})_2\text{Rh}(\text{NH}_2\text{Ph})_2][\text{OTf}]_3$  (**3**) (Scheme 2.2). In order to verify the coordination of aniline to the transition metal center, we synthesized the  $^{15}\text{N}$  labeled version of complex **3**,  $[(^t\text{bpy})_2\text{Rh}(^{15}\text{NH}_2\text{Ph})_2][\text{OTf}]_3$  (**3- $^{15}\text{N}$** ) using  $^{15}\text{NH}_2\text{Ph}$  (98%  $^{15}\text{N}$ ). The  $^1\text{H}$  NMR spectrum of **3- $^{15}\text{N}$**  contains a doublet of doublets at 7.88 ppm ( $^1J_{\text{N-H}} = 71$  Hz,  $^2J_{\text{H-N}} = 11$  Hz) for the aniline  $^{15}\text{N-H}$  protons. The phenyl hydrogen atoms of coordinated aniline are observed as two triplets and a doublet at 7.11 ppm, 6.96 ppm and 6.59 ppm in the  $^1\text{H}$  NMR spectrum of the complex **3** (Figure 2.5).

A metathesis reaction of  $[(^t\text{bpy})_2\text{Rh}(\text{NH}_2\text{Ph})_2][\text{OTf}]_3$  (**3**) with  $\text{NaBAR}'_4$  leads to the formation of  $[(^t\text{bpy})_2\text{Rh}(\text{NH}_2\text{Ph})_2][\text{BAR}'_4]_3$  (**4**). Crystals of  $[(^t\text{bpy})_2\text{Rh}(\text{NH}_2\text{Ph})_2][\text{BAR}'_4]_3$  suitable for an X-ray diffraction study were obtained by slow diffusion of hexanes into a solution of **4** in DCM (Figure 2.6). The solid state structure of **4** will be discussed below (see Section 2.2.4).



**Scheme 2.4.** Synthesis of  $[(^t\text{bpy})_2\text{Rh}(\text{NH}_2\text{Ph})_2][\text{OTf}]_3$  (**3**).

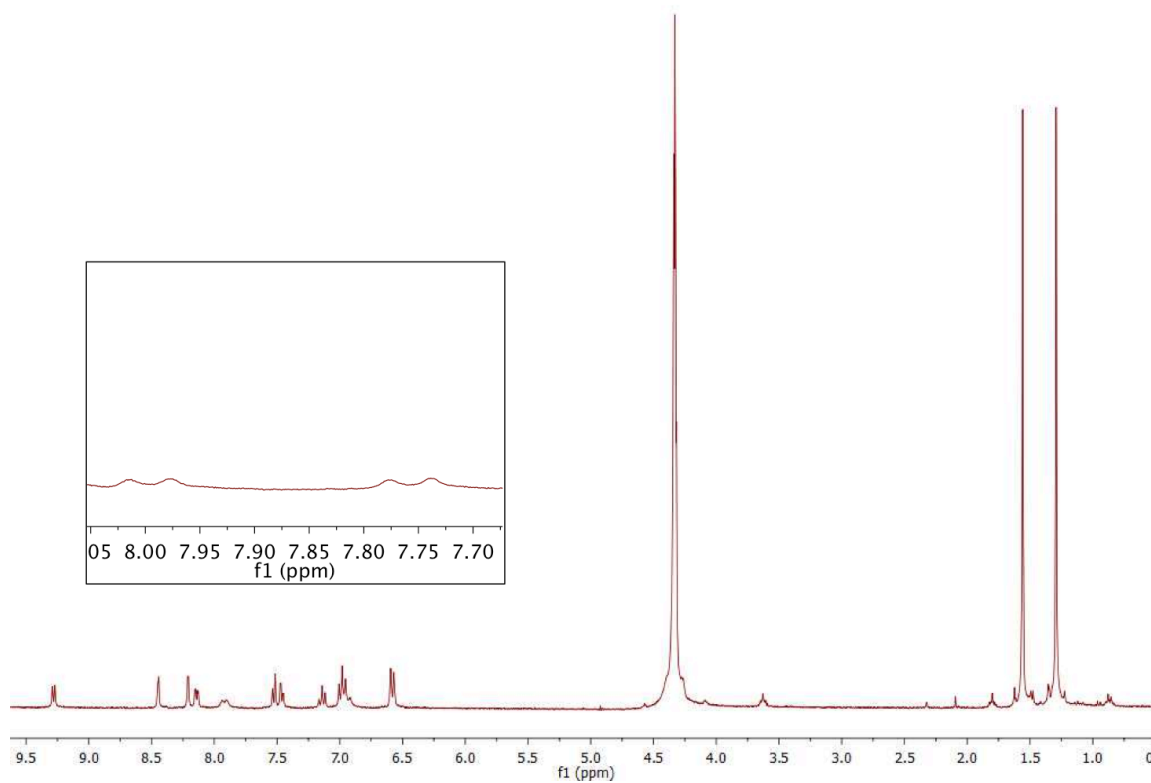


**Figure 2.5.**  $^1\text{H}$  NMR spectrum of  $[(^1\text{bpy})_2\text{Rh}(\text{NH}_2\text{Ph})_2][\text{OTf}]_3$  (**3**) in  $\text{CD}_3\text{NO}_2$ .  $^{15}\text{NH}_2\text{Ph}$  resonance  $[(^1\text{bpy})_2\text{Rh}(^{15}\text{NH}_2\text{Ph})_2][\text{OTf}]_3$  (**3**- $^{15}\text{N}$ ) is shown in the inset.

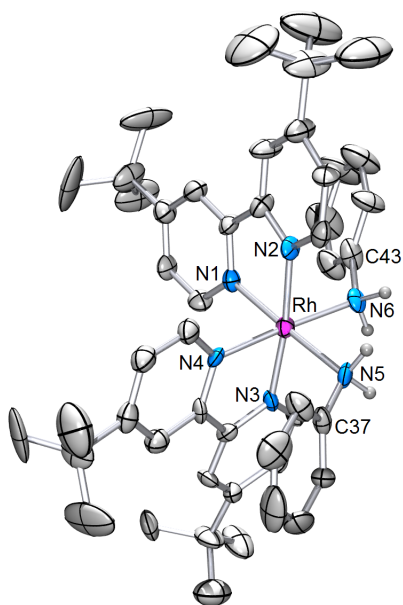
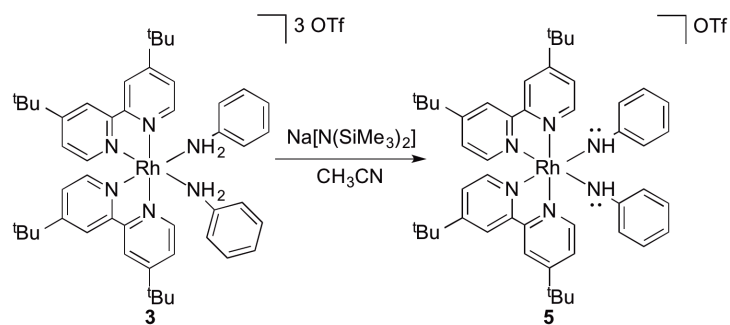


**Figure 2.6.** ORTEP diagram (50% probability) of  $[(^1\text{bpy})_2\text{Rh}(\text{NH}_2\text{Ph})_2][\text{BAR}'_4]_3$  (**4**). Counterions and most hydrogen atoms are omitted for clarity. Selected bond lengths (Å): Rh–N1, 2.02(1); Rh–N2, 2.054(9); Rh–N3, 2.055(9); Rh–N4, 2.036(9); Rh–N5, 2.120(9); Rh–N6, 2.132(8), N5–C37, 1.44(2); N6–C43, 1.45(2). Selected bond angles ( $^\circ$ ): Rh–N5–C37, 120.1(7); Rh–N6–C43, 118.2(6).

Deprotonation of both aniline ligands of the colorless complex **4** with  $\text{Na}[\text{N}(\text{SiMe}_3)_2]$  (2 equiv.) gives the deep-red bis-anilido complex  $[(^1\text{bpy})_2\text{Rh}(\text{NHPH})_2][\text{OTf}]$  (**5**) in 86% isolated yield (Scheme 2.5 and Figure 2.7). The  $^{15}\text{N}$  labeled variant (**5**- $^{15}\text{N}$ ) of complex **5** was also prepared, and the anilido NH proton is observed as a doublet at 5.11 ppm ( $^1J_{\text{N-H}} = 54$  Hz) in the  $^1\text{H}$  NMR spectrum of **5**- $^{15}\text{N}$  (inset Figure 2.7). Relative to the starting bisaniline complex **4** the NH protons of **5** have shifted upfield by 2.67 ppm. A similar upfield shift has been observed upon deprotonation of  $(^1\text{bpy})\text{Pt}(\text{NH}_2\text{Ph})_2$  complexes.<sup>34</sup> A metathesis reaction of complex **5** with  $\text{NaBAR}'_4$  gave  $[(^1\text{bpy})_2\text{Rh}(\text{NHPH})_2][\text{BAR}'_4]$  (**6**). The solid-state structure of complex **6** was

determined by single crystal X-ray diffraction (Figure 2.8). A discussion of the X-ray structure for complex **6** is presented below in Section 2.2.4.



**Scheme 2.5.** Deprotonation of  $[(\text{tBu})_2\text{bpy}]_2\text{Rh}(\text{NH}_2\text{Ph})_2][\text{OTf}]_3$  (**3**) to give  $[(\text{tBu})_2\text{bpy}]_2\text{Rh}(\text{NHPh})_2][\text{OTf}]$  (**5**).

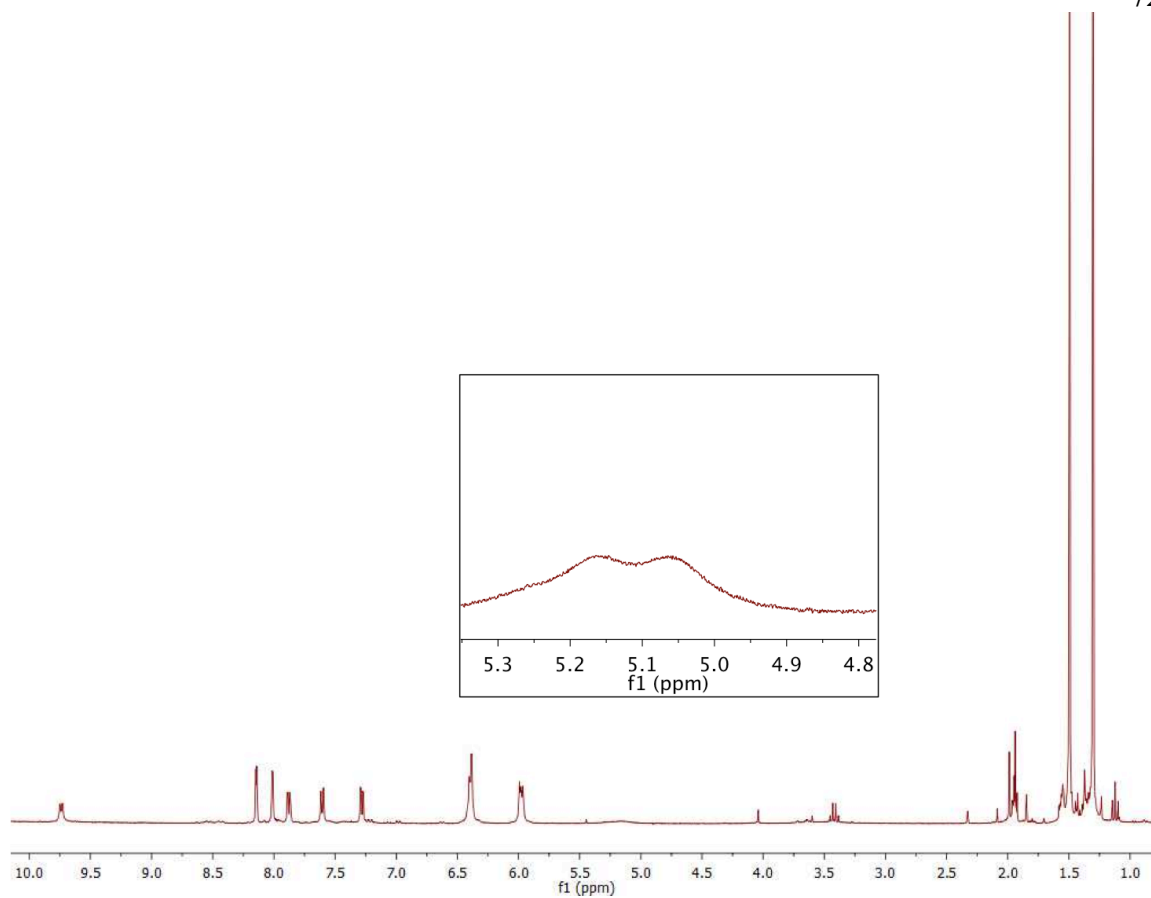


**Figure 2.7.**  $^1\text{H}$  NMR spectrum of  $[(\text{bpy})_2\text{Rh}(\text{NH}_2\text{Ph})_2][\text{OTf}]$  (**5**) in  $\text{CD}_3\text{CN}$ .  $^{15}\text{NHP}$  resonance  $[(\text{bpy})_2\text{Rh}(^{15}\text{NHP})_2][\text{OTf}]$  (**5- $^{15}\text{N}$** ) is shown in the inset.

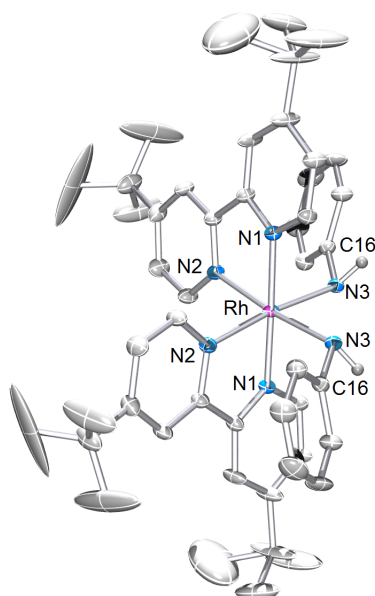
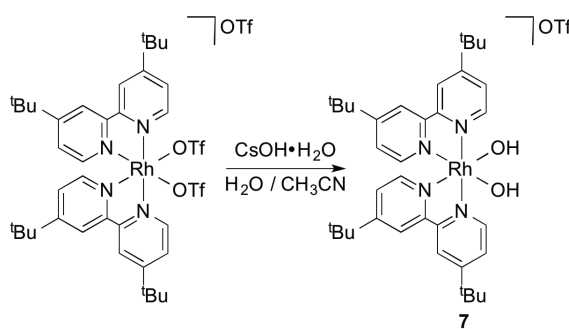


**Figure 2.8.** ORTEP diagram (30% probability) of  $[(^t\text{bpy})_2\text{Rh}(\text{NHPH})_2][\text{BAR}'_4]$  (**6**). Counterions and most hydrogen atoms are omitted for clarity. Selected bond lengths (Å): Rh–N1, 2.021(5); Rh–N2, 2.058(5); Rh–N3, 2.076(5); N3–C16, 1.390(8). Selected bond angles (°): C16–Rh–N3, 119.5(4).

### 2.2.2 Synthesis of Rh(III)–hydroxide, Aqua, Methoxide and Methanol Compounds

In addition to the  $(^t\text{bpy})_2\text{Rh}(\text{III})$  aniline and anilido complexes described above, a series of  $(^R\text{bpy})_2\text{Rh}(\text{III})$  ( $R = ^t\text{Bu}$ , or H) hydroxide, aqua, methoxide and methanol complexes have been synthesized. The addition of  $\text{CsOH}\cdot\text{H}_2\text{O}$  in  $\text{H}_2\text{O}$  to a solution of  $[(^t\text{bpy})_2\text{Rh}(\text{OTf})_2][\text{OTf}]$  in  $\text{CH}_3\text{CN}$  leads to the formation of the pale yellow solid  $[(^t\text{bpy})_2\text{Rh}(\text{OH})_2][\text{OTf}]$  (**7**) (Scheme 2.6). The  $^1\text{H}$  NMR spectrum of **7** is consistent with  $\text{C}_2$  symmetry because 6  $^t\text{bpy}$  aryl resonances and 2  $^t\text{Bu}$  resonances are observed. A broad singlet for the OH resonance of  $[(^t\text{bpy})_2\text{Rh}(\text{OH})_2][\text{OTf}]$  is observed at  $-1.82$  ppm (Figure 2.9). A broad absorption is observed at  $3443\text{ cm}^{-1}$  in the IR spectrum, which is assigned to  $\nu_{\text{OH}}$ . Crystals of **7** suitable for X-ray diffraction were obtained (Figure 2.10). The Rh–O

bond length of complex **7** was found to be 2.010(2) Å. This is similar in the length to the Rh–O bond length of previously reported [(terpy)Rh(OH)(H<sub>2</sub>O)<sub>2</sub>][NO<sub>3</sub>]<sub>2</sub> (terpy = 2,2':6',2''-terpyridine).<sup>35</sup>



**Scheme 2.6.** Synthesis of [(<sup>t</sup>bpy)<sub>2</sub>Rh(OH)<sub>2</sub>][OTf] (**7**).

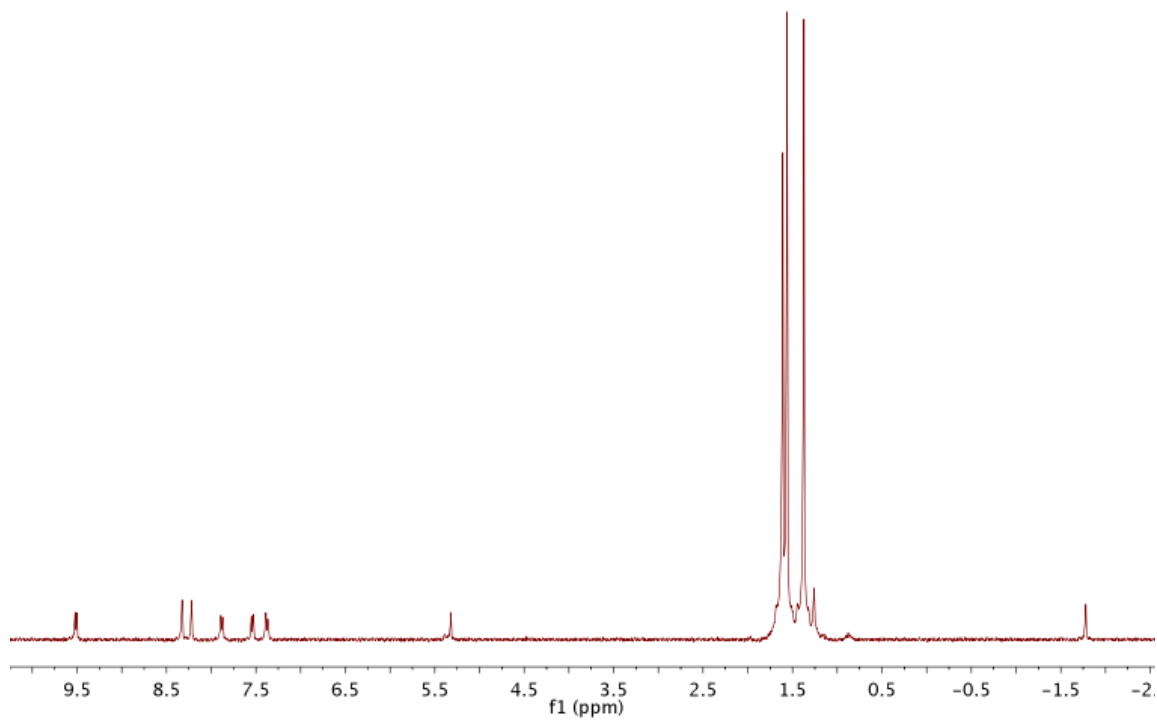


**Figure 2.9.** <sup>1</sup>H NMR spectrum of [(<sup>t</sup>bpy)<sub>2</sub>Rh(OH)<sub>2</sub>][OTf] (**7**) in CD<sub>2</sub>Cl<sub>2</sub>. H<sub>2</sub>O is observed at 1.61 ppm.

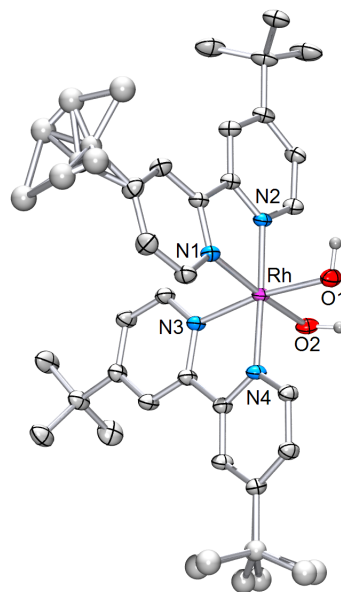
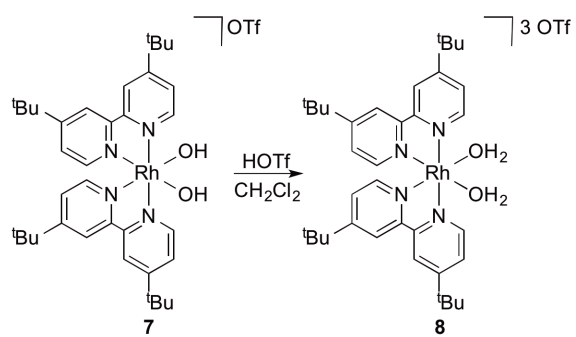


**Figure 2.10.** ORTEP diagram (50% probability) of  $[(^t\text{bpy})_2\text{Rh}(\text{OH})_2][\text{OTf}]$  (**7**). Counterions and hydrogen atoms are omitted for clarity. Selected bond lengths (Å): Rh–N1, 2.043(2); Rh–N2, 2.020(2); Rh–N3, 2.036(2); Rh–N4, 2.022(2); Rh–O1, 2.010(2); Rh–O2, 2.010(2). Selected bond angles ( $^\circ$ ): O1–Rh–O2 87.48(9); O1–Rh–N2, 89.63(9); O2–Rh–N4, 86.74(9). Eight non-H atoms have not been anisotropically refined.

$[(^t\text{bpy})_2\text{Rh}(\text{H}_2\text{O})_2][\text{OTf}]_3$  (**8**) is formed by the addition of HOTf (2 equiv.) to a solution of  $[(^t\text{bpy})_2\text{Rh}(\text{OH})_2][\text{OTf}]$  (**7**) in DCM (Scheme 2.7). In the  $^1\text{H}$  NMR spectrum of **8** a resonance for coordinated  $\text{H}_2\text{O}$  is observed at 7.21 ppm (Figure 2.9). A broad absorption at  $3086\text{ cm}^{-1}$  in the IR spectrum of **8** indicates the presence of an aqua ligand.



**Scheme 2.7.** Synthesis of [(<sup>t</sup>bpy)<sub>2</sub>Rh(H<sub>2</sub>O)<sub>2</sub>][OTf]<sub>3</sub> (**8**).

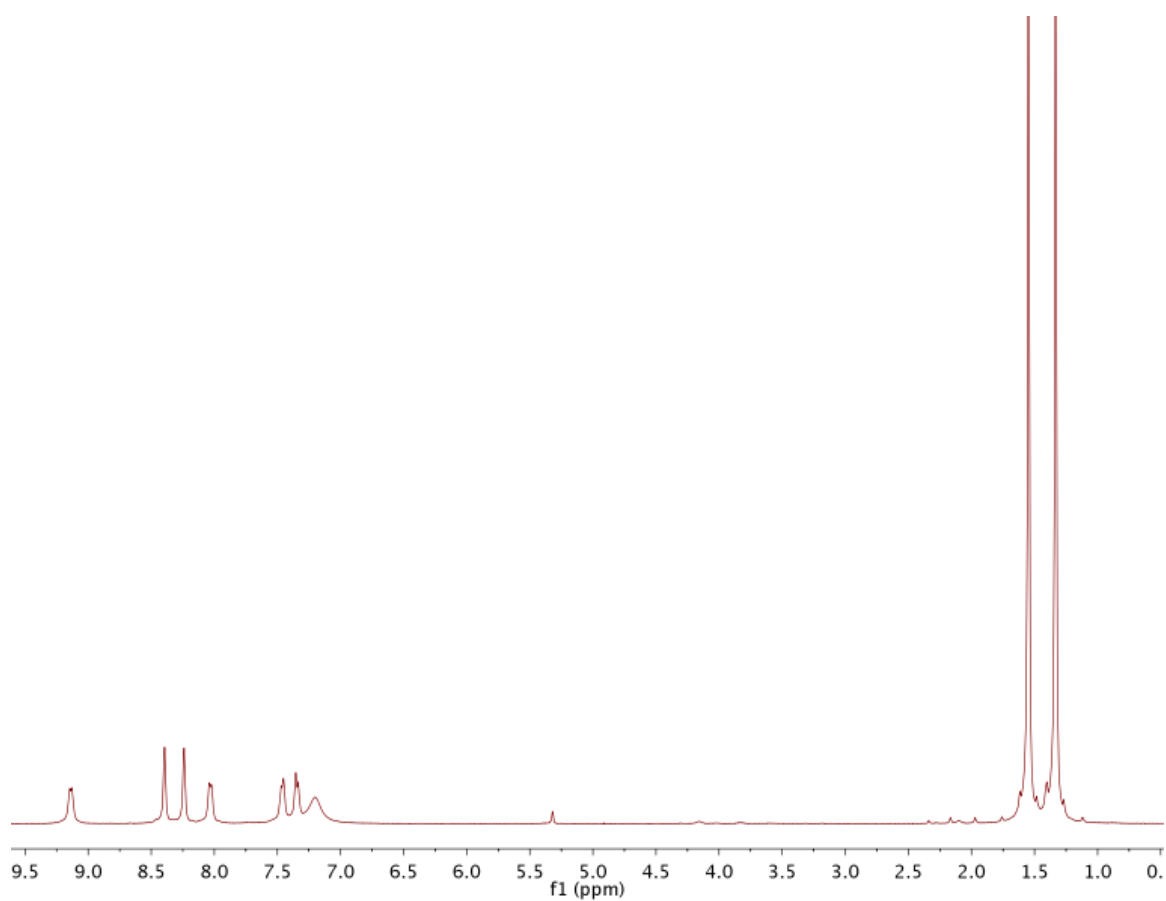
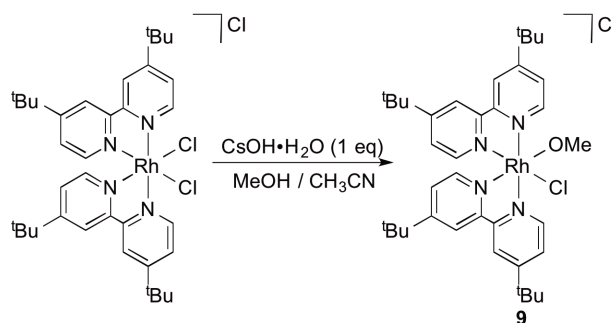


**Figure 2.11.** <sup>1</sup>H NMR spectrum of [(<sup>t</sup>bpy)<sub>2</sub>Rh(H<sub>2</sub>O)<sub>2</sub>][OTf]<sub>3</sub> (**8**) in CD<sub>2</sub>Cl<sub>2</sub>.

The reaction of a solution of  $[(^t\text{bpy})_2\text{Rh}(\text{Cl})_2]\text{Cl}$  in  $\text{CH}_3\text{CN}$  with  $\text{CsOH}\cdot\text{H}_2\text{O}$  (1 equiv.) in  $\text{MeOH}$  leads to the formation of  $[(^t\text{bpy})_2\text{Rh}(\text{OMe})(\text{Cl})]\text{Cl}$  (**9**) (Scheme 2.8). The  $^1\text{H}$  NMR spectrum for complex **9** contains 12  $^t\text{bpy}$  aryl resonances and is therefore consistent with a loss of  $\text{C}_2$  symmetry that is present in the starting material (Figure 2.12). A methoxide resonance is observed at 2.78 ppm. The solid-state structure of  $[(^t\text{bpy})_2\text{Rh}(\text{OMe})(\text{Cl})]\text{Cl}$  (**9**) shows the expected pseudo octahedral coordination sphere (Figure 2.13). The  $\text{Rh}-\text{Cl}$  bond distance is 2.324(2) Å. The  $\text{Rh}-\text{O}$  bond distance is 2.000(3) Å, which is similar to the  $\text{Rh}-\text{O}$  bond distance of  $[(^t\text{bpy})_2\text{Rh}(\text{OMe})(\text{MeOH})][\text{OTf}][\text{TFA}]_2$  [1.994(3) Å] and within the limit of uncertainty of the  $\text{Rh}-\text{O}$  bond distance of  $[(^t\text{bpy})_2\text{Rh}(\text{OMe})_2][\text{BAR}'_4]$  [2.003(2) Å and 2.002(2) Å] (see Chapter 3). The  $\text{Rh}-\text{O}-\text{C}$  bond angle for the methoxide ligand of complex **9** is 118.0(2) $^\circ$ , which is similar in magnitude to those of  $[(^t\text{bpy})_2\text{Rh}(\text{OMe})(\text{MeOH})][\text{OTf}][\text{TFA}]$  [119.4(3) $^\circ$ ] and  $[(^t\text{bpy})_2\text{Rh}(\text{OMe})_2][\text{BAR}'_4]$  [117.8(2) $^\circ$  and 117.2(2) $^\circ$ ] (see Chapter 3).



**Scheme 2.8.** Synthesis of  $[(^t\text{bpy})_2\text{Rh}(\text{OMe})(\text{Cl})]\text{Cl}$  (**9**).

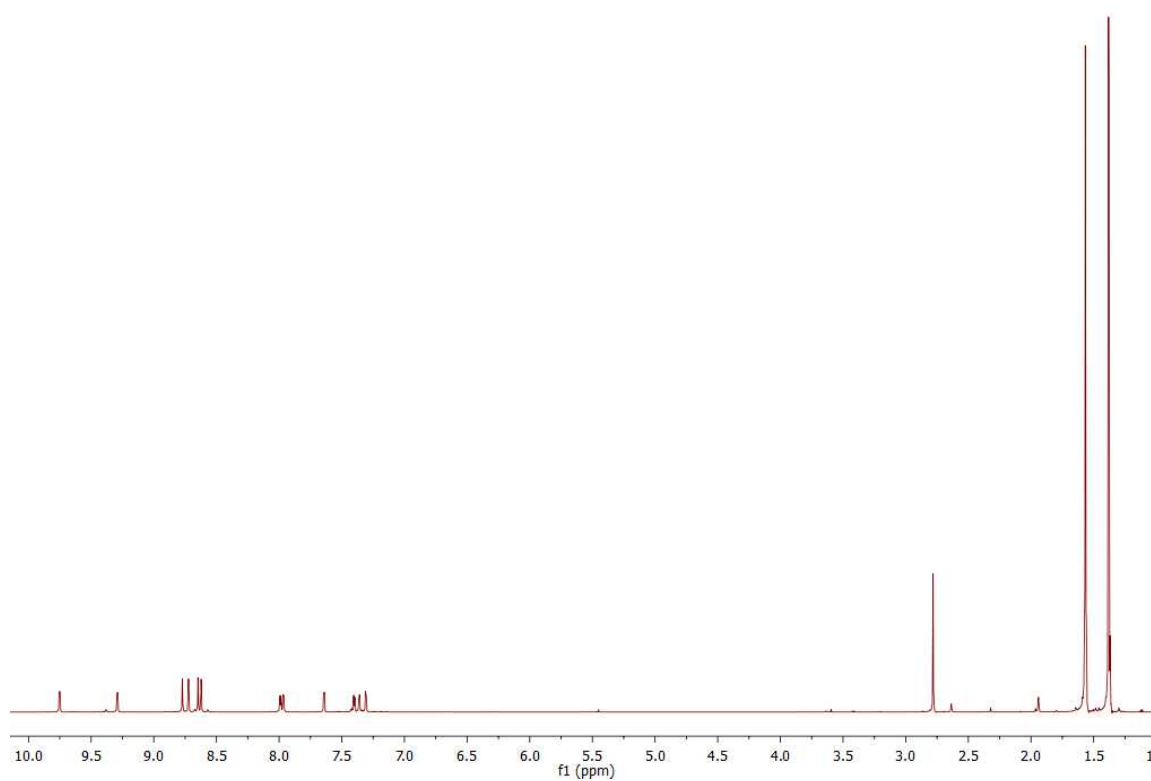


**Figure 2.12.**  $^1\text{H}$  NMR spectrum of  $[(^4\text{bpy})_2\text{Rh}(\text{OMe})(\text{Cl})]\text{Cl}$  (**9**) in  $\text{CD}_3\text{CN}$ .

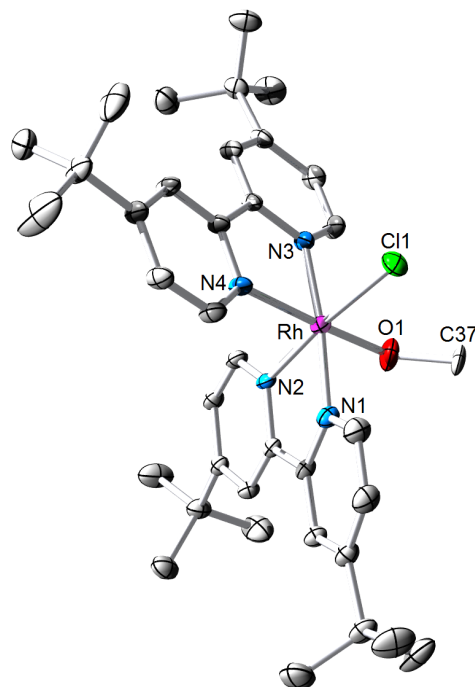


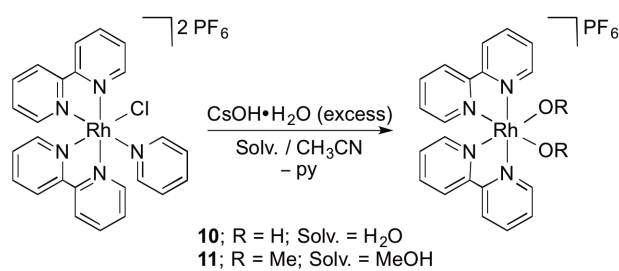
**Figure 2.13.** ORTEP diagram (50% probability) of  $[(\text{tbpy})_2\text{Rh}(\text{OMe})(\text{Cl})]\text{Cl}$  (**9**). Counterion and hydrogen atoms are omitted for clarity. The methoxide and chloride ligands were disordered in two sites and the ratio of the conformers was 60 to 40. The higher occupancy is shown. Selected bond lengths (Å): Rh–N1, 2.022(1); Rh–N2, 2.037(1); Rh–N3, 2.009(1); Rh–N4, 2.039(1); Rh–O1, 2.000(3); Rh–Cl1, 2.324(1); O1–C37, 1.463(4). Select bond angles (°): Rh–O1–C37, 118.0(2); Cl1–Rh–O1, 96.6(1); N4–Rh–N3, 79.79(5); N1–Rh–N4, 97.13(5); N2–Rh–N4, 97.13(5).

The addition of excess  $\text{CsOH}\cdot\text{H}_2\text{O}$  in  $\text{H}_2\text{O}$  or  $\text{MeOH}$  to a  $\text{CH}_3\text{CN}$  solution of  $[(\text{bpy})_2\text{Rh}(\text{py})(\text{Cl})][\text{PF}_6]^{36}$  leads to the formation of  $[(\text{bpy})_2\text{Rh}(\text{OH})_2][\text{PF}_6]$  (**10**) and  $[(\text{bpy})_2\text{Rh}(\text{OMe})_2][\text{PF}_6]$  (**11**), respectively (Scheme 2.9). When only 1 equiv. of  $\text{CsOH}\cdot\text{H}_2\text{O}$  was utilized unreacted starting material and  $[(\text{bpy})_2\text{Rh}(\text{OR})_2][\text{PF}_6]$  ( $\text{R} = \text{H}, \text{Me}$ ) were observed.

The  $^1\text{H}$  NMR spectra for complexes **10** and **11** are consistent with  $\text{C}_2$  symmetric complexes with 6 bpy aryl resonances and 2  $^t\text{Bu}$  aliphatic resonances observed. The  $^1\text{H}$

NMR spectrum of  $[(\text{bpy})_2\text{Rh}(\text{OH})_2][\text{PF}_6]$  (**11**) contains an OH resonance at  $-1.33$  ppm ( $\nu_{\text{OH}}$ ) and a characteristic absorption at  $3396\text{ cm}^{-1}$  in the IR spectrum (Figure 2.14). The methoxide resonance of complex **10** is observed as a doublet in the  $^1\text{H}$  NMR spectrum at  $2.70$  ppm ( $^3J_{\text{Rh-H}} = 1$  Hz) (Figure 2.15).

A single crystal of  $[(\text{bpy})_2\text{Rh}(\text{OMe})_2][\text{PF}_6]$  suitable for X-ray diffraction study was grown by the diffusion of  $\text{Et}_2\text{O}$  into a solution of complex **11** in  $\text{CH}_3\text{CN}$  (Figure 2.16). The Rh–O bond distances for the methoxide ligands of complex **11** are  $2.011(2)$  Å and  $2.010(2)$  Å. These are in close agreement with  $[(^t\text{bpy})_2\text{Rh}(\text{OMe})_2][\text{BAr}'_4]$  [ $2.003(2)$  Å and  $2.002(2)$  Å] (see Chapter 3). The Rh–O–CH<sub>3</sub> bond angles of complex **11** [ $121.3(2)^\circ$  and  $119.2(2)^\circ$ ] are slightly larger than that of  $[(^t\text{bpy})_2\text{Rh}(\text{OMe})_2][\text{BAr}'_4]$  [ $117.8(2)^\circ$  and  $117.3(2)^\circ$ ] (see Chapter 3).



**Scheme 2.9.** Synthesis of  $[(\text{bpy})_2\text{Rh}(\text{OR})_2][\text{PF}_6]$  (R = H, Me) by addition of excess  $\text{CsOH}\cdot\text{H}_2\text{O}$  to  $[(\text{bpy})_2\text{Rh}(\text{py})(\text{Cl})][\text{PF}_6]$ .

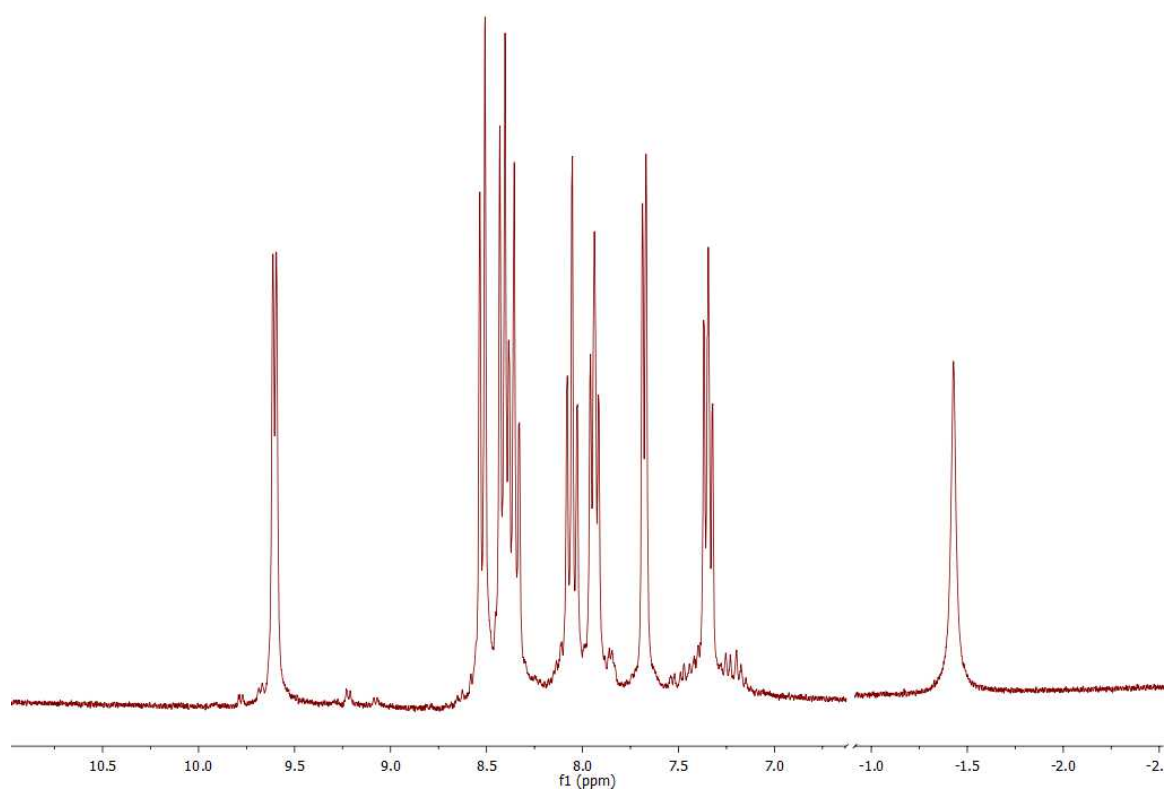


**Figure 2.14.**  $^1\text{H}$  NMR spectrum of  $[(\text{bpy})_2\text{Rh}(\text{OH})_2][\text{PF}_6]$  (**10**) in  $\text{CD}_3\text{CN}$ . The spectrum is cut between ~6.5 ppm and -1.0 ppm.

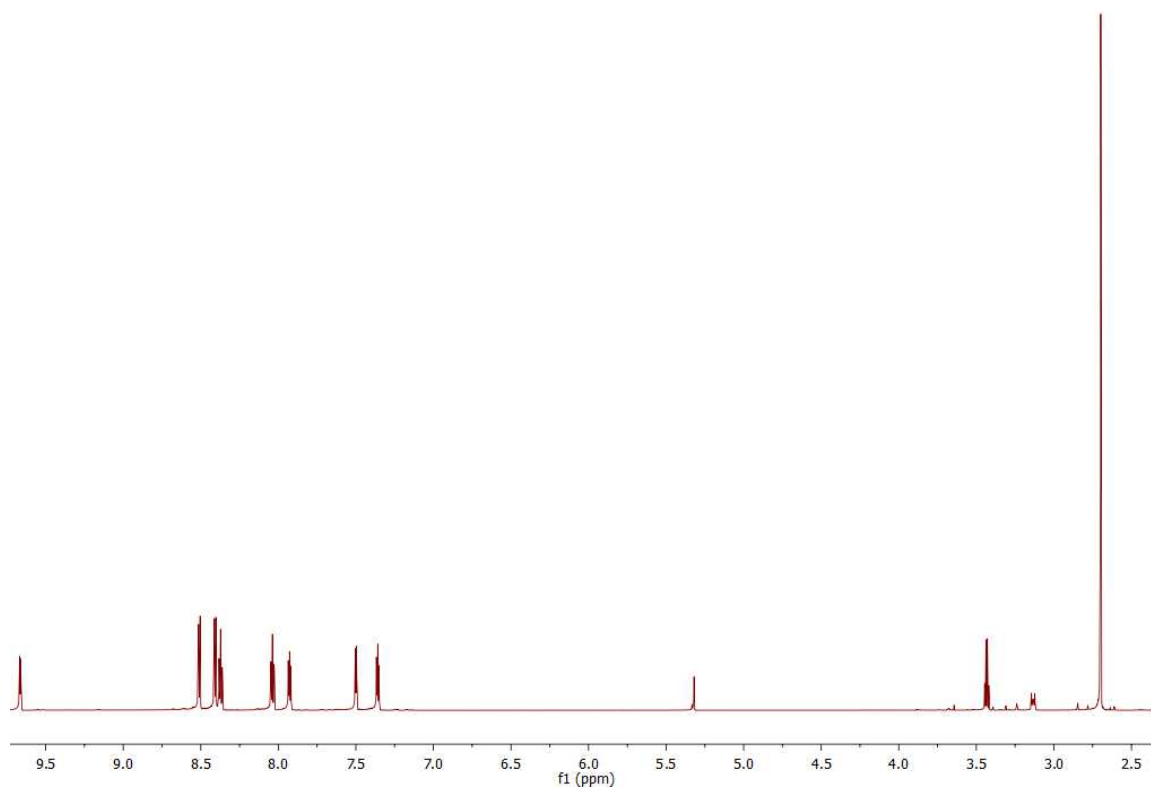


**Figure 2.15.**  $^1\text{H}$  NMR spectrum of  $[(\text{bpy})_2\text{Rh}(\text{OMe})_2][\text{PF}_6]$  (**11**) in  $\text{CD}_2\text{Cl}_2$ .

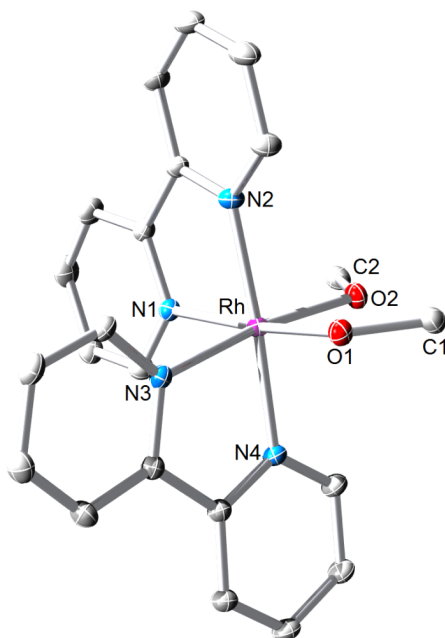


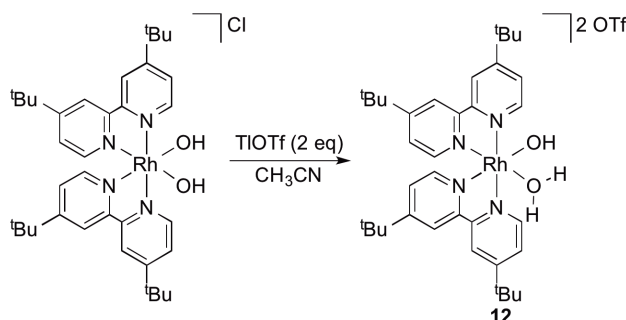
**Figure 2.16.** ORTEP diagram (30% probability) of  $[(bpy)_2Rh(OMe)_2][PF_6]$  (**11**). Counterions and hydrogen atoms omitted for clarity. Selected bond lengths (Å): Rh–N1, 2.053(2); Rh–N2, 2.017(2); Rh–N3, 2.055(3); Rh–N4, 2.015(2); Rh–O1, 2.011(2); Rh–O2, 2.010(2), O1–C1, 1.392(4); O2–C2, 1.399(4). Selected bond angles ( $^\circ$ ): Rh–O1–C1, 121.3(2); Rh–O2–C2, 119.2(2).

### 2.2.3 Reactivity of $[(^t\text{bpy})_2Rh(X)_2]^+$ (X = NPh, OH, OMe) with MOTf (M = Ag, Tl, Na) Salts

We had an interest in oxidation of  $[(^t\text{bpy})_2Rh(X)_2]^+$  (X = OH, NHR) complexes. Initial reaction with AgOTf prompted us to also explore reactions with NaOTf and TlOTf. These reactions are described below.

The addition of 2 equiv. of TlOTf to  $[(^t\text{bpy})_2Rh(OH)_2]Cl$  results in the formation of  $[(^t\text{bpy})_2Rh(OH)(OH_2)][OTf]_2$  (**12**) via protonation of one of the hydroxide ligands. We assume that the proton source is a result of *in situ* generated HOTf or from residual water

in the solvent (Scheme 2.9). Complex **12** appears  $C_2$  symmetric by room temperature  $^1\text{H}$  and  $^{13}\text{C}$  NMR spectroscopy, which suggests a fast proton exchange between the hydroxide and aqua ligands (Figure 2.17). A broad resonance is observed at  $-0.07$  ppm in the  $^1\text{H}$  NMR spectrum of **12**, which could be due to the  $-\text{OH}$  moiety. It is also possible that the resonances due to coordinated  $\text{H}_2\text{O}$  and  $-\text{OH}$  are too broad to observe. A low temperature  $^1\text{H}$  NMR study was performed on complex **12**. At  $-83$   $^\circ\text{C}$ , the proton transfer between the hydroxide and aqua ligands was too rapid to observe broadening of the  $^1\text{bpy}$  resonances or decoalescence of the resonance at  $-0.07$  ppm. A broad absorption in the IR spectrum at  $3462\text{ cm}^{-1}$  has been assigned to  $\nu_{\text{OH}}$ . A broad absorption in the IR spectrum at  $3082\text{ cm}^{-1}$  has been assigned to  $\nu_{\text{OH}}$  for the aqua ligand.



**Scheme 2.10.** The synthesis of  $[(^t\text{bpy})_2\text{Rh}(\text{OH})(\text{H}_2\text{O})][\text{OTf}]_2$  (**12**) is achieved using *in situ* generated HOTf. It is presumed that HOTf is generated by adventitious  $\text{H}_2\text{O}$ .

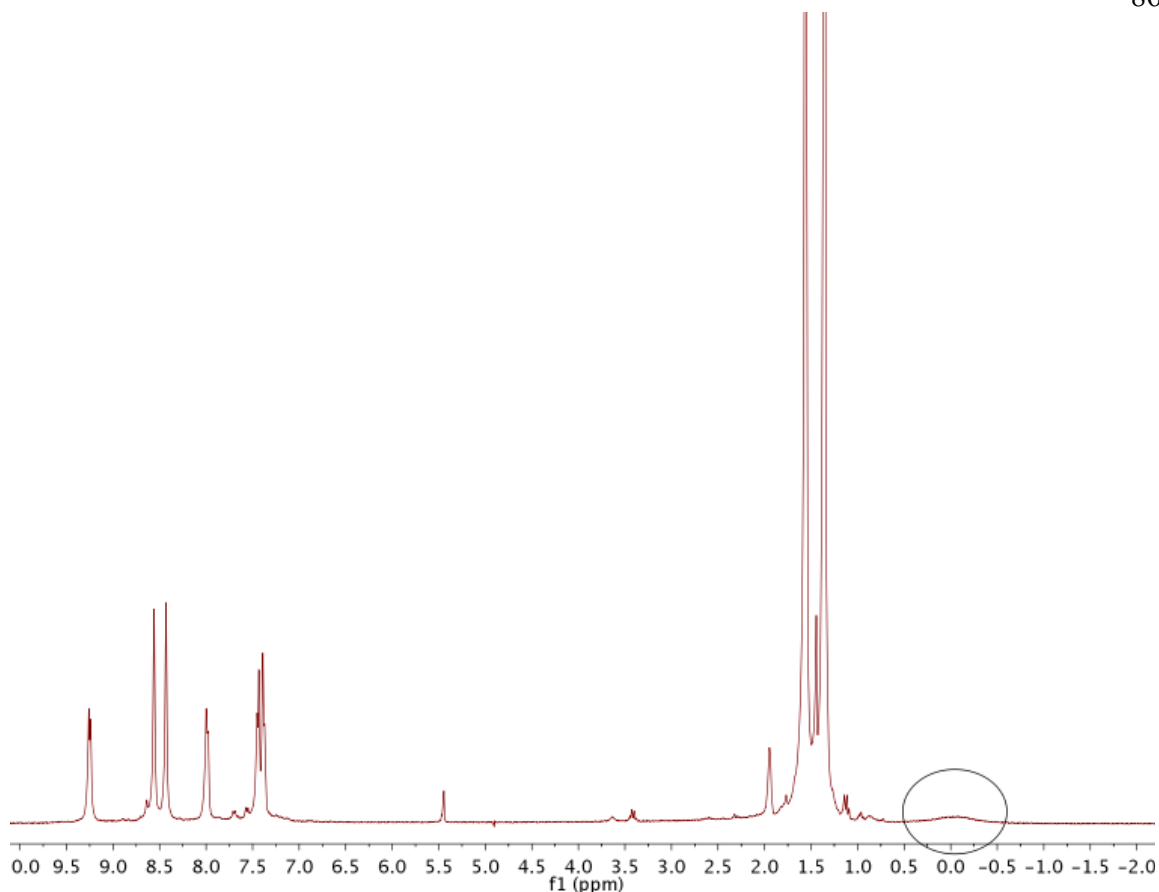


**Figure 2.17.**  $^1\text{H}$  NMR spectrum of  $[(^4\text{bpy})_2\text{Rh}(\text{OH})(\text{H}_2\text{O})][\text{OTf}]_2$  (**12**) in  $\text{CD}_3\text{CN}$ .

The reaction of  $\text{MOTf}$  ( $\text{M} = \text{Ag}, \text{Tl}$  or  $\text{Na}$ ) with  $[(^4\text{bpy})_2\text{Rh}(\text{OMe})_2]\text{Cl}$  produces  $[(^4\text{bpy})_2\text{Rh}(\text{OMe})(\text{MeOH})][\text{OTf}]_2$  (**13**).  $^1\text{H}$  NMR data show that the methoxide resonance of complex **13** shifts slightly relative to starting material and that there is a slight variation in chemical shift depending on the identity of the metal triflate salt used (Figure 2.18). Minor differences are observed for the  $^4\text{bpy}$  aryl resonances when using different  $\text{MOTf}$  salts. The larger shifts for the methoxide resonances are believed to be a result of varying degrees of protonation. We speculate that a rapid equilibrium between  $[(^4\text{bpy})_2\text{Rh}(\text{OMe})_2]\text{Cl}$  and  $[(^4\text{bpy})_2\text{Rh}(\text{OMe})(\text{MeOH})][\text{OTf}]_2$  leads to the appearance of a

single methoxide/ methanol CH<sub>3</sub> peak. The starting material and product are perhaps in rapid equilibrium and the percentage of protonation from the reactions of [(<sup>1</sup>bpy)<sub>2</sub>Rh(OMe)<sub>2</sub>]Cl with different MOTf salts leads to slight changes in chemical shifts.

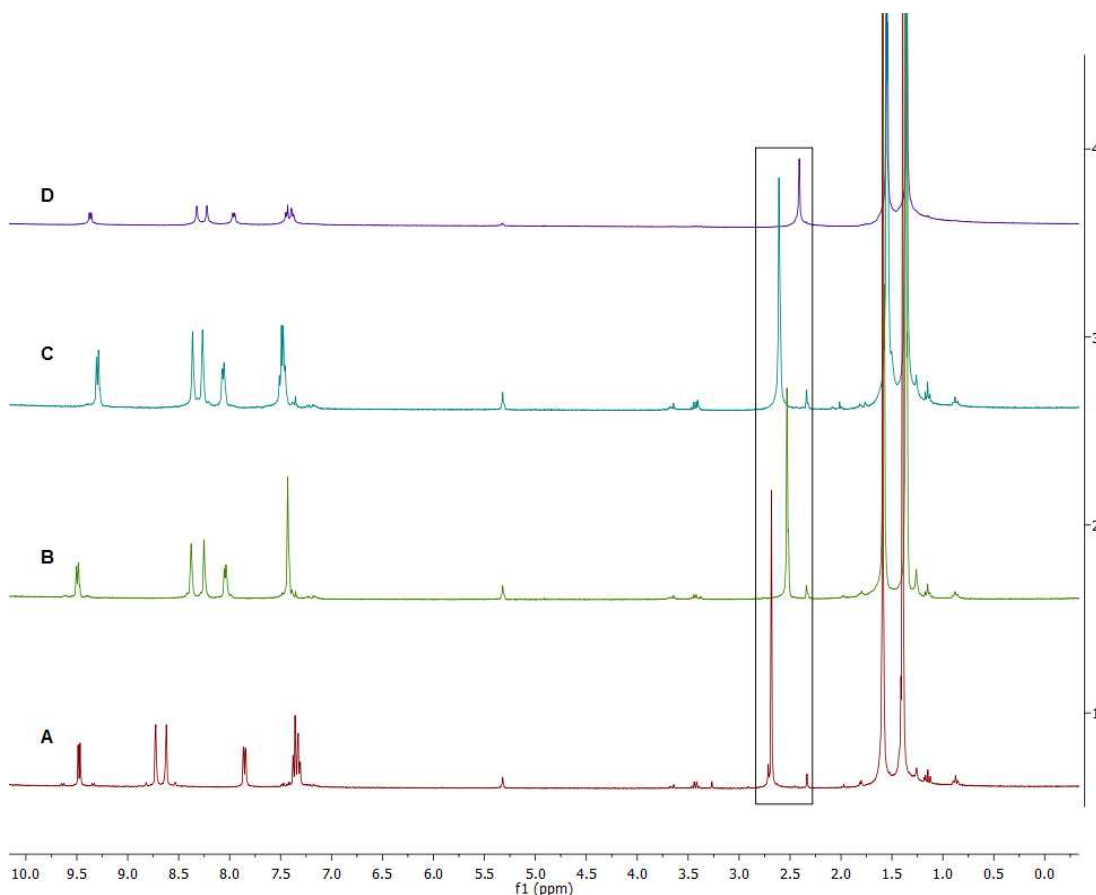


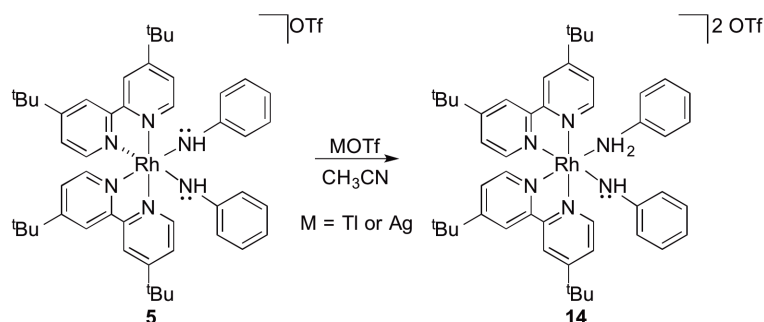
**Figure 2.18.** <sup>1</sup>H NMR spectra demonstrating the slight differences in the chemical shifts of the methoxide resonance of [(<sup>1</sup>bpy)<sub>2</sub>Rh(OMe)(MeOH)][OTf]<sub>2</sub> (**13**) for the reaction of [(<sup>1</sup>bpy)<sub>2</sub>Rh(OMe)<sub>2</sub>]Cl with different MOTf salts (M = Tl, Ag or Na). A = [(<sup>1</sup>bpy)<sub>2</sub>Rh(OMe)<sub>2</sub>]Cl (starting material); B = [(<sup>1</sup>bpy)<sub>2</sub>Rh(OMe)<sub>2</sub>]Cl + 2 equiv. of TlOTf; C = [(<sup>1</sup>bpy)<sub>2</sub>Rh(OMe)<sub>2</sub>]Cl + 2 equiv. of AgOTf; D = [(<sup>1</sup>bpy)<sub>2</sub>Rh(OMe)<sub>2</sub>]Cl + 2 equiv. of NaOTf. Methoxide resonance is indicated by the box. <sup>1</sup>H NMR spectra were acquired in CD<sub>2</sub>Cl<sub>2</sub>.

Complexes **12** and **13** are formed by protonation, but an alternative pathway is single electron oxidation to a Rh(IV) complex  $[(^t\text{bpy})_2\text{Rh}(\text{R})_2]^{+2}$  (R = H or Me) can be envisioned. Hydrogen atom abstraction by AgOTf or TlOTf could generate **12** or **13**. Also, the production of **13** upon reaction of  $[(^t\text{bpy})_2\text{Rh}(\text{OMe})_2]\text{Cl}$  with NaOTf argues against a redox pathway.

In an analogous manner to the synthesis of complex **12**, the addition of 1 equiv. of MOTf (M = Tl or Ag) to a solution of  $[(^t\text{bpy})_2\text{Rh}(\text{NHPh})_2][\text{OTf}]$  (**5**) produces  $[(^t\text{bpy})_2\text{Rh}(\text{NHPh})(\text{NH}_2\text{Ph})][\text{OTf}]_2$  (**14**) in 70% isolated yield (Scheme 2.11). By  $^1\text{H}$  NMR spectroscopy, complex **14** appears to be  $\text{C}_2$  symmetric, which is likely a result of fast proton exchange between the aniline/anilido ligands (Figure 2.19). This is consistent with  $[(^t\text{bpy})_2\text{Rh}(\text{OH})(\text{H}_2\text{O})][\text{OTf}]_2$  reported in this chapter and with  $[(^t\text{bpy})_2\text{Rh}(\text{OMe})(\text{MeOH})][\text{OTf}][\text{TFA}]$ , which will be discussed in detail in Chapter 3. When a  $^1\text{H}$  NMR spectrum of complex **14** is acquired in THF- $d_8$ , all the resonances are broad, which is consistent with a fluxional process. A sharper  $^1\text{H}$  NMR spectrum of complex **14** is acquired in  $\text{CD}_3\text{CN}$ . Two broad singlets are observed at 7.58 and 7.14 ppm for the aniline and anilido NH protons of  $[(^t\text{bpy})_2\text{Rh}(\text{NHPh})(\text{NH}_2\text{Ph})][\text{OTf}]_2$  (Figure 2.19). The rate constant for chemical exchange at coalescence is equal to  $(\pi\Delta\nu)/\sqrt{2}$  where  $\Delta\nu$  is the distance between the two resonances in Hertz. A plausible explanation for why the aniline and anilido NH protons are observed as separate resonances is that the  $\Delta\nu$  at slow exchange could be significantly large compared to the  $\Delta\nu$  of the other resonances. Resonances will broaden and coalesce at different temperatures depending on

the magnitude of  $\Delta\nu$ . A high temperature  $^1\text{H}$  NMR study was performed on complex

**14**. Unfortunately, coalescence of the aniline and anilido NH studies could not be observed because substantial decomposition into multiple species was occurred at temperatures greater than 91 °C. A crystal of  $[(^t\text{bpy})_2\text{Rh}(\text{NHPh})(\text{NH}_2\text{Ph})][\text{OTf}]_2$  suitable for an X-ray crystal diffraction study was obtained by slow diffusion of  $\text{Et}_2\text{O}$  into a solution of complex **14** in  $\text{CH}_3\text{CN}$ . The solid-state structure confirms identity of complex **14** (Figure 2.20). Details of the X-ray crystal structure will be described in Section 2.2.4.



**Scheme 2.11.** Addition of  $\text{MOTf}$  ( $\text{M} = \text{Tl}$  or  $\text{Ag}$ ) to a  $\text{CH}_3\text{CN}$  solution of  $[(^t\text{bpy})_2\text{Rh}(\text{NHPh})_2][\text{OTf}]$  (**5**) leads to formation of  $[(^t\text{bpy})_2\text{Rh}(\text{NHPh})(\text{NH}_2\text{Ph})][\text{OTf}]_2$  (**14**) via *in situ* generated  $\text{HOTf}$ . It is presumed that  $\text{HOTf}$  is generated by adventitious  $\text{H}_2\text{O}$ .

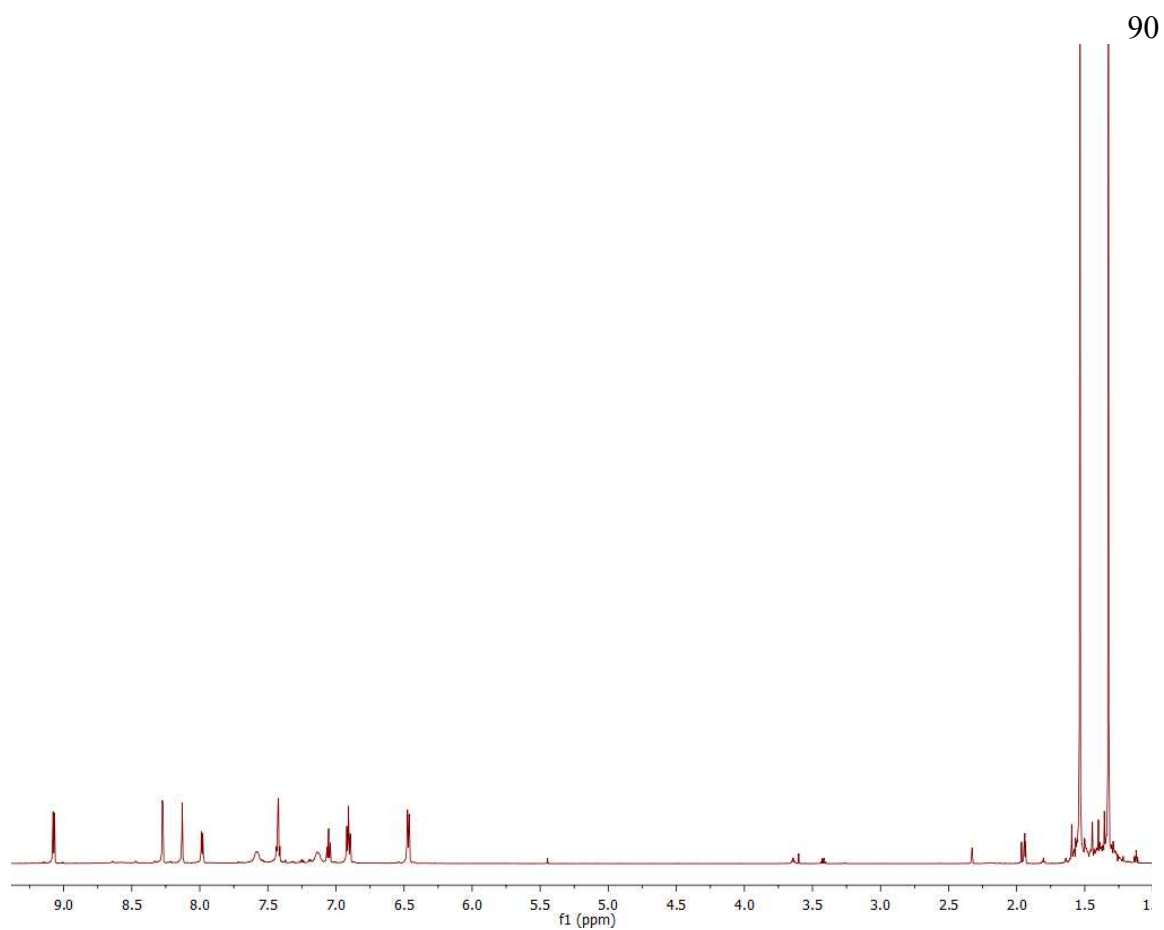


**Figure 2.19.**  $^1\text{H}$  NMR spectrum of  $[(^4\text{bpy})_2\text{Rh}(\text{NHPh})(\text{NH}_2\text{Ph})][\text{OTf}]_2$  (**14**) in  $\text{CD}_3\text{CN}$ .

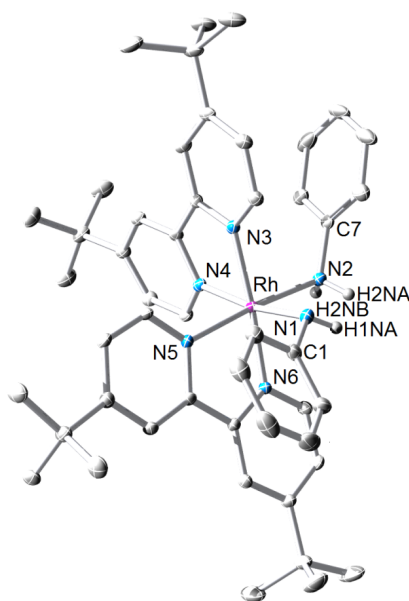


**Figure 2.20.** ORTEP diagram (30% probability) of  $[(bpy)_2Rh(NHPh)(NH_2Ph)][OTf]_2$  (**14**). Counterions and most hydrogen atoms are omitted for clarity. Selected bond lengths (Å): Rh–N1, 2.053(3); Rh–N2, 2.117(3); Rh–N3, 2.088(3); Rh–N4, 2.032(3); Rh–N5, 2.037(3); Rh–N6, 2.022(3); N1–C1, 1.401(4); N2–C7, 1.443(4). Selected bond angles (°): Rh–N1–C1, 121.3(2); Rh–N2–C7, 119.2(2).

#### 2.2.4 Discussion of X-ray Crystal Data for Aniline and Anilido Complexes

A comparison of the Rh–N and N–C bond lengths and the Rh–N–C bond angles for the solid-state structures of  $[(^t\text{bpy})_2Rh(\text{Me})(\text{NH}_2\text{Ph})][\text{BAr}'_4][\text{OTf}]$  (**1**),  $[(^t\text{bpy})_2Rh(\text{NH}_2\text{Ph})_2][\text{BAr}'_4]_3$  (**4**),  $[(^t\text{bpy})_2Rh(\text{NHPh})_2][\text{BAr}'_4]$  (**6**), and  $[(^t\text{bpy})_2Rh(\text{NHPh})(\text{NH}_2\text{Ph})][\text{OTf}]_2$  (**14**) is shown in Figure 2.21. The solid-structure of complexes **1**, **4**, **6** and **14** all reveal pseudo-octahedral coordination spheres. The N–C bond distances for coordinated aniline in the bisaniline complex **4** are 1.44(2) Å and 1.46(2) Å. These values are in close agreement to that of  $[(^t\text{bpy})_2Rh(\text{Me})(\text{NH}_2\text{Ph})][\text{BAr}'_4][\text{OTf}]$  (**1**) [1.429(5) Å]. The Rh–N–C aniline bond angles

of  $[(^t\text{bpy})_2\text{Rh}(\text{NH}_2\text{Ph})_2][\text{BAR}'_4]_3$  are  $120.1(7)^\circ$  and  $118.2(6)^\circ$ , which are in close agreement to that observed for  $[(^t\text{bpy})_2\text{Rh}(\text{Me})(\text{NH}_2\text{Ph})][\text{BAR}'_4][\text{OTf}]$  (**1**) [ $119.4(2)^\circ$ ].

The observed Rh–NHPH and NH–C<sub>ipsoanilido</sub> bond lengths for the bisanilido complex **6** are 1.290(8) Å and 1.390(8) Å, respectively. The Rh–NHPH and the anilido N–C bond lengths are shorter than the Rh–NH<sub>2</sub>Ph and aniline N–C bond lengths of both  $[(^t\text{bpy})_2\text{Rh}(\text{NH}_2\text{Ph})_2][\text{BAR}'_4]_3$  (**4**) [1.44(2) Å and 1.46(2) Å] and  $[(^t\text{bpy})_2\text{Rh}(\text{Me})(\text{NH}_2\text{Ph})][\text{BAR}'_4][\text{OTf}]$  (**1**) [1.429(5) Å]. The shorter N–C anilido bond length is likely a result of increased delocalization of the nitrogen lone pair into the phenyl  $\pi^*$  system.<sup>37</sup> The phenyl rings of the anilido ligand are oriented for  $\pi$ -interaction since the Rh–N–C<sub>phenyl</sub> is not orthogonal to the anilido phenyl plane. The dihedral angle is approximately 80°. As a result, the nitrogen lone pair of the anilido is aligned to back donate into the  $\pi$  system of the aromatic ring. Overlap exists between the p orbital of the nitrogen atom with the  $\pi$  system of the aromatic. Shorter Rh–N bond distances are observed for Rh–N<sub>anilido</sub> versus Rh–N<sub>aniline</sub>. For example, for complex **4** the Rh–N<sub>aniline</sub> bond distances are 2.20(9) Å and 2.132(8) Å while the Rh–N<sub>anilido</sub> bond distance for complex **6** is 2.076(5) Å.

Relatedly, the Rh–N<sub>anilido</sub> bond [2.053(3) Å] of complex **14** is shorter than the Rh–N<sub>aniline</sub> bond [2.117(3) Å], which is consistent with the predicted delocalization of the nitrogen lone pair into the phenyl  $\pi^*$  system for anilido ligand. The Rh–N<sub>anilido</sub> bond of **14** is slightly shorter than the corresponding bond of  $[(^t\text{bpy})_2\text{Rh}(\text{NHPH})_2][\text{BAR}'_4]$  (**6**) [2.076(5) Å]. The Rh–N<sub>aniline</sub> bond length of  $[(^t\text{bpy})_2\text{Rh}(\text{NHPH})(\text{NH}_2\text{Ph})][\text{OTf}]_2$  (**14**) [2.117(3) Å] is similar to those of  $[(^t\text{bpy})_2\text{Rh}(\text{NH}_2\text{Ph})_2][\text{BAR}'_4]_3$  (**4**) [2.120(9) Å and

2.132(8) Å]. Comparison of the Rh–N<sub>aniline</sub> and Rh–N<sub>anilido</sub> bond distance in complex

**14**, indicate that the Rh–N<sub>anilido</sub> bond length is shorter by approximately 0.064 Å.

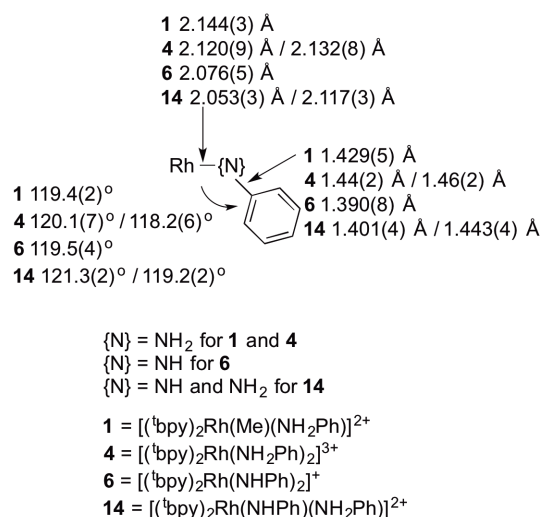
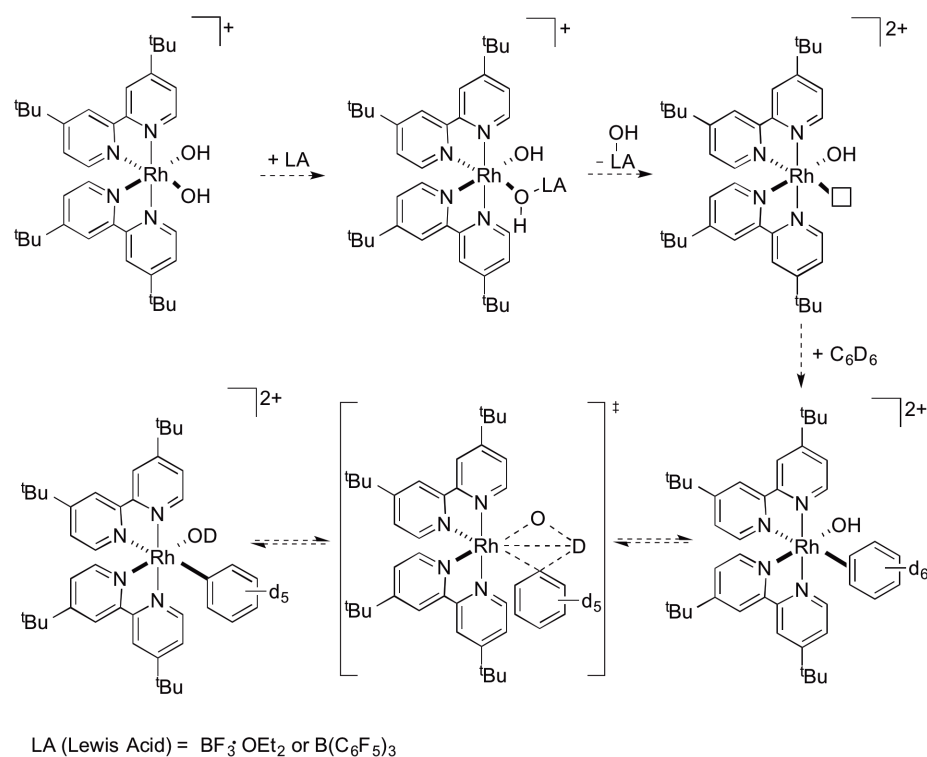


**Figure 2.21.** Comparison of bond angles and lengths data from X-ray crystal structures of the synthesized Rh(III) aniline and anilido complexes [(<sup>t</sup>bpy)<sub>2</sub>Rh(Me)(NH<sub>2</sub>Ph)<sub>2</sub>][OTf][BAR'<sub>4</sub>] (**1**) [(<sup>t</sup>bpy)<sub>2</sub>Rh(NH<sub>2</sub>Ph)<sub>2</sub>][BAR'<sub>4</sub>]<sub>3</sub> (**4**), [(<sup>t</sup>bpy)<sub>2</sub>Rh(NHPh)<sub>2</sub>][BAR'<sub>4</sub>] (**6**) and [(<sup>t</sup>bpy)<sub>2</sub>Rh(NHPh)(NH<sub>2</sub>Ph)][OTf]<sub>2</sub> (**14**).

### 2.3 Attempted Arene H/D Exchange using (<sup>t</sup>bpy)<sub>2</sub>Rh(OH)<sub>2</sub>[OTf] (**7**)

Examples of late transition metal hydroxide complexes for the activation of C–H bonds have been reported.<sup>7,21-31</sup> We investigated the ability of [(<sup>t</sup>bpy)<sub>2</sub>Rh(OH)<sub>2</sub>][OTf] (**7**) to activate benzene C–H bonds. We were particularly interested in studying whether complex **7** could perform the 1,2-addition of C–H bonds across the Rh–OH bonds. Complex **7** was treated with a Lewis acid, either BF<sub>3</sub>·OEt<sub>2</sub> or B(C<sub>6</sub>F<sub>5</sub>)<sub>3</sub> in an effort to remove one of the hydroxide ligands and create an open coordination site (Scheme 2.12 and Table 2.1). <sup>1</sup>H NMR spectroscopy suggested the formation of an asymmetric species, but no H/D exchange was observed with C<sub>6</sub>D<sub>6</sub>.



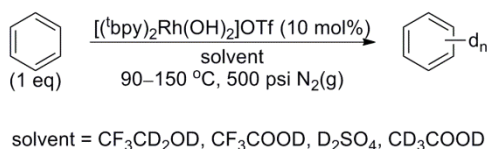
**Scheme 2.12.** Proposed benzene H/D exchange using  $[(^t\text{bpy})_2\text{Rh}(\text{OH})_2]\text{OTf}$  (**7**) and a Lewis acid (LA).

**Table 2.1.** Conditions investigated for benzene H/D exchange using  $[(^t\text{bpy})_2\text{Rh}(\text{OH})_2][\text{OTf}]$  (**7**) in the presence of Lewis acid.

Lewis acid	mol% acid	Solvent	Temperature (°C)
$\text{BF}_3 \cdot \text{OEt}_2$	10	$\text{C}_6\text{D}_6$	50
$\text{B}(\text{C}_6\text{F}_5)_3$	10	$\text{C}_6\text{D}_6$	50 – 75
$\text{B}(\text{C}_6\text{F}_5)_3$	10	$\text{C}_6\text{D}_6 / \text{THF-d}_8$	50
$\text{B}(\text{C}_6\text{F}_5)_3$	20	$\text{C}_6\text{D}_6 / \text{THF-d}_8$	50 – 60
$\text{B}(\text{C}_6\text{F}_5)_3$	100 (1 equiv)	$\text{C}_6\text{D}_6 / \text{THF-d}_8$	75

Several examples of late transition metal mediated C–H activation under acidic conditions have been reported.<sup>38-44</sup> This led us to investigate the ability of  $[(^t\text{bpy})_2\text{Rh}(\text{OH})_2][\text{OTf}]$  (**7**) to activate benzene C–H bonds by 1,2-CH-addition mechanism in acidic media. Benzene H/D exchange using  $[(^t\text{bpy})_2\text{Rh}(\text{OH})_2][\text{OTf}]$  (**10**)

mol% relative to benzene) in deuterated acidic solvents (TFA- $d_1$ ,  $D_2SO_4$ , acetic acid- $d_4$  and  $CF_3CD_2OD$ ) was investigated (Scheme 2.13). Minimal deuterium incorporation into benzene was observed by GC-MS (Table 2.2); however, control experiments in the absence of **7** showed that the exchange is due to direct reaction of the deuterated acids with benzene.



**Scheme 2.13.** General depiction of reaction conditions for H/D exchange reactions between benzene and deuterated solvents in the presence of 10 mol%  $[(t^bpy)_2Rh(OH)_2]OTf$ .

**Table 2.2.** Deuterium incorporation into  $C_6D_6$  using  $[(t^bpy)_2Rh(OH)_2]OTf$  (**7**) (10 mol% relative to benzene) in acidic solvents at 180 °C.

Solvent	Time (h)	$C_6H_6$ (mol%)	$C_6H_5D$ (mol%)	$C_6H_4D_2$ (mol%)	$C_6H_3D_3$ (mol%)	$C_6H_2D_4$ (mol%)	$C_6HD_5$ (mol%)	$C_6D_6$ (mol%)
$CF_3CD_2OD$	18	99.5	0.0	0.2	0.1	0.0	0.0	0.1
Acetic acid- $d_4$	6	98.7	1.2	0.1	0.0	0.0	0.0	0.0
Acetic acid- $d_4$	18	99.9	0.0	0.0	0.1	0.0	0.0	0.0
Acetic acid- $d_4$	24	100.0	0.0	0.0	0.0	0.0	0.0	0.0
TFA- $d_1$	18	89.1	9.1	1.5	0.1	0.1	0.0	0.0
TFA- $d_1$	24	82.6	15.0	1.0	0.4	0.4	0.4	0.2

## 2.4 Conclusions

A series of (<sup>R</sup>bpy)<sub>2</sub>Rh(III) (R = H, <sup>t</sup>Bu) complexes with anionic oxygen- (-OR, -OH) and nitrogen- (-NHPh) based heteroatom ligands have been synthesized. A comparison of the solid state structure data for [(<sup>t</sup>bpy)<sub>2</sub>Rh(Me)(NH<sub>2</sub>Ph)][OTf][BAR'<sub>4</sub>] (**2**), [(<sup>t</sup>bpy)<sub>2</sub>Rh(NH<sub>2</sub>Ph)<sub>2</sub>]<sup>2+</sup> (**4**), [(<sup>t</sup>bpy)<sub>2</sub>Rh(NHPh)<sub>2</sub>]<sup>+</sup> (**6**) and [(<sup>t</sup>bpy)<sub>2</sub>Rh(NHPh)(NH<sub>2</sub>Ph)][OTf]<sub>2</sub> (**14**) is reported. These data provided insight into late transition metal heteroatom bonding. The synthesis of the (<sup>R</sup>bpy)<sub>2</sub>Rh(III) heteroatom complexes reported herein was directed at the elucidation of a Rh(III) heteroatom complex for 1,2-CH-addition. Unfortunately, under the conditions investigated, the desired C–H activation was not observed.

## 2.5 Experimental Section

**General Considerations.** Unless otherwise noted, all synthetic procedures were performed under anaerobic conditions in a nitrogen-filled glovebox or by using standard Schlenk techniques. Glovebox purity was maintained by periodic nitrogen purges and was monitored by an oxygen analyzer (O<sub>2</sub> (g) < 15 ppm for all reactions). Toluene and tetrahydrofuran, were dried by distillation from sodium/benzophenone. Pentane was distilled over P<sub>2</sub>O<sub>5</sub>. Diethyl ether, acetonitrile, and methanol were dried by distillation from CaH<sub>2</sub>. Hexanes, benzene, and dichloromethane were purified by passage through a column of activated alumina. Acetonitrile-*d*<sub>3</sub>, methylene chloride-*d*<sub>2</sub>, *ortho*-dichlorobenzene-*d*<sub>4</sub>, nitromethane-*d*<sub>3</sub>, and THF-*d*<sub>8</sub> were stored under a N<sub>2</sub> atmosphere over 4 Å molecular sieves. <sup>1</sup>H and <sup>13</sup>C NMR spectra were recorded on a Varian Mercury Plus 300 (75 MHz operating frequency for <sup>13</sup>C NMR), Varian Inova 500 MHz

spectrometer (125 MHz operating frequency for  $^{13}\text{C}$  NMR), Bruker Avance DRX 600 MHz spectrometer (150 MHz operative frequency for  $^{13}\text{C}$  NMR), or Bruker Avance III 800 MHz spectrometer (201 MHz operative frequency for  $^{13}\text{C}$  NMR). All  $^1\text{H}$  and  $^{13}\text{C}$  NMR spectra are referenced against residual proton signals ( $^1\text{H}$  NMR) or the  $^{13}\text{C}$  resonances of the deuterated solvent ( $^{13}\text{C}$  NMR). All  $^{31}\text{P}$  NMR were obtained on a Varian Mercury Plus 300 MHz spectrometer (operating frequency 121 MHz) and referenced against an external standard of  $\text{H}_3\text{PO}_4$  ( $\delta = 0$ ). All  $^{19}\text{F}$  NMR spectra were obtained on a Varian Mercury Plus 300 MHz spectrometer (operating frequency 282 MHz) and referenced against an external standard of hexafluorobenzene ( $\delta = -164.9$ ). IR spectra were obtained on a Shimadzu IRAffinity-1 Fourier transform infrared spectrometer. Samples were prepared in solution flow cells or KBr pellets. Elemental analyses were performed by Atlantic Microlabs, Inc. High resolution mass spectra were acquired in ESI mode, from samples dissolved in a 3:1 acetonitrile/water solution containing sodium trifluoroacetate (NaTFA). Mass spectra are reported for  $\text{M}^+$  for monocationic complexes, or for  $[\text{M}+\text{H}^+]$  or  $[\text{M}+\text{Na}^+]$  for neutral complexes, using  $[\text{Na}(\text{NaTFA})_x]^+$  clusters as an internal standard. In all cases, observed isotopic envelopes were consistent with the molecular composition reported. Spectra were collected on either a Bruker BioTOF-Q, Shimadzu IT-TOF or an Agilent 6230 TOF. Dr. William H. Myers from the University of Richmond collected and interpreted the HRMS data. Dr. Michal Sabat at the University of Virginia solved the reported X-ray crystallography data. The preparation, isolation, and characterization of  $\text{NaBAR}'_4$  has been previously reported. The  $^t\text{bpy}$  version of  $[(\text{bpy})_2\text{Rh}(\text{Cl})_2]\text{Cl}$  was synthesized following the published procedure.<sup>45</sup>

$[(^t\text{bpy})_2\text{Rh}(\text{OTf})_2][\text{OTf}]$ ,<sup>45</sup>  $[(^t\text{bpy})_2\text{Rh}(\text{Cl})_2][\text{BAR}'_4]$ ,<sup>33</sup>  $[(^t\text{bpy})_2\text{Rh}(\text{Me})_2][\text{BAR}'_4]$ ,<sup>33</sup>  
 $[(^t\text{bpy})_2\text{Rh}(\text{Me})(\text{OTf})][\text{BAR}'_4]$ ,<sup>33</sup>  $[(^t\text{bpy})_2\text{Rh}(\text{OMe})_2]\text{Cl}$ ,<sup>46</sup>  
 $[(^t\text{bpy})_2\text{Rh}(\text{OMe})(\text{MeOH})][\text{OTf}][\text{TFA}]$ ,<sup>46</sup>  $[(\text{bpy})_2\text{Rh}(\text{py})(\text{Cl})][\text{PF}_6]$ <sup>36</sup> were prepared according to the published procedures. All other reagents were purchased from commercial sources and used without further purification.

**$[(^t\text{bpy})_2\text{Rh}(\text{Me})(\text{NH}_2\text{Ph})][\text{BAR}'_4][\text{OTf}]$  (1).**  $[(^t\text{bpy})_2\text{Rh}(\text{Me})(\text{OTf})][\text{BAR}'_4]$  (0.0678 g, 0.0407 mmol) was dissolved in  $\text{CH}_3\text{NO}_2$  (10 mL). Aniline (3.7  $\mu\text{L}$ , 0.041 mmol) was added, and the solution was refluxed overnight. The volatiles were removed *in vacuo* yielding a yellow-brown solid (0.057 g, 80% yield). X-ray quality crystals were obtained by layering a concentrated DCM solution of **1** with hexanes at room temperature.  $^1\text{H}$  NMR (500 MHz,  $\text{CD}_3\text{NO}_2$ )  $\delta$  8.96 (d,  $^3J_{\text{H5-H6}} = 6$  Hz, 1H,  $^t\text{bpy}$  6), 8.91 (d,  $^3J_{\text{H5-H6}} = 6$  Hz, 1H,  $^t\text{bpy}$  6), 8.80 (d,  $^3J_{\text{H5-H6}} = 6$  Hz, 1H,  $^t\text{bpy}$  6), 8.62 (d,  $^4J_{\text{H3-H5}} = 2$  Hz, 1H,  $^t\text{bpy}$  3), 8.43 (s, 1H,  $^t\text{bpy}$  3), 8.30 (d,  $^4J_{\text{H3-H5}} = 2$  Hz, 2H,  $^t\text{bpy}$  3), 8.07 (dd,  $^3J_{\text{H5-H6}} = 6$  Hz,  $^4J_{\text{H3-H5}} = 2.1$  Hz, 1H,  $^t\text{bpy}$  5), 7.94 (d,  $^3J_{\text{H5-H6}} = 6$  Hz, 1H,  $^t\text{bpy}$  6), 7.85 (br s, 8H, *ortho*-BAR'<sub>4</sub>), 7.72 (dd,  $^3J_{\text{H5-H6}} = 6$  Hz,  $^4J_{\text{H3-H5}} = 2$  Hz, 1H,  $^t\text{bpy}$  5), 7.65 (br s, 4H, *para*-BAR'<sub>4</sub>), 7.53 (dd,  $^3J_{\text{H5-H6}} = 6$  Hz,  $^4J_{\text{H3-H5}} = 3$  Hz, 2H,  $^t\text{bpy}$  5), 6.97 (t,  $^3J_{\text{H2-H3}} = 7$  Hz, 1H, *para*-NH<sub>2</sub>Ph), 6.89 (t,  $^3J = 8$  Hz, 2H, *meta*-NH<sub>2</sub>Ph), 6.43 (t,  $^3J = 12$  Hz, 2H, *ortho*-NH<sub>2</sub>Ph), 6.19 (d,  $^2J_{\text{H-H}} = 11$  Hz, 1H, NH<sub>2</sub>Ph), 5.85 (d,  $^2J_{\text{H-H}} = 11$  Hz, 1H, NH<sub>2</sub>Ph), 1.50 (s, 3H, Rh-CH<sub>3</sub>), 1.55, 1.45, 1.33, 1.27 (each a s, 9H,  $^t\text{bpy}$   $^t\text{Bu}$ ).  $^{13}\text{C}$  NMR (125.75 MHz,  $\text{CD}_3\text{NO}_2$ )  $\delta$  166.0, 165.9, 165.1, 164.9, 156.9, 155.7, 155.1, 153.2, 150.3, 149.8, 149.4, 148.9, 125.7, 125.6, 125.5, 124.6, 121.9, 121.8, 121.4, 120.6, (each a s,  $^t\text{bpy}$  aromatic C's), 139.5 (s, *ipso*-NH<sub>2</sub>Ph), 129.1 (s, *para*-NH<sub>2</sub>Ph), 124.8 (s, *meta*-NH<sub>2</sub>Ph), 120.5 (s, *ortho*-NH<sub>2</sub>Ph), 161.8

(q,  $^1J_{B-C} = 50$ , *ipso*-BAr'<sub>4</sub>), 134.8 (s, *ortho*-BAr'<sub>4</sub>), 128.9 (q,  $^2J_{C-F} = 26$  Hz, *meta*-BAr'<sub>4</sub>), 124.5 (q,  $^1J_{C-F} = 272$  Hz, CF<sub>3</sub>-BAr'<sub>4</sub>), 35.6, 35.3, 35.2, 35.2 (each a s, <sup>t</sup>Bu C(CH<sub>3</sub>)<sub>3</sub>), 29.1, 29.0, 29.0, 28.8 (each a s, <sup>t</sup>Bu C(CH<sub>3</sub>)<sub>3</sub>), 5.6 (d,  $^1J_{Rh-C} = 22$  Hz, Rh-CH<sub>3</sub>). <sup>19</sup>F NMR (281.95 MHz, CD<sub>3</sub>CN)  $\delta$  -63.6 (BAr'<sub>4</sub>), -79.7 (OTf). Anal. Calcd for C<sub>76</sub>H<sub>70</sub>BF<sub>27</sub>N<sub>5</sub>O<sub>3</sub>RhS: C, 51.86; H, 4.01; N, 3.98. Found: C, 51.50; H, 4.07; N, 4.39.

**[(<sup>t</sup>bpy)<sub>2</sub>Rh(Me)(NHPh)][BAr'<sub>4</sub>] (2).** [(<sup>t</sup>bpy)<sub>2</sub>Rh(Me)(NH<sub>2</sub>Ph)][BAr'<sub>4</sub>][OTf] (1) (0.0465 g, 0.264 mmol) was dissolved in THF (~5 mL). Na[N(SiMe<sub>3</sub>)<sub>2</sub>] (2 M in THF, 13.5  $\mu$ L) was added via a microsyringe, which resulted in the clear yellow solution turning dark red with a precipitate. The solution stirred at room temperature for 15 minutes before reducing to dryness under vacuum. The red solid residue was reconstituted in Et<sub>2</sub>O and filtered through a fine porosity frit containing Celite to remove NaOTf. The Celite was washed with Et<sub>2</sub>O, and the filtrate was reduced to dryness under vacuum. The residue was redissolved in THF and filtered through a fine porosity frit containing basic alumina. The filtrate was reduced to dryness under vacuum to give a red solid (0.0422 g, 97%). <sup>1</sup>H NMR (600 MHz, CD<sub>3</sub>CN)  $\delta$  9.07 (d,  $^3J_{H5-H6} = 6$  Hz, 1H, <sup>t</sup>bpy 6), 8.56 (d,  $^3J_{H5-H6} = 6$  Hz, 1H, <sup>t</sup>bpy 6), 8.46 (d,  $^4J_{H3-H5} = 2$  Hz, 1H, <sup>t</sup>bpy 3), 8.31 (d,  $^4J_{H3-H5} = 2$  Hz, 1H, <sup>t</sup>bpy 3), 8.23 (d,  $^4J_{H3-H5} = 2$  Hz, 1H, <sup>t</sup>bpy 3), 8.17 (d,  $^4J_{H3-H5} = 2$  Hz, 1H, <sup>t</sup>bpy 3), 7.85 (d,  $^3J_{H5-H6} = 6$  Hz, 1H, <sup>t</sup>bpy 6), 7.72 (d,  $^3J_{H5-H6} = 6$  Hz, 1H, <sup>t</sup>bpy 6), 7.69 (s, 8H, *ortho* BAr'<sub>4</sub>), 7.66 (s, 4H, *para* BAr'<sub>4</sub>), 7.51 (dd,  $^3J_{H5-H6} = 6$  Hz,  $^4J_{H3-H5} = 2$  Hz, 1H, <sup>t</sup>bpy 5), 7.47 (dd,  $^3J_{H5-H6} = 6$  Hz,  $^4J_{H3-H5} = 2$  Hz, 1H, <sup>t</sup>bpy 5), 7.24 (dd,  $^3J_{H5-H6} = 6$  Hz,  $^4J_{H3-H5} = 2$  Hz, 1H, <sup>t</sup>bpy 5), 7.09 (d,  $^3J_{H5-H6} = 6$  Hz, 1H, <sup>t</sup>bpy 5), 6.89 (t,  $^3J_{H-H} = 7$  Hz, 2H, *para*-NHPh), 6.83 (t,  $^3J_{H-H} = 8$  Hz, 2H, *meta*-NHPh), 6.40 (d,  $J = 7$  Hz, 2H, *ortho*-

NHPh), 5.88 (bs, 1H, *NHPh*), 1.38 (d,  $^2J_{\text{Rh-H}} = 2$  Hz, 3H, CH<sub>3</sub>), 1.52, 1.44, 1.37, 1.30 (each a s, 9H, <sup>t</sup>Bu). <sup>13</sup>C NMR (201 MHz, CD<sub>3</sub>CN)  $\delta$  166.5, 166.4, 165.8, 165.6, 157.7, 156.6, 155.9, 154.2, 151.4, 151.2, 150.5, 150.0, 126.2, 126.0, 125.8, 123.0, 122.7, (each a s, <sup>t</sup>bpy aromatic C's, 3 signals missing presumably due to coincidental overlap), 129.8 (s, *meta*-NHPh), 127.5 (s, *ipso*-NHPh), 125.3 (s, *para*-NH<sub>2</sub>Ph), 121.4 (s, *ortho*-NH<sub>2</sub>Ph), 162.6 (q,  $^1J_{\text{B-C}} = 50$  Hz, *ipso*-BAr'<sub>4</sub>), 135.6 (s, *ortho*-BAr'<sub>4</sub>), 129.9 (m, *meta*-BAr'<sub>4</sub>), 124.0 (q,  $^1J_{\text{C-F}} = 272$  Hz, CF<sub>3</sub>-BAr'<sub>4</sub>), 118.6 (p,  $J = 4$  Hz, *para*-BAr'<sub>4</sub>), 36.8, 36.5, 36.4 (each a s, <sup>t</sup>Bu-C(CH<sub>3</sub>)<sub>3</sub>, 1 signal missing presumably due to coincidental overlap), 30.4, 30.9, 30.4, 30.2 (each a s, <sup>t</sup>Bu-C(CH<sub>3</sub>)<sub>3</sub>), 6.6 (d,  $^1J_{\text{Rh-C}} = 23$ , Rh-CH<sub>3</sub>). <sup>19</sup>F NMR (281.95 MHz, CD<sub>3</sub>CN)  $\delta$  -63.5 (BAr'<sub>4</sub>), -79.7 (OTf). Note: Both OTf and BAr'<sub>4</sub> are present. M<sup>+</sup> = [C<sub>43</sub>H<sub>57</sub>N<sub>5</sub>Rh]<sup>+</sup>; obs'd, calc'd, ppm; 746.3659, 746.3664, -0.7.

**[(<sup>t</sup>bpy)<sub>2</sub>Rh(NH<sub>2</sub>Ph)<sub>2</sub>][OTf]<sub>3</sub> (3).** [(<sup>t</sup>bpy)<sub>2</sub>Rh(OTf)<sub>2</sub>][OTf] (0.2528 g, 0.2326 mmol), aniline (126  $\mu$ L, 1.38 mmol) and THF (~125 mL) were combined in a round bottom flask. The solution was heated at reflux overnight. A white solid precipitated during heating. The solvent was reduced to ~1 mL *in vacuo*. Hexanes were added to complete precipitation. The white solid was collected by filtration through a fine porosity frit. The solid was washed with DCM (2 x 5 mL) to remove starting material and a byproduct, [(<sup>t</sup>bpy)<sub>2</sub>Rh][OTf]<sub>3</sub>, formed during the reaction. The solid was washed with hexanes (~5 mL) and dried under vacuum (0.2265 g, 76%). <sup>1</sup>H NMR (300 MHz, CD<sub>3</sub>NO<sub>2</sub>)  $\delta$  9.29 (d,  $^3J_{\text{H5-H6}} = 6$  Hz, 2H, <sup>t</sup>bpy 6/6'), 8.45 (d,  $^4J_{\text{H3-H5}} = 2$  Hz, 2H, <sup>t</sup>bpy 3/3'), 8.21 (d,  $^4J_{\text{H3-H5}} = 2$  Hz, 2H, <sup>t</sup>bpy 3/3'), 8.14 (dd,  $^3J_{\text{H5-H6}} = 6$  Hz,  $^4J_{\text{H3-H5}} = 2$  Hz, 2H, <sup>t</sup>bpy 5/5'), 7.87 (d,  $^2J_{\text{H-H}} = 12$  Hz, 4H, NH<sub>2</sub>Ph), 7.53 (d,  $^3J_{\text{H5-H6}} = 6$  Hz, 2H, <sup>t</sup>bpy 6/6'), 7.47

(dd,  $^3J_{H5-H6} = 6$  Hz,  $^4J_{H3-H5} = 2$  Hz, 2H,  $^1\text{bpy}$  5/5'), 7.14 (t,  $^3J_{H-H} = 8$  Hz, 2H, *para*-NH<sub>2</sub>Ph), 6.98 (t,  $^3J_{H-H} = 8$  Hz, 4H, *meta*-NH<sub>2</sub>Ph), 6.58 (d,  $^3J_{H-H} = 8$  Hz, 4H, *ortho*-NH<sub>2</sub>Ph), 1.56, 1.30 (each a s, 18H,  $^1\text{Bu}$ ). [( $^1\text{bpy}$ )<sub>2</sub>Rh( $^{15}\text{NH}_2\text{Ph}$ )<sub>2</sub>][OTf]<sub>3</sub>: (300 MHz, CD<sub>3</sub>CN)  $\delta$  7.88 (dd,  $^1J_{N-H} = 71$  Hz,  $^2J_{H-H} = 11$  Hz, 4H, NH<sub>2</sub>). <sup>13</sup>C NMR (125.75 MHz CD<sub>3</sub>NO<sub>2</sub>)  $\delta$  168.8, 167.7, 155.2, 154.7, 151.1, 150.8, 127.1, 126.6, 123.4, 122.7, (each a s,  $^1\text{bpy}$  aromatic C's), 137.3 (s, *ipso*-NH<sub>2</sub>Ph), 129.8, 121.3 (each s, *meta/para*-NH<sub>2</sub>Ph), 127.2 (s, *ortho*-NH<sub>2</sub>Ph), 35.9, 35.5 (each a s,  $^1\text{Bu}$  C(CH<sub>3</sub>)<sub>3</sub>), 29.0, 28.8 (each a s,  $^1\text{Bu}$  C(CH<sub>3</sub>)<sub>3</sub>). <sup>19</sup>F NMR (281.95 MHz, CD<sub>3</sub>CN)  $\delta$  -79.6 (s, OTf). Anal. Calcd for C<sub>51</sub>H<sub>62</sub>F<sub>9</sub>N<sub>6</sub>O<sub>9</sub>RhS<sub>3</sub>: C, 48.19; H 4.91; N 6.61. Found: C, 48.33; H, 5.11; N, 6.56.

[( $^1\text{bpy}$ )<sub>2</sub>Rh(NH<sub>2</sub>Ph)<sub>2</sub>][BAR'<sub>4</sub>]<sub>3</sub> (**4**). [( $^1\text{bpy}$ )<sub>2</sub>Rh(NH<sub>2</sub>Ph)<sub>2</sub>][OTf]<sub>3</sub> (**3**) (0.1039 g, 0.08161 mmol) was dissolved in 15 mL of a 2:1 (V:V) mixture of CH<sub>3</sub>CN to THF. NaBAR'<sub>4</sub> (0.2170 g, 0.2449 mmol) in THF (~ 5 mL) was added slowly. After stirring at room temperature for 2 h, the volatiles were removed *in vacuo*. The residue was dissolved in DCM and filtered through Celite. The filtrate was reduced to dryness *in vacuo* to yield a low-density off-white solid (0.2762 g, 99% yield). X-ray quality crystals were grown by layering a concentrated solution of **4** in DCM with hexanes. <sup>1</sup>H NMR (600 MHz, CD<sub>3</sub>NO<sub>2</sub>)  $\delta$  9.23 (d,  $^3J_{H5-H6} = 6$  Hz, 2H,  $^1\text{bpy}$  6/6'), 8.47 (d,  $^4J_{H3-H5} = 2$  Hz, 2H,  $^1\text{bpy}$  3/3'), 8.22 (d,  $^4J_{H3-H5} = 2$  Hz, 2H,  $^1\text{bpy}$  3/3'), 8.17 (dd,  $^3J_{H5-H6} = 6$  Hz,  $^4J_{H3-H5} = 2$  Hz, 2H,  $^1\text{bpy}$  5/5'), 7.87 (br s, 8H, BAR'<sub>4</sub> *ortho* position), 7.67 (s, 4H, BAR'<sub>4</sub> *para* position), 7.52 (d,  $^3J_{H5-H6} = 6$  Hz, 2H,  $^1\text{bpy}$  6/6'), 7.46 (dd,  $^3J_{H5-H6} = 6$  Hz,  $^4J_{H3-H5} = 2$  Hz, 2H,  $^1\text{bpy}$  5/5'), 7.16 (t,  $^3J_{H-H} = 8$  Hz, 2H, *para*-NH<sub>2</sub>Ph), 6.99 (t,  $^3J_{H-H} = 8$  Hz, 4H, *meta*-NH<sub>2</sub>Ph), 6.63 (d,  $^2J_{H-H} = 11$  Hz, 4H, NH<sub>2</sub>Ph), 6.56 (d,  $^3J_{H-H} = 8$  Hz, 4H, *ortho*-NH<sub>2</sub>Ph), 1.55, 1.27

(each a s, 18H, <sup>t</sup>Bu). <sup>13</sup>C NMR (151 MHz, CD<sub>3</sub>NO<sub>2</sub>) δ 170.9, 169.7, 156.8, 156.2, 151.8, 151.7, 128.1, 125.3, 125.1, 124.5 (each a s, <sup>t</sup>bpy aromatic), 138.4 (s, *ipso*-NH<sub>2</sub>Ph), 131.5, 129.0 (each s, *meta/para*-NH<sub>2</sub>Ph), 123.3 (s, *ortho*-NH<sub>2</sub>Ph), 163.2 (four line pattern, <sup>1</sup>J<sub>CB</sub> = 50 Hz, BAr'<sub>4</sub>), 136.2 (s, BAr'<sub>4</sub>), 130.4 (q, <sup>1</sup>J<sub>CF</sub> = 31 Hz, BAr'<sub>4</sub>C-CF<sub>3</sub>), 124.9 (q, <sup>1</sup>J<sub>CF</sub> = 273 Hz, BAr'<sub>4</sub>, CF<sub>3</sub>), 119.0 (s, BAr'<sub>4</sub>), 37.5, 37.0 (each a s, <sup>t</sup>Bu-C(CH<sub>3</sub>)<sub>3</sub>), 30.4, 30.2 (each a s, <sup>t</sup>Bu-C(CH<sub>3</sub>)<sub>3</sub>). <sup>19</sup>F NMR (282 MHz, CD<sub>3</sub>NO<sub>2</sub>) δ -63.71 (s, BAr'<sub>4</sub>). M<sup>3+</sup> = [C<sub>48</sub>H<sub>62</sub>N<sub>6</sub>Rh]<sup>3+</sup> obs'd. calc'd, ppm: 275.1352, 275.1358, -2.2. M<sup>2+</sup> = [C<sub>48</sub>H<sub>61</sub>N<sub>6</sub>Rh]<sup>2+</sup> obs'd. calc'd, ppm: 412.2013, 412.2001, 2.9. M<sup>+</sup> = [C<sub>48</sub>H<sub>60</sub>N<sub>6</sub>Rh]<sup>+</sup> obs'd. calc'd, ppm: 823.3936, 823.3929, 0.9.

[(<sup>t</sup>bpy)<sub>2</sub>Rh(NHPh)<sub>2</sub>][OTf] (**5**). [(<sup>t</sup>bpy)<sub>2</sub>Rh(NH<sub>2</sub>Ph)<sub>2</sub>][OTf]<sub>3</sub> (**3**) (0.1748 g, 0.1373 mmol) was dissolved in CH<sub>3</sub>CN (~25 mL) in a round bottom flask. Na[N(SiMe<sub>3</sub>)<sub>2</sub>] (2 M in THF, 152 μL, 0.300 mmol) was slowly added via a microsyringe. The colorless solution turned deep red upon addition of base. The solution was stirred at room temperature for 1 h before reducing *in vacuo* to ~1 mL. Et<sub>2</sub>O was added dropwise until precipitation of off-white NaOTf ceased. The solution was filtered through a fine porosity frit containing Celite. The solid was washed with Et<sub>2</sub>O, and the red filtrate was reduced *in vacuo* to dryness (0.1150 g, 86%). <sup>1</sup>H NMR (300 MHz, CD<sub>3</sub>CN) δ 9.74 (d, <sup>3</sup>J<sub>H5-H6</sub> = 6 Hz, 2H, <sup>t</sup>bpy 6/6'), 8.14 (d, <sup>4</sup>J<sub>H3-H5</sub> = 2 Hz, 2H, <sup>t</sup>bpy 3/3'), 8.01 (d, <sup>4</sup>J<sub>H3-H5</sub> = 2 Hz, 2H, <sup>t</sup>bpy 3/3'), 7.88, 7.28 (each a dd, <sup>3</sup>J<sub>H5-H6</sub> = 6 Hz, <sup>4</sup>J<sub>H3-H5</sub> = 2.0 Hz, 2H each, <sup>t</sup>bpy 5/5'), 7.61 (d, <sup>3</sup>J<sub>H5-H6</sub> = 6 Hz, 2H, <sup>t</sup>bpy 6/6'), 6.39 (d, <sup>3</sup>J<sub>H-H</sub> = 7 Hz, 4H, *para*-NH<sub>2</sub>Ph), 6.06 – 5.92 (m, 3H, *ortho/meta*-NHPh), 5.16 (s, 2H, NH), 1.49, 1.30 (each a s, 18H, <sup>t</sup>Bu). [(<sup>t</sup>bpy)<sub>2</sub>Rh(<sup>15</sup>NHPh)<sub>2</sub>][OTf]: <sup>1</sup>H NMR (500 MHz, CD<sub>3</sub>CN) δ 9.77 (d, <sup>3</sup>J<sub>H5-H6</sub> = 6 Hz, 2H,

<sup>1</sup>H NMR (400 MHz, CD<sub>3</sub>CN) δ 8.14 and 8.04 (each a d, <sup>4</sup>J<sub>H3-H5</sub> = 2 Hz, 2H, <sup>1</sup>bpy 3/3'), 7.86 (dd, <sup>3</sup>J<sub>H5-H6</sub> = 6 Hz, <sup>4</sup>J<sub>H3-H5</sub> = 2.1, 2H, <sup>1</sup>bpy 5/5'), 7.61 (d, <sup>3</sup>J<sub>H5-H6</sub> = 6 Hz, 2H, <sup>1</sup>bpy 6/6'), 7.28 (dd, <sup>3</sup>J<sub>H5-H6</sub> = 6 Hz, <sup>4</sup>J<sub>H3-H5</sub> = 2 Hz, 2H, <sup>1</sup>bpy 5/5'), 6.38 (d, <sup>3</sup>J = 7 Hz, 4H, *para*-NHPH), 6.06 – 5.85 (m, 3H, *ortho/meta*-NHPH), 5.11 (d, <sup>1</sup>J<sub>15N-H</sub> = 54 Hz, 2H, <sup>15</sup>NH), 1.49, 1.30 (each a s, 18H, <sup>1</sup>bpy <sup>1</sup>Bu). <sup>13</sup>C NMR (75 MHz, CD<sub>3</sub>CN) δ 165.1, 164.7, 156.3, 155.2, 151.0, 150.1, 124.5, 124.3 (each a s, <sup>1</sup>bpy aromatic C's, 2 signals missing presumably due to coincidental overlap), 128.2 (s, *ipso*-NHPH), 121.3 (each s, *meta/ para*-NHPH), 117.6 (s, *ortho*-NHPH), 35.8, 35.6, (each a s, <sup>1</sup>Bu C(CH<sub>3</sub>)<sub>3</sub>), 29.8, 29.6 (each a s, <sup>1</sup>Bu C(CH<sub>3</sub>)<sub>3</sub>). <sup>19</sup>F NMR (281.95 MHz, CD<sub>3</sub>CN) δ -79.6 (s, OTf). M<sup>+</sup> = [C<sub>48</sub>H<sub>60</sub>N<sub>6</sub>Rh]<sup>+</sup>; ppm: 823.3919, 823.3920, -0.1.

[(<sup>1</sup>bpy)<sub>2</sub>Rh(NHPH)<sub>2</sub>][BAr'<sub>4</sub>] (**6**). [(<sup>1</sup>bpy)<sub>2</sub>Rh(NHPH)<sub>2</sub>][OTf] (**5**) (0.0900 g, 0.0925 mmol) was suspended in THF (~15 mL). NaBAr'<sub>4</sub> (0.0801 g, 0.903 mmol) in THF (~5 mL) was slowly added, and a homogeneous solution resulted. After stirring at room temperature for 2 h, the volatiles were removed under vacuum. The red residue was dissolved in Et<sub>2</sub>O and filtered through Celite. The filtrate was reduced to dryness to yield a red solid (0.1084 g, 69%). X-ray quality crystals were grown by layering a concentrated solution of complex **6** in Et<sub>2</sub>O with pentane. <sup>1</sup>H NMR (600 MHz, CD<sub>3</sub>CN) δ 9.60 (d, <sup>3</sup>J<sub>H5-H6</sub> = 5 Hz, 2H, <sup>1</sup>bpy 6/6'), 8.16 (d, <sup>4</sup>J<sub>H3-H5</sub> = 2 Hz, 2H, <sup>1</sup>bpy 3/3'), 8.04 (d, <sup>4</sup>J<sub>H3-H5</sub> = 2 Hz, 2H, <sup>1</sup>bpy 3/3'), 7.86 (dd, <sup>3</sup>J<sub>H5-H6</sub> = 6 Hz, <sup>4</sup>J<sub>H3-H5</sub> = 2 Hz, 2H, <sup>1</sup>bpy 5/5'), 7.69 (br s, 8H, BAr'<sub>4</sub> *ortho* position), 7.66 (s, 4H, BAr'<sub>4</sub> *para* position), 7.58 (d, <sup>3</sup>J<sub>H5-H6</sub> = 6 Hz, 1H, <sup>1</sup>bpy 6/6'), 7.29 (dd, <sup>3</sup>J<sub>H5-H6</sub> = 6 Hz, <sup>4</sup>J<sub>H3-H5</sub> = 2 Hz, 2H, <sup>1</sup>bpy 5/5'), 6.48 (m, 8H, *para* and *meta*-NH<sub>2</sub>Ph overlapping), 6.05 (d, <sup>3</sup>J<sub>H-H</sub> = 7 Hz, 4H, *ortho*-NH<sub>2</sub>Ph), 1.49, 1.29 (each a s, 18H,

<sup>t</sup>Bu). <sup>13</sup>C NMR (151 MHz, CD<sub>3</sub>CN) δ 166.3, 165.84, 156.9, 155.9, 151.8, 151.1, 129.21, 125.5, 125.3, 122.7 (each a s, <sup>t</sup>bpy and NPh carbons, 4 resonances missing presumably due to coincidental overlap with the CD<sub>3</sub>CN resonance), 162.6 (four line pattern, <sup>1</sup>J<sub>CB</sub> = 50 Hz, BAr'<sub>4</sub>), 135.65 (s, BAr'<sub>4</sub>), 129.9 (q, <sup>1</sup>J<sub>CF</sub> = 32 Hz, BAr'<sub>4</sub> C–CF<sub>3</sub>), 125.5 (q, <sup>1</sup>J<sub>CF</sub> = 273 Hz, BAr'<sub>4</sub>, CF<sub>3</sub>), 113.5 (s, BAr'<sub>4</sub>), 36.6, 36.4 (each a s, <sup>t</sup>Bu C(CH<sub>3</sub>)<sub>3</sub>), 30.6, 30.4 (each a s, <sup>t</sup>Bu C(CH<sub>3</sub>)<sub>3</sub>). <sup>19</sup>F NMR (282 MHz, CD<sub>3</sub>CN) δ –63.6 (s, BAr'<sub>4</sub>). Anal. Cald. For C<sub>80</sub>H<sub>72</sub>BF<sub>24</sub>N<sub>6</sub>Rh C, 56.95; H, 4.30; N, 4.98. Found: C, 56.87; H, 4.17; N, 4.86.

**[(<sup>t</sup>bpy)<sub>2</sub>Rh(OH)<sub>2</sub>][OTf] (7).** A solution of [(<sup>t</sup>bpy)<sub>2</sub>Rh(OTf)<sub>2</sub>][OTf] (0.2225 g, 0.2047 mmol) in CH<sub>3</sub>CN (~5 mL) was prepared in a Schlenk flask. CsOH·H<sub>2</sub>O (0.0791, 0.4710 mmol) was added to a second Schlenk flask. On a Schlenk line, H<sub>2</sub>O (2 mL) was de-gassed with N<sub>2</sub>(g). H<sub>2</sub>O was transferred via a cannula to the Schlenk flask containing CsOH·H<sub>2</sub>O. After stirring for ~5 minutes, the CsOH solution was transferred via cannula to the Schlenk flask containing [(<sup>t</sup>bpy)<sub>2</sub>Rh(OTf)<sub>2</sub>][OTf]. Upon the addition of the CsOH solution, the yellow solution became slightly darker in color. The reaction was stirred at room temperature for 1.5 h before the solvent was removed under vacuum. Inside a positive pressure N<sub>2</sub>(g) glovebox, the solid was re-dissolved in CH<sub>2</sub>Cl<sub>2</sub> and filtered through Celite. The Celite was washed with CH<sub>2</sub>Cl<sub>2</sub> (3 x 5 mL). The filtrate was reduced to ~1.5 mL under vacuum and Et<sub>2</sub>O (5 mL) was added to precipitate a yellow solid. The solid was collected by filtration through a fine porosity frit and then dried under vacuum (0.1402 g, 83% yield). X-ray quality crystals were grown by layering a CH<sub>2</sub>Cl<sub>2</sub> solution of complex **7** with Et<sub>2</sub>O. <sup>1</sup>H NMR (300 MHz, CD<sub>2</sub>Cl<sub>2</sub>) δ 9.49 (d, <sup>3</sup>J<sub>H5-H6</sub> = 6 Hz, 2H, <sup>t</sup>bpy

6/6'), 8.33 (s, 2H, <sup>1</sup>bpy 3/3'), 8.25 (s, 2H, <sup>1</sup>bpy 3/3'), 7.86 (d, <sup>3</sup>J<sub>H5-H6</sub> = 6 Hz, 2H, <sup>1</sup>bpy 5/5'), 7.52 (d, <sup>3</sup>J<sub>H5-H6</sub> = 6 Hz, 2H, <sup>1</sup>bpy 6/6'), 7.37 (d, <sup>3</sup>J<sub>H5-H6</sub> = 6 Hz, 2H, <sup>1</sup>bpy 5/5'), 1.57, 1.32 (each a s, 18H, <sup>1</sup>Bu), -1.26 (bs, 2H, OH). <sup>13</sup>C NMR (75 MHz, CD<sub>2</sub>Cl<sub>2</sub>) δ 165.6, 164.6, 156.4, 155.6, 150.2, 149.5, 125.1, 124.8, 120.8 (each a s, <sup>1</sup>bpy aromatic C's, 1 signal missing presumably due to coincidental overlap), 36.1, 35.8 (each a s, <sup>1</sup>Bu C(CH<sub>3</sub>)<sub>3</sub>), 30.4, 30.2 (each a s, <sup>1</sup>Bu C(CH<sub>3</sub>)<sub>3</sub>). <sup>19</sup>F NMR (281.96 MHz, CD<sub>2</sub>Cl<sub>2</sub>) δ -79.1 (s, OTf). IR (KBr): ν<sub>OH</sub> = 3449 cm<sup>-1</sup>. M<sup>+</sup> = [C<sub>36</sub>H<sub>50</sub>N<sub>4</sub>O<sub>2</sub>Rh]<sup>+</sup>; obsd, calc'd, ppm: 673.2962, 673.2983, -3.1

**[(<sup>1</sup>bpy)<sub>2</sub>Rh(OH)<sub>2</sub>]Cl.** [(<sup>1</sup>bpy)<sub>2</sub>Rh(Cl)<sub>2</sub>]Cl (0.1536 g, 0.2059 mmol) was suspended in CH<sub>3</sub>CN (~15 mL) in a Schlenk flask. CsOH·H<sub>2</sub>O (0.3423 g, 2.038 mmol) was added to a second Schlenk flask. Both Schlenk flasks were sealed and removed from the glovebox. On a Schlenk line, H<sub>2</sub>O (1 mL) was degassed with N<sub>2</sub>(g). The H<sub>2</sub>O was transferred via a cannula to the Schlenk flask containing CsOH·H<sub>2</sub>O. The white solid dissolved upon stirring. The CsOH solution was transferred via cannula to the flask containing the [(<sup>1</sup>bpy)<sub>2</sub>Rh(Cl)<sub>2</sub>]Cl causing the metal complex to dissolve completely. The resulting solution was stirred under N<sub>2</sub>(g) for 1 hour 15 minutes before reducing to dryness under vacuum. Inside a glovebox, the yellow solid was re-constituted in CH<sub>2</sub>Cl<sub>2</sub> and filtered through a fine porosity frit containing Celite. The Celite was washed with CH<sub>2</sub>Cl<sub>2</sub> (5 x 25 mL). The filtrate was reduced to ~1 mL *in vacuo*. Et<sub>2</sub>O was added to precipitate a yellow solid, which was collected by filtration through a fine porosity frit and dried in an evacuated desiccator (0.1391 g, 96% yield). <sup>1</sup>H NMR (300 MHz, CD<sub>2</sub>Cl<sub>2</sub>) δ 9.52 (d, <sup>3</sup>J<sub>H5-H6</sub> = 6, 2H, <sup>1</sup>bpy 6/6'), 8.64 (d, <sup>4</sup>J<sub>H3-H5</sub> = 2, 2H, <sup>1</sup>bpy 3/3'), 8.53 (d, <sup>4</sup>J<sub>H3-H5</sub> = 2, 2H, <sup>1</sup>bpy

3/3'), 7.86 (dd,  $^3J_{\text{H5-H6}} = 6$ ,  $^4J_{\text{H3-H5}} = 2.0$ , 2H,  $^1\text{bpy } 5/5'$ ), 7.52 (d,  $^3J_{\text{H5-H6}} = 6$ , 2H,  $^1\text{bpy } 6/6'$ ), 7.35 (dd,  $^3J_{\text{H5-H6}} = 6$ ,  $^4J_{\text{H3-H5}} = 2$ , 2H,  $^1\text{bpy } 5/5'$ ), 1.58, 1.40 (each a s, 18H each,  $^1\text{Bu}$ ), -1.81 (bs, 2H, *OH*).  $^{13}\text{C}$  NMR (151 MHz,  $\text{CD}_2\text{Cl}_2$ )  $\delta$  166.3, 165.2, 156.8, 156.2, 150.3, 149.8, 124.9, 121.9 (each a s,  $^1\text{bpy}$ , 2 signals missing presumably due to coincidental overlap), 36.6, 36.3 (each a s,  $^1\text{Bu } \text{C}(\text{CH}_3)_3$ ), 30.9, 30.6 (each a s,  $^1\text{Bu } \text{C}(\text{CH}_3)_3$ ). IR (KBr):  $\nu_{\text{OH}} = 3396 \text{ cm}^{-1}$ .  $[\text{C}_{36}\text{H}_{50}\text{N}_4\text{O}_2\text{Rh}]^+$  obs'd. calc'd, ppm: 673.2984, 673.2983, 0.2.

**$[(^1\text{bpy})_2\text{Rh}(\text{H}_2\text{O})_2][\text{OTf}]_3$  (8).**  $[(^1\text{bpy})_2\text{Rh}(\text{OH})_2][\text{OTf}]$  (7) (0.086 g, 0.105 mmol) was dissolved in  $\text{CH}_2\text{Cl}_2$ . HOTf (18  $\mu\text{L}$ , 0.20 mmol) was added via a microsyringe. After 15 minutes,  $\text{Et}_2\text{O}$  was added to precipitate the product. The solid was washed with  $\text{Et}_2\text{O}$  and dried under vacuum to give a white solid (0.110 g, 94%).  $^1\text{H}$  NMR (300 MHz,  $\text{CD}_2\text{Cl}_2$ )  $\delta$  9.14 (d,  $^3J_{\text{H-H}} = 6 \text{ Hz}$ , 2H,  $^1\text{bpy } 6/6'$ ), 8.42, 8.26 (each a s, 2H,  $^1\text{bpy } 3/3'$ ), 8.03 (d,  $^3J_{\text{H-H}} = 6 \text{ Hz}$ , 2H,  $^1\text{bpy } 6/6'$ ), 7.45 (d,  $^3J_{\text{H-H}} = 6 \text{ Hz}$ , 2H,  $^1\text{bpy } 5/5'$ ), 7.37 (d,  $^3J_{\text{H-H}} = 7 \text{ Hz}$ , 2H,  $^1\text{bpy } 5/5'$ ), 7.21 (bs, 4H,  $\text{H}_2\text{O}$ ), 1.55, 1.33 (each a s, 18H).  $^{13}\text{C}$  NMR (75 MHz,  $\text{CD}_2\text{Cl}_2$ )  $\delta$  168.9, 168.3, 156.4, 155.0, 150.4, 127.2, 123.2, 122.9 (each a s,  $^1\text{bpy}$ , 2 signals missing presumably due to coincidental overlap), 36.6, 36.2 (each a s,  $\text{C}(\text{CH}_3)_3$ ), 30.2, 29.9 (each a s,  $\text{C}(\text{CH}_3)_3$ ).  $^{19}\text{F}$  NMR (281.96 MHz,  $\text{CD}_2\text{Cl}_2$ )  $\delta$  -79.3 (s, OTf). IR (KBr):  $\nu_{\text{OH}} = 3086 \text{ cm}^{-1}$ . Anal. Calcd for  $\text{C}_{39}\text{H}_{52}\text{F}_9\text{N}_4\text{O}_{11}\text{RhS}_3$ : C, 41.71; H, 4.67; N, 4.99. Found: C, 41.97; H, 4.71; N, 5.06.

**$[(^1\text{bpy})_2\text{Rh}(\text{OMe})(\text{Cl})]\text{Cl}$  (9).**  $\text{CsOH}\cdot\text{H}_2\text{O}$  (0.0241 g, 0.144 mmol) was dissolved in MeOH (~2 mL) in a round bottom flask. The solution was allowed to stir at room temperature for ~5 minutes before addition of a  $\text{CH}_3\text{CN}$  (~5 mL) solution of  $[(^1\text{bpy})_2\text{Rh}(\text{Cl})_2]\text{Cl}$  (0.1001 g, 0.1342 mmol). The solution was stirred at room

temperature for 2 h before reducing the dryness under vacuum. The yellow-orange solid was reconstituted in DCM and filtered through Celite. The Celite was washed with DCM (5 x 5 mL) and the filtrate was reduced to ~1 mL *in vacuo*. Et<sub>2</sub>O was added to precipitate a yellow solid which, was collected by filtration through a fine porosity frit, washed with Et<sub>2</sub>O and dried under vacuum (0.0972 g, 98%). X-ray quality crystals were grown by layering a concentrated solution of complex **9** in acetonitrile with Et<sub>2</sub>O. <sup>1</sup>H NMR (800 MHz, CD<sub>3</sub>CN) δ 9.75 (d, <sup>3</sup>J<sub>H5-H6</sub> = 6 Hz, 1H, <sup>t</sup>bpy 6), 9.29 (d, <sup>3</sup>J<sub>H5-H6</sub> = 6 Hz, 1H, <sup>t</sup>bpy 6), 8.77 (d, <sup>4</sup>J<sub>H3-H5</sub> = 2 Hz, 1H, <sup>t</sup>bpy 3), 8.72 (d, <sup>4</sup>J<sub>H3-H5</sub> = 2 Hz, 1H, <sup>t</sup>bpy 3), 8.65 (d, <sup>4</sup>J<sub>H3-H5</sub> = 2 Hz, 1H, <sup>t</sup>bpy 3), 8.62 (d, <sup>4</sup>J<sub>H3-H5</sub> = 2 Hz, 1H, <sup>t</sup>bpy 3), 7.99 (dd, <sup>3</sup>J<sub>H5-H6</sub> = 6 Hz, <sup>4</sup>J<sub>H3-H5</sub> = 2 Hz, 1H, <sup>t</sup>bpy 5), 7.96 (dd, <sup>3</sup>J<sub>H5-H6</sub> = 6 Hz, <sup>4</sup>J<sub>H3-H5</sub> = 2 Hz, 1H, <sup>t</sup>bpy 5), 7.64 (d, <sup>3</sup>J<sub>H5-H6</sub> = 6 Hz, 1H, <sup>t</sup>bpy 6), 7.40 (dd, <sup>3</sup>J<sub>H5-H6</sub> = 6 Hz, <sup>4</sup>J<sub>H3-H5</sub> = 2 Hz, 1H, <sup>t</sup>bpy 5), 7.36 (dd, <sup>3</sup>J<sub>H5-H6</sub> = 6 Hz, <sup>4</sup>J<sub>H3-H5</sub> = 2 Hz, 1H, <sup>t</sup>bpy 5), 7.31 (d, <sup>3</sup>J<sub>H5-H6</sub> = 6 Hz, 1H, <sup>t</sup>bpy 6), 2.78 (s, 3H, OCH<sub>3</sub>), 1.57, 1.56, 1.38, 1.38 (each a s, 18H, <sup>t</sup>Bu) <sup>13</sup>C NMR (201 MHz, CD<sub>3</sub>CN) δ 166.9, 166.8, 166.3, 165.9, 157.2, 156.97, 156.9, 156.4, 152.2, 151.4, 150.2, 149.9, 126.1, 125.8, 125.6, 125.5, 123.3, 123.2, 123.1, 123.0 (each a s, <sup>t</sup>bpy aromatic C's), 57.7 (s, <sup>-</sup>OCH<sub>3</sub>), 36.8, 36.8, 36.6, 36.5 (each a s, C(CH<sub>3</sub>)), 30.6, 30.6, 30.3, 30.3 (each a s, C(CH<sub>3</sub>)<sub>3</sub>). [C<sub>37</sub>H<sub>51</sub>N<sub>4</sub>OClRh]<sup>+</sup> obs'd (%), calc'd (%), ppm: 705.2775 (100), 705.2801 (100), -3.7; 706.2816 (47), 706.2833 (46), -2.4; 707.2764 (47), 707.2791 (46), -4.0.

**[(bpy)<sub>2</sub>Rh(OH)<sub>2</sub>][PF<sub>6</sub>] (10).** [(bpy)<sub>2</sub>Rh(py)(Cl)][PF<sub>6</sub>] (0.0990 g, 0.121 mmol) was dissolved in CH<sub>3</sub>CN (~5 mL) in a Schlenk flask. CsOH·H<sub>2</sub>O (0.1629 g, 0.9700 mmol) was added to a second Schlenk flask. On a Schlenk line, H<sub>2</sub>O (1/2 mL) was degassed with N<sub>2</sub>(g). The H<sub>2</sub>O was transferred via a cannula to the Schlenk flask containing

CsOH·H<sub>2</sub>O. An acetonitrile solution of [(bpy)<sub>2</sub>Rh(py)(Cl)][PF<sub>6</sub>] was transferred via cannula to the flask containing the CsOH solution. The resulting clear colorless solution was stirred under N<sub>2</sub>(g) for 2 h before reducing to dryness under vacuum. The yellow solid was redissolved in CH<sub>2</sub>Cl<sub>2</sub> and filtered through Celite. The Celite was washed with CH<sub>2</sub>Cl<sub>2</sub> (3 x 5 mL). The filtrate was reduced to ~1 mL *in vacuo*, and Et<sub>2</sub>O (5 mL) was added to precipitate a yellow solid. The solid was collected by filtration through a fine porosity frit, washed with pentane and dried under vacuum (0.0428 g, 60%). <sup>1</sup>H NMR (600 MHz, CD<sub>2</sub>Cl<sub>2</sub>) δ 9.71 (d, <sup>3</sup>J<sub>H-H</sub> = 5 Hz, 2H, bpy 3/3' or 6/6'), 8.58 (d, <sup>3</sup>J<sub>H-H</sub> = 8 Hz, 2H, bpy 3/3' or 6/6'), 8.47 (d, <sup>3</sup>J<sub>H-H</sub> = 8 Hz, 2H, bpy 3/3' or 6/6'), 8.37 (td, <sup>3</sup>J<sub>H-H</sub> = 9 Hz, <sup>3</sup>J<sub>H-H</sub> = 8, 1 Hz, 2H, bpy 4/4' or 5/5'), 8.07 (td, <sup>3</sup>J<sub>H-H</sub> = 8 Hz, <sup>4</sup>J<sub>H-H</sub> = 2 Hz, 2H, bpy 4/4' or 5/5'), 7.92 (t, <sup>3</sup>J<sub>H-H</sub> = 7 Hz, 2H, bpy 4/4' or 5/5'), 7.62 (d, <sup>3</sup>J<sub>H-H</sub> = 6 Hz, 2H, bpy 3/3' or 6/6'), 7.38 (t, <sup>3</sup>J<sub>H-H</sub> = 7 Hz, 2H, bpy 4/4' or 5/5'), -1.63 (bs, 2H, OH). <sup>13</sup>C NMR (201 MHz, CD<sub>3</sub>CN) δ 157.6, 156.7, 151.8, 150.8, 150.7, 141.2, 140.4, 128.3, 124.9, 124.8 (each a s, bpy). <sup>19</sup>F NMR (282 MHz, CD<sub>2</sub>Cl<sub>2</sub>) δ -74.4 (d, <sup>1</sup>J<sub>F-P</sub> = 711 Hz, PF<sub>6</sub>). <sup>31</sup>P NMR (121 MHz, CD<sub>2</sub>Cl<sub>2</sub>) δ -144.0 (m, PF<sub>6</sub>). IR (KBr): ν<sub>OH</sub> = 3396 cm<sup>-1</sup>. Anal. Calcd for C<sub>20</sub>H<sub>18</sub>F<sub>6</sub>N<sub>4</sub>O<sub>2</sub>PRh: C, 40.42; H, 3.05; N, 9.43. Found: C, 40.05; H, 3.44; N, 8.91. M<sup>+</sup> = [C<sub>20</sub>H<sub>18</sub>N<sub>4</sub>O<sub>2</sub>Rh]<sup>+</sup> obs'd. calc'd, ppm: 449.0481, 449.0479, 0.4.

**[(bpy)<sub>2</sub>Rh(OMe)<sub>2</sub>][PF<sub>6</sub>] (11).** [(bpy)<sub>2</sub>Rh(py)(Cl)][PF<sub>6</sub>] (0.0603 g, 0.0736 mmol) was dissolved in CH<sub>3</sub>CN (~5 mL) and added dropwise to a stirring solution of CsOH·H<sub>2</sub>O (0.0247 g, 0.147 mmol) in MeOH (~½ mL). The resulting bright yellow solution was stirred at room temperature for ½ h before reducing to dryness under vacuum. The solid was reconstituted in CH<sub>2</sub>Cl<sub>2</sub> and filtered through Celite. The Celite

was washed with  $\text{CH}_2\text{Cl}_2$  (3 x 5 mL). The filtrate was reduced to ~1 mL *in vacuo*.

$\text{Et}_2\text{O}$  (5 mL) was added to precipitate a yellow-brown solid that was collected by filtration through a fine porosity frit and then dried under vacuum (0.0341 g, 75%). X-ray quality crystals were grown by layering a solution of complex **11** in  $\text{CH}_3\text{CN}$  with  $\text{Et}_2\text{O}$ .  $^1\text{H}$  NMR (600 MHz,  $\text{CD}_2\text{Cl}_2$ )  $\delta$  9.67 (d,  $^3J_{\text{H-H}} = 6$  Hz, 2H, bpy 3/3' or 6/6'), 8.50 (t,  $^3J_{\text{H-H}} = 8$  Hz, 2H, bpy 4/4' or 5/5'), 8.40 (d,  $^3J_{\text{H-H}} = 8$  Hz, 2H, bpy 3/3' or 6/6'), 8.37 (td,  $^3J_{\text{H-H}} = 8$  Hz,  $^4J_{\text{H-H}} = 2$  Hz, 2H, bpy 4/4' or 5/5'), 8.04 (td,  $^3J_{\text{H-H}} = 8$  Hz,  $^4J_{\text{H-H}} = 2$  Hz, 2H, bpy 4/4' or 5/5'), 7.93 (m, 2H, bpy 4/4' or 5/5'), 7.50 (d,  $^3J_{\text{H-H}} = 6$  Hz, 2H, bpy 3/3' or 6/6'), 7.36 (ddd,  $^3J_{\text{H-H}} = 7$  Hz,  $^3J_{\text{H-H}} = 6$  Hz,  $^4J_{\text{H-H}} = 1$  Hz, 2H, 4/4' or 5/5'), 2.70 (d, 6H,  $^3J_{\text{Rh-H}} = 1$  Hz,  $-\text{OCH}_3$ ).  $^{13}\text{C}$  NMR (201.25 MHz,  $\text{CD}_2\text{Cl}_2$ )  $\delta$  156.9, 155.9, 150.6, 150.4, 141.0, 140.0, 128.3, 127.8, 124.4, 124.2 (each a s, bpy aromatic C's, 2 signals missing presumably due to coincidental overlap), 56.1 (s,  $\text{OCH}_3$ ).  $^{19}\text{F}$  NMR (281.96 MHz,  $\text{CD}_2\text{Cl}_2$ )  $\delta$  -74.2 (d,  $^1J_{\text{F-P}} = 711$ ,  $\text{PF}_6$ ).  $^{31}\text{P}$  NMR (121 MHz,  $\text{CD}_2\text{Cl}_2$ )  $\delta$  -140.9 (m,  $\text{PF}_6$ ). Anal. Calcd for  $\text{C}_{22}\text{H}_{22}\text{F}_6\text{N}_4\text{O}_2\text{PRh}$ : C, 42.46; H, 3.56; N, 9.00. Found: C, 42.31; H, 4.06; N, 8.54.

**$[(^t\text{bpy})_2\text{Rh}(\text{OH})(\text{H}_2\text{O})][\text{OTf}]_2$  (**12**)**.  $[(^t\text{bpy})_2\text{Rh}(\text{OH})_2]\text{Cl}$  (0.0572 g, 0.0786 mmol) was dissolved in  $\text{CH}_2\text{Cl}_2$  (~10 mL) in a round bottom flask.  $\text{TiOTf}$  (0.0559 g, 0.158 mmol) in  $\text{CH}_3\text{CN}$  (~5 mL) was added to the flask. The clear yellow solution formed a precipitate upon addition of  $\text{TiOTf}$ . The solution was stirred at room temperature for 45 minutes before it was reduced to dryness under vacuum. The residue was reconstituted in  $\text{CH}_2\text{Cl}_2$  and filtered through Celite. The Celite was washed with  $\text{CH}_2\text{Cl}_2$  (2 x 5 mL). The filtrate was reduced to ~2 mL under vacuum and a pale yellow solid was precipitated

with Et<sub>2</sub>O. The solid was collected by filtration through a fine porosity frit, washed with Et<sub>2</sub>O and dried under vacuum (0.0679 g, 89%). <sup>1</sup>H NMR (300 MHz, CD<sub>3</sub>CN) δ 9.24 (d, <sup>3</sup>J<sub>H5-H6</sub> = 6 Hz, 2H, <sup>t</sup>bpy 6/6'), 8.55 (d, <sup>4</sup>J<sub>H3-H5</sub> = 2 Hz, 2H, <sup>t</sup>bpy 3/3'), 8.42 (s, 2H, <sup>t</sup>bpy 3/3'), 7.98 (d, <sup>3</sup>J<sub>H5-H6</sub> = 6 Hz, 2H, <sup>t</sup>bpy 6/6'), 7.47 – 7.35 (m, 4H, <sup>t</sup>bpy 5/5'), 1.35, 1.55 (each a s, 18 H, <sup>t</sup>Bu), –0.07 (bs, 1H, OH moieties). <sup>13</sup>C NMR (75 MHz, CD<sub>2</sub>Cl<sub>2</sub>) δ 167.0, 166.0, 156.1, 155.6, 150.6, 149.0, 127.0, 126.1, 122.6, 122.0, 121.7, 118.4 (s, <sup>t</sup>bpy), 36.2, 35.9 (s, <sup>t</sup>Bu C(CH<sub>3</sub>)<sub>3</sub>), 30.2, 29.9 (s, each <sup>t</sup>Bu C(CH<sub>3</sub>)<sub>3</sub>). <sup>19</sup>F NMR (282 MHz, CD<sub>2</sub>Cl<sub>2</sub>) δ -78.5 (s, OTf). IR (KBr): ν<sub>OH</sub> = 3462 cm<sup>-1</sup>, ν<sub>OH</sub> = 3082 cm<sup>-1</sup>. [C<sub>36</sub>H<sub>50</sub>N<sub>4</sub>O<sub>2</sub>Rh]<sup>+</sup> obs'd, calc'd, ppm; 673.2965, 673.2983, -2.7. HRMS data are consistent with loss of a proton to obtain [(<sup>t</sup>bpy)<sub>2</sub>Rh(OH)<sub>2</sub>]<sup>+</sup>.

**[(<sup>t</sup>bpy)<sub>2</sub>Rh(OMe)(MeOH)[OTf]<sub>2</sub> (13).** [(<sup>t</sup>bpy)<sub>2</sub>Rh(OMe)<sub>2</sub>][OTf] (0.0926 g, 0.109 mmol) was dissolved in CH<sub>2</sub>Cl<sub>2</sub> (~10 mL) in a round bottom flask. TlOTf (0.0389 g, 0.110 mmol) in CH<sub>2</sub>Cl<sub>2</sub> (~5 mL) was added to the clear yellow solution causing the solution to turn cloudy. The reaction mixture was stirred at room temperature for 1 h before reducing to dryness *in vacuo*. The yellow solid was reconstituted in CH<sub>2</sub>Cl<sub>2</sub> and filtered through ~2 inches of Celite in a fine porosity frit. The Celite was washed with CH<sub>2</sub>Cl<sub>2</sub> (5 x 5 mL). The filtrate was reduced to ~1 mL *in vacuo* and Et<sub>2</sub>O was added to precipitate a yellow solid. The yellow solid was collected by filtration through a fine porosity frit. The solid was washed with Et<sub>2</sub>O and dried under vacuum (0.1074 g). <sup>1</sup>H NMR (600 MHz, CD<sub>2</sub>Cl<sub>2</sub>) δ 9.29 (d, <sup>3</sup>J<sub>H5-H6</sub> = 6 Hz, 2H, <sup>t</sup>bpy 6/6'), 8.38, 8.27 (each a s, 2H each, <sup>t</sup>bpy 3/3'), 8.03 (s, 2H, <sup>t</sup>bpy 5/5'), 7.48 (d, <sup>3</sup>J<sub>H5-H6</sub> = 6 Hz, 4H, <sup>t</sup>bpy 6/6', 5/5'), 2.48 (bs, 6H, OCH<sub>3</sub>) 1.55, 1.36 (each a s, 18H each, <sup>t</sup>Bu). <sup>13</sup>C NMR (75 MHz, CD<sub>3</sub>CN) δ

169.8, 169.9, 159.2, 159.0, 154.0, 152.3, 128.6, 126.9, 125.7 (each a s, <sup>1</sup>bpy aromatic C's, 1 signal missing presumably due to coincidental overlap), 59.9 (s, 2C, OCH<sub>3</sub>), 39.5, 39.2 (each a s, <sup>t</sup>Bu C(CH<sub>3</sub>)<sub>3</sub>), 33.2, 32.9 (each a s, <sup>t</sup>Bu C(CH<sub>3</sub>)<sub>3</sub>). <sup>19</sup>F NMR (281.96 MHz, CD<sub>3</sub>CN) δ -79.6 (s, OTf). Anal. Calcd for C<sub>41</sub>H<sub>56</sub>F<sub>9</sub>N<sub>4</sub>O<sub>11</sub>RhS<sub>3</sub>: C, 42.78; H, 4.90; N, 4.87. Found: C, 42.54; H, 4.88; N, 5.00. EA data is consistent with loss of a proton to from [(<sup>1</sup>bpy)<sub>2</sub>Rh(MeOH)<sub>2</sub>][OTf]<sub>3</sub>.

[(<sup>1</sup>bpy)<sub>2</sub>Rh(NHPh)(NH<sub>2</sub>Ph)][OTf]<sub>2</sub> (**14**). [(<sup>1</sup>bpy)<sub>2</sub>Rh(NHPh)<sub>2</sub>][OTf] (**5**) (0.05090 g, 0.05231 mmol) was dissolved in THF (~10 mL). TlOTf (0.0219 g, 0.0620 mmol) in THF (~2 mL) was added to the [(<sup>1</sup>bpy)<sub>2</sub>Rh(NHPh)<sub>2</sub>][OTf] solution. The red solution was allowed to stir at room temperature for 0.5 h before reducing to dryness *in vacuo*. The red solid was re-constituted in THF and filtered through Celite. The Celite was washed with THF (3 x 5 mL) and the filtrate was reduced to ~1 mL *in vacuo*. Hexanes were added to precipitate a red-orange solid, which was collected by filtration through a fine porosity frit and dried under vacuum overnight. The solid was dissolved in THF, layered with pentane and placed in the freezer (-34 °C). Red crystalline material was collected by filtration through a fine porosity frit and washed with pentane and Et<sub>2</sub>O. The solid was dried under vacuum (0.0409 g, 70%). X-ray quality crystals grown by layering a concentrated solution of complex **14** in CH<sub>3</sub>CN with Et<sub>2</sub>O. <sup>1</sup>H NMR (600 MHz, CD<sub>3</sub>CN) δ 9.07 (d, <sup>3</sup>J<sub>H5-H6</sub> = 6 Hz, 2H, <sup>1</sup>bpy 6/6'), (d, <sup>4</sup>J<sub>H3-H5</sub> = 2 Hz, 2H, <sup>1</sup>bpy 3/3'), 8.13 (d, <sup>4</sup>J<sub>H3-H5</sub> = 2 Hz, 2H, <sup>1</sup>bpy 3/3'), 7.98 (dd, <sup>3</sup>J<sub>H5-H6</sub> = 6 Hz, <sup>4</sup>J<sub>H3-H5</sub> = 2 Hz, 2H, <sup>1</sup>bpy 5/5'), 7.58 (bs, 1H, NH), 7.43 (m, 4H, <sup>1</sup>bpy 6/6' and <sup>1</sup>bpy 5/5' coincidental overlap), 7.14 (bs, 1H, NH), 7.05 (t, <sup>3</sup>J<sub>H-H</sub> = 8 Hz, 4H, *para*-NHPh), 6.91 (t, <sup>3</sup>J<sub>H-H</sub> = 8 Hz, 4H, *meta*-NHPh), 6.47 ((t,

$^3J_{\text{H-H}} = 8$  Hz, 4H, *ortho*-NHPH)), 1.54, 1.33 (each a s, each 18H,  $^t\text{Bu}$ ).  $^{13}\text{C}$  NMR (75 MHz,  $\text{CD}_3\text{CN}$ )  $\delta$  169.4, 168.5, 156.0, 155.5, 152.3, 152.0, 127.3, 124.8, 124.3 (each a s,  $^t\text{bpy}$  aromatic C's, 1 signal missing presumably due to coincidental overlap presumably), 138.4 (s, *ipso*-NHPH), 130.6 (s, *meta*-NHPH), 127.9 (s, *para*-NHPH), 122.4 (s, *ortho*-NHPH), 37.1, 36.7 (each a s,  $^t\text{Bu}$  C( $\text{CH}_3$ ) $_3$ ), 30.3, 30.1 (each a s,  $^t\text{Bu}$  C( $\text{CH}_3$ ) $_3$ ).  $^{19}\text{F}$  NMR (281.96 MHz,  $\text{CD}_3\text{CN}$ )  $\delta$  -79.5 (s, OTf).  $[\text{C}_{48}\text{H}_{60}\text{N}_6\text{Rh}]^+$ ; obs'd, calc'd, ppm; 823.3915, 823.3929, -3.0. HRMS data is consistent with loss of a proton to give  $[(^t\text{bpy})_2\text{Rh}(\text{NHPH})_2]^+$ .

## 2.6 References

1. Fulton, J. R.; Holland, A. W.; Fox, D. J.; Bergman, R. G. *Acc. Chem. Res.* **2002**, *35*, 44.
2. Gunnoe, T. B. *Eur. J. Inorg. Chem.* **2007**, 1185.
3. Conner, D.; Jayaprakash, K. N.; Cundari, T. R.; Gunnoe, T. B. *Organometallics* **2004**, *23*, 2724.
4. Mayer, J. M. *Comments Inorg. Chem.* **1988**, *8*, 125.
5. Caulton, K. G. *New J. Chem.* **1994**, *18*, 25.
6. Holland, P. L.; Andersen, R. A.; Bergman, R. G. *Comments Inorg. Chem.* **1999**, *21*, 115.
7. Webb, J. R.; Burgess, S. A.; Cundari, T. R.; Gunnoe, T. B. *Dalton Trans.* **2013**, *42*, 16646.
8. Chao, Y.-W.; Rodgers, P. M.; Wigley, D. E. *J. Am. Chem. Soc.* **1991**, *113*, 6326.
9. Lin, Z.; Hall, M. B. *Coord. Chem. Rev.* **1993**, *123*, 149.

10. Fulton, J. R.; Sklenak, S.; Bouwkamp, M. W.; Bergman, R. G. *J. Am. Chem. Soc.* **2002**, *124*, 4722.
11. Conner, D.; Jayaprakash, K. N.; Wells, M. B.; Manzer, S.; Gunnoe, T. B.; Boyle, P. D. *Inorg. Chem.* **2003**, *42*, 4759.
12. Goj, L. A.; Blue, E. D.; Delp, S. A.; Gunnoe, T. B.; Cundari, T. R.; Pierpont, A. W.; Petersen, J. L.; Boyle, P. D. *Inorg. Chem.* **2006**, *45*, 9032.
13. Askevold, B.; Friedrich, A.; Buchner, M. R.; Lewall, B.; Filippou, A. C.; Herdtweck, E.; Schneider, S. *J. Organomet. Chem.* **2013**, *744*, 35.
14. Kohl, S. W.; Weiner, L.; Schwartsburd, L.; Konstantinovski, L.; Shimon, L. J. W.; Ben-David, Y.; Iron, M. A.; Milstein, D. *Science* **2009**, *324*, 74.
15. Choi, K. S.; Lai, T. H.; Lee, S. Y.; Chan, K. S. *Organometallics* **2011**, *30*, 2633.
16. Fryzuk, M. D.; Montgomery, C. D.; Rettig, S. J. *Organometallics* **1991**, *10*, 467.
17. Abdur-Rashid, K.; Faatz, M.; Lough, A. J.; Morris, R. H. *J. Am. Chem. Soc.* **2001**, *123*, 7473.
18. Fulmer, G. R.; Muller, R. P.; Kemp, R. A.; Goldberg, K. I. *J. Am. Chem. Soc.* **2009**, *131*, 1346.
19. Fulmer, G. R.; Herndon, A. N.; Kaminsky, W.; Kemp, R. A.; Goldberg, K. I. *J. Am. Chem. Soc.* **2011**, *133*, 17713.
20. Webb, J. R.; Pierpont, A. W.; Munro-Leighton, C.; Gunnoe, T. B.; Cundari, T. R.; Boyle, P. D. *J. Am. Chem. Soc.* **2010**, *132*, 4520.
21. Feng, Y.; Lail, M.; Barakat, K. A.; Cundari, T. R.; Gunnoe, T. B.; Petersen, J. L. *J. Am. Chem. Soc.* **2005**, *127*, 14174.

22. Feng, Y.; Lail, M.; Foley, N. A.; Gunnoe, T. B.; Barakat, K. A.; Cundari, T. R.; Petersen, J. L. *J. Am. Chem. Soc.* **2006**, *128*, 7982.
23. Cundari, T. R.; Grimes, T. V.; Gunnoe, T. B. *J. Am. Chem. Soc.* **2007**, *129*, 13172.
24. Tenn, I., W. J.; Young, K. J. H.; Bhalla, G.; Oxgaard, J.; Goddard III, W. A.; Periana, R. A. *J. Am. Chem. Soc.* **2005**, *127*, 14172.
25. Tenn, I., W. J.; Young, K. J. H.; Oxgaard, J.; Nielson, R. J.; Goddard III, W. A.; Periana, R. A. *Organometallics* **2006**, *25*, 5173.
26. Hashiguchi, B. G.; Young, K. J. H.; Yousufuddin, M.; Goddard, W. A.; Periana, R. A. *J. Am. Chem. Soc.* **2010**, *132*, 12542.
27. Kloek, S. M.; Heinekey, D. M.; Goldberg, K. I. *Angew. Chem., Int. Ed.* **2007**, *46*, 4736.
28. Hanson, S. K.; Heinekey, D. M.; Goldberg, K. I. *Organometallics* **2008**, *27*, 1454.
29. Bercaw, J. E.; Hazari, N.; Labinger, J. A. *Organometallics* **2009**, *28*, 5489.
30. Ahmed, T. S.; Tonics, I. A.; Labinger, J. A.; Bercaw, J. E. *Organometallics* **2013**, *32*, 3322.
31. Lohr, T. L.; Piers, W. E.; Parvez, M. *Chem. Sci.* **2013**, *4*, 770.
32. Bolaño, T. B. *Unpublished Results* **2011**.
33. Webb, J. R.; Figg, T. M.; Otten, B. M.; Cundari, T. R.; Gunnoe, T. B.; Sabat, M. *Eur. J. Inorg. Chem.* **2013**, *2013*, 4515.
34. Webb, J. R.; Munro-Leighton, C.; Pierpont, A. W.; Gurkin, J. T.; Gunnoe, T. B.; Cundari, T. R.; Sabat, M.; Petersen, J. L.; Boyle, P. D. *Inorg. Chem.* **2011**, *50*, 4195.

35. Inoki, D.; Matsumoto, T.; Hayashi, H.; Takashita, K.; Nakai, H.; Ogo, S. *Dalton Trans.* **2012**, *41*, 4328.
36. Kim, M. Y.; Seok, W. K.; Lee, H. N.; Han, S. H.; Dong, Y. K.; Yun, H. Z. *Naturforsch., B: Chem. Sci.* **2001**, *56*, 747.
37. Conner, D.; Jayaprakash, K. N.; Gunnoe, T. B.; Boyle, P. D. *Inorg. Chem.* **2002**, *41*, 3042.
38. Periana, R. A.; Taube, D. J.; Evitt, E. R.; Loffler, D. G.; Wentreck, P. R.; Voss, G.; Masuda, T. *Science* **1993**, *259*, 340.
39. Periana, R. A.; Taube, D. J.; Gamble, S.; Taube, H.; Satoh, T.; Fuji, H. *Science* **1998**, *280*, 560.
40. Ahlquist, M.; Periana, R. A.; Goddard, W. A. *Chem. Commun.* **2009**, 2373.
41. Bischof, S. M.; Ess, D. H.; Meier, S. K.; Oxgaard, J.; Nielsen, R. J.; Bhalla, G.; Goddard, W. A.; Periana, R. A. *Organometallics* **2010**, *29*, 742.
42. Hickman, A. J.; Villalobos, J. M.; Sanford, M. S. *Organometallics* **2009**, *28*, 5316.
43. Rhinehart, J. L.; Manbeck, K. A.; Buzak, S. K.; Lippa, G. M.; Brennessel, W. W.; Goldberg, K. I.; Jones, W. D. *Organometallics* **2012**, *31*, 1943.
44. Hashiguchi, B. G.; Konnick, M. M.; Bischof, S. M.; Gustafson, S. J.; Devarajan, D.; Gunsalus, N.; Ess, D. H.; Periana, R. A. *Science* **2014**, *343*, 1232.
45. Bolinger, C. M.; Story, N.; Sullivan, B. P.; Meyer, T. J. *Inorg. Chem.* **1988**, *27*, 4582.

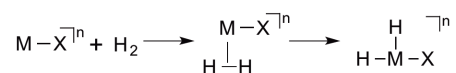
46. Burgess, S. A.; Devarajan, D.; Bolaño, T.; Ess, D. H.; Gunnoe, T. B.; Sabat, M.; Myers, W. H. *Inorg. Chem.* **2014**, *53*, 5328.

### 3 1,2-Addition of Dihydrogen Across Rh(III)–OMe Bonds

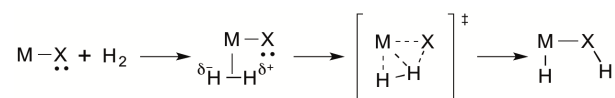
#### 3.1 Introduction

The activation of covalent bonds (*e.g.*, H–H, Si–H and C–H bonds) is relevant to the development of catalytic reactions using dihydrogen, silanes and hydrocarbons. For example, catalytic hydrogenations are among the most versatile and important synthetic processes.<sup>1,2,3</sup> Wilkinson's catalyst, RhCl(PPh<sub>3</sub>)<sub>3</sub>, is used to hydrogenate alkenes to alkanes.<sup>2</sup> In 2001, the Nobel Prize in chemistry was awarded to William S. Knowles and Ryoji Noyori for their work on enantioselective hydrogenation, a reaction that the chemical industry heavily relies to set the stereochemistry of tertiary stereocenters.<sup>2</sup>

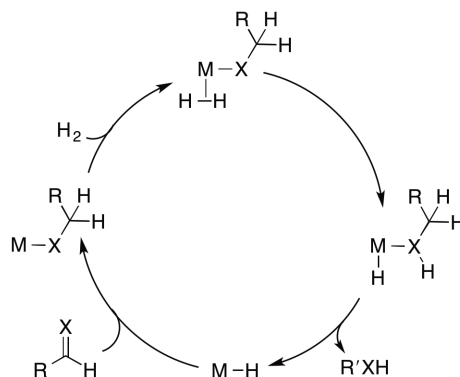
For transition metal catalyzed hydrogenation reactions, the dihydrogen activation step usually occurs by oxidative addition to the metal to form a bis-hydride complex (Scheme 3.1) or by 1,2-addition across a M–X (X = OR, NR<sub>2</sub>, SR, etc.) bond to produce (H)M–X(H). The latter reaction is often considered a heterolytic cleavage with formal transfer of a proton to the ligand X and transfer of a hydride to the metal (Scheme 3.2). Heterolytic cleavage of dihydrogen is likely involved in hydrogenations of aldehydes, ketones and imines and in the generation of Stryker's reagent (Scheme 3.3).<sup>4,5,6</sup> Furthermore, net dihydrogen addition across M–OR bonds could play a role in deoxygenation of biomass (or compounds that model biomass) via hydrogenolysis of ethers (Scheme 3.4).<sup>7,8</sup>



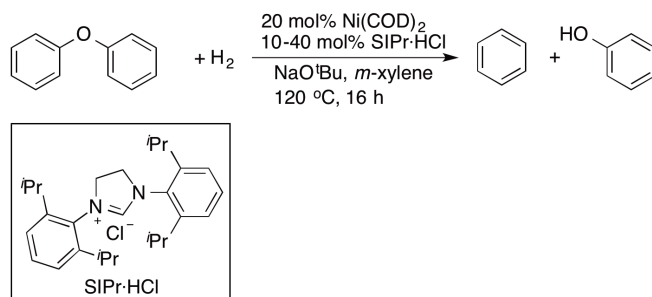
**Scheme 3.1.** The oxidative addition of dihydrogen across M–X (X = OR, NR<sub>2</sub> or SR) bonds.



**Scheme 3.2.** The 1,2-addition of dihydrogen across M–X (X = OR, NR<sub>2</sub> or SR) bonds.



**Scheme 3.3.** Mechanism for metal mediated heterolytic cleavage of H<sub>2</sub> in the hydrogenation of aldehydes, ketone and imines. (X = O, N).



**Scheme 3.4.** A reported example of hydrogenolysis of diaryl ethers.<sup>7</sup>

Examples of stoichiometric dihydrogen or related C–H activations by d<sup>6</sup> hydroxide and amido complexes have been reported (Figure 3.1). For example, d<sup>6</sup> complexes have been demonstrated to activate dihydrogen and/or arene C–H bonds.<sup>9-10,11,12</sup> More specifically, the Ru(II) complexes RuCl(PPh<sub>3</sub>)[κ<sup>3</sup>-N(SiMe<sub>2</sub>PPh<sub>2</sub>)<sub>2</sub>]<sup>9</sup> and *trans*-RuH<sub>2</sub>(diphosphine)(tmen)<sup>13</sup> (where diphosphine = *R*- or *S*-binap and tmen = NHCMe<sub>2</sub>CMe<sub>2</sub>NH<sub>2</sub>) both activate H<sub>2</sub>. Additionally, our group has reported that (PCP)Ru(CO)(NH<sub>2</sub>) [PCP = 2,6-(CH<sub>2</sub>P<sup>t</sup>Bu)<sub>2</sub>C<sub>6</sub>H<sub>3</sub>, R = H, CH<sub>3</sub>] adds H<sub>2</sub> across the Ru–NH<sub>2</sub> bond to form (PCP)Ru(CO)(H) and free ammonia

(Figure 3.1).<sup>14</sup> H/D exchange between the hydroxide or anilido ligand of  $\text{TpRu}(\text{PMe}_3)_2\text{X}$  ( $\text{X} = \text{OH}, \text{NHPh}$ ;  $\text{Tp} = \text{hydridotris}(\text{pyrazolyl})\text{borate}$ ) and  $\text{C}_6\text{D}_6$  was observed upon heating (80 to 130 °C).<sup>15,16,17</sup> Additionally, Periana, Goddard and coworkers have reported an Ir(III) methoxide complex  $(\text{acac})_2\text{Ir}(\text{OMe})(\text{L})$  ( $\text{acac} = \kappa^2\text{-O,O-acetylacetonate}$ ,  $\text{L} = \text{pyridine}$  or  $\text{CH}_3\text{OH}$ ) that performs stoichiometric benzene C–H activation.

Complexes with  $d^8$  configurations have also been shown to perform stoichiometric activation of H–H and in some cases, C–H bonds. Goldberg, Kemp and co-workers have reported dihydrogen activation by the  $d^8$  Pd(II) complexes  $(\text{PCP})\text{Pd}(\text{OR})$  ( $\text{PCP} = 2,6\text{-}(\text{CH}_2\text{PBU}_2)_2\text{C}_6\text{H}_3$ ;  $\text{R} = \text{OH}, \text{CH}_3$ )<sup>18,19</sup> and benzene C–H activation by  $d^8$  Rh(I) complexes  $(\text{PNP})\text{Rh}(\text{X})$  ( $\text{PNP} = 2,6\text{-di-tert-butylphosphinomethylpyridine}$ ;  $\text{X} = \text{OR}, \text{OCH}_2\text{CF}_3$ ).<sup>20,21</sup> Furthermore, the Ir(I) and Rh(I) complexes  $[(\kappa^4\text{-COD})\text{M}(\mu\text{-OH})]_2$  ( $\text{M} = \text{Rh}, \text{Ir}$ ;  $\text{COD} = 1,5\text{-cyclooctadiene}$ ) activate C–H bonds of indene to give  $[(\text{COD})\text{Rh}(\eta^3\text{-indenyl})]$ .<sup>22,23</sup> Examples of both H–H activation and C–H activation across  $d^8$  Pt(II)–X bonds accelerated by Pt(0) particles are also known. We reported that the net addition of H–H across the Pt–NHPh bond of  $[(^t\text{bpy})\text{Pt}(\text{Me})(\text{NHPh})]$  is catalyzed by Pt(s).<sup>24</sup> Piers and co-workers reported benzene C–H addition across the Pt(II)–OH bonds of  $(\text{BIAN})\text{Pt}(\text{OH})_2$  ( $\text{BIAN} = \text{bis}(3,5\text{-bis}(2,6\text{-diisopropylphenyl})\text{benzene})\text{-acenaphthenequinonediimine}$ ), which is also accelerated by *in situ* generated Pt(0) particles.<sup>25</sup>

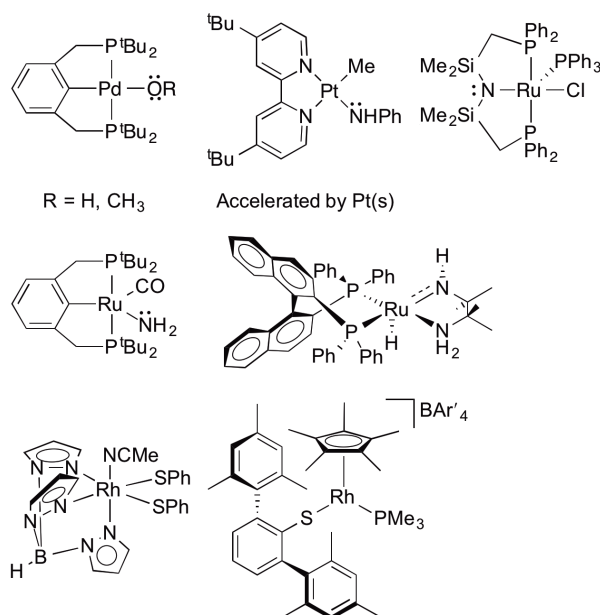


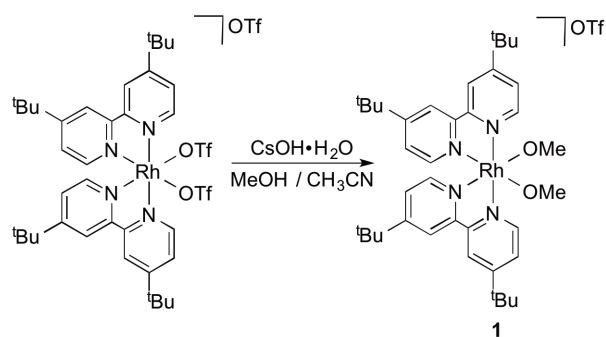
**Figure 3.1.** Transition metal heteroatom complexes that have been reported to mediate dihydrogen activation.

The half sandwich complexes  $[\text{Cp}^*\text{M}(\text{PMe}_3)(\text{SDmp})][\text{BAR}'_4]$  ( $\text{M} = \text{Rh}, \text{Ir}$ ;  $\text{Dmp} = 2,6$ -(mesityl)<sub>2</sub>C<sub>6</sub>H<sub>3</sub>;  $\text{BAR}'_4 = \text{tetrakis}[(3,5\text{-trifluoromethyl})\text{phenyl}]\text{borate}$ ) mediate heterolysis of dihydrogen to form  $[\text{Cp}^*\text{Rh}(\text{PMe}_3)(\text{H})(\text{HSDmp})][\text{BAR}'_4]$ , which hydrogenates benzaldehyde, *N*-benzylideneaniline and cyclohexanone.<sup>26</sup> The heterolytic activation of dihydrogen by  $[\text{Tp}^{\text{Me}2}\text{Rh}(\text{SPh})_2(\text{NCMe})]$  ( $\text{Tp}^{\text{Me}2} = \text{hydrotris}(3,5\text{-dimethylpyrazoyl})\text{borate}$ ) to form  $\text{Tp}^{\text{Me}2}\text{Rh}(\text{H})(\text{SPh})(\text{NCMe})$  and PhSH has been reported.<sup>27,28</sup> In the presence of an amine base, the dithiolate complex  $\text{Tp}^{\text{Me}2}\text{Rh}(\text{bdt})(\text{NCMe})$  ( $\text{bdt} = 1,2\text{-C}_6\text{H}_4\text{S}_2$ ) reacts with H<sub>2</sub> to form  $[\text{Tp}^{\text{Me}2}\text{Rh}(\text{H})(\text{bdt})]^-$  and ammonium cations.<sup>27</sup> The dithiolate complex also serves as a chemoselective catalysis for the hydrogenation of imines.<sup>28</sup> We sought a robust Rh(III) complex supported by *N*-based ligands to study dihydrogen addition across Rh(III)–OR

bonds. Herein, we report the preparation of  $[(^t\text{bpy})_2\text{Rh}(\text{OMe})_2]^+$  and its use as a precursor for heterolytic dihydrogen activation across a Rh(III)–OMe bond.<sup>29</sup>

### 3.2 Results and Discussion

The reaction of  $[(^t\text{bpy})_2\text{Rh}(\text{OTf})_2][\text{OTf}]$  in  $\text{CH}_3\text{CN}$  with 2.5 equiv of  $\text{CsOH}\cdot\text{H}_2\text{O}$  in MeOH at room temperature produces  $[(^t\text{bpy})_2\text{Rh}(\text{OMe})_2][\text{OTf}]$  (**1**) in 90% isolated yield (Scheme 3.5). The  $^1\text{H}$  NMR spectrum of **1** shows six  $^t\text{bpy}$  aromatic resonances, two  $^t\text{Bu}$  singlets and one methoxide resonance (2.6 ppm), which is consistent with the expected  $\text{C}_2$  symmetry (Figure 3.2). A metathesis reaction of  $[(^t\text{bpy})_2\text{Rh}(\text{OMe})_2]\text{Cl}$  with  $\text{NaBAR}'_4$  leads to the formation of  $[(^t\text{bpy})_2\text{Rh}(\text{OMe})_2]\text{BAR}'_4$  (**2**). A crystal of complex **2** suitable for an X-ray diffraction study was obtained (Figure 3.3). The structure of **2** confirms the expected pseudo-octahedral coordination sphere. The Rh–O1 and Rh–O2 bond lengths are 2.003(2) Å and 2.002(2) Å, respectively. These are in close agreement with  $[(\text{bpy})_2\text{Rh}(\text{OMe})_2]\text{PF}_6$  [2.011(2) Å and 2.010(2) Å] and within the limits of uncertainty for the Rh–O bond distance of  $[(^t\text{bpy})_2\text{Rh}(\text{OMe})(\text{Cl})]\text{Cl}$  [2.324(2) Å] (see Chapter 2). The Rh–O1–C1 bond angles of **2** are 117.8(2)° and 117.2(2)° and are smaller than those of  $[(\text{bpy})_2\text{Rh}(\text{OMe})_2]\text{PF}_6$  [121.3(2)° and 119.2(2)°] (See Chapter 2). The Rh–O–C bond angle for  $[(^t\text{bpy})_2\text{Rh}(\text{OMe})(\text{Cl})]\text{Cl}$  is 118.0(2)°, which is similar in magnitude to those of  $[(^t\text{bpy})_2\text{Rh}(\text{OMe})_2]\text{BAR}'_4$  [117.8(2)° and 117.2(2)°] (see Chapter 2).



**Scheme 3.5.** Synthesis of  $[(^t\text{Bu})_2\text{bpy}]_2\text{Rh}(\text{OMe})_2\text{OTf}$  (**1**).

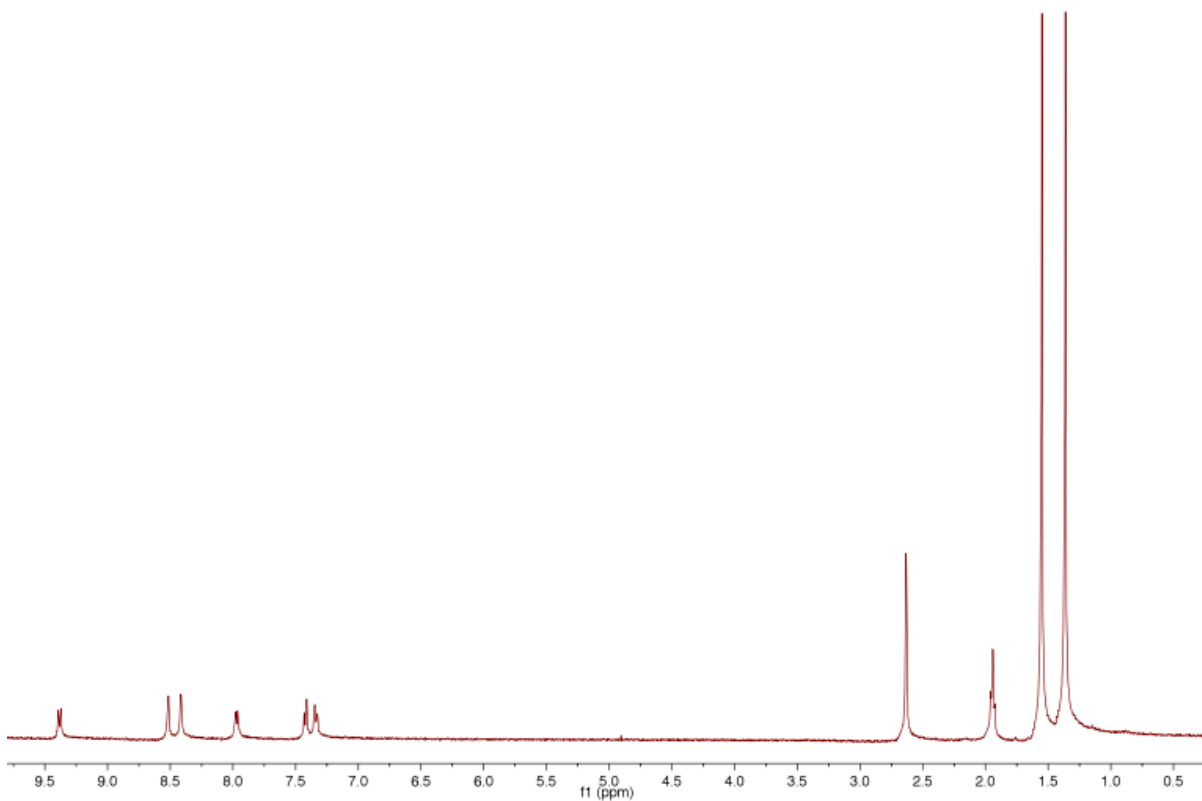


**Figure 3.2.**  $^1\text{H}$  NMR spectrum of  $[(^t\text{Bu})_2\text{bpy}]_2\text{Rh}(\text{OMe})_2\text{OTf}$  (**1**) in  $\text{CD}_3\text{CN}$ .

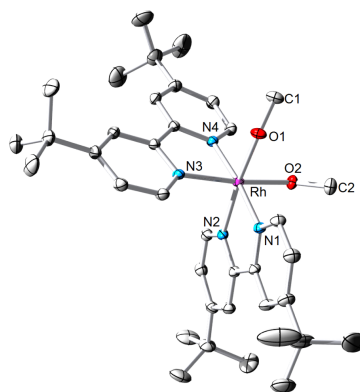
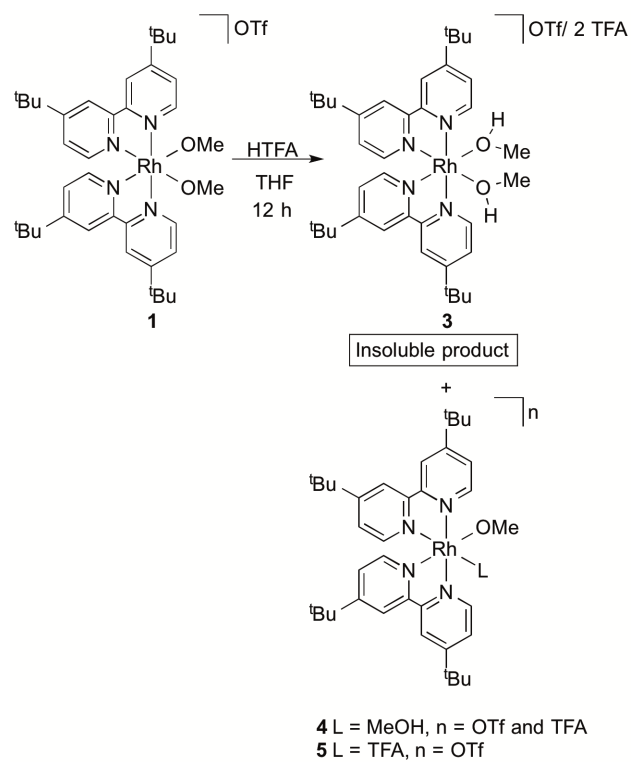


**Figure 3.3.** ORTEP diagram (50% probability) of  $[(^4\text{bpy})_2\text{Rh}(\text{OMe})_2]\text{BARf}_4$  (**2**). Counterions and hydrogen atoms omitted for clarity. Selected bond lengths (Å): Rh–N1, 2.048(2); Rh–N2, 2.017(2); Rh–N3, 2.049(2); Rh–N4, 2.022(2); Rh–O1, 2.003(2); Rh–O2, 2.002(2), O1–C1, 1.396(3); O2–C2, 1.402(3). Selected bond angles (°): Rh–O1–C1, 117.8(2); Rh–O2–C2, 117.2(2); N4–Rh–N3, 96.84(9); O1–Rh–O2, 91.73(8); N1–Rh–N2, 79.68(9); N1–Rh–N4, 95.97(8), N2–Rh–N3, 96.84(9).

The addition of one equivalent of HTFA (trifluoroacetic acid) to a suspension of complex **1** in THF results in a homogeneous solution (Scheme 3.6). After stirring for 12 h at room temperature,  $[(^4\text{bpy})_2\text{Rh}(\text{MeOH})_2][\text{OTf}][\text{TFA}]_2$  (**3**) precipitates from solution as a yellow solid. The  $^1\text{H}$  and  $^{13}\text{C}$  NMR spectrum of **3** shows a  $C_2$  symmetric molecule with 6  $^4\text{bpy}$  aryl and  $^t\text{Bu}$  resonances (Figure 3.4). The methanol  $\text{CH}_3$  resonance for complex **3** is observed as a broad singlet at 2.79 ppm in the  $^1\text{H}$  NMR spectrum and at 53.11 ppm in the  $^{13}\text{C}$  NMR spectrum. Two resonances at -77.02 and -80.01 ppm are observed in the  $^{19}\text{F}$  NMR spectrum of  $[(^4\text{bpy})_2\text{Rh}(\text{MeOH})_2][\text{OTf}][\text{TFA}]_2$  for the TFA and OTf counterions respectively.  $^1\text{H}$  NMR analysis of the filtrate after removing **3** by filtration indicates a mixture of the two  $(^4\text{bpy})_2\text{Rh}$  complexes  $[(^4\text{bpy})_2\text{Rh}(\text{OMe})(\text{MeOH})][\text{OTf}][\text{TFA}]$  (**4**) and  $[(^4\text{bpy})_2\text{Rh}(\text{OMe})(\text{TFA})][\text{OTf}]$  (**5**) in an approximate 2:1 ratio (Figure 3.5). The  $^{19}\text{F}$  NMR spectrum of the mixture of **4** and **5** contains a single OTf resonance at -80.1 ppm and two TFA resonances at -77.0 ppm and -77.3 ppm.



**Scheme 3.6.** The reaction of  $[(^t\text{bpy})_2\text{Rh}(\text{OMe})_2][\text{OTf}]$  (**1**) with HTFA (1 equivalent) leads to the formation of three products.

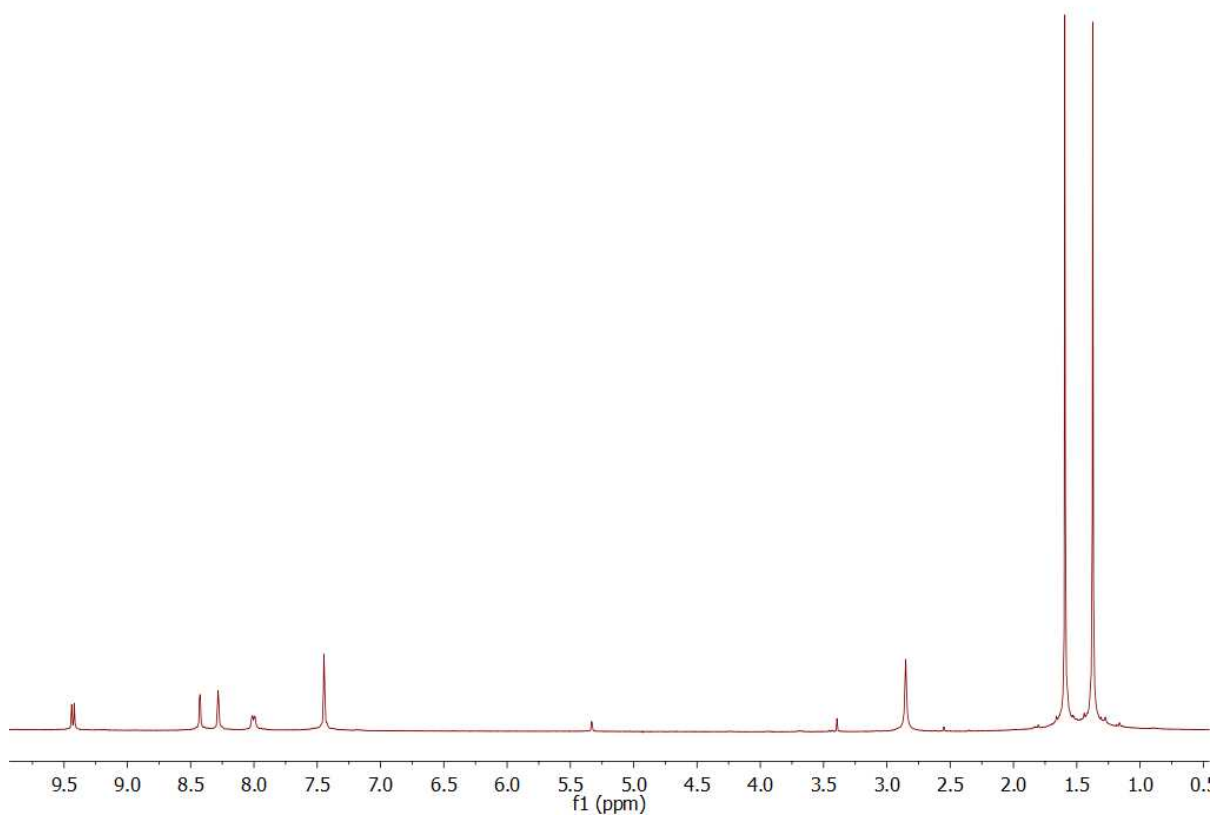


**Figure 3.4.**  $^1\text{H}$  NMR spectrum of  $[(\text{tbpy})_2\text{Rh}(\text{MeOH})_2][\text{OTf}][\text{TFA}]_2$  (**3**) in  $\text{CD}_2\text{Cl}_2$ .

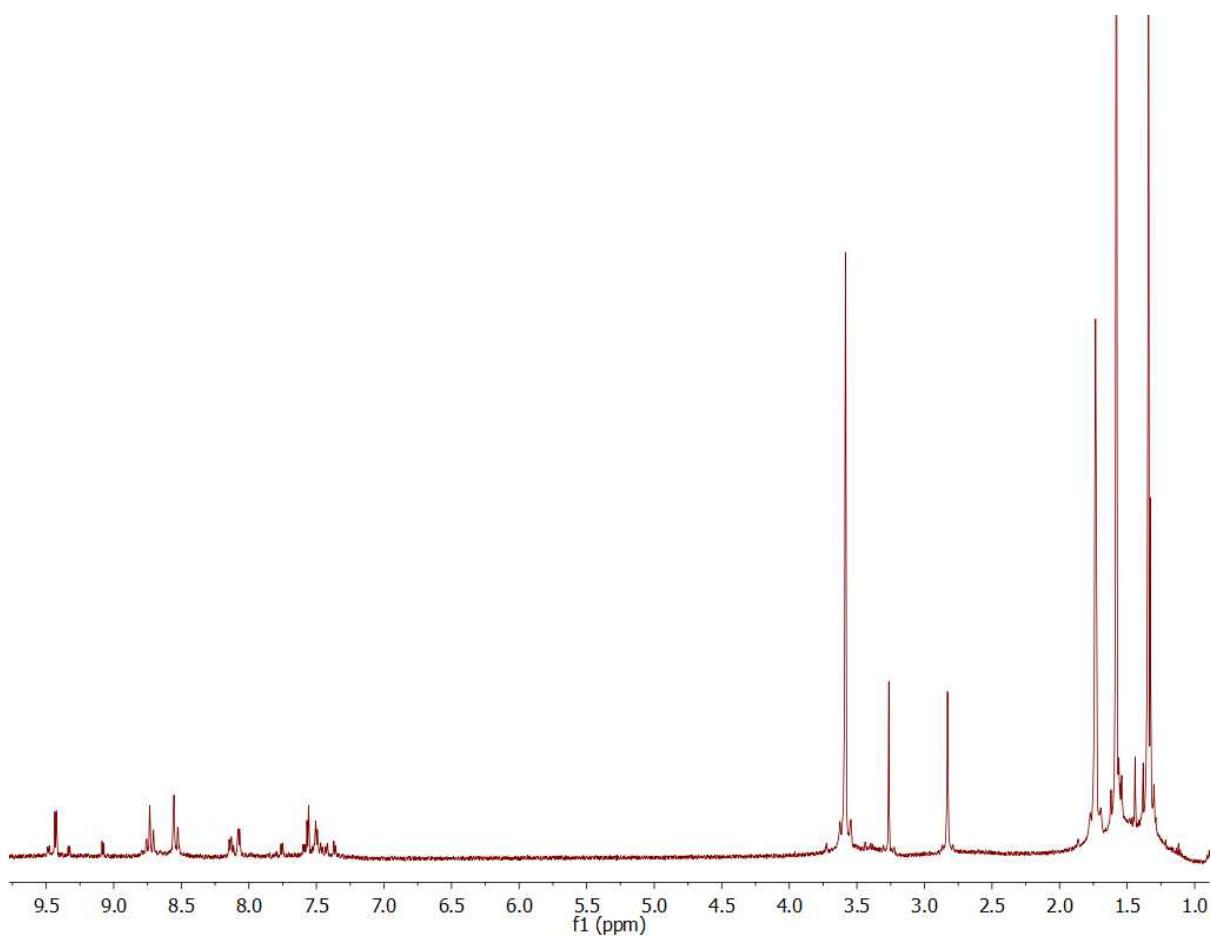


**Figure 3.5.**  $^1\text{H}$  NMR spectrum of soluble protonation products  $[(^t\text{bpy})_2\text{Rh}(\text{OMe})(\text{MeOH})][\text{OTf}][\text{TFA}]$  (**4**) and  $[(^t\text{bpy})_2\text{Rh}(\text{OMe})(\text{TFA})][\text{OTf}]$  (**5**) in  $\text{THF-}d_8$ .

A crystal of complex **4** suitable for an X-ray diffraction study was obtained by layering a methylene chloride solution of complexes **3**, **4** and **5** with pentane (Figure 3.6). The Rh–O bond length of the methoxide ligand (Rh–O1 = 1.994(3) Å) is slightly shorter than that of the methanol ligand (Rh–O2 = 2.062(3) Å), and the O–C bond distance for the methoxide ligand (O1–C1 = 1.396(6) Å) is slightly shorter than the O–C bond distance for the methanol ligand (O2–C2 = 1.427(6) Å). The Rh–O–C bond angles for the methoxide and methanol ligands are 119.4(3)° and 121.0(3)°, respectively. When crystals of **4** are dissolved

in THF- $d_8$ , the  $^1\text{H}$  NMR spectrum shows a mixture of **4** and **5**. This result is consistent with the rapid establishment of an equilibrium between **4** and **5**.

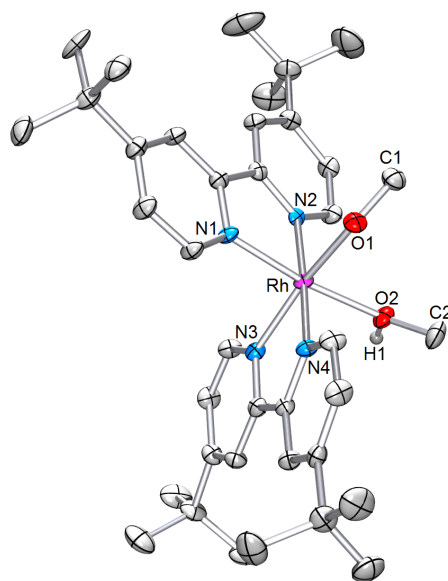
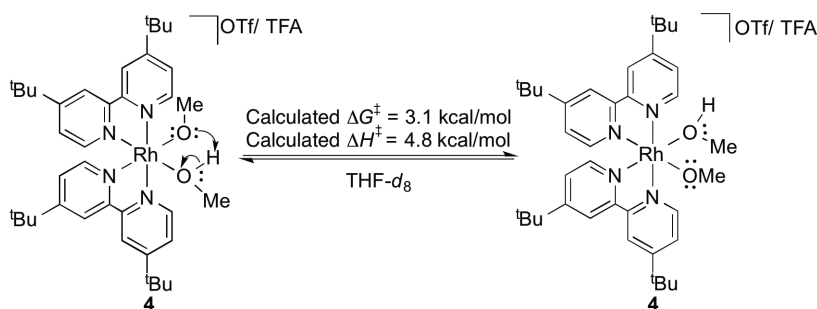


**Figure 3.6.** ORTEP diagram (50% probability) of  $[(^t\text{bpy})_2\text{Rh}(\text{OMe})(\text{MeOH})][\text{OTf}][\text{TFA}]$  (**4**). Counterions and most hydrogen atoms omitted for clarity. Selected bond lengths (Å): Rh–N1, 2.002(4); Rh–N2, 2.026(4); Rh–N3, 2.063(4); Rh–N4, 2.016(4); Rh–O1, 1.994(3); Rh–O2, 2.062(3); O1–C1, 1.396(6); O2–C2, 1.427(6). Selected bond angles (°): Rh–O1–C1, 119.4(3); Rh–O2–C2, 121.0(3); N4–Rh–N3, 79.4(1); O1–Rh–O2, 89.4(1); N1–Rh–N2, 80.2(1); N1–Rh–N4, 97.4(1); N2–Rh–N3, 100.1(1).

The room temperature  $^1\text{H}$  NMR spectrum of  $[(^t\text{bpy})_2\text{Rh}(\text{OMe})(\text{MeOH})][\text{OTf}][\text{TFA}]$  (**4**) contains a single resonance for the methoxide and methanol  $\text{CH}_3$  groups, which is inconsistent with a static asymmetric complex. However, variable temperature NMR spectroscopy revealed a dynamic process that is consistent with rapid proton exchange between the methanol and methoxide ligands. Below room temperature, the sharp singlet at 2.83 ppm assigned to the methoxide and methanol  $\text{CH}_3$  protons in the room temperature  $^1\text{H}$  NMR spectrum broadens (the coalescence temperature is observed  $-46\text{ }^\circ\text{C}$ ) and resolves into two broad resonances at  $\sim 3.0$  ppm and  $\sim 2.7$  ppm, which we assigned as resonances due to the

methoxide and methanol ligands (Figure 3.7). Although a definitive assignment cannot be made, we assume the downfield resonance ( $\sim 3.0$  ppm) is due to the methanol ligand. The slow exchange limit was not reached at  $-94$  °C. The response of the aromatic and  $^t\text{Bu}$  resonances is also consistent with the proposed fluxional process. The six sharp aryl  $^t\text{bpy}$  resonances and the two aliphatic  $^t\text{Bu}$  singlets broadened as the temperature was lowered. The coordinated MeOH ligand of **4** does not exchange with free MeOH on the same timescale. Thus, the fluxional process does not likely involve MeOH dissociation. Instead, we are likely observing an exchange of the OH protons between the MeOH and OMe ligands.

At the coalescence temperature for the intramolecular proton exchange, the rate of exchange ( $k_{\text{obs}}$ ) is equal to  $\pi\Delta\nu/\sqrt{2}$  where  $\Delta\nu$  is the difference in energy between the resonances at slow exchange. Although the slow exchange regime was not reached in variable temperature NMR experiment described above, a low limit on  $\Delta\nu$  can be derived from the data at  $-94$  °C ( $\Delta\nu \geq 165$  Hz). Thus,  $k_{\text{obs}} \geq 366$  Hz for the intramolecular proton exchange. Using the Eyring equation and the rate for proton exchange,  $\Delta G^\ddagger \leq 11$  kcal/mol at the coalescence temperature ( $-46$  °C). DFT calculations indicate a  $\Delta H^\ddagger$  of 3.1 kcal/mol and a  $\Delta G^\ddagger$  of 4.8 kcal/mol (298 K) for the intramolecular proton transfer (Scheme 3.7).



**Scheme 3.7.** Intramolecular proton transfer between the methoxide and methanol ligands of  $[(^t\text{bpy})_2\text{Rh}(\text{OMe})(\text{MeOH})][\text{OTf}][\text{TFA}]$  (**4**).

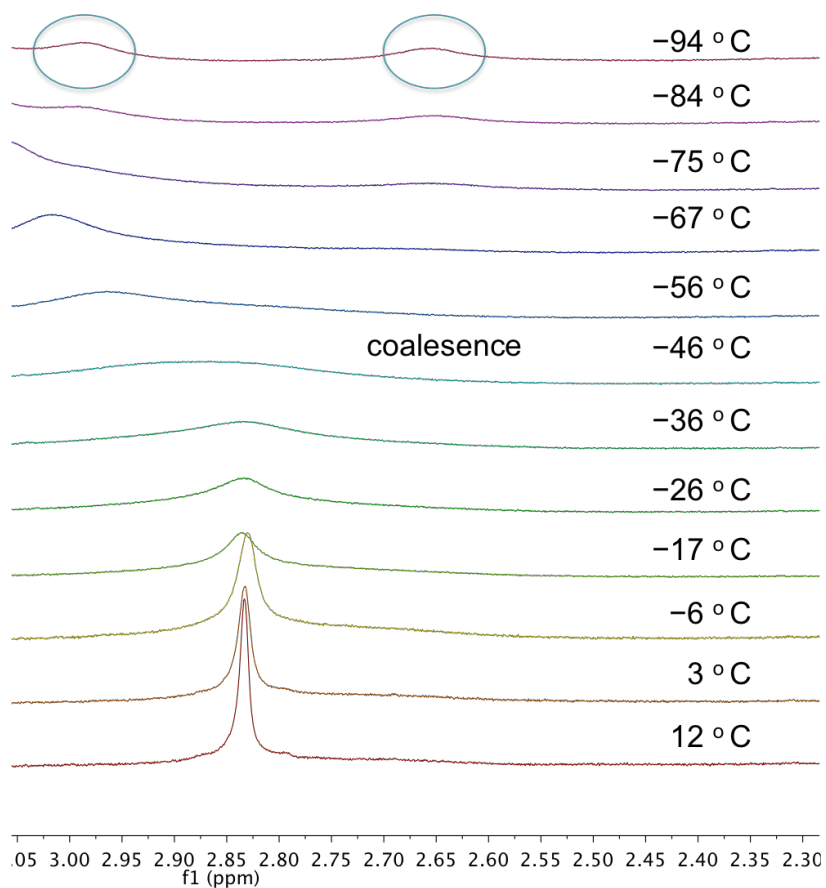


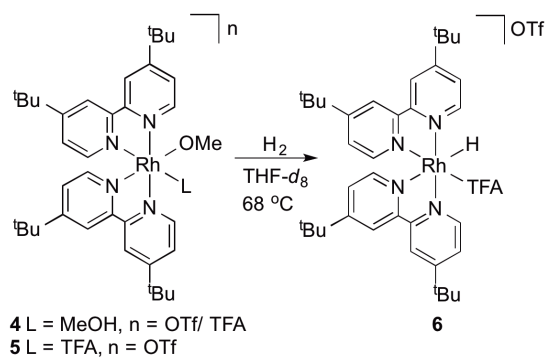
**Figure 3.7.** Stacked  $^1\text{H}$  NMR spectra plot for the variable temperature  $^1\text{H}$  NMR study of  $[(^t\text{bpy})_2\text{Rh}(\text{OMe})(\text{MeOH})][\text{OTf}][\text{TFA}]$  (**4**).

Heating (68 °C) a mixture of complexes **4** and **5** with dihydrogen (15 to 55 psig) produces free MeOH and  $[(^t\text{bpy})_2\text{Rh}(\text{H})(\text{TFA})]^+$  (**6**) (Scheme 3.8). Complex **5** is quickly consumed after pressurizing with dihydrogen and heating to 68 °C. The hydride complex  $[(^t\text{bpy})_2\text{Rh}(\text{H})(\text{TFA})][\text{OTf}]$  (**6**) has been independently synthesized via the oxidative addition of HTFA to the Rh(I) complex  $[(^t\text{bpy})_2\text{Rh}]^+$  (Scheme 3.9). The  $^1\text{H}$  NMR spectrum of **6** contains a characteristic Rh–H doublet at -13.36 ppm (d,  $^1J_{\text{Rh-H}} = 13$  Hz) (Figure 3.8).

Other acids besides HTFA were investigated for the protonation of  $[(^t\text{bpy})_2\text{Rh}(\text{OMe})_2]\text{OTf}$  (**1**) to generate the active species **4** and **5**.  $\text{HBF}_4 \cdot \text{Et}_2\text{O}$  resulted in decomposition to intractable material. Acetic acid was determined to be too weak of an acid and resulted in no reaction.  $\text{HBAr}'_4$  proved to be of adequate strength to form **4** and **5** with  $\text{BAr}'_4$  anion. Subsequent heating of **4** and **5** with  $\text{BAr}'_4$  anion under dihydrogen pressure resulted in the formation of the desired hydride product but also multiple decomposition products.  $\text{HCl}$  was tested but due to the sensitivity of  $[(^t\text{bpy})_2\text{Rh}(\text{H})(\text{TFA})][\text{OTf}]$  to halogens the formation of multiple hydride products was observed (see below).

Under rigorous anaerobic conditions, complex **6** is stable in  $\text{THF-}d_8$ . However, over a period of several hours at room temperature without rigorous protection from air, complex **6** decomposes to  $[(^t\text{bpy})_3\text{Rh}]^{3+}$  and unknown products. In addition, the hydride complex **6** is sensitive to halide sources. Failure to remove residual  $\text{CH}_2\text{Cl}_2$  from the synthesis of  $[(^t\text{bpy})_2\text{Rh}(\text{OMe})_2][\text{OTf}]$  results in the reaction of **6** with  $\text{CH}_2\text{Cl}_2$  to produce  $[(^t\text{bpy})_2\text{Rh}(\text{H})(\text{Cl})]^+$ . The hydride resonance of  $[(^t\text{bpy})_2\text{Rh}(\text{H})(\text{Cl})][\text{TFA}]$  (**7**) is observed at -14.42 ppm (d,  $^1J_{\text{Rh-H}} = 12$  Hz) (Figure 3.9).  $[(^t\text{bpy})_2\text{Rh}(\text{H})(\text{Cl})][\text{TFA}]$  has been independently synthesized by the oxidative addition of  $\text{HCl}$  to  $[(^t\text{bpy})_2\text{Rh}][\text{TFA}]$  (Scheme 3.9). When  $[(^t\text{bpy})_2\text{Rh}(\text{H})(\text{TFA})][\text{OTf}]$  is dissolved in THF and  $\text{CH}_2\text{Cl}_2$  (~5 equiv) is added, pressurized with dihydrogen (25 psig) and heated at 70 °C for 24 h complete conversion to  $[(^t\text{bpy})_2\text{Rh}(\text{Cl})_2][\text{TFA}]$  (**8**) is observed (Scheme 3.10). Also, the hydride complex **6** reacts (6.5 h, 70 °C) with excess  $\text{CH}_2\text{Br}_2$  (19 equiv) to generate  $[(^t\text{bpy})_2\text{Rh}(\text{Br})_2][\text{TFA}]$  (**9**). The identity of **9** has been confirmed by independent synthesis (Scheme 3.11). The  $^1\text{H}$  NMR

spectra for complex **8** and **9** are consistent with  $C_2$  symmetric complexes with 6 <sup>t</sup>Bu aryl resonances and two <sup>t</sup>Bu aliphatic singlets (Figure 3.10 and Figure 3.11).



**Scheme 3.8.** The reaction of complexes **4** and **5** ultimately leads to the formation of  $[(^t\text{bpy})_2\text{Rh}(\text{H})(\text{TFA})][\text{OTf}]$  (**6**).

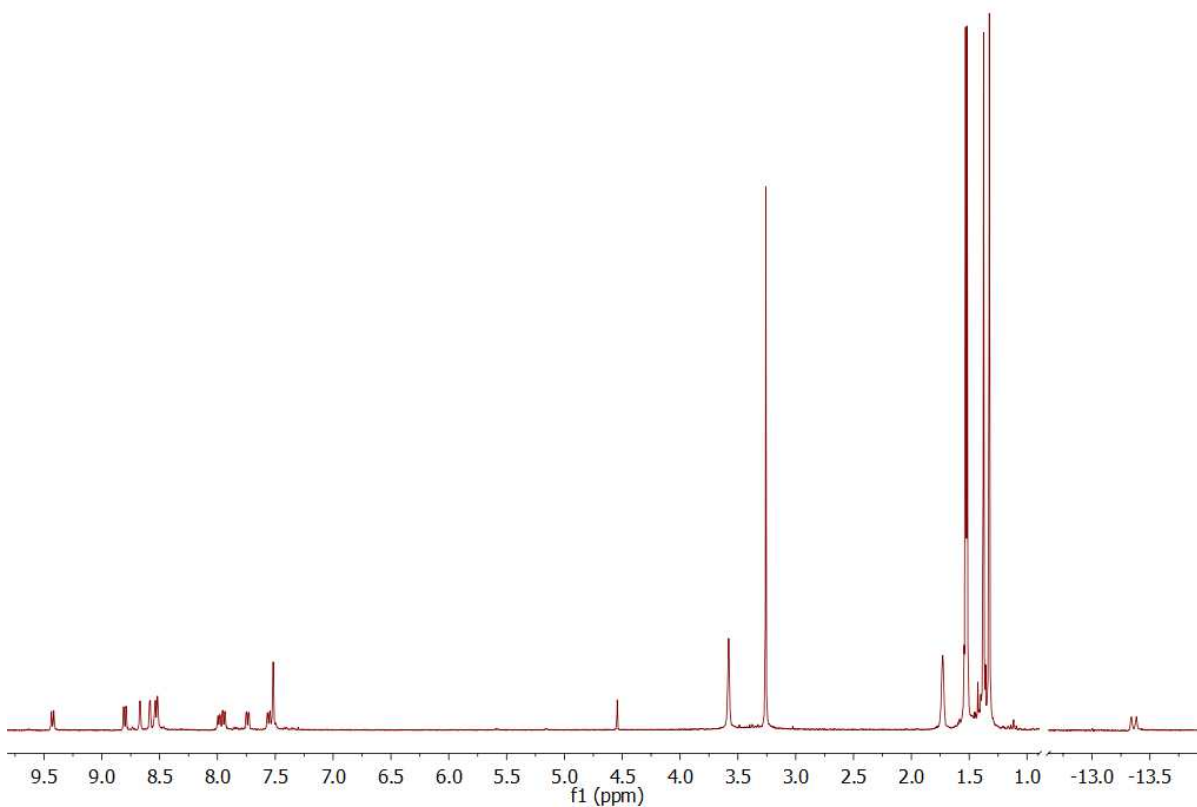
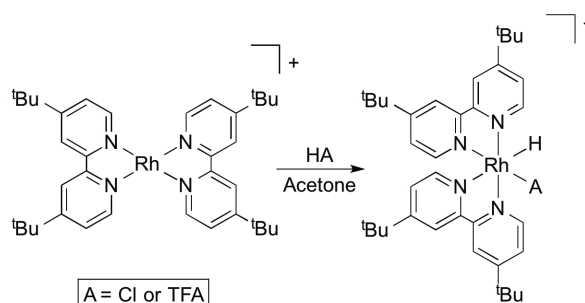
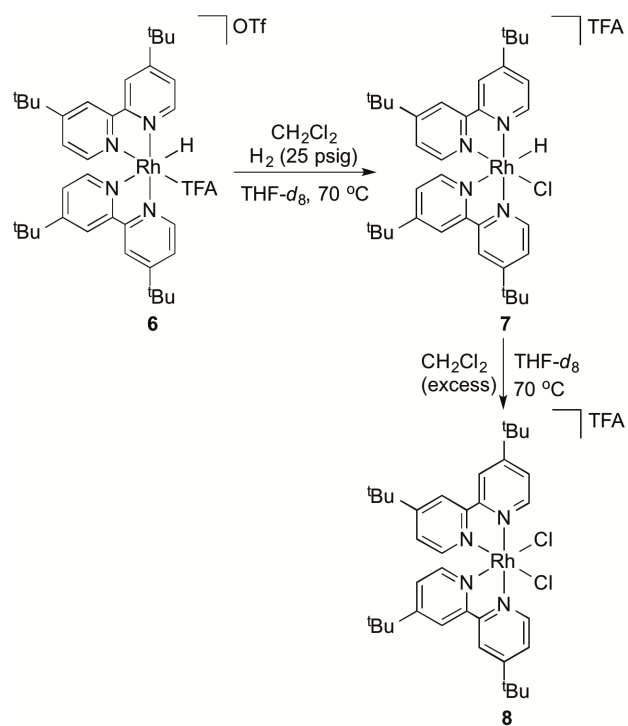


**Figure 3.8**  $^1\text{H}$  NMR spectrum of  $[(\text{tbpy})_2\text{Rh}(\text{H})(\text{TFA})][\text{OTf}]$  (**6**) in  $\text{THF-}d_8$ . The resonance at 4.54 ppm corresponds to  $\text{H}_2$ . Free MeOH is observed at 3.26 ppm. The hydride resonance is shifted upfield to  $-13.36$  (d,  $^1J_{\text{Rh-H}} = 12.8$  Hz).



**Scheme 3.9.** The oxidative addition of HTFA or HCl to the Rh(I) complexes  $[(\text{tbpy})_2\text{Rh}]^+$  gives the hydride complexes  $[(\text{tbpy})_2\text{Rh}(\text{H})(\text{TFA})]^+$  and  $[(\text{tbpy})_2\text{Rh}(\text{H})(\text{Cl})]^+$  respectively.



**Scheme 3.10.** The reaction of  $[(^t\text{bpy})_2\text{Rh}(\text{H})(\text{TFA})][\text{OTf}]$  (**6**) with  $\text{CH}_2\text{Cl}_2$  leads to the formation of a second hydride species,  $[(^t\text{bpy})_2\text{Rh}(\text{H})(\text{Cl})][\text{TFA}]$  (**7**), and excess  $\text{CH}_2\text{Cl}_2$  leads to the formation of  $[(^t\text{bpy})_2\text{Rh}(\text{Cl})_2][\text{TFA}]$  (**8**). The reaction is performed in the presence of  $\text{H}_2$  to suppress decomposition of complex **6**.

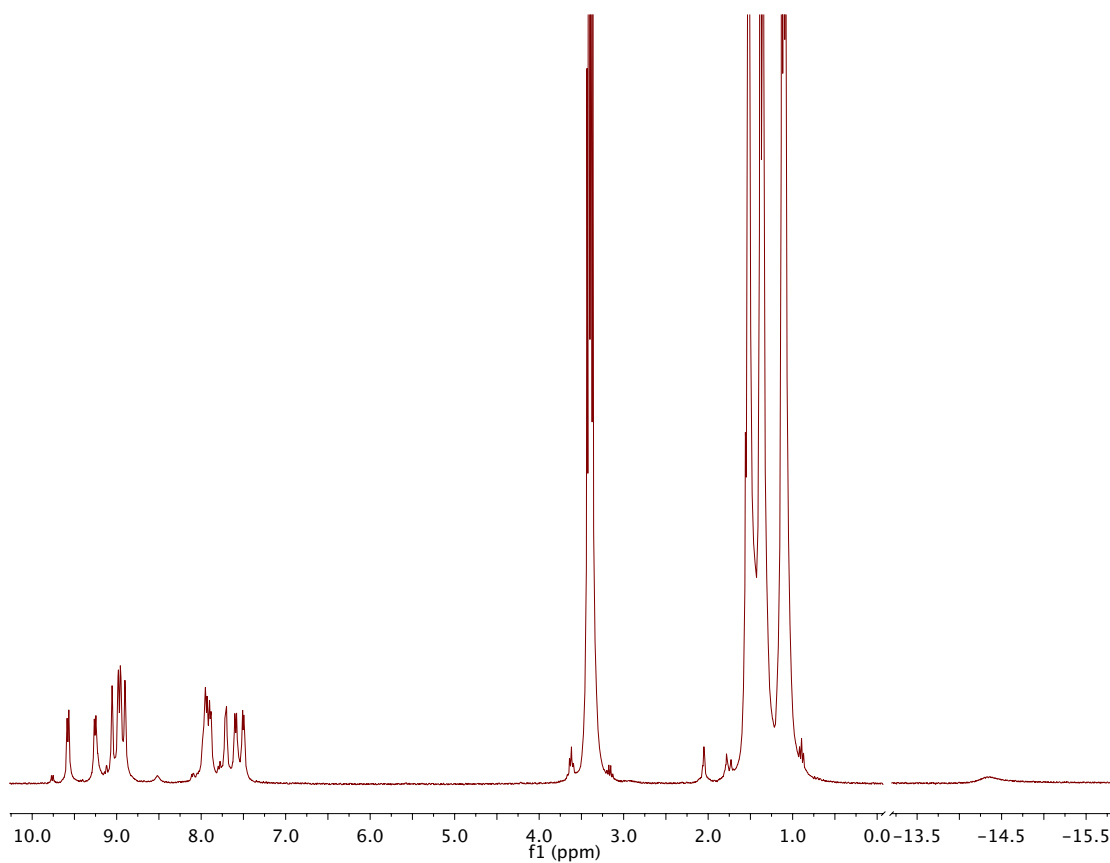


**Figure 3.9.** <sup>1</sup>H NMR spectrum of [(<sup>t</sup>bpy)<sub>2</sub>Rh(H)(Cl)][TFA] (**7**) in acetone-*d*<sub>6</sub> with the baseline cropped between -0.40 to -13.20 ppm. The quartet at 3.40 ppm and triplet at 1.11 ppm correspond to diethyl ether (HCl used in the synthesis of **7** was a 1 N solution in Et<sub>2</sub>O).

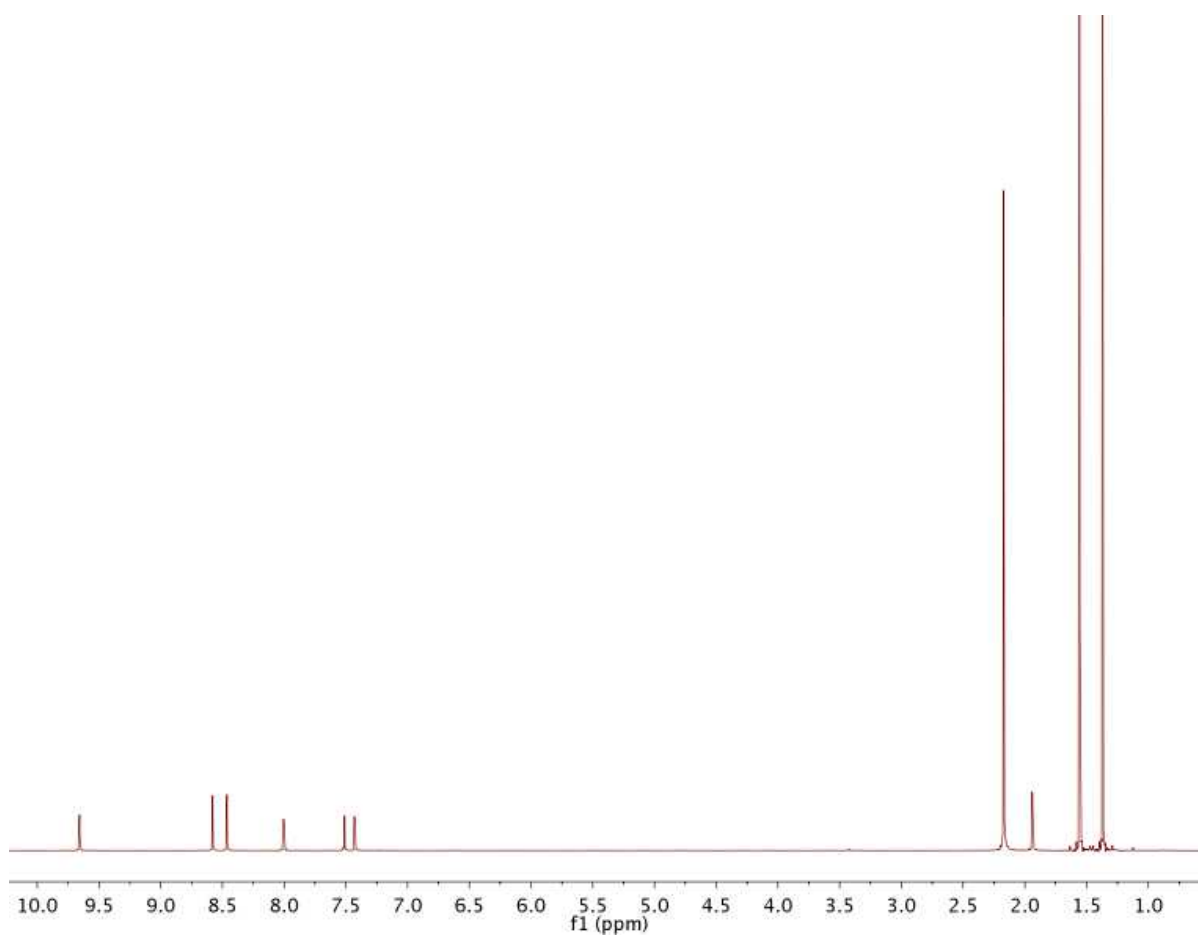
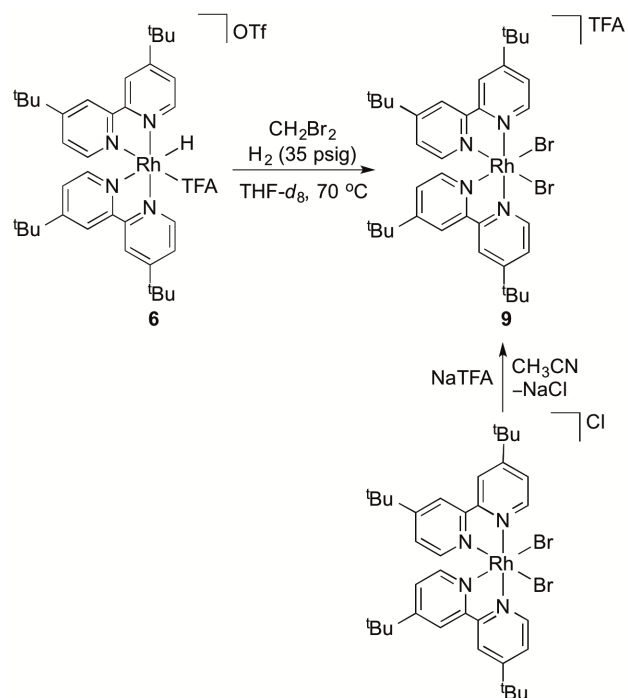


**Figure 3.10.** <sup>1</sup>H NMR spectrum of [(bpy)<sub>2</sub>Rh(Cl)<sub>2</sub>][TFA] (**8**) in CD<sub>3</sub>CN.



**Scheme 3.11.** The reaction of  $[(^t\text{bpy})_2\text{Rh}(\text{H})(\text{TFA})][\text{OTf}]$  (**6**) with excess  $\text{CH}_2\text{Br}_2$  leads to the formation of  $[(^t\text{bpy})_2\text{Rh}(\text{Br})_2][\text{TFA}]$  (**9**) without observation of an intermediate hydride species. The reaction is performed in the presence of  $\text{H}_2$  to suppress decomposition of complex **6**.

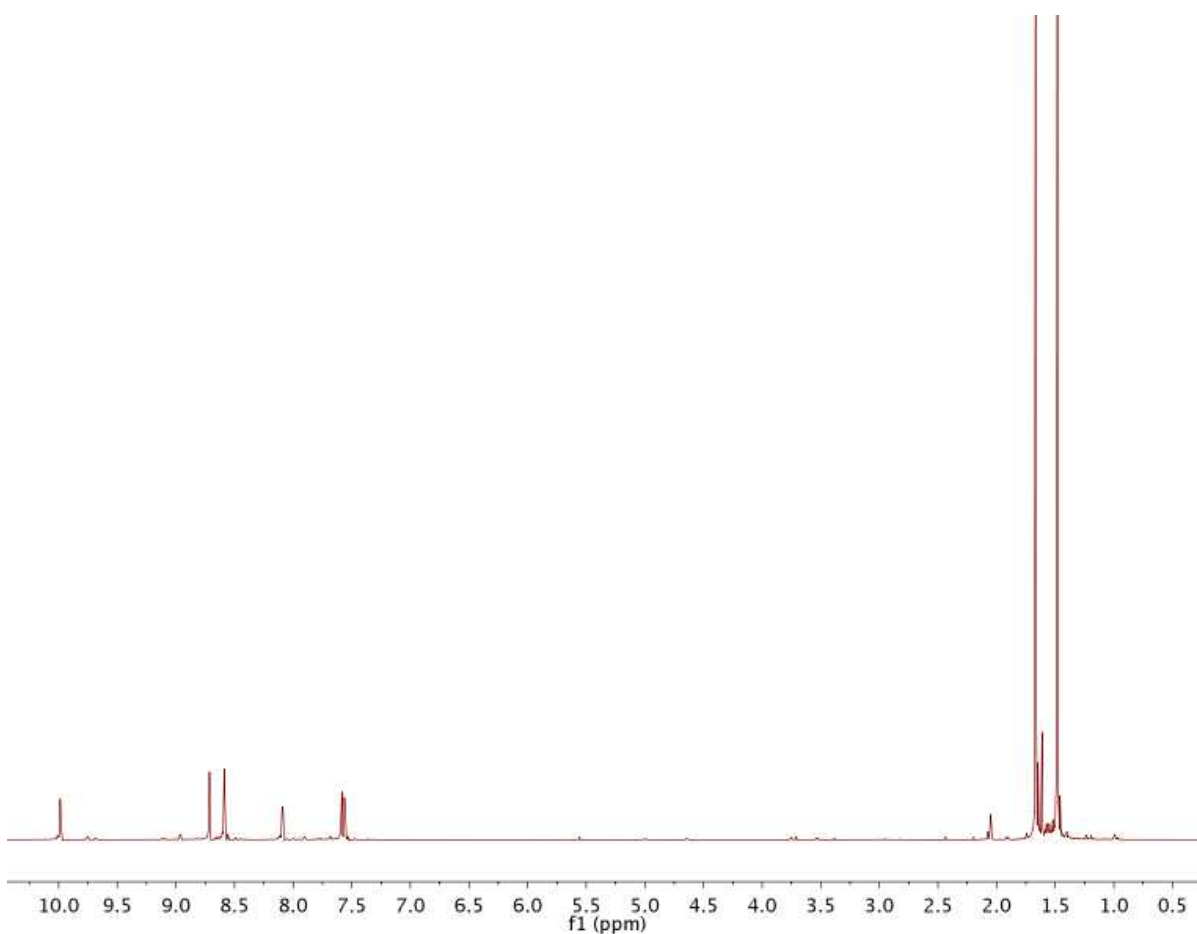


**Figure 3.11.**  $^1\text{H}$  NMR spectrum of  $[(\text{bpy})_2\text{Rh}(\text{Br})_2][\text{TFA}]$  (**9**) in  $\text{CD}_3\text{CN}$ .

$^1\text{H}$  NMR spectroscopy was used to monitor the reaction of **4** and **5** with hydrogen over a range of hydrogen pressures (15, 30, 45 and 55 psig). Unless otherwise noted, all kinetic experiments were performed at least in triplicate. Intermediates were not observed. Representative kinetic plots of concentration of Rh starting material versus time are shown in Figure 3.12. The range of initial hydrogen concentrations is  $6.3 \times 10^{-3}$  M (15 psig) to  $1.8 \times 10^{-2}$  M (55 psig), which gives an approximate 2.9-fold change in initial concentration from 15 psig to 55 psig. The dependence of rate of dihydrogen activation using complexes **4** and **5** on hydrogen concentration is not definitive. Two observations are consistent with a process

that is zero-order in dihydrogen and first-order in Rh complex. First, good fits ( $R^2 = 0.96$  to  $0.99$ ) for a first-order exponential decay are obtained as well as natural log plots (Table 3.1, Figure 3.12, Figure 3.13). Second, within deviations of the experiments, the rates of reaction show little dependence on concentration of dihydrogen between 15 and 45 psi (Figure 3.12 and Table 3.1). However,  $k_{\text{obs}}$  values (taken from first-order fits) indicate that the rate of reaction increases by a factor of  $\sim 1.5$  with a 2.9-fold increase in initial hydrogen concentration (comparing the results using 15 psig to 55 psig). Thus, the kinetic data point to a dependence on hydrogen concentration that is intermediate between zero- and first-order (see below). A Hg poisoning test was performed to test for possible formation of Rh nanoparticles,<sup>30</sup> but the rate of disappearance of complexes **4** and **5** was not significantly altered in the presence of Hg.

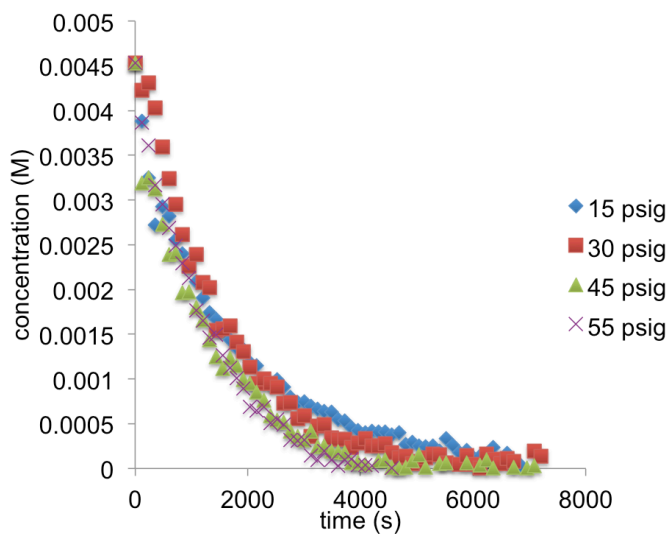


**Figure 3.12.** Disappearance of starting material (complexes **4** and **5**) under variable pressure of dihydrogen.

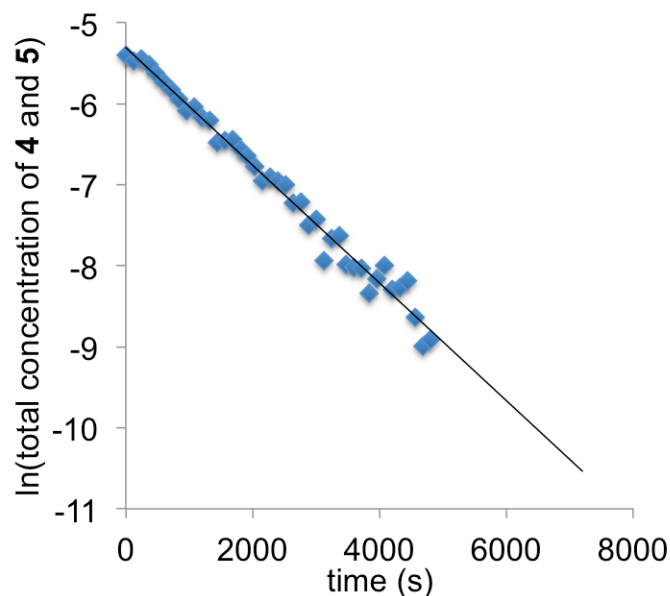


**Figure 3.13.** Representative plot of  $\ln$  of total starting material (complexes **4** and **5**) versus time under 30 psig dihydrogen ( $R^2 = 0.98$ ).

**Table 3.1.** Average  $k_{\text{obs}}$  from the first-order fits to kinetic plots for the reaction of **4** and **5** with  $\text{H}_2$  at 68 °C (see Figure 3.12).

psig $\text{H}_2$	$k_{\text{obs}} (\text{s}^{-1})^{\text{a}}$
15	$5.4(7) \times 10^{-4}$
30	$6.8(9) \times 10^{-4}$
45	$5.1(9) \times 10^{-4}$
55	$8.0(8) \times 10^{-4}$

<sup>a</sup> $k_{\text{obs}}$  values are the average from at least 3 independent reactions.

We probed the influence of free methanol on the rate of dihydrogen activation (Table 3.2 and Figure 3.14). The reaction rate increases by a factor of approximately two from 0.002 M MeOH to 0.011 M of free MeOH. A plot of  $k_{\text{obs}}$  versus concentration of MeOH reveals a non-first-order acceleration (Figure 3.14). This is surprising since MeOH dissociation likely precedes dihydrogen coordination to Rh (see below). This possibly suggests that two factors are at play for the influence of MeOH on the rate of hydrogen activation: 1) coordination to

Rh, and 2) adjusting solvent polarity (see below). Efforts to perform the reaction in other polar solvents (e.g.,  $\text{CH}_3\text{NO}_2$ ,  $\text{CH}_3\text{CN}$ , acetone) to probe the influence of solvent polarity resulted in decomposition of complexes **4** and **5** without production of **6**. When dihydrogen activation was attempted in the presence of 0.15 M to 0.32 M added MeOH large deviations in rate were observed. An inhibition was observed between 0.18 M and 0.22 M of added MeOH but rate acceleration was observed between 0.23 M and 0.26 M of added MeOH.

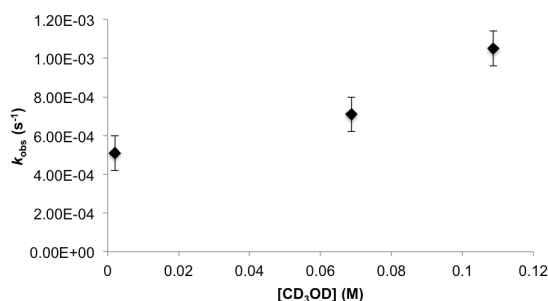


**Figure 3.14.** A plot of  $k_{\text{obs}}$  versus concentration of methanol for the activation of dihydrogen by complexes **4** and **5**.

**Table 3.2.** Average  $k_{\text{obs}}$  from the first-order decay plots of the reaction of protonation product with  $\text{H}_2$  (45 psig) and added MeOH (0, 3, and 5 equiv.) at 68 °C.

equiv. MeOH	[MeOH] (M)	$k_{\text{obs}}$ (s <sup>-1</sup> ) <sup>a</sup>
0	0.002	5.1(9) × 10 <sup>-4</sup>
3	0.07	7.1(9) × 10 <sup>-4</sup>
5	0.11	1.05(9) × 10 <sup>-3</sup>

<sup>a</sup> $k_{\text{obs}}$  values are the average from at least 3 independent reactions.

The rate of degenerate exchange between coordinated and free methanol was determined under pseudo-first-order conditions. In separate experiments,  $\text{CD}_3\text{OD}$  (5, 10 and

20 equiv. relative Rh) was added to a solution of complex **4** in THF-*d*<sub>8</sub>. A plot of  $k_{\text{obs}}$  values (obtained from first-order fits for disappearance of the resonance for coordinated MeOH for **4**) versus the concentration of CD<sub>3</sub>OD provides support that the reaction is zero-order in MeOH (Figure 3.15). This is consistent with rate limiting dissociation of MeOH (Scheme 3.12). The  $k$  values obtained for the fits of the first-order exponential decay plots (Table 3.3) are statistically identical or very similar to the  $k_{\text{obs}}$  for the dihydrogen activation reaction ( $k_{\text{obs}} = 5.1(9) \times 10^{-4} \text{ s}^{-1}$ ) in the absence of added MeOH (0.002 M free MeOH, see Table 3.2). To test for a KIE for degenerate methanol exchange from  $[(^t\text{bpy})_2\text{Rh}(\text{CH}_3\text{OH})(\text{OCH}_3)]^{2+}$ , we prepared  $[(^t\text{bpy})_2\text{Rh}(\text{CD}_3\text{OD})(\text{OCD}_3)]^{2+}$  and measured the rate of exchange between coordinated CD<sub>3</sub>OD and free CH<sub>3</sub>OH (Scheme 3.13). From three independent experiments  $[\text{CH}_3\text{OH}] = 0.1 \text{ M}$  the first-order  $k_{\text{obs}} = 2.6(5) \times 10^{-4} \text{ s}^{-1}$ . Thus, a KIE of  $k_{\text{H}}/k_{\text{D}} = 2.2(4)$  is observed for degenerate exchange of coordinated and free methanol using  $[(^t\text{bpy})_2\text{Rh}(\text{CH}_3\text{OH})(\text{OCH}_3)]^{2+}/\text{CD}_3\text{OD}$  ( $k_{\text{H}}$ ) and  $[(^t\text{bpy})_2\text{Rh}(\text{CD}_3\text{OD})(\text{OCD}_3)]^{2+}/\text{CH}_3\text{OH}$  ( $k_{\text{D}}$ ).



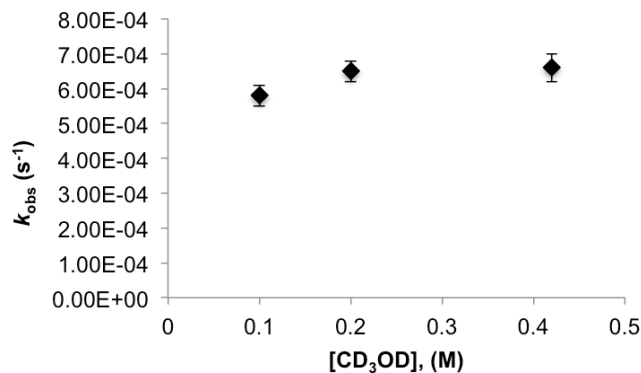
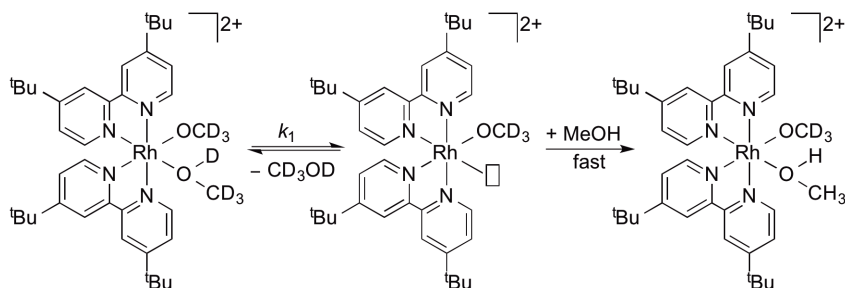


**Figure 3.15.** Plot of  $k_{\text{obs}}$  versus  $[\text{CD}_3\text{OD}]$  for the exchange of coordinated MeOH of  $[(\text{t-bpy})_2\text{Rh}(\text{OMe})(\text{MeOH})][\text{OTf}][\text{TFA}]$  (**4**) with free  $\text{CD}_3\text{OD}$ .

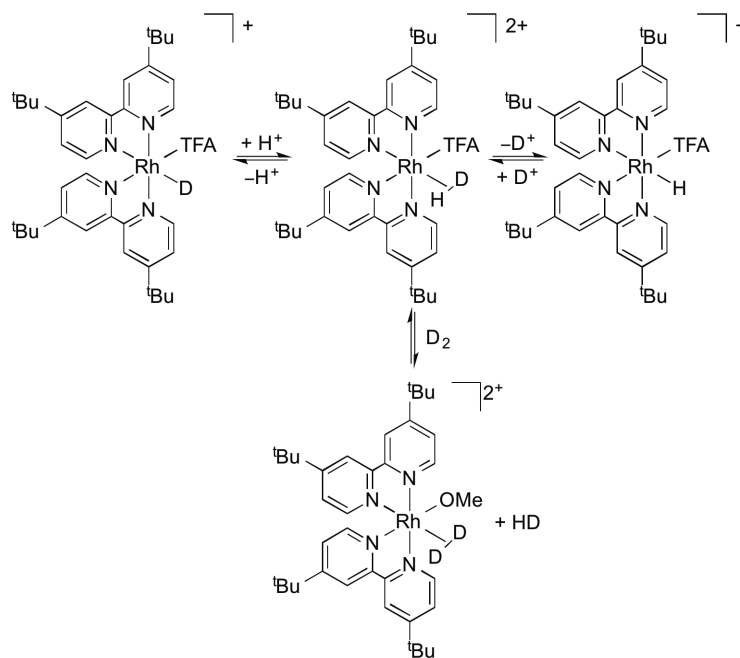


**Scheme 3.13.** Monitoring the rate of MeOH exchange with coordinated  $\text{CD}_3\text{OD}$  of  $[(\text{t-bpy})_2\text{Rh}(\text{OCD}_3)(\text{CD}_3\text{OD})][\text{OTf}][\text{TFA}]$  gives the rate of  $\text{CD}_3\text{OD}$  dissociation.

In order to determine whether or not a kinetic isotope effect (KIE) is observed when activating  $\text{D}_2$ , we reacted the mixture of **4** and **5** with  $\text{D}_2$ . The average  $k_{\text{obs}}$  from the first-order exponential decay plots for the reaction using 45 psig  $\text{D}_2$  ( $k_{\text{obs}} = 3.2(5) \times 10^{-4} \text{ s}^{-1}$ ) indicate that the reaction proceeds at a slightly faster rate with  $\text{H}_2$  ( $k_{\text{obs}} = 5.1(9) \times 10^{-4} \text{ s}^{-1}$ ). Thus, the data are consistent with a small KIE with  $k_{\text{H}}/k_{\text{D}} = 1.6(4)$ . No appreciable change in rate was observed upon varying the pressure of  $\text{D}_2$  [we could not obtain the concentration of  $\text{D}_2$  in the  $^1\text{H}$  NMR experiments;  $k_{\text{obs}} = 5.1 \times 10^{-4} \text{ s}^{-1}$  (20 psig),  $4.9 \times 10^{-4} \text{ s}^{-1}$  (30 psig),  $4.9 \times 10^{-4} \text{ s}^{-1}$  (55 psig)]. The high-pressure ( $> 20$  psig) experiments with  $\text{D}_2$  were performed once. Similarly,

the half-life for H<sub>2</sub> activation by [(<sup>4</sup>bpy)<sub>2</sub>Rh(CD<sub>3</sub>OD)(OCD<sub>3</sub>)]<sup>2+</sup> is approximately 2.5 greater than that using [(<sup>4</sup>bpy)<sub>2</sub>Rh(CH<sub>3</sub>OH)(OCH<sub>3</sub>)]<sup>2+</sup>.

When D<sub>2</sub> is used in place of H<sub>2</sub>, the final deuteride product should be [(<sup>4</sup>bpy)<sub>2</sub>Rh(D)(TFA)][OTf] (Scheme 3.14). As expected, the hydride resonance at -13.3 ppm is initially absent in the <sup>1</sup>H NMR spectrum of the reactions using D<sub>2</sub> (Figure 3.16). Eventually, the appearance of HD (4.50 ppm, <sup>1</sup>J<sub>HD</sub> = 42 Hz) occurs simultaneously with the formation of the protio Rh–H complex [(<sup>4</sup>bpy)<sub>2</sub>Rh(H)(TFA)][OTf]. Additionally, free H<sub>2</sub> is observed. A source of H<sup>+</sup> (e.g., free MeOH) likely results in the formation of Rh–H, HD and H<sub>2</sub>. As shown in Scheme 3.14, the initial product from the reaction with D<sub>2</sub>, [(<sup>4</sup>bpy)<sub>2</sub>Rh(D)(TFA)]<sup>+</sup>, can be protonated to form [(<sup>4</sup>bpy)<sub>2</sub>Rh(η<sup>2</sup>-HD)(TFA)]<sup>2+</sup>, and the loss of D<sup>+</sup> would give [(<sup>4</sup>bpy)<sub>2</sub>Rh(H)(TFA)]<sup>+</sup>. Exchange of D<sub>2</sub> with coordinated HD of [(<sup>4</sup>bpy)<sub>2</sub>Rh(η<sup>2</sup>-HD)(TFA)]<sup>2+</sup> would produce free HD.



**Scheme 3.14.** Proposed pathway for the formation of HD, H<sub>2</sub> and Rh-H during the reaction of  $[(t\text{bpy})_2\text{Rh}(\text{OMe})(\text{MeOH})][\text{OTf}][\text{TFA}]$  (**4**) with D<sub>2</sub> after the initial formation of  $[(t\text{bpy})_2\text{Rh}(\text{D})(\text{TFA})]^+$ .

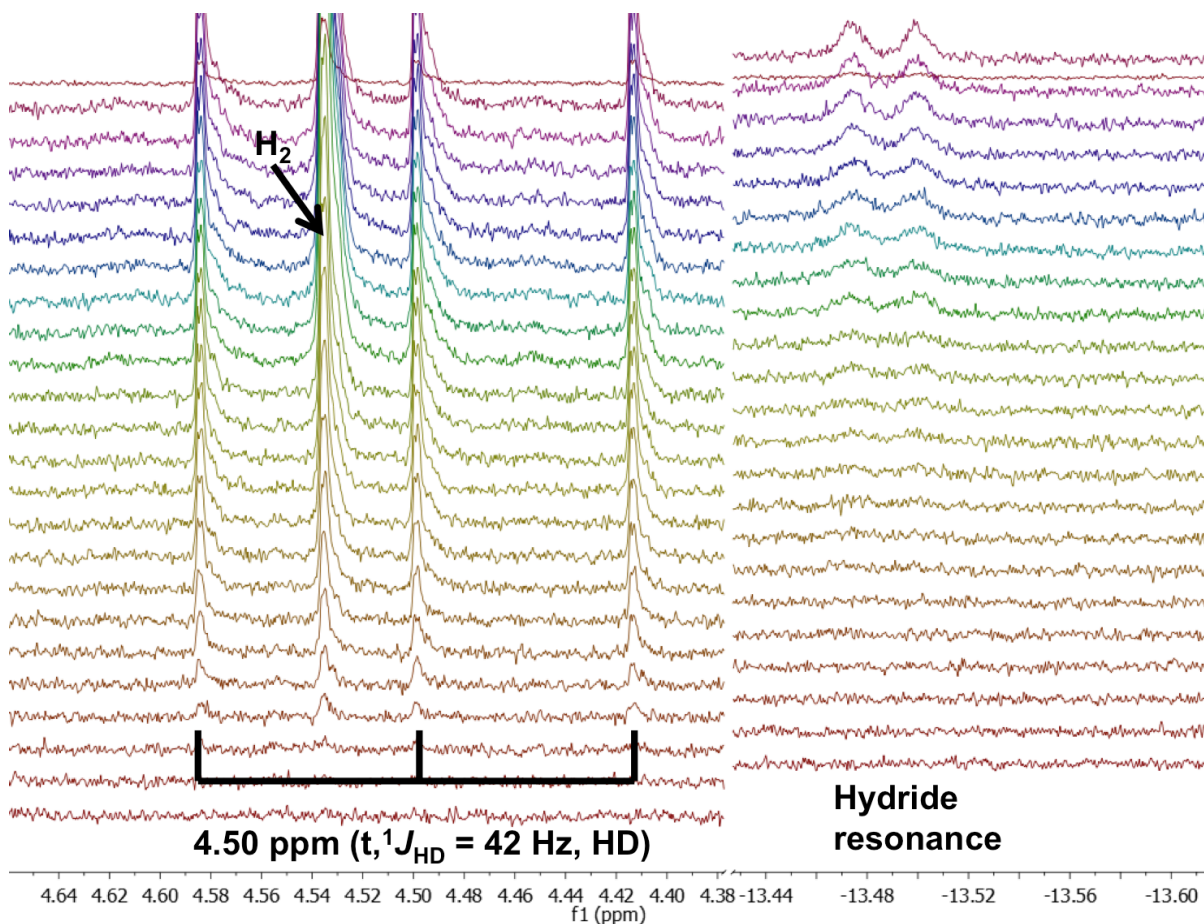
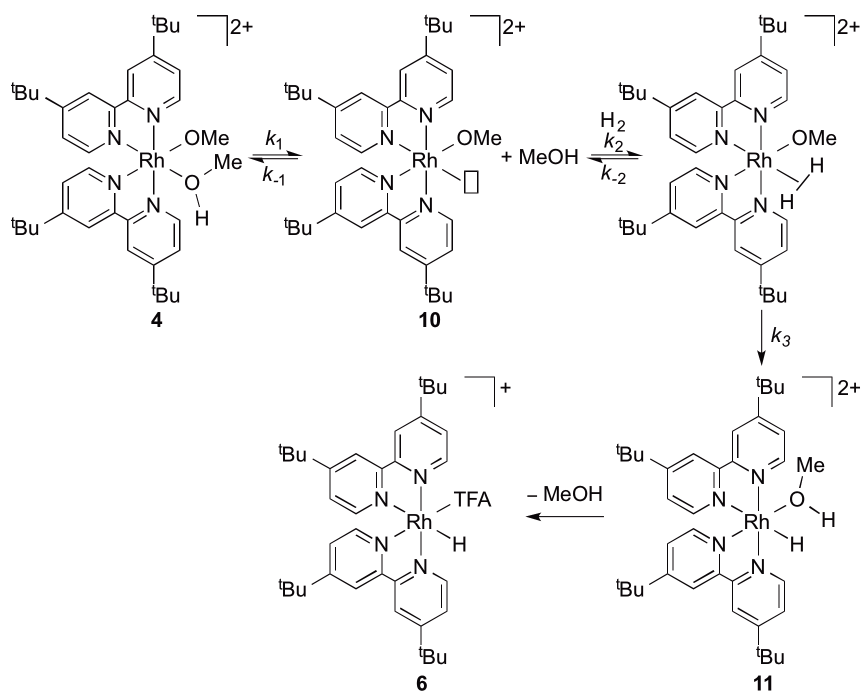


**Figure 3.16.**  $^1\text{H}$  NMR stack plot showing the formation of HD,  $\text{H}_2$ , and the hydride resonance of  $[(^t\text{bpy})_2\text{Rh}(\text{H})(\text{TFA})]\text{OTf}$  (**6**) for the reaction of complexes **4** and **5** with  $\text{D}_2$ .

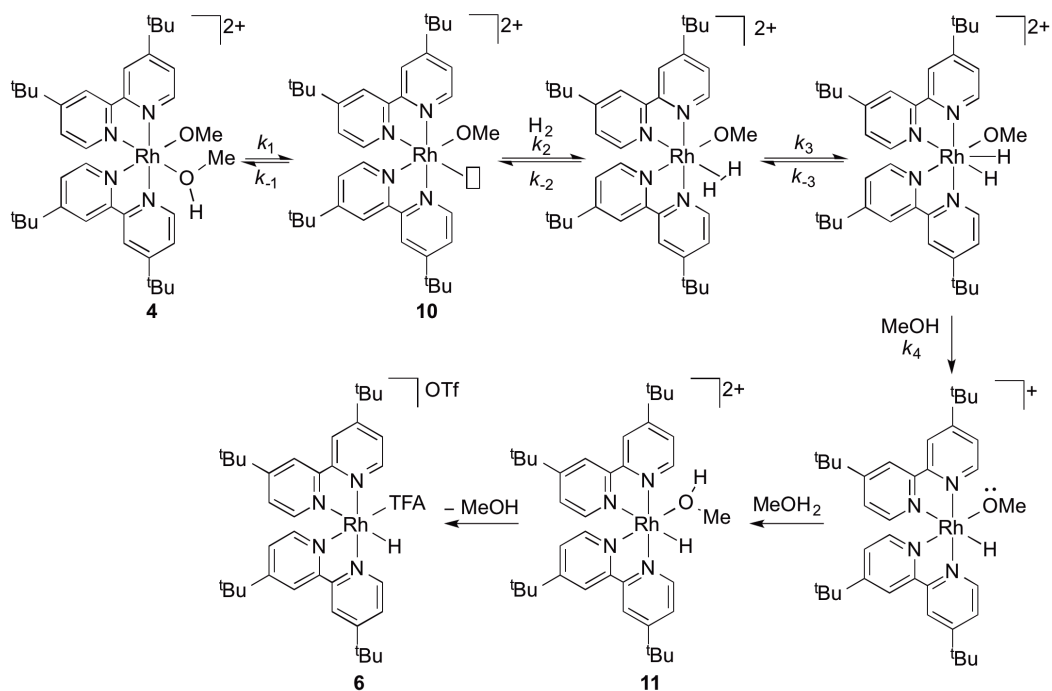
Scheme 3.15 shows a likely pathway for the net 1,2-addition of  $\text{H}_2$  across the Rh–OMe bond to form complex **6**. Methanol dissociation from  $[(^t\text{bpy})_2\text{Rh}(\text{OMe})(\text{MeOH})]^{2+}$  (**4**) would form the five-coordinate species  $[(^t\text{bpy})_2\text{Rh}(\text{OMe})]^{2+}$  (**10**). Dihydrogen coordination gives  $[(^t\text{bpy})_2\text{Rh}(\text{OMe})(\eta^2\text{-H}_2)][\text{OTf}][\text{TFA}]$ , and 1,2-addition across the Rh–OMe bond produces the Rh–hydride product  $[(^t\text{bpy})_2\text{Rh}(\text{H})(\text{MeOH})]^{2+}$  (**11**). Complex **11** can convert to **6**, which is the final Rh product, by loss of MeOH and coordination of TFA.

Two alternative mechanisms for  $\text{H}_2$  activation from the 5-coordinate complex  $[(^t\text{bpy})_2\text{Rh}(\text{OMe})]^{2+}$  (**10**) can be envisioned. As shown in Scheme 3.16,  $\text{H}_2$  activation could

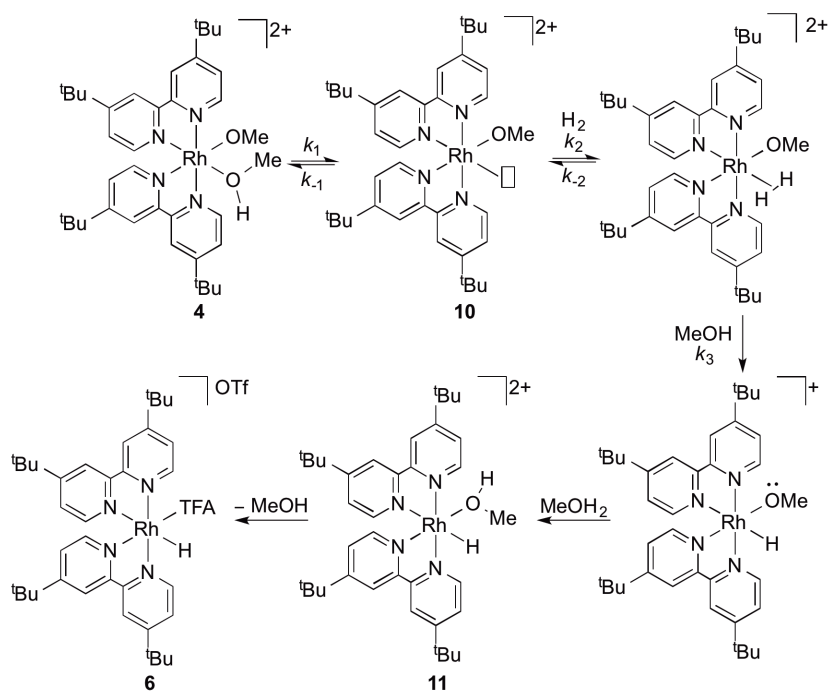
occur by oxidative addition of dihydrogen to complex **10** to give a Rh(V) bis-hydride complex followed by proton loss to give  $[(^t\text{bpy})_2\text{Rh}(\text{H})(\text{OMe})]^+$ . Subsequent protonation of the methoxide ligand would give  $[(^t\text{bpy})_2\text{Rh}(\text{H})(\text{MeOH})]^{2+}$ , and dissociation of MeOH would yield the final product  $[(^t\text{bpy})_2\text{Rh}(\text{H})(\text{TFA})]^+$ . Alternatively, coordination of dihydrogen to **10** and deprotonation by free MeOH would give  $[(^t\text{bpy})_2\text{Rh}(\text{H})(\text{OMe})]^+$  (Scheme 3.17). Protonation of the methoxide ligand would give  $[(^t\text{bpy})_2\text{Rh}(\text{H})(\text{MeOH})]^{2+}$ , and dissociation of MeOH would lead to the formation of the final hydride complex **6** (Scheme 3.17). These mechanisms are discussed with our proposed pathway below.



**Scheme 3.15.** Proposed mechanism for H<sub>2</sub> activation by  $[(^t\text{bpy})_2\text{Rh}(\text{OMe})(\text{MeOH})[\text{TFA}][\text{OTf}]]$  (**4**).



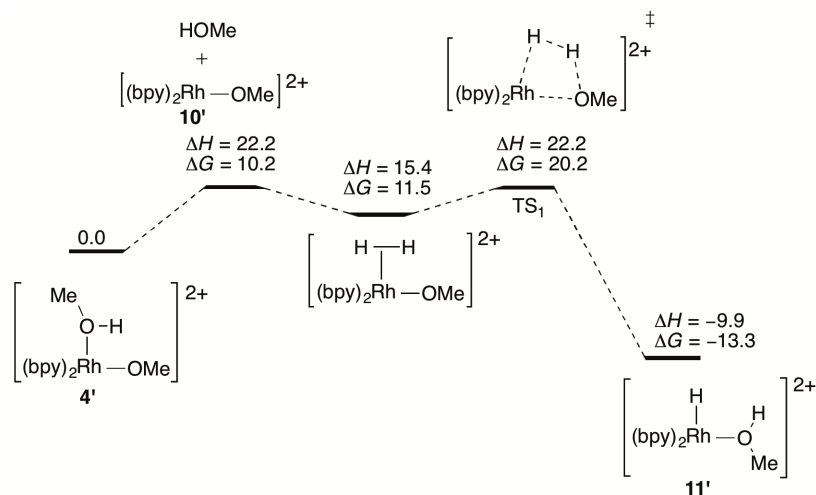
**Scheme 3.16.** Alternative mechanism for dihydrogen activation involving the oxidative addition of dihydrogen.



**Scheme 3.17.** Alternative mechanism for dihydrogen activation involving deprotonation of  $\eta^2\text{-H}_2$  by free MeOH.

In addition to experimental rate and isotope effects, we have also carried out density functional calculations to examine the structures and energy landscape for 1,2-addition of dihydrogen to complex **4**. Deepa Devarajan and Prof. Dan Ess at Brigham Young University performed the DFT calculations. All calculations were carried out in Gaussian 09.<sup>31</sup> Complex **4** was modeled without <sup>t</sup>Bu groups on the bpy ligands (**4'**). The M06<sup>32,33</sup> functional with the 6-31G(d,p)[LANL2DZ for Rh] basis set and pseudopotential was used to optimize all ground-state and transition-state structures. The larger 6-311++G(2d,2p)[LANL2TZ(f) for Rh] was used for further refinement of energies. THF solvent effects were modeled with the implicit SMD model.<sup>34</sup>

To begin, we examined the energetics for MeOH loss to create a vacant coordination site on the Rh metal center in complex **4'** (Scheme 3.18). We did not examine associative mechanisms since the Rh complex is an octahedral 18-electron species. As somewhat expected, on the solvated potential energy surface no transition structure was located for direct MeOH dissociation. Therefore, the  $\Delta H^\ddagger$  for MeOH dissociation and H<sub>2</sub> coordination is estimated by the thermodynamic enthalpy penalty for complete MeOH dissociation to give **10'**. The  $\Delta H$  for MeOH dissociation is 22.2 kcal/mol relative to complex **4'**. We also examined the possibility that added MeOH can facilitate MeOH dissociation from the Rh coordination sphere. The calculations suggest no acceleration of this process with added MeOH.



**Scheme 3.18.** Calculated reaction pathway for H<sub>2</sub> activation by the model [(bpy)<sub>2</sub>Rh(OMe)(MeOH)]<sup>2+</sup> complex (kcal/mol).

After the five-coordinate complex **10'** is generated, dihydrogen can form a weak interaction with the Rh metal center to give the [(bpy)<sub>2</sub>Rh(OMe)(H<sub>2</sub>)]<sup>2+</sup> complex with ΔH = 15.4 kcal/mol (Figure 3.17). Thus, coordination of hydrogen to **10'** is calculated to be exothermic by 6.8 kcal/mol. Similar to many other metal–H<sub>2</sub> coordination intermediates, the H–H bond length is stretched from its equilibrium bond length of 0.74 Å to 0.80 Å,<sup>35,36</sup> and the Rh–hydrogen interaction distances are between 1.87 Å and 1.89 Å.

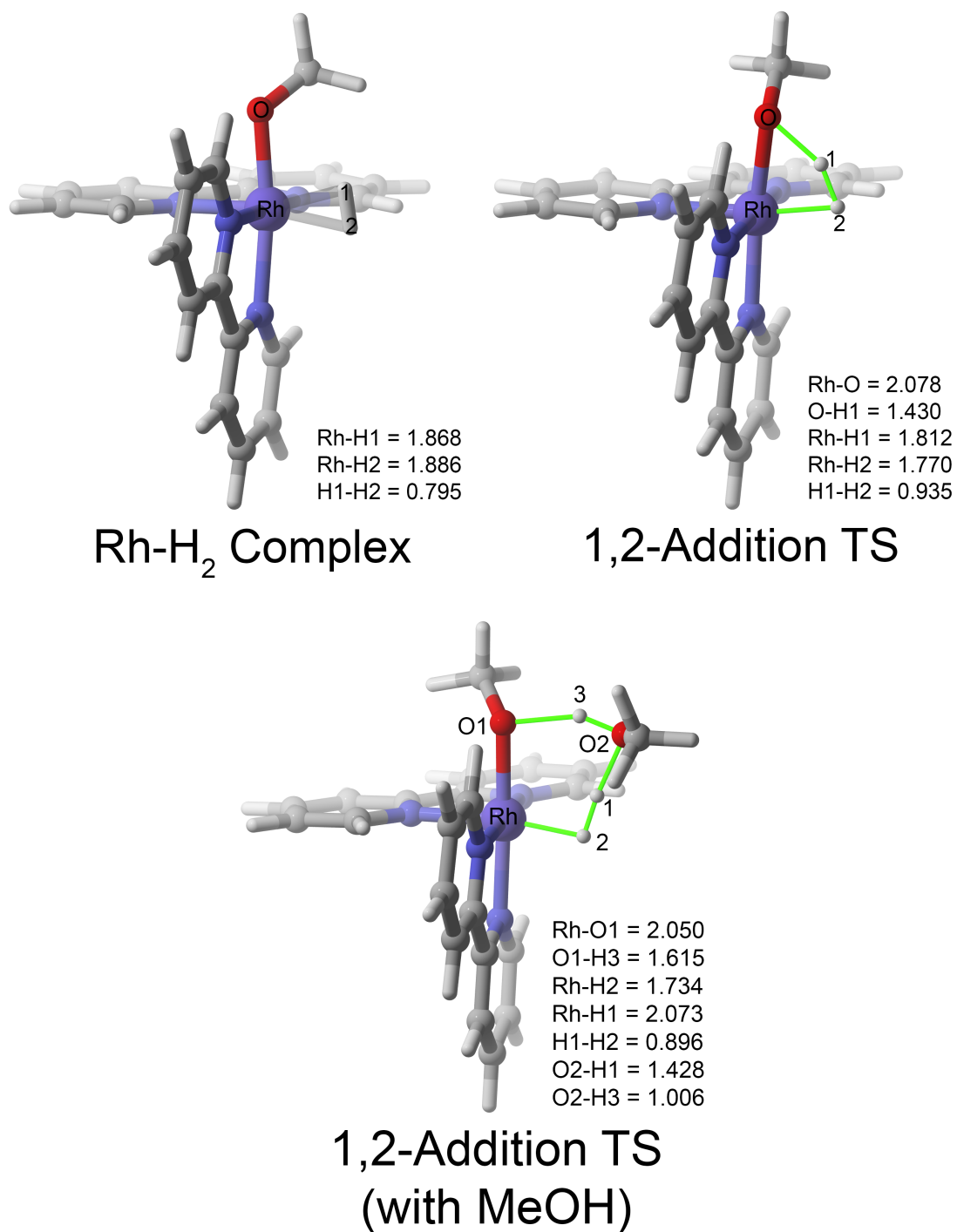


**Figure 3.17.** Dihydrogen coordination and 1,2-addition transition-state structures (bond lengths are in Å).

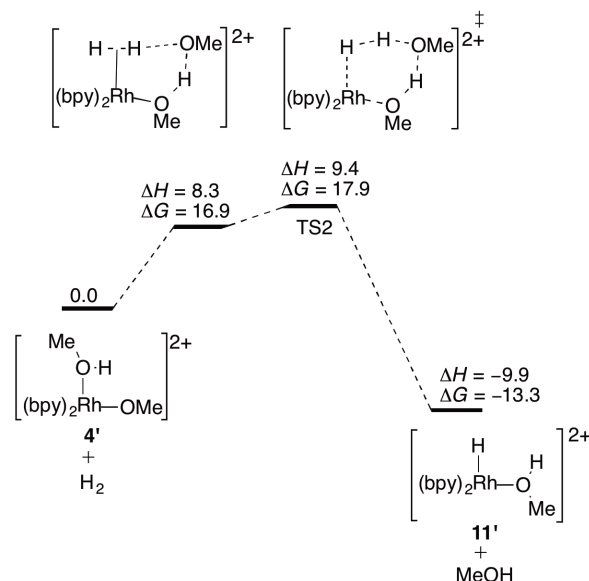
After dihydrogen coordination there is a concerted transition state for 1,2-addition of H–H across the Rh–OMe bond that results in the Rh–H complex **11'** (Scheme 3.18). In this transition state, the H–H is stretched to a partial bond length of 0.94 Å. The other geometrics, including the forming O–H bond and forming Rh–H bond, are similar to previously reported 1,2-addition transition states to metal alkoxide species.<sup>14,18-19,24,37-38</sup> In the transition state there is also a short Rh–H interaction distance (1.81 Å) between the Rh metal center and the hydrogen that migrates from coordinated H<sub>2</sub> to the methoxide ligand.

The calculated  $\Delta H^\ddagger$  for 1,2-addition is 22.2 kcal/mol relative to complex **4'** and dihydrogen, and the resulting Rh–H species is –9.9 kcal/mol exothermic. While the Rh–H<sub>2</sub> coordination complex is stabilized by ~7 kcal/mol relative to complex **10'**, overall the dihydrogen activation energy surface is flat for both coordination and cleavage of the H–H bond. Based on the enthalpy surface, dissociation of MeOH from complex **4'** is equal in energy to the dihydrogen activation transition state. This enthalpy landscape qualitatively matches the experimentally determined first-order rate dependence on Rh complexes and non-first-order rate dependence on dihydrogen pressure and could simultaneously explain the small KIE value observed. However, because a fully optimized transition state was not found for MeOH dissociation from complex **4'**, caution should be taken in the interpretation of a rate-limiting reaction step from this enthalpy surface.

While the calculated enthalpy landscape for dihydrogen coordination and 1,2-addition is in reasonable accordance with experiment, the free energy landscape is challenging to interpret. The  $\Delta G$  for MeOH dissociation and the energy of intermediate **10'** is 10.2 kcal/mol. However, this free energy value cannot be used to approximate the  $\Delta G^\ddagger$  for H<sub>2</sub> coordination

since MeOH is fully dissociated and highly overestimates translational entropy. In cases like this where the enthalpy surface is flat in the region for bond coordination and activation caution should be used when interpreting the free energy landscape and it is likely best to examine the enthalpy landscape.

We have also examined the impact of added MeOH on the 1,2-addition transition state for dihydrogen activation. Figure 3.17 shows this transition state and how MeOH acts to shuttle the hydrogen during formation of the Rh–H species. Methanol has been previously shown to act as a proton shuttle in the isomerization of Ru hydrido alkynyl intermediates to Ru vinylidene complexes.<sup>39</sup> The  $\Delta H^\ddagger$  and  $\Delta G^\ddagger$  values for the MeOH-assisted pathway are 9.4 and 17.9 kcal/mol, respectively (Scheme 3.19). This suggests that on the enthalpy surface there is a significant energetic advantage for MeOH to assist hydrogen transfer. However, this enthalpy advantage is significantly mitigated by an entropy penalty. On the free energy surface the MeOH-assisted transition state is ~2 kcal/mol lower in energy than the transition state without MeOH. Corrections for the small concentration of added MeOH at 0.43 M shows that this MeOH assistance likely only accounts for an ~1 kcal/mol lower activation free energy, which is possibly in accordance with the modest rate enhancement.



**Scheme 3.19.** Methanol assisted H<sub>2</sub> activation and M06/6-311++G(2d,2p)[LANL2TZ(f)] energies in THF solvent. (kcal/mol).

Rate law I in Scheme 3.20 is derived from the pathway in Scheme 3.15 using the steady-state approximation, and rate law II is the variant in which MeOH serves as a catalyst in the dihydrogen activation step ( $k_3$ ). Rate law III is derived assuming that free MeOH aids in the dissociation of coordinated MeOH ( $k_1$  step in Scheme 3.15). Rate laws I, II and III are consistent with the observed dependence on H<sub>2</sub> if the magnitude of  $k_2k_3[H_2]$  is sufficiently large. That is, the  $k_2k_3[H_2]$  term can cancel (or partially cancel) the first-order [H<sub>2</sub>] term in the numerator and, thus, the observed dependence on dihydrogen that is intermediate between zero- and first-order. The DFT calculations predict that the  $\Delta H^\ddagger$  for methanol dissociation and dihydrogen activation will be similar (Scheme 3.15). Thus, it is not unreasonable that the  $k_2k_3[H_2]$  term could compete with other terms in the denominators. The non-zero/non-first order dependence on [H<sub>2</sub>] is also consistent with a small KIE for H<sub>2</sub> versus D<sub>2</sub> activation. Rate laws IV and V are based on the alternative mechanisms involving oxidative addition and

$\eta^2$  coordination of  $H_2$  followed by proton loss as shown in Scheme 3.16 and Scheme 3.17, respectively. These predict a similar dependence on concentration of dihydrogen and methanol as rate laws I-III and, thus, the mechanisms shown in Schemes 3.15, 3.16 and 3.17 cannot be distinguished using the rate as a function of dihydrogen concentration.

$$I. \text{ If } k_3 \text{ is RDS: Rate} = \frac{k_1 k_2 k_3 [Rh][H_2]}{k_{-1} k_{-2} [MeOH] + k_{-1} k_3 [MeOH] + k_2 k_3 [H_2]}$$

$$\frac{k_1 k_2 k_3 [Rh][H_2]}{k_{-1} k_{-2} + k_{-1} k_3 [MeOH] + k_2 k_3 [H_2]}$$

$$III. \text{ } k_3 \text{ is RDS and MeOH assists in } k_1: \text{ Rate} = \frac{k_1 k_2 k_3 [Rh][MeOH][H_2]}{k_{-1} k_{-2} [MeOH] + k_{-1} k_3 [MeOH] + k_2 k_3 [H_2]}$$

$$IV. \text{ Oxidative addition, } k_4 \text{ is RDS: Rate} = \frac{k_1 k_2 k_3 k_4 [Rh][H_2]}{k_{-1} k_{-2} k_{-3} + k_{-1} k_{-2} k_4 [MeOH] + k_{-1} k_2 k_4 [MeOH][H_2] + k_2 k_3 k_4 [H_2]}$$

$$V. \text{ } \eta^2\text{-}H_2 \text{ coordination followed by proton loss, } k_4 \text{ is RDS: Rate} = \frac{k_1 k_2 k_3 [Rh][H_2]}{k_{-1} k_{-2} + k_{-1} k_3 [MeOH] + k_2 k_3 [H_2]}$$

**Scheme 3.20.** Rate law I is based on the proposed pathway shown in Scheme 3.15 rate law II is the variant with methanol catalyzed  $H_2$  activation, and rate law III is a variant where free MeOH assists in  $k_1$  and MeOH catalyzed the  $H_2$  addition. Rate law IV is based on the oxidative addition mechanism in Scheme 3.16. Rate law V is based on the mechanism involving coordination of  $H_2$  followed by proton loss as shown in Scheme 3.17.

Rate laws I and II predict a straightforward inverse dependence on concentration of MeOH, which is inconsistent with experimental observations. However, rate law III is more complex. Under low concentration of MeOH, if the  $k_2 k_3 [H_2]$  term dominates, a first-order dependence on MeOH is predicted, and eventually saturation kinetics would be expected. Again, this rate law is not fully consistent with experimental observations. Note that inclusion of MeOH in the  $k_1$  step of the pathways leading to rate laws IV and V would give similar dependence for these mechanisms. Thus, none of the mechanisms and rate laws are fully consistent with experimental observations. It is possible that the dependence of reaction rate on MeOH concentration is a combination of intimate involvement of MeOH in the reaction pathway (i.e., MeOH assisted ligand dissociation and  $H_2$  activation) and solvent

polarity effects. As indicated above, we attempted to compare the rate of dihydrogen activation in THF with more polar solvents ( $\text{CH}_3\text{NO}_2$ ,  $\text{CH}_3\text{CN}$ , acetone), but the reactions resulted in decomposition of complexes **4** and **5** without production of **6**. Another possibility is that the added MeOH aids dissociation of MeOH ( $k_1$ ) via hydrogen-bonding. To test this, we compared the impact of added  $\text{CD}_3\text{OD}$  on the activation of  $\text{H}_2$  to that of  $\text{CH}_3\text{OH}$ . We cannot conclude whether or not there is an isotope effect for the MeOH-acceleration for the reaction of **4** and **5** with dihydrogen in the presence of three equiv of MeOH versus three equiv  $\text{CD}_3\text{OD}$  because the deviations are too large.

A small KIE is observed for activation of  $\text{D}_2$  versus  $\text{H}_2$ . The activation of  $\text{D}_2$  leads to the formation of  $\text{CH}_3\text{OD}$  (methanol- $d_1$ ), and we hypothesized that coordination of  $\text{CH}_3\text{OD}$  to Rh might impact the rate of methanol dissociation ( $k_1$  in Scheme 3.12). Thus, if the reaction of **4** and **5** with  $\text{D}_2$  leads to the formation of  $[(^t\text{bpy})_2\text{Rh}(\text{CH}_3\text{OD})(\text{OCH}_3)]^{2+}$ , the  $k_{\text{H}}/k_{\text{D}}$  observed for  $\text{H}_2/\text{D}_2$  activation might be explained. However, our results suggest that  $[(^t\text{bpy})_2\text{Rh}(\text{CH}_3\text{OD})(\text{OCH}_3)]^{2+}$  likely does not form during  $\text{D}_2$  activation by **4** and **5**. The activation of  $\text{D}_2$  by **4** or **5** would produce  $[(^t\text{bpy})_2\text{Rh}(\text{CH}_3\text{OD})(\text{H})]^{2+}$ , which then dissociates  $\text{CH}_3\text{OD}$  to form **6**. Exchange of coordinated  $\text{CH}_3\text{OH}$  and free  $\text{CH}_3\text{OD}$  would likely require formation of the five-coordinate intermediate  $[(^t\text{bpy})_2\text{Rh}(\text{OCH}_3)]^{2+}$ , and our kinetic analysis suggests that this intermediate should react more rapidly with dihydrogen than free methanol. But it is possible to rationalize the small KIE for  $\text{H}_2$  versus  $\text{D}_2$  activation if the dependence on  $\text{H}_2$  is intermediate between zero- and first-order. Thus, a relatively large KIE for  $\text{H}_2$  versus  $\text{D}_2$  would be attenuated by the non-first-order dependence. This scenario is consistent with a slight increase in rate of  $\text{H}_2$  activation when the initial concentration is increased by a

factor 2.9 (see above). Unfortunately, the large deviations do not allow a quantified determination of the impact of H<sub>2</sub> concentration on rate.

### 3.3 Conclusions

The addition of one equivalent of HTFA to [(<sup>t</sup>bpy)<sub>2</sub>Rh(OMe)<sub>2</sub>][OTf] leads to the formation of [(<sup>t</sup>bpy)<sub>2</sub>Rh(OMe)(MeOH)][OTf][TFA] and [(<sup>t</sup>bpy)<sub>2</sub>Rh(OMe)(TFA)][OTf], which activate dihydrogen by net 1,2-addition of H–H across the Rh(III)–OMe bond. The reaction displays non-first-order dependence on concentration of dihydrogen and a first-order dependence on concentration of Rh starting material. The calculated  $\Delta H^\ddagger$  for the H<sub>2</sub> activation step is only 6.8 kcal/mol from the dihydrogen adduct. In contrast, the calculated  $\Delta H$  for MeOH dissociation from [(bpy)<sub>2</sub>Rh(OMe)(MeOH)[TFA][OTf] (**4'**) is 22.2 kcal/mol. Thus, we propose that the dicationic charge of the [(<sup>t</sup>bpy)<sub>2</sub>Rh(OMe)]<sup>2+</sup> fragment impacts the energetics of overall H<sub>2</sub> activation in two ways: 1) the enthalpy for dissociation of the Lewis basic methanol is relatively large, 2) the electrophilic character of the Rh(III) results in a very small  $\Delta H^\ddagger$  for the 1,2-addition of H<sub>2</sub> across the Rh–OMe bond. Thus, dihydrogen coordination to Rh(III) enhances its acidity,<sup>35,40</sup> and the basic methoxide can easily deprotonate the coordinated dihydrogen ligand. The addition of free MeOH provides a slight rate acceleration, and calculations predict that the participation of MeOH in the core unit for H<sub>2</sub> activation can lower the  $\Delta H^\ddagger$  substantially. These results show promise for the use of highly electrophilic late transition metals with basic heteroatomic ligands (e.g., hydroxide, alkoxide, amido) for dihydrogen activation chemistry and the use of basic additives as co-catalysts.

### 3.4 Experimental Section

**General Considerations.** Unless otherwise noted, all synthetic procedures were performed under anaerobic conditions in a nitrogen-filled glovebox or by using standard Schlenk techniques. Glovebox purity was maintained by periodic nitrogen purges and was monitored by an oxygen analyzer ( $O_2$  (g) < 15 ppm for all reactions). Toluene, tetrahydrofuran and diethyl ether were dried by distillation from sodium/benzophenone. Pentane was distilled over  $P_2O_5$ . Acetonitrile and methanol were dried by distillation from  $CaH_2$ . Hexanes, benzene and dichloromethane were purified by passage through a column of activated alumina. Acetonitrile- $d_3$ , methylene chloride- $d_2$ , acetone- $d_6$  and THF- $d_8$  were stored under a  $N_2$  atmosphere over 4 Å molecular sieves.  $H_2$  and  $D_2$  were purchased from Matheson Gas and Cambridge Isotope Labs, respectively, and used as received.  $^1H$  and  $^{13}C$  NMR spectra were recorded on a Varian Mercury Plus 300 MHz (75 MHz operating frequency for  $^{13}C$  NMR), Varian Inova 500 MHz spectrometer (125 MHz operating frequency for  $^{13}C$  NMR), Bruker Avance DRX 600 MHz spectrometer (150 MHz operative frequency for  $^{13}C$  NMR), or Bruker Avance III 800 MHz spectrometer (201 MHz operative frequency for  $^{13}C$  NMR). All  $^1H$  and  $^{13}C$  NMR spectra are referenced against residual proton signals ( $^1H$  NMR) or the  $^{13}C$  resonances of the deuterated solvent ( $^{13}C$  NMR).  $^{19}F$  NMR (operating frequency 282 MHz) spectra were obtained on a Varian Mercury Plus 300 MHz spectrometer and referenced against an external standard of hexafluorobenzene ( $\delta = -164.9$ ). Elemental analyses were performed by Atlantic Microlabs, Inc. High-resolution mass spectra were acquired in ESI mode from samples dissolved in a 3:1 acetonitrile/water solution containing sodium trifluoroacetate (NaTFA). Mass spectra are reported as  $M^+$  for monocationic complexes, or as  $[M+H^+]$  or  $[M+Na^+]$  for neutral complexes, using  $[Na(NaTFA)_x]^+$  clusters

as an internal standard. In all cases, observed isotopic envelopes were consistent with the molecular composition reported. For products with a simple spectrum, the monoisotopic ion is reported; for products with a complicated spectrum, the major peaks in the isotopic envelope are reported. Spectra were collected on either a Shimadzu IT-TOF or an Agilent 6230 TOF. Dr. William H. Myers from the University of Richmond collected and interpreted the HRMS data. Dr. Michal Sabat at the University of Virginia solved the reported X-ray crystallography data. DFT calculations were performed by Dr. Daniel H. Ess and Deepa Devarajan at Brigham Young University. The preparation of NaBAR<sub>4</sub> has been previously reported.<sup>41</sup> The <sup>t</sup>bpy version of [(bpy)<sub>2</sub>Rh(X)<sub>2</sub>]X (X = Cl, Br) were synthesized following the published procedure.<sup>42</sup> (COE)<sub>2</sub>Rh(TFA) (COE = cyclooctene) was made following the literature procedure using AgTFA instead of AgPF<sub>6</sub>.<sup>43</sup> The synthesis of [(bpy)<sub>2</sub>Rh(H)(OTf)]<sup>+</sup> has been previously reported without full experimental details or characterization data.<sup>44</sup> The oxidative additions of HTFA and HCl to [(<sup>t</sup>bpy)<sub>2</sub>Rh]<sup>+</sup>, to form [(<sup>t</sup>bpy)<sub>2</sub>Rh(H)(TFA)]<sup>+</sup> and [(<sup>t</sup>bpy)<sub>2</sub>Rh(H)(Cl)]<sup>+</sup>, respectively, were based on this synthesis.

**[(<sup>t</sup>bpy)<sub>2</sub>Rh(OTf)<sub>2</sub>][OTf].** This complex was prepared with modification to the procedure reported by Meyer and co-workers.<sup>42</sup> The complex [(<sup>t</sup>bpy)<sub>2</sub>RhCl<sub>2</sub>]Cl (0.4995 g, 0.6695 mmol) was dissolved in 1,2-dichlorobenzene (24 mL). HOTf (355 μL, 4.01 mmol) was added via a microsyringe. The yellow solution was heated at reflux overnight. Upon cooling to room temperature, Et<sub>2</sub>O (20 mL) was added through the condenser. The reaction mixture was placed in the freezer for several hours to allow maximum precipitation. The solid was collected by filtration through a fine porosity frit, washed with Et<sub>2</sub>O, and dried under vacuum for approximately 1 h. In air, the solid was reconstituted in CH<sub>2</sub>Cl<sub>2</sub> and washed with H<sub>2</sub>O (3 x 100 mL). The combined organic extracts were washed with brine (1 x

100 mL), dried over Na<sub>2</sub>SO<sub>4</sub>, and reduced to dryness using a rotary evaporator. The yellow solid was dried under vacuum overnight. The solid was reconstituted in CH<sub>2</sub>Cl<sub>2</sub> and reprecipitated with Et<sub>2</sub>O. The solid was collected over a fine porosity frit, washed with Et<sub>2</sub>O, and dried under vacuum (0.522 g, 72%). <sup>1</sup>H NMR (300 MHz, CD<sub>3</sub>CN) δ 9.19 (d, <sup>3</sup>J<sub>H5-H6</sub> = 6 Hz, 2H, <sup>t</sup>bpy 6/6'), 8.65 (d, <sup>4</sup>J<sub>H3-H5</sub> = 2 Hz, 2H, <sup>t</sup>bpy 3/3'), 8.47 (d, <sup>4</sup>J<sub>H3-H5</sub> = 2 Hz, 2H, <sup>t</sup>bpy 3/3'), 8.21 (dd, <sup>3</sup>J<sub>H5-H6</sub> = 6 Hz, <sup>4</sup>J<sub>H3-H5</sub> = 2 Hz, 2H, <sup>t</sup>bpy 5/5'), 7.45 (dd, <sup>3</sup>J<sub>H5-H6</sub> = 6 Hz, <sup>4</sup>J<sub>H3-H5</sub> = 2 Hz, 2H, <sup>t</sup>bpy 5/5'), 7.36 (d, <sup>3</sup>J<sub>H5-H6</sub> = 7 Hz, 2H, <sup>t</sup>bpy 6/6'), 1.58, 1.37 (each a s, 18H, <sup>t</sup>Bu). <sup>13</sup>C NMR (75 MHz, CD<sub>3</sub>CN) δ 169.7, 169.1, 158.6, 156.5, 152.9, 150.9, 127.8, 127.2, 124.4, 124.2 (each a s, <sup>t</sup>bpy aromatic C's), 37.3, 36.9 (each a s, <sup>t</sup>Bu C(CH<sub>3</sub>)<sub>3</sub>) 30.5, 30.2 (each a s, <sup>t</sup>Bu C(CH<sub>3</sub>)<sub>3</sub>). A quartet for O<sub>3</sub>SCF<sub>3</sub> was not observed in the <sup>13</sup>C NMR spectrum. <sup>19</sup>F NMR (282 MHz, CD<sub>3</sub>CN) δ -79.7 (s, OTf). Anal. Calcd for C<sub>39</sub>H<sub>48</sub>F<sub>9</sub>N<sub>4</sub>O<sub>9</sub>RhS<sub>3</sub>: C, 43.10; H, 4.45; N, 5.15. Found: C, 42.61; H, 4.25; N, 5.04.

**[(<sup>t</sup>bpy)<sub>2</sub>Rh(OMe)<sub>2</sub>][OTf] (1).** A solution of [(<sup>t</sup>bpy)<sub>2</sub>Rh(OTf)<sub>2</sub>][OTf] (0.1999 g, 0.1839 mmol) in CH<sub>3</sub>CN (~10 mL) was slowly added to a solution of CsOH•H<sub>2</sub>O (0.0775 g, 0.462 mmol) in methanol (~5 mL). The yellow solution was stirred at room temperature for 1 h before the solvent was removed under vacuum. The yellow solid was dissolved in CH<sub>2</sub>Cl<sub>2</sub> and filtered through a plug of Celite. The Celite was washed with CH<sub>2</sub>Cl<sub>2</sub> (5 x 5 mL). The filtrate was reduced to ~2 mL under vacuum. Pentane (5 mL) was added to precipitate a yellow solid. The solid was collected over a fine porosity frit and then dried under vacuum before transferring to a pressure tube. Pentane (~20 mL) was added, and the heterogeneous solution was stirred at room temperature overnight. The pressure tube was sonicated for 1 h. The solid was collected over a fine porosity frit, washed with additional pentane (2 x 5 mL) and dried under vacuum (0.142 g, 90%). <sup>1</sup>H NMR (300 MHz, CD<sub>3</sub>CN) δ 9.37 and 7.42 (each

a d,  $^3J_{\text{H5-H6}} = 6$  Hz, 2H each,  $^1\text{bpy}$  6/6'), 8.51, 8.41 (each a d,  $^4J_{\text{H3-H5}} = 2$  Hz, 2H each,  $^1\text{bpy}$  3/3'), 7.9, 7.35 (dd,  $^3J_{\text{H5-H6}} = 6$  Hz,  $^4J_{\text{H3-H5}} = 2$  Hz, 2H each,  $^1\text{bpy}$  5/5'), 2.62 (bs, 6H,  $\text{OCH}_3$ ), 1.55, 1.36 (each a s, 18H each,  $^t\text{Bu}$ ).  $^{13}\text{C}$  NMR (75 MHz,  $\text{CD}_2\text{Cl}_2$ )  $\delta$  165.9, 164.6, 156.6, 155.7, 150.2, 149.7, 125.5, 124.9, 120.9, 120.7 (each a s,  $^1\text{bpy}$  aromatic C's), 56.7 (s,  $\text{OCH}_3$ ), 36.4, 36.1 (each a s,  $\text{C}(\text{CH}_3)_3$ ), 30.8, 30.5 (each a s,  $\text{C}(\text{CH}_3)_3$ ).  $^{19}\text{F}$  NMR (281.96 MHz,  $\text{CD}_2\text{Cl}_2$ )  $\delta$  -79.1 (s, OTf). Anal. Calcd for  $\text{C}_{39}\text{H}_{54}\text{F}_3\text{N}_4\text{O}_5\text{Rh}$ : C, 55.05; H, 6.40; N, 6.58. Found: C, 55.22; H, 6.40; N, 6.49.

**$[(^1\text{bpy})_2\text{Rh}(\text{OMe})_2]\text{Cl}$ .** A procedure analogous to the synthesis of  $[(^1\text{bpy})_2\text{Rh}(\text{OMe})_2][\text{OTf}]$  was employed except  $[(^1\text{bpy})_2\text{Rh}(\text{Cl})_2]\text{Cl}$  (0.2529 g, 0.3390 mmol) was used as the starting material (0.2288 g, 92%).  $^1\text{H}$  NMR (300 MHz,  $\text{CD}_3\text{CN}$ )  $\delta$  9.38 (d,  $^3J_{\text{H5-H6}} = 6$  Hz, 2H,  $^1\text{bpy}$  6/6'), 8.53 (d,  $^4J_{\text{H3-H5}} = 2$  Hz, 2H,  $^1\text{bpy}$  3/3'), 8.43 (d,  $^4J_{\text{H3-H5}} = 2$  Hz, 2H,  $^1\text{bpy}$  3/3'), 7.97 (dd,  $^3J_{\text{H5-H6}} = 6$  Hz,  $^4J_{\text{H3-H5}} = 2$  Hz, 2H,  $^1\text{bpy}$  5/5'), 7.42 (d,  $^3J_{\text{H5-H6}} = 6$  Hz, 2H,  $^1\text{bpy}$  6/6'), 7.33 (dd,  $^3J_{\text{H5-H6}} = 6$  Hz,  $^4J_{\text{H3-H5}} = 2$  Hz, 2H,  $^1\text{bpy}$  5/5'), 2.63 (s, 6H,  $\text{OCH}_3$ ), 1.55, 1.36 (each a s, 18H each,  $^t\text{Bu}$ ).  $^{13}\text{C}$  NMR (151 MHz,  $\text{CD}_2\text{Cl}_2$ )  $\delta$  166.18, 164.95, 156.74, 155.99, 149.91, 149.67, 125.18, 124.71, 121.93, 121.78 (each a s,  $^1\text{bpy}$  aromatic C's), 56.0 ( $\text{OCH}_3$ ), 36.6, 36.3 (each a s,  $\text{C}(\text{CH}_3)_3$ ), 30.9, 30.6 (each a s,  $\text{C}(\text{CH}_3)_3$ ).  $\text{M}^+ = \text{C}_{38}\text{H}_{54}\text{N}_4\text{O}_2\text{Rh}^+$ ; obs'd (%), calc'd (%), ppm: 701.3308, 701.3296, 1.7.

**$[(^1\text{bpy})_2\text{Rh}(\text{OMe})_2][\text{BAr}'_4]$  (2).**  $[(^1\text{bpy})_2\text{Rh}(\text{OMe})_2]\text{Cl}$  (0.1877 g, 0.2546 mmol) was partially dissolved in THF (~20 mL).  $\text{NaBAr}'_4$  (0.2256 g, 0.2546 mmol) in THF (~5 mL) was added dropwise. The resulting solution was stirred at room temperature for 1 h before reducing solvent volume to 10 mL under vacuum. The solution was filtered through Celite to remove NaCl. The Celite was washed with THF (5 x 10 mL). The filtrate was reduced to dryness *in vacuo*. The resulting yellow solid was taken up in  $\text{Et}_2\text{O}$  and transferred to a vial.

The Et<sub>2</sub>O was removed under vacuum to yield an orange-yellow low-density solid. The solid was dried further under vacuum (0.3789 g, 95%). X-ray quality crystals were grown by layering a solution of complex **2** in Et<sub>2</sub>O with hexane. <sup>1</sup>H NMR (300 MHz, CD<sub>3</sub>CN) δ 9.38 (d, <sup>3</sup>J<sub>H5-H6</sub> = 6 Hz, 2H, <sup>t</sup>bpy 6/6'), 8.51 (s, 2H, <sup>t</sup>bpy 3/3'), 8.41 (s, 2H, <sup>t</sup>bpy 3/3'), 7.97 (dd, <sup>3</sup>J<sub>H5-H6</sub> = 6 Hz, <sup>4</sup>J<sub>H3-H5</sub> = 2 Hz, 2H, <sup>t</sup>bpy 5/5'), 7.73 – 7.63 (m, 12H, BAr'<sub>4</sub>), 7.42 (d, <sup>3</sup>J<sub>H5-H6</sub> = 6 Hz, 2H, <sup>t</sup>bpy 6/6'), 7.33 (dd, <sup>3</sup>J<sub>H5-H6</sub> = 6 Hz, <sup>4</sup>J<sub>H3-H5</sub> = 2 Hz, 2H, <sup>t</sup>bpy 5/5'), 2.63 (s, 6H, OCH<sub>3</sub>), 1.55, 1.35 (each a s, 18H, <sup>t</sup>Bu). <sup>13</sup>C NMR (201 MHz, CD<sub>3</sub>CN) δ 166.3, 165.2, 125.3, 125.3, 122.2, 122.2, 157.1, 156.5, 150.8, 149.8 (each a s, <sup>t</sup>bpy aromatic C's), 162.6 (q, <sup>1</sup>J<sub>B-Cipso</sub> = 50 Hz, BAr'<sub>4</sub>), 135.6 (BAr'<sub>4</sub>), 129.9 (q, <sup>2</sup>J<sub>C-F</sub> = 32 Hz, 31 Hz, *m*-BAr'<sub>4</sub>), 125.4 (q, <sup>1</sup>J<sub>C-F</sub> = 272 Hz, CF<sub>3</sub>-BAr'<sub>4</sub>), 118.7 (BAr'<sub>4</sub>), 55.9 (s, OCH<sub>3</sub>), 36.7, 36.4 (each a s, C(CH<sub>3</sub>)<sub>3</sub>), 30.6, 30.3 (each a s, C(CH<sub>3</sub>)<sub>3</sub>). <sup>19</sup>F NMR (282 MHz, CD<sub>3</sub>CN) δ –63.6 (s, BAr'<sub>4</sub>). M<sup>+</sup> = C<sub>38</sub>H<sub>54</sub>N<sub>4</sub>O<sub>2</sub>Rh<sup>+</sup>; obs'd, calc'd, ppm: 701.3304, 701.3296, 1.1

**[(<sup>t</sup>bpy)<sub>2</sub>Rh(OMe)<sub>2</sub>][TFA].** [(<sup>t</sup>bpy)<sub>2</sub>Rh(OMe)<sub>2</sub>]Cl (0.2288 g, 0.3104 mmol) was suspended in CH<sub>3</sub>CN (~25 mL). NaTFA (0.0425 g, 0.312 mmol) in CH<sub>3</sub>CN (~ 5 mL) was added dropwise. [(<sup>t</sup>bpy)<sub>2</sub>Rh(OMe)<sub>2</sub>]Cl dissolved completely upon addition of NaTFA and the solution became slightly cloudy. The resulting mixture was allowed to stir at room temperature for 1 h before evaporating to dryness *in vacuo*. The yellow residue was dissolved in CH<sub>2</sub>Cl<sub>2</sub> and filtered through Celite. The Celite was washed with CH<sub>2</sub>Cl<sub>2</sub> (5 x 5 mL). The filtrate was reduced to dryness under vacuum. The yellow solid was reconstituted in CH<sub>2</sub>Cl<sub>2</sub> and precipitated with pentane. The solid was combined with pentane (~15 mL) and sonicated for 1 h. The solid was collected by filtration through a fine porosity frit, washed with additional pentane and dried under vacuum (0.2200 g, 87%). <sup>1</sup>H NMR (800 MHz, CD<sub>3</sub>CN) δ 9.38 (d, <sup>3</sup>J<sub>H5-H6</sub> = 6 Hz, 2H, <sup>t</sup>bpy 6/6'), 8.53 (d, <sup>4</sup>J<sub>H3-H5</sub> = 2 Hz, 2H, <sup>t</sup>bpy 3/3'), 8.43 (d, <sup>4</sup>J<sub>H3-H5</sub> =

2 Hz, 2H, <sup>1</sup>bpy 3/3'), 7.97 (dd, <sup>3</sup>J<sub>H5-H6</sub> = 6 Hz, <sup>4</sup>J<sub>H3-H5</sub> = 2 Hz, 2H, <sup>1</sup>bpy 5/5'), 7.42 (d, <sup>3</sup>J<sub>H5-H6</sub> = 6 Hz, 2H, <sup>1</sup>bpy 6/6'), 7.34 (dd, <sup>3</sup>J<sub>H5-H6</sub> = 6 Hz, <sup>4</sup>J<sub>H3-H5</sub> = 2 Hz, 2H, <sup>1</sup>bpy 5/5'), 2.62 (s, 3H, OCH<sub>3</sub>), 1.55, 1.36 (each a s, 18H, <sup>1</sup>Bu). <sup>13</sup>C NMR (201 MHz, CD<sub>3</sub>CN) δ 166.3, 165.2, 157.1, 156.5, 150.8, 149.9, 125.4, 125.3, 122.3, 122.2 (each a s, <sup>1</sup>bpy aromatic C's), 55.9 (s, OCH<sub>3</sub>), 36.7, 36.4 (each a s, C(CH<sub>3</sub>)<sub>3</sub>), 30.7, 30.3 (each a s, 3C, C(CH<sub>3</sub>)<sub>3</sub>). <sup>19</sup>F NMR (282 MHz, CD<sub>3</sub>CN) δ -75.5 (s, TFA).

**[(<sup>1</sup>bpy)<sub>2</sub>Rh(H)(TFA)][OTf] (6). Method 1.** Exclusion of chlorinated solvents is critical for the synthesis of complex **6**. THF was freshly distilled prior to use. [(<sup>1</sup>bpy)<sub>2</sub>Rh(OMe)<sub>2</sub>][OTf] (0.0606 g, 0.0712 mmol) was suspended in THF (~15 mL) in a glass Fisher-Porter reactor. HTFA (5.5 μL, 0.072 mmol) was added via a microsyringe. Upon addition of acid, [(<sup>1</sup>bpy)<sub>2</sub>Rh(OMe)<sub>2</sub>][OTf] dissolved and the solution changed from a bright yellow to a lighter yellow color. The vessel was pressurized with 30 psig of H<sub>2</sub> and heated at 70 °C in an oil bath for 17 h. After heating, the solution was a dark purple. After cooling to room temperature, the solvent was removed *in vacuo* to yield a dark purple solid that was dried further under vacuum (0.059 g, 91%). **Method 2.** [(<sup>1</sup>bpy)<sub>2</sub>Rh][TFA] (0.0050 g, 0.0066 mmol) was dissolved in acetone-*d*<sub>6</sub> in a screw cap NMR tube. HTFA (10.2 μL of solution, 0.00663 mmol, 0.65 M in acetone-*d*<sub>6</sub>) was slowly added via a microsyringe. The purple solution turned brown and then black. The product was analyzed by <sup>1</sup>H NMR spectroscopy but was not isolated. The <sup>1</sup>H NMR (300 MHz, THF-*d*<sub>8</sub>) δ 9.43 (d, <sup>3</sup>J<sub>H5-H6</sub> = 6 Hz, 1H, <sup>1</sup>bpy 6), 8.80 (d, <sup>3</sup>J<sub>H5-H6</sub> = 6 Hz, 1H, <sup>1</sup>bpy 6), 8.66 (d, <sup>4</sup>J<sub>H3-H5</sub> = 2 Hz, 1H, <sup>1</sup>bpy 3), 8.58 (d, <sup>4</sup>J<sub>H3-H5</sub> = 2 Hz, 1H, <sup>1</sup>bpy 3), 8.52 (d, <sup>3</sup>J<sub>H5-H6</sub> = 6 Hz, 2H, <sup>1</sup>bpy 6), 7.99 (dd, <sup>3</sup>J<sub>H5-H6</sub> = 5 Hz, <sup>4</sup>J<sub>H3-H5</sub> = 2 Hz, 1H, <sup>1</sup>bpy 5), 7.95 (dd, <sup>3</sup>J<sub>H5-H6</sub> = 6 Hz, <sup>4</sup>J<sub>H3-H5</sub> = 2 Hz, 1H, <sup>1</sup>bpy 5), 7.74 (dd, <sup>3</sup>J<sub>H5-H6</sub> = 6 Hz, <sup>4</sup>J<sub>H3-H5</sub> = 2 Hz, 1H, <sup>1</sup>bpy 5), 7.55 (dd, <sup>3</sup>J<sub>H5-H6</sub> = 6 Hz, <sup>4</sup>J<sub>H3-H5</sub> = 2 Hz, 1H, <sup>1</sup>bpy 5), 7.52 (d, <sup>4</sup>J<sub>H3-</sub>

$_{\text{H5}} = 1 \text{ Hz}$ , 2H,  $^1\text{bpy}$  3), 1.53 (s, 9H,  $^t\text{Bu}$ ), 1.52 (s, 9H,  $^t\text{Bu}$ ), 1.38 (s, 9H,  $^t\text{Bu}$ ), 1.33 (s, 9H,  $^t\text{Bu}$ ), -13.36 (d,  $^1J_{\text{Rh-H}} = 13 \text{ Hz}$ , 1H, Rh-H).  $^{13}\text{C}$  NMR (201 MHz, THF- $d_8$ )  $\delta$  162.8, 162.2, 161.9, 161.7, 156.2, 154.8, 154.4, 154.3, 152.2, 148.8, 146.4, 146.2, 123.3, 122.5, 122.5, 122.4, 119.6, 119.6, 118.7 (each a s,  $^1\text{bpy}$  aromatic C's, one signal missing presumably due to coincidental overlap), 33.9, 33.6, 33.5, 33.4 (each a s,  $\text{C}(\text{CH}_3)_3$ ), 27.7, 27.7, 27.6, 27.5 (each a s,  $\text{C}(\text{CH}_3)_3$ ).  $^{19}\text{F}$  NMR (282 MHz, THF- $d_8$ )  $\delta$  -76.5 (s, TFA), -79.9 (s, OTf).

**$[(^1\text{bpy})_2\text{Rh}(\text{H})(\text{Cl})][\text{TFA}]$  (7). Method 1.**  $[(^1\text{bpy})_2\text{Rh}(\text{H})(\text{TFA})][\text{OTf}]$  (0.0049 g, 0.0057 mmol) was dissolved in THF- $d_8$  (350  $\mu\text{L}$ ) in a J. Young tube.  $\text{CH}_2\text{Cl}_2$  (1.8  $\mu\text{L}$ , 0.028 mmol) was added via a microsyringe. Hexamethyldisilane (HMDS, 0.2  $\mu\text{L}$ ) was added as an internal standard. The tube was pressurized with 25 psig  $\text{H}_2(\text{g})$ . The reaction was placed in a 70  $^\circ\text{C}$  oil bath for 6 days. During this time, the reaction progress was monitored by  $^1\text{H}$  NMR spectroscopy until 100% conversion was observed (91% yield by  $^1\text{H}$  NMR spectroscopy).

**Method 2.**  $[(^1\text{bpy})_2\text{Rh}][\text{TFA}]$  (0.0214 g, 0.0284 mmol) was dissolved in acetone- $d_6$  (1 mL) in a J. Young NMR tube. The tube was placed in the freezer (-34  $^\circ\text{C}$ ) for 2 h. HCl (25.5  $\mu\text{L}$ , 0.0255 mmol, 1 N in  $\text{Et}_2\text{O}$ ) was added via a microsyringe to the tube containing the cold solution. The purple solution became a darker blackish-purple color upon addition of acid. After  $\frac{1}{2}$  h the solvent was removed *in vacuo* to yield a dark black-purple solid (0.0125 g, 56%).  $^1\text{H}$  NMR (300 MHz, Acetone- $d_6$ )  $\delta$  9.58 (d,  $^3J_{\text{H5-H6}} = 6 \text{ Hz}$ , 1H,  $^1\text{bpy}$  6), 9.26 (d,  $^3J_{\text{H5-H6}} = 6 \text{ Hz}$ , 1H,  $^1\text{bpy}$  6), 9.05, 8.98, 8.96, 8.90 (each a s, 1H,  $^1\text{bpy}$  3), 7.97-7.94 (m, partially buried under d at 7.94, 1H,  $^1\text{bpy}$  5), 7.94 (d,  $^3J_{\text{H5-H6}} = 6 \text{ Hz}$ , 2H,  $^1\text{bpy}$  5), 7.89 (d,  $^3J_{\text{H5-H6}} = 6 \text{ Hz}$ , 1H,  $^1\text{bpy}$  5), 7.71 (d,  $^3J_{\text{H5-H6}} = 6 \text{ Hz}$ , 1H,  $^1\text{bpy}$  6), 7.59 (d,  $^3J_{\text{H5-H6}} = 6 \text{ Hz}$ , 1H,  $^1\text{bpy}$  6), 7.50 (m, 1H,  $^1\text{bpy}$  5), 1.52 (s, 18H,  $^t\text{Bu}$ ), 1.38, 1.35 (each a s, 9H,  $^t\text{Bu}$ ), -14.37 (bs, 1H, Rh-H). Note: In THF- $d_8$  the hydride resonance is observed as a doublet with  $^1J_{\text{Rh-H}} = 12 \text{ Hz}$ .  $^1\text{H}$

NMR (300 MHz, THF- $d_8$ )  $\delta$  -14.42 (d,  $^1J_{\text{Rh-H}} = 12$  Hz, 1H, Rh-H).  $^{13}\text{C}$  NMR (201 MHz, Acetone- $d_6$ )  $\delta$  165.4, 165.0, 165.0, 164.8, 157.9, 157.4, 157.3, 154.9, 152.3, 150.8, 148.7, 126.2, 125.4, 125.0, 124.9, 122.9, 122.8, 122.7, 122.1 (each a s,  $^1\text{bpy}$  aromatic C's, one signal missing presumably due to coincidental overlap), 36.6, 36.5, 36.4, 36.3 (each a s,  $\text{C}(\text{CH}_3)_3$ ), 30.6, 30.6, 30.5, 30.4 (each a s,  $\text{C}(\text{CH}_3)_3$ ).  $^{19}\text{F}$  NMR (282 MHz, Acetone- $d_6$ )  $\delta$  -74.9 (s, TFA).

**$[(^1\text{bpy})_2\text{Rh}][\text{TFA}]$ .**  $(\text{COE})_2\text{Rh}(\text{TFA})$  (0.0685 g, 0.152 mmol) was dissolved in THF (~5 mL).  $^1\text{bpy}$  (0.0815 g, 0.304 mmol) in THF (~2 mL) was slowly added causing the golden-yellow solution to turn dark purple. After stirring for 30 min, the solvent was removed under vacuum. The dark purple solid was further dried under vacuum for approximately 3 h. The solid was transferred to a fine porosity frit and washed with benzene (5 x 2 mL) to remove free  $^1\text{bpy}$ . The dark purple solid was dried under vacuum overnight (0.0908 g, 79%).  $^1\text{H}$  NMR (300 MHz, Acetone- $d_6$ )  $\delta$  9.22 (d,  $^3J_{\text{H}_5\text{-H}_6} = 6$  Hz, 4H,  $^1\text{bpy}$  6/6'), 8.46 (s, 4H,  $^1\text{bpy}$  3/3'), 7.77 (dd,  $^3J_{\text{H}_5\text{-H}_6} = 6$  Hz,  $^4J_{\text{H}_3\text{-H}_5} = 2$  Hz, 4H,  $^1\text{bpy}$  5/5'), 1.46 (s, 36H,  $^1\text{Bu}$ ).  $^{13}\text{C}$  NMR (201 MHz, Acetone- $d_6$ )  $\delta$  160.7, 156.0, 151.3, 123.9, 119.8 (each a s,  $^1\text{bpy}$  aromatic C's), 35.4 (s,  $\text{C}(\text{CH}_3)_3$ ), 29.5 (s,  $\text{C}(\text{CH}_3)_3$ ).  $^{19}\text{F}$  NMR (282 MHz, Acetone- $d_6$ )  $\delta$  -75.0 (s, TFA).  $\text{M}^+ = \text{C}_{36}\text{H}_{48}\text{N}_4\text{Rh}^+$ ; obs'd (%), calc'd (%), ppm: 639.2899, 639.2929, -4.7.

**$[(^1\text{bpy})_2\text{Rh}(\text{Cl})_2][\text{TFA}]$  (8). Method 1.**  $[(^1\text{bpy})_2\text{RhCl}_2]\text{Cl}$  (0.2536 g, 0.3399 mmol) was dissolved in 1,2-dichlorobenzene (12 mL). HTFA (155  $\mu\text{L}$ , 2.02 mmol) was added via a microsyringe. The yellow solution was heated at reflux overnight. Upon cooling to room temperature  $\text{Et}_2\text{O}$  (~25 mL) was added via the condenser. The reaction mixture was placed in the freezer (-34  $^\circ\text{C}$ ) for several hours to allow for maximum precipitation. The reaction mixture was filtered through a fine porosity frit, washed with  $\text{Et}_2\text{O}$ , and the solid was dried under vacuum for approximately 1 h. The solid was reconstituted in  $\text{CH}_2\text{Cl}_2$  (~30 mL) and

washed with H<sub>2</sub>O (3 x 75 mL). The combined organic extracts were washed with NaHCO<sub>3</sub> (1 x 75 mL), dried over Na<sub>2</sub>SO<sub>4</sub>, and then reduced to dryness using a rotary evaporator. The yellow solid was dried under vacuum overnight. The solid was reconstituted in CH<sub>2</sub>Cl<sub>2</sub> and precipitated with Et<sub>2</sub>O. The solid was collected by filtering through a fine porosity frit, washed with Et<sub>2</sub>O, and dried under vacuum (0.207 g, 75%). **Method 2.** [(<sup>t</sup>bpy)<sub>2</sub>Rh(OMe)<sub>2</sub>][TFA] (0.296 g, 0.0363 mmol) was suspended in THF (~8 mL). HTFA stock solution in THF (56 μL, 0.65 M) was added via a microsyringe. The reaction mixture was stirred to dissolve the complex. The yellow solution was transferred to a glass Fisher Porter reaction vessel. The vessel was sealed and removed from the glovebox. The Fisher Porter was pressurized with 40 psig H<sub>2</sub>(g) and placed in a 70 °C oil bath for 16.5 h. The solution was a dark brown color upon removal from the oil bath. After cooling to room temperature, the solution was degassed and brought into the glovebox. The solvent was removed under vacuum. The hydride product mixture was dissolved in CH<sub>2</sub>Cl<sub>2</sub>. The vessel was sealed and removed from the glovebox. The vessel was pressurized with 25 psig H<sub>2</sub>(g) and placed in a 70 °C oil bath to heat for 23.5 h. After cooling to room temperature, the solution was degassed and brought into the glovebox. The yellow solution was reduced to dryness under vacuum. The residue was reconstituted in DCM, and Et<sub>2</sub>O was added to precipitate a pale yellow solid, which was collected by filtration through a fine porosity frit, washed with Et<sub>2</sub>O and dried under vacuum (0.0125 g, 42%). <sup>1</sup>H NMR (800 MHz, CD<sub>3</sub>CN) δ 9.66 (d, <sup>3</sup>J<sub>H5-H6</sub> = 6 Hz, 2H, <sup>t</sup>bpy 6/6'), 8.58 (d, <sup>4</sup>J<sub>H3-H5</sub> = 2 Hz, 2H, <sup>t</sup>bpy 3/3'), 8.46 (d, <sup>4</sup>J<sub>H3-H5</sub> = 2 Hz, 2H, <sup>t</sup>bpy 3/3'), 8.01 (dd, <sup>3</sup>J<sub>H5-H6</sub> = 6 Hz, <sup>4</sup>J<sub>H3-H5</sub> = 2 Hz, 2H, <sup>t</sup>bpy 5/5'), 7.51 (d, <sup>3</sup>J<sub>H5-H6</sub> = 6 Hz, 2H, <sup>t</sup>bpy 6/6'), 7.43 (dd, <sup>3</sup>J<sub>H5-H6</sub> = 6 Hz, 2 Hz, 2H, <sup>t</sup>bpy 5/5'), 1.56 (s, 18H, <sup>t</sup>Bu), 1.37 (s, 18H, <sup>t</sup>Bu). <sup>13</sup>C NMR (201 MHz, CD<sub>3</sub>CN) δ 167.3, 166.9, 156.9, 156.8, 152.3, 150.8, 126.9,

126.3, 123.5, 123.5 (each a s, <sup>1</sup>bpy aromatic C's), 36.9, 36.6 (each a s, C(CH<sub>3</sub>)<sub>3</sub>), 30.5, 30.3 (each a s, C(CH<sub>3</sub>)<sub>3</sub>). <sup>19</sup>F NMR (282 MHz, CD<sub>3</sub>CN) δ -75.6 (s, TFA). Anal. Calcd for C<sub>38</sub>H<sub>48</sub>Cl<sub>2</sub>F<sub>3</sub>N<sub>4</sub>O<sub>2</sub>Rh: C, 55.41; H, 5.87; N, 6.80. Found: C, 55.13; H, 5.85; N, 6.93. M<sup>+</sup> = C<sub>36</sub>H<sub>48</sub>Cl<sub>2</sub>N<sub>4</sub>Rh<sup>+</sup> obs'd (%), calc'd (%), ppm: 709.2306, 709.2318, -1.7.

**[(<sup>1</sup>bpy)<sub>2</sub>Rh(Br)<sub>2</sub>][TFA] (9). Method 1.** [(<sup>1</sup>bpy)<sub>2</sub>Rh(Br)<sub>2</sub>]Br (0.0253 g, 0.0288 mmol) was suspended in CH<sub>3</sub>CN (~5 mL). NaTFA (0.0040 g, 0.029 mmol) in CH<sub>3</sub>CN (~2 mL) was added dropwise. The Rh starting material dissolved upon addition of the NaTFA solution; however, the solution was slightly turbid because of the NaCl precipitate. The solution was stirred at room temperature for 1 h before reducing to dryness under vacuum. The pale yellow solid was reconstituted in CH<sub>3</sub>CN and filtered through Celite to remove NaCl. The Celite was washed with CH<sub>3</sub>CN. The filtrate was reduced to 1 mL in vacuo. Pentane was added to precipitate a yellow solid that was collected by filtration through a fine porosity frit, washed with pentane and dried under vacuum (0.0231 g, 88%). **Method 2.** [(<sup>1</sup>bpy)<sub>2</sub>Rh(OMe)<sub>2</sub>][TFA] (0.0509 g, 0.0625 mmol) was suspended in THF (~15 mL). HTFA (4.8 μL, 0.063 mmol) was added via a microsyringe. The reaction mixture was stirred to dissolve the complex. The yellow solution was transferred to a Fisher Porter reaction vessel. The vessel was sealed and removed from the glovebox. The Fisher Porter reactor was pressurized with 35 psig H<sub>2</sub>(g) and placed in a 70 °C oil bath for 6 h and 15 min. The solution was a dark brown color upon removal from the oil bath. After cooling to room temperature, the Fisher Porter was degassed and brought into the glovebox. CH<sub>2</sub>Br<sub>2</sub> (86 μL, 1.2 mmol) was added via a microsyringe. The vessel was sealed and removed from the glovebox. The vessel was pressurized with 20 psig H<sub>2</sub>(g) and placed in a 70 °C oil bath to heat for 6.5 h. The THF insoluble yellow solid was collected by filtration and washed with hexanes and pentane.

The filtrate was reduced to 1 mL in vacuo. Hexanes were added to the filtrate to precipitate a yellow solid, which was collected in the same frit as the initial solid. The solid was washed with hexanes and dried under vacuum (0.0392 g, 69%).  $^1\text{H}$  NMR (800 MHz,  $\text{CD}_3\text{CN}$ )  $\delta$  9.98 (d,  $^3J_{\text{H5-H6}} = 6$  Hz, 2H,  $^t\text{bpy}$  6/6'), 8.71 (s, 2H,  $^t\text{bpy}$  3/3'), 8.59 (s, 2H,  $^t\text{bpy}$  3/3'), 8.09 (dd,  $^3J_{\text{H5-H6}} = 6$  Hz,  $^4J_{\text{H3-H5}} = 2$  Hz, 2H,  $^t\text{bpy}$  5/5'), 7.59 (d,  $^3J_{\text{H5-H6}} = 6$  Hz, 2H,  $^t\text{bpy}$  6/6'), 7.56 (dd,  $^3J_{\text{H5-H6}} = 6$  Hz,  $^4J_{\text{H3-H5}} = 2$  Hz, 2H,  $^t\text{bpy}$  5/5'), 1.67 (s, 18H,  $^t\text{Bu}$ ), 1.48 (s, 18H,  $^t\text{Bu}$ ).  $^{13}\text{C}$  NMR (201 MHz,  $\text{CD}_3\text{CN}$ )  $\delta$  167.1, 166.9, 156.9, 156.8, 154.2, 150.4, 127.2, 126.3, 123.7, 123.6 (each a s,  $^t\text{bpy}$  aromatic C's), 36.9, 36.6 (each a s,  $\text{C}(\text{CH}_3)_3$ ), 30.5, 30.3 (each a s,  $\text{C}(\text{CH}_3)_3$ ).  $^{19}\text{F}$  NMR (282 MHz, Acetone- $d_6$ )  $\delta$  -75.4 (s, TFA).  $\text{M}^+ = \text{C}_{36}\text{H}_{48}\text{Br}_2\text{N}_4\text{Rh}^+$  obs'd, calc'd, ppm: 797.1330 (46.5), 797.1295 (49.4), 4.4; 798.1340 (19.4), 798.1327 (20.2), 1.6; 799.1306 (100), 799.1278 (100), 3.5; 800.1320 (40.3), 800.1308 (39.9), 1.5; 801.1284 (56.6), 801.1267 (54.6), 2.1; 802.1305 (20.2), 802.1290 (20.2), 1.9.

**$[(^t\text{bpy})_2\text{Rh}(\text{MeOH})_2][\text{OTf}][\text{TFA}]_2$  (**3**).** This complex is obtained as an insoluble by-product from the protonation of  $[(^t\text{bpy})_2\text{Rh}(\text{OMe})_2][\text{OTf}]$  with one equivalent of HTFA. Complex **3** has been independently synthesized as follows.  $[(^t\text{bpy})_2\text{Rh}(\text{OMe})_2][\text{OTf}]$  (0.0385 g, 0.0452 mmol) was suspended in THF (~5 mL). HTFA (7  $\mu\text{L}$ , 0.091 mmol) was added slowly. The addition of HTFA results in dissolution of  $[(^t\text{bpy})_2\text{Rh}(\text{OMe})_2][\text{OTf}]$ . After stirring for 4 h, the solvent was removed in vacuo. The yellow solid was redissolved in  $\text{CH}_2\text{Cl}_2$  and precipitated with pentane. The pale yellow solid was collected via filtration through a fine porosity frit, washed with pentane (2 x 2.5 mL) and dried under vacuum (0.0267 g, 55%).  $^1\text{H}$  NMR (300 MHz,  $\text{CD}_2\text{Cl}_2$ )  $\delta$  9.42 (d,  $^3J_{\text{H5-H6}} = 6$  Hz, 2H, 6/6'), 8.41 (s, 2H,  $^t\text{bpy}$  3/3'), 8.27 (s, 2H,  $^t\text{bpy}$  3/3'), 7.99 (d,  $^3J_{\text{H5-H6}} = 6$  Hz, 2H, 6/6'), 7.43 (s, 4H,  $^t\text{bpy}$  5/5'), 2.84 (s, 6H,  $\text{CH}_3\text{OH}$ ), 1.58 (s, 18H,  $^t\text{Bu}$ ), 1.36 (s, 18H,  $^t\text{Bu}$ ).  $^{13}\text{C}$  NMR (151 MHz,  $\text{CD}_2\text{Cl}_2$ )  $\delta$

167.7, 166.4, 156.7, 156.1, 151.5, 150.0, 126.3, 126.1, 122.2, 122.0 (each a s, <sup>4</sup>bpy aromatic C's), 36.7, 36.3 (each a s, C(CH<sub>3</sub>)<sub>3</sub>), 30.8, 30.4 (each a s, C(CH<sub>3</sub>)<sub>3</sub>). A HSQC experiment confirms that the CH<sub>3</sub>OH resonance is missing due to coincidental overlap with the solvent resonance. <sup>13</sup>C NMR (201 MHz, Acetone-*d*<sub>6</sub>) δ 167.6, 166.4, 157.0, 157.0, 152.0, 150.2, 126.3, 126.2, 123.3, 123.1 (each a s, <sup>4</sup>bpy aromatic C's), 53.1 (s, CH<sub>3</sub>OH), 36.9, 36.4 (each a s, C(CH<sub>3</sub>)<sub>3</sub>), 30.6, 30.2 (each a s, C(CH<sub>3</sub>)<sub>3</sub>). <sup>19</sup>F NMR (282 MHz, CD<sub>2</sub>Cl<sub>2</sub>) δ -77.0 (s, TFA), -80.0 (s, OTf). Anal. Calcd for C<sub>43</sub>H<sub>56</sub>F<sub>9</sub>N<sub>4</sub>O<sub>9</sub>RhS: C, 47.87; H, 5.23; N, 5.19. Found: C, 47.81; H, 5.27; N, 5.33.

**H<sub>2</sub> Activation: Kinetic Studies.** A representative catalytic reaction is described. [(<sup>4</sup>bpy)<sub>2</sub>Rh(OMe)<sub>2</sub>][OTf] (0.0360 g, 0.0423 mmol) was suspended in THF-*d*<sub>8</sub> (2 mL) in a volumetric flask. The mixture was stirred to dissolve as much solid as possible. HTFA (3.2 μL, 0.042 mmol) was added slowly dropwise. The solution was stirred causing all of the [(<sup>4</sup>bpy)<sub>2</sub>Rh(OMe)<sub>2</sub>][OTf] to dissolve. HMDS (1 μL, 0.0049 mmol) was added as an internal standard. The homogeneous yellow solution was transferred to a tube. A stir bar was added, the tube was capped, and the solution was stirred (300 rpm) for 12 h. Within 15 minutes, a yellow solid precipitated. After 12 h, the tube was removed from the glovebox and centrifuged for 5 minutes. The tube was taken into a glovebox where the yellow solution was decanted from the yellow solid. The solution (300 μL each) was added to five J. Young tubes. For some experiments, MeOH was added at this point. Either 3 equiv of methanol (0.8 μL, 0.02 mmol), or 5 equiv of methanol (1.3 μL, 0.032 mmol) was added to each tube. The equiv of methanol were based on the moles of [(<sup>4</sup>bpy)<sub>2</sub>Rh(OMe)<sub>2</sub>][OTf] added to the volumetric flask and how much of this stock solution was added to each tube (0.0063 mmol/tube). The tubes were all frozen with N<sub>2</sub>(*l*). Before inserting into the NMR probe, each

tube was degassed using 3 freeze pump thaw cycles. The tubes were left under vacuum for 30 s during these cycles. The tubes were then pressurized with H<sub>2</sub> (15, 30, 45, or 55 psig) or D<sub>2</sub> for 15 s and inverted several times to ensure adequate mixing. The tubes were placed into a temperature calibrated Varian 500 MHz spectrometer probe (equilibrated at 68 °C). The temperature was determined using 80% ethylene glycol in DMSO-*d*<sub>6</sub> and the following equation provided by Bruker Instruments, Inc. VT-Calibration Manual:  $T(K) = (4.218 - \Delta)/0.009132$ , where  $\Delta$  is the shift difference (ppm) between CH<sub>2</sub> and OH resonance of ethylene glycol. <sup>1</sup>H NMR arrays were collected. Eight scans were acquired for each spectrum. The delay time was set to 12.8 s and the acquisition time was set to 2.2 s. Each spectrum required 2 minutes to complete. Depending on the experiment, collection of a new data point began every 120 s or 180 s. Each set of conditions was run at least in triplicate, except for the 20 psig and 30 psig D<sub>2</sub> which were only performed once.

**[(<sup>1</sup>bpy)<sub>2</sub>Rh(OMe)(MeOH)][OTf][TFA] (4).** Complex 4 is generated *in situ* during the experimental set up for H<sub>2</sub> activation (see above). X-ray quality crystals were grown in the crystal tube containing the [(<sup>1</sup>bpy)<sub>2</sub>Rh(MeOH)<sub>2</sub>][OTf][TFA]<sub>2</sub> from which the stock solution was decanted and any residual solution remaining in the crystal tube after decanting (hence, there is some [(<sup>1</sup>bpy)<sub>2</sub>Rh(OMe)(MeOH)][OTf][TFA] present). DCM was added to the crystal tube, and the solution was layered with pentane. <sup>1</sup>H NMR (300 MHz, THF-*d*<sub>8</sub>)  $\delta$  9.43 (d, <sup>3</sup>*J*<sub>H5-H6</sub> = 6 Hz, 2H, <sup>1</sup>bpy 6/6'), 8.83 (d, <sup>4</sup>*J*<sub>H3-H5</sub> = 2 Hz, 2H, <sup>1</sup>bpy 3/3'), 8.65 (d, <sup>4</sup>*J*<sub>H3-H5</sub> = 2 Hz, 2H, <sup>1</sup>bpy 3/3'), 8.07 (dd, <sup>3</sup>*J*<sub>H5-H6</sub> = 6, <sup>4</sup>*J*<sub>H3-H5</sub> = 2 Hz, 2H, <sup>1</sup>bpy 5/5'), 7.56 (d, <sup>3</sup>*J*<sub>H5-H6</sub> = 6 Hz, 2H, <sup>1</sup>bpy 6/6'), 7.49 (dd, <sup>3</sup>*J*<sub>H5-H6</sub> = 6 Hz, <sup>4</sup>*J*<sub>H3-H5</sub> = 2 Hz, 2H), 2.84 (s, 6H, OCH<sub>3</sub>/CH<sub>3</sub>OH), 1.58, 1.34 (each a s, 18H, <sup>1</sup>bpy). <sup>13</sup>C NMR (201 MHz, THF-*d*<sub>8</sub>)  $\delta$  167.4, 165.8, 157.5, 157.0, 152.3, 150.1, 126.4, 125.9, 123.3, 123.1 (each a s, <sup>1</sup>bpy), 54.85 (s, OCH<sub>3</sub>), 36.90, 36.43 (each

a s, C(CH<sub>3</sub>)<sub>3</sub>), 30.60, 30.33 (each a s, C(CH<sub>3</sub>)<sub>3</sub>). <sup>19</sup>F NMR (282 MHz, THF-*d*<sub>8</sub>) δ -76.8 (s, TFA), -80.1 (OTf). Anal. Calcd for C<sub>41</sub>H<sub>55</sub>F<sub>6</sub>N<sub>4</sub>O<sub>7</sub>RhS C, 51.04; H, 5.75; N, 5.81. Found: C, 50.46; H, 5.61; N, 5.71. [(<sup>t</sup>bpy)<sub>2</sub>Rh(OMe)(TFA)][OTf] (**5**) is obtained as the minor soluble product from the reaction of [(<sup>t</sup>bpy)<sub>2</sub>Rh(OMe)<sub>2</sub>][OTf] (**1**) with HTFA (1 equiv). Complex **5** has not been isolated. <sup>1</sup>H NMR (500 MHz, THF-*d*<sub>8</sub>) δ 9.48 (d, <sup>3</sup>J<sub>H5-H6</sub> = 6 Hz, 1H, <sup>t</sup>bpy 6), 9.33 (d, <sup>3</sup>J<sub>H5-H6</sub> = 6 Hz, 1H, <sup>t</sup>bpy 6), 9.08 (d, <sup>3</sup>J<sub>H5-H6</sub> = 6 Hz, 1H, <sup>t</sup>bpy 6), 8.76 (s, 1H, <sup>t</sup>bpy 3), 8.71 (s, 1H, <sup>t</sup>bpy 3), 8.52 (s, 2H, <sup>t</sup>bpy 3), 8.14 (dd, <sup>3</sup>J<sub>H5-H6</sub> = 6 Hz, <sup>4</sup>J<sub>H3-H5</sub> = 2 Hz, 1H, <sup>t</sup>bpy 5), 7.76 (d, *J* = 6 Hz, 1H, <sup>t</sup>bpy 6), 7.59 (unresolved dd, 1H, <sup>t</sup>bpy 5), 7.43 (dd, <sup>3</sup>J<sub>H5-H6</sub> = 6 Hz, <sup>4</sup>J<sub>H3-H5</sub> = 2 Hz, 1H, <sup>t</sup>bpy 5), 7.36 (d, <sup>3</sup>J<sub>H5-H6</sub> = 6 Hz, 1H, <sup>t</sup>bpy 5), 1.44 (s, 9H, <sup>t</sup>Bu), 1.38 (s, 9H, <sup>t</sup>Bu). Remaining two <sup>t</sup>Bu resonances and OMe resonance are missing presumably due to coincidental overlap with resonances for [(<sup>t</sup>bpy)<sub>2</sub>Rh(OMe)(MeOH)][OTf][TFA] (**4**).

**Methanol Exchange.** The general procedure described above for the H<sub>2</sub> activation kinetic studies was utilized with the following modifications. After the solution (300 μL each) was added to five J. Young tubes, either 5 equiv (1.3 μL, 0.032 mmol), 10 equiv (2.6 μL, 0.064 mmol) or 20 equiv of CD<sub>3</sub>OD (5.3 μL, 0.13 mmol) relative to [(<sup>t</sup>bpy)<sub>2</sub>Rh(OMe)<sub>2</sub>][OTf] was added to each tube. Room temperature <sup>1</sup>H NMR spectra were acquired. The tubes were placed into a temperature calibrated Varian 500 MHz spectrometer probe (equilibrated at 68 °C). The temperature was determined as described above. <sup>1</sup>H NMR arrays were collected. 8 scans were acquired for each spectrum. The delay time was set to 12.8 s and the acquisition time was set to 2.2 s. Each spectrum required 2 minutes to complete. Acquisition of a new data point began every 180 s. The procedure was repeated using 5 and 10 equiv of CD<sub>3</sub>OD.

**Methanol Exchange – Coordinated CD<sub>3</sub>OD with CH<sub>3</sub>OH.** The general procedure described above for the H<sub>2</sub> activation kinetic studies was utilized with the following modifications. [(<sup>1</sup>bpy)<sub>2</sub>Rh(OCD<sub>3</sub>)<sub>2</sub>][OTf] was prepared using the procedure for the synthesis of complex **1** except CD<sub>3</sub>OD was used instead of protio methanol. The <sup>1</sup>H NMR data for [(<sup>1</sup>bpy)<sub>2</sub>Rh(OCD<sub>3</sub>)<sub>2</sub>][OTf] are identical to that of perprotio complex **1** except the methoxide peak is absent. The deuterated complex [(<sup>1</sup>bpy)<sub>2</sub>Rh(OCD<sub>3</sub>)<sub>2</sub>][OTf] was treated with 1 equivalent of DTFA. The solution (300 μL each) was divided equally into five J. Young NMR tubes, and five equiv (1.3 μL, 0.032 mmol) of MeOH were added to each tube. Room temperature <sup>1</sup>H NMR spectra were acquired. The tubes were placed into a temperature calibrated Varian 500 MHz spectrometer probe (equilibrated at 68 °C). The temperature was determined as described above. <sup>1</sup>H NMR arrays were collected. Eight scans were acquired for each spectrum. The delay time was set to 12.8 s and the acquisition time was set to 2.2 s. Acquisition of a new data point began every 180 s. The appearance for the coordinated MeOH resonance was monitored and analyzed using first-order fits.

**Hg Poisoning Test.** The general procedure described above for the H<sub>2</sub> activation kinetic studies was utilized with the following modifications. After the solution (300 μL each) was added to five J. Young tubes, a drop of Hg was added to each tube. Before inserting into the NMR probe, the tube was degassed using 3 freeze pump thaw cycles. The tube was left under vacuum for 30 s during these cycles. The tube was pressurized with H<sub>2</sub> (45 psig) for 15 s and inverted several times to ensure adequate mixing. The tube was placed into a temperature calibrated Varian 500 MHz spectrometer probe (equilibrated at 68 °C). The temperature was determined as described above. A <sup>1</sup>H NMR array was collected. 8 scans were acquired for each spectrum. The delay time was set to 12.8 s and the acquisition time

was set to 2.2 s. Each spectrum required 2 minutes to complete. Acquisition of a new data point began every 180 s.

### 3.5 References

1. Hartwig, J. F. *Organotransition Metal Chemistry: From Bonding to Catalysis*. University Science Books: Sausalito, CA, 2010.
2. Crabtree, R. H. *The Organometallic Chemistry of the Transition Metals*. 4th ed.; John Wiley & Sons: New York, NY, 2005.
3. *Handbook of Homogeneous Hydrogenation*. Wiley-VCH: Weinheim, Germany, 2007.
4. Clapham, S. E.; Hadzovic, A.; Morris, R. H. *Coord. Chem. Rev.* **2004**, *248*, 2201.
5. Deutsch, C.; Krause, N.; Lipshutz, B. H. *Chem. Rev.* **2008**, *108*, 2916.
6. Ito, M.; Ikariya, T. *Chem. Commun.* **2007**, 5134.
7. Sergeev, A. G.; Hartwig, J. F. *Science* **2011**, *332*, 439.
8. Furimsky, E. *Appl. Catal., A* **2000**, *199*, 147.
9. Fryzuk, M. D.; Montgomery, C. D.; Rettig, S. J. *Organometallics* **1991**, *10*, 467.
10. Tenn, I., W. J.; Young, K. J. H.; Oxgaard, J.; Nielson, R. J.; Goddard III, W. A.; Periana, R. A. *Organometallics* **2006**, *25*, 5173.
11. Webb, J. R.; Burgess, S. A.; Cundari, T. R.; Gunnoe, T. B. *Dalton Trans.* **2013**, *42*, 16646.
12. Webb, J. R.; Bolaño, T. B.; Gunnoe, T. B. *ChemSusChem* **2011**, *4*, 37.
13. Abdur-Rashid, K.; Faatz, M.; Lough, A. J.; Morris, R. H. *J. Am. Chem. Soc.* **2001**, *123*, 7473.

14. Conner, D.; Jayaprakash, K. N.; Cundari, T. R.; Gunnoe, T. B. *Organometallics* **2004**, *23*, 2724.
15. Feng, Y.; Lail, M.; Barakat, K. A.; Cundari, T. R.; Gunnoe, T. B.; Petersen, J. L. *J. Am. Chem. Soc.* **2005**, *127*, 14174.
16. Feng, Y.; Lail, M.; Foley, N. A.; Gunnoe, T. B.; Barakat, K. A.; Cundari, T. R.; Petersen, J. L. *J. Am. Chem. Soc.* **2006**, *128*, 7982.
17. Cundari, T. R.; Grimes, T. V.; Gunnoe, T. B. *J. Am. Chem. Soc.* **2007**, *129*, 13172.
18. Fulmer, G. R.; Muller, R. P.; Kemp, R. A.; Goldberg, K. I. *J. Am. Chem. Soc.* **2009**, *131*, 1346.
19. Fulmer, G. R.; Herndon, A. N.; Kaminsky, W.; Kemp, R. A.; Goldberg, K. I. *J. Am. Chem. Soc.* **2011**, *133*, 17713.
20. Kloek, S. M.; Heinekey, D. M.; Goldberg, K. I. *Angew. Chem., Int. Ed.* **2007**, *46*, 4736.
21. Hanson, S. K.; Heinekey, D. M.; Goldberg, K. I. *Organometallics* **2008**, *27*, 1454.
22. Bercaw, J. E.; Hazari, N.; Labinger, J. A. *Organometallics* **2009**, *28*, 5489.
23. Ahmed, T. S.; Tonics, I. A.; Labinger, J. A.; Bercaw, J. E. *Organometallics* **2013**, *32*, 3322.
24. Webb, J. R.; Pierpont, A. W.; Munro-Leighton, C.; Gunnoe, T. B.; Cundari, T. R.; Boyle, P. D. *J. Am. Chem. Soc.* **2010**, *132*, 4520.
25. Lohr, T. L.; Piers, W. E.; Parvez, M. *Chem. Sci.* **2013**, *4*, 770.
26. Sakamoto, M.; Ohki, Y.; Kehr, G.; Erker, G.; Tatsumi, K. *J. Organomet. Chem.* **2009**, *694*, 2820.
27. Seino, H.; Misumi, Y.; Hojo, Y.; Mizobe, Y. *Dalton Trans.* **2010**, *39*, 3072.

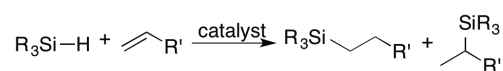
28. Misumi, Y.; Seino, H.; Mizobe, Y. *J. Am. Chem. Soc.* **2009**, *131*, 14636.
29. Burgess, S. A.; Devarajan, D.; Bolano, T.; Ess, D. H.; Gunnoe, T. B.; Sabat, M.; Myers, W. H. *Inorg. Chem.* **2014**, *53*, 5328. Portions of this chapter were adapted from this manuscript.
30. Widegren, J. A.; Finke, R. G. *J. Mol. Cat. A: Chem.* **2003**, *198*, 317.
31. Frisch, M. J.; et al. *Gaussian 09, Revision B.01*, Gaussian Inc.: Wallingford, CT, 2009.
32. Zhao, Y.; Truhlar, D. G. *Theor. Chem. Acc.* **2008**, *120*, 215.
33. Zhao, Y.; Truhlar, D. G. *Acc. Chem. Res.* **2008**, *41*, 157.
34. Marenich, A. V.; Cramer, C. J.; Truhlar, D. G. *J. Phys. Chem. B* **2009**, *113*, 6378.
35. Kubas, G. J. *Metal Dihydrogen and  $\sigma$ -Bond Complexes*. Kluwer Academic/Plenum Publishers: New York, 2001; p 259.
36. Jessop, P. G.; Morris, R. H. *Coord. Chem. Rev.* **1992**, *121*, 155.
37. Ess, D. H.; Bischof, S. M.; Oxgaard, J.; Periana, R. A.; Goddard, W. A. *Organometallics* **2008**, *27*, 6440.
38. Webb, J. R.; Munro-Leighton, C.; Pierpont, A. W.; Gurkin, J. T.; Gunnoe, T. B.; Cundari, T. R.; Sabat, M.; Petersen, J. L.; Boyle, P. D. *Inorg. Chem.* **2011**, *50*, 4195.
39. Jimenez-Tenorio, M.; Puerta, M. C.; Valerga, P.; Ortuno, M. A.; Ujaque, G.; Lledos, A. *Inorg. Chem.* **2013**, *52*, 8919.
40. Morris, R. H. *J. Am. Chem. Soc.* **2014**, *136*, 1948.
41. Yakelis, N. A.; Bergman, R. G. *Organometallics* **2005**, *24*, 3579.
42. Bolinger, C. M.; Story, N.; Sullivan, B. P.; Meyer, T. J. *Inorg. Chem.* **1988**, *27*, 4582.
43. Schrock, R. R.; Osborn, J. A. *J. Am. Chem. Soc.* **1971**, *93*, 3089.

44. Yan, S. G.; Brunschwig, B. S.; Creutz, C.; Fujita, E.; Sutin, N. *J. Am. Chem. Soc.* **1998**, *120*, 10553.

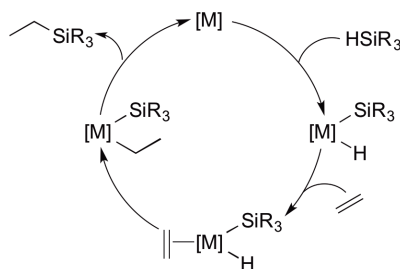
## 4 Work in Progress: Si–H Activation Across Rh(III)–OMe Bonds

### 4.1 Introduction

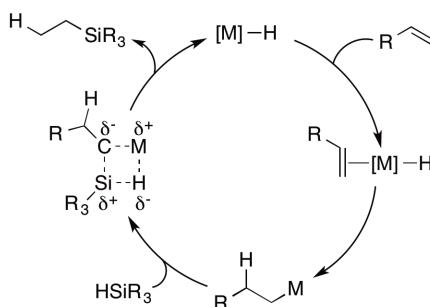
Hydrosilylation of multiple bonds is of interest in polymer and organic chemistry due to the wide utility of organosilicon compounds in the synthesis of silicon rubbers, adhesives, sealants and conductive polymers (Scheme 4.1).<sup>1</sup> Two mechanisms are most commonly invoked for transition metal catalyzed olefin hydrosilylation. Olefin hydrosilylation reactions involving late transition-metals are typically thought to function by a Chalk-Harrod oxidative addition-type mechanism (Scheme 4.2).<sup>2,3</sup> Two frequently used Pt hydrosilylation catalysts that are proposed to function by this mechanism include Speier's catalyst ( $\text{H}_2\text{PtCl}_6/\text{iPrOH}$ ) and Karstedt's catalyst ( $\text{Pt}_2[(\text{Me}_2\text{SiCH}=\text{CH}_2)_2\text{O}]_3$ ).<sup>4,5</sup> These catalysts suffer from multiple drawbacks, including the inability to recover or recycle the catalyst (Speier's) and low selectivity (Karstedt's).<sup>2,6</sup> Olefin hydrosilylation using  $d^0$  early transition-metals is thought to occur via a  $\sigma$ -bond metathesis mechanism (Scheme 4.3).<sup>7,8,9</sup> Reactions that proceed by this mechanism are often more selective than those that function by a Chalk-Harrod-type mechanism because of the regioselectivity of olefin insertion into the metal–hydride bond.<sup>7-10</sup>



**Scheme 4.1.** Hydrosilylation of olefins is used to synthesize alkylsilanes.



**Scheme 4.2.** Chalk-Harrod mechanism for transition metal catalyzed hydrosilylation.

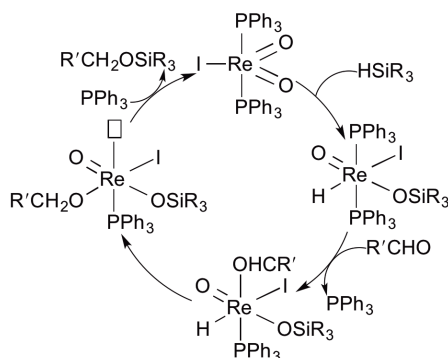


**Scheme 4.3.** Mechanism for  $d^0$  transition metal catalyzed hydrosilylation involving  $\sigma$ -bond metathesis.

While most hydrosilylation catalysts perform Si–H activation by oxidative addition or  $\sigma$ -bond metathesis, complexes bearing multiply-bonded heteroatomic ligands have been shown to exhibit reactivity that may be inconsistent with these established pathways.<sup>11-15</sup> One example was reported by Toste and co-workers, who found that the reaction of aldehydes and ketones with tertiary silanes in the presence of the Re(V) catalyst  $(PPh)_3Re(O)_2I$  did not proceed by the predicted Chalk-Harrod-type mechanism.<sup>14,16</sup> The proposed alternative mechanism involves the initial addition of the Si–H bond across the Re=O bond to form a siloxyrhenium hydride intermediate (Scheme 4.4). Subsequent insertion of a carbonyl substrate into the Re–H bond of the siloxyrhenium hydride intermediate leads to the formation of a siloxyrhenium alkoxide and a retro-[2 + 2] reaction between the siloxy and alkoxy ligand releases the silyl ether

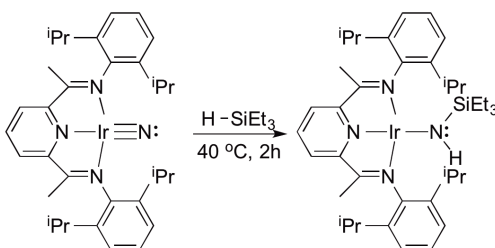
product. However, there has been debate over Toste's proposed mechanism.<sup>13</sup>

Stoichiometric deuterium labeling experiments for the reaction of equimolar mixture of benzaldehyde,  $\text{DSiMe}_2\text{Ph}$  and  $(\text{PhMe}_2\text{SiO})\text{Re}(\text{PPh}_3)_2(\text{I})(\text{H})$  provide results inconsistent with the mechanism proposed by Toste and co-workers.<sup>13</sup>



**Scheme 4.4.** Toste and co-workers proposed mechanism for hydrosilylation using  $(\text{PPh}_3)_3\text{Re}(\text{O})_2\text{I}$ .

Sieh and Burger reported the activation of Si–H bonds of triethyl and triaryl silanes using an Ir(III) nitrido complex  $(^i\text{Pr}_3\text{NNN})\text{Ir}\equiv\text{N}$  ( $^i\text{Pr}_3\text{NNN} = 2,6$ -diacetylpyridinebis(2,6-diisopropylaniline)) to give the corresponding Ir silyl amido complexes (Scheme 4.5).<sup>15</sup> Experimental and computational evidence suggest the Si–H bond activation occurs via the concerted electrophilic attack by the silane ( $\delta^+$ ) on the nitride ( $\delta^-$ ).<sup>15</sup>



**Scheme 4.5.** Si–H bond activation using  $(^i\text{Pr}_3\text{NNN})\text{Ir}\equiv\text{N}$ .

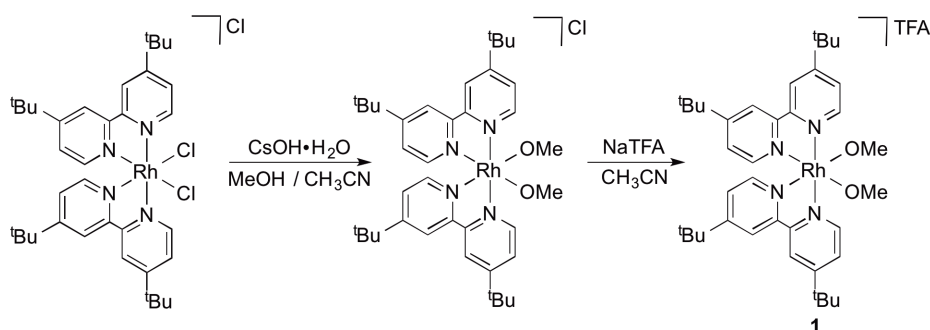
It is possible that Si–H activation by metal oxo complexes proceeds by 1,2-addition of Si–H bonds across M=O bonds. Heterolytic cleavage of a Si–H bond by the Ru–S bond of a tethered SDmp (DMP = 2,6-dimesitylphenyl) Ru(II) complex has been reported.<sup>17</sup> In Chapter 3, the activation of dihydrogen using the Rh(III) methoxide complexes  $[(^t\text{bpy})_2\text{Rh}(\text{OMe})(\text{MeOH})][\text{OTf}][\text{TFA}]$  and  $[(^t\text{bpy})_2\text{Rh}(\text{OMe})(\text{TFA})][\text{OTf}]$  ( $^t\text{bpy}$  = 4,4'-di-*tert*-butyl-2,2'-bipyridyl; OTf = trifluoromethanesulfonate; TFA = trifluoroacetate) was described. Given that Si–H bonds (BDE = 75 kcal/mol) are slightly polar and weaker than strong non-polar H–H bonds (BDE = 104 kcal/mol), we hypothesized that  $[(^t\text{bpy})_2\text{Rh}(\text{OMe})]^{2+}$  would also be able activate Si–H bonds.<sup>18</sup> Herein, we report initial findings for the activation of Si–H bonds using  $[(^t\text{bpy})_2\text{Rh}(\text{OMe})(\text{MeOH})]^{2+}$ .

## 4.2 Results and Discussion

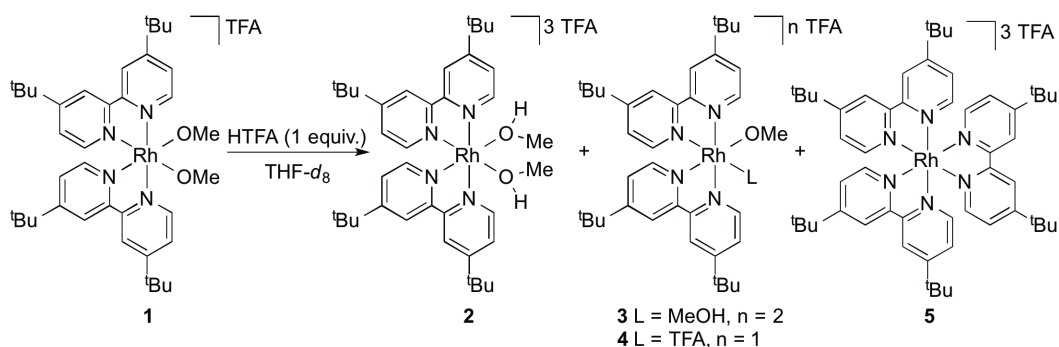
The precursor to these active species,  $[(^t\text{bpy})_2\text{Rh}(\text{OMe})_2][\text{TFA}]$ , has a trifluoroacetate counterion rather than the triflate counterion utilized in Chapter 3. The TFA counterion was utilized for the work in this chapter instead of OTf because a shorter reaction time for the Si–H activation reaction was observed when using a trifluoroacetate counterion.

The synthesis of  $[(^t\text{bpy})_2\text{Rh}(\text{OMe})_2][\text{TFA}]$  (**1**) was reported in Chapter 3. Briefly, complex **1** is synthesized in two steps (Scheme 4.6). First, the addition of CsOH·H<sub>2</sub>O in MeOH to previously reported  $[(^t\text{bpy})_2\text{Rh}(\text{Cl})_2]\text{Cl}$  gives  $[(^t\text{bpy})_2\text{Rh}(\text{OMe})_2]\text{Cl}$ . A subsequent salt metathesis reaction of  $[(^t\text{bpy})_2\text{Rh}(\text{OMe})_2]\text{Cl}$  with NaTFA gives the desired  $[(^t\text{bpy})_2\text{Rh}(\text{OMe})_2][\text{TFA}]$  (**1**).

The active species for Si–H activation are prepared in a manner identical to the species for H<sub>2</sub> activation. The addition of HTFA (1 equiv.) to [(<sup>t</sup>bpy)<sub>2</sub>Rh(OMe)<sub>2</sub>][TFA] gives multiple products including [(<sup>t</sup>bpy)<sub>2</sub>Rh(MeOH)<sub>2</sub>][TFA]<sub>3</sub> (**2**), [(<sup>t</sup>bpy)<sub>2</sub>Rh(OMe)(MeOH)][TFA]<sub>2</sub> (**3**), [(<sup>t</sup>bpy)<sub>2</sub>Rh(OMe)(TFA)][TFA] (**4**) and some [(<sup>t</sup>bpy)<sub>3</sub>Rh][TFA]<sub>3</sub> (**5**) (Scheme 4.7). Insoluble complex **2** and sparingly soluble complex **5** are separated after centrifugation of the reaction mixture and decanting of the solution from the insoluble products. <sup>1</sup>H NMR analysis of the filtrate after removing **2** and **5** by filtration indicates a mixture of complexes **3** and **4** in approximately a 1:1 ratio.



**Scheme 4.6.** Synthesis of [(<sup>t</sup>bpy)<sub>2</sub>Rh(OMe)<sub>2</sub>][TFA] (**1**).



**Scheme 4.7.** The addition of HTFA (1 equiv.) to [(<sup>t</sup>bpy)<sub>2</sub>Rh(OMe)<sub>2</sub>][TFA] (**1**) leads to the formation of four products.

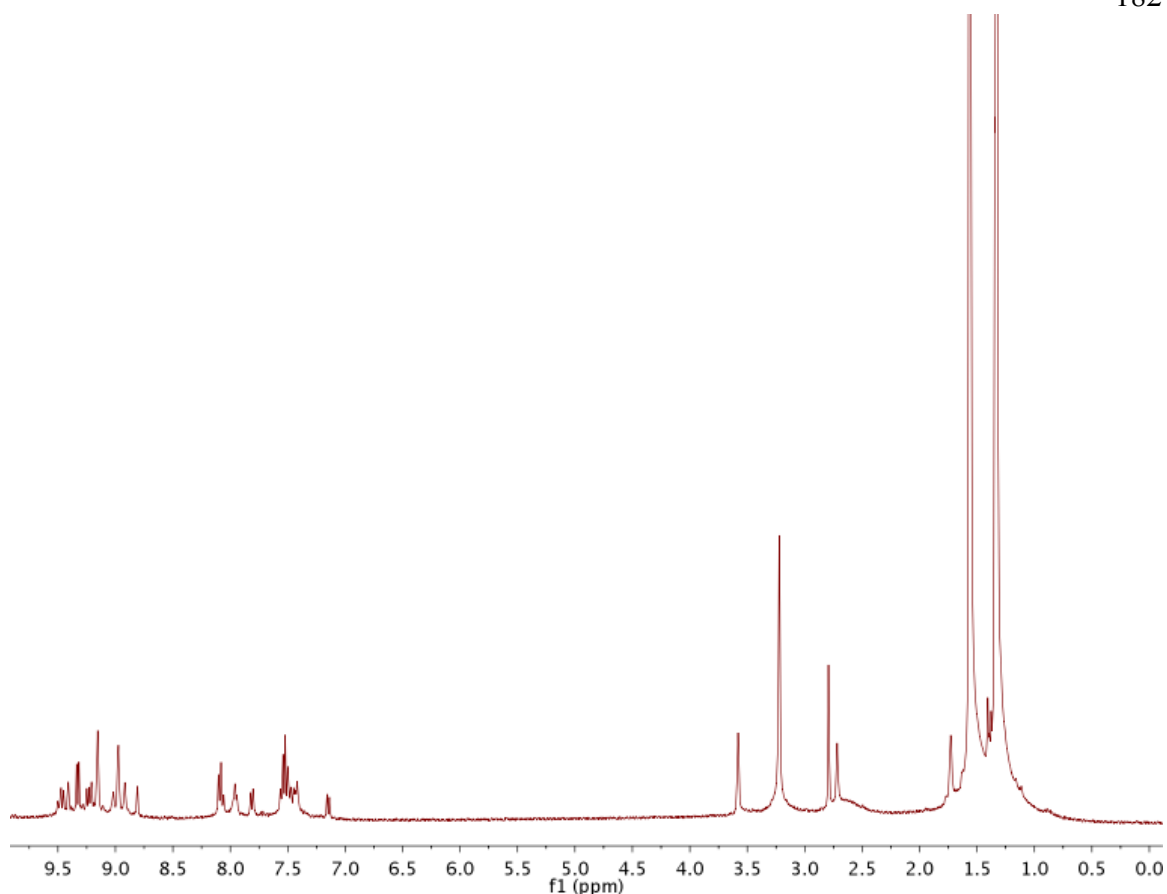
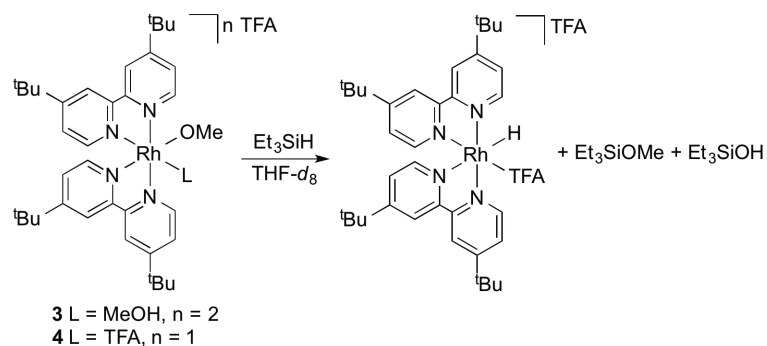


**Figure 4.1.**  $^1\text{H}$  NMR spectrum of soluble protonation products  $[(^t\text{bpy})_2\text{Rh}(\text{OMe})(\text{MeOH})][\text{TFA}]_2$  (**3**) and  $[(^t\text{bpy})_2\text{Rh}(\text{OMe})(\text{TFA})][\text{TFA}]$  (**4**) in  $\text{THF-}d_8$ .

A solution of complexes **3** and **4** reacts immediately at room temperature with  $\text{Et}_3\text{SiH}$  (1 equiv.) to generate  $\text{Et}_3\text{SiOMe}$ ,  $\text{Et}_3\text{SiOH}$  and a new Rh hydride complex ( $-14.43$  ppm, d,  $^1J_{\text{Rh-H}} = 27$  Hz). The identity of this intermediate Rh–H has not been determined, but possibilities will be discussed below. After  $\sim 12$  h at room temperature, complete conversion to a final hydride product ( $-13.36$  ppm, d,  $^1J_{\text{Rh-H}} = 13$  Hz) is observed, which is consistent with  $[(^t\text{bpy})_2\text{Rh}(\text{H})(\text{TFA})][\text{TFA}]$  (**6**) (see Scheme 4.8, Figure 4.2 and Chapter 3).



**Scheme 4.8.** The final products from the reaction of  $[(\text{tBu}_4\text{bpy})_2\text{Rh}(\text{OMe})(\text{L})]^{n+}$  ( $\text{L} = \text{MeOH}$ ,  $n = 2$  TFA, **(3)**;  $\text{L} = \text{TFA}$ ,  $n = 1$  TFA, **(4)**) with  $\text{Et}_3\text{SiH}$  are  $[(\text{tBu}_4\text{bpy})_2\text{Rh}(\text{H})(\text{TFA})][\text{TFA}]$ ,  $\text{Et}_3\text{SiOMe}$  and  $\text{Et}_3\text{SiOH}$ .

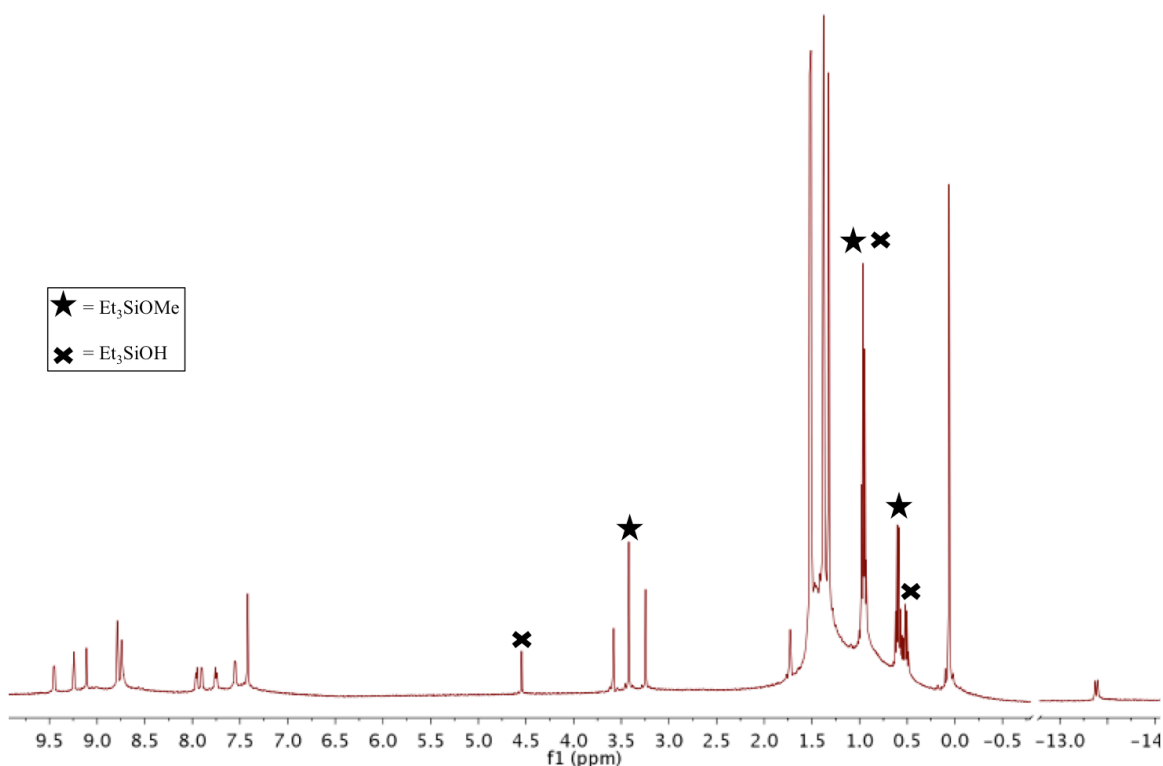
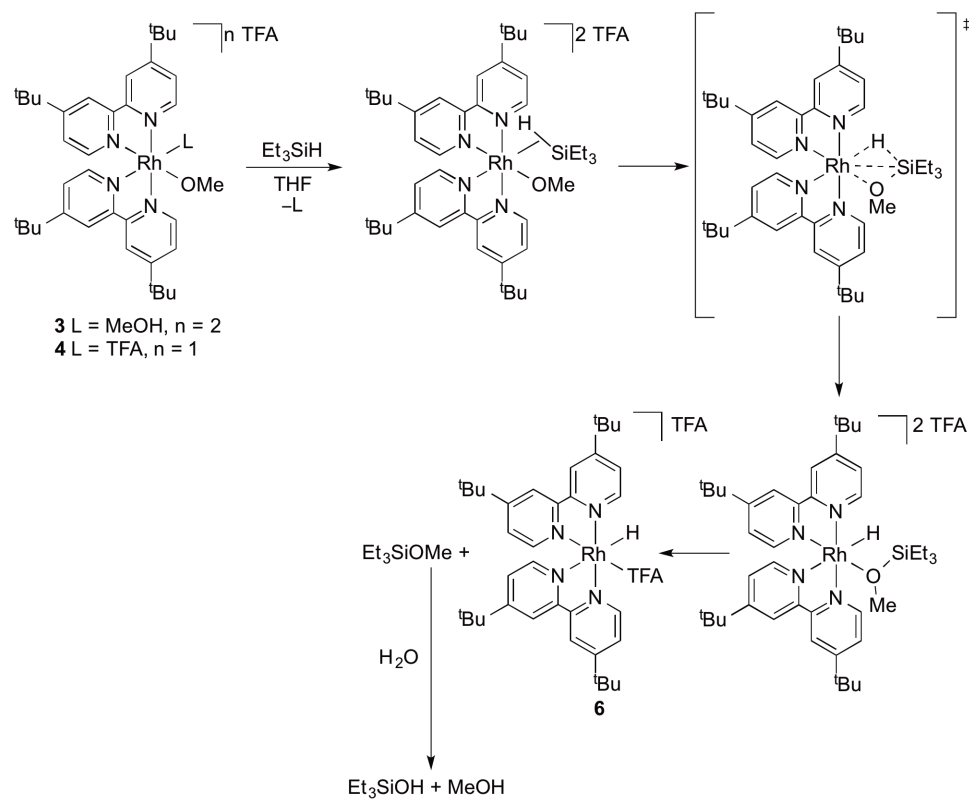


**Figure 4.2.**  $^1\text{H}$  NMR spectrum in  $\text{THF-}d_8$  of the final product mixture from the reaction of  $\text{Et}_3\text{SiH}$  with  $[(\text{tBu}_4\text{bpy})_2\text{Rh}(\text{OMe})(\text{L})]^{n+}$  ( $\text{L} = \text{MeOH}$ ,  $n = 2$  TFA, **(3)**;  $\text{L} = \text{TFA}$ ,  $n = 1$  TFA, **(4)**). Free  $\text{CH}_3\text{OH}$  is observed at 3.27 ppm and hexamethyldisilane (HMDS, added as an internal standard) is observed at 0.0 ppm. Resonances for the organic products are observed at 4.54 ppm, 3.42 ppm, 0.96 ppm, 0.60 ppm, and 0.52 ppm.

#### 4.2.1 Characterization of the Organic Reaction Products

The identity of the organic products from the activation of  $\text{Et}_3\text{SiH}$  by the Rh(III) methoxide complexes **3** and **4** are  $\text{Et}_3\text{SiOMe}$  and  $\text{Et}_3\text{SiOH}$ . The formation of  $\text{Et}_3\text{SiOMe}$  is consistent with Si–H activation by 1,2-SiH-addition across the Rh–OMe bond (Scheme 4.9). The characteristic peaks for  $\text{Et}_3\text{SiOMe}$  observed in the  $^1\text{H}$  NMR spectrum include a singlet for the OMe (3.42 ppm), a triplet at 0.96 ppm ( $^3J_{\text{H-H}} = 8$  Hz) and a quartet at 0.60 ppm ( $^3J_{\text{H-H}} = 8$  Hz) (Figure 4.3). There is some coincidental overlap of the methyl triplet for  $\text{Et}_3\text{SiOMe}$  and  $\text{Et}_3\text{SiOH}$  (Figure 4.3).  $\text{Et}_3\text{SiOH}$  is presumably formed by hydrolysis of  $\text{Et}_3\text{SiOMe}$  by residual proton sources in the reaction mixture (Scheme 4.9). Addition of  $\text{H}_2\text{O}$  to the mixture of  $\text{Et}_3\text{SiOMe}$  and  $\text{Et}_3\text{SiOH}$  allows for full conversion to  $\text{Et}_3\text{SiOH}$ . The hydroxyl resonance of  $\text{Et}_3\text{SiOH}$  is observed at 4.54 ppm. The ethyl resonances for  $\text{Et}_3\text{SiOH}$  are observed as a triplet at 0.93 ppm ( $^3J_{\text{H-H}} = 8$  Hz) and a quartet at 0.51 ( $^3J_{\text{H-H}} = 8$  Hz) (Figure 4.4). The production of  $\text{Et}_3\text{SiOH}$  has been confirmed by GC/MS and  $^1\text{H}$  NMR spectroscopy by comparison to an authentic sample. An authentic sample of  $\text{Et}_3\text{SiOMe}$  could not be purchased; however, NMR data of the reaction mixture are consistent with previously reported data.<sup>19</sup>



**Scheme 4.9.**  $\text{Et}_3\text{SiOMe}$  and  $\text{Et}_3\text{SiOH}$  are observed as the organic products from the activation of  $\text{Et}_3\text{SiH}$  using  $[(^t\text{bpy})_2\text{Rh}(\text{OMe})(\text{L})]^{n+}$  [L = MeOH, n = 2 TFA, (3); L = TFA, n = TFA, (4)].

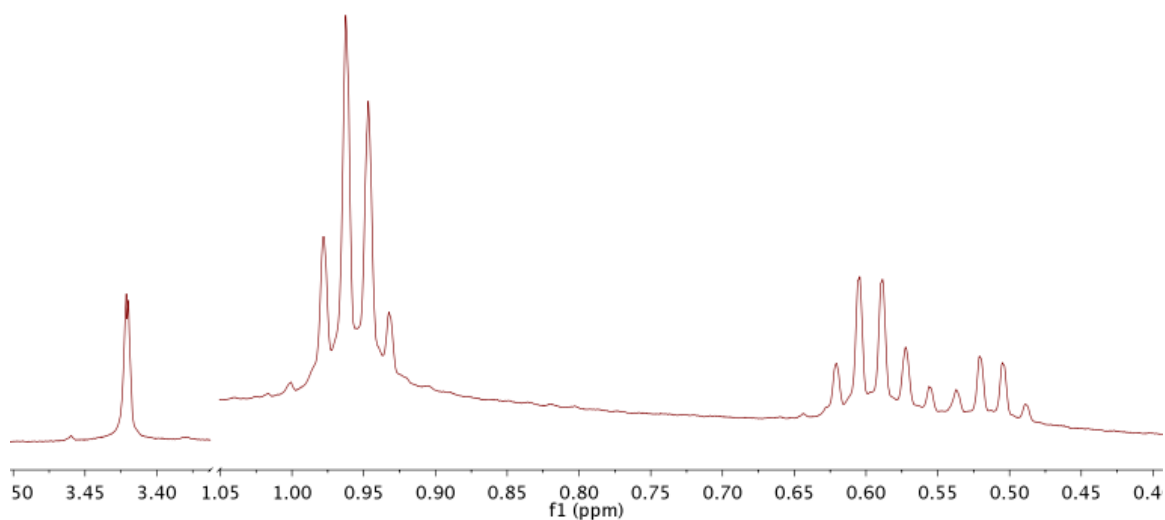


**Figure 4.3.** Partial  $^1\text{H}$  NMR spectrum for the product mixture from the activation of Si–H of  $\text{Et}_3\text{SiH}$  by  $[(^t\text{bpy})_2\text{Rh}(\text{OMe})(\text{L})]^{n+}$  ( $\text{L} = \text{MeOH}$ ,  $n = 2$  TFA, **(3)**;  $\text{L} = \text{TFA}$ ,  $n = \text{TFA}$ , **(4)**). The methyl peaks of  $\text{Et}_3\text{SiOMe}$  and  $\text{Et}_3\text{SiOH}$  overlap (0.98 – 0.93 ppm). The resonances due to the methylene groups appear at 0.60 ppm for  $\text{Et}_3\text{SiOMe}$  and 0.51 ppm for  $\text{Et}_3\text{SiOH}$ . The resonance for the OMe group of  $\text{Et}_3\text{SiOMe}$  is observed at 3.42 ppm

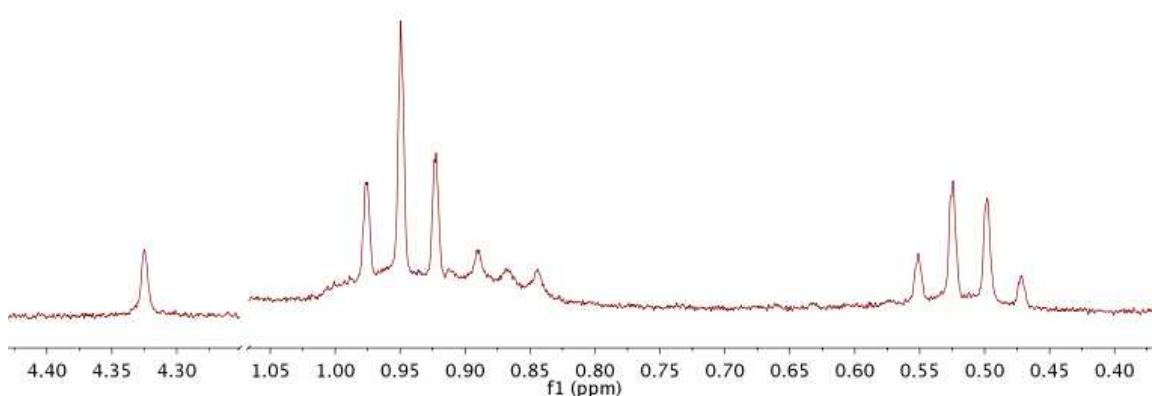


**Figure 4.4.**  $^1\text{H}$  NMR spectrum of  $\text{Et}_3\text{SiOH}$  in  $\text{THF-}d_8$ .

#### 4.2.2 Identity of the Rh–H Complexes

Possible identities of the new Rh–H complex that gives a hydride resonance at –14.4 ppm ( $^1J_{\text{Rh-H}} = 27$  Hz) are shown in Figure 4.5. It is believed that this first observed hydride is not  $[(^1\text{bpy})_2\text{Rh}(\eta^2\text{-H-SiEt}_3)(\text{OMe})][\text{TFA}]_2$  because it is anticipated that the Rh–H resonance for  $[(^1\text{bpy})_2\text{Rh}(\eta^2\text{-H-SiEt}_3)(\text{OMe})][\text{TFA}]_2$  would appear further downfield. For the Rh(I) complex  $(\text{CO})_2\text{ClRh}(\eta^2\text{-SiHCl}_3)$  a broad resonances at –8.26 ppm is observed in the room temperature  $^1\text{H}$  NMR spectrum for  $\eta^2\text{-SiH}$ .<sup>20</sup> At 248 K, a doublet with was observed with  $^{29}\text{Si}$  satellites consistent with a  $\eta^2\text{-silane}$  ( $^1J_{\text{Rh-H}} = 13$  Hz,  $^1J_{\text{Si-H}} = 49$  Hz).<sup>20</sup> Resonance for  $\eta^2\text{-SiH}$  groups for Ru complexes are typically observed between

-7.75 ppm and -10.30 ppm.<sup>21,22,23</sup> For the  $\text{Ru}(\eta^2\text{-SiHR}_3)$  complexes, satellites ranging in magnitude from ~30 to 50 Hz are observed for  $^{29}\text{Si}$  coupling to the hydride.<sup>21,22,23</sup> No satellites were observed for the -14 ppm hydride resonances. Since there is no resonance in the  $^1\text{H}$  NMR spectrum that appears to correspond to coordinated MeOH, we suspect that the identity of the intermediate hydride is not  $[(^t\text{bpy})_2\text{Rh}(\text{H})(\text{MeOH})][\text{TFA}]_2$ . Instead, it is proposed that the hydride complex at -14.43 ppm is  $[(^t\text{bpy})_2\text{Rh}(\text{H})(\text{Et}_3\text{SiOMe})][\text{TFA}]$  (**7**). When the Si-H bond activation reaction is performed at 12 °C another intermediate hydride is observed at -14.32 (d,  $^1J_{\text{Rh-H}} = 24$  Hz). Since free  $\text{Et}_3\text{SiOMe}$  is hydrolyzed to  $\text{Et}_3\text{SiOH}$  by residual proton sources (*i.e.* free MeOH), we propose that below room temperature  $\text{Et}_3\text{SiOMe}$  likely dissociates from  $[(^t\text{bpy})_2\text{Rh}(\text{H})(\text{Et}_3\text{SiOMe})][\text{TFA}]$  and free  $\text{Et}_3\text{SiOMe}$  is then hydrolyzed to  $\text{Et}_3\text{SiOH}$  and free  $\text{Et}_3\text{SiOH}$ , which can coordinate to Rh to form  $[(^t\text{bpy})_2\text{Rh}(\text{H})(\text{Et}_3\text{SiOH})][\text{TFA}]$  (**8**) (Scheme 4.10). Changes in the ethyl resonances are observed over time suggesting that the -14 ppm hydride species likely involve coordinated  $\text{Et}_3\text{SiOH}$  and  $\text{Et}_3\text{SiOMe}$  (Figure 4.6). The addition of one equiv. of  $\text{Et}_3\text{SiOH}$  to putative  $[(^t\text{bpy})_2\text{Rh}(\text{H})(\text{Et}_3\text{SiOMe})][\text{TFA}]$  does not result in the formation of a second hydride providing experimental evidence to suggest that  $[(^t\text{bpy})_2\text{Rh}(\text{H})(\text{Et}_3\text{SiOH})][\text{TFA}]$  is not the identity of the second -14 ppm hydride species.

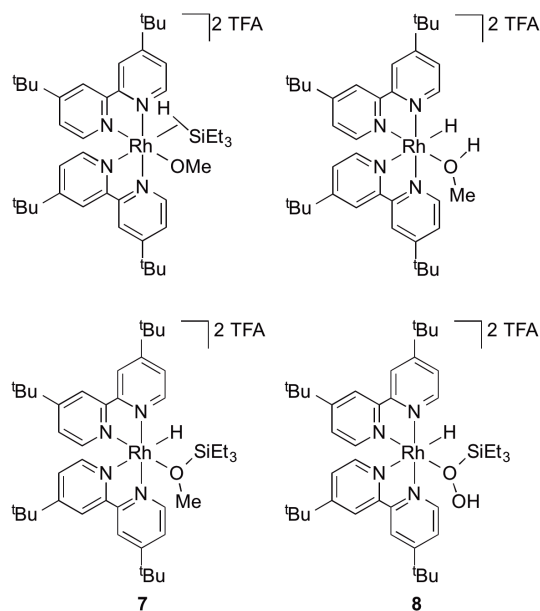


**Figure 4.5.** Possible identities of the hydride complex with observed resonance at  $-14$  ppm.

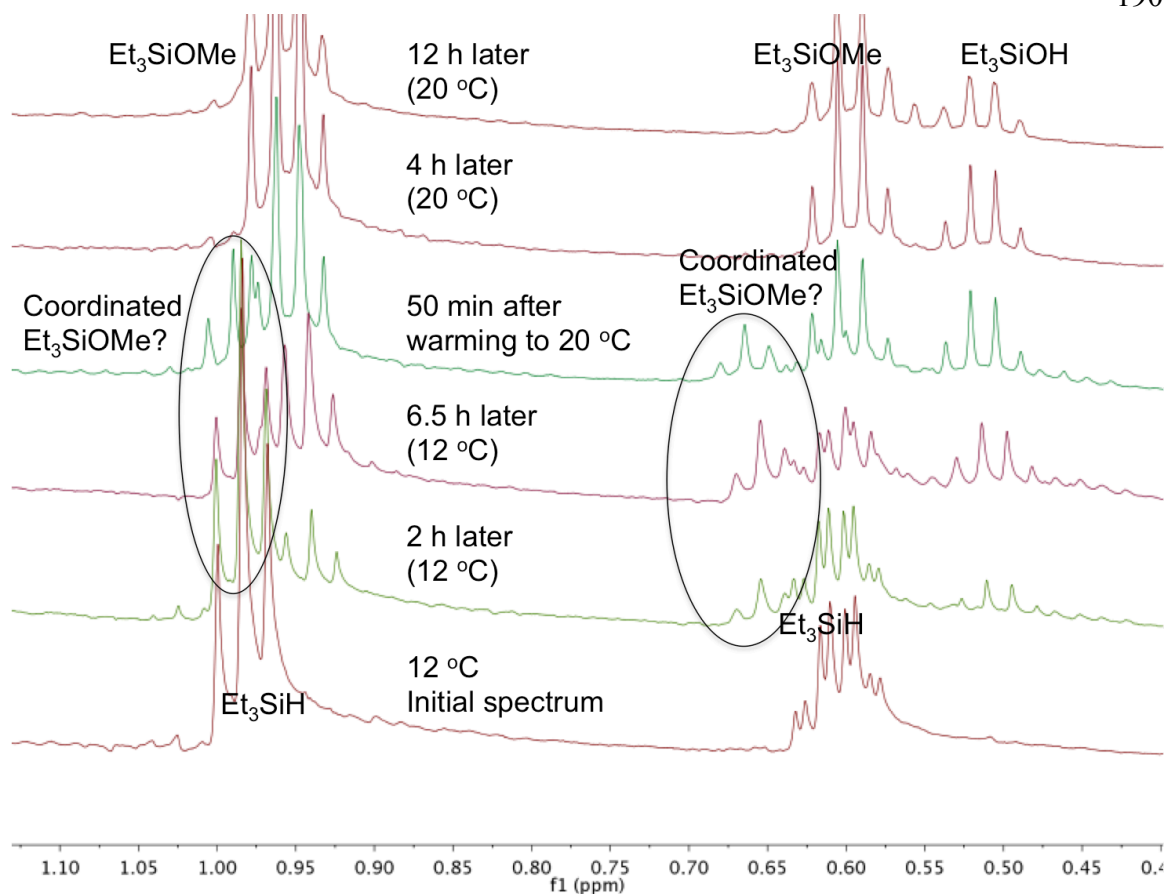
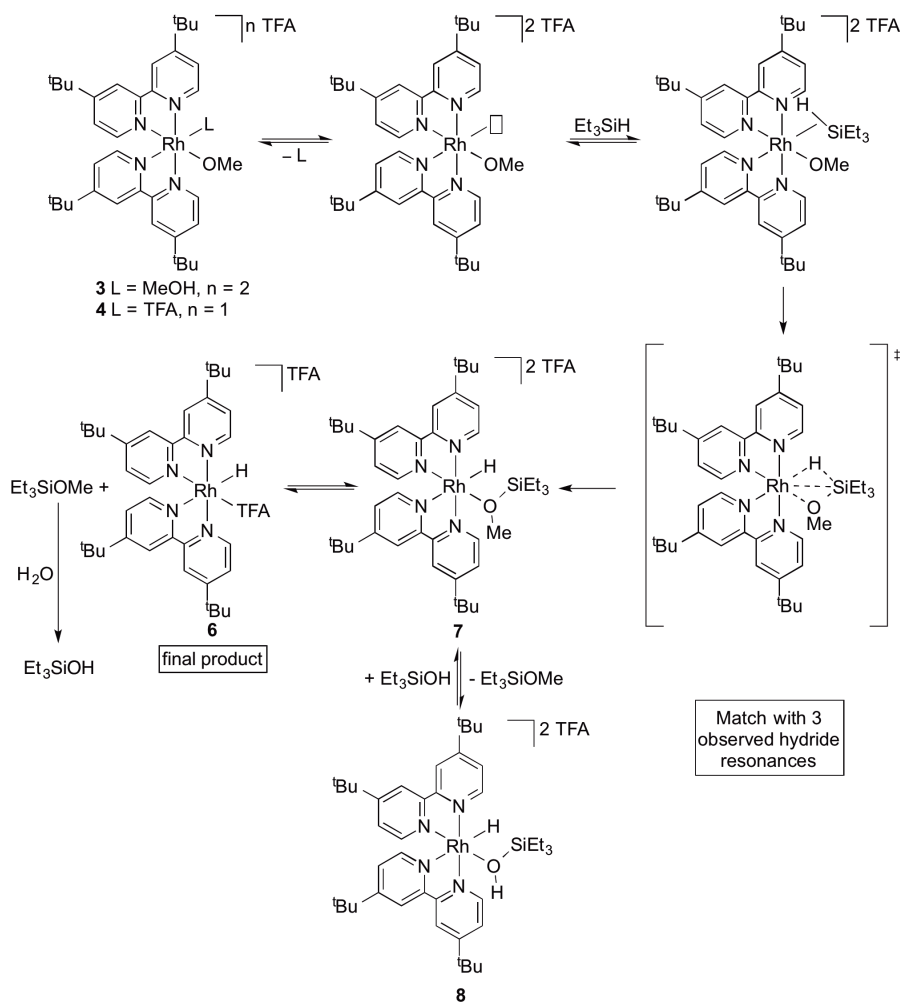


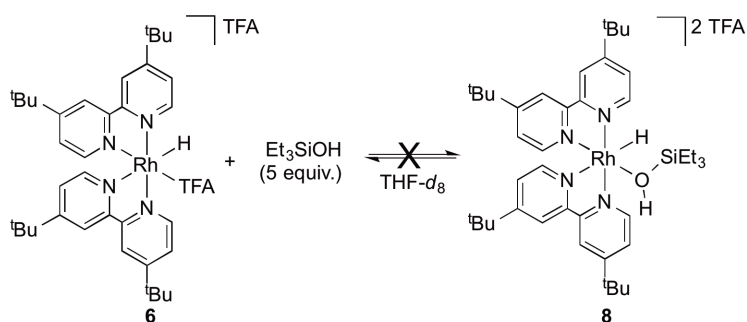
**Figure 4.6.** Stacked  $^1\text{H}$  NMR spectra plot for the activation of Si-H bonds of  $\text{Et}_3\text{SiH}$  by  $[(^1\text{bpy})_2\text{Rh}(\text{OMe})(\text{MeOH})][\text{TFA}]_2$  (**3**) and  $[(^1\text{bpy})_2\text{Rh}(\text{OMe})(\text{TFA})][\text{TFA}]$  (**4**) showing the changes in the ethyl resonances with time.



**Scheme 4.10.** Proposed mechanism for the reaction of  $\text{Et}_3\text{SiH}$  with  $[(^t\text{bpy})_2\text{Rh}(\text{OME})(\text{MeOH})][\text{TFA}]_2$  (**3**), and  $[(^t\text{bpy})_2\text{Rh}(\text{OME})(\text{TFA})][\text{TFA}]$  (**4**).

To gather evidence to either confirm or refute the identity of the two  $-14$  ppm hydrides,  $\text{Et}_3\text{SiOH}$  (5 equiv.) was added to the final reaction solution containing complex **6**,  $\text{Et}_3\text{SiOMe}$  and  $\text{Et}_3\text{SiOH}$ . No changes were observed by  $^1\text{H}$  NMR spectroscopy after sitting at room temperature for 4 h. The solution was put in an ice bath for 30 min and no changes were observed in a  $^1\text{H}$  NMR spectrum acquired immediately after removing the sample from the ice bath. The tube was then heated at  $60^\circ\text{C}$  for 1 h. A variable temperature  $^1\text{H}$  NMR study was performed on  $[(^t\text{bpy})_2\text{Rh}(\text{H})(\text{TFA})][\text{TFA}]$  (**6**). In this

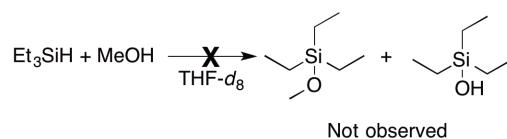
experiment, no resonances for the  $-14$  ppm hydrides appeared upon cooling a solution of complex **6**,  $\text{Et}_3\text{SiOMe}$  and  $\text{Et}_3\text{SiOH}$  to  $12$  °C or  $3$  °C. These results suggest that there is no equilibrium between  $[(^t\text{bpy})_2\text{Rh}(\text{H})(\text{TFA})][\text{TFA}]$  and complex **8** or **7** (Scheme 4.11). Perhaps, instead, the two  $-14$  hydrides are rotamers of  $[(^t\text{bpy})_2\text{Rh}(\text{H})(\text{Et}_3\text{SiOMe})][\text{TFA}]$ . In another experiment, the reaction was monitored until the formation of complex **7** was observed, and  $\text{Et}_3\text{SiOH}$  (1 equiv.) was added. The formation of complex **8** was not observed.



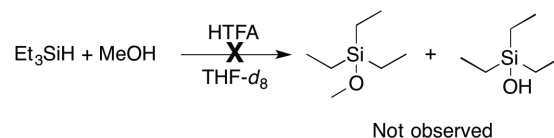
**Scheme 4.11.**  $[(^t\text{bpy})_2\text{Rh}(\text{H})(\text{TFA})][\text{TFA}]$  (**6**) and  $[(^t\text{bpy})_2\text{Rh}(\text{H})(\text{Et}_3\text{SiOH})][\text{TFA}]$  (**8**) are not in equilibrium.

### 4.2.3 Control Reactions

Control reactions were performed to ensure that the observed Si–H activation involves  $[(^t\text{bpy})_2\text{Rh}(\text{OMe})(\text{L})]^{n+}$  ( $\text{L} = \text{MeOH}$ ,  $n = 2$  TFA, **3**;  $\text{L} = \text{TFA}$ ,  $n = \text{TFA}$ , **4**). Combining  $\text{Et}_3\text{SiH}$  with  $\text{MeOH}$  in THF does not lead to the formation of  $\text{Et}_3\text{SiOMe}$  or  $\text{Et}_3\text{SiOH}$  (Scheme 4.12). Additionally, neither  $\text{Et}_3\text{SiOMe}$  nor  $\text{Et}_3\text{SiOH}$  were observed when  $\text{Et}_3\text{SiH}$ ,  $\text{MeOH}$ , and HTFA are combined in THF (Scheme 4.13). Collectively, these control reactions suggest that the formation of  $\text{Et}_3\text{SiOMe}$  and  $\text{Et}_3\text{SiOH}$  involves  $[(^t\text{bpy})_2\text{Rh}(\text{OMe})(\text{L})]^{n+}$  ( $\text{L} = \text{MeOH}$ ,  $n = 2$  TFA, **3**;  $\text{L} = \text{TFA}$ ,  $n = \text{TFA}$ , **4**).



**Scheme 4.12.** Control reaction between Et<sub>3</sub>SiH and MeOH.



**Scheme 4.13.** Control reaction between Et<sub>3</sub>SiH and MeOH in the presence of HTFA.

### 4.3 Summary and Future Work

The Rh(III) methoxide complexes [(<sup>t</sup>bpy)<sub>2</sub>Rh(OMe)(L)]<sup>n+</sup> (L = MeOH, n = 2 TFA, **3**; L = TFA, n = TFA, **4**) activate the Si–H bond of Et<sub>3</sub>SiH to ultimately form [(<sup>t</sup>bpy)<sub>2</sub>Rh(H)(TFA)][TFA] and Et<sub>3</sub>SiOMe. Hydrolysis of Et<sub>3</sub>SiOMe leads to the formation of Et<sub>3</sub>SiOH. Based on the results from the activation of H<sub>2</sub> reported in Chapter 3, we hypothesize that the Si–H activation occurs via the 1,2-addition of Si–H bonds across Rh(III) methoxide bonds; however, mechanistic details of the Si–H activation reaction remain unknown. Two intermediate hydrides are observed by <sup>1</sup>H NMR spectroscopy, which are tentatively assigned as [(<sup>t</sup>bpy)<sub>2</sub>Rh(H)(Et<sub>3</sub>SiOMe)][TFA]<sub>2</sub> and [(<sup>t</sup>bpy)<sub>2</sub>Rh(H)(Et<sub>3</sub>SiOH)][TFA]<sub>2</sub>. Alternatively the intermediate hydrides could be [(<sup>t</sup>bpy)<sub>2</sub>Rh(η<sup>2</sup>-H–SiEt<sub>3</sub>)(OMe)][TFA]<sub>2</sub> and [(<sup>t</sup>bpy)<sub>2</sub>Rh(H)(MeOH)][TFA]<sub>2</sub> however spectroscopic data suggests provides evidence against these two species (see above). Detailed kinetic studies will be performed to determine the dependence on Rh methoxide complex and concentration of silane. The activation of other alkyl and aryl silanes will also be investigated. Additionally, we would like to test complexes

$[(^t\text{bpy})_2\text{Rh}(\text{OMe})(\text{L})]^{n+}$  (L = MeOH, n = 2 TFA, **3**; L = TFA, n = TFA, **4**) for catalytic hydrosilylation of aldehydes, ketones, and imines as well as catalytic silane oxidation.

#### 4.4 Experimental Section

**General Considerations.** Unless otherwise noted, all synthetic procedures were performed under anaerobic conditions in a nitrogen-filled glovebox or by using standard Schlenk techniques. Glovebox purity was maintained by periodic nitrogen purges and was monitored by an oxygen analyzer ( $\text{O}_2$  (g) < 15 ppm for all reactions). Toluene, tetrahydrofuran, pentane and diethyl ether were dried by distillation from sodium/benzophenone. Pentane was distilled over  $\text{P}_2\text{O}_5$ . Acetonitrile and methanol were dried by distillation from  $\text{CaH}_2$ . Hexanes, benzene and dichloromethane were purified by passage through a column of activated alumina. Acetonitrile- $d_3$ , methylene chloride- $d_2$ , acetone- $d_6$  and THF- $d_8$  were stored under a  $\text{N}_2$  atmosphere over 4 Å molecular sieves.  $\text{H}_2$  and  $\text{D}_2$  were purchased from Matheson Gas and Cambridge Isotope Labs, respectively, and used as received.  $^1\text{H}$  and  $^{13}\text{C}$  NMR spectra were recorded on a Varian Mercury Plus 300 MHz (75 MHz operating frequency for  $^{13}\text{C}$  NMR), Varian Inova 500 MHz spectrometer (125 MHz operating frequency for  $^{13}\text{C}$  NMR), Bruker Avance DRX 600 MHz spectrometer (150 MHz operative frequency for  $^{13}\text{C}$  NMR), or Bruker Avance III 800 MHz spectrometer (201 MHz operative frequency for  $^{13}\text{C}$  NMR). All  $^1\text{H}$  and  $^{13}\text{C}$  NMR spectra are referenced against residual proton signals ( $^1\text{H}$  NMR) or the  $^{13}\text{C}$  resonances of the deuterated solvent ( $^{13}\text{C}$  NMR).  $^{19}\text{F}$  NMR (operating frequency 282 MHz) spectra were obtained on a Varian Mercury Plus 300 MHz spectrometer and referenced against an external standard of hexafluorobenzene ( $\delta = -164.9$ ). The preparation of  $\text{NaBAR}'_4$ <sup>24</sup> and  $[(^t\text{bpy})_3\text{Rh}][\text{OTf}]_3$ <sup>25</sup> have been previously reported. The  $^t\text{bpy}$

version of [(bpy)<sub>2</sub>Rh(Cl)<sub>2</sub>]Cl was synthesized following the published procedure.<sup>26</sup> The synthesis of [(<sup>t</sup>bpy)<sub>2</sub>Rh(OMe)<sub>2</sub>][TFA] and [(<sup>t</sup>bpy)<sub>2</sub>Rh(H)(TFA)][OTf] were reported in Chapter 3.

**Representative Et<sub>3</sub>SiH Activation Reaction.** [(<sup>t</sup>bpy)<sub>2</sub>Rh(OMe)<sub>2</sub>][TFA] (**1**) (0.0100 g, 0.0136 mmol) was suspended in THF-*d*<sub>8</sub> (500 μL), and HTFA (1.0 μL, 0.013 mmol) was slowly added. HMDS (0.2 μL, 0.001 mmol) was added as an internal standard. Within 15 min, a yellow solid precipitated. The yellow reaction mixture was stirred (300 rpm) for 12 h. After 12 h, the tube was removed from the glovebox and centrifuged for 5 min. The tube was taken into a glovebox where the dark yellow solution was decanted from the yellow solid. The solution was added to a screw-cap NMR tube. Et<sub>3</sub>SiH (2.2 μL, 0.014 mmol) was added via a microsyringe. The reaction was monitored periodically by <sup>1</sup>H NMR spectroscopy. During the course of the reaction the solution changes from dark yellow to dark purple.

[(<sup>t</sup>bpy)<sub>2</sub>Rh(H)(TFA)] (**6**). <sup>1</sup>H NMR (600 MHz, THF-*d*<sub>8</sub>) δ 9.78 (d, <sup>3</sup>J<sub>H5-H6</sub> = 6 Hz, 1H, <sup>t</sup>bpy 6), 9.64 (d, <sup>4</sup>J<sub>H3-H5</sub> = 2 Hz, 1H, <sup>t</sup>bpy 3), 9.51 (s, 1H, <sup>t</sup>bpy 3), 9.14 (d, <sup>4</sup>J<sub>H3-H5</sub> = 2 Hz, 1H, <sup>t</sup>bpy 3), 9.11 (d, <sup>3</sup>J<sub>H5-H6</sub> = 6 Hz, 1H, <sup>t</sup>bpy 6), 9.09 (d, <sup>4</sup>J<sub>H3-H5</sub> = 2 Hz, 1H, <sup>t</sup>bpy 3), 8.30 (dd, <sup>3</sup>J<sub>H5-H6</sub> = 6 Hz, <sup>4</sup>J<sub>H3-H5</sub> = 2 Hz, 1H, <sup>t</sup>bpy 5), 8.23 (dd, <sup>3</sup>J<sub>H5-H6</sub> = 6 Hz, <sup>4</sup>J<sub>H3-H5</sub> = 2 Hz, 1H, <sup>t</sup>bpy 5), 8.09 (dd, <sup>3</sup>J<sub>H5-H6</sub> = 6 Hz, <sup>4</sup>J<sub>H3-H5</sub> = 2 Hz, 1H, <sup>t</sup>bpy 5), 7.89 (dd, <sup>3</sup>J<sub>H5-H6</sub> = 6 Hz, <sup>4</sup>J<sub>H3-H5</sub> = 2 Hz, 1H, <sup>t</sup>bpy 5), 7.76 (s, 2H, <sup>t</sup>bpy 6), 1.86, 1.85, 1.72, 1.66 (each a s, 9H, <sup>t</sup>Bu), -13.04 (d, <sup>1</sup>J<sub>Rh-H</sub> = 3 Hz, 1H, Rh-H). <sup>13</sup>C NMR (151 MHz, THF-*d*<sub>8</sub>) δ 166.29, 165.49, 165.45, 165.10, 159.41, 157.85, 157.81, 157.51, 155.32, 151.06, 149.28, 149.03, 125.44, 125.38, 125.29, 124.99, 124.17, 122.87, 122.04 (each a s, <sup>t</sup>bpy, one signal missing presumably due to coincidental overlap), 37.05, 36.74, 36.68, 36.53 (each a s,

<sup>t</sup>Bu-C(CH<sub>3</sub>)<sub>3</sub>, 30.85, 30.70, 30.65, 30.63 (each a s, <sup>t</sup>Bu-C(CH<sub>3</sub>)<sub>3</sub>). <sup>19</sup>F NMR (282 MHz, THF-*d*<sub>8</sub>) δ -76.40 (s, TFA), -76.76 (s, TFA). Attempts to isolate complex **6** were unsuccessful. We speculate the decomposition product is [(<sup>t</sup>bpy)<sub>2</sub>Rh(TFA)<sub>2</sub>][TFA].

**Et<sub>3</sub>SiOH.** <sup>1</sup>H NMR (500 MHz, THF-*d*<sub>8</sub>) δ 4.54 (s, 1H, OH), 0.93 (t, <sup>3</sup>J<sub>H-H</sub> = 8 Hz, 9H, CH<sub>2</sub>CH<sub>3</sub>), 0.51 (q, <sup>3</sup>J<sub>H-H</sub> = 8 Hz, 6H, CH<sub>2</sub>CH<sub>3</sub>). <sup>13</sup>C NMR (201 MHz, THF) δ 7.3 (s, CH<sub>2</sub>CH<sub>3</sub>), 7.0 (s, CH<sub>2</sub>CH<sub>3</sub>).

**Et<sub>3</sub>SiOMe.** <sup>1</sup>H NMR (500 MHz, THF-*d*<sub>8</sub>) δ 3.42 (s, OCH<sub>3</sub>), 0.96 (t, <sup>3</sup>J<sub>H-H</sub> = 8 Hz, 9H, CH<sub>2</sub>CH<sub>3</sub>), 0.60 (q, <sup>3</sup>J<sub>H-H</sub> = 8 Hz, 6H, CH<sub>2</sub>CH<sub>3</sub>). <sup>13</sup>C NMR (201 MHz, THF-*d*<sub>8</sub>) δ 50.9 (s, OCH<sub>3</sub>), 7.2 (s, CH<sub>2</sub>CH<sub>3</sub>), 5.0 (s, CH<sub>2</sub>CH<sub>3</sub>).

#### 4.5 References

1. Brook, M. A. *Silicon in Organic, Organometallic, and Polymer Chemistry*. John Wiley & Sons, Inc.: New York, 2000.
2. Crabtree, R. H. *The Organometallic Chemistry of the Transition Metals*. 4th ed.; John Wiley & Sons: New York, NY, 2005.
3. Hartwig, J. F. *Organotransition Metal Chemistry: From Bonding to Catalysis*. University Science Books: Sausalito, CA, 2010.
4. Speier, J. L. *Adv. Organometc. Chem.* **1979**, *17*, 407.
5. Hitchcock, P. B.; Lappert, M. F.; Warhurst, N. J. W. *Angew. Chem. Int. Ed.* **1991**, *30*, 438.
6. Marko, I. E.; Sterin, S.; Buisine, O.; Mignani, G.; Branlard, P.; Tinant, B.; Declercq, J. *Science* **2002**, *298*, 202.
7. Molander, G. A.; Julius, M. *J. Org. Chem.* **1992**, *57*, 6347.
8. Fu, P. F.; Brard, L.; Li, Y. W.; Marks, T. J. *J. Am. Chem. Soc.* **1995**, *117*, 7157.

9. Gountchev, T. I.; Tilley, T. D. *Organometallics* **1999**, *18*, 5661.
10. Glaser, P. B.; Tilley, T. D. *J. Am. Chem. Soc.* **2003**, *125*, 13640.
11. Fernandes, A. C.; Fernandes, R.; Romao, C. C.; Royo, B. *Chem. Commun.* **2005**, 213.
12. Reis, P. M.; Romao, C. C.; Royo, B. *Dalton Trans.* **2006**, 1842.
13. Shirobokov, O. G.; Kuzmina, L. G.; Nikonov, G. I. *J. Am. Chem. Soc.* **2011**, *133*, 6487.
14. Nolin, K. A.; Krumper, J. R.; Pluth, M. D.; Bergman, R. G.; Toste, F. D. *J. Am. Chem. Soc.* **2007**, *129*, 14684.
15. Sieh, D.; Burger, P. *J. Am. Chem. Soc.* **2013**, *135*, 3971.
16. Kennedy-Smith, J. J.; Nolin, K. A.; Gunterman, H. P.; Toste, F. D. *J. Am. Chem. Soc.* **2003**, *125*, 4056.
17. Klare, H. F. T.; Oestreich, M.; Ito, J.; Nishiyama, H.; Ohki, Y.; Tatsumi, K. *J. Am. Chem. Soc.* **2011**, *133*, 3312.
18. Luo, Y.-R. *Handbook of Bond Dissociation Energies in Organic Compounds*. CRC Press: Boca Raton, 2003.
19. Ojima, Y.; Yamaguchi, K.; Mizuno, N. *Adv. Synth. Catal.* **2009**, *351*, 1405.
20. Yu, M. M.; Jing, H. Z.; Fu, X. F. *Inorg. Chem.* **2013**, *52*, 10741.
21. Freeman, S. T. N.; Lemke, F. R.; Brammer, L. *Organometallics* **2002**, *21*, 2030.
22. Gutsulyak, D. V.; Churakov, A. V.; Kuzmina, L. G.; Howard, J. A. K.; Nikonov, G. I. *Organometallics* **2009**, *28*, 2655.
23. Gutsulyak, D. V.; Vyboishchikov, S. F.; Nikonov, G. I. *J. Am. Chem. Soc.* **2010**, *132*, 5950.

24. Yakelis, N. A.; Bergman, R. G. *Organometallics* **2005**, *24*, 3579.
25. Cline, E. D.; Adamson, S. E.; Bernhard, S. *Inorg. Chem.* **2008**, *47*, 10378.
26. Bolinger, C. M.; Story, N.; Sullivan, B. P.; Meyer, T. J. *Inorg. Chem.* **1988**, *27*, 4582.

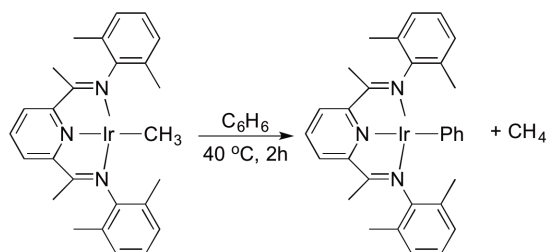
## 5 Synthesis of Rh–Heteroatom Complexes with Pyridine-Diimine Ligand

### 5.1 Introduction

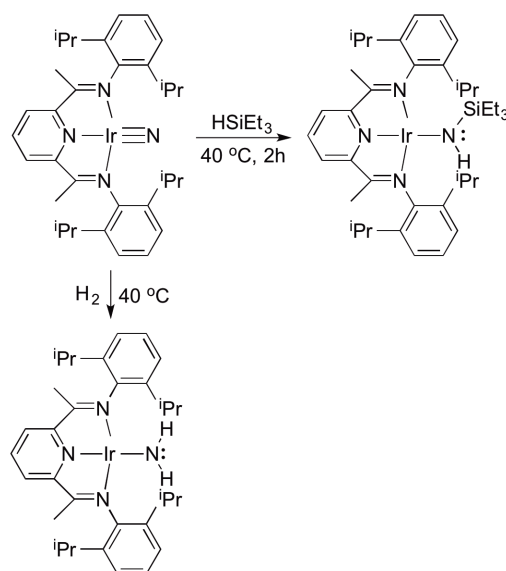
The  $[(^R\text{bpy})_2\text{RhX}_2]^+$   $[(^R\text{bpy})_2\text{Rh}(\text{HX})_2]^{3+}$  and  $[(^R\text{bpy})_2\text{Rh}(\text{X})(\text{L})]^{2+}$  (R = H, <sup>t</sup>Bu; X = OH, OR, NPh; L = NH<sub>2</sub>Ph, MeOH, H<sub>2</sub>O, Me, Cl) complexes discussed in Chapters 2, 3 and 4 were unable to activate C–H bonds under the conditions investigated. As a result, we sought to modify the ancillary ligand with hopes of obtaining an active Rh–X complex for C–H activation reactions. Our focus remained on Rh(III) hoping to combine an acidic metal with a basic ligand X for C–H activation. Tridentate aryl-substituted pyridine-diimine (NNN) complexes were targeted because these ligands are sterically demanding, and we believed this would inhibit the formation of  $\mu$ -X dimers.

Late transition metal complexes supported by NNN ligands are known.<sup>1-10</sup> The Pd(II) and Ni(II) complexes  $[(\text{ArN}=\text{C}(\text{R})\text{C}(\text{R})=\text{NAr})\text{M}(\text{CH}_3)(\text{OEt}_2)] [\text{BAR}'_4]$  (M = Pd, Ni; R = H, Me; Ar = 2,6-C<sub>6</sub>H<sub>3</sub>(<sup>i</sup>Pr)<sub>2</sub>, 2,6-C<sub>6</sub>H<sub>3</sub>Me<sub>2</sub>; BAR'<sub>4</sub> = tetrakis[(3,5-trifluoromethyl)phenyl]borate) have been reported to act as “robust” catalysts for ethylene polymerization.<sup>11</sup> Upon activation with methylaluminoxane (MAO), NNN Fe(II), Fe(III), and Co(II) complexes (NNN = 2,6-(ArNCR')C<sub>5</sub>H<sub>3</sub>N; Ar = 2,6-diisopropyl, 2,6-dimethyl, 2,6-diethyl; R = H, Me) serve as catalyst for ethylene polymerization.<sup>1,2</sup> Higher activity was observed when ketimine-based NNN ligands were used over aldimine-based systems (R = Me versus H) and Fe ketimine NNN complexes were more reactive than Co.<sup>2</sup> Intermolecular benzene C–H activation is observed upon heating (40 °C) (<sup>i</sup>PrNNN)Ir(Me) [<sup>i</sup>PrNNN = 2,6-diacetylpyridinebis(2,6-diisopropylaniline)] in benzene to give (<sup>i</sup>PrNNN)Ir(Ph) and CH<sub>4</sub> (Scheme 5.1).<sup>3</sup> The activation of Si–H bonds of triethyl and triaryl silanes by (<sup>i</sup>PrNNN)Ir≡N to give the corresponding Ir

silyl amido complexes has been reported (Scheme 5.2).<sup>4</sup> Experimental and computational studies suggest that Si–H activation proceeds via electrophilic attack of the silane on the nucleophilic nitrido nitrogen. The addition of dihydrogen to the electrophilic nitrogen atom of the Ir nitrido complex ( $^{i\text{Pr}}\text{NNN})\text{Ir}\equiv\text{N}$  to give the corresponding Ir amido complex has also been observed (Scheme 5.2).<sup>5</sup> The activation of dihydrogen is accelerated by acid because the lone pair on the nitrido helps to lower the activation barrier. Collectively between the Si–H and dihydrogen activation, the nitrido unit of ( $^{i\text{Pr}}\text{NNN})\text{Ir}\equiv\text{N}$  has been shown to have both nucleophilic and electrophilic properties depending on whether a Si–H or H–H bond is being broken.<sup>4,5</sup> Si–H bond activation requires nucleophilic attack of the nitrido ligand on the silane while the nitrido acts as an electrophile when activating  $\text{H}_2$ .

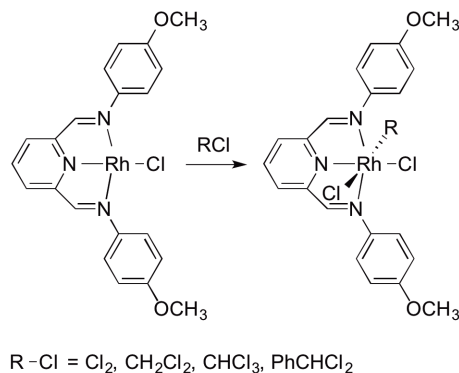


**Scheme 5.1.** Benzene C–H activation by ( $^{i\text{Pr}}\text{NNN})\text{IrMe}$ .



**Scheme 5.2.** Si–H and H<sub>2</sub> activation by (<sup>iPr</sup>NNN)Ir≡N.

Several examples of Rh(I) and Rh(III) complexes with NNN ligands have been reported.<sup>6-10,12</sup> The (NNN)Rh complexes are not active for ethylene polymerization.<sup>6</sup> Rh(I) complexes with NNN ligands undergo facile oxidative addition reactions.<sup>7,12</sup> For example, the oxidative additions of C–Cl bonds of CH<sub>2</sub>Cl<sub>2</sub>, CHCl<sub>3</sub>, benzyl chloride, and α,α-dichlorotoluene to (<sup>p-anisyl</sup>NNN)Rh(Cl) (<sup>p-anisyl</sup>NNN = 2,6-diacetylpyridinebis(4-methoxyaniline)] have been reported (Scheme 5.3).<sup>7</sup> This chapter will describe the synthesis, characterization and reactivity studies of NNN Rh(I) and Rh(III) heteroatom complexes.

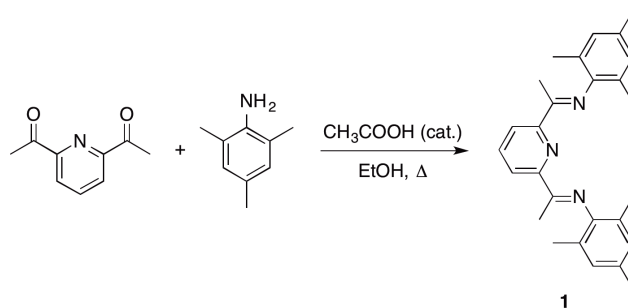


**Scheme 5.3.** Oxidative addition of C–Cl bonds to (<sup>p-anisyl</sup>NNN)Rh(Cl).

## 5.2 Results and Discussion

### 5.2.1 Synthesis of 2,6-diacetylpyridinebis(2,4,6-trimethylaniline)

The terdentate aryl-substituted pyridine diimine ligand 2,6-diacetylpyridinebis(2,4,6-trimethylaniline) (<sup>Mes</sup>NNN, **1**) was prepared using the previously reported method for the synthesis of 2,6-bis(imino)pyridyl ligands.<sup>2</sup> As shown in Scheme 5.4, the condensation of 2,6-diacetylpyridine with 2,4,6-trimethylaniline (2 equiv.) in the presence of a catalytic amount of glacial acetic acid gave yellow crystalline solid **1** upon cooling. Complex **1** was obtained in a 50% isolated yield. The <sup>1</sup>H NMR spectrum of **1** (Figure 5.1) shows a doublet at 7.97 ppm (<sup>3</sup>J<sub>H-H</sub> = 8 Hz) and a triplet at 7.97 (<sup>3</sup>J<sub>H-H</sub> = 8 Hz) for the pyridyl 3 and 4 position protons, respectively. A singlet is observed at 6.86 ppm for the protons on the mesityl ring. A singlet is observed at 2.26 ppm for the methyl group on the imine. The mesityl methyls are observed as singlets at 2.21 ppm (6H) and 1.97 ppm (12H), respectively.



**Scheme 5.4** Synthesis of 2,6-diacetylpyridinebis(2,4,6-trimethylaniline) (<sup>Mes</sup>NNN) (**1**).

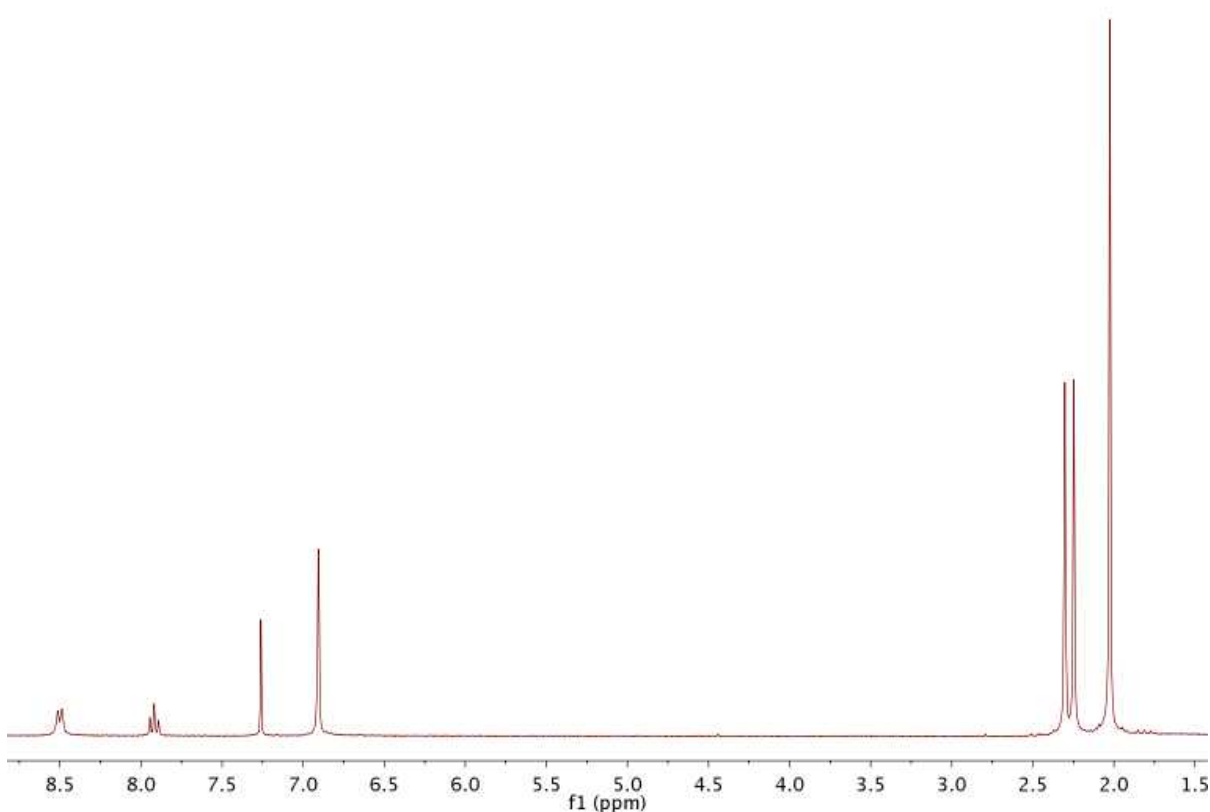
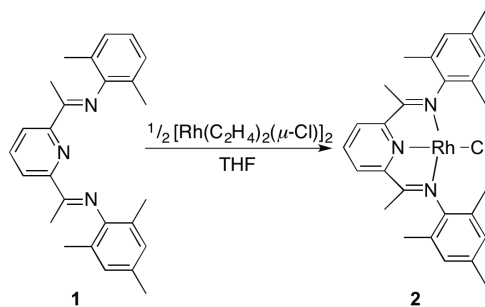


**Figure 5.1**  $^1\text{H}$  NMR spectrum of 2,6-diacetylpyridinebis(2,4,6-trimethylaniline) ( $^{\text{Mes}}\text{NNN}$ ) (**1**) in  $\text{CDCl}_3$ .

### 5.2.2 Synthesis of ( $^{\text{Mes}}\text{NNN}$ )Rh(Cl) and Oxidation to ( $^{\text{Mes}}\text{NNN}$ )Rh(Me)(OTf) $_2$

( $^{\text{Mes}}\text{NNN}$ )Rh(Cl) (**2**) was prepared using the procedure reported by Nuckel and Burger for related complexes (Scheme 5.5).<sup>12</sup> Compound **1** was suspended in THF, and dropwise addition of a THF solution of  $[\text{Rh}(\text{C}_2\text{H}_4)(\mu\text{-Cl})_2]$  resulted in an immediate color change from yellow to dark green. ( $^{\text{Mes}}\text{NNN}$ )Rh(Cl) (**2**) was recrystallized in THF/pentane at room temperature to give a clean product in 21% isolated yield. Relative to the  $^1\text{H}$  NMR spectrum of free ligand (Figure 5.1), the resonance for the aromatic protons of complex **2** are shifted downfield. A triplet at 8.51 ppm ( $^3J_{\text{H-H}} = 8$  Hz) and a doublet at 7.80 ppm ( $^3J_{\text{H-H}} = 8$  Hz)

are observed for the pyridyl 3 and 4 position protons, respectively (Figure 5.2). In addition, a singlet is observed at 6.85 ppm for the mesityl aromatic protons. The resonance for the methyl of the imine carbon is observed as a singlet at 2.27 ppm. The methyl groups of the mesityl are observed as singlets at 2.03 (12H) and 1.53 (6H) ppm.



**Scheme 5.5.** Synthesis of (<sup>Mes</sup>NNN)Rh(Cl) (**2**).

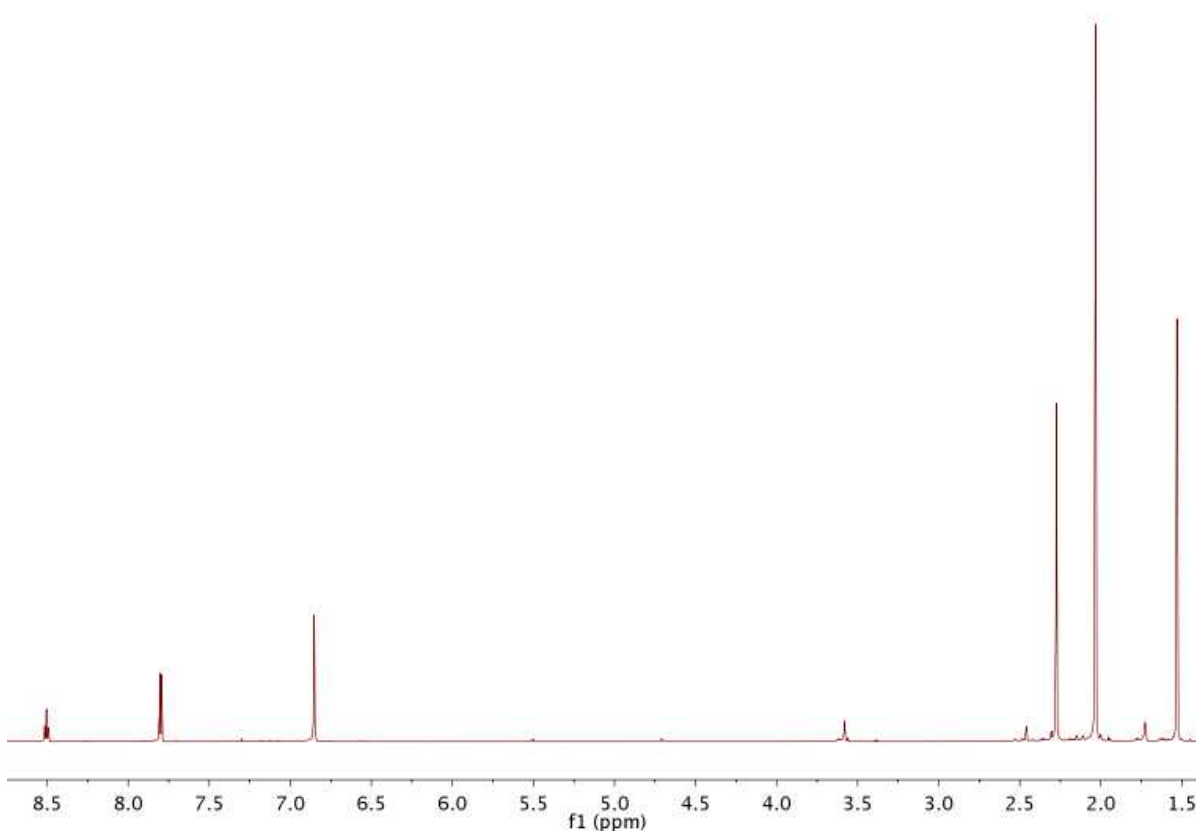
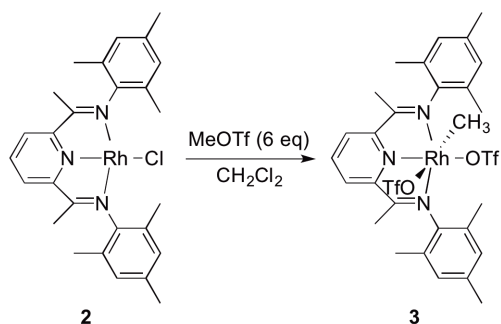


**Figure 5.2.**  $^1\text{H}$  NMR spectrum of  $(^{\text{Mes}}\text{NNN})\text{Rh}(\text{Cl})$  (**2**) in  $\text{THF-}d_8$ .

Using the procedure reported by Nuckel and Burger<sup>12</sup> for a similar complex, oxidation of the dark green  $(^{\text{Mes}}\text{NNN})\text{Rh}(\text{Cl})$  (**2**) with excess  $\text{MeOTf}$  ( $\text{OTf} =$  trifluoromethanesulfonate) gave the yellow Rh(III) complex  $(^{\text{Mes}}\text{NNN})\text{Rh}(\text{Me})(\text{OTf})_2$  (**3**) in 74% isolated yield (Scheme 5.6). The resonance for the methyl ligand is observed in the  $^1\text{H}$  NMR spectrum of complex **3** at 1.87 ppm (d,  $^3J_{\text{Rh-Me}} = 2$  Hz) (Figure 5.3). A characteristic Rh–Me doublet is observed in the  $^{13}\text{C}$  NMR spectrum at 4.4 ppm ( $^1J_{\text{Rh-C}} = 24$  Hz). Complex **3** is  $\text{C}_s$  symmetric and because of the trans methyl and triflate groups, the mesityl methyl peaks and aromatic protons within an individual mesityl rings are no longer equivalent. These methyl groups are observed in the  $^1\text{H}$  NMR spectrum as singlets at 2.39 ppm, 2.27

ppm and 2.08 ppm, and the inequivalent aromatic resonances are observed at 6.96 ppm and 6.94 ppm.



**Scheme 5.6.** Synthesis of (<sup>Mes</sup>NNN)Rh(Me)(OTf)<sub>2</sub> (**3**).

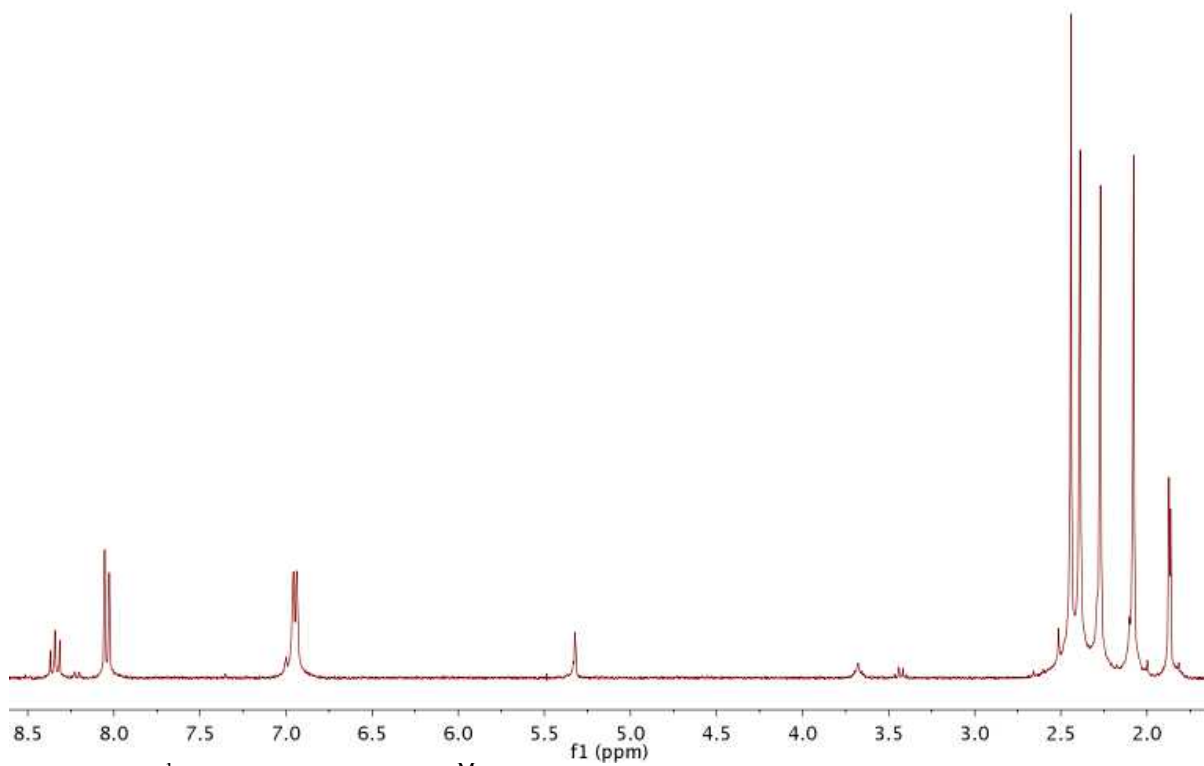
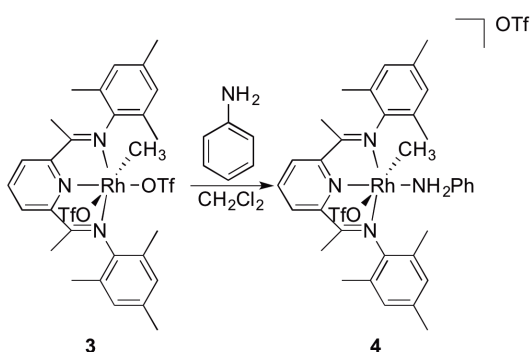


**Figure 5.3.** <sup>1</sup>H NMR spectrum of (<sup>Mes</sup>NNN)Rh(Me)(OTf)<sub>2</sub> (**3**) in CD<sub>2</sub>Cl<sub>2</sub>.

### 5.2.3 Synthesis of $[(^{\text{Mes}}\text{NNN})\text{Rh}(\text{Me})(\text{OTf})(\text{NH}_2\text{Ph})][\text{OTf}]$ (**4**)

The addition of aniline to a solution of complex **3** in  $\text{CH}_2\text{Cl}_2$  leads to the formation of a new complex,  $[(^{\text{Mes}}\text{NNN})\text{Rh}(\text{Me})(\text{NH}_2\text{Ph})(\text{OTf})][\text{OTf}]$  (**4**), in a 97% isolated yield (Scheme 5.7). The  $^1\text{H}$  and  $^{13}\text{C}$  NMR spectra of complex **4** show doublets corresponding to the methyl ligand at 0.99 ppm ( $^2J_{\text{Rh-H}} = 2$  Hz) and 7.3 ppm ( $^1J_{\text{Rh-C}} = 25$  Hz), respectively. A broad singlet is observed in the  $^1\text{H}$  NMR spectrum of **4** at 4.77 ppm for the aniline  $\text{NH}_2$  protons (Figure 5.4). The observation of a single resonance for the  $\text{NH}_2$  unit, other than resonance for a diastereotopic group, is consistent with  $C_s$  symmetry. In addition, the aniline aromatic protons resonate as a triplet at 7.00 ppm ( $^3J_{\text{H-H}} = 7$  Hz), a triplet at 6.84 ( $^3J_{\text{H-H}} = 8$  Hz), and a doublet at 5.05 ( $^2J_{\text{H-H}} = 8$  Hz). The resonance due to the *ortho*- $\text{NH}_2\text{Ph}$  protons is shifted upfield at 5.05 ppm, which is likely a result of shielding by the mesityl rings of  $^{\text{Mes}}\text{NNN}$ . This assignment of the peak due to the *ortho*- $\text{NH}_2\text{Ph}$  protons was confirmed by correlations in the COSY 2D NMR spectrum. Correlations were observed between the *meta* and *para*-aniline resonances (triplets at 7.00 ppm and 6.84 ppm) with the *ortho*-aniline resonance confirming the upfield chemical shift of the *ortho*-aniline protons.



**Scheme 5.7.** Synthesis of  $[(^{\text{Mes}}\text{NNN})\text{Rh}(\text{Me})(\text{NH}_2\text{Ph})(\text{OTf})][\text{OTf}]$  (**4**).

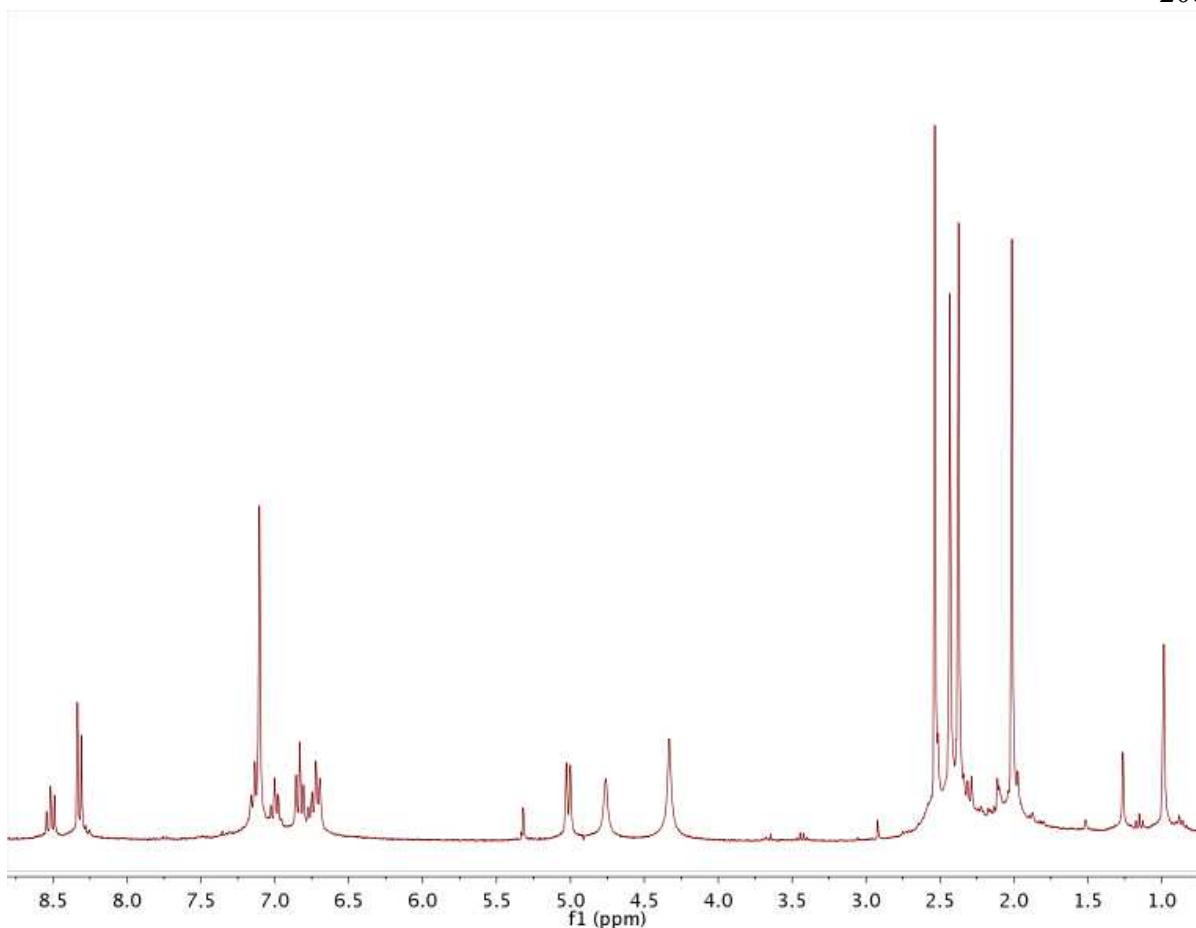


**Figure 5.4.**  $^1\text{H}$  NMR spectrum of  $[(^{\text{Mes}}\text{NNN})\text{Rh}(\text{Me})(\text{NH}_2\text{Ph})(\text{OTf})][\text{OTf}]$  (**4**) in  $\text{CD}_2\text{Cl}_2$ .

Crystals of  $[(^{\text{Mes}}\text{NNN})\text{Rh}(\text{Me})(\text{NH}_2\text{Ph})(\text{OTf})][\text{OTf}]$  (**4**) suitable for a X-ray diffraction study were obtained by layering a solution of **4** in THF with pentane (Figure 5.5). The crystal structure confirms a pseudo octahedral coordination sphere. The  $\text{Rh}-\text{C}_{\text{Me}}$  bond length [2.034(2) Å] is 0.025 Å shorter than that of the related complex  $[(^{\text{t}}\text{bpy})_2\text{Rh}(\text{Me})(\text{NH}_2\text{Ph})][\text{BAR}'_4][\text{OTf}]$  [ $\text{Rh}-\text{C}_{\text{Me}} = 2.063(3)$  Å] (see Chapter 2) and is 0.055 Å shorter than the  $\text{Rh}-\text{C}_{\text{Me}}$  bond length of  $[(^{\text{t}}\text{bpy})_2\text{Rh}(\text{Me})_2][\text{BAR}'_4]$ .<sup>13</sup> A possible explanation for the difference in  $\text{Rh}-\text{C}_{\text{Me}}$  bond strength is the trans influence of OTF (trans to methyl ligand of **4**) is less than that of a pyridyl ligand. The  $\text{Rh}-\text{N}_{\text{aniline}}$  bond length of **4** is 2.117(2) Å, which is statistically identical to the same  $\text{Rh}-\text{N}$  bond length of

$[(^t\text{bpy})_2\text{Rh}(\text{Me})(\text{NH}_2\text{Ph})][\text{BAR}'_4][\text{OTf}]$  [2.114(3) Å] (see Chapter 2). The Rh–N–C bond angle of the aniline ligand of complex **4** was determined to be 119.9(1)°, which is also statistically identical to the Rh–N–C bond angle of  $[(^t\text{bpy})_2\text{Rh}(\text{Me})(\text{NH}_2\text{Ph})][\text{BAR}'_4][\text{OTf}]$  [119.4(2)°] (see Chapter 2).

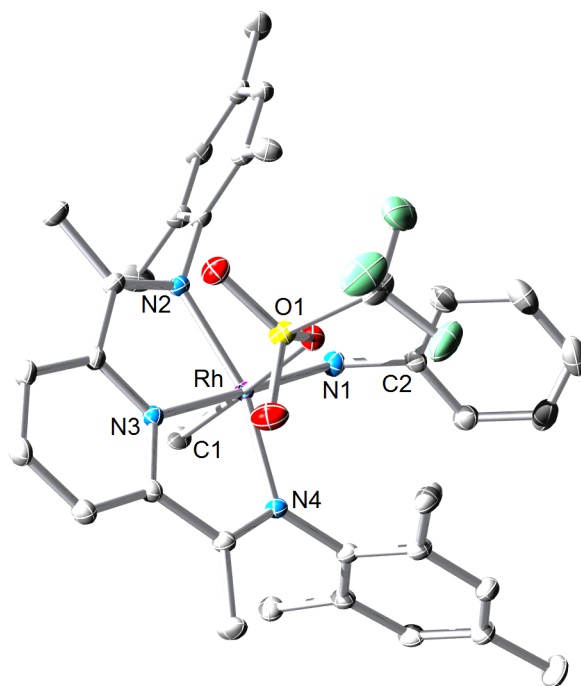
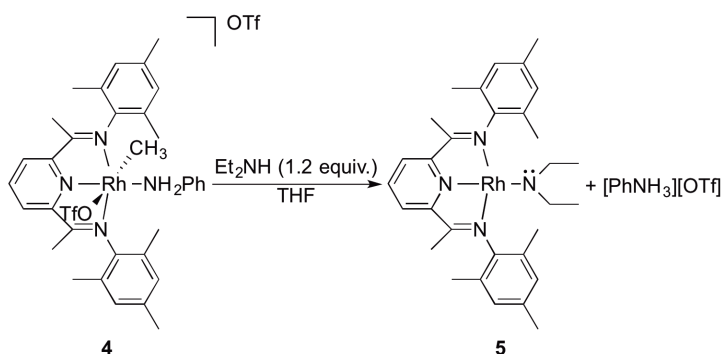


**Figure 5.5.** ORTEP diagram (30% probability) of  $[(^{\text{Mes}}\text{NNN})\text{Rh}(\text{Me})(\text{NH}_2\text{Ph})(\text{OTf})][\text{OTf}]$  (**4**). Counterion and hydrogen atoms omitted for clarity. Selected bond lengths (Å): Rh–C1, 2.034(2); Rh–N1, 2.117(2); Rh–N2, 2.089(2); Rh–N3, 1.931(2); Rh–N4, 2.082(2); Rh–O1, 2.304(1); N1–C2, 1.449(3). Selected bond angles (°): C1–Rh–O1, 174.22(7); C2–N1–Rh, 119.9(1).

#### 5.2.4 Synthesis of $(^{\text{Mes}}\text{NNN})\text{Rh}(\text{NEt}_2)$ (**5**)

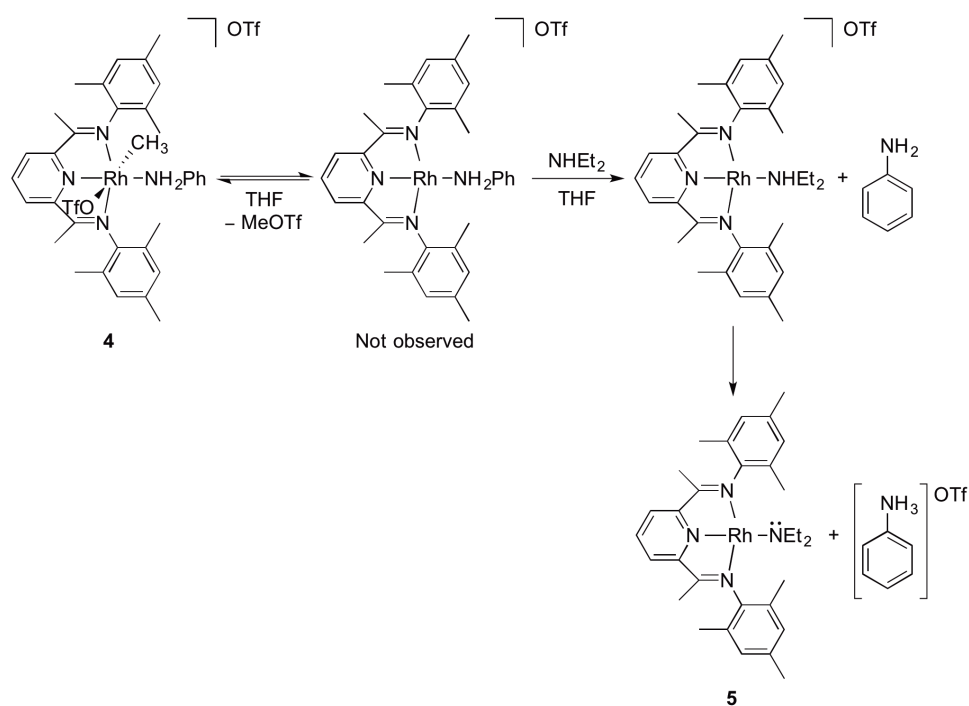
The addition of  $\text{Et}_2\text{NH}$  to a yellow solution of the Rh(III) complex **4** in THF results in the immediate formation of the dark green Rh(I) complex  $(^{\text{Mes}}\text{NNN})\text{Rh}(\text{NEt}_2)$  (**5**) (Scheme 5.8). The solution becomes slightly viscous, possibly because  $\text{MeOTf}$ , which is a proposed product (see below) oligomerizes or polymerizes THF. The  $^1\text{H}$  NMR spectrum of the reaction mixture prior to work up shows free aniline and  $[\text{Et}_2\text{NH}_2][\text{OTf}]$ . No  $\text{CH}_4$  was

observed by  $^1\text{H}$  NMR spectroscopy when performing the reaction in a sealed J. Young NMR tube. The formation of complex **5** does not occur in 1,4-dioxanes, presumably due to poor solubility of the starting material in 1,4-dioxane. No reaction was observed when trying to synthesize complex **5** in  $\text{CH}_3\text{CN}$ .



**Scheme 5.8.** The addition of  $\text{Et}_2\text{NH}$  to  $[(^{\text{Mes}}\text{NNN})\text{Rh}(\text{Me})(\text{NH}_2\text{Ph})(\text{OTf})][\text{OTf}]$  (**4**) leads to the formation of the Rh(I)–amido complex  $(^{\text{Mes}}\text{NNN})\text{Rh}(\text{NEt}_2)$  (**5**).

The proposed mechanism for the formation of  $(^{\text{Mes}}\text{NNN})\text{Rh}(\text{NEt}_2)$  (**5**) from  $[(^{\text{Mes}}\text{NNN})\text{Rh}(\text{Me})(\text{NH}_2\text{Ph})(\text{OTf})][\text{OTf}]$  (**4**) and  $\text{Et}_2\text{NH}$  is shown in Scheme 5.9. The first step involves the reductive elimination of  $\text{MeOTf}$ . In the second step, ligand exchange occurs between coordinated aniline and free  $\text{NHET}_2$ . In the third step, free aniline deprotonates coordinated  $\text{NHET}_2$  to give complex **5** and anilinium triflate. Attempts to trap  $\text{MeOTf}$  using 2,6-lutidine were unsuccessful, possibly because the  $\text{MeOTf}$  reacts more rapidly with THF.



**Scheme 5.9.** Proposed mechanism for the formation of (<sup>Mes</sup>NNN)Rh(NEt<sub>2</sub>) (**5**).

In order to gain evidence for the loss of MeOTf in the first step of the proposed mechanism shown in Scheme 5.9, complex **4** was dissolved in HTFA. If reversible reductive elimination of MeOTf occurs, the Rh(I) complex [<sup>Mes</sup>NNN)Rh(NH<sub>2</sub>Ph)][OTf] should be trapped by HTFA to form [<sup>Mes</sup>NNN)Rh(NH<sub>2</sub>Ph)(H)(TFA)][OTf]. Disappearance of a coordinated methyl resonance is observed in the <sup>1</sup>H NMR spectrum after heating for 2 h at 60 °C. However, a peak for free MeOTf was absent in the <sup>1</sup>H NMR spectrum. In addition, neither a singlet for CH<sub>4</sub> or a Rh–H resonance are observed by <sup>1</sup>H NMR spectroscopy. GC-MS analysis of the headspace did not detect CH<sub>4</sub> suggesting that HTFA did not protonate the methyl ligand leading to the release of CH<sub>4</sub>. The observed peaks did not coincide with anilinium TFA or free ligand. When the reaction was repeated with 1 equiv. of HTFA in

THF- $d_8$  or  $CD_2Cl_2$ , free ligand was observed after heating at 60 °C for 2 h but MeOTf was not observed.

The  $^1H$  NMR spectrum of complex **5** (Figure 5.6) shows a triplet at 8.47 ppm (t,  $^3J_{H-H} = 8$  Hz) and a doublet at 8.09 ppm (d,  $^3J_{H-H} = 8$  Hz) for the protons on the pyridyl ring. A singlet is observed at 7.08 ppm for the protons of the mesityl groups. The imine methyls are observed at 2.31 ppm, and the two singlets for the methyl groups on the mesityl groups resonate at 2.21 ppm (12H) and 1.94 ppm (6H). The ethyl resonances of the coordinated diethyl amido ligand appear at 3.05 ppm (q,  $^3J_{H-H} = 7$  Hz) and 1.29 ppm (t,  $^3J_{H-H} = 7$  Hz). The peaks for the ethyl groups of the coordinated diethyl amido ligand are shifted downfield relative to free diethyl amine by 0.48 ppm for the methylene resonance and 0.92 ppm for the methyl [free diethyl amine: 2.57 ppm (q,  $^3J_{H-H} = 7$  Hz) 1.02 ppm (t,  $^3J_{H-H} = 7$  Hz)].

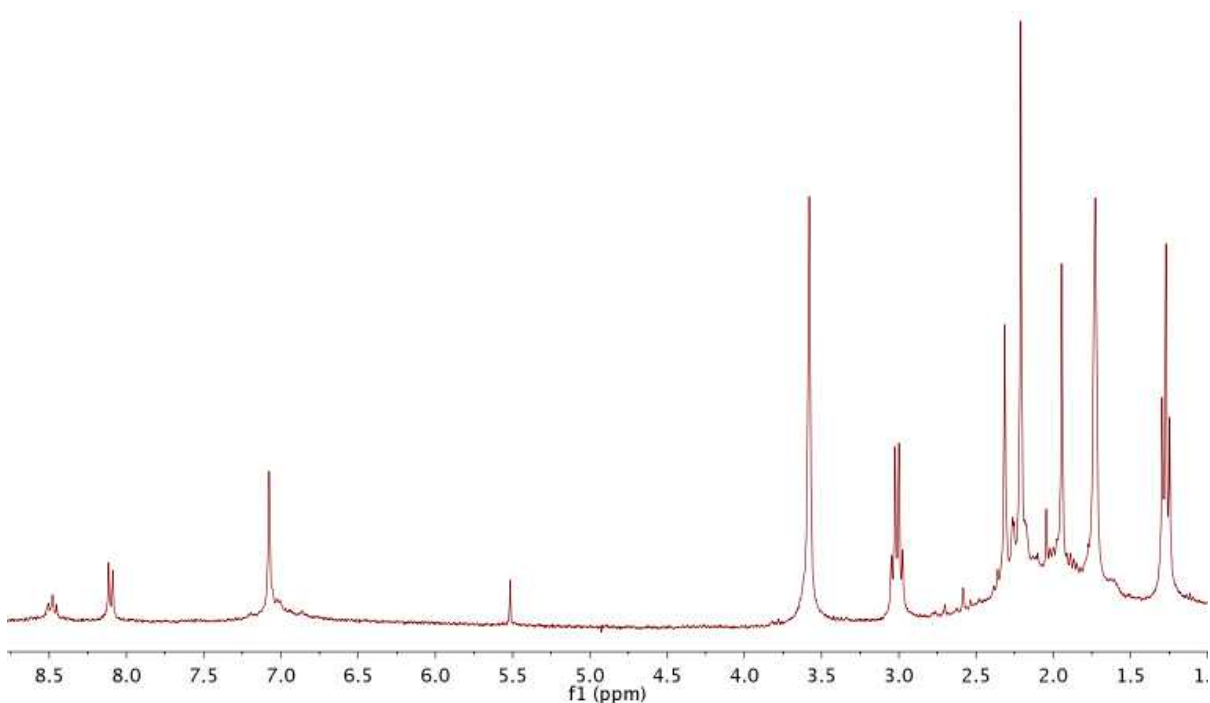
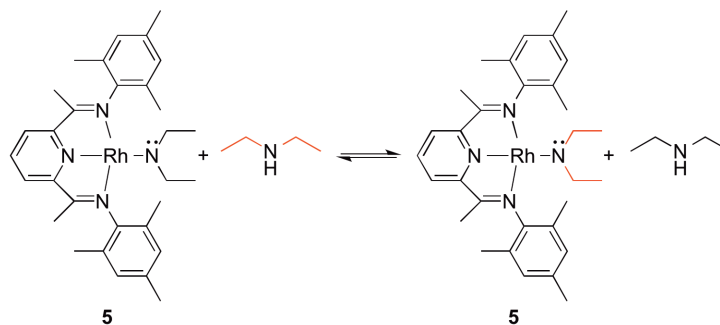


**Figure 5.6.**  $^1\text{H}$  NMR spectrum of  $(^{\text{Mes}}\text{NNN})\text{Rh}(\text{NEt}_2)$  (**5**) in  $\text{THF-}d_8$ .

The synthesis of complex **5** can also be achieved by addition of  $\text{Et}_2\text{NH}$  (1.2 equiv.) to  $(^{\text{Mes}}\text{NNN})\text{Rh}(\text{Me})(\text{OTf})_2$  (**3**). Excess  $\text{Et}_2\text{NH}$  is required for the synthesis of **5** from  $[(^{\text{Mes}}\text{NNN})\text{Rh}(\text{Me})(\text{NH}_2\text{Ph})(\text{OTf})][\text{OTf}]$  or  $(^{\text{Mes}}\text{NNN})\text{Rh}(\text{Me})(\text{OTf})_2$ . When only one equiv. is utilized a mixture of starting material and product is obtained and only a single set of resonances are observed for the ethyl group of **5** and free  $\text{Et}_2\text{NH}$  in the room temperature  $^1\text{H}$  NMR spectrum of crude product. This indicates a rapid fluxional process that exchanges the amide ligand and free  $\text{Et}_2\text{NH}$  (Scheme 5.10). However, separate resonances are observed for the amido ligand and free  $\text{Et}_2\text{NH}$  in the room temperature  $^{13}\text{C}$  NMR spectrum. When excess

free  $\text{Et}_2\text{NH}$  is added to a THF- $d_8$  solution of crude **5** the ethyl resonances for the coordinated diethylamido ligand are observed to shift upfield by  $^1\text{H}$  NMR spectroscopy closer to the chemical shift of free diethylamine but, separate peaks for free diethylamine are not observed. The product is purified by recrystallization from a THF solution of **5** layered with hexanes. The  $^{19}\text{F}$  NMR spectrum of the crystallized product does not contain signals, confirming that MeOTf and HOTf have been removed. The absence of a OTf resonance in the  $^{19}\text{F}$  NMR spectrum provides support that that complex **5** is a Rh(I) amido complex and not  $[(^{\text{Mes}}\text{NNN})\text{Rh}(\text{NH}\text{Et}_2)][\text{OTf}]$ . Ultimately, the best support that complex **5** is a diethylamido complex is the crystallographic data obtained for complex **5**.



**Scheme 5.10.** Free  $\text{Et}_2\text{NH}$  is in rapid chemical exchange with the coordinated amido ligand of  $(^{\text{Mes}}\text{NNN})\text{Rh}(\text{NEt}_2)$  (**5**).

A single crystal of  $(^{\text{Mes}}\text{NNN})\text{Rh}(\text{NEt}_2)$  suitable for X-ray diffraction study was obtained (Figure 5.7). The structure shows the expected pseudo square planar coordination sphere about Rh. There is a highly disordered triflate that is likely HOTf. The nitrogen of the diethyl amido ligand is planar indicating that no proton is present on this nitrogen atom confirming that complex **5** is Rh(I) diethylamido complex and not a Rh(I) diethylamine complex. The bond angles around the amido nitrogen are  $120^\circ$ . The diethylamido ligand is planar because the p-orbital on the amido nitrogen is orthogonal to the filled Rh  $d\pi$  orbital

and the nitrogen p-orbital of the pyridine as shown in Scheme 5.11. The orthogonal orientation of the amido nitrogen results in a two-center interaction that gives no net bond (Scheme 5.11). If the p-orbital of the amido nitrogen was instead in the same plane as the Rh  $d\pi$  and pyridyl nitrogen p-orbital then a three-center interaction would be observed and the amido would not be planar (Scheme 5.12). A planar structure has also been reported for  $\text{LiNH}_2$ .<sup>14</sup>

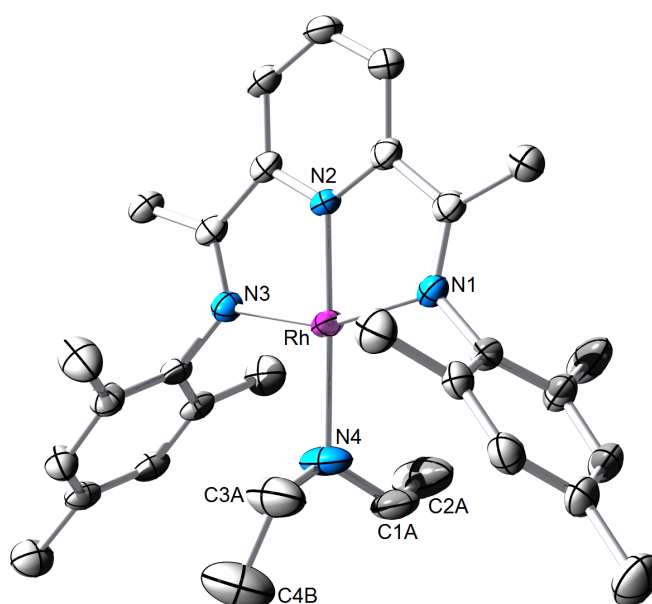
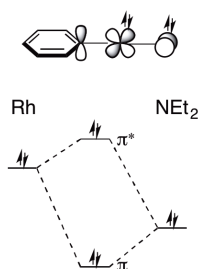
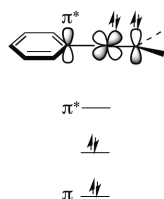


**Figure 5.7.** ORTEP diagram (50% probability) of  $(^{\text{Mes}}\text{NNN})\text{Rh}(\text{NEt}_2)$  (**5**). Omitted is a highly disordered  $\text{OTf}^-$ . Disorder about  $\text{Et}_2\text{N}$  was modeled and higher occupancy is shown. Selected bond lengths ( $\text{\AA}$ ): Rh–N1, 2.048(3); Rh–N2, 1.906(3); Rh–N3, 2.033(3); Rh–N4, 2.139(3); N4–C1A, 1.39(1); N4–C3A, 1.438(6). Selected bond angles ( $^\circ$ ): N2–Rh–N3, 79.1(1); N2–Rh–N1, 79.10(12); N3–Rh–N1, 158.2(1); N2–Rh–N4, 178.4(2); N3–Rh–N4, 99.4(2); N1–Rh–N4, 102.4(1); C1A–N4–Rh, 118.9(4); C3A–N4–Rh, 113.2(3); C3A–N4–C1A, 120.5(5).



**Scheme 5.11.** The planar geometry of amido ligand is a result of the orthogonal orientation of the nitrogen p-orbital for the amido. The orthogonal orientation leads to a two-center interaction giving not net bond.



**Scheme 5.12.** A three-center interaction would be observed if the p-orbital of the pyridyl nitrogen, Rh  $d\pi$  and p-orbital of the amido nitrogen are coplanar.

### 5.3 Treatment of $[(^{\text{Mes}}\text{NNN})\text{Rh}(\text{Me})(\text{OTf})(\text{NH}_2\text{Ph})][\text{OTf}]$ (**4**) with Base

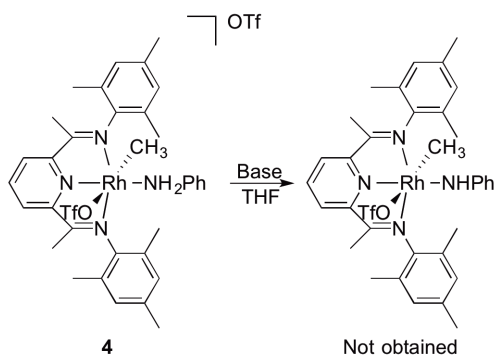
As discussed above, we have been targeting a complex to directly compare affinity for 1,2-CH or H<sub>2</sub> addition across M–R versus M–X (X = OR, NHR) bonds. The complex  $[(^{\text{Mes}}\text{NNN})\text{Rh}(\text{Me})(\text{NHPh})(\text{OTf})]$  should have a labile OTf ligand for CH or H<sub>2</sub> coordination and competition between 1,2-addition across Rh–Me versus Rh–NHPh could be directly determined. As a result, a considerable effort was extended towards the synthesis of  $[(^{\text{Mes}}\text{NNN})\text{Rh}(\text{Me})(\text{NHPh})(\text{OTf})]$  from complex **4** (Scheme 5.13). Several bases were investigated to deprotonate **4** (Table 4.1), but successful conversion to the anilido complex was not achieved. MeLi, KH and Na[N(TMS)<sub>2</sub>] proved to be too reactive and led to decomposition of the Rh complex. With less basic substrates, no reactivity was observed (*e.g.* Et<sub>3</sub>N, 2-cyclohexylamine, 2,6-lutidine, K<sub>2</sub>CO<sub>3</sub> or Ph<sub>2</sub>NH).

Deprotonation of  $[(^{\text{Mes}}\text{NNN})\text{Rh}(\text{Me})(\text{NH}_2\text{Ph})(\text{OTf})][\text{OTf}]$  using bases whose conjugate acids have pK<sub>a</sub> between 17.0 and 12.0 also proved unsuccessful. For example, no reactivity was observed with either 1,8-bis(dimethylamino)naphthalene (“Proton Sponge”) or 1,8-diazabicyclo[5.4.0]undec-7-ene (DBU). It was hypothesized that “Proton Sponge” and DBU were unable to deprotonate complex **4** because they are perhaps too sterically bulky. NaOH was investigated as a comparably less sterically encumbering base. Unfortunately, the reaction of complex **4** with NaOH results in the formation of multiple products. As a result, it was determined that bases that are small may displace the coordinated OTf ligand. For this reason, mid-sized and mid-strength bases, which are less likely to interact with ligands on Rh other than coordinated aniline, were investigated.

Treatment of complex **4** with KO<sup>t</sup>Bu appeared promising; the resonances for the protons on coordinated aniline disappeared and changes were also observed for the aromatic

protons suggesting successful deprotonation of aniline. Unfortunately, upon attempted isolation of the product decomposition occurred. It was hypothesized that a Rh–OH species was formed since H<sub>2</sub>O was used to dissolve the KO<sup>t</sup>Bu. For this reason, attention was directed away from bases that would require the use H<sub>2</sub>O for dissolution. The heterogeneous reaction of complex **4** with KO<sup>t</sup>Bu was unsuccessful.

Investigation of Et<sub>2</sub>NH was warranted due to its intermediate basicity and moderate steric bulk. As described above, treatment of [(<sup>Mes</sup>NNN)Rh(Me)(NH<sub>2</sub>Ph)(OTf)][OTf] (**4**) with Et<sub>2</sub>NH leads to reductive elimination of MeOTf and displacement of coordinated aniline with Et<sub>2</sub>NH to generate the Rh(I) complex, (<sup>Mes</sup>NNN)Rh(NEt<sub>2</sub>) (**5**). Using the conditions investigated, the synthesis of (<sup>Mes</sup>NNN)Rh(Me)(NHPh)(OTf) was unsuccessful.



**Scheme 5.13.** Attempted synthesis of (<sup>Mes</sup>NNN)Rh(Me)(NHPh)(OTf).

**Table 5.1.** Investigated bases for the synthesis of [(<sup>Me</sup>sNNN)Rh(Me)(NHPh)(OTf)].

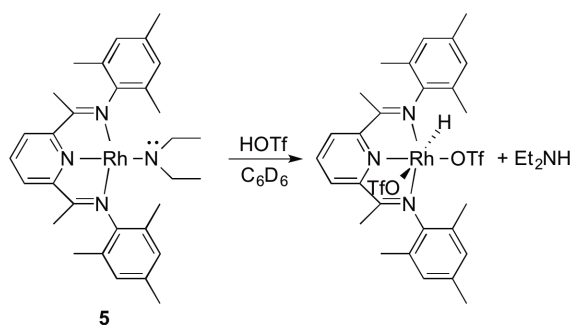
Base	pK <sub>a</sub> <sup>a</sup>
MeLi <sup>a</sup>	pK <sub>a</sub> CH <sub>4</sub> = 48 (H <sub>2</sub> O), 56 (DMSO)
KH <sup>a</sup>	pK <sub>a</sub> H <sub>2</sub> = ~36 (H <sub>2</sub> O)
Na[N(TMS) <sub>2</sub> ] <sup>a</sup>	pK <sub>a</sub> HMDS = 26 (THF), 30 (DMSO)
KO <sup>t</sup> Bu <sup>a</sup>	pK <sub>a</sub> <sup>t</sup> BuOH = 17.0 (H <sub>2</sub> O), 29.4 (DMSO)
NaOH <sup>a</sup>	pK <sub>a</sub> H <sub>2</sub> O = 15.7 (H <sub>2</sub> O), 32 (DMSO)
1,8-Bis(dimethylamino)naphthalene (Proton Sponge) <sup>a</sup>	pK <sub>a</sub> for conjugate acid = -9.0, 12 (H <sub>2</sub> O)
1,8-diazabicyclo[5.4.0]undec-7-ene (DBU) <sup>a</sup>	pK <sub>a</sub> for conjugate acid = ~12 (DMSO)
<sup>i</sup> Pr <sub>2</sub> NH <sup>a,b</sup>	pK <sub>a</sub> <sup>i</sup> Pr <sub>2</sub> NH = 11.05 (H <sub>2</sub> O) pK <sub>a</sub> <sup>i</sup> Pr <sub>2</sub> NH = 36 (THF)
Et <sub>2</sub> NH <sup>b</sup>	pK <sub>a</sub> Et <sub>2</sub> NH = 10.98 (H <sub>2</sub> O)
Et <sub>3</sub> N <sup>b</sup>	pK <sub>a</sub> Et <sub>3</sub> N = 10.65 (H <sub>2</sub> O)
Cyclohexyl amine <sup>b</sup>	pK <sub>a</sub> cyclohexyl amine = 10.64 (H <sub>2</sub> O)
2,6-lutidine <sup>a</sup>	pK <sub>a</sub> for conjugate acid = 6.75 (H <sub>2</sub> O), 4,46 (DMSO)
K <sub>2</sub> CO <sub>3</sub> <sup>c</sup>	pK <sub>a1</sub> H <sub>2</sub> CO <sub>3</sub> = 6.4 (H <sub>2</sub> O) pK <sub>a2</sub> = 10.3 (H <sub>2</sub> O)
Ph <sub>2</sub> NH <sup>a</sup>	pK <sub>a</sub> Ph <sub>2</sub> NH = 25.0 (DMSO)

<sup>a</sup>pK<sub>a</sub> values taken from Bordwell pK<sub>a</sub> table<sup>15</sup><sup>b</sup>pK<sub>a</sub> values taken from reference 5<sup>c</sup>pK<sub>a</sub> values taken from reference 16

### 5.3.1 Reactivity of (MesNNN)Rh(NEt<sub>2</sub>) (**5**)

The ability of (MesNNN)Rh(NEt<sub>2</sub>) (**5**) to activate dihydrogen to form (MesNNN)Rh(H) and NHEt<sub>2</sub> was investigated. Unfortunately no H<sub>2</sub> activation was observed. Heating (50 °C to 90 °C) complex **5** in THF under H<sub>2</sub>(g) (20 psig) resulted in decomposition after 48 h at 90 °C.

The addition of HOTf to (MesNNN)Rh(NEt<sub>2</sub>) (**5**) resulted in oxidation to the Rh(III) species (MesNNN)Rh(H)(OTf)<sub>2</sub> along with release of Et<sub>2</sub>NH (Scheme 5.14). The reaction proceeded instantaneously at room temperature without the observation of [(MesNNN)Rh(H)(NHEt<sub>2</sub>)(OTf)][OTf] as an intermediate. A characteristic Rh–H doublet is observed at –22.30 ppm (d, <sup>2</sup>J<sub>Rh–H</sub> = 24 Hz) in the <sup>1</sup>H NMR spectrum of (MesNNN)Rh(H)(OTf)<sub>2</sub>. The synthesis of (iPrNNN)Rh(H)(OTf)<sub>2</sub> by addition of HOTf to (iPrNNN)Rh(Cl) has previously been reported.<sup>12</sup> The <sup>1</sup>H NMR data for (MesNNN)Rh(H)(OTf)<sub>2</sub> was in agreement with the previously reported data. When MeOTf is added to a solution of (MesNNN)Rh(NEt<sub>2</sub>) a mixture of several species is obtained. No characteristic Rh–Me doublet could be identified suggesting that the simple oxidative addition of MeOTf to complex **5** was not successful.



**Scheme 5.14.** Oxidation of (MesNNN)Rh(NEt<sub>2</sub>) (**5**) by HOTf to form the Rh(III) complex (MesNNN)Rh(H)(OTf)<sub>2</sub>.

#### 5.4 Initial Exploration of Other NNN Complexes

The synthesis of (*p*-anisyl<sup>1</sup>NNN)RhCl<sub>3</sub> has previously been achieved by the oxidative addition of Cl<sub>2</sub>(g) to (*p*-anisyl<sup>1</sup>NNN)Rh(Cl) or by bubbling O<sub>2</sub>(g) through a solution of (*p*-anisyl<sup>1</sup>NNN)Rh(CH<sub>2</sub>Cl)Cl<sub>2</sub> in refluxing H<sub>2</sub>O.<sup>7</sup> (<sup>Mes</sup>NNN)RhCl<sub>3</sub> can be synthesized by refluxing a solution of <sup>Mes</sup>NNN with RhCl<sub>3</sub>·H<sub>2</sub>O in a MeOH/THF solution. It was anticipated that (<sup>Mes</sup>NNN)RhCl<sub>3</sub> would serve as an entry into an (NNN)RhX<sub>2</sub>(NHR) complexes. Unfortunately the solubility of (<sup>Mes</sup>NNN)RhCl<sub>3</sub> was limited to polar solvents such as methanol and ethanol, and this complex was unstable both as a solid and in solution. In solution, (<sup>Mes</sup>NNN)RhCl<sub>3</sub> decomposes within ~30 minutes and as a solid (<sup>Mes</sup>NNN)RhCl<sub>3</sub> decomposes over several days at room temperature.

In an effort to find an alternative entryway to the desired complex, the previously reported five-coordinate complex (<sup>*i*Pr</sup>NNN)Rh(Me)(I)[BAR'<sub>4</sub>] [<sup>*i*Pr</sup>NNN = 2,6-diacetylpyridinebis(2,6-diisopropylaniline)] was prepared.<sup>6</sup> Some exploratory reactions have been performed using this complex in an effort to exchange the iodine ligand for a hydroxide, alkoxide or anilido. The addition of CsOH in H<sub>2</sub>O or MeOH to a CH<sub>3</sub>CN solution of (<sup>*i*Pr</sup>NNN)Rh(Me)(I)[BAR'<sub>4</sub>] resulted in the formation of multiple products. Furthermore, the reaction of (<sup>*i*Pr</sup>NNN)Rh(Me)(I)[BAR'<sub>4</sub>] with NaOMe led to decomposition. Treatment of (<sup>*i*Pr</sup>NNN)Rh(Me)(I)[BAR'<sub>4</sub>] with MOTf (M = Tl, Ag) and aniline resulted in the formation of numerous products and (<sup>*i*Pr</sup>NNN)Rh(Me)(NH<sub>2</sub>Ph)[BAR'<sub>4</sub>][OTf] could not be identified.

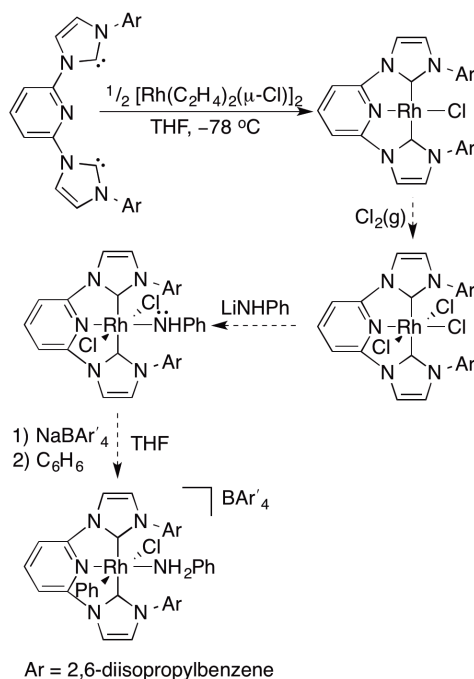
#### 5.5 Conclusions

[(<sup>Mes</sup>NNN)Rh(Me)(NH<sub>2</sub>Ph)(OTf)][OTf] (**4**) was synthesized by addition of aniline to a solution of (<sup>Mes</sup>NNN)Rh(Me)(OTf)<sub>2</sub> (**3**). Attempted deprotonation of [(<sup>Mes</sup>NNN)Rh(Me)(NH<sub>2</sub>Ph)(OTf)][OTf] was unsuccessful because the coordinated aniline is

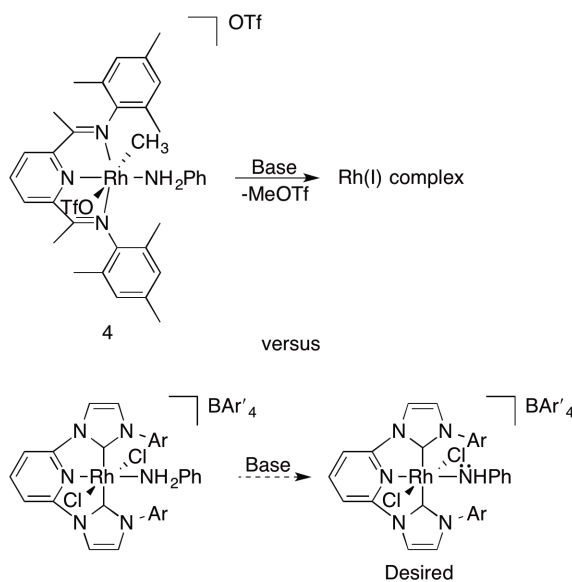
labile and the complex is easily reduced. The Rh(I) complex (<sup>Mes</sup>NNN)Rh(NEt<sub>2</sub>) (**5**) can be synthesized by addition of Et<sub>2</sub>NH to either [<sup>Mes</sup>NNN)Rh(Me)(NH<sub>2</sub>Ph)(OTf)][OTf] or (<sup>Mes</sup>NNN)Rh(Me)(OTf)<sub>2</sub>. Complex **5** does not activate H<sub>2</sub> at room temperature, and decomposition is observed upon heating. In general, the synthesized (NNN)Rh complexes have proven to be very air sensitive and prone to decomposition, especially at elevated temperatures, and are not well suited for C–H activation.

## 5.6 Possible Future Work

Future work could involve additional modification of the ligand set on Rh. Rh(III) complexes bearing the “pincer” *N*-heterocyclic carbene ligand, 3,3'-diaryl-1,1'-pyridine-2,6-diylbis(imidazole-2-ylidene), have been reported.<sup>17</sup> Rh(III) heteroatom complexes bearing this ligand could serve as the next synthetic target (Scheme 5.15). It was evident from the difficulty experienced when trying to deprotonate [<sup>Mes</sup>NNN)Rh(Me)(NH<sub>2</sub>Ph)(OTf)][OTf] (**4**), that the (NNN)Rh(III) complexes are easily reduced to Rh(I). Substituting the NNN ligands for a “pincer” *N*-heterocyclic carbene ligand will help increase electron density on the Rh metal center and thus stabilize the complexes at the Rh(III) oxidation state (Scheme 5.16).

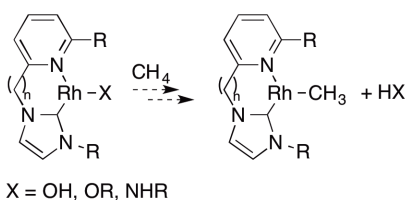


**Scheme 5.15.** 1,2-CH-addition of benzene by a proposed [3,3'-diaryl-1,1'-pyridine-2,6-diylbis(imidazole-2-ylidene)]Rh(NHPh)Cl<sub>2</sub> complex.



**Scheme 5.16.** Attempted deprotonation of [(<sup>Mes</sup>NNN)Rh(Me)(NH<sub>2</sub>Ph)(OTf)][OTf] (**4**) results in reduction to yield a Rh(I) complex. The increased electron density around the metal center for the proposed [3,3'-diaryl-1,1'-pyridine-2,6-diylbis(imidazole-2-ylidene)]Rh complex will hopefully result in the successful formation of Rh(III) heteroatom complex upon treatment with base.

The synthesized Rh(I) four-coordinate species heteroatom complex, (<sup>Mes</sup>NNN)Rh(NEt<sub>2</sub>), reported in this chapter does not activate dihydrogen. As a result, three-coordinate Rh(I) heteroatom complexes containing neutral bidentate ligands will serve as a future synthetic target. The bidentate ligand should be bulky to prevent dimerization. The ligand should also be strongly donating. A potential example is a pyridyl carbene. Furthermore, to prevent ligand cyclometalation the ligand should not have any C–H bonds that could be activated.



**Scheme 5.17.** Proposed Rh(I) heteroatom complex for 1,2-CH-addition.

## 5.7 Experimental

**General Considerations.** Unless otherwise noted, all synthetic procedures were performed under anaerobic conditions in a nitrogen-filled glovebox or by using standard Schlenk techniques. Glovebox purity was maintained by periodic nitrogen purges and was monitored by an oxygen analyzer ( $O_2$  (g) < 15 ppm for all reactions). Toluene, tetrahydrofuran, diethyl ether and pentane were dried by distillation from sodium/benzophenone. Acetonitrile and methanol were dried by distillation from CaH<sub>2</sub>. Hexanes, benzene and dichloromethane were purified by passage through a column of activated alumina. Acetonitrile-*d*<sub>3</sub>, methylene chloride-*d*<sub>2</sub>, C<sub>6</sub>D<sub>6</sub> and THF-*d*<sub>8</sub> were stored under a N<sub>2</sub> atmosphere over 4 Å molecular sieves. <sup>1</sup>H and <sup>13</sup>C NMR spectra were recorded on a Varian Mercury Plus 300 (75 MHz operating frequency for <sup>13</sup>C NMR), Varian Inova 500 MHz spectrometer (125 MHz operating frequency for <sup>13</sup>C NMR), Bruker Avance DRX 600

MHz spectrometer (150 MHz operative frequency for  $^{13}\text{C}$  NMR), or Bruker Avance III 800 MHz spectrometer (201 MHz operative frequency for  $^{13}\text{C}$  NMR). All  $^1\text{H}$  and  $^{13}\text{C}$  NMR spectra are referenced against residual proton signals ( $^1\text{H}$  NMR) or the  $^{13}\text{C}$  resonances of the deuterated solvent ( $^{13}\text{C}$  NMR). All  $^{19}\text{F}$  NMR spectra were obtained on a Varian Mercury Plus 300 MHz spectrometer (operating frequency 282 MHz) and referenced against an external standard of hexafluorobenzene ( $\delta = -164.9$ ). Elemental analyses were performed by Atlantic Microlabs, Inc. High resolution mass spectra were acquired in ESI mode, from samples dissolved in a 3:1 acetonitrile/water solution containing sodium trifluoroacetate (NaTFA). Mass spectra are reported for  $\text{M}^+$  for monocationic complexes, or for  $[\text{M}+\text{H}^+]$  or  $[\text{M}+\text{Na}^+]$  for neutral complexes, using  $[\text{Na}(\text{NaTFA})_x]^+$  clusters as an internal standard. In all cases, observed isotopic envelopes were consistent with the molecular composition reported. For organic products, the monoisotopic ion is reported; for complexes, the major peaks in the isotopic envelope are reported. Spectra were collected on an Agilent 6230. Dr. William H. Myers from the University of Richmond collected and interpreted the HRMS data. Dr. Michal Sabat at the University of Virginia solved the reported X-ray crystallography data. ( $^{\text{Mes}}\text{NNN}$ ) (**1**) was prepared using the general procedure for NNN compounds.<sup>2</sup> All other reagents were purchased from commercial sources and used as is.

**( $^{\text{Mes}}\text{NNN}$ )Rh(Cl) (2).** The complex was prepared using the previously reported procedure for an analogous complex with a 2,6-dimethyl NNN and 2,6-diisopropyl NNN ligands.<sup>12</sup>  $^{\text{Mes}}\text{NNN}$  (**1**, 0.0978 g, 0.246 mmol) was dissolved in THF (~15 mL) and added slowly to a stirring solution of  $[(\text{C}_2\text{H}_4)_2\text{Rh}(\mu\text{-Cl})_2]$  (0.0478 g, 0.122 mmol) in THF (~5 mL). Upon combination, the yellow solution immediately turned dark green. After stirring at room temperature for 1 h, the solvent was removed under vacuum. The dark green residue was

washed with pentane (2 x 5 mL) and dried under vacuum. The solid was recrystallized at room temperature from THF and pentane (0.0542 g, 21% yield).  $^1\text{H}$  NMR (800 MHz, THF- $d_8$ )  $\delta$  8.50 (t,  $^3J_{\text{H-H}} = 8$  Hz, 1H, py 4), 7.80 (d,  $^3J_{\text{H-H}} = 8$  Hz, 2H, py 3,5), 6.85 (s, 4H,  $\text{CH}_{\text{arom}}$ ), 2.27 (s, 6H,  $\text{CN-CH}_3$ ), 2.03 (s, 12H,  $\text{CH}_3$ ), 1.53 (s, 6H,  $\text{CH}_3$ ).  $^{13}\text{C}$  NMR (201 MHz, THF- $d_8$ )  $\delta$  168.4 (C=N), 157.4, 147.8, 135.2, 130.7, 129.4, 125.9, 123.5 (each a s, aromatic C), 21.3, 19.0 (each a s,  $\text{CH}_3$ ), 16.9 (C=N- $\text{CH}_3$ ). Anal. Calcd for  $\text{C}_{27}\text{H}_{31}\text{ClN}_3\text{Rh}$ : C, 60.51; H, 5.83; N, 7.84. Found: C, 59.78; H, 5.97; N, 7.24.

**(<sup>Mes</sup>NNN)Rh(Me)(OTf)<sub>2</sub> (3).** The complex was synthesized using a reported procedure for the 2,6-dimethylaniline variant of this complex.<sup>12</sup> (<sup>Mes</sup>NNN)Rh(Cl) (**2**, 0.1038 g, 0.1937 mmol) was dissolved in  $\text{CH}_2\text{Cl}_2$  (~10 mL). MeOTf (110  $\mu\text{L}$ , 0.972 mmol) was added via a microsyringe causing the green solution to turn red-orange. After stirring for 0.5 h, volatiles were removed *in vacuo*. The resulting orange solid was redissolved in DCM and precipitated with  $\text{Et}_2\text{O}$ . The solid was collected by filtration through a fine porosity frit, washed with  $\text{Et}_2\text{O}$ , and dried under vacuum (0.1298 g, 74%).  $^1\text{H}$  NMR (300 MHz,  $\text{CD}_2\text{Cl}_2$ )  $\delta$  8.35 (t,  $^3J_{\text{H-H}} = 8$  Hz, 1H, py 4), 8.05 (d,  $^3J_{\text{H-H}} = 8$  Hz, 2H, py 3,5), 6.96 (d,  $^3J_{\text{H-H}} = 7$  Hz, 4H,  $\text{CH}_{\text{arom}}$ ), 2.46 (s, 6H, C=N- $\text{CH}_3$ ), 2.41 (s, 3H,  $\text{CH}_3$ ), 2.29, 2.09 (each a s, 6H,  $\text{CH}_3$ ), 1.89 (d,  $^2J_{\text{Rh-H}} = 3$  Hz, 3H, Rh- $\text{CH}_3$ ).  $^{13}\text{C}$  NMR (201 MHz,  $\text{CD}_2\text{Cl}_2$ )  $\delta$  179.0 (s, C=N), 159.4, 140.8, 139.9, 138.1, 133.1, 130.8, 129.2, 128.2, 127.8 (each a s, aromatic C), 20.6, 19.6, 18.6 (each a s,  $\text{CH}_3$ ), 18.5 (s, C=N- $\text{CH}_3$ ), 4.4 (d,  $^1J_{\text{Rh-C}} = 24$  Hz, Rh- $\text{CH}_3$ ).  $^{19}\text{F}$  NMR (282 MHz,  $\text{CD}_2\text{Cl}_2$ )  $\delta$  -80.5 (s, OTf), -81.4 (s, OTf). Anal. Calcd for  $\text{C}_{30}\text{H}_{34}\text{F}_6\text{N}_3\text{O}_6\text{RhS}_2$ : C, 44.29; H, 4.21; N, 5.16. Found: C, 43.65; H, 4.18; N, 4.97.

**[(<sup>Mes</sup>NNN)Rh(Me)(NH<sub>2</sub>Ph)(OTf)][OTf] (4).** (<sup>Mes</sup>NNN)Rh(Me)(OTf)<sub>2</sub> (**3**, 0.0499 g, 0.0602 mmol) was dissolved in  $\text{CH}_2\text{Cl}_2$  (~5 mL). Aniline (5.8  $\mu\text{L}$ , 0.064 mmol) was added

via microsyringe. The reaction solution was stirred at room temperature for 1 h during which time the reaction changed from orange to yellow. The solvent was reduced to ~ 1 mL under vacuum. A yellow solid was precipitated from solution with Et<sub>2</sub>O. The solid was collected by filtration through a fine porosity frit, washed with Et<sub>2</sub>O and dried under vacuum (0.0539 g, 97%). X-ray quality crystals were grown by layering a solution of complex **4** in THF with pentane. <sup>1</sup>H NMR (800 MHz, CD<sub>2</sub>Cl<sub>2</sub>) δ 8.52 (t, <sup>3</sup>J<sub>H-H</sub> = 8 Hz, 1H, py 4), 8.31 (d, <sup>3</sup>J<sub>H-H</sub> = 8 Hz, 2H, py 3/5), 7.10 (s, 4H, CH<sub>arom</sub> mesityl), 7.00 (t, <sup>3</sup>J<sub>H-H</sub> = 7 Hz, 1H, *para*-NH<sub>2</sub>Ph), 6.84 (t, <sup>3</sup>J<sub>H-H</sub> = 8 Hz, 2H, *meta*-NH<sub>2</sub>Ph), 5.05 (d, <sup>3</sup>J<sub>H-H</sub> = 8 Hz, 2H, *ortho*-NH<sub>2</sub>Ph), 4.77 (bs, 1H, NH<sub>2</sub>Ph), 2.54 (s, 6H, C=N-CH<sub>3</sub>), 2.44 (s, 3H, CH<sub>3</sub>), 2.38, 2.02 (each a s, 6H, CH<sub>3</sub>), 0.99 (d, <sup>2</sup>J<sub>Rh-H</sub> = 2 Hz, Rh-CH<sub>3</sub>). <sup>13</sup>C NMR (201.25 MHz, CD<sub>2</sub>Cl<sub>2</sub>) δ 182.5 (s, C=N), 157.3 (s, py 2 + 6), 141.6 (s, py 4), 140.7, 139.1 (each a s, C *ipso*- N C<sub>arom</sub> or C<sub>aniline</sub>), 137.3, 131.2, 130.9, 130.4, 129.5 (each a s, C<sub>arom</sub>), 130.1 (s, py 3/5), 129.1 (s, *meta*-NH<sub>2</sub>Ph), 125.8 (s, *para*-NH<sub>2</sub>Ph), 120.0 (s, *ortho*-NH<sub>2</sub>Ph), 20.5 (s, C=N-CH<sub>3</sub>), 19.0, 19.0, 18.8 (each a s, mesityl CH<sub>3</sub>), 7.3 (d, <sup>1</sup>J<sub>Rh-C</sub> = 25 Hz, Rh-CH<sub>3</sub>). <sup>19</sup>F NMR (281.95 MHz, CD<sub>2</sub>Cl<sub>2</sub>) δ -80.2 (s, OTf). Anal. Calcd for C<sub>36</sub>H<sub>41</sub>F<sub>6</sub>N<sub>4</sub>O<sub>6</sub>RhS<sub>2</sub>: C, 47.69; H, 4.56; N, 6.18. Found: C, 47.41; H, 4.50; N, 6.07.

(<sup>Mes</sup>NNN)Rh(NEt<sub>2</sub>) (**5**). (<sup>Mes</sup>NNN)Rh(Me)(OTf)<sub>2</sub> (**4**, 0.0501 g, 0.0605 mmol) was dissolved in THF (~ 5 mL). Et<sub>2</sub>NH (15.6 μL, 0.151 mmol) was added to the yellow solution via a microsyringe causing the solution to immediately turn dark green. The solution was stirred at room temperature for 1 h before reducing to dryness under vacuum. The dark green solid was washed with pentane (2 x 5 mL) and then dried under vacuum overnight. The solid was purified by crystallization from a concentrated solution of complex **5** in THF layered with hexanes (0.021 g, 62%). <sup>1</sup>H NMR (800 MHz, THF-*d*<sub>8</sub>) δ 8.47 (t, <sup>3</sup>J<sub>H-H</sub> = 8 Hz, 1H, py

4), 8.09 (d,  $^3J_{\text{H-H}} = 8$  Hz, 2H, py 3,5), 7.08 (s, 4H, CH Ar mesityl), 3.05 (q,  $^3J_{\text{H-H}} = 7$  Hz, 4H,  $\text{CH}_2\text{CH}_3$ ), 2.31 (s, 6H,  $\text{C}=\text{N}-\text{CH}_3$ ), 2.21 (s, 12H,  $\text{CH}_3$ ), 1.94 (s, 6H,  $\text{CH}_3$ ), 1.29 (t,  $^3J_{\text{H-H}} = 7$  Hz, 6H,  $\text{CH}_2\text{CH}_3$ ).  $^{13}\text{C}$  NMR (201 MHz,  $\text{THF}-d_8$ )  $\delta$  173.2 (s,  $\text{C}=\text{N}$ ), 157.2, 145.5, 137.6, 132.5, 130.7, 130.6, 127.1 (py and  $\text{C}_{\text{arom}}$ ), 46.8 ( $\text{NCH}_2\text{CH}_3$ ), 21.2, 18.2 ( $\text{C}_{\text{arom}} \text{CH}_3$ ), 17.1 ( $\text{NCH}_2\text{CH}_3$ ), 15.8 ( $\text{C}=\text{N}-\text{CH}_3$ ).  $[\text{M}-(\text{NEt}_2^-)]^+ = [\text{C}_{27}\text{H}_{31}\text{N}_3\text{Rh}]^+$  obs'd. calc'd, ppm: 500.1569, 500.1568, 0.0.  $\text{M}-(\text{NEt}_2^-)+\text{CH}_3\text{CN}]^+ = [\text{C}_{29}\text{H}_{34}\text{N}_4\text{Rh}]^+$  obs'd. calc'd, ppm: 541.1855, 541.1833, 0.4. No signal was observed at 572  $[\text{C}_{31}\text{H}_{41}\text{N}_4\text{Rh}]^+$ .

## 5.8 References

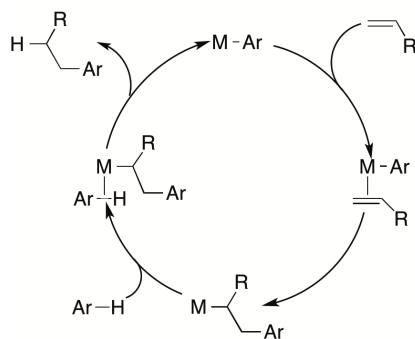
1. Small, B. L.; Brookhart, M.; Bennett, A. M. A. *J. Am. Chem. Soc.* **1998**, *120*, 4049.
2. Britovsek, G. J. P.; Bruce, M.; Gibson, V. C.; Kimberley, B. S.; Maddox, P. J.; Mastroianni, S.; McTavish, S. J.; Redshaw, C.; Solan, G. A.; Stromberg, S.; White, A. J. P.; Williams, D. J. *J. Am. Chem. Soc.* **1999**, *121*, 8728.
3. Nuckel, S.; Burger, P. *Angew. Chem. Int. Ed.* **2003**, *42*, 1632.
4. Sieh, D.; Burger, P. *J. Am. Chem. Soc.* **2013**, *135*, 3971.
5. Schoffel, J.; Rogachev, A. Y.; George, S. D.; Burger, P. *Angew. Chem. Int. Ed.* **2009**, *48*, 4734.
6. Dias, E. L.; Brookhart, M.; White, P. S. *Organometallics* **2000**, *19*, 4995.
7. Haarman, H. F.; Ernsting, J. M.; Kranenburg, M.; Kooijman, H.; Veldman, N.; Spek, A. L.; vanLeeuwen, P. W. N. M.; Vrieze, K. *Organometallics* **1997**, *16*, 887.
8. Haarman, H. F.; Kaagman, J. W. F.; Smeets, W. J. J.; Spek, A. L.; Vrieze, K. *Inorg. Chim. Acta* **1998**, *270*, 34.
9. Schoffel, J.; Susnjar, N.; Nuckel, S.; Sieh, D.; Burger, P. *Eur. J. Inorg. Chem.* **2010**, 4911.

10. Sieh, D.; Schlimm, M.; Andernach, L.; Angersbach, F.; Nuckel, S.; Schoffel, J.; Susnjar, N.; Burger, P. *Eur. J. Inorg. Chem.* **2012**, 444.
11. Johnson, L. K.; Killian, C. M.; Brookhart, M. *J. Am. Chem. Soc.* **1995**, *117*, 6414.
12. Nuckel, S.; Burger, P. *Organometallics* **2001**, *20*, 4345.
13. Webb, J. R.; Figg, T. M.; Otten, B. M.; Cundari, T. R.; Gunnoe, T. B.; Sabat, M. *Eur. J. Inorg. Chem.* **2013**, *2013*, 4515.
14. Grotjahn, D. B.; Sheridan, P. M.; Al Jihad, I.; Ziurys, L. M. *J. Am. Chem. Soc.* **2001**, *123*, 5489.
15. Reich, H. J. Bordwell pKa Data. <http://www.chem.wisc.edu/areas/reich/pkatable/>.
16. Zumdhal, S. S.; Zumdhal, S. A. *Chemistry*. 5th ed.; Houghton Mifflin Company: Boston, 2000.
17. Wright, J. A.; Danopoulos, A. A.; Motherwell, W. B.; Carroll, R. J.; Ellwood, S.; Sassmannshausen, J. *Eur. J. Inorg. Chem.* **2006**, 4857.

## 6 Hydrophenylation of Ethylene using a Cationic Ru(II) Catalyst: Comparison to a Neutral Ru(II) Catalyst

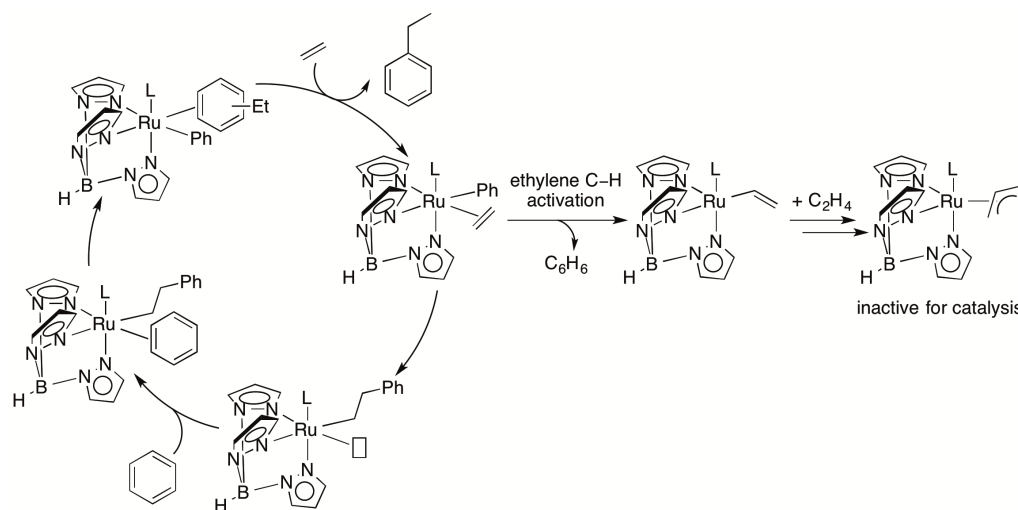
### 6.1 Introduction

Alkyl arenes are produced on a large scale from arenes and olefins using acid-based catalysts (either zeolites or Friedel-Crafts catalysts).<sup>1-5</sup> In recent years, substantial advances have been made in transition metal-catalyzed functionalization of C–H bonds.<sup>6-</sup><sup>16</sup> Transition metal catalyzed olefin hydroarylation provides a complementary route for the alkylation of aromatic substrates that can proceed by a pathway that is different from acid catalyzed aromatic alkylation.<sup>17-36</sup> For some transition metal mediated olefin hydroarylation reactions, olefin insertion into a metal-aryl bond is followed by aromatic C–H activation and liberation of alkylated aromatic arene (Scheme 6.1).<sup>17,18,37</sup> Potential benefits of this method include the selective production of linear alkyl arenes when using  $\alpha$ -olefins, selective synthesis of mono-alkyl arenes, regioselective synthesis of dialkyl arenes, and direct synthesis of vinyl arenes using oxidative hydroarylation.<sup>17,18,21-36</sup> Examples of catalysts that are active for unactivated hydrocarbons (e.g., benzene and ethylene) are limited, but catalysts based on Pd, Ru, Ir, Re and Pt have been reported.<sup>17,22-</sup>



**Scheme 6.1.** Catalytic cycle for transition metal catalyzed olefin hydroarylation that incorporates olefin insertion and aromatic C–H activation.

Our group has previously reported  $\text{TpRu(L)(NCMe)Ph}$  [ $\text{Tp} =$  hydridotris(pyrazolyl)borate;  $\text{L} = \text{CO}, \text{PMe}_3, \text{P}(\text{OCH}_2)_3\text{CEt}$  or  $\text{P}(\text{OCH}_2)_2(\text{OCCH}_3)$ ] complexes for catalytic ethylene hydrophenylation.<sup>36,38,39,40-42</sup> These studies have indicated a trend in the catalytic efficiency as the donor ability of the ligand “L” is varied.<sup>17,39</sup> For more strongly donating ligands (e.g.,  $\text{PMe}_3, \text{P}(\text{OCH}_2)_3\text{CEt}$ ), ethylene C–H activation competes with catalytic ethylene hydrophenylation and results in the formation of  $\text{TpRu(L)}(\eta^3\text{-C}_3\text{H}_4\text{Me})$  and catalyst deactivation (Scheme 6.2).<sup>38,39,41</sup> As a result, the more electron-rich  $\text{TpRu(L)(NCMe)Ph}$  complexes are relatively poor catalysts for olefin hydroarylation. Table 6.1 shows a summary of turnover numbers (TONs) for hydrophenylation of ethylene using a series of  $\text{TpRu(L)(NCMe)Ph}$  complexes. Ru(III/II) potentials (vs. NHE), which have been used to compare the impact of L on the electron density of  $\text{TpRu(L)(NCMe)Ph}$  catalyst precursors, are also shown in Table 6.1.<sup>17,39</sup> Based on these results, it is anticipated that less electron-rich Ru(II) complexes would provide catalysts that give higher TONs than  $\text{TpRu(L)(NCMe)Ph}$  complexes.



**Scheme 6.2.** Formation of the complexes  $\text{TpRu(L)}(\eta^3\text{-C}_3\text{H}_4\text{Me})$  [ $\text{L} = \text{CO}$ ,  $\text{PMe}_3$ ,  $\text{P}(\text{OCH}_2)_3\text{CEt}$ , and  $\text{P}(\text{OCH}_2)_2(\text{OCCH}_3)$ ], which are inactive for ethylene hydrophenylation, results from ethylene C–H activation.

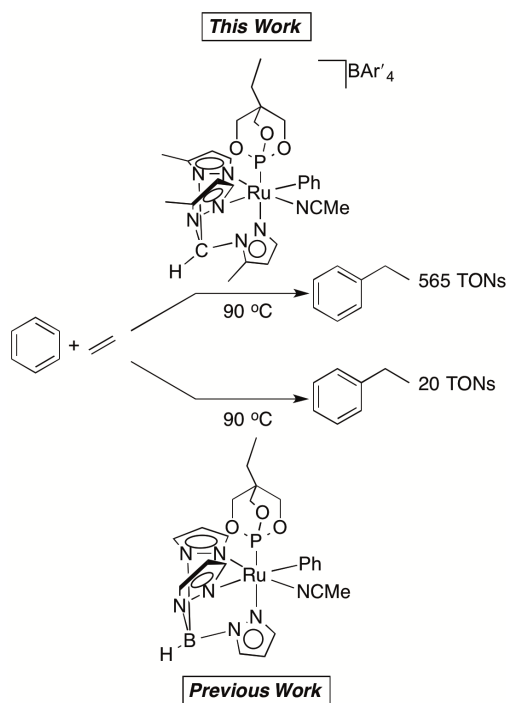
**Table 6.1.** Comparison of Ru(III/II) potentials and TONs for ethylene hydrophenylation using  $\text{TpRu(L)}(\text{NCMe})(\text{Ph})$  [ $\text{L} = \text{CO}$ ,  $\text{PMe}_3$ ,  $\text{P}(\text{OCH}_2)_3\text{CEt}$  or  $\text{P}(\text{OCH}_2)_2(\text{OCCH}_3)$ ] complexes.<sup>17,39</sup>

L	$E_{1/2}$ (V vs NHE)	TON <sup>a</sup>
$\text{PMe}_3$	0.29	0 <sup>b</sup>
$\text{P}(\text{OCH}_2)_3\text{CEt}$	0.54	20 <sup>b</sup>
$\text{P}(\text{OCH}_2)_2(\text{OCCH}_3)$	0.69	90 <sup>b</sup>
CO	1.03	415 <sup>c</sup>

<sup>a</sup>90 °C, 15 psi  $\text{C}_2\text{H}_4$ , and 0.025 mol% catalyst. <sup>b</sup>Catalyst deactivates by forming  $\text{TpRu(L)}(\eta^3\text{-C}_3\text{H}_4\text{Me})$ . <sup>c</sup>The identity of the catalyst decomposition products are unknown.

One strategy to access less electron-rich Ru(II) catalysts, compared to  $\text{TpRu(L)}(\text{NCMe})\text{Ph}$  complexes, is to produce cationic variants. For example, replacement of anionic Tp with charge-neutral poly(pyrazolyl)alkanes provides a method to generate

cationic complexes that are structurally similar to  $\text{TpRu(L)(NCMe)Ph}$  but less electron-rich.<sup>43</sup> To test this strategy, we have synthesized a cationic Ru(II) catalyst that is similar to  $\text{TpRu(P(OCH}_2)_3\text{CEt)(NCMe)Ph}$ , a known ethylene hydrophenylation catalyst with low TON ( $\leq 20$ ).<sup>39,41</sup> Under optimized conditions, the new cationic Ru(II) catalyst provides an increase in TON by a factor of nearly 30-fold compared to  $\text{TpRu(P(OCH}_2)_3\text{CEt)(NCMe)Ph}$  (Scheme 6.3). Although the new cationic Ru(II) complex is slightly less active than its TpRu variant, its increased thermal stability allows reactions to be carried out at higher temperatures at which much faster catalysis is accessible.



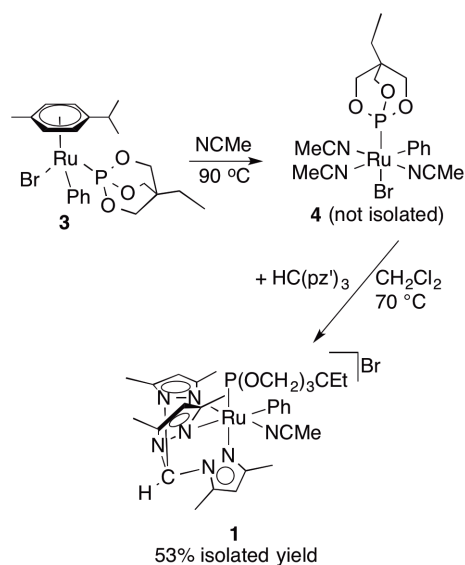
**Scheme 6.3.** Previously reported  $\text{TpRu(P(OCH}_2)_3\text{CEt)(NCMe)Ph}$  gives 20 TONs of ethylbenzene at 90 °C whereas the catalyst described in this work,  $[(\text{HC(pz}^5)_3)\text{Ru(P(OCH}_2)_3\text{CEt)(NCMe)Ph}][\text{BAR}'_4]$ , gives 565 TONs of ethylbenzene.

## 6.2 Results and Discussion

### 6.2.1 Synthesis of Ru(II) Poly(pyrazolyl) Alkane Complexes

A brief overview of the synthesis and characterization of Ru(II) poly(pyrazolyl) alkanes complexes first prepared by Dr. Evan Joslin is included as introductory material. The sections that follow will focus on catalysis using one of these complexes,  $[(\text{HC}(\text{pz}^5)_3)\text{Ru}(\text{P}(\text{OCH}_2)_3\text{CEt})(\text{NCMe})\text{Ph}][\text{BAr}'_4]$ .

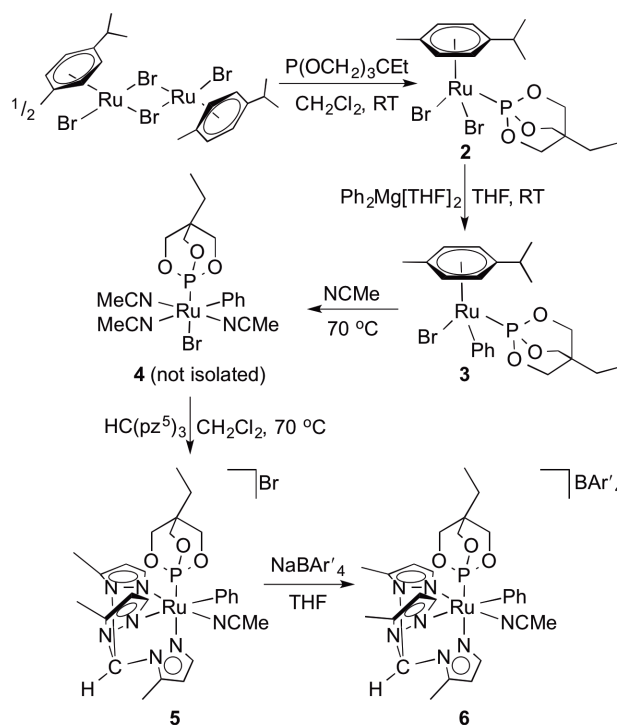
Heating the Ru(II) cation  $[(\text{C}(\text{pz})_4)\text{Ru}(\text{P}(\text{OCH}_2)_3\text{CEt})(\text{NCMe})\text{Me}]^+$  (pz = pyrazolyl) results in intramolecular C–H activation of a pyrazoyl 5-position C–H bond.<sup>44</sup> As a result,  $[(\text{C}(\text{pz})_4)\text{Ru}(\text{P}(\text{OCH}_2)_3\text{CEt})(\text{NCMe})\text{Me}]^+$  is inactive for catalytic hydrophenylation of benzene.<sup>44</sup> Thus, Dr. Evan Joslin synthesized the 3,5-dimethyl variant  $[(\text{HC}(\text{pz}')_3)\text{Ru}(\text{P}(\text{OCH}_2)_3\text{CEt})(\text{NCMe})\text{Ph}][\text{BAr}'_4]$  (**1**) [ $\text{HC}(\text{pz}')_3$  = tris(3,5-dimethylpyrazolyl)methane] to protect against C–H activation of the pyrazolyl 5-position C–H bond (Scheme 6.4).<sup>45</sup> Cyclic voltammetry of  $[(\text{HC}(\text{pz}')_3)\text{Ru}(\text{P}(\text{OCH}_2)_3\text{CEt})(\text{NCMe})\text{Ph}][\text{BAr}'_4]$  (**1**) shows a reversible wave [Ru(III/II)] at 0.82 V (vs NHE), which is close to the Ru(III/II) potential (1.03 V) of  $\text{TpRu}(\text{CO})(\text{NCMe})\text{Ph}$  and is approximately a +0.28 V shift compared to  $\text{TpRu}(\text{P}(\text{OCH}_2)_3\text{CEt})(\text{Ph})(\text{NCMe})$  (0.54 V vs. NHE).<sup>41</sup> Complex **1** was investigated as a catalyst for ethylene hydrophenylation between 90 °C and 125 °C with 15 to 25 psi of ethylene.<sup>45</sup> No production of ethylbenzene or styrene was observed.



**Scheme 6.4.** Synthesis of  $[(\text{HC}(\text{pz}')_3)\text{Ru}(\text{P}(\text{OCH}_2)_3\text{CEt})(\text{NCMe})\text{Ph}]\text{Br}$  (**1**).

Assuming that the steric bulk of the  $(\text{HC}(\text{pz}')_3)$  ligand is likely responsible for the inability of complex **1** to catalyze ethylene hydrophenylation, Dr. Evan Joslin incorporated the 5-methyl variant and prepared  $[(\text{HC}(\text{pz}^5)_3)\text{Ru}(\text{P}(\text{OCH}_2)_3\text{CEt})(\text{NCMe})\text{Ph}][\text{BAR}'_4]$  (**6**) [ $\text{HC}(\text{pz}^5)_3$  = tris(5-methylpyrazolyl)methane] (Scheme 6.5).<sup>45</sup> The addition of  $\text{Ph}_2\text{Mg}[\text{THF}]_2$  (0.8 equivalents) to a heterogeneous mixture of  $(\eta^6\text{-}p\text{-cymene})\text{Ru}(\text{P}(\text{OCH}_2)_3\text{CEt})\text{Br}_2$  (**2**) in THF gives  $(\eta^6\text{-}p\text{-cymene})\text{Ru}(\text{P}(\text{OCH}_2)_3\text{CEt})(\text{Br})\text{Ph}$  (**3**) in a 95% isolated yield.<sup>44</sup> Heating  $(\eta^6\text{-}p\text{-cymene})\text{Ru}(\text{P}(\text{OCH}_2)_3\text{CEt})(\text{Br})\text{Ph}$  (**3**) in NCMe at 70 °C for 3.5 h leads to the formation of putative  $(\text{NCMe})_2\text{Ru}(\text{P}(\text{OCH}_2)_3\text{CEt})(\text{Br})\text{Ph}$  (**4**).<sup>45</sup> Complex **4** has not been isolated or fully characterized. The reaction of **4** with  $\text{HC}(\text{pz}^5)_3$  at 70 °C gives  $[(\text{HC}(\text{pz}^5)_3)\text{Ru}(\text{P}(\text{OCH}_2)_3\text{CEt})(\text{NCMe})\text{Ph}]\text{Br}$  (**5**) in 87% isolated yield (Scheme 6.5). A crystal of **5** suitable for X-ray diffraction was obtained (Figure 6.1). The structure reveals a pseudo octahedral coordination sphere. The O–P–O bond angles of the phosphite are

101.7(2)°, 101.1(1)° and 100.9(2)°. The O–P–O bond angles for previously reported  $\text{TpRu}(\text{PPh}_3)(\text{P}(\text{OCH}_2)_3\text{CEt})\text{Cl}$  [101.4(1)°, 101.3(1)°, 100.8(1)°] and  $\text{TpRu}(\text{PPh}_3)(\text{P}(\text{OCH}_2)_3\text{CEt})\text{OTf}$  [102.43(8)°, 102.78(8)°, and 99.88(8)°] are in good agreement with those of complex **5**. The Ru–P bond distances of the previously reported complexes  $\text{TpRu}(\text{PPh}_3)(\text{P}(\text{OCH}_2)_3\text{CEt})\text{Cl}$  and  $\text{TpRu}(\text{PPh}_3)(\text{P}(\text{OCH}_2)_3\text{CEt})\text{OTf}$  are 2.202(1) Å and 2.212(1) Å, respectively, which are comparable to the Ru–P [2.1889(9) Å] bond distance for the cationic complex **5**.<sup>41</sup> A metathesis reaction of **5** with  $\text{NaBAR}'_4$  gave  $[(\text{HC}(\text{pz}^5)_3)\text{Ru}(\text{P}(\text{OCH}_2)_3\text{CEt})(\text{NCMe})\text{Ph}][\text{BAR}'_4]$  (**6**) in 97% isolated yield (Scheme 6.5). The  $E_{1/2}$  [Ru(III/II)] of  $[(\text{HC}(\text{pz}^5)_3)\text{Ru}(\text{P}(\text{OCH}_2)_3\text{CEt})(\text{NCMe})\text{Ph}][\text{BAR}'_4]$  (**6**) is 0.83 V versus NHE.



**Scheme 6.5.** Synthesis of  $[(\text{HC}(\text{pz}^5)_3)\text{Ru}(\text{P}(\text{OCH}_2)_3\text{CET})(\text{NCMe})\text{Ph}][\text{BAR}'_4]$  (**6**).

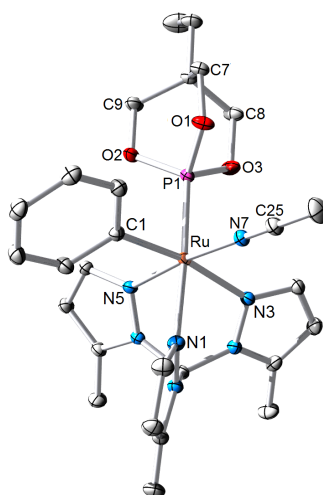


**Figure 6.1.** ORTEP diagram of  $[(\text{HC}(\text{pz}^5)_3)\text{Ru}(\text{P}(\text{OCH}_2)_3\text{CET})(\text{NCMe})\text{Ph}]\text{Cl}$  (**5-Cl**) (35% probability with hydrogen atoms and chloride omitted). During crystallization from  $\text{CH}_2\text{Cl}_2$ , bromide counterion was replaced with chloride. Selected bond lengths ( $\text{\AA}$ ): Ru–P1, 2.1889(9); P1–O1, 1.602(3); P1–O2, 1.614(3); P1–O3, 1.624(3); Ru–C1, 2.069(4); Ru–N1, 2.133(3); Ru–N3, 2.172(3); Ru–N5, 2.071(3); Ru–N7, 2.023(3); N7–C25, 1.140(5). Selected bond angles (deg): O3–P1–O2, 100.93(15); O1–P1–O3, 101.1(1); O1–P1–O2, 101.7(2); N7–Ru–C1, 89.4(1); P1–Ru–N7, 92.19(9); C1–Ru–P1, 89.3(1); Ru–N7–C25, 178.0(3).

## 6.2.2 Catalytic Ethylene Hydrophenylation

The efficiency of complex **6** (0.01 mol%) as a catalyst for ethylene hydrophenylation was investigated at several different temperatures using 15 psi of C<sub>2</sub>H<sub>4</sub> (Figure 6.2). The reactors were recharged with 15 psi ethylene after each time point recorded. The highest turnovers (TOs) of ethylbenzene (~400) were obtained after 36 h at 150 °C, after which the catalyst is deactivated. Using the ideal gas law, the maximum theoretical number of TO with 15 psi of ethylene is ~600.

Under optimized conditions (0.025 mol% catalyst, 15 psi C<sub>2</sub>H<sub>4</sub> and 90 °C), TpRu(P(OCH<sub>2</sub>)<sub>3</sub>CEt)(NCMe)Ph gives only 20 TONs of ethylbenzene.<sup>39,41</sup> For a direct comparison of catalytic hydrophenylation of ethylene using **6** versus TpRu(P(OCH<sub>2</sub>)<sub>3</sub>CEt)(NCMe)Ph, complex **6** (0.025 mol% relative to benzene) was heated in benzene at 90 °C with 15 psi of ethylene for this reaction, ethylene was not recharged at any time point between 0 h and 131 h. After 131 h, 565 TONs of ethylbenzene are produced using complex **6**, which is ~95% yield based on ethylene (Scheme 6.6). This represents a 28-fold improvement compared to TpRu(P(OCH<sub>2</sub>)<sub>3</sub>CEt)(NCMe)Ph.<sup>39</sup>

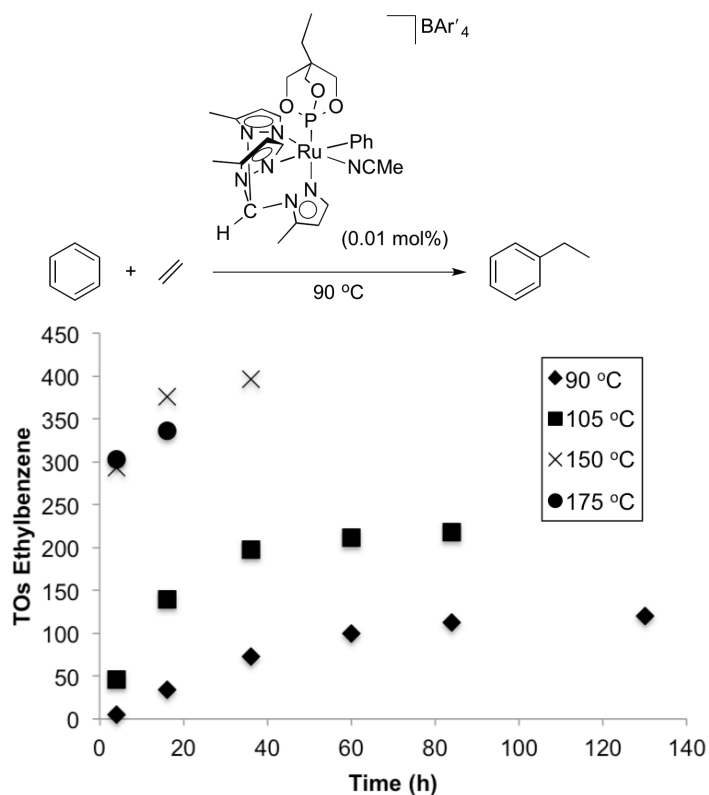
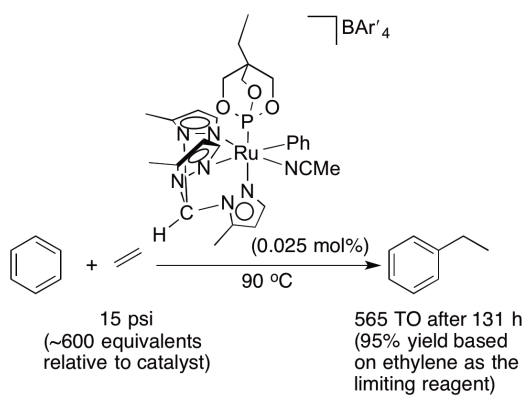


**Figure 6.2.** Catalytic hydrophenylation of ethylene (15 psi) using 0.01 mol% (relative to benzene)  $[(\text{HC}(\text{pz}^5)_3)\text{Ru}(\text{P}(\text{OCH}_2)_3\text{CEt})(\text{NCMe})\text{Ph}][\text{BAR}'_4]$  (**6**) at 90, 105, 150 and 175 °C.



**Scheme 6.6.** Ethylene hydrophenylation using  $[(\text{HC}(\text{pz}^5)_3)\text{Ru}(\text{P}(\text{OCH}_2)_3\text{CEt})(\text{NCMe})\text{Ph}][\text{BAR}'_4]$  (**6**) (0.025 mol%) gives ethylbenzene in 95% yield based on ethylene as a limiting reagent after 131 h at 90 °C.

In order to directly compare the activity of complex **6** to  $\text{TpRu}(\text{P}(\text{OCH}_2)_3\text{CEt})(\text{NCMe})(\text{Ph})$ , the turnover frequency (TOF) for ethylene hydrophenylation catalyzed by **6** was calculated after 4 h of reaction at 90 °C, 105 °C, 150 °C and 175 °C (Figure 6.2). For reactions at 90 °C and 105 °C, catalyst deactivation at 4 h is minimal (see Figure 6.2). However, at 150 °C and 175 °C some catalyst deactivation occurs after 4 h. Thus, the calculated TOFs at 150 °C and 175 °C are lower limits on catalyst activity. The TOF using **6** at 90 °C is  $3.6 \times 10^{-4} \text{ s}^{-1}$  (Table 6.2). Under the same conditions, at 90 °C a TOF of  $4.8 \times 10^{-4} \text{ s}^{-1}$  is observed for  $\text{TpRu}(\text{P}(\text{OCH}_2)_3\text{CEt})(\text{NCMe})\text{Ph}$ .<sup>39</sup> Thus,  $\text{TpRu}(\text{P}(\text{OCH}_2)_3\text{CEt})(\text{NCMe})\text{Ph}$  is only 1.3 times more active than complex **6** at 90 °C (Table 6.2). The increased stability of **6** compared to  $\text{TpRu}(\text{P}(\text{OCH}_2)_3\text{CEt})(\text{NCMe})\text{Ph}$  allows catalysis at higher temperatures. At 150 °C, the TOF using **6** ( $\geq 2 \times 10^{-2} \text{ s}^{-1}$ ) is  $\geq 42$  times greater than the TOF using  $\text{TpRu}(\text{P}(\text{OCH}_2)_3\text{CEt})(\text{NCMe})\text{Ph}$  at 90 °C. Attempted catalysis using  $\text{TpRu}(\text{P}(\text{OCH}_2)_3\text{CEt})(\text{NCMe})\text{Ph}$  at temperatures greater than 100 °C leads to rapid deactivation with minimal ethylbenzene product ( $< 20 \text{ TONs}$ ).<sup>41</sup>

**Table 6.2.** Comparison of TOF for ethylbenzene production for catalytic ethylene hydrophenylation using Ru(II) complexes.

Catalyst	Temp (°C)	TOF (s <sup>-1</sup> )	rel TOF
[(HC(pz <sup>5</sup> ) <sub>3</sub> Ru(P(OCH <sub>2</sub> ) <sub>3</sub> CEt)(NCMe)Ph)[BAR' <sub>4</sub> ] <sup>a</sup>	90	3.6 x 10 <sup>-4</sup>	1
TpRu(P(OCH <sub>2</sub> ) <sub>3</sub> CEt)(NCMe)Ph <sup>a</sup>	90	4.8 x 10 <sup>-4</sup>	1.3
[(HC(pz <sup>5</sup> ) <sub>3</sub> Ru(P(OCH <sub>2</sub> ) <sub>3</sub> CEt)(NCMe)Ph)[BAR' <sub>4</sub> ] <sup>b</sup>	105	3.2 x 10 <sup>-3</sup>	9
[(HC(pz <sup>5</sup> ) <sub>3</sub> Ru(P(OCH <sub>2</sub> ) <sub>3</sub> CEt)(NCMe)Ph)[BAR' <sub>4</sub> ] <sup>b</sup>	150 <sup>c</sup>	2.0 x 10 <sup>-2</sup>	56
[(HC(pz <sup>5</sup> ) <sub>3</sub> Ru(P(OCH <sub>2</sub> ) <sub>3</sub> CEt)(NCMe)Ph)[BAR' <sub>4</sub> ] <sup>b</sup>	175 <sup>c</sup>	2.1 x 10 <sup>-2</sup>	58

<sup>a</sup>TOF calculated after 4 h at 90 °C with 15 psi C<sub>2</sub>H<sub>4</sub> and 0.025 mol% of catalyst. <sup>b</sup>TOF calculated after 4 h with 15 psi C<sub>2</sub>H<sub>4</sub> and 0.01 mol% of catalyst. <sup>c</sup>Catalyst deactivation is significant, and TOF is a lower limit.

For TpRu(L)(NCMe)Ph complexes with L = P(OCH<sub>2</sub>)<sub>2</sub>(OCCH<sub>3</sub>), P(OCH<sub>2</sub>)<sub>3</sub>CEt or PMe<sub>3</sub>, catalyst deactivation occurs through ethylene C–H activation to form a Ru–vinyl complex, which undergoes olefin insertion and isomerization to form η<sup>3</sup>-allyl complexes (Scheme 6.1).<sup>17,39</sup> Also, for TpRu(L)(NCMe)Ph catalysts, TONs increase as the donating ability of L decreases.<sup>39</sup> We have interpreted experimental and computational studies to determine that increased donor ability of L retards the rate of ethylene insertion, which allows olefin C–H activation to compete with olefin hydroarylation.<sup>17,39</sup> The catalyst deactivation products are TpRu(L)(η<sup>3</sup>-C<sub>3</sub>H<sub>4</sub>Me) complexes.<sup>17,39</sup> Likewise, the <sup>1</sup>H NMR spectra of the non-volatile material from catalytic reactions using **6** show resonances consistent with an η<sup>3</sup>-allyl complex (Figure 6.4 and Figure 6.5). Characteristic allyl peaks include a triplet of triplets at 4.47 ppm (<sup>3</sup>J<sub>AC</sub> = 7 Hz) (for labels see Figure 6.3), a doublet of triplets at 2.56 ppm (<sup>3</sup>J<sub>AC</sub> = 7 Hz, <sup>2</sup>J<sub>AB</sub> = 2 Hz), a doublet of quartets at 1.86 ppm (<sup>3</sup>J<sub>CD</sub> = 12 Hz, <sup>3</sup>J<sub>DMe</sub> = 6 Hz) and a doublet of doublets at 0.80 ppm (<sup>3</sup>J<sub>BC</sub> = 11 Hz, <sup>2</sup>J<sub>AB</sub> = 2 Hz). The resonance due to the allyl methyl is observed as a doublet (<sup>3</sup>J<sub>DMe</sub> = 6 Hz) at 1.54

ppm. The allyl complex  $[(\text{HC}(\text{pz}^5)_3)\text{Ru}(\text{P}(\text{OCH}_2)_3\text{CEt})(\eta^3\text{-C}_3\text{H}_4\text{Me})][\text{BAr}'_4]$  (**7**) was independently synthesized by heating a solution of complex **6** in THF at 105 °C under 215 psi  $\text{C}_2\text{H}_4$  (Scheme 6.7). The deactivation of complex **6** occurs by a similar pathway to  $\text{TpRu}(\text{L})(\text{NCMe})\text{Ph}$  [ $\text{L} = \text{CO}, \text{P}(\text{OCH}_2)_3\text{CEt}, \text{PMe}_3$  and  $\text{P}(\text{OCH}_2)_2(\text{OCCH}_3)$ ] complexes (Scheme 6.8). For  $\text{TpRu}(\text{PMe}_3)(\text{NCMe})\text{Ph}$ , the formation of the vinyl complex occurs from  $\text{TpRu}(\text{PMe}_3)(\eta^2\text{-C}_2\text{H}_4)\text{Ph}$ .<sup>17,38</sup> For complex **6**, we have not differentiated whether formation of the putative vinyl complex occurs from  $[(\text{HC}(\text{pz}^5)_3)\text{Ru}(\text{P}(\text{OCH}_2)_3\text{CEt})(\eta^2\text{-C}_2\text{H}_4)\text{Ph}][\text{BAr}'_4]$  or  $[(\text{HC}(\text{pz}^5)_3)\text{Ru}(\text{P}(\text{OCH}_2)_3\text{CEt})(\eta^2\text{-C}_2\text{H}_4)(\text{CH}_2\text{CH}_2\text{Ph})][\text{BAr}'_4]$ .

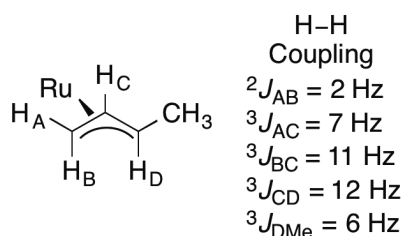
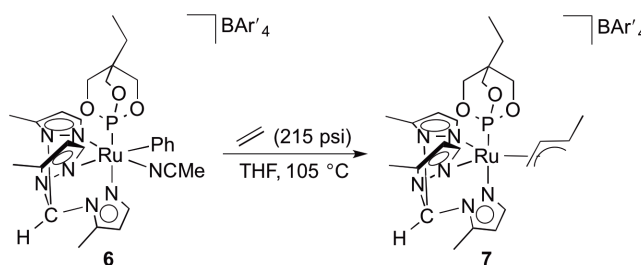
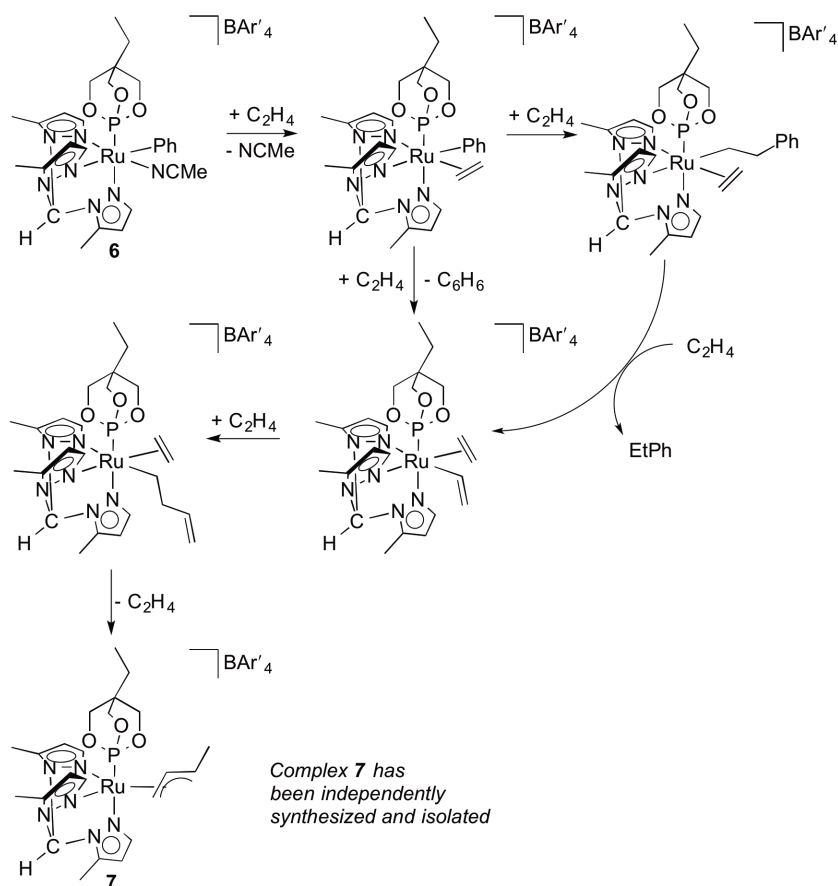


**Figure 6.3.** Allyl Coupling Diagram for  $[(\text{HC}(\text{pz}^5)_3)\text{Ru}(\text{P}(\text{OCH}_2)_3\text{CEt})(\eta^3\text{-C}_3\text{H}_4\text{Me})][\text{BAr}'_4]$  (**7**).



**Scheme 6.7.** Independent synthesis of  $[(\text{HC}(\text{pz}^5)_3)\text{Ru}(\text{P}(\text{OCH}_2)_3\text{CEt})(\eta^3\text{-C}_3\text{H}_4\text{Me})][\text{BAr}'_4]$  (**7**).



**Scheme 6.8.** The proposed deactivation pathway for  $[(\text{HC}(\text{pz}^5)_3)\text{Ru}(\text{P}(\text{OCH}_2)_3\text{CEt})(\text{NCMe})\text{Ph}][\text{BAr}'_4]$  (**6**) involves ethylene C–H activation.

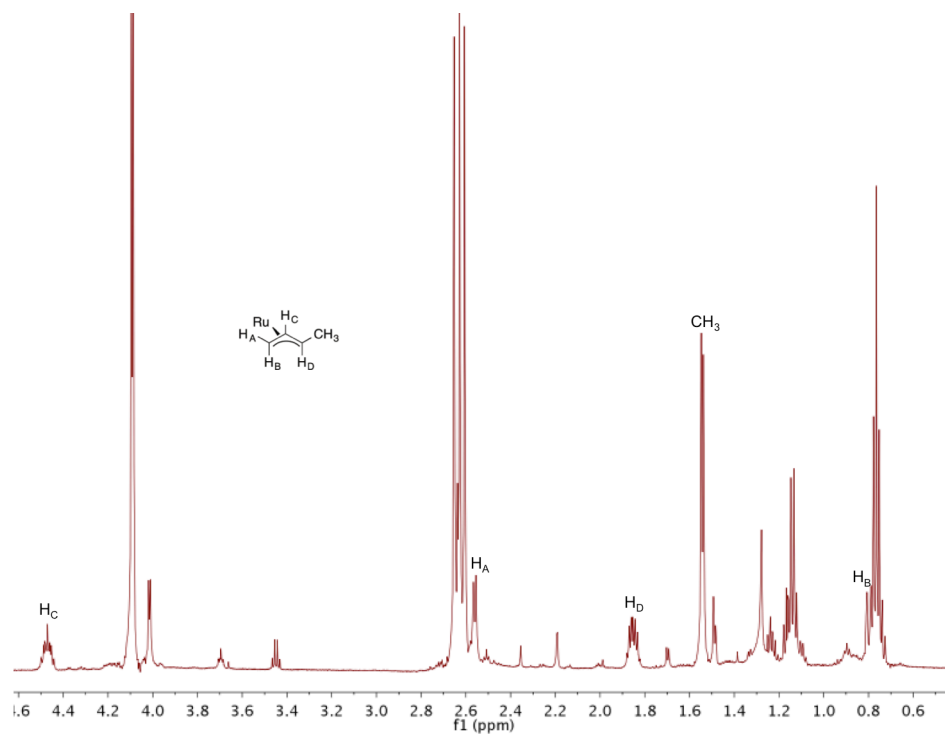


**Figure 6.4.** Partial  $^1\text{H}$  NMR spectrum of the non-volatiles from a catalytic ethylene hydrophenylation reaction using  $[(\text{HC}(\text{pz}^5)_3)\text{Ru}(\text{P}(\text{OCH}_2)_3\text{CEt})(\text{NCMe})\text{Ph}][\text{BAr}'_4]$  (**6**). The allyl resonances of  $[(\text{HC}(\text{pz}^5)_3)\text{Ru}(\text{P}(\text{OCH}_2)_3\text{CEt})(\eta^3\text{-C}_3\text{H}_4\text{Me})][\text{BAr}'_4]$  (**7**) are labeled.

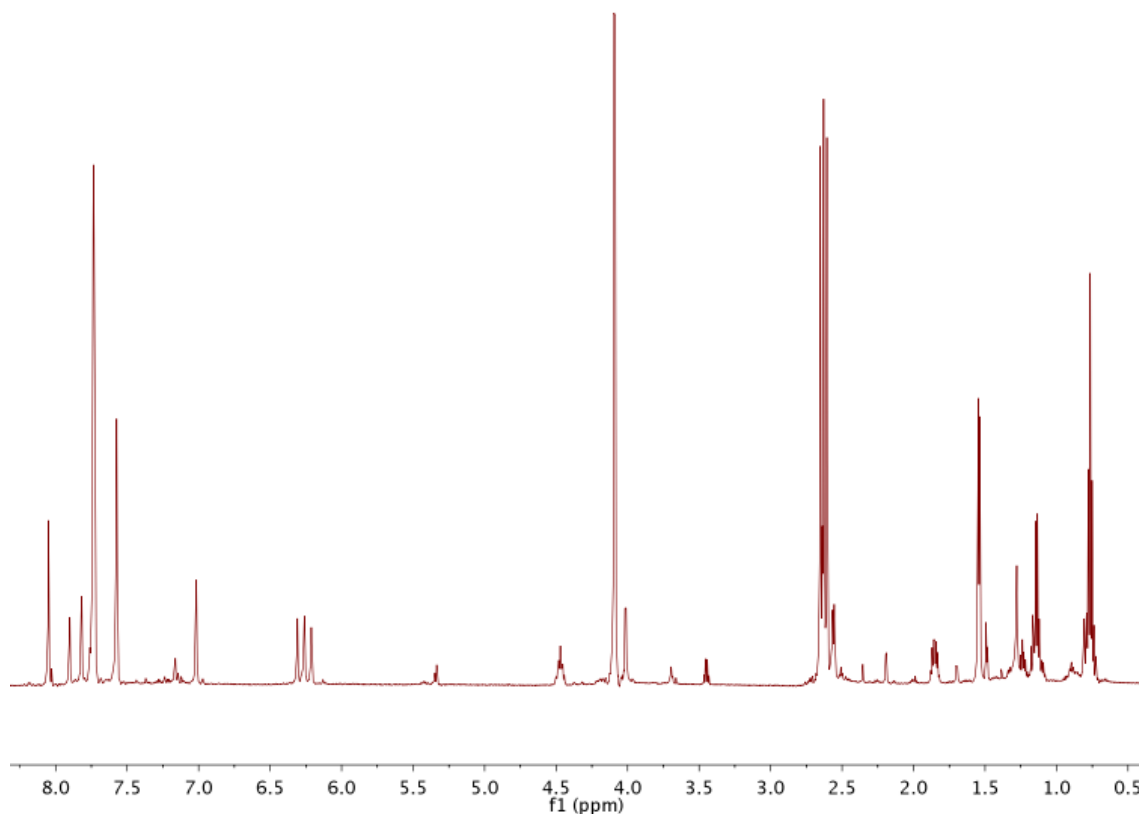


**Figure 6.5.**  $^1\text{H}$  NMR spectrum of  $[(\text{HC}(\text{pz}^5)_3\text{Ru}(\text{P}(\text{OCH}_2)_3\text{CET})(\eta^3\text{-C}_3\text{H}_4\text{Me}))][\text{BAR}'_4]$  (**7**) in  $\text{CD}_2\text{Cl}_2$ .

Ethylene hydrophenylation was carried out at 90 °C with 0.01 mol% complex **6** under different ethylene pressures. Similar to  $\text{TpRu}(\text{L})(\text{NCMe})\text{Ph}$  catalysts,<sup>17,39</sup> higher ethylene pressures reduce the TONs and TOF (Figure 6.6 and Table 6.3). A plot of TOF versus  $\text{C}_2\text{H}_4$  pressure reveals an inverse dependence (Figure 6.7), for which previous studies of the mechanism of ethylene hydrophenylation by  $\text{TpRu}(\text{L})(\text{NCMe})\text{Ph}$  complexes provide a plausible explanation (Scheme 6.9).<sup>17</sup> Initial exchange of coordinated NCMe with ethylene forms  $[(\text{HC}(\text{pz}^5)_3\text{Ru}(\text{P}(\text{OCH}_2)_3\text{CET})(\eta^2\text{-C}_2\text{H}_4)\text{Ph})][\text{BAR}'_4]$ . Subsequent olefin insertion gives

$[(HC(pz^5)_3)Ru(P(OCH_2)_3CEt)(CH_2CH_2Ph)][BAR'_4]$ , and coordination of ethylene forms  $[(HC(pz^5)_3)Ru(P(OCH_2)_3CEt)(CH_2CH_2Ph)(\eta^2-C_2H_4)][BAR'_4]$ . For  $TpRu(L)(NCMe)Ph$  catalysts, we have evidence that  $TpRu(L)(CH_2CH_2Ph)(\eta^2-C_2H_4)$  complexes are the likely catalyst resting states.<sup>17</sup> An inverse dependence of the rate of catalysis on ethylene concentration is expected since ethylene removes the active catalyst from the catalytic cycle.

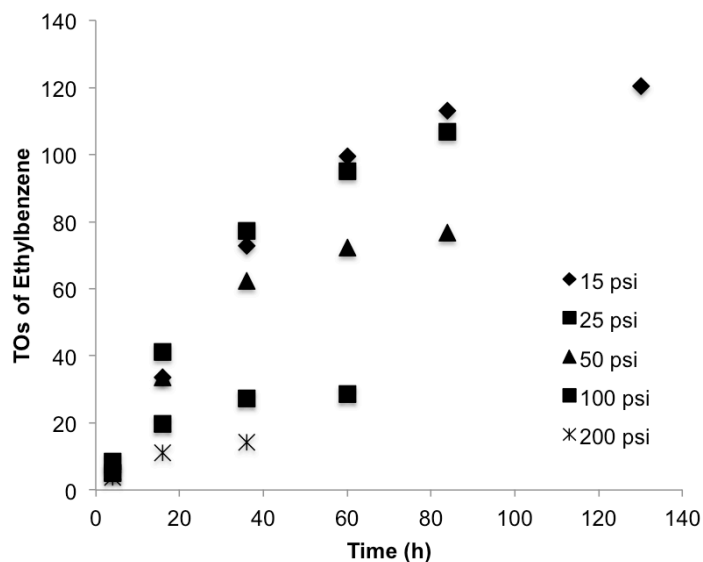


**Figure 6.6.** Catalytic ethylene hydrophenylation by  $[(HC(pz^5)_3)Ru(P(OCH_2)_3CEt)(NCMe)Ph][BAR'_4]$  (6) (0.01 mol%, 90 °C) at variable ethylene pressures.

**Table 6.3.** Comparison of TOF for ethylbenzene production for catalytic ethylene hydrophenylation using  $[(HC(pz^5)_3)Ru(P(OCH_2)_3CEt)(NCMe)Ph][BAR'_4]$  (**6**) (0.01 mol%) and varying pressures of  $C_2H_4$ .

$C_2H_4$ (psi)	TOF ( $s^{-1}$ ) <sup>a</sup>
15	$3.07 \times 10^{-4}$
25	$2.54 \times 10^{-4}$
50	$2.39 \times 10^{-4}$
100	$5.88 \times 10^{-5}$
200	$1.82 \times 10^{-5}$

<sup>a</sup>TOF calculated after 4 h at 90 °C and 0.01 mol% of catalyst.

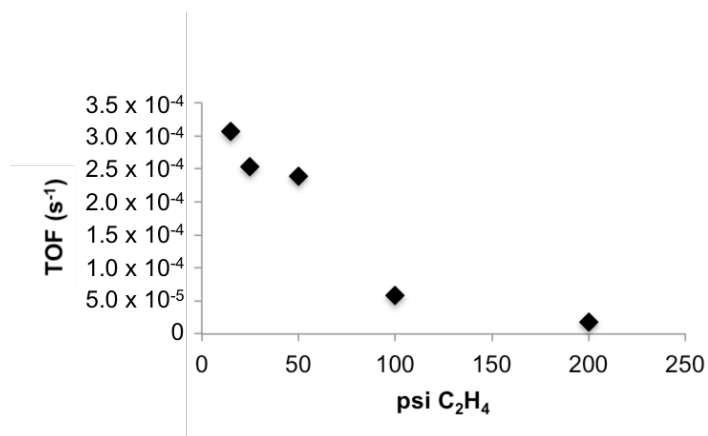
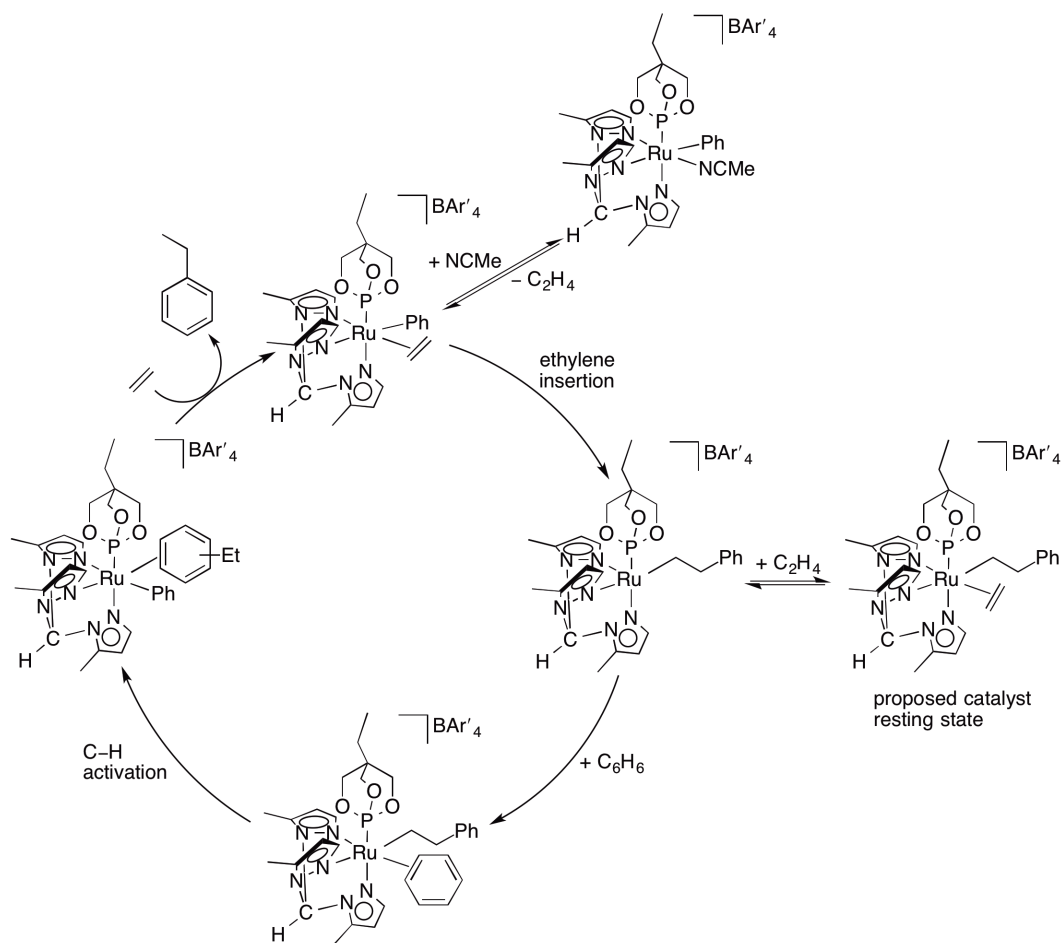


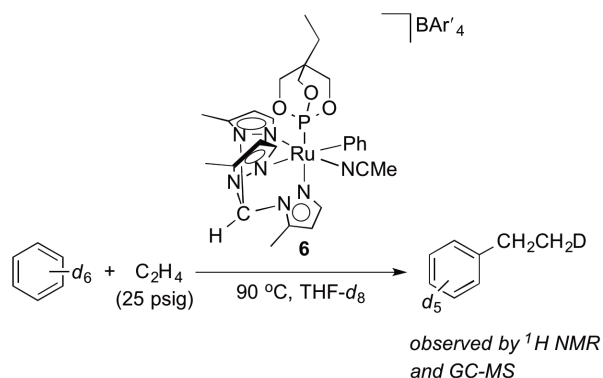
**Figure 6.7.** TOF for ethylbenzene production for catalytic ethylene hydrophenylation using  $[(HC(pz^5)_3)Ru(P(OCH_2)_3CEt)(NCMe)Ph][BAR'_4]$  (**6**) (0.01 mol%) versus psi  $C_2H_4$ . TOFs were calculated using TO after 4 h at 90 °C.



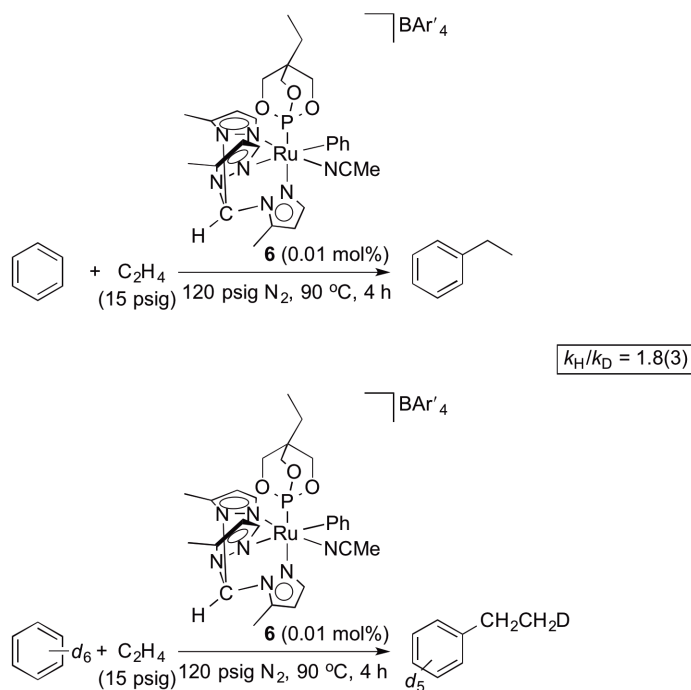
**Scheme 6.9.** Proposed catalytic cycle for ethylene hydrophenylation using  $[(\text{HC}(\text{pz}^5)_3)\text{Ru}(\text{P}(\text{OCH}_2)_3\text{Ct})(\text{NCMe})\text{Ph}][\text{BAR}'_4]$  (**6**).

For the catalytic reaction of complex **6** with  $\text{C}_6\text{D}_6$  and  $\text{C}_2\text{H}_4$ , GC-MS and  $^1\text{H}$  NMR data indicate the primary product is  $\text{C}_6\text{D}_5\text{CH}_2\text{CH}_2\text{D}$  (Scheme 6.10). Resonances ( $^1\text{H}$  NMR) for  $\text{C}_6\text{D}_5\text{CH}_2\text{CH}_2\text{D}$  can be observed when monitoring a catalytic reaction of complex **6** with  $\text{C}_6\text{D}_6$  and 25 psig  $\text{C}_2\text{H}_4$  in  $\text{THF-}d_8$  at  $90^\circ\text{C}$ . Multiplets are observed at 1.19 ppm for the mono-deuterated methyl and at 2.60 ppm for the benzylic methylene resonances. GC-MS shows  $\text{EtPh-}d_6$  as the major product, and a primary fragment

consistent with  $-\text{CH}_2\text{CH}_2\text{D}$  ( $m/z = 30$ ) is observed. We compared the TOF for ethylbenzene production (determined using the TOs after 4 h at 90 °C with 15 psi  $\text{C}_2\text{H}_4$ ) for catalytic reactions performed with  $\text{C}_6\text{D}_6$  to separate experiments using  $\text{C}_6\text{H}_6$ , and a KIE ( $k_{\text{H}}/k_{\text{D}}$ ) of 1.8(3) was determined (Scheme 6.11). This is consistent with rate limiting benzene C–H activation in the catalytic cycle.



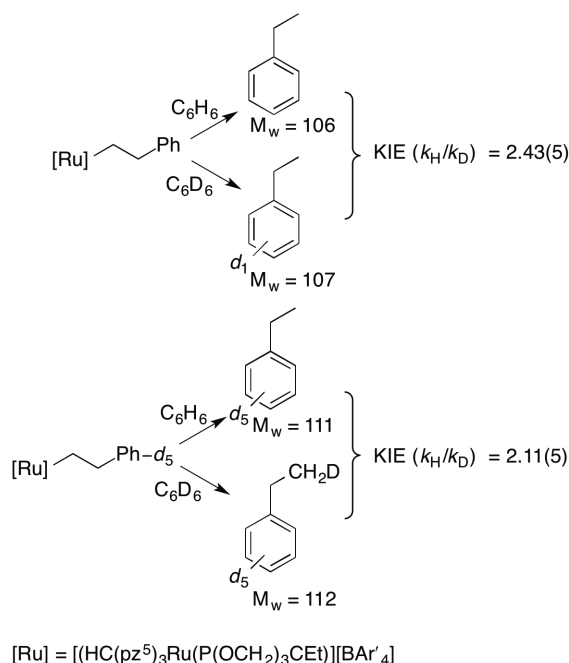
**Scheme 6.10.**  $\text{C}_6\text{D}_5\text{CH}_2\text{CH}_2\text{D}$  is the major product from the catalytic reaction of  $[(\text{HC}(\text{pz}^5)_3)\text{Ru}(\text{P}(\text{OCH}_2)_3\text{CEt})(\text{NCMe})\text{Ph}][\text{BAR}'_4]$  (**6**) with  $\text{C}_6\text{D}_6$  and 25 psig  $\text{C}_2\text{H}_4$ .



**Scheme 6.11.** A KIE ( $k_{\text{H}}/k_{\text{D}}$ ) of 1.8(3) was determined by comparing the TOF for ethylbenzene product for identical catalytic reactions one using  $\text{C}_6\text{H}_6$  and the other using  $\text{C}_6\text{D}_6$ .

Catalytic ethylene hydrophenylation using complex **6** (0.01 mol%) was also performed using a 1:1 molar ratio of  $\text{C}_6\text{H}_6$  to  $\text{C}_6\text{D}_6$ . Presumably, this leads to the formation of both  $[(\text{HC}(\text{pz}^5)_3)\text{Ru}(\text{P}(\text{OCH}_2)_3\text{CEt})(\text{CH}_2\text{CH}_2\text{Ph})][\text{BAR}'_4]$  and  $[(\text{HC}(\text{pz}^5)_3)\text{Ru}(\text{P}(\text{OCH}_2)_3\text{CEt})(\text{CH}_2\text{CH}_2\text{Ph-}d_5)][\text{BAR}'_4]$  as catalytic intermediates. These species can react with either  $\text{C}_6\text{H}_6$  or  $\text{C}_6\text{D}_6$  to generate four possible isotopologues (Scheme 6.12). These four ethylbenzene isotopologues are the primary products observed by GC-MS from the reaction in a 1:1 mixture of  $\text{C}_6\text{D}_6$  and  $\text{C}_6\text{H}_6$ . After heating for 4 h at 90 °C, a KIE ( $k_{\text{H}}/k_{\text{D}}$ ) of 2.11(5) was determined by comparing the ratios of  $M_{\text{w}}$  111/112 in the GC-MS of the reaction mixture. This KIE is statistically identical to the KIE determined by comparison of TOF from catalysis in  $\text{C}_6\text{H}_6$  versus  $\text{C}_6\text{D}_6$  ( $k_{\text{H}}/k_{\text{D}}$ ) of 1.8(3)

(see above). A KIE of 2.1(1) was previously determined for catalytic hydrophenylation of ethylene using  $\text{TpRu}(\text{CO})(\text{NCMe})\text{Ph}$  as the catalyst.<sup>36</sup> The same KIE values for complex **6** and  $\text{TpRu}(\text{CO})(\text{NCMe})\text{Ph}$  are consistent with similar mechanisms.



**Scheme 6.12.** The reaction of  $[(\text{HC}(\text{pz}^5)_3\text{Ru}(\text{P}(\text{OCH}_2)_3\text{CEt})(\text{NCMe})\text{Ph})][\text{BAR}'_4]$  (**6**) with a 1:1 molar ratio  $\text{C}_6\text{H}_6$  to  $\text{C}_6\text{D}_6$  leads to the formation of four isotopologues of ethylbenzene.

### 6.2.3 Degenerate $\text{NCMe}/\text{NCCD}_3$ Exchange

Previously, we reported evidence that stoichiometric C–D activation of  $\text{C}_6\text{D}_6$  by  $\text{TpRu}(\text{L})(\text{NCMe})\text{Ph}$  [ $\text{L} = \text{CO}$ ,  $\text{PMe}_3$ ,  $\text{P}(\text{OCH}_2)_3\text{CEt}$  or  $\text{P}(\text{OCH}_2)_2(\text{OCCH}_3)$ ] complexes occurs by the pathway shown in Scheme 6.13.<sup>17</sup> We expected that the cationic nature of **6** might result in strong coordination of  $\text{NCMe}$  (compared to  $\text{TpRu}(\text{L})(\text{NCMe})\text{Ph}$

complexes), which could slow the rate of C–D activation of C<sub>6</sub>D<sub>6</sub>. The rate of exchange between coordinated NCCH<sub>3</sub> of **6** and free NCCD<sub>3</sub> confirms this. The rate of degenerate NCCH<sub>3</sub>/NCCD<sub>3</sub> exchange for complex **6** was determined using <sup>1</sup>H NMR spectroscopy by heating a solution of complex **6** in NCCD<sub>3</sub> at 70 °C (Scheme 6.14). A *k*<sub>obs</sub> value of 5.7(7) x 10<sup>-6</sup> s<sup>-1</sup> was determined from first order plots. This rate is slower by ~5.6 fold than the rate of exchange for TpRu(CO)(NCMe)Ph under similar conditions (*k*<sub>obs</sub> = 3.2(2) x 10<sup>-5</sup> s<sup>-1</sup> at 70 °C).<sup>17</sup> The rate of degenerate NCMe/NCCD<sub>3</sub> exchange for complex **6** was also determined at 80, 88 and 95 °C. Values for *k*<sub>obs</sub> of 3.3(3) x 10<sup>-5</sup> s<sup>-1</sup>, 5.4(3) x 10<sup>-5</sup> s<sup>-1</sup> and 2.48(7) x 10<sup>-4</sup> s<sup>-1</sup>, respectively, were determined (Figure 6.8). An Eyring plot gave activation parameters of Δ*H*<sup>‡</sup> = 35(5) kcal/mol and Δ*S*<sup>‡</sup> = 19(13) eu for the NCMe/NCCD<sub>3</sub> exchange reaction (Figure 6.9). The rate of degenerate NCMe/NCCD<sub>3</sub> exchange for a THF-*d*<sub>8</sub> solution of complex **6** at 95 °C with 10, 20 and 30 equivalents (0.1 M, 0.2 M, and 0.3 M) of added NCCD<sub>3</sub> showed statistically identical rates (*k*<sub>obs</sub> = 1.1(1) x 10<sup>-4</sup> s<sup>-1</sup>), consistent with a dissociative mechanism.

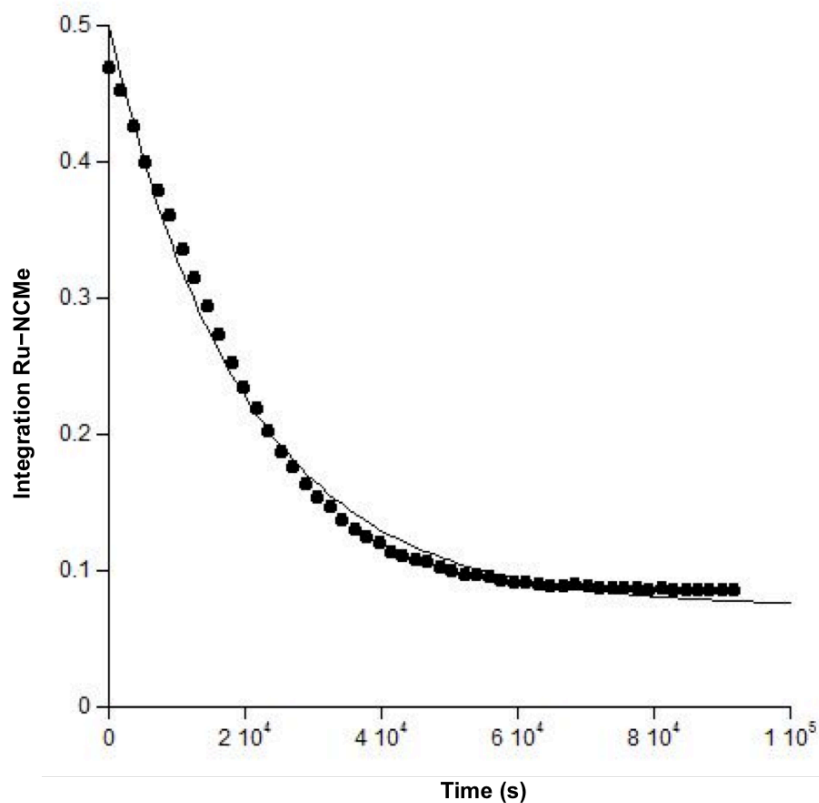
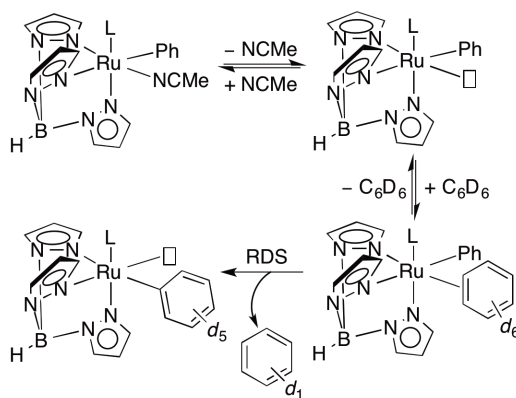
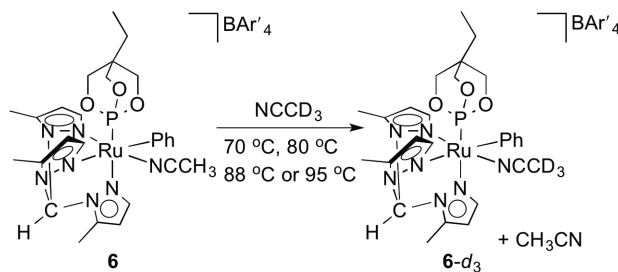


**Figure 6.8.** Representative plot of degenerate  $\text{NCCH}_3/\text{NCCD}_3$  exchange for  $[(\text{HC}(\text{pz}^5)_3)\text{Ru}(\text{P}(\text{OCH}_2)_3\text{CEt})(\text{NCMe})\text{Ph}][\text{BAR}'_4]$  (**6**) at  $88^\circ\text{C}$  ( $k_{\text{obs}} = 5.4(3) \times 10^{-5} \text{ s}^{-1}$ ,  $R^2 = 0.99$ ).



**Scheme 6.13.** Proposed pathway for C–D activation of benzene by  $\text{TpRu}(\text{L})(\text{NCMe})\text{Ph}$  [ $\text{L} = \text{CO}$ ,  $\text{P}(\text{OCH}_2)_3\text{CEt}$ , and  $\text{P}(\text{OCH}_2)_2(\text{OCCH}_3)$ ].



**Scheme 6.14.** Degenerate NCMethyl/NCCD<sub>3</sub> exchange using [(HC(pz<sup>5</sup>)<sub>3</sub>)Ru(P(OCH<sub>2</sub>)<sub>3</sub>CEt)(NCMe)Ph][BAR'<sub>4</sub>] (**6**).

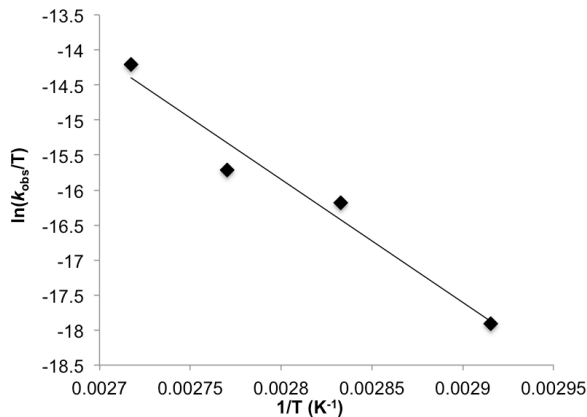


**Figure 6.9.** Eyring plot of degenerate NCMethyl / NCCD<sub>3</sub> exchange for [(HC(pz<sup>5</sup>)<sub>3</sub>)Ru(P(OCH<sub>2</sub>)<sub>3</sub>CEt)(NCMe)Ph][BAR'<sub>4</sub>] (**6**) ( $R^2 = 0.96$ ; 70 °C to 95 °C).

#### 6.2.4 Stoichiometric C–D Activation of C<sub>6</sub>D<sub>6</sub>

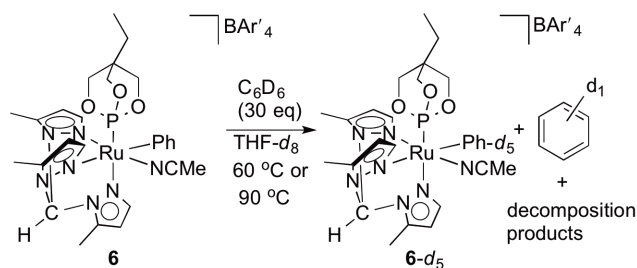
For TpRu(L)(NCMe)Ph complexes [L = CO, PMe<sub>3</sub>, P(pyr)<sub>3</sub>, P(OCH<sub>2</sub>)<sub>3</sub>CEt, and P(OCH<sub>2</sub>)<sub>2</sub>(OCCH<sub>3</sub>)], the rate of stoichiometric C–D activation of C<sub>6</sub>D<sub>6</sub> to produce TpRu(L)(NCMe)(C<sub>6</sub>D<sub>5</sub>) and C<sub>6</sub>H<sub>5</sub>D decreases as the Ru(III/II) potential becomes more positive.<sup>17,39</sup> The Ru(III/II) potential of **6** is negative of TpRu(CO)(NCMe)Ph (1.03 V)

and positive of  $\text{TpRu}[\text{P}(\overline{\text{OCH}_2})_2(\overline{\text{OCCH}_3})](\text{NCMe})\text{Ph}$  (0.69 V). Thus, it was anticipated that the rate of  $\text{C}_6\text{D}_6$  C–D activation by **6** would be faster than  $\text{TpRu}(\text{CO})(\text{NCMe})\text{Ph}$  but slower than  $\text{TpRu}[\text{P}(\overline{\text{OCH}_2})_2(\overline{\text{OCCH}_3})](\text{NCMe})\text{Ph}$ . The  $k_{\text{obs}}$  values for C–D activation of  $\text{C}_6\text{D}_6$  for  $\text{TpRu}(\text{CO})(\text{NCMe})\text{Ph}$  and  $\text{TpRu}(\text{P}(\text{OCH}_2)_3\text{CEt})(\text{NCMe})\text{Ph}$  (with 0.065 mmol NCMe added to prevent decomposition) at 60 °C are  $4.62(3) \times 10^{-6} \text{ s}^{-1}$  and  $1.20(2) \times 10^{-5} \text{ s}^{-1}$ , respectively.<sup>39</sup>

In the absence of added NCMe, competitive decomposition is observed when monitoring stoichiometric C–D activation of  $\text{C}_6\text{D}_6$  using complex **6**. As a result, a detailed kinetic analysis of  $\text{C}_6\text{D}_6$  activation by **6** is not possible. Less decomposition is observed with added NCMe (1 equivalent); however, the rate of C–D activation is significantly slowed. We are unable to monitor stoichiometric C–D activation of  $\text{C}_6\text{D}_6$  using complex **6** in neat  $\text{C}_6\text{D}_6$ . As a result, the following experiments were performed in the absence of added NCMe.

Monitoring ( $^1\text{H}$  NMR spectroscopy) a solution of complex **6** in  $\text{THF-}d_8$  with 30 equivalents of  $\text{C}_6\text{D}_6$  at 60 °C for two weeks shows ~50% conversion to  $[(\text{HC}(\text{pZ}^5)_3)\text{Ru}(\text{P}(\text{OCH}_2)_3\text{CEt})(\text{NCMe})\text{Ph-}d_5][\text{BAR}'_4]$  and  $\text{C}_6\text{H}_5\text{D}$  (Scheme 6.15). GC-MS analysis of the reaction mixture confirmed  $\text{C}_6\text{H}_5\text{D}_1$  as the primary organic product. Using an approximate  $t_{1/2}$  of 2 weeks for the reaction of **6** with  $\text{C}_6\text{D}_6$  gives  $k_{\text{obs}} \sim 5.7 \times 10^{-7} \text{ s}^{-1}$ . Thus, the rate of  $\text{C}_6\text{D}_6$  activation by complex **6** is ~80 times slower than  $\text{TpRu}(\text{CO})(\text{NCMe})\text{Ph}$  and ~200 times slower than  $\text{TpRu}(\text{P}(\text{OCH}_2)_3\text{CEt})(\text{NCMe})\text{Ph}$ . Keeping in mind the limits on this analysis due to partial decomposition of **6**, the rate of  $\text{C}_6\text{D}_6$  activation by **6** is likely an upper limit. A solution of complex **6** in  $\text{THF-}d_8$  with 30

equivalents of  $C_6D_6$  was heated at 90 °C. First order exponential decay plots from the integration for the *ortho*-phenyl resonance of complex **6** versus time gave a  $k_{obs}$  value of  $8.6(6) \times 10^{-6} \text{ s}^{-1}$  (Figure 6.10). Despite that complex **6** has a more negative Ru(III/II) potential than  $TpRu(CO)(NCMe)Ph$ , benzene C–D activation is much slower for **6**. These results demonstrate the trend observed for rate of benzene activation by  $TpRu(L)(NCMe)Ph$  complexes as a function of Ru(III/II) potential likely cannot be extended to cationic variants, even those that are structurally related to the  $TpRu(L)(NCMe)Ph$  complexes.



**Scheme 6.15.** Stoichiometric C–D Activation of  $C_6D_6$  using  $[(HC(pz^5)_3)Ru(P(OCH_2)_3CEt)(NCMe)Ph][[BAR'_4]]$  (**6**).

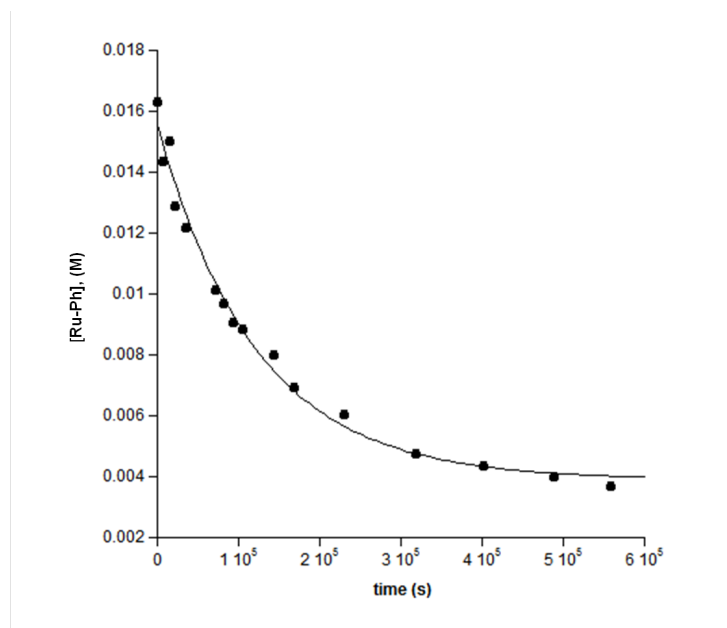
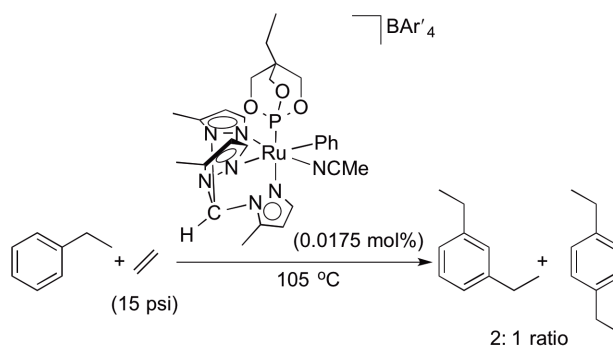


**Figure 6.10.** Representative plot of stoichiometric C–D activation of  $C_6D_6$  by  $[(HC(pz^5)_3Ru(P(OCH_2)_3CEt)(NCMe)Ph)][BAR'_4]$  (**6**) in THF- $d_8$  with 30 equivalents of  $C_6D_6$  at 90 °C ( $k_{obs} = 8.6(6) \times 10^{-6} s^{-1}$ ,  $R^2 = 0.99$ ).

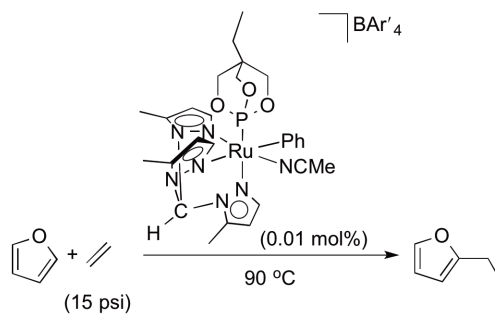
### 6.2.5 Other Olefin Hydroarylation Reactions

Due to the poor electronic influence of alkyl groups, dialkylbenzene production using Friedel–Crafts catalysis produces a mixture of 1,2- 1,3- and 1,4-dialkylbenzenes.<sup>4</sup> To test the ability of **6** to regioselectively produce dialkylbenzenes, we examined the hydroarylation reaction of ethylbenzene with ethylene (15 psi) at 105 °C using 0.0175 mol% complex **6** (Scheme 6.16). A 2:1 distribution of 1,3-diethylbenzene to 1,4-diethylbenzene (18 and 9 TO after 4 h, respectively) was observed (Scheme 6.16). 86 TOs were observed after 36 h. The TOF for the formation of diethylbenzene after 4 h was  $1.9 \times 10^{-4} s^{-1}$  which is 1.7 times slower than the formation of ethylbenzene from benzene.



**Scheme 6.16.** Catalysis with ethylbenzene gives 1,3 and 1,4-diethylbenzene in a 2 to 1 ratio.

The catalytic formation of 2-ethylfuran from the hydroarylation reaction of furan and ethylene was also investigated. C–H activation of furan by  $[(\text{HC}(\text{pz}^5)_3)\text{Ru}(\text{P}(\text{OCH}_2)_3\text{CET})(\text{NCMe})\text{Ph}][\text{BAR}'_4]$  (**6**) readily occurs at 90 °C to give  $[(\text{HC}(\text{pz}^5)_3)\text{Ru}(\text{P}(\text{OCH}_2)_3\text{CET})(\text{NCMe})(2\text{-furyl})][\text{BAR}'_4]$  as observed by  $^1\text{H}$  NMR spectroscopy. The catalytic reaction between furan and  $\text{C}_2\text{H}_4$  (15 psi) at 90 °C in the presence of complex **6** (0.01 mol%) gives ~10 TOs of 2-ethylfuran after 84 h at which point, the catalyst has deactivated (Scheme 6.17).



**Scheme 6.17.** Catalytic reaction between ethylene and furan.

One of the potential benefits of transition metal catalyzed olefin hydroarylation over traditional Friedel–Crafts catalysis is potential for selective synthesis of linear alkyl olefins when using  $\alpha$ -olefins.<sup>17</sup> Catalytic propylene hydrophenylation using complex **6** (0.01 mol%) and 15, 50, and 100 psig propylene at 105 °C was investigated. Unfortunately, cumene was observed as the major product with the best conditions (15 psig) giving only 3 TOs after 36 h. Minimal production of n-propylbenzene (approximately 1 TO) was observed under these conditions. The steric bulk of HC(pz<sup>5</sup>)<sub>3</sub> likely hinders propylene from coordinating to Ru.

### 6.3 Conclusion

Detailed studies of olefin hydroarylation using TpRu(L)(NCMe)Ph [L = CO, PMe<sub>3</sub>, P(OCH<sub>2</sub>)<sub>3</sub>CEt and P(OCH<sub>2</sub>)<sub>2</sub>(OCCH<sub>3</sub>)] catalysts led us to propose that cationic Ru(II) variants would provide greater TONs. Comparison of the TONs for ethylene hydrophenylation by TpRu(P(OCH<sub>2</sub>)<sub>3</sub>CEt)(NCMe)Ph and [(HC(pz<sup>5</sup>)<sub>3</sub>)Ru(P(OCH<sub>2</sub>)<sub>3</sub>CEt)(NCMe)Ph][BAR'<sub>4</sub>] (**6**) confirms this hypothesis. The best TON for TpRu(P(OCH<sub>2</sub>)<sub>3</sub>CEt)(NCMe)Ph is 20 (24 h, 90 °C, 0.025 mol% catalyst, 15 psi C<sub>2</sub>H<sub>4</sub>).<sup>39</sup> In contrast, complex **6** gives 565 TONs under these same conditions, which is a 28-fold improvement upon replacing Tp with a charge neutral tris(pyrazolyl)alkane ligand. Furthermore, the increased stability of **6** allows catalysis at higher temperatures, which can be used to overcome the slightly lower activity for **6** compared to TpRu(P(OCH<sub>2</sub>)<sub>3</sub>CEt)(NCMe)Ph at 90 °C. At 150 °C, complex **6** is an effective catalyst,

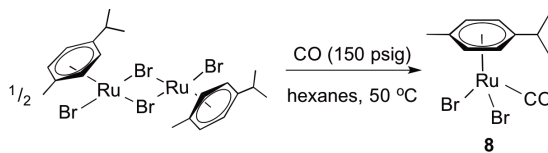
and the rate is ~60 times faster than using  $\text{TpRu}(\text{P}(\text{OCH}_2)_3\text{CEt})(\text{NCMe})\text{Ph}$  at the optimal 90 °C.

A TON of ~400 and  $\text{TOF} \geq 2 \times 10^{-2} \text{ s}^{-1}$  at 150 °C places complex **6** among the more active and long lived transition metal catalysts for ethylene hydrophenylation.<sup>25</sup> Periana, Goddard and co-workers have reported that  $[\text{Ir}(\mu\text{-acac})\text{-}O,O,C^3)(\text{acac}\text{-}O,O)(\text{acac})\text{-}O,O,C^3)]_2$  (acac = acetylacetonate) catalyzes ethylene hydrophenylation with a TON of 455 (3h) at 180 °C, which corresponds to a TOF of  $4.2 \times 10^{-2} \text{ s}^{-1}$ .<sup>46,47</sup> We have previously reported that  $[(\text{dpm})\text{Pt}(\text{Ph})(\text{THF})]^+$  (dpm = 2,6'-dipyridylmethane) catalyzes ethylene hydrophenylation with a TOF of  $\sim 1.8 \times 10^{-2} \text{ s}^{-1}$  (120 °C) with a TON of 469 (100 °C).<sup>25</sup> The results reported herein suggest even less electron rich Ru(II) catalysts than **6** are promising targets.

#### 6.4 Future Work

For the  $\text{TpRu}(\text{L})(\text{NCMe})\text{Ph}$  [L = CO,  $\text{PMe}_3$ ,  $\text{P}(\text{OCH}_2)_3\text{CEt}$ , or  $\text{P}(\text{OCH}_2)_2(\text{OCCH}_3)$ ] complexes, catalyst efficiency increases as the donor ability of L decreases.<sup>17,39</sup> As described above, an increase in catalyst longevity is achieved by replacing Tp with a charge neutral tris(pyrazolyl) alkane ligand. These results point to  $[(\text{HC}(\text{pz}^5)_3)\text{Ru}(\text{CO})(\text{NCMe})\text{Ph}]^+$  as a catalyst with potential to achieve even greater TONs than complex **6**. Preliminary attempts to synthesize  $[(\text{HC}(\text{pz}^5)_3)\text{Ru}(\text{CO})(\text{NCMe})\text{Ph}][\text{BAR}'_4]$  have been made. Progress towards the synthesis of  $[(\text{HC}(\text{pz}^5)_3)\text{Ru}(\text{CO})(\text{NCMe})\text{Ph}][\text{BAR}'_4]$  is described below.

As previously reported, heating (50 °C) a heterogeneous mixture of  $[(\eta^6\text{-}p\text{-cymene})\text{Ru}(\mu\text{-Br})(\text{Br})]_2$  in hexanes under 150 psig of CO for 2 h led to the formation of deep red  $(\eta^6\text{-}p\text{-cymene})\text{Ru}(\text{CO})\text{Br}_2$  (**8**) (Scheme 6.18). A CO absorption is observed at  $1994\text{ cm}^{-1}$  in the IR spectrum of complex **8**, and the  $^1\text{H}$  NMR spectrum of complex **8** is consistent with mirror symmetry (Figure 6.11).



**Scheme 6.18.** Synthesis of  $(\eta^6\text{-}p\text{-cymene})\text{Ru}(\text{CO})\text{Br}_2$  (**8**).

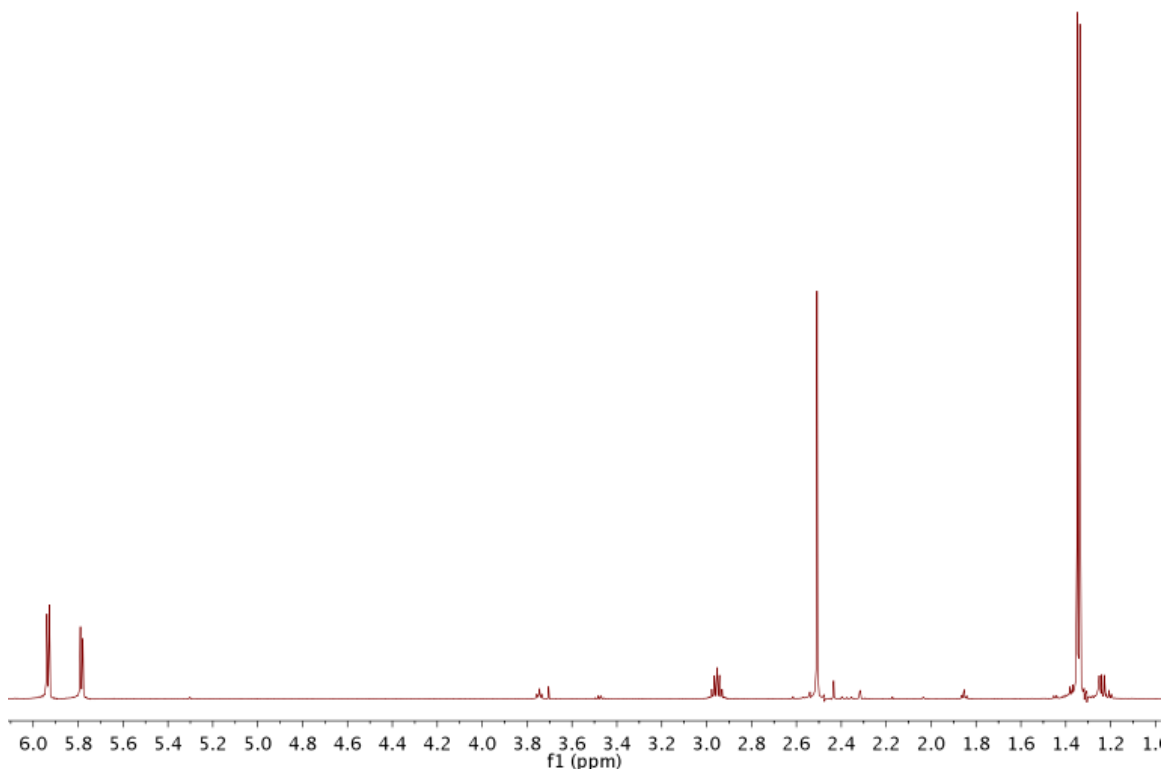
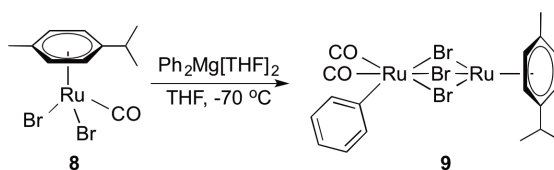


**Figure 6.11.**  $^1\text{H}$  NMR spectrum of  $(\eta^6\text{-}p\text{-cymene})\text{Ru}(\text{CO})\text{Br}_2$  (**8**) in  $\text{CDCl}_3$ .

In an effort to make  $(\eta^6\text{-}p\text{-cymene})\text{Ru}(\text{CO})(\text{Br})\text{Ph}$ ,  $(\eta^6\text{-}p\text{-cymene})\text{Ru}(\text{CO})\text{Br}_2$  was reacted with  $\text{Ph}_2\text{Mg}[\text{THF}]_2$ . Two CO absorptions were observed by IR spectroscopy ( $2048\text{ cm}^{-1}$  and  $1979\text{ cm}^{-1}$ ), for the product suggesting two complexes or a dicarbonyl complex. A single doublet ( $1.38\text{ ppm}$   $^3J_{\text{HH}} = 3\text{ Hz}$ ) was observed for the isopropyl methyl of the  $p$ -cymene, which is consistent with a mirror plane of symmetry (Figure 6.13). X-ray quality crystals grown by slow evaporation in  $\text{CH}_2\text{Cl}_3$  showed that product is the asymmetrical Ru binuclear complex  $(\eta^6\text{-}p\text{-cymene})\text{Ru}(\mu\text{-Br})_3\text{Ru}(\text{CO})_2\text{Ph}$  (**9**) (Figure 6.12). The Ru atoms are bridged by three bromide ligands. One Ru atom has an  $\eta^6$ -coordinated  $p$ -cymene ligand while the other Ru atom has two CO ligands and a coordinated phenyl (Scheme 6.19).



**Scheme 6.19.** The reaction of  $(\eta^6\text{-}p\text{-cymene})\text{Ru}(\text{CO})\text{Br}_2$  (**8**) with  $\text{Ph}_2\text{Mg}[\text{THF}]_2$  leads to the formation of an asymmetric Ru binuclear complex (**9**).

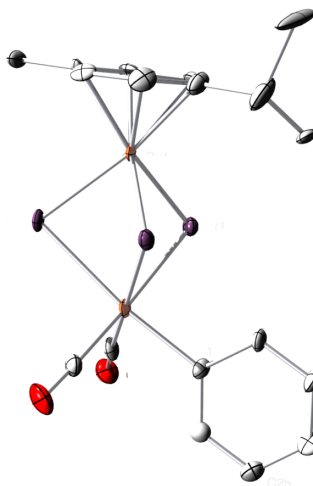


**Figure 6.12.** ORTEP diagram of  $(\eta^6\text{-}p\text{-cymene})\text{Ru}(\mu\text{-Br})_3\text{Ru}(\text{CO})_2\text{Ph}$  (**9**). Note: final refinement was not performed.

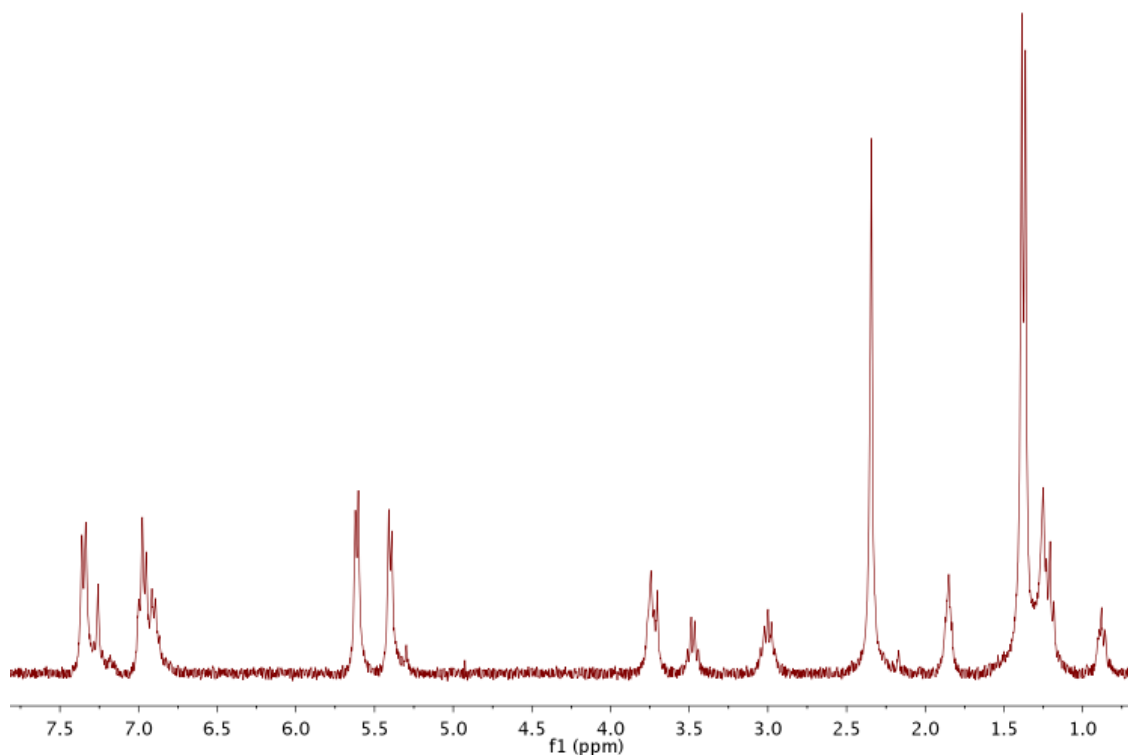
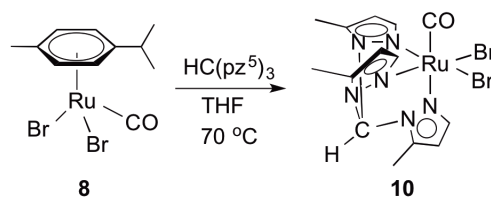


**Figure 6.13.**  $^1\text{H}$  NMR spectrum of  $(\eta^6\text{-}p\text{-cymene})\text{Ru}(\mu\text{-Br})_3\text{Ru}(\text{CO})_2(\text{Ph})$  (**9**) in  $\text{CDCl}_3$ .

To help avoid formation of a dimer upon phenylation, the *p*-cymene ligand of  $(\eta^6\text{-}p\text{-cymene})\text{Ru}(\text{CO})\text{Br}_2$  (**8**) was replaced with  $\text{HC}(\text{pz}^5)_3$  prior to phenylation. Heating ( $70^\circ\text{C}$ ) a solution of complex **8** and  $\text{HC}(\text{pz}^5)_3$  in THF results in the precipitation of the beige solid  $(\text{HC}(\text{pz}^5)_3)\text{Ru}(\text{CO})\text{Br}_2$  (**10**) (Scheme 6.20). Complex **10** exhibits  $\nu_{\text{CO}} = 1958\text{ cm}^{-1}$  in the IR spectrum. The  $^1\text{H}$  NMR  $(\text{HC}(\text{pz}^5)_3)\text{Ru}(\text{CO})\text{Br}_2$  is consistent with  $\text{C}_s$  symmetry as only 2 resonances are observed for both the 3- and 4-position protons on the pyrazolyl rings and methyl groups (Figure 6.14).



**Scheme 6.20.** Synthesis of  $(\text{HC}(\text{pz}^5)_3)\text{Ru}(\text{CO})\text{Br}_2$  (**10**).

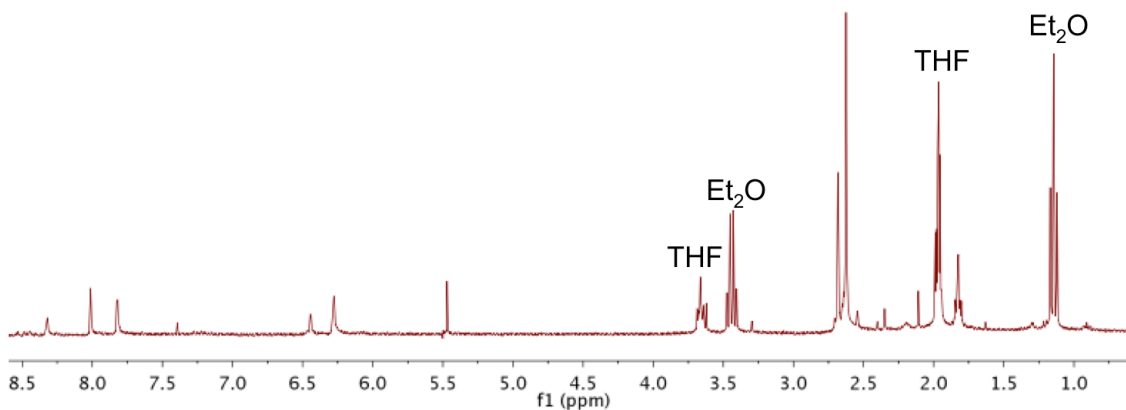
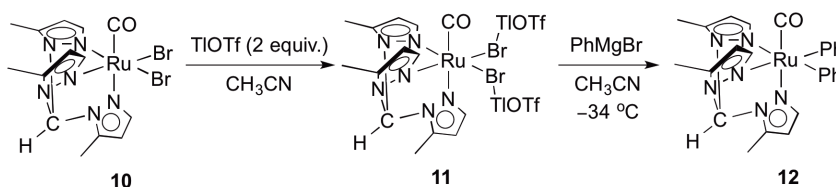


**Figure 6.14.**  $^1\text{H}$  NMR spectrum of  $(\text{HC}(\text{pz}^5)_3)\text{Ru}(\text{CO})\text{Br}_2$  (**10**) in  $\text{CD}_3\text{CN}$ . The poor solubility of **10** made it difficult to obtain a high quality  $^1\text{H}$  NMR spectrum.

$(\text{HC}(\text{pz}^5)_3)\text{Ru}(\text{CO})\text{Br}_2$  (**10**) has poor solubility in common organic solvents. It is sparingly soluble in NCMe. Attempts were made to phenylate  $(\text{HC}(\text{pz}^5)_3)\text{Ru}(\text{CO})\text{Br}_2$ ; however, due to the low solubility these reactions were unsuccessful. In an effort to improve the solubility of  $(\text{HC}(\text{pz}^5)_3)\text{Ru}(\text{CO})\text{Br}_2$ , TlOTf (2 equivalents) was added to a

suspension of complex **10** in NCMe. The  $^1\text{H}$  NMR of the product revealed new resonances, but HRMS data are consistent with a TlOTf adduct of  $(\text{HC}(\text{pz}^5)_3)\text{Ru}(\text{CO})\text{Br}_2$  (Scheme 6.21). Reaction of  $[(\text{HC}(\text{pz}^5)_3)\text{Ru}(\text{CO})\text{Br}_2][\text{TlOTf}]_2$  (**11**) with  $\text{PhMgBr}$  at  $-34\text{ }^\circ\text{C}$  lead to the formation of what is believed to be  $(\text{HC}(\text{pz}^5)_3)\text{Ru}(\text{CO})(\text{Ph})_2$  (**12**) (Scheme 6.21). A CO absorption is observed in the KBr IR spectrum at  $1959\text{ cm}^{-1}$ . The extremely poor solubility of complex **12** has made both characterization and purification difficult. Treatment of the putative  $(\text{HC}(\text{pz}^5)_3)\text{Ru}(\text{CO})(\text{Ph})_2$  with  $\text{HCl}$  in  $\text{Et}_2\text{O}$  results in the observation of free benzene and a decomposed Ru product.



**Scheme 6.21.** Possible synthesis of  $[(\text{HC}(\text{pz}^5)_3)\text{Ru}(\text{CO})\text{Br}_2][\text{TlOTf}]_2$  (**11**) and  $[(\text{HC}(\text{pz}^5)_3)\text{Ru}(\text{CO})(\text{NCMe})(\text{Ph})_2]\text{Br}$  (**12**).

## 6.5 Experimental

**General Methods.** Unless otherwise noted, all synthetic procedures were performed under anaerobic conditions in a nitrogen-filled glovebox or by using standard Schlenk techniques. Glovebox purity was maintained by periodic nitrogen purges and was monitored by an oxygen analyzer ( $\text{O}_2$  (g) < 15 ppm for all reactions). Toluene, tetrahydrofuran, pentane and diethyl ether were dried by distillation from sodium/benzophenone. Acetonitrile was dried by distillation from  $\text{CaH}_2$ . Hexanes, benzene and dichloromethane were purified by passage through a column of activated

alumina. Chloroform- $d_1$ , benzene- $d_6$ , acetonitrile- $d_3$ , methylene chloride- $d_2$  and THF- $d_8$  were stored under a  $N_2$  atmosphere over 4 Å molecular sieves.  $^1H$  and  $^{13}C$  NMR spectra were recorded on a Varian Mercury Plus 300 (126 MHz operating frequency for  $^{13}C$  NMR), Varian Inova 500 MHz spectrometer (125 MHz operating frequency for  $^{13}C$  NMR), Bruker Avance DRX 600 MHz spectrometer (150 MHz operative frequency for  $^{13}C$  NMR) or Bruker Avance III 800 MHz spectrometer (201 MHz operative frequency for  $^{13}C$  NMR). All  $^1H$  and  $^{13}C$  NMR spectra are referenced against residual proton signals ( $^1H$  NMR) or the  $^{13}C$  resonances of the deuterated solvent ( $^{13}C$  NMR). All  $^{31}P$  NMR were obtained on a Varian Mercury Plus 300 MHz spectrometer (operating frequency 121 MHz) and referenced against an external standard of  $H_3PO_4$  ( $\delta = 0$ ).  $^{19}F$  NMR (operating frequency 282 MHz) spectra were obtained on a Varian Mercury Plus 300 MHz spectrometer and referenced against an external standard of hexafluorobenzene ( $\delta = -164.9$ ). IR spectra were obtained on a Shimadzu IRAffinity-1 Fourier transform infrared spectrometer. KBr pellets of the samples were prepared. Elemental analyses were performed by Atlantic Microlabs, Inc. Electrochemical experiments were performed under a nitrogen atmosphere using a BAS Epsilon Potentiostat. Cyclic voltammograms were recorded in  $CH_3CN$  using a standard three electrode cell from  $-1700$  to  $1700$  mV at  $100$  mV/s with a glassy carbon working electrode and tetrabutylammonium hexafluorophosphate as the electrolyte. All potentials are reported versus NHE (normal hydrogen electrode) using ferrocene as the internal standard. High resolution mass spectra were acquired in ESI mode from samples dissolved in a 3:1 acetonitrile/water solution containing sodium trifluoroacetate (NaTFA). Mass spectra are reported for  $M^+$

for monocationic complexes or for  $[M+H^+]$  or  $[M+Na^+]$  for neutral complexes using  $[Na(NaTFA)_x]^+$  clusters as an internal standard. In all cases, observed isotopic envelopes were consistent with the molecular composition reported. Mass spectra were collected on a Waters Xevo G2Qtof or Agilent 6230 TOF. GC-MS was performed using a Shimadzu GCMS-QP2012 Plus system with a 30 m x 0.25 mm SHRXI-5MS column with 0.25 mm film thickness using electron impact ionization (EI). Dr. William H. Myers from the University of Richmond collected and interpreted the HRMS data. Dr. Michal Sabat at the University of Virginia solved the reported X-ray crystallography data. The preparation, isolation and characterization of  $[\eta^6\text{-}p\text{-cymene})Ru(Br)(\mu\text{-}Br)]_2$ ,<sup>48</sup>  $NaBAR'_4$ ,<sup>49</sup>  $Ph_2Mg[THF]_2$ ,<sup>50</sup>  $HC(pz^5)_3$ ,<sup>51</sup>  $(\eta^6\text{-}p\text{-cymene})Ru(P(OCH_2)_3CEt)(Br)Ph$  **(3)**,<sup>44</sup>  $[(HC(pz^5)_3)Ru(P(OCH_2)_3CEt)(NCMe)Ph]Br$  **(1)**,<sup>45</sup>  $[(HC(pz^5)_3)Ru(P(OCH_2)_3CEt)(NCMe)Ph]Br$  **(5)**,<sup>45</sup>  $[(HC(pz^5)_3)Ru(P(OCH_2)_3CEt)(NCMe)Ph][BAR'_4]$  **(6)**<sup>45</sup> have been previously reported.  $(\eta^6\text{-}p\text{-cymene})Ru(P(OCH_2)_3CEt)Br_2$  was prepared using the procedure reported for the synthesis of  $(\eta^6\text{-}p\text{-cymene})Ru(P(OCH_2)_3CEt)Cl_2$  using the bromide analogue,  $[(\eta^6\text{-}p\text{-cymene})Ru(Br)(\mu\text{-}Br)]_2$ , as the starting material.<sup>52</sup>  $(\eta^6\text{-}p\text{-cymene})Ru(CO)Br_2$  was synthesized following the method for the synthesis of  $(\eta^6\text{-}p\text{-cymene})Ru(CO)(Cl)_2$ .<sup>53</sup>  $P(OCH_2)_3CEt$  was obtained from a commercial source and purified by dissolution in hexanes and filtration through Celite. The filtrate was concentrated to dryness to yield a white solid. All other reagents were used as purchased from commercial sources.



$[(HC(pz^5)_3)Ru(P(OCH_2)_3CEt)(NCMe)Ph][BAR'_4]$  **(6)** (0.785 g, 0.0523 mmol) was

dissolved in THF (~10 mL) in a stainless steel pressure reactor. The reactor was purged three times with C<sub>2</sub>H<sub>4</sub> and then charged with 200 psig C<sub>2</sub>H<sub>4</sub>. The reactor was placed in a temperature-regulated aluminum block set to 105 °C. After 54 h of heating, the reactor was removed from the aluminum block, cooled to room temperature and degassed. The yellow solution was filtered through a pad of Celite. The filtrate was reduced to dryness *in vacuo* to give a low-density yellow-brown solid (0.063 g, 83%). <sup>1</sup>H NMR (600 MHz, CD<sub>2</sub>Cl<sub>2</sub>) δ 8.05 (s, 1H, HC(pz<sup>5</sup>)<sub>3</sub>), 7.90, 7.82 (each a d, <sup>3</sup>J<sub>HH</sub> = 2 Hz, 1H, HC(pz<sup>5</sup>)<sub>3</sub> 5-position), 7.73 (br s, 8H, BAr'<sub>4</sub> *ortho* position), 7.57 (br s, 4H, BAr'<sub>4</sub> *para* position), 7.02 (s, 1H, HC(pz<sup>5</sup>)<sub>3</sub> 5-position), 6.31, 6.26 (each a dd, <sup>3</sup>J<sub>HH</sub> = 1 Hz, 1H, HC(pz<sup>5</sup>)<sub>3</sub> 4-position), 6.21 (s, 1H, HC(pz<sup>5</sup>)<sub>3</sub> 4-position), 4.47 (tt, <sup>3</sup>J<sub>BC</sub> = 11 Hz, <sup>3</sup>J<sub>AC</sub> = 7 Hz, see Figure 6.3 for designations, 2H, allyl H<sub>c</sub>), 4.09 (d, <sup>3</sup>J<sub>CP</sub> = 5 Hz, 6H, P(OCH<sub>2</sub>)<sub>3</sub>CCH<sub>2</sub>CH<sub>3</sub>), 2.65, 2.63, 2.61 (each a s, 3H, HC(pz<sup>5</sup>)<sub>3</sub> 5-methyl position), 2.56 (dt, <sup>3</sup>J<sub>AC</sub> = 7 Hz, <sup>2</sup>J<sub>AB</sub> = 2 Hz, 1H, allyl H<sub>A</sub>), 1.86 (dq, <sup>3</sup>J<sub>CD</sub> = 12 Hz, <sup>3</sup>J<sub>DMe</sub> = 6 Hz, 1H, allyl H<sub>D</sub>), 1.54 (d, <sup>3</sup>J<sub>DMe</sub> = 6 Hz, 3H, allyl CH<sub>3</sub>), 1.13 (q, <sup>3</sup>J<sub>HH</sub> = 8 Hz, 2H, P(OCH<sub>2</sub>)<sub>3</sub>CCH<sub>2</sub>CH<sub>3</sub>), 0.80 (dd, <sup>3</sup>J<sub>BC</sub> = 11 Hz, <sup>2</sup>J<sub>AB</sub> = 2 Hz, 1H, allyl H<sub>B</sub>), 0.76 (t, <sup>3</sup>J<sub>HH</sub> = 8 Hz, 3H, P(OCH<sub>2</sub>)<sub>3</sub>CCH<sub>2</sub>CH<sub>3</sub>). <sup>13</sup>C NMR (201 MHz, CD<sub>2</sub>Cl<sub>2</sub>) δ 162.3 (four line pattern, <sup>1</sup>J<sub>CB</sub> = 50 Hz, BAr'<sub>4</sub>), 149.0, 146.9, 141.8, 141.3, 140.9, 140.9, 108.8, 108.7, 108.5, (each a s, HC(pz<sup>5</sup>)<sub>3</sub>), 135.4 (s, BAr'<sub>4</sub>), 129.7 (q, <sup>1</sup>J<sub>CF</sub> = 32 Hz, BAr'<sub>4</sub> C-CF<sub>3</sub>), 118.1 (s, BAr'<sub>4</sub>), 125.2 (q, <sup>1</sup>J<sub>CF</sub> = 273 Hz, BAr'<sub>4</sub> CF<sub>3</sub>), 88.2 (allyl-CH<sub>2</sub>CHCHCH<sub>3</sub>), 74.9 (d, <sup>2</sup>J<sub>CP</sub> = 7 Hz, P(OCH<sub>2</sub>)<sub>3</sub>CCH<sub>2</sub>CH<sub>3</sub>), 69.0 (s, HC(pz<sup>5</sup>)<sub>3</sub>), 55.0 (d, <sup>2</sup>J<sub>CP</sub> = 3 Hz, allyl-CH<sub>2</sub>CHCHCH<sub>3</sub>), 35.6 (d, <sup>3</sup>J<sub>CP</sub> = 29 Hz, P(OCH<sub>2</sub>)<sub>3</sub>CCH<sub>2</sub>CH<sub>3</sub>), 33.3 (d, <sup>2</sup>J<sub>CP</sub> = 5 Hz, allyl-CH<sub>2</sub>CHCHCH<sub>3</sub>), 23.8 (s, P(OCH<sub>2</sub>)<sub>3</sub>CCH<sub>2</sub>CH<sub>3</sub>), 18.4 (s, allyl-CH<sub>2</sub>CHCHCH<sub>3</sub>), 11.5, 11.5, 11.5 (each a s,

HC(pz<sup>5</sup>)<sub>3</sub>-CH<sub>3</sub> groups), 7.3 (s, P(OCH<sub>2</sub>)<sub>3</sub>CCH<sub>2</sub>CH<sub>3</sub>). <sup>31</sup>P{<sup>1</sup>H} NMR (121 MHz, CD<sub>2</sub>Cl<sub>2</sub>) δ 139.8. <sup>19</sup>F NMR (282 MHz, CD<sub>2</sub>Cl<sub>2</sub>) δ -64.2. M<sup>+</sup> = [C<sub>23</sub>H<sub>34</sub>N<sub>6</sub>O<sub>3</sub>PRu]<sup>+</sup> obsd (%), calcd (%), ppm: 569.1502 (12), 569.1501 (15), 0.3; 572.1483 (33), 572.1485 (36), -0.3; 573.1477 (41), 573.1477 (44), 0.0; 574.1482 (56), 574.1484 (57), -0.4; 575.1471 (100), 575.1474 (100), -0.6; 576.1500 (27), 576.1500 (26), -0.1; 577.1480 (57), 577.1482 (54), -0.4.

**( $\eta^6$ -*p*-cymene)Ru(CO)(Br)<sub>2</sub> (8).** The complex was synthesized using the same method reported for the synthesis of the chloride analogue, ( $\eta^6$ -*p*-cymene)Ru(CO)(Cl)<sub>2</sub>.<sup>53</sup> [( $\eta^6$ -*p*-cymene)Ru( $\mu$ -Br)(Br)]<sub>2</sub> (0.2301 g, 0.2912 mmol) was suspended in hexanes (~30 mL) in a Fisher Porter. The reaction vessel was pressurized with CO (150 psig) and heated at 50 °C for 2 h in a temperature controlled oil bath while stirring. The reaction mixture remained heterogeneous. The Fisher Porter was removed from the oil bath, cooled to room temperature and degassed. Inside the glovebox, the solvent was removed in vacuo. The pinkish-red solid was dissolved in DCM and precipitated with hexanes. The pink-red shiny solid was collected over a fine porosity frit, washed with hexanes (2 x 5 mL) and dried under vacuum (0.2328 g, 94%). <sup>1</sup>H NMR (800 MHz, CDCl<sub>3</sub>) δ 5.92 (d, <sup>3</sup>J<sub>HH</sub> = 7 Hz, 2H, Cy-C<sub>Ar</sub>), 5.77 (d, <sup>3</sup>J<sub>HH</sub> = 6 Hz, 2H, Cy-C<sub>Ar</sub>), 2.95 (p, <sup>3</sup>J<sub>HH</sub> = 8 Hz, 1H, Cy-CH(CH)<sub>3</sub>), 2.51 (s, 2H, Cy-CH<sub>3</sub>), 1.37 – 1.31 (d, <sup>3</sup>J<sub>HH</sub> = 8 Hz, 6H, Cy-CH(CH<sub>3</sub>)<sub>2</sub>). <sup>13</sup>C NMR (201 MHz, CDCl<sub>3</sub>) δ 189.3 (s, C≡O), 114.70, 114.5, 93.7, 92.7 (each a s, Cy-C<sub>Ar</sub>) 31.9 (s, Cy-CH<sub>3</sub>), 29.9 (s, Cy-CH(CH<sub>3</sub>)<sub>2</sub>) 22.8 (s, Cy-CH(CH<sub>3</sub>)<sub>2</sub>). IR (KBr): ν<sub>CO</sub> = 1994 cm<sup>-1</sup>. Anal. Calcd for C<sub>11</sub>H<sub>14</sub>Br<sub>2</sub>ORu: C, 31.23 ; H, 3.34. Found: C, 31.19; H, 3.28.

**( $\eta^6$ -*p*-cymene)Ru( $\mu$ -Br)<sub>3</sub>Ru(CO)<sub>2</sub>Ph (9).** ( $\eta^6$ -*p*-cymene)Ru(CO)Br<sub>2</sub> (8)

(0.2303 g, 0.5443 mmol) was suspended in THF (~15 mL). Ph<sub>2</sub>Mg[THF]<sub>2</sub> (0.1395 g, 0.4322 mmol) was dissolved in THF (~15 mL). The Ph<sub>2</sub>Mg was added dropwise to the round bottom flask containing the Ru species. The reaction was stirred at room temperature for 1 h and reaction changed from pink to black. The THF was removed in vacuo. Benzene (~30 mL) was added to the flask containing the residue. The benzene mixture was stirred for 15 min then filtered through Celite. The filtrate was passed through ½ inch of silica. The silica was washed with THF. All solvent was removed and ~5 mL of CH<sub>2</sub>Cl<sub>2</sub> was added followed by hexanes to induce a precipitate. The precipitate was collected on a fine porosity frit and dried in vacuo. The solid was redissolved in DCM and passed through ½ inch of silica. The silica was washed with DCM. The filtrate was reduced to ~1 mL in vacuo. Hexanes was added to precipitate a yellow-orange solid. The solid was collected on a fine porosity frit and dried in vacuo (0.0052 g, 3% yield). X-ray quality crystals were grown by slow evaporation from CHCl<sub>3</sub>. <sup>1</sup>H NMR (300 MHz, CDCl<sub>3</sub>)  $\delta$  7.36 (d, <sup>3</sup>J<sub>HH</sub> = 8 Hz, 2H, *ortho*-C<sub>6</sub>H<sub>6</sub>), 6.99 (t, <sup>3</sup>J<sub>HH</sub> = 7 Hz, 2H, *meta*-C<sub>6</sub>H<sub>6</sub>), 6.91 (d, <sup>3</sup>J<sub>HH</sub> = 8 Hz, 2H, *para*-C<sub>6</sub>H<sub>6</sub>), 5.62 (d, <sup>3</sup>J<sub>HH</sub> = 6 Hz, 2H, *p*-cymene Ar), 5.41 (d, <sup>3</sup>J<sub>HH</sub> = 6 Hz, 2H, *p*-cymene Ar), 3.02 (sept, <sup>2</sup>J<sub>HH</sub> = 7 Hz, 1H, (CH<sub>3</sub>C<sub>6</sub>H<sub>4</sub>(CH)(CH<sub>3</sub>)<sub>2</sub>) 2.36 (s, 3H, C<sub>6</sub>H<sub>4</sub>-CH<sub>3</sub>), 1.38 (d, <sup>3</sup>J<sub>HH</sub> = 7 Hz, 6H, CH<sub>3</sub>C<sub>6</sub>H<sub>4</sub>(CH)(CH<sub>3</sub>)<sub>2</sub>). IR (KBr):  $\nu_{\text{CO}}$  = 2048 cm<sup>-1</sup> and 1979 cm<sup>-1</sup>.

**(HC(pz<sup>5</sup>)<sub>3</sub>)Ru(CO)Br<sub>2</sub> (10).** ( $\eta^6$ -*p*-cymene)Ru(CO)Br<sub>2</sub> (8) (0.0522 g, 0.123 mmol) and HC(pz<sup>5</sup>)<sub>3</sub> (0.0317 g, 0.124 mmol) were combined in THF (~ 20 mL) in a pressure tube. The solution was heated in a temperature control oil bath at 70 °C for 6.5

h. A beige solid precipitated from solution during heating. The solid was collected over a fine porosity frit. The solid was washed with pentane and dried under vacuum (0.0610 g, 91%).  $^1\text{H}$  NMR (300 MHz,  $\text{CD}_3\text{CN}$ )  $\delta$  8.30 (d,  $^4J = 2$  Hz, 1H,  $\text{HC}(\text{pz}^5)_3$ ), 7.99 (s, 2H,  $\text{HC}(\text{pz}^5)_3$  3-position), 7.80 (d,  $^3J_{\text{HH}} = 2$  Hz, 2H,  $\text{HC}(\text{pz}^5)_3$  3-position), 6.42 (m, 1H,  $\text{HC}(\text{pz}^5)_3$  4-position), 6.26 (m, 2H,  $\text{HC}(\text{pz}^5)_3$  4-position), 2.66 (s, 3H,  $\text{HC}(\text{pz}^5)_3$  5-methyl), 2.60 (s, 6H,  $\text{HC}(\text{pz}^5)_3$  5-methyl).  $^{13}\text{C}$  NMR (201 MHz,  $\text{CD}_3\text{CN}$ )  $\delta$  147.9, 145.7, 143.9, 108.1, 107.8 (each a s,  $\text{HC}(\text{pz}^5)_3$ , one missing presumably due to coincidental overlap), 69.0, (s,  $\text{HC}(\text{pz}^5)_3$ ), 10.5, 10.2 (each a s,  $\text{HC}(\text{pz}^5)_3$  5-methyl).  $\text{C}\equiv\text{O}$  was not observed due to the extremely poor solubility of the complex. IR (KBr):  $\nu_{\text{CO}} = 1958$   $\text{cm}^{-1}$ . obsd (%), calcd (%), ppm: 564.8694 (28), 564.8688 (24), 1.0; 565.8723 (36), 565.8692 (45), 5.4; 566.8666 (69), 566.8682 (65), -2.9; 567.8668 (45), 567.8681 (56), -2.4; 568.8660 (100), 568.8674 (100), -2.5; 569.8721 (16), 569.8679 (33), 7.3; 570.8642 (60), 570.8666 (70), -4.3.

**$[(\text{HC}(\text{pz}^5)_3)\text{Ru}(\text{CO})\text{Br}_2][\text{TiOTf}]_2$  (11).**  $(\text{HC}(\text{pz}^5)_3)\text{Ru}(\text{CO})\text{Br}_2$  (0.0334 g, 0.0613 mmol) was suspended in  $\text{CH}_3\text{CN}$  (~3 mL).  $\text{TiOTf}$  (0.0434 g, 0.123 mmol) in  $\text{CH}_3\text{CN}$  (~2 mL) was added dropwise. The homogeneous yellow solution was stirred at room temperature for 1 h. The resulting light-brown solution was filtered through celite. The filtrate was reduced to dryness in vacuo (0.0786 g, 102% yield, contains excess  $\text{TiOTf}$ ).  $^1\text{H}$  NMR (600 MHz,  $\text{CD}_3\text{CN}$ )  $\delta$  8.52 (d,  $^4J_{\text{HH}} = 2$  Hz, 1H,  $\text{HC}(\text{pz}^5)_3$ ), 8.01 (s, 2H,  $\text{HC}(\text{pz}^5)_3$  3-position), 7.72 (d,  $^3J_{\text{HH}} = 2$  Hz, 1H,  $\text{HC}(\text{pz}^5)_3$  3-position), 6.52 (m, 1H,  $\text{HC}(\text{pz}^5)_3$  4-position), 6.28 (m, 2H,  $\text{HC}(\text{pz}^5)_3$  4-position), 2.69 (s, 3H,  $\text{HC}(\text{pz}^5)_3$  5-methyl), 2.61 (s, 6H,  $\text{HC}(\text{pz}^5)_3$  5-methyl).  $^{13}\text{C}$  NMR (151 MHz,  $\text{CD}_3\text{CN}$ )  $\delta$  218.4 ( $\text{C}\equiv\text{O}$ ), 148.9,

147.0, 145.8, 144.60, 109.6, 109.3 (each a s, HC(pz<sup>5</sup>)<sub>3</sub>), 70.1 (s, HC(pz<sup>5</sup>)<sub>3</sub>), 11.7, 11.5 (each a s, HC(pz<sup>5</sup>)<sub>3</sub> 5-methyl). <sup>19</sup>F NMR (282 MHz, CD<sub>3</sub>CN) δ -79.8 (s, OTf). IR (KBr): ν<sub>CO</sub> = 1991 cm<sup>-1</sup>.

**[(HC(pz<sup>5</sup>)<sub>3</sub>)Ru(CO)(Ph)<sub>2</sub>]Br (12).** [(HC(pz<sup>5</sup>)<sub>3</sub>)Ru(CO)Br<sub>2</sub>] TlOTf adduct (0.0145 g, 0.0116 mmol) was dissolved in CH<sub>3</sub>CN. The solution was cooled to -34 °C. PhMgBr (22 μL, 0.022 mmol, 1 M in THF) was slowly added. The solution was allowed to warm to room temperature before filtering through Celite. The Celite was washed with CH<sub>3</sub>CN and the filtrate was reduced to dryness under vacuum to give a brown solid (0.0155g). A <sup>19</sup>F NMR spectrum of the isolated material indicates residual TlOTf is still present. This likely explains why the yield is greater than 200%. Purification of the solid has not been successful. The reported <sup>1</sup>H NMR data is for the crude product. <sup>1</sup>H NMR (300 MHz, CD<sub>3</sub>CN) δ 8.30 (d, <sup>4</sup>J<sub>HH</sub> = 2 Hz, 1H, HC(pz<sup>5</sup>)<sub>3</sub>), 7.99 (s, 2H, HC(pz<sup>5</sup>)<sub>3</sub> 3-position), 7.80 (d, <sup>3</sup>J<sub>HH</sub> = 2 Hz, 1H, HC(pz<sup>5</sup>)<sub>3</sub> 3-position), 7.66 (d, <sup>4</sup>J<sub>HH</sub> = 8 Hz, 4H, *ortho*-phenyl), 7.18 (m, 6H, *meta* and *para*-phenyl overlapping), (dd, <sup>3</sup>J<sub>HH</sub> = 2 Hz, <sup>3</sup>J<sub>HH</sub> = 1 Hz, 2H, HC(pz<sup>5</sup>)<sub>3</sub> 4-position), 6.26 (dd, <sup>3</sup>J<sub>HH</sub> = 2 Hz, <sup>3</sup>J<sub>HH</sub> = 1 Hz, 1H, HC(pz<sup>5</sup>)<sub>3</sub> 4-position), 2.66 (s, 3H, HC(pz<sup>5</sup>)<sub>3</sub> 5-methyl), 2.60 (s, 6H, HC(pz<sup>5</sup>)<sub>3</sub> 5-methyl). IR (KBr) ν<sub>CO</sub> = 1959 cm<sup>-1</sup>.

**Rate of Stoichiometric C<sub>6</sub>D<sub>6</sub> Activation by [(HC(pz<sup>5</sup>)<sub>3</sub>)Ru(P(OCH<sub>2</sub>)<sub>3</sub>CEt)(NCMe)Ph][BAR'<sub>4</sub>] (6).**

[(HC(pz<sup>5</sup>)<sub>3</sub>)Ru(P(OCH<sub>2</sub>)<sub>3</sub>CEt)(NCMe)Ph][BAR'<sub>4</sub>] (6) (0.014 g, 0.0095 mmol), C<sub>6</sub>D<sub>6</sub> (26 μL, 0.29 mmol) and hexamethyldisilane (HMDS) (1 μL, 0.005 mmol, as an internal standard) were combined in 1 mL of THF-*d*<sub>8</sub>. To three separate screw-cap NMR tubes 300 μL of this solution were added. The tubes were heated to 60 °C in a temperature-

controlled oil bath.  $^1\text{H}$  NMR spectra using a 12.8 s pulse delay time were periodically acquired. Relative to the internal standard, HMDS, the rate of the reaction was monitored by integration of the ortho phenyl resonance (6.96 ppm). Changes were observed in the  $\text{P}(\text{OCH}_2)_3\text{CEt}$  resonances over time.

**Degenerate**  $\text{NCCH}_3/\text{NCCD}_3$  **Exchange** **for**  
 $[(\text{HC}(\text{pz}^5)_3)\text{Ru}(\text{P}(\text{OCH}_2)_3\text{CEt})(\text{NCMe})\text{Ph}][\text{BAr}'_4]$  (**6**). In a 1 mL volumetric flask  $[(\text{HC}(\text{pz}^5)_3)\text{Ru}(\text{P}(\text{OCH}_2)_3\text{CEt})(\text{NCMe})\text{Ph}][\text{BAr}'_4]$  (**6**) (0.016 g, 0.011 mmol) was dissolved in  $\text{CD}_3\text{CN}$ . Hexamethyldisilane (HMDS) (1  $\mu\text{L}$ , 0.005 mmol) was added as an internal standard. The solution was divided between three J. Young NMR tubes (300  $\mu\text{L}$ /tube). The tubes were placed into a temperature calibrated Varian 500 MHz spectrometer probe (equilibrated at 88  $^\circ\text{C}$ ). The temperature was determined using 80% ethylene glycol in  $\text{DMSO-}d_6$  and the following equation provided by Bruker Instruments, Inc. VT-Calibration Manual:  $T(\text{K}) = (4.218 - \Delta)/0.009132$ , where  $\Delta$  is the shift difference (ppm) between  $\text{CH}_2$  and  $\text{OH}$  resonance of ethylene glycol. The reaction was monitored by  $^1\text{H}$  NMR spectroscopy using automated data acquisition. Eight scans were acquired for each spectrum. The delay time was set to 12.8 s, and the acquisition time was set to 2.2 s. Each spectrum required 2 min to complete and the acquisition of a new data point began every 30 min. The exchange reaction was repeated at 70  $^\circ\text{C}$ , 80  $^\circ\text{C}$  and 95  $^\circ\text{C}$  only the tubes were heated in a temperature-controlled oil bath.  $^1\text{H}$  NMR spectra using a 12.8 s pulse delay time were periodically acquired. All reactions were monitored through at least three half-lives.

**Dependence of Degenerate  $\text{NCCH}_3/\text{NCCD}_3$  Exchange for**

**$[(\text{HC}(\text{pz}^5)_3)\text{Ru}(\text{P}(\text{OCH}_2)_3\text{CEt})(\text{NCMe})\text{Ph}][\text{BAr}'_4]$  (6) on  $\text{NCCD}_3$  Concentration.** In a 1 mL volumetric flask  $[(\text{HC}(\text{pz}^5)_3)\text{Ru}(\text{P}(\text{OCH}_2)_3\text{CEt})(\text{NCMe})\text{Ph}][\text{BAr}'_4]$  (6) (0.016 g, 0.011 mmol) was dissolved in  $\text{THF-}d_8$ . 10 equivalents (0.3 mmol, 0.1 M), 20 equivalents (0.2 mmol, 0.2 M) or 30 equivalents (0.3 mmol, 0.3 M) of  $\text{NCCD}_3$  was added. Hexamethyldisilane (HMDS) (1  $\mu\text{L}$ , 0.005 mmol) was added as an internal standard. The solution was divided between three J. Young NMR tubes (300  $\mu\text{L}$ /tube). The tubes were heated to 95  $^\circ\text{C}$  in a temperature-controlled oil bath.  $^1\text{H}$  NMR spectra using a 12.8 s pulse delay time were periodically acquired. All reactions were monitored through at least three half-lives.

**Representative**

**Catalytic**

**Reaction.**

$[(\text{HC}(\text{pz}^5)_3)\text{Ru}(\text{P}(\text{OCH}_2)_3\text{CEt})(\text{NCMe})\text{Ph}][\text{BAr}'_4]$  (6) (0.017 g, 0.011 mmol) was dissolved in  $\text{C}_6\text{H}_6$  (10 mL) (with decane added as an internal standard). The solution was stirred for 5 min to ensure homogeneity before transferring 3 mL each to three stainless steel pressure reactors. The reactors were charged with 15 psi of  $\text{C}_2\text{H}_4$  followed by  $\text{N}_2$  to give a total pressure of 120 psig. The reactors were placed in a temperature-regulated aluminum block set to 105  $^\circ\text{C}$ . After 4, 16, 36, 60, and 84 h the reactors were degassed, sampled under  $\text{N}_2$  and then re-pressurized before returning to the aluminum block. The reaction mixture was analyzed by GC-MS using peak areas of the products and the internal standard to calculate product yields. Ethylbenzene production was quantified using linear regression analysis of gas chromatograms of standard samples. A set of ten known standards consisting of 1:5, 3:5, 5:5, 7.5:5, 10:5, 50:5, 100:5, 150:5, 300:5, 600:5

molar ratios of ethylbenzene to decane in methylene chloride were prepared. A plot of peak area ratios versus molar ratios gave a regression line.

**Monitoring Ethylene Hydrophenylation using  $C_6D_6$  by  $^1H$  NMR Spectroscopy.**  $[(HC(pz^5)_3)Ru(P(OCH_2)_3CEt)(NCMe)Ph][BAR'_4]$  (**6**) (0.010 g, 0.0067 mmol) was dissolved in THF- $d_8$  (300  $\mu$ L) in a J. Young NMR tube.  $C_6D_6$  (59  $\mu$ L 0.67 mmol) was added to the tube using a microsyringe. The tube was pressurized with 25 psig of  $C_2H_4$  and placed in a temperature regulated oil bath set to 90 °C. The reaction was monitored periodically by  $^1H$  and  $^{31}P$  NMR spectroscopy. Resonances for  $C_6D_5CH_2CH_2D$  were observed by  $^1H$  NMR spectroscopy. A multiplet at 1.19 ppm is observed for the mono-deuterated methyl and a multiplet at 2.60 ppm is observed for the benzylic methylene resonances of  $C_6D_5CH_2CH_2D$ . Unfortunately, the resonance at 2.60 ppm overlaps with the 5-position methyl resonances of coordinated  $HC(pz^5)_3$ , which prevents a detailed analysis of splitting. GC-MS analysis shows two major peaks with  $m/z$  of 96 and 112, which is consistent with production of  $C_6D_5CH_2CH_2D$ . The ethyl fragment is consistent with predominant  $-CH_2CH_2D$ .

**Determination of Kinetic Isotope Effect. Method 1.**  $[(HC(pz^5)_3)Ru(P(OCH_2)_3CEt)(NCMe)Ph][BAR'_4]$  (**6**) (0.017 g, 0.011 mmol) was dissolved in 7 mL of  $C_6D_6$  (with decane added as an internal standard). The solution was stirred for 5 min to ensure homogeneity before transferring 2 mL each to three stainless steel pressure reactors. The reactors were charged with 15 psi of  $C_2H_4$  followed by  $N_2$  to give a total pressure of 120 psig. The reactors were placed in a temperature-regulated aluminum block set to 90 °C. After 4 h the reactors were degassed and sampled under  $N_2$ .

The reaction mixture was analyzed by GC-MS using peak areas of the products and the internal standard to calculate product yields. GC-MS data indicate the major product is  $C_6D_5CH_2CH_2D$ . The MS spectrum for ethyl benzene contains parent peaks at  $m/z$  91 and 106. The major peak for the ethyl fragment is observed at 29  $m/z$ . For the catalytic reaction using  $C_6D_6$ , parent peaks in the mass spectrum are observed at 106 and 112  $m/z$ , which is consistent with the formation of  $C_6D_5CH_2CH_2D$ . In addition, enrichment of  $m/z$  of 30 is observed for ethyl chain supporting formation of  $CH_2CH_2D$ . The  $k_H/k_D$  was determined by dividing the ratio average (data collected in triplicate) peak areas for ethylbenzene to internal standard for a catalytic reaction under identical conditions (0.01 mol% complex **6**, 90 °C, 4 h) in  $C_6H_6$  by the ratio of peak areas of the average  $C_6D_5CH_2CH_2D$  integrations to internal standard for the three runs using  $C_6D_6$ . **Method 2.**  $[(HC(pz^5)_3)Ru(P(OCH_2)_3CEt)(NCMe)Ph][BAR'_4]$  (**6**) (0.012 g, 0.0079 mmol) was dissolved in 3.5 mL of  $C_6D_6$  and 3.5 mL of  $C_6H_6$  (with decane added as an internal standard). The solution was stirred for 5 min to ensure homogeneity before transferring 2 mL each to three stainless steel pressure reactors. The reactors were charged with 15 psi of  $C_2H_4$  followed by  $N_2$  to give a total pressure of 120 psig. The reactors were placed in a temperature-regulated aluminum block set to 90 °C. After 4 h the reactors were degassed and sampled under  $N_2$ . The reaction mixture was analyzed by GC-MS. A KIE was determined by dividing the intensities for  $M_w = 111$  by the intensities for  $M_w = 112$ .

## 6.6 References

1. Gerzeliev, I. M.; Khadzhiev, S. N.; Sakharova, I. E. *Petroleum Chemistry* **2011**, *51*, 39.

2. Perego, C.; Ingallina, P. *Green Chem.* **2004**, *6*, 274.
3. Macquarrie, D. J., Industrial Friedel–Crafts Chemistry. In *Catalytic Asymmetric Friedel-Crafts Alkylations*, Bandini, M.; Umani-Ronchi, A., Eds. Wiley-VCH: Weinheim, Germany, 2009.
4. G. A. Olah, A. M. *Hydrocarbon Chemistry*. 2nd ed.; Wiley-Intersciences: New York, 2003.
5. C. Perego, P. P., Advances in Aromatics Processing Using Zeolite Catalysts. In *Advances in Nanoporous Materials*, Elsevier B. V. : Great Britain, 2009; Vol. 1, pp 97.
6. Goldberg, K. I.; Goldman, A. S., *Activation and Functionalization of C-H Bonds*. American Chemical Society: Washington, DC, 2004; Vol. 885.
7. Kuhl, N.; Hopkinson, M. N.; Wencel-Delord, J.; Glorius, F. *Angew. Chem. Int. Ed.* **2012**, *51*, 10236.
8. Colby, D. A.; Bergman, R. G.; Ellman, J. A. *Chem. Rev.* **2010**, *110*, 624.
9. Cheng, C.; Kim, B. G.; Guironnet, D.; Brookhart, M.; Guan, C.; Wang, D. Y.; Krogh-Jespersen, K.; Goldman, A. S. *J. Am. Chem. Soc.* **2014**, *136*, 6672.
10. Neufeldt, S. R.; Sanford, M. S. *Acc. Chem. Res.* **2012**, *45*, 936.
11. Dobereiner, G. E.; Yuan, J.; Schrock, R. R.; Goldman, A. S.; Hackenberg, J. D. *J. Am. Chem. Soc.* **2013**, *135*, 12572.
12. Bowring, M. A.; Bergman, R. G.; Tilley, T. D. *J. Am. Chem. Soc.* **2013**, *135*, 13121.
13. Lian, Y. J.; Bergman, R. G.; Lavis, L. D.; Ellman, J. A. *J. Am. Chem. Soc.* **2013**, *135*, 7122.

14. Howell, J. M.; Liu, W.; Young, A. J.; White, M. C. *J. Am. Chem. Soc.* **2014**, *136*, 5750.
15. Chan, K. S. L.; Wasa, M.; Chu, L.; Laforteza, B. N.; Miura, M.; Yu, J. Q. *Nat Chem* **2014**, *6*, 146.
16. Cheng, G.-J. Y., Yun-Fang; Liu, Peng; Chen, Ping; Sun, Tian-Yu; Li, Gang; Zhang, Xinhao; Houk, K. N.; Yu, Jin-Quan; Wu, Yun-Dong *J. Am. Chem. Soc.* **2014**, *136*, 894.
17. Foley, N. A.; Lee, J. P.; Ke, Z. F.; Gunnoe, T. B.; Cundari, T. R. *Acc. Chem. Res.* **2009**, *42*, 585.
18. Andreatta, J. R.; McKeown, B. A.; Gunnoe, T. B. *J. Organomet. Chem.* **2011**, *696*, 305.
19. Lewis, J. C.; Bergman, R. G.; Ellman, J. A. *Acc. Chem. Res.* **2008**, *41*, 1013.
20. Ritleng, V.; Sirlin, C.; Pfeffer, M. *Chem. Rev.* **2002**, *102*, 1731.
21. Goj, L. A.; Gunnoe, T. B. *Curr. Org. Chem.* **2005**, *9*, 671.
22. McKeown, B. A.; Foley, N. A.; Lee, J. P.; Gunnoe, T. B. *Organometallics* **2008**, *27*, 4031.
23. McKeown, B. A.; Gonzalez, H. E.; Friedfeld, M. R.; Gunnoe, T. B.; Cundari, T. R.; Sabat, M. *J. Am. Chem. Soc.* **2011**, *133*, 19131.
24. McKeown, B. A.; Gonzalez, H. E.; Friedfeld, M. R.; Brosnahan, A. M.; Gunnoe, T. B.; Cundari, T. R.; Sabat, M. *Organometallics* **2013**, *32*, 2857.
25. McKeown, B. A.; Gonzalez, H. E.; Gunnoe, T. B.; Cundari, T. R.; Sabat, M. *ACS Catal.* **2013**, *3*, 1165.

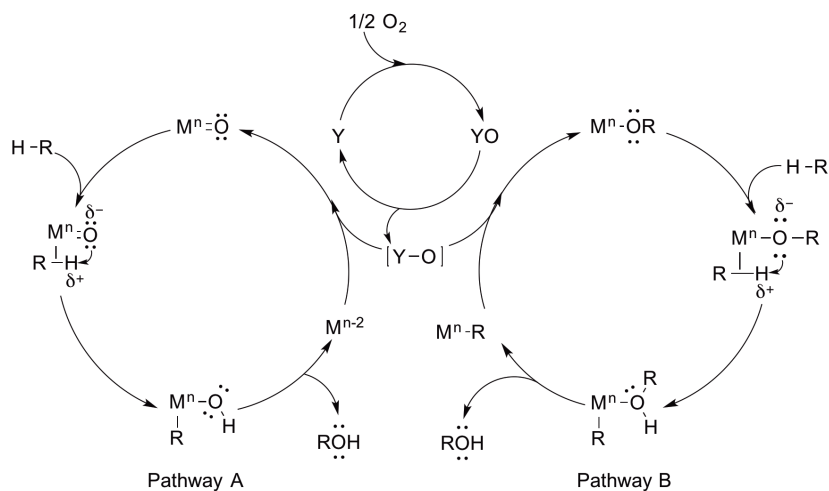
26. McKeown, B. A.; Gonzalez, H. E.; Michaelos, T.; Gunnoe, T. B.; Cundari, T. R.; Crabtree, R. H.; Sabat, M. *Organometallics* **2013**, *32*, 3903.
27. Karshtedt, D.; Bell, A. T.; Tilley, T. D. *Organometallics* **2004**, *23*, 4169.
28. Karshtedt, D.; McBee, J. L.; Bell, A. T.; Tilley, T. D. *Organometallics* **2006**, *25*, 1801.
29. Cucciolito, M. E.; D'Amora, A.; Tuzi, A.; Vitagliano, A. *Organometallics* **2007**, *26*, 5216.
30. Bowring, M. A.; Bergman, R. G.; Tilley, T. D. *Organometallics* **2011**, *30*, 1295.
31. Oxgaard, J.; Goddard, W. A. *J. Am. Chem. Soc.* **2004**, *126*, 442.
32. Oxgaard, J.; Periana, R. A.; Goddard, W. A. *J. Am. Chem. Soc.* **2004**, *126*, 11658.
33. Luedtke, A. T.; Goldberg, K. I. *Angew. Chem. Int. Ed.* **2008**, *47*, 7694.
34. Jones, W. D.; Maguire, J. A.; Rosini, G. P. *Inorg. Chim. Acta* **1998**, *270*, 77.
35. Periana, R. A.; Liu, X. Y.; Bhalla, G. *Chem. Commun.* **2002**, *24*, 3000.
36. Lail, M.; Bell, C. M.; Conner, D.; Cundari, T. R.; Gunnoe, T. B.; Petersen, J. L. *Organometallics* **2004**, *23*, 5007.
37. Oxgaard, J.; Muller, R. P.; Goddard III, W. A.; Periana, R. A. *J. Am. Chem. Soc.* **2004**, *126*, 352.
38. Foley, N. A.; Lail, M.; Lee, J. P.; Gunnoe, T. B.; Cundari, T. R.; Petersen, J. L. *J. Am. Chem. Soc.* **2007**, *129*, 6765.
39. Joslin, E. E.; McMullin, C. L.; Gunnoe, T. B.; Cundari, T. R.; Sabat, M.; Myers, W. H. *Organometallics* **2012**, *31*, 6851.
40. Lail, M.; Arrowood, B. N.; Gunnoe, T. B. *J. Am. Chem. Soc.* **2003**, *125*, 7506.

41. Foley, N. A.; Ke, Z. F.; Gunnoe, T. B.; Cundari, T. R.; Petersen, J. L. *Organometallics* **2008**, *27*, 3007.
42. Foley, N. A.; Lail, M.; Gunnoe, T. B.; Cundari, T. R.; Boyle, P. D.; Petersen, J. L. *Organometallics* **2007**, *26*, 5507.
43. Dias, H. V. R.; Lovely, C. J. *Chem. Rev.* **2008**, *108*, 3223.
44. Joslin, E. E.; Quillian, B.; Gunnoe, T. B.; Cundari, T. R.; Sabat, M.; Myers, W. H. *Inorg. Chem.* **2014**, *53*, 6270.
45. Joslin, E. E. *Unpublished Results, PhD Thesis* **2013**.
46. Matsumoto, T.; Taube, D. J.; Periana, R. A.; Taube, H.; Yoshida, H. *J. Am. Chem. Soc.* **2000**, *122*, 7414.
47. Matsumoto, T.; Periana, R. A.; Taube, D. J.; Yoshida, H. *J. Mol. Catal. A.: Chem.* **2002**, *180*, 1.
48. Mendoza-Ferri, M. G.; Hartinger, C. G.; Nazarov, A. A.; Eichinger, R. E.; Jakupec, M. A.; Severin, K.; Keppler, B. K. *Organometallics* **2009**, *28*, 6260.
49. Yakelis, N. A.; Bergman, R. G. *Organometallics* **2005**, *24*, 3579.
50. Lühder, K.; Nehls, D.; Madeja, K. *J. Prakt. Chem.* **1983**, *325*, 1027.
51. Goodman, M. A.; Nazarenko, A. Y.; Casavant, B. J.; Li, Z. J.; Brennessel, W. W.; DeMarco, M. J.; Long, G.; Goodman, M. S. *Inorg. Chem.* **2012**, *51*, 1084.
52. Joslin, E. E.; McMullin, C. L.; Gunnoe, T. B.; Cundari, T. R.; Sabat, M.; Myers, W. H. *Inorg. Chem.* **2012**, *51*, 4791.
53. Hodson, E.; Simpson, S. J. *Polyhedron* **2004**, *23*, 2695.

## 7 Summary and Future Outlook

### 7.1 Activation of Nonpolar Bonds by 1,2-Addition across Rh–X (X = OR, NHR) Bonds

Hydrocarbon functionalization is generally broken down into two key steps: C–H bond cleavage followed by C–X (X = OR, NHR, halide, etc.) bond formation. We have proposed a catalytic cycle for the functionalization of hydrocarbons that involves C–H activation via 1,2-CH-addition across a metal–oxo or metal–imido bond followed by C–O (or C–N) reductive elimination to release the functionalized product (Scheme 7.1, Pathway A, metal–oxo is shown). Oxidation of the metal center leads to the regeneration of the starting metal–oxo or imido complex. Alternatively, as shown in Pathway B of Scheme 7.1, 1,2-CH-addition across a M–OR or M–NHR bond would lead to the formation of an alcohol or amine, respectively. Net oxygen atom or nitrene insertion into the newly formed metal–hydrocarbyl bond regenerates the starting metal alkoxide or amido complex.



**Scheme 7.1.** Proposed catalytic cycles for hydrocarbon functionalization incorporating 1,2-CH-addition across M=O or M–OR bonds.

The 1,2-CH-addition of both arene and alkane C–H bonds has been reported for early transition metal imido complexes with  $d^0$  electron configurations.<sup>1</sup> But, for electropositive early transition metals, activation barriers for C–N reductive elimination to release functionalized product are likely to be prohibitively large. The 1,2-addition of arene C–H bonds across late (*i.e.*, group 6 or later) transition metal–X (X = OH, OR, NHR) bonds has also been reported; however, due to the limited number of examples, little is known about these transformations.<sup>1,2</sup>

### 7.1.1 Rh(III) Heteroatom Complexes Supported by Bipyridyl and Pyridine-Diimine Ligands for 1,2-Addition of C–H, H–H and Si–H Bonds

As discussed in Chapters 2, 3, 4 and 5, the development of Rh alkoxide and amido complexes for the 1,2-addition of non-polar bonds (*e.g.*, H–H, C–H, Si–H) across Rh–X bonds was investigated. Octahedral Rh(III) aniline, anilido, hydroxide, aqua, methoxide and methanol complexes supported by 2,2'-bipyridyl (bpy) or 4,4'-di-*tert*-butyl-2,2'-bipyridyl (<sup>t</sup>bpy) ligands have been synthesized and characterized. The ability of such complexes to activate C–H bonds was examined under a range of conditions without success. In contrast, the activation of dihydrogen was achieved using the complexes  $[(^t\text{bpy})_2\text{Rh}(\text{OMe})(\text{MeOH})][\text{OTf}][\text{TFA}]$  and  $[(^t\text{bpy})_2\text{Rh}(\text{OMe})(\text{TFA})][\text{OTf}]$  (OTf = trifluoromethanesulfonate, TFA = trifluoroacetate). Experimental and computational data are consistent with a mechanism involving the dissociation of methanol to generate a coordination site for  $\eta^2\text{-H}_2$  coordination. The 1,2-addition of dihydrogen across the Rh(III)–OMe bond results in the formation of unobserved  $[(^t\text{bpy})_2\text{Rh}(\text{H})(\text{MeOH})][\text{OTf}][\text{TFA}]$ . Dissociation of MeOH and coordination of the TFA

counterion leads to the formation of  $[(^t\text{bpy})_2\text{Rh}(\text{H})(\text{TFA})][\text{OTf}]$ . Studies indicate that the activation of dihydrogen has a first-order dependence on the Rh(III) methoxide complex and a dependence on hydrogen that is between zero- and first-order. Slight rate acceleration is observed upon addition of free MeOH. Density functional theory calculations are consistent with a decreased  $\Delta H^\ddagger$  through participation of MeOH in the transition state.

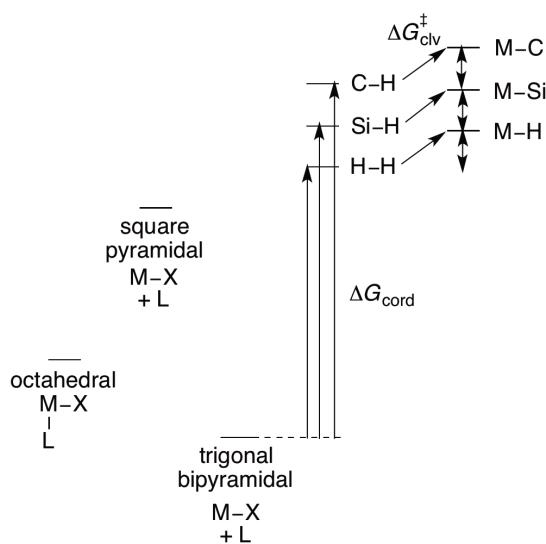
The activation of the Si–H bond of  $\text{Et}_3\text{SiH}$  by  $[(^t\text{bpy})_2\text{Rh}(\text{OMe})(\text{MeOH})][\text{TFA}]_2$  and  $[(^t\text{bpy})_2\text{Rh}(\text{OMe})(\text{TFA})][\text{TFA}]$  to produce  $\text{Et}_3\text{SiOMe}$  and  $[(^t\text{bpy})_2\text{Rh}(\text{H})(\text{TFA})][\text{TFA}]$  has been observed. The details of this transformation are still under investigation. Future work will be focused on the identification of all hydride products in addition to kinetic studies.

In Chapter 5 the synthesis of Rh(I) and Rh(III) amido complexes bearing terdentate aryl-substituted pyridine-diimine (NNN) ligands was discussed. Unfortunately, the (NNN)Rh complexes proved to be unstable. Attempts to activate  $\text{H}_2$  with the Rh(I) amido complex  $(^{\text{Mes}}\text{NNN})\text{Rh}(\text{NEt}_2)$  ( $^{\text{Mes}}\text{NNN}$  = 2,6-diacetylpyridinebis(2,4,6-trimethylanilize)) resulted in decomposition to multiple intractable products.

### 7.1.2 Future Synthetic Targets

The primary focus of the research described in Chapters 2 through 5 was the synthesis of Rh(III) heteroatom complexes for the activation of covalent bonds. Successful activation of H–H and Si–H bonds has been achieved, but activation of C–H bonds was not observed. Perhaps the lack of C–H activation stems from weak coordination of C–H bonds.<sup>3</sup> The strong C–H bond and weak  $\sigma$ -donor ability of methane cause methane to be a poor ligand.<sup>4,5</sup> Thus it is expected that a substantial portion of the

overall activation barrier for C–H activation is the coordination of the C–H bond (Scheme 7.2). Starting from an 18-electron octahedral complex, loss of a ligand gives a five-coordinate intermediate. The five-coordinate intermediate may be undergoing a geometry change from square pyramidal to trigonal bipyramidal. If accessed, the trigonal bipyramidal geometry could be stabilized by Rh–OMe  $\pi$ -donation. From the trigonal bipyramidal intermediate  $\Delta G_{\text{act}}^{\ddagger} = \Delta G_{\text{coord}} + \Delta G_{\text{clv}}^{\ddagger}$ . We propose that  $\Delta G_{\text{coord}}$  for C–H bond is larger than the  $\Delta G_{\text{coord}}$  for H–H and Si–H bonds. We believe that once coordinated, the  $\Delta G_{\text{clv}}^{\ddagger}$  for H–H versus Si–H versus C–H will be similar in magnitude. Consequently, we believe C–H activation was not observed because C–H bond coordination was not accessible. Coordination of methane to a transition metal would involve reorientation of a  $sp^3$  hybrid orbital whereas no reorientation would be required for dihydrogen which bonds to a metal using a sigma orbital.<sup>3</sup>



**Scheme 7.2.** Energy level diagram to showing the predicted differences in  $\Delta G_{\text{coord}}$  for C–H, Si–H and H–H bonds.

Perhaps the methoxide ligand was insufficiently basic to activate C–H bonds. The heteroatom ligand needs to be electron rich and sizable polarization of the M–X is critical. Taking these explanations into consideration, future synthetic targets can be proposed. Rh–amido and anilido complexes will be targeted instead of methoxide because these nitrogen based heteroatom ligands will be more basic than methoxide.  $[(^t\text{bpy})_2\text{Rh}(\text{NH}_2)(\text{OTf})][\text{OTf}]$  could serve as a potential target molecule. However, modification of the ancillary ligands could also help achieve C–H activation. Future synthetic targets could be designed to enhance the basicity of the heteroatom ligand by selecting strongly donating ancillary ligands such as those shown in Figure 7.1. Strongly donating ligands will also serve to increase the nucleophilicity of the Rh(III) metal center. The proposed ligands are bulky to avoid dimerization when accessing a 5-coordinate intermediate and do not contain any C–H bonds that could be activated.

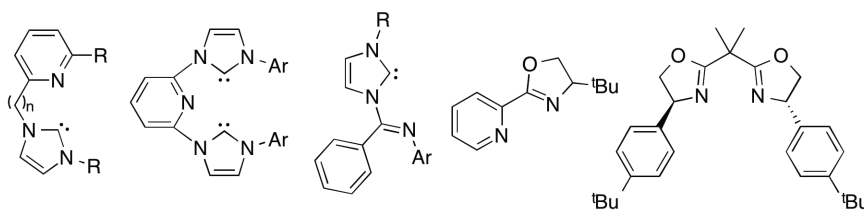


**Figure 7.1.** Ligands for future Rh(III) synthetic targets.

## 7.2 Ethylene Hydrophenylation Using a Ru(II) Complex Supported by a Charge Neutral Poly(pyrazolyl) Alkane Ligands

In Chapter 6, the functionalization of benzene C–H bonds using the cationic Ru(II) complex  $[(\text{HC}(\text{pz}^5)_3)\text{Ru}(\text{P}(\text{OCH}_2)_3\text{CEt})(\text{NCMe})\text{Ph}][\text{BAR}'_4]$  [ $\text{HC}(\text{pz}^5)_3 = \kappa^3\text{-tris}(5\text{-methylpyrazolyl})\text{methane}$ ;  $\text{Ar}' = 3,5\text{-CF}_3\text{-C}_6\text{H}_3$ ] was discussed. This project was focused on the development of catalysts for olefin hydroarylation, the addition of aromatic C–H bonds

across olefin C=C bonds, which provides an alternative method to acid-based catalysis for the synthesis of alkyl or vinyl arenes.<sup>6,7,8</sup> Transition metal-mediated olefin hydroarylation often involves  $\eta^2$ -olefin coordination to the metal followed by olefin insertion into the metal–aryl bond. Ensuing aromatic C–H activation and subsequent liberation of alkyl arene regenerates the starting metal complex.

The catalytic activity of the cationic Ru(II) complex  $[(\text{HC}(\text{pz}^5)_3)\text{Ru}(\text{P}(\text{OCH}_2)_3\text{CEt})(\text{NCMe})\text{Ph}][\text{BAR}'_4]$  for the hydrophenylation of ethylene was compared to our previously reported neutral Ru(II) complexes  $\text{TpRu}(\text{L})(\text{NCMe})\text{Ph}$  [ $\text{Tp}$  = hydridotris(pyrazoyl)borate;  $\text{L}$  = CO,  $\text{PMe}_3$ ,  $\text{P}(\text{OCH}_2)_3\text{CEt}$ , and  $\text{P}(\text{OCH}_2)_2(\text{OCCH}_3)$ ].<sup>9,10</sup> Based on our studies of  $\text{TpRu}(\text{L})(\text{NCMe})\text{Ph}$  catalysts, we predicted that less electron-rich Ru(II) complexes would give higher TONs. As a result, we targeted a cationic variant. Replacement of  $\text{Tp}$  with a charge neutral poly(pyrazolyl) alkane ligand allowed the synthesis of a cationic Ru(II) complex,  $[(\text{HC}(\text{pz}^5)_3)\text{Ru}(\text{P}(\text{OCH}_2)_3\text{CEt})(\text{NCMe})\text{Ph}][\text{BAR}'_4]$ , that is structurally similar to  $\text{TpRu}(\text{P}(\text{OCH}_2)_3\text{CEt})(\text{NCMe})\text{Ph}$  but less electron-rich.

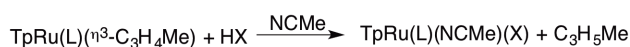
The reaction of  $[(\text{HC}(\text{pz}^5)_3)\text{Ru}(\text{P}(\text{OCH}_2)_3\text{CEt})(\text{NCMe})\text{Ph}][\text{BAR}'_4]$  (0.025 mol% relative to benzene) in benzene with  $\text{C}_2\text{H}_4$  (15 psi) gave 565 TONs of ethylbenzene with no significant production of styrene or dialkylbenzene after 131 h at 90 °C. This corresponds to 28-fold improvement compared to optimized conditions for  $\text{TpRu}(\text{P}(\text{OCH}_2)_3\text{CEt})(\text{NCMe})\text{Ph}$ . The stability of  $[(\text{HC}(\text{pz}^5)_3)\text{Ru}(\text{P}(\text{OCH}_2)_3\text{CEt})(\text{NCMe})\text{Ph}][\text{BAR}'_4]$  is enhanced relative to  $\text{TpRu}(\text{L})(\text{NCMe})\text{Ph}$  complexes allowing catalysis at higher temperatures. The TOF for ethylene hydrophenylation using  $[(\text{HC}(\text{pz}^5)_3)\text{Ru}(\text{P}(\text{OCH}_2)_3\text{CEt})(\text{NCMe})\text{Ph}][\text{BAR}'_4]$  at 150

$^{\circ}\text{C} \geq 2.0 \times 10^{-2} \text{ s}^{-1}$ , which is  $\sim 42$  times greater than the TOF for  $\text{TpRu}(\text{P}(\text{OCH}_2)_3\text{CEt})(\text{NCMe})\text{Ph}$  at  $90^{\circ}\text{C}$  ( $4.8 \times 10^{-4} \text{ s}^{-1}$ ).

### 7.2.1 Future Directions

These results suggest that even less electron-rich Ru(II) complexes could exhibit enhanced longevity. As a result, efforts towards the synthesis of  $[(\text{HC}(\text{pz}^5)_3)\text{Ru}(\text{CO})(\text{NCMe})\text{Ph}][\text{BAR}'_4]$  are underway. The synthesis of this complex is proving challenging due to poor solubility of the synthetic precursors in organic solvents and the potential for these species to form dimers.

Ethylene C–H activation to form Ru–vinyl complexes results in the deactivation of  $\text{TpRu}(\text{L})(\text{NCMe})(\text{Ph})$  [ $\text{L} = \text{PMe}_3$ ,  $\text{P}(\text{OCH}_2)_3\text{CEt}$ , and  $\text{P}(\text{OCH}_2)_2(\text{OCCH}_3)$ ] catalysts.<sup>9,10</sup> The deactivation of  $[(\text{HC}(\text{pz}^5)_3)\text{Ru}(\text{P}(\text{OCH}_2)_3\text{CEt})(\text{NCMe})\text{Ph}][\text{BAR}'_4]$  to form an  $\eta^3$ -allyl complex  $[(\text{HC}(\text{pz}^5)_3)\text{Ru}(\text{P}(\text{OCH}_2)_3\text{CEt})(\eta^3\text{-C}_3\text{H}_4\text{Me})][\text{BAR}'_4]$  occurs by an analogous pathway. A previous student, Dr. Evan Joslin, indicated that the allyl can be liberated with Brønsted acids:



Thus, if  $\text{TpRu}(\text{L})(\text{NCMe})(\text{X})$ , and related cationic complex can activate benzene, perhaps assisted by added base, the active catalyst can be regenerated. Such regeneration would likely require removal of the liberated acid, and a heterogeneous catalyst would be advantageous. Consequently, one direction is to support the molecular Ru(II) catalyst on solid, insoluble material (Figure 7.2 and Scheme 7.3).

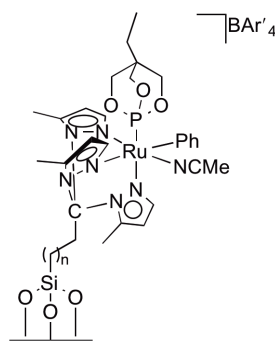
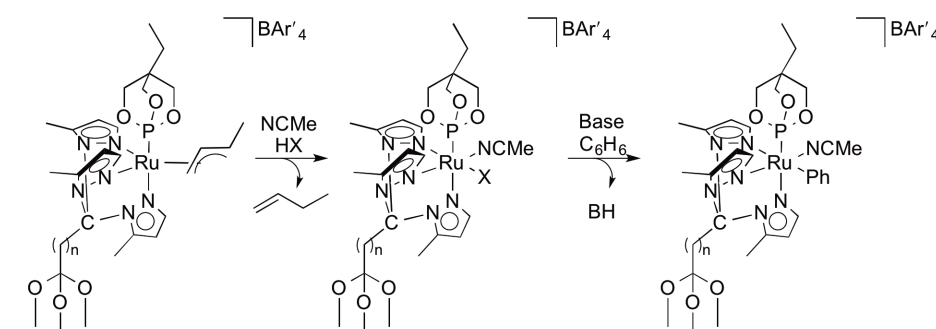


**Figure 7.2.**  $[(\text{HC}(\text{pz}^5)_3)\text{Ru}(\text{P}(\text{OCH}_2)_3\text{CET})(\text{NMe})\text{Ph}][\text{BAR}'_4]$  supported on a mesoporous silica nanoparticle (MSN).



**Scheme 7.3.** Proposed catalyst recycling of MSN-supported  $[(\text{HC}(\text{pz}^5)_3)\text{Ru}(\text{P}(\text{OCH}_2)_3\text{CET})(\text{NMe})\text{Ph}][\text{BAR}'_4]$ .

### 7.3 References

1. Webb, J. R.; Burgess, S. A.; Cundari, T. R.; Gunnoe, T. B. *Dalton Trans.* **2013**, 42, 16646.
2. Webb, J. R.; Bolaño, T. B.; Gunnoe, T. B. *ChemSusChem* **2011**, 4, 37.
3. Gunnoe, T. B., Metal-Mediated Carbon-Hydrogen Bond Activation. In *Physical Inorganic Chemistry: Reactions, Processes, and Applications*, Bakac, A., Ed. Wiley-VCH: Hoboken, N. J, 2010; pp 495.
4. Bernskoetter, W. H.; Schauer, C. K.; Goldberg, K. I.; Brookhart, M. *Science* **2009**, 326, 553.

5. Perutz, R. N.; Turner, J. J. *J. Am. Chem. Soc.* **1975**, *97*, 4791.
6. C. Perego, P. P., Advances in Aromatics Processing Using Zeolite Catalysts. In *Advances in Nanoporous Materials*, Elsevier B. V. : Great Britain, 2009; Vol. 1, pp 97.
7. Perego, C.; Ingallina, P. *Green Chem.* **2004**, *6*, 274.
8. Gerzeliev, I. M.; Khadzhiev, S. N.; Sakharova, I. E. *Petroleum Chemistry* **2011**, *51*, 39.
9. Joslin, E. E.; McMullin, C. L.; Gunnoe, T. B.; Cundari, T. R.; Sabat, M.; Myers, W. H. *Organometallics* **2012**, *31*, 6851.
10. Foley, N. A.; Lee, J. P.; Ke, Z. F.; Gunnoe, T. B.; Cundari, T. R. *Acc. Chem. Res.* **2009**, *42*, 585.